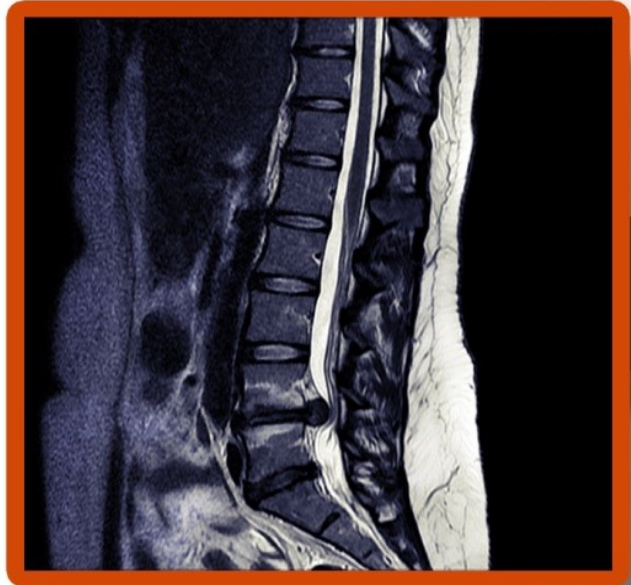


THE LUMBAR MRI IN CLINICAL PRACTICE

WILLIAM E. MORGAN

*A Survey of
Lumbar MRI for
Musculoskeletal
Clinicians*



EDITED BY
CLARE P. MORGAN

“He who studies medicine without books sails an uncharted sea, but he who studies medicine without patients does not go to sea at all.”

William Osler Canadian Physician, 1849-1919

The Lumbar MRI in Clinical Practice

A Survey of Lumbar MRI for Musculoskeletal Clinicians

William E. Morgan





Bethesda Spine Institute LLC,
11117 Innsbrook Way
Ijamsville, Maryland, 21754

Copyright © 2013. Text by William E. Morgan, DC

All rights reserved. No part of this book may be reproduced in any form, or by any electronic, mechanical, or other means without prior permission in writing from the publisher.

Editor: Clare P. Morgan

All rights reserved

Copies of this eBook can be purchased through <http://drmorgan.info/home/>

Disclaimer

The views expressed in this book are those of the author and do not necessarily reflect the official policy or position of the Department of the Navy, Department of the Army, Department of Defense, nor the U.S. Government.

Nothing in the presentation implies any Federal/DOD/DON endorsement.

The information within this guide represents the views of the author at the date of publication. Due to the rapid increase in knowledge, the author reserves the right to update and modernize his views as science uncovers more information. While every attempt has been made to verify the information, the author cannot accept responsibility for inaccuracies or oversights. Any perceived disrespect against organizations or individual persons is unintentional. The author makes no guarantee or warranty pertaining to the success of the reader using this material.

The Cost of Piracy

The ability to rapidly share information is part of what makes living in the twenty-first century so extraordinary. So extraordinary that many people forget that much of what is passed from person to person is protected by copyright. Reproducing copyright-protected electronic literature is illegal and is, in a word, stealing. Reproducing copyright protected material is morally wrong and is illegal.

But more disturbing than the legality of piracy is the fact that doctors and students continue to steal the intellectual property of others. When a doctor or student bootlegs intellectual property, it costs them. It costs them their integrity; it costs them their self-respect; and it costs them their shame. If you cannot afford these costs, I would ask you to pay for the labor of others rather than steal it. It is the right thing to do, and our patients deserve to be treated by doctors who have retained their integrity.

Preface

While there are books written on the subject of systematic interpretation of lumbar MRI, they are written from a radiologist's perspective. This presentation seeks to help practitioners who actually treat lumbar spinal conditions to understand how the radiologist's interpretation relates to their patients. This book is not intended to be a replacement for using a radiologist; it is intended to magnify the effectiveness of the practitioner-radiologist relationship. My background is not radiology, but manual treatment of spinal conditions. I learned long ago the value and limitations of a radiologist's report. The value is in their expert interpretation, the ability to identify pathology, injury, and anatomical variance. With the advent of computer-enhanced imagery such as CT and MRI, the amount of data available to a radiologist has increased exponentially. Because of this increase, the radiologist must decide what information is important and what information is incidental. I have seen MRI studies in which a ten-page report would not be sufficient to describe the specific findings. The quality of MRI has improved so much that it is difficult to find images that are totally unremarkable.

The knowledge gained in this book is not a replacement for the many years of training and experience that create board certified radiologists.

This book is intended to be used within the safety net of a qualified radiologist.

The Physics of MR

“Never worry about theory as long as the machinery does what it's supposed to do.”

Robert A. Heinlein, *Waldo & Magic, Inc.* (1950)

The physical science behind MRI was intentionally omitted from this manual. While I do understand the importance of knowing the science behind this medium, I do not have the inclination nor the background to discuss the physics of MRI in this book. I would encourage those interested in knowing more about this aspect of MRI to delve deeper into this subject through another author. This book will concentrate on the clinician's need to extract clinical data from the images, rather than learn how MRI works. I would compare my approach to driving a car with no intricate knowledge of how the engine works, as opposed to learning the mechanics and engineering theories of the automobile before driving. In short, you can drive the car without understanding how the engine works, and for our needs you can understand some diagnostic principles of MRI (within the safety net provided by a qualified radiologist) without knowing the detailed physics.

For those interested in understanding the physics of MR more fully, I recommend the work of Joseph P. Hornak, Ph.D. who offers a free online eBook on the physics of MRI at:

<http://www.cis.rit.edu/htbooks/mri/>

Contents

Chapter	Page
1 The Clinician's Perspective	1
2 Introduction to the Systematic Interpretation of the Lumbar MRI	9
3 Anatomic Atlas of the Lumbar Spine on MRI	24
4 Standardized Anatomic Reference Descriptions	46
5 Classification of Disc Derangements	54
6 Classification of Annular Tears	88
7 Gallery of Lumbar Disc Derangements	96
8 Spondylolysis and Spondylolisthesis	150
9 Spondylosis	180
10 Central Canal Stenosis	187
11 Fractures	202
12 Modic Changes on MRI: Vertebral Body Marrow Morphology	214
13 Lumbar Facets	224
14 Vertebral Hemangiomas	243
15 Conjoined Nerve Roots	249
16 Classification of Spinal Cord Tumors and Masses by Location	258
17 Perineural (Tarlovs) Cysts	268
18 Hematomas	276
19 Metastasis	283
20 Tumors: Schwannomas/Ependymoma	291
21 Inflammatory Joint Disease	297
22 Fat	303
23 Gadolinium Enhancement	323
24 Post-Surgical Findings	330
25 Arachnoiditis and Arachnoid Cysts	347
26 Incidental Visceral Findings	357
27 Other Assorted Findings on MRI	379
28 Upright MRI	394
29 Artifacts	400
30 Systematic Sequence of Interpretation	406
Appendix	410

To return to this page from
anywhere in this book, click this icon:



Introduction

Before beginning this book you should know my peculiar perspective on the duty of the clinician to know the tools of his or her trade and why my perspective is so geared toward the training of clinicians in the various diagnostic tools that they use to make clinical decisions.

When I had been in practice for about ten years, a young man was referred to my office with neck pain and headaches. He had fallen and struck his head three months prior and subsequently had been seen by five different physicians. Cervical spine X-rays along with CTs of the head and cervical spine were taken at the time of injury, but the radiologist's reports were negative. I accepted this referral and the radiographic reports at face value and began a treatment plan. Early in the care I sensed that something was not right with this patient even though he was neurologically intact. I requested another set of x-rays, something the insurance company balked at because it was not compliant with their guidelines for care. I insisted and provided a compelling enough argument that the insurance company acquiesced and authorized a second set of X-rays. Soon I received a call from the radiologist, a friend of mine, who was very energetic on the phone. "Bill," he said, "I read the x-rays on the patient that you sent over this afternoon. He needs to be transported to the ER in a rigid cervical collar as soon as possible. He has a hangman's fracture of C2 and an anterior dislocation of C2 on C3."

We transported the patient to the ER of the hospital, but the orthopedic surgeon on call refused to come down for a patient who had been injured three months prior. I never will forget his words on the phone, "If his head hasn't fallen off in the last three months, it's not going to fall off tonight." Thank God he was right since I could not get a physician with admitting privileges to admit this young man. He spent the night in the ER before being admitted the next morning. The orthopedic surgeon was astounded at the sight of the new images and was a little sheepish around me for some time after this event. The young man subsequently received three corrective surgeries.

When we reviewed the original X-rays and CT scans, the fractures were clearly visible, though the anterior dislocation was not. Another set of eyes or two may have been able to spot the fractures and get this patient to the appropriate level of care sooner. Since that day I have been committed to reviewing the actual images of my patients and not just the written report. This book is intended to help you to be another set of eyes in screening those images. It will also help you to understand what the radiologist is saying in his or her report.

William E. Morgan

The Clinician's Perspective

1



Why Should a Clinician Study Lumbar MRI?

It has been said that a picture is worth a thousand words. I believe that this adage is true if you understand what you are observing. The radiology report is an attempt to describe in words what is seen in a radiographic image. This will work well for describing overt pathology, injury, or obvious clinically significant findings. A picture is worth a thousand words, yet the average radiologist report fails to have even a thousand words.

Radiologists are economical in the use of words in their reports, so by necessity the radiologist must triage what findings reach the written report. With advanced imagery technology such as CT and MRI, so much information is available that if a radiologist were to describe everything visible in every slice of imagery, the report could conceivably be ten to twenty pages long. A report of that length would be impractical for both the radiologist and the requesting provider. As a result the radiologist must try to determine which findings are clinically significant, and then concisely pass these on to the requesting provider.

Prior to the innovation of MRI and CT, spinal specialists used clinical findings correlated to X-rays and myelograms. (Myelograms use a contrast media and an X-ray to identify spinal lesions.) When MRIs became available with their increased specificity and sensitivity, a high percentage of the studies yielded the identification of disc herniation. This resulted in an increase in the number of lumbar disc surgeries until it was determined that in many people a disc herniation and other spinal lesions are considered an incidental finding. Just because you find a derangement or anomaly, it does not mean that it is clinically significant. Analyzing the patient history and physical examination along with an MRI will help to determine the clinical relevance of a finding on MRI.

We can expect the radiologist to identify most pathology, diagnostic findings such as disc derangements, and findings that have the potential of being clinically significant. What they do lack, however, is first-hand knowledge of the patient.

Below is the description of a famous work of art. It is written from a detached point of view that is uninformed about the people and events in the painting. It is accurate in every way, but lacks sufficient background knowledge to clearly state what is happening.

Image Report

This painting appears to be an oil on plaster painting. This image demonstrates a well-developed white male reclining on a green slope leaning on his right elbow. He is nude and devoid of body hair. This man is located on the left side of the painting and is looking at another older man on the right side of the painting. The man on the left is casually reaching his left hand toward the older man. The older man has long gray hair and a beard, but is well-muscled. The older man is surrounded by eleven nude young children and is shrouded in a red cloth. He is wearing a shear short-sleeved tunic. The older man is reaching his right arm with an extended index finger toward the hand of the younger man.

Here is the painting that was described on the previous page. With a historical perspective you may clearly see that image is the romanticized duplication of God reaching out to Adam during Creation painted on the ceiling of the Sistine Chapel by Michelangelo di Lodovico Buonarroti Simoni. While the description of this painting on the previous page was accurate in every way, it lacked the historic and visual perspective that provides the viewer with the immediate knowledge of the significance of the painting.

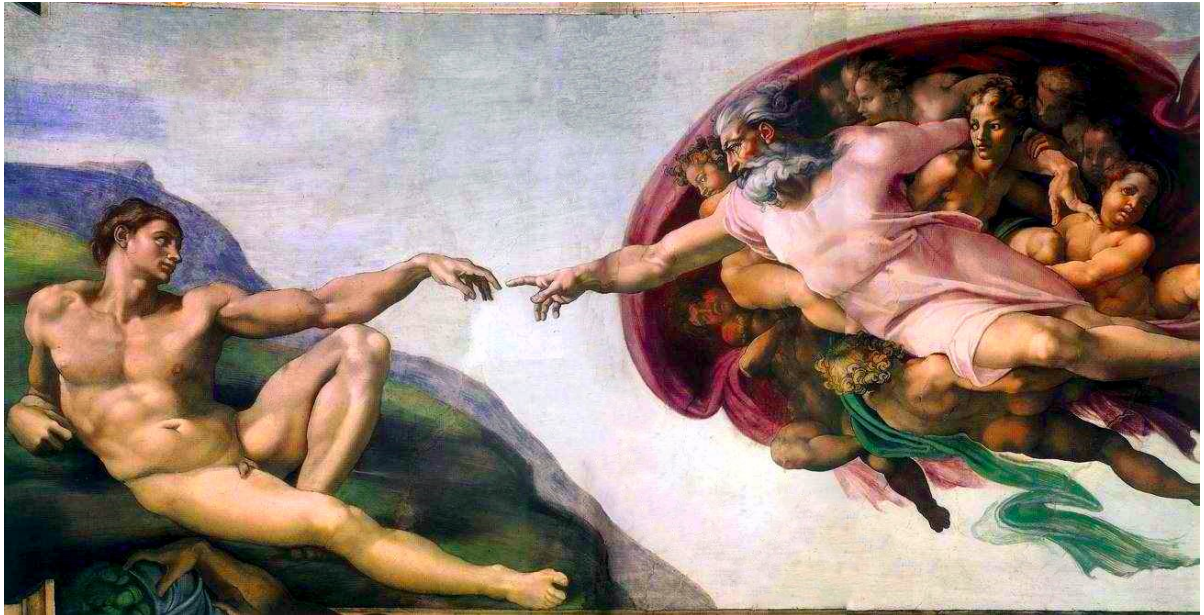


Figure 1:1. The Creation of Adam by Michelangelo di Lodovico Buonarroti Simoni 1512, Sistine Chapel

It is my contention that the historical perspective is important in obtaining information of clinical significance. Having watched many neurosurgical morning reports, it is quite obvious that while they defer to the opinion of the neuroradiologist, the neuro-surgeons connect their history and physical exam with their own interpretation of MRIs to obtain a specific diagnosis. The MRI is a tool that should be in the hands of everyone who treats the spine, and a clinician-radiologist collaborative team is far preferable to having two distinct and non-conversing professions. That collaboration begins with the clinician providing the radiologist with adequate historic and clinical perspective to help the radiologist understand why the study was requested and progresses to the radiologist correlating the radiographic findings to the clinical profile of the patient. For most cases this level of communication is sufficient, but there will be times where only direct interaction between the clinician and the radiologist will suffice. The radiologist may need more clinical information or recommend another study or protocol to better visualize what the clinician wants to see. The clinician may ask the radiologist to expound on the findings or to elaborate on a nuance found in the image. The clinician-radiologist relationship should be a healthy relationship built on clear communication.

What Makes it into a Radiology Report?

The amount of information to a radiologist on a single MRI study is vast, that to attempt to record all findings is not practical and would add confusion to the average practitioner. What is on a radiology report is most pathology and most clinically significant findings, as deemed significant by the radiologist, and a smattering of other details that may be pertinent to the requesting provider. This pyramid represents the findings that are visible on MRIs. It shows that the findings with less of a clinical impact are more common, and the more clinically significant findings are less common. Normal findings and anatomical variants are on the bottom while pathology and diagnostic findings are at the top.

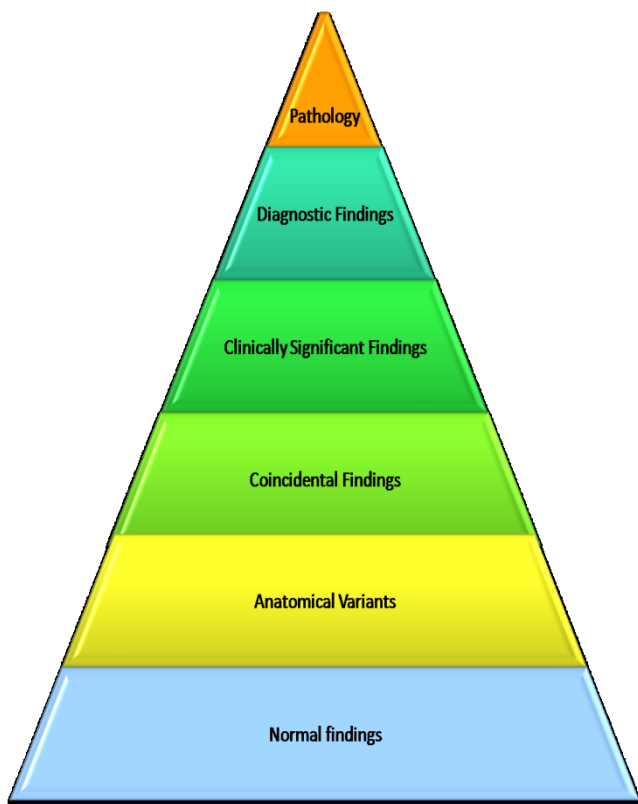


Figure 1:2.

The red inverted triangle represents what is included in a radiology report. Since a report that includes everything could consume an hour of dictation and a ream of paper, the radiologist must prioritize and economize what is reported. Of course all pathology and diagnostically significant findings should be included and most are included. The radiologist will also include a smattering of other findings that have potential significance: coincidental findings, anatomical variants, and the like. This book will not replace the radiology report, and certainly every MRI should be interpreted by a board certified radiologist. But it will aid clinicians in expanding their use of the lumbar MRI past the limitations of a written MRI report.

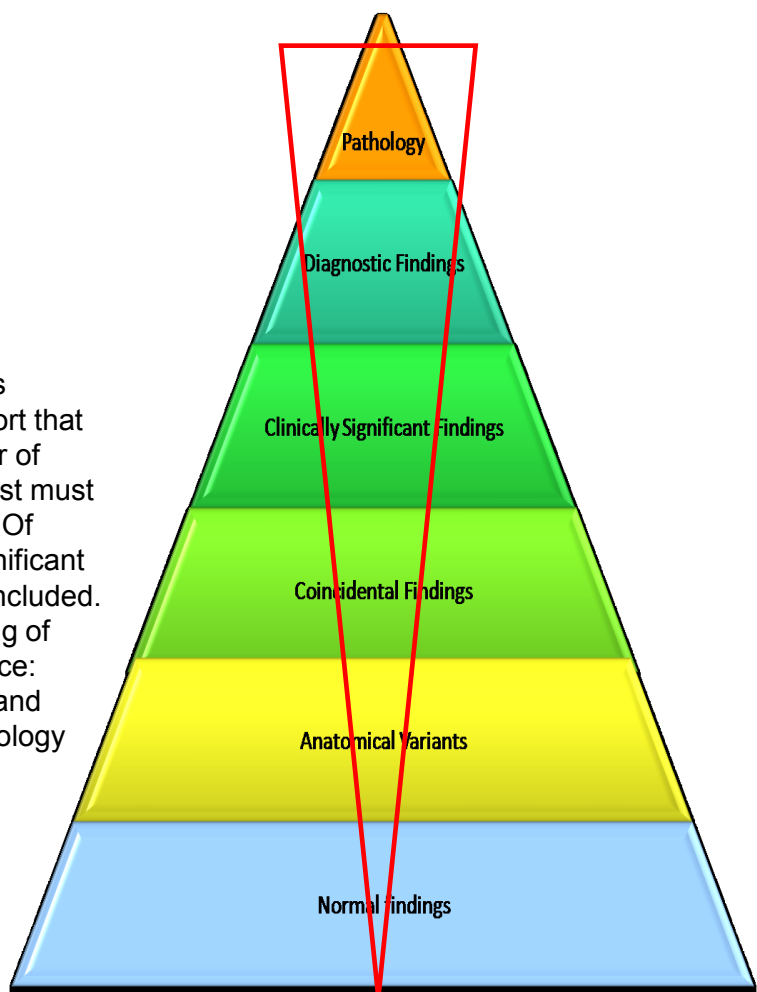


Figure 1:3.

MRI Findings in Asymptomatic Patients

There have been several studies over the years that have found significant MRI findings in asymptomatic subjects. Many of these findings on MR had previously been considered to cause pain and infirmity. Jensen and associates performed scans on 98 asymptomatic individuals. Of the 98 individuals without symptoms, only 36% had normal lumbar discs at every level, 27% had disc protrusions, 1% had an extrusion, 52% had disc bulges at one or more levels, and annular tears were present in 14%.

In another study performed by Boden et al., 67 people who never had lower back pain received lumbar MRIs. Of those individuals younger than 60 years old, 20% had a disc herniation, while those older than 60 had a herniation rate of 36%, and 21% had spinal stenosis.

Weishagupt studied 60 asymptomatic people between the ages of 20 and 50. In this population, 62-67% had lumbar disc bulges or herniations, 32-33% had annular tears, and 18% had disc extrusions.

These and other studies clearly demonstrate the need to correlate a patient's clinical presentation with the findings on lumbar MRI. Coincidental or incidental findings can lead the practitioner on a grand wild goose chase while creating anxiety in the patient. We need to be careful in discerning between findings that have clinical implications and those findings which are merely incidental.

Balancing the Weight of Clinical and Radiographic Findings

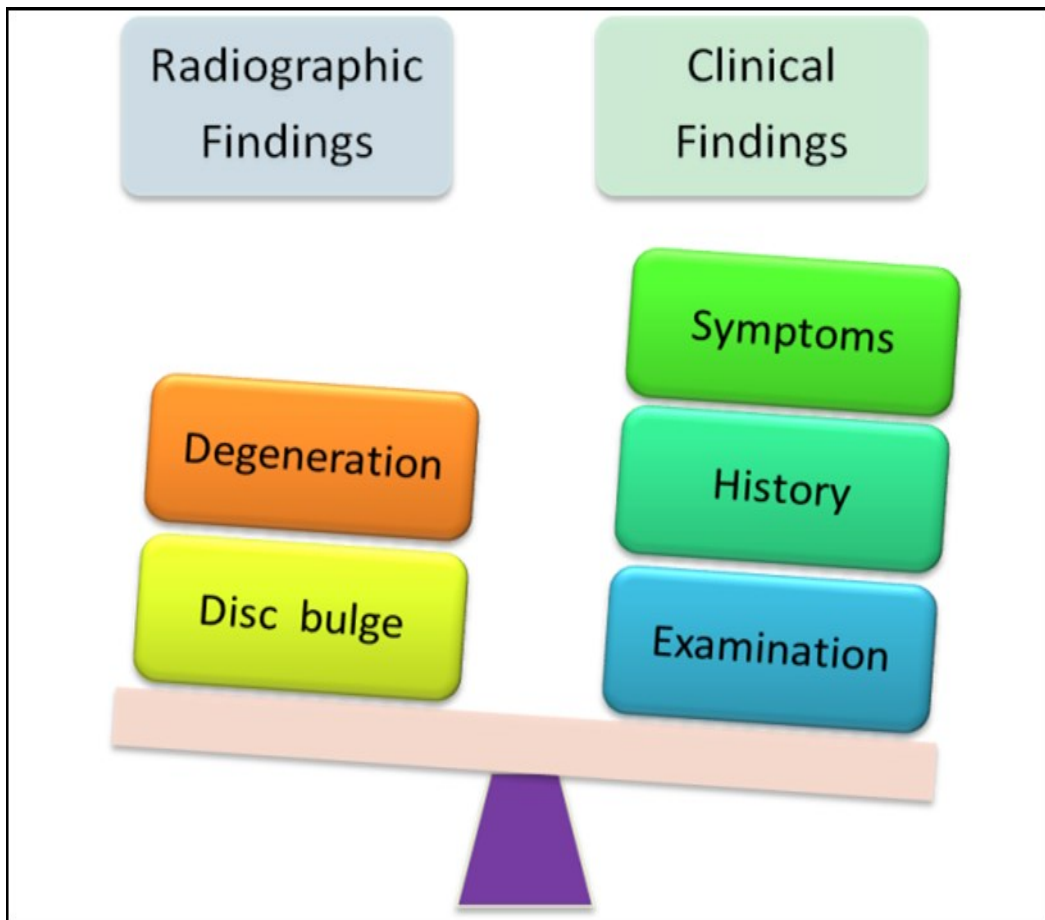


Figure 1:4.

With the amount of detail that is visible on an MRI, it would be easy to get bogged down with the incidental findings on an MRI. Just because there is a finding visible on MRI does not mean that it is clinically significant. *Herniated discs are often seen on MRIs of patients with no clinical manifestation of the condition.* The flip side of learning to read MRI is that the sensitivity of this technology is so great that there can be too much information. All radiographic findings must be correlated to history and clinical findings. So I offer a word of warning to the non-radiologists: Do not jump to conclusions; most MRI findings should be corroborated by the patient's complaints and findings on clinical examination. The exception is the finding of pathologies which may lie dormant clinically, but still require intervention.

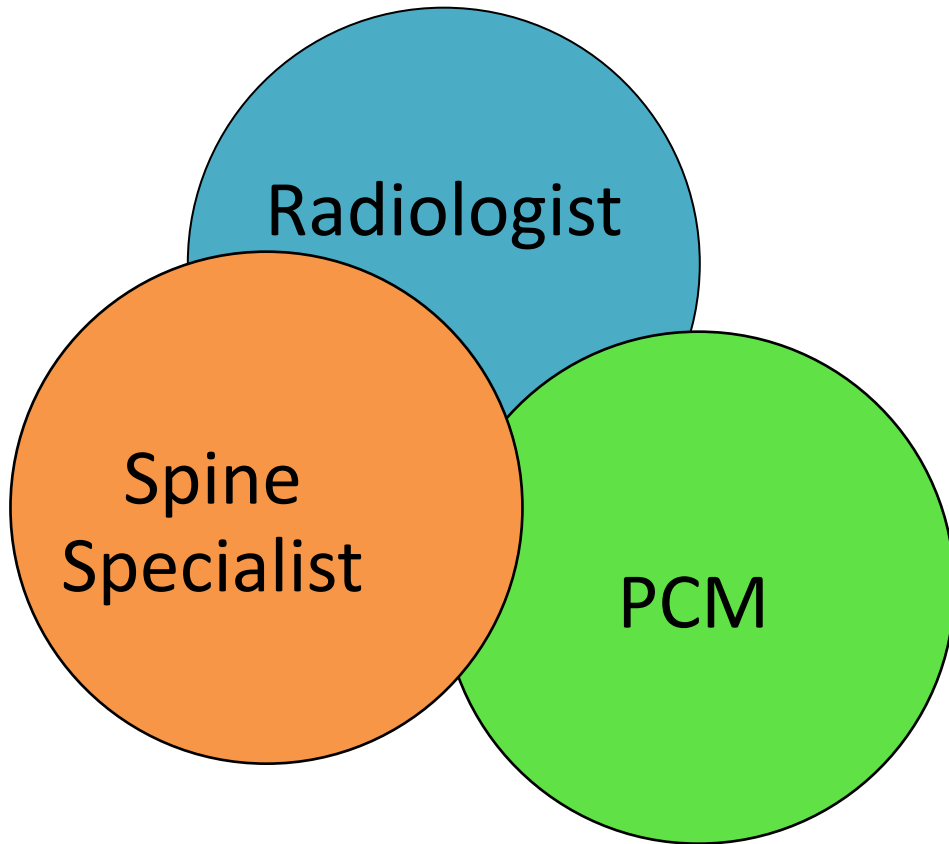


Figure 1:5.

This Venn diagram illustrates the relationships and knowledge overlap of radiologists, spinal specialists, and primary care managers (PCM). The spine specialists and the radiologists (particularly neuroradiologists) have an intersecting body of knowledge. The spine care practitioner has some knowledge of radiology, and the radiologist has some knowledge of spinal care procedures and diagnosis. The primary care manager will have some overlay of knowledge, but it would be to a lesser degree. The PCM would be much more reliant on the written report than someone who primarily treats spinal conditions.

What is not shared with the other providers is the radiologist's in-depth knowledge of radiologic diagnostics and interventions, the spine specialist's in-depth knowledge of spinal conditions and treatments, and the PCM's broad base of medical knowledge. These three team members are reliant on the others for providing optimal patient care.

Suggested Reading

Jensen et al. (1994). Magnetic resonance imaging of the lumbar spine in people without back pain. *New England Journal of Medicine*, Jul 14;331(2):69-73.

Boden et al. (1990). Abnormal magnetic-resonance scans of the lumbar spine in asymptomatic subjects. A prospective investigation. *J Bone Joint Surg Am*. 1990 Mar;72(3):403-8.

Weishaupt et al. (1998). MR imaging of the lumbar spine: prevalence of intervertebral disk extrusion and sequestration, nerve root compression, end plate abnormalities, and osteoarthritis of the facet joints in asymptomatic volunteers. *Radiology*. 1998 Dec;209(3):661-6.

Introduction to the Systematic Interpretation of the Lumbar MRI



Orientation and Sequencing of the Lumbar MRI

Without a systematic approach, endeavoring to interpret MRIs would be a daunting task. Efficient interpretation of the lumbar MRI entails several components: identification of the image orientation, the MRI image type (T2W, T1W, fat suppressed T2W, etc.), the knowledge of the anatomical structures (normal and variants of normal), and the ability to identify injury, abnormality, and pathology. This chapter will introduce a simple system for analyzing lumbar MRI studies.

Image Orientation

There are three planes of orientation that are common in MRI studies: sagittal, axial, and coronal.

1.Sagittal Images- Sagittal images are oriented in a lengthwise view allowing the visualization of the entire lumbar spine in one image. In some aspects the sagittal image resembles a lateral lumbar X-ray. The difference is that the sagittal image shows a slice through the body at a particular anterior to posterior slice. After identifying the sagittal image, determine the left-right orientation.

2.Axial Images- Axial images reveal cross-sectional anatomy of the spine and paraspinal structures. In the axial image the structures appear reversed. The structures from the left side of the body will appear on the right side of the axial image. This is easier to remember and conceptualize if you envision the patient's feet being toward the viewer.

3.Coronal Images- Coronal images are full length studies that show the left-to-right width of the structures studied. These images are usually only included in the spotting/orientation views and are not commonly included in the detailed bulk of the lumbar MRI studies.



Figure 2:1. Sagittal view



Figure 2:2. Axial view

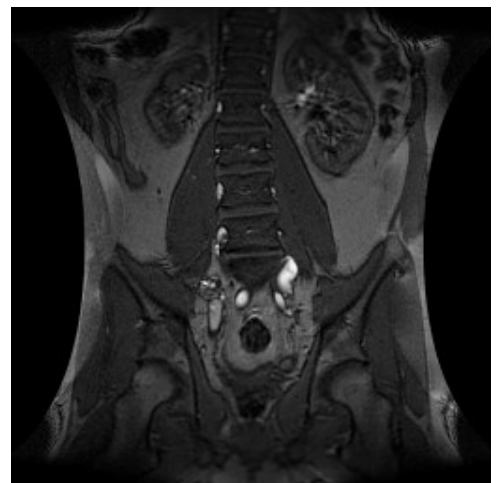


Figure 2:3. Coronal view

Orientation of Axial Images

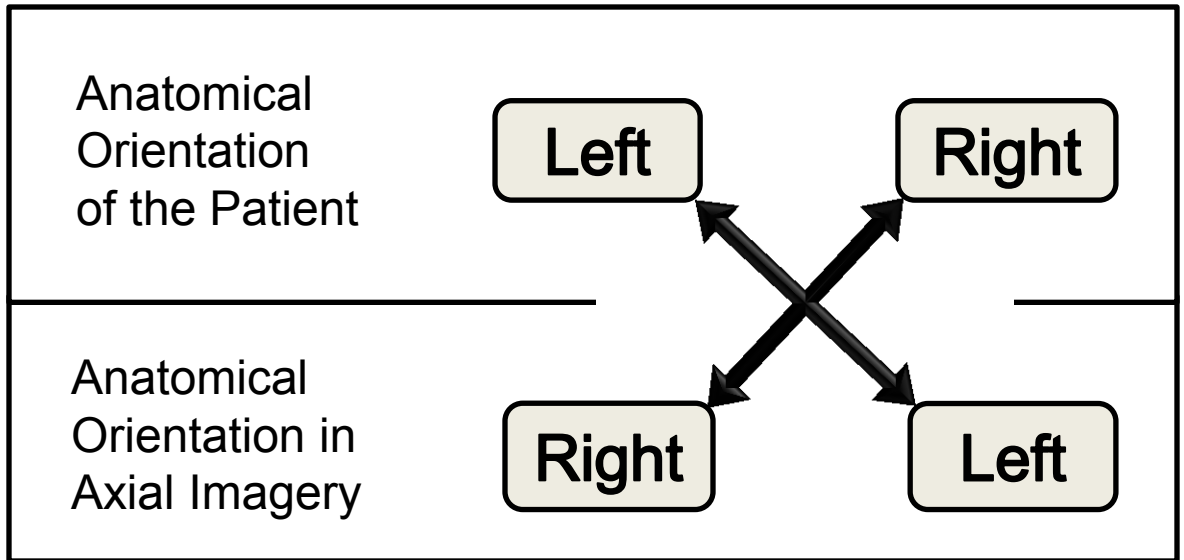


Figure 2:4.



Figure 2:5.

It is important to remember that when viewing axial MRIs left and right are reversed. If a structure is visualized on the right of the axial image, it is found on the left side of the patient. You may notice that in the image above there is a simple cyst in this patient's right kidney. This is seen on the left side of the MRI (yellow arrow).

Image Orientation and Location Descriptors

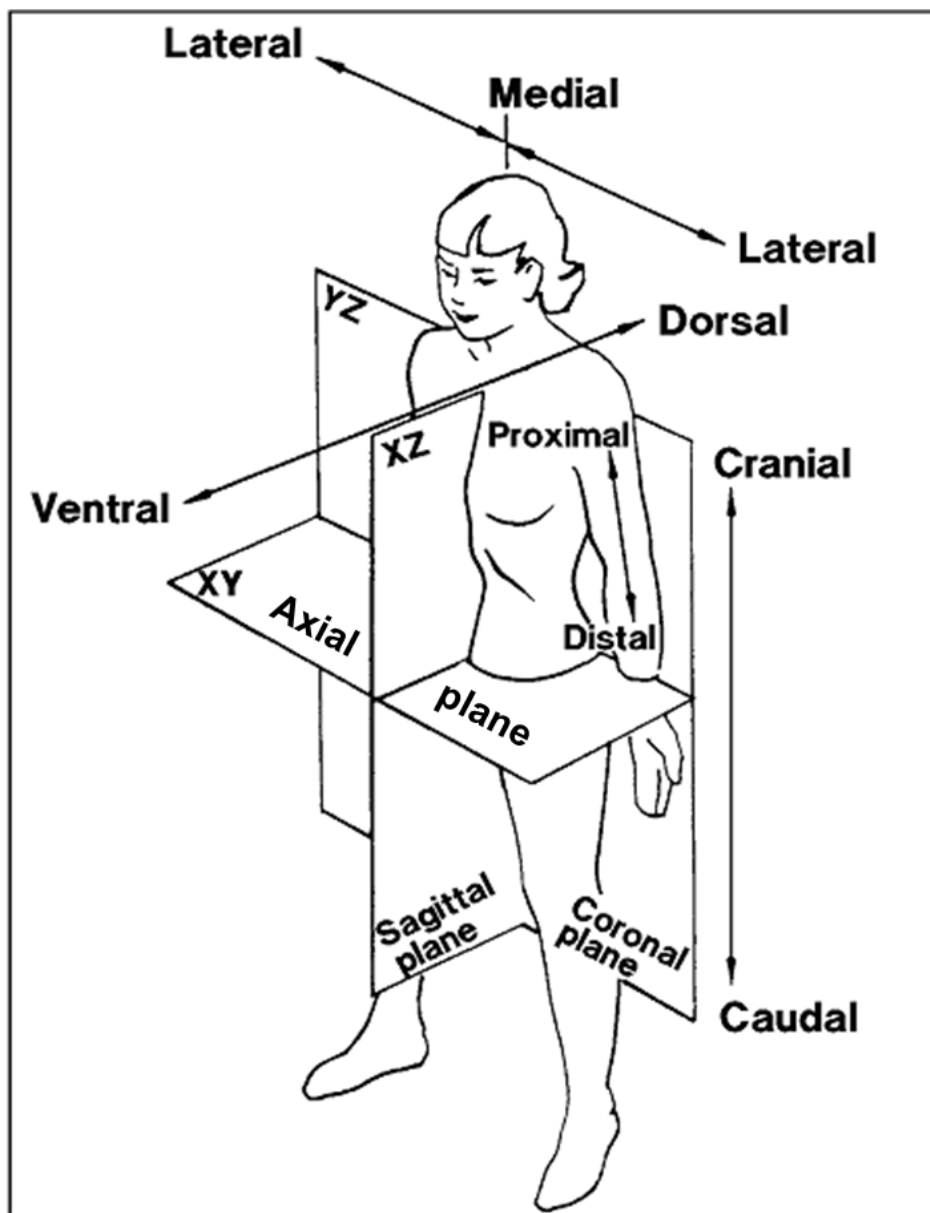


Figure 2:6.

This diagram clearly illustrates the planes available in MRI: axial, sagittal, and coronal. It also clarifies several other terms that are commonly used in anatomical, biomechanical, and radiographic discussions. In describing locations seen on imagery, this standardized terminology will give more complete descriptions of location. There are variations in the use of these descriptors. It is common to see cephalad rather than cranial, or anterior and posterior rather than ventral and dorsal in reports, and transverse rather than axial.

This schematic was adapted from NASA: Reference: 16, pp. III-78; NASA-STD-3000 260 (Rev A)
<http://msis.jsc.nasa.gov/images/Section03/Image64.gif>

Identifying Image Sequences

MRI studies typically include scout films which identify and label the slices. Understanding how to use scout films to identify image locations is fundamental to interpreting MRI studies.



Figure 2:7. The scout image for identifying the axial slices is a sagittal film with lines through it. These lines present each of the axial images available for viewing. This particular image identifies and labels 30 different axial slices. When viewing an axial image, the level can be identified by finding the corresponding identifying markers. These slices are uniform and made horizontally, regardless of the angles of the vertebral anatomy.

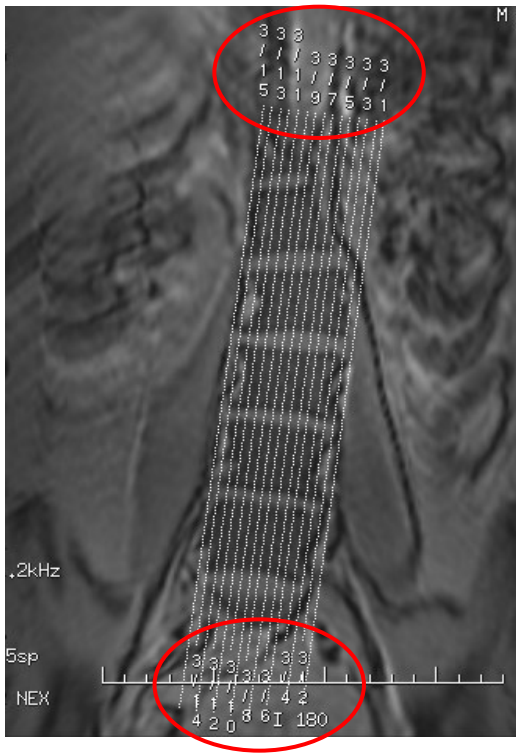


Figure 2:8. For sagittal images the scout film is a coronal film with lines through it. These lines correspond to each of the sagittal images available for viewing. This particular image identifies and labels 15 different sagittal slices. The key to viewing sagittal imagery is to know which side of the spine you are viewing: left or right.

In viewing MRI in an electronic format sequence, identification is simplified by the use of scout lines and linking images together and scrolling.



Figure 2:9. Uniform horizontal slices

In most lumbar MRIs the axial slices will be evenly spaced intervals (figure 2:9). Some studies will emphasize special regions of anatomy or a site of concern, such as the site of an injury, degeneration, or disease; or a study may be limited to the disc spaces (figure 2:10). They may even be angled to correlate to the angles of the vertebrae and disc spaces. These spotting or scout films indicate that the technician selected slices through the disc spaces and through an area of particular concern. The technician also made sure that the slice angles aligned with the anatomic variations of the lumbar segments. Note that there are areas of the lumbar vertebrae which are not visualized at all.

The red lines in the scout film of figure 2:11 reveal large areas of the lumbar spine that are not represented in axial imagery. This study was particularly intended to visualize a condition affecting the L3-4 vertebrae and disc along with the intervertebral disc spaces of the rest of the lumbar spine.



Figure 2:10. Slices along the disc planes.

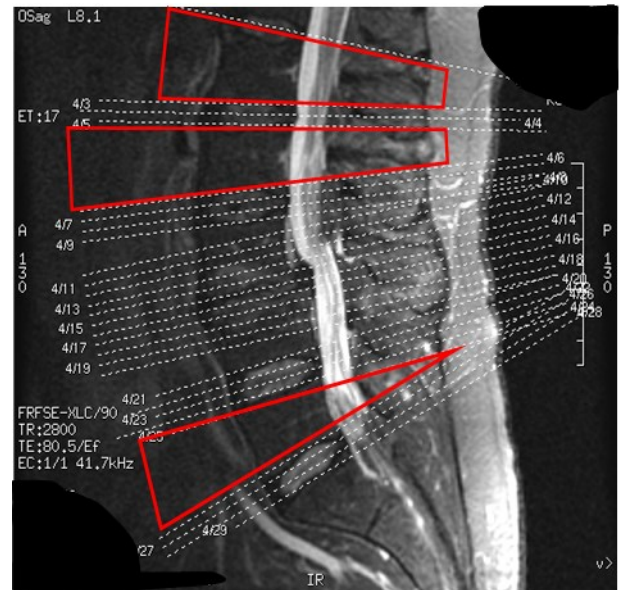


Figure 2:11. Selective slices of anatomy of particular interest. Note the red bordered sections with no slices.

MRI Image Type

MRI image types enhance various tissue types differently. This allows the differentiation of tissues by the specialist. The various types of MRI images are as follows:

1. T1 Weighted Image: Water densities are dark, and fat densities are bright. T1WI have greater anatomic detail than T2WI.

2. T2 Weighted Image: Water and fat densities are bright, while muscle appears intermediate in intensity.

3. Fat Suppressed T2 Weighted Image: Water densities are bright, whereas fat is suppressed and dark.

4. Intermediate T2 Weighted Image: Ligaments and cartilage are viewed as very dark.

5. Gadolinium Enhanced T1 Weighted Image: Gadolinium is an injected contrast media. It is used to identify pathology.

6. Fast Spin Echo (FSE): Frequently used in musculoskeletal imaging, FSE allows quicker image acquisition of T2 weighed images. Fat is bright on T2 weighted images. Marrow or subcutaneous pathology may not show up unless fat suppression is used.

7. FSE STIR (Short T1 Inversion Recovery): This image has a decreased signal intensity (brightness) from fat and an increased signal from fluid and edema. It is useful in identifying soft tissue and marrow pathologies.

8. Proton Density: Proton density uses a mixture of T1 and T2 images. It is characterized by enhanced anatomical detail and poor tissue contrast.

9. Fat Saturation: Fat saturation employs a “spoiler” pulse that neutralizes the fat signal without affecting the water and gadolinium signal. Fat saturation can be used with T1 weighted images to distinguish a hemorrhage from a lipoma. When used with FSE T2 weighted images, fat saturation can enhance marrow or soft tissue pathology.

10. FIESTA (Fast Imaging Employing Steady sTate Acquisition): This method of image acquisition captures structures rapidly and provides high quality images of fluid-filled structures.

Comparing T1 to T2 Weighted Images

MRI Image Characteristics

For practical purposes the most commonly utilized types of MRI images by non-radiologists are T1 and T2 weighted images. T1 has greater anatomic detail, but T2 tends to be the favored image type for observing the intervertebral disc and the spinal cord. The chart below reflects the characteristics of each image type. These images highlight the characteristics of T1 and T2 images.

Tissue	T1	T2
Bone	Neutral	Neutral
Air	Dark	Dark
Fat	Bright	Light
Water	Dark	Bright

Figure 2:12. Tissue characteristics on MR with T1 and T2 weighted imagery.

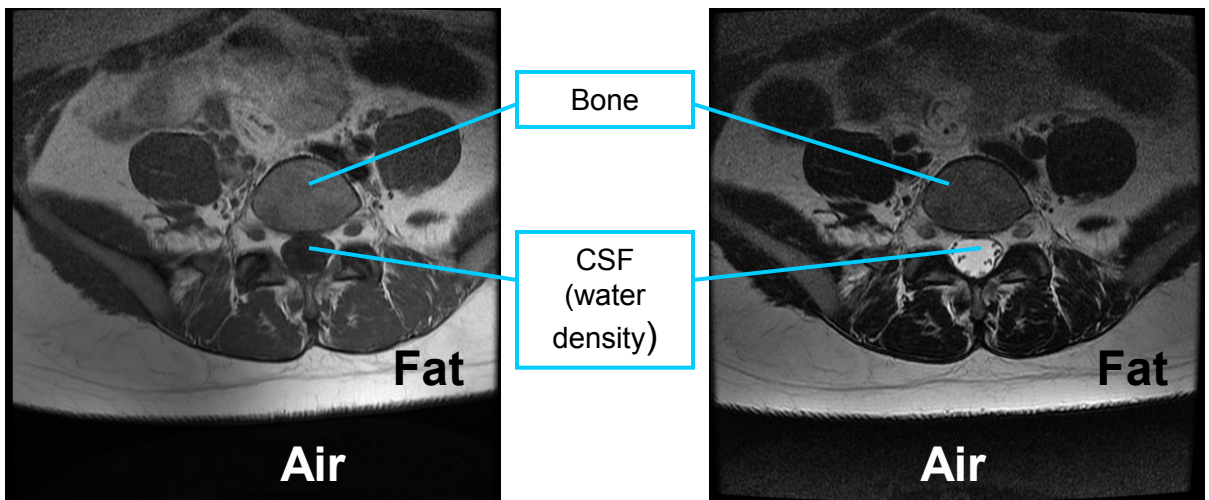


Figure 2:13. T1W Axial Image

Figure 2:14. T2W Axial Image

Note that some tissues are dark (low intensity signal) on both image types. These include: gas, cortical bone, calcification, tendons/ligaments, and menisci.

How are T1 and T2 Weighted Images Alike?

For comparison purposes the two sagittal images have been placed side by side with T1 on the left and T2 on the right. Note that on both images the vertebral bodies are a neutral gray color, the muscles and ligaments are dark, air is black, and fat is light-colored.

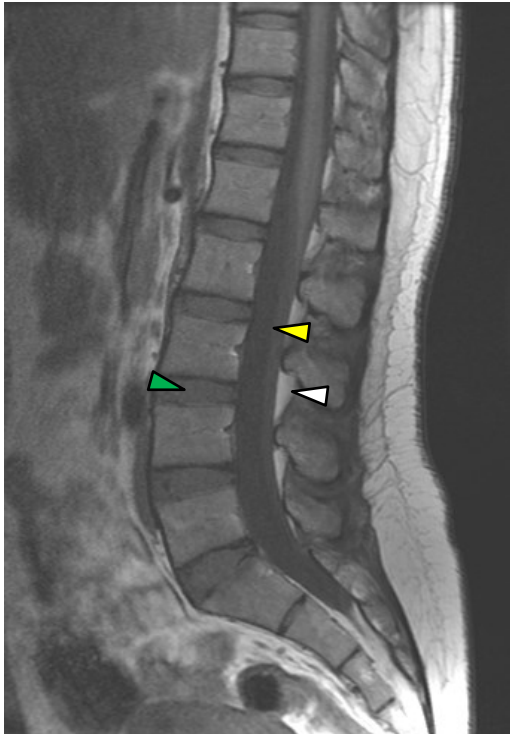


Figure 2:15. T1 Weighted Sagittal Image. The green arrow points to the dark (hypointense) disc, the white arrow points to the fat of the posterior recess, and the yellow arrow points to the fluid of the CSF.



Figure 2:16. T2 Weighted Sagittal Image. The blue arrow points to the hyperintense signal, indicative of a well-hydrated disc. The yellow arrow points to the bright signal, characteristic of fluid in the CSF.

How Do T1 and T2 Weighted Images Differ?

The difference is black and white. In T1 images water is black, while T2 images display water as white. The blackness of water in a T1 image makes it more difficult to differentiate the cerebral spinal fluid from the nerves, and likewise, the disc from the contents of the central canal. However, the T1 image aids in discerning the details of other anatomic structures.

Characteristics of T1 and T2 Weighted Images and Fluid-Filled Lesions



These two images are from a patient with multiple benign renal cysts. Note the large light colored ovoid lesions in the kidneys in the T2 weighted image (figure 2:17). The cysts are easy to distinguish from the soft tissue of the kidneys.

In the T1 weighted image (figure 2:18) the water-density cysts are dark and more difficult to distinguish from the kidneys.

Fat is light-colored in both T1 and T2, while muscles, ligaments, and tendons are dark.

Figure 2:17. T2 weighted axial image reveals multiple large renal cysts. These cysts are ovoid and light-colored.

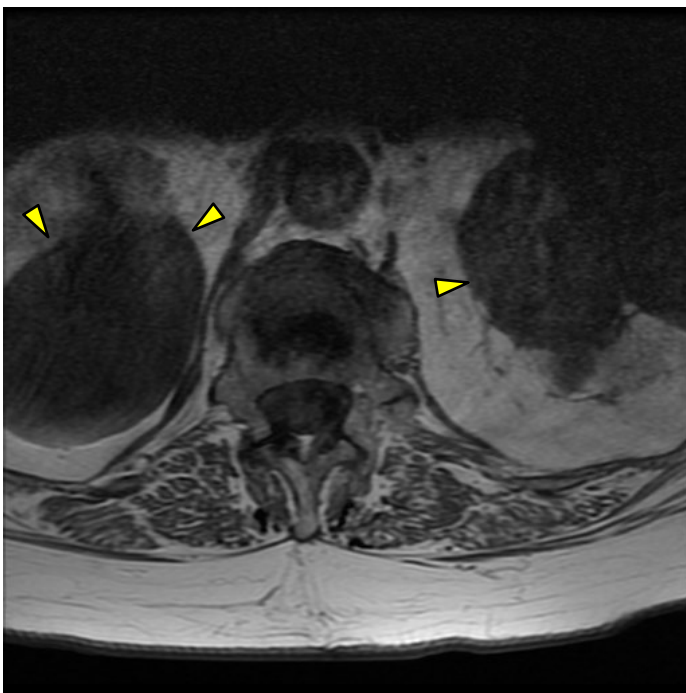


Figure 2:18. In this T1 weighted axial image the renal cysts are dark.

Systematic Interpretation of the Lumbar MRI

There are several methods for systematically reviewing lumbar MRIs. This method ensures that you cover the images in a logical manner. The next two pages expand on how to analyze axial and sagittal sequences in detail. As you develop an eye for the subtleties found in lumbar MRI, you will find that sticking to a systematic procedure of observation will help you to avoid missing important findings.

Sequence of Systematic Interpretation of Lumbar MRI Images

1. Verify patient identifiers and date of examination.
2. Confirm that the images and the studies are in order if using film rather than digitized images.
3. View the sagittal T2 weighted images from left to right.
4. View the sagittal T1 weighted images from left to right.
5. View and analyze the T2 weighted axial images from caudal to cephalad.
6. View and analyze the T1 weighted axial images from caudal to cephalad.
7. Review your findings and compare to the radiologist's report.
8. Determine if the radiographic findings are clinically significant or coincidental findings.
9. Integrate collaborative MRI findings into patient care.

Sequential Analysis of Sagittal Images

1. Identify the left-right orientation. Sagittal images represent anatomic slices in a vertical plane which travel through the body from posterior to anterior and divide the body into right and left components. Scroll from left to right. If you are unable to identify the orientation of the sagittal images, remember that the aorta is on the left while the inferior vena cava is on the right. The aorta typically has a greater girth and a more symmetrically round appearance.

2. Analyze the spine from a global view. Scan through the sagittal images and look for larger, more obvious findings:

Alignment of the spine - Spondylolisthesis and retrolisthesis can be usually be discerned on sagittal inspection. Scoliosis can be a little more difficult. On sagittal imagery a scoliosis will present with partial views of structures and a contorted view of the spinal canal and vertebral bodies.

Vertebral body shape- Identify endplate disruption, Schmorl's nodes, compression fractures, block vertebrae, and fusion.

Vertebral body content- Analyze for edema, tumors, fatty infiltration, and hemangiomas.

Posterior elements- Evaluate the facets, the pars, the spinous processes, the pedicles, and the lamina.

Endplates- Look for sclerotic changes and alterations in signal intensity as well as disruptions or fractures of the endplates.

3. Intervertebral foramina:

The IVF should be a light-colored peanut-shaped image with a gray dot in the middle. The light color is due to the fat that is in the foramina. When displaced, the light-colored fat will alter in shape. The gray dot in the foramina is the exiting nerve root.

4. The discs and the spinal canal:

Look for alterations in disc height. Increased disc height may occur with discitis. Loss of disc height and reduced water content is indicative of degeneration. Disc tears and derangements may also be observed in sagittal imagery. Note disruptions of the thecal sac, the cauda equina, and nerve roots.

High intensity zones (HIZ) may be observed in T2 weighted images. These bright-colored zones indicate the presence of disc tears, scarring, or vascularization of the annulus.

The cord should terminate at about the level of L1. Increased signal (brightness) on T2 weighted images may indicate cysts, tumors, syrinxes, or demyelination.

Sequential Analysis of Axial Images

1. Identify left and right. Axial images are backwards; structures seen on the left of an axial image represent structures found on the right side of the patient.
2. Begin your analysis caudally proceeding cephalad. The sacrum will be easily recognizable. Observe the S1 nerve roots. Look for perineural (Tarlov's cysts) which occur most commonly at the S2 and S1 nerve roots.
3. As you scroll superiorly, observe the L5-S1 disc. Note the circumferential margin of the disc and inspect it for derangement. Scroll past the disc to the L5 vertebra. Note that L5 is commonly shaped like a lemon when viewed axially. Observe the bony integrity of L5. Look for elongation of the central canal which may be indicative of a spondylolisthesis.
4. The canal should be intact and not effaced. Look for effacement or disruption of the thecal sac by discs, osteophytes, spondylosis, or other space-occupying lesions.
5. Look at the lumbar discs and evaluate for tears, herniations, nerve compression, and degeneration.
6. Identify the ligamentum flavum, and look for signs of hypertrophy and subsequent stenosis.
7. Evaluate the posterior elements of the vertebrae. Look for pars defects, spina bifida, facet hypertrophy, and overall posterior ring integrity.
8. Examine the retroperitoneal space.
9. In addition to examining the spinal structures, evaluate and note the paraspinal muscles, multifidus muscles, iliopsoas muscles, the great vessels, and the kidneys.
10. After scrolling up the lumbar spine, reverse directions and descend the spine to follow the course of the nerve roots. Start cephalad and scroll (if using a computer) caudally. If looking at film, move from slide to slide. Follow the migration of the nerve rootlets from the cauda equina from their posterior central location to the lateral anterior portion of the thecal sac and then leaving the sac as traversing nerve roots.

Which Radiological Studies Should You Order?

Develop a relationship with your radiologist and be willing to consult with the radiologist prior to ordering radiological studies. Explain the history and work with the radiologist to determine the best study for each patient.

Trauma	<ul style="list-style-type: none">•Plain films may be used initially to determine if there is an unstable injury or displacement•Non-contrast CT•MRI to evaluate cord integrity
Tumors	MRI with contrast enhancement
Inflammation and Vascular Disorders	MRI with contrast enhancement
Scoliosis	Plain-film X-rays unless pathology is suspected; then MRI
Congenital anomalies	MRI without contrast enhancement
Infections	MRI with contrast enhancement
Nerve Root Compression	MRI
Spondylolisthesis	<ul style="list-style-type: none">•Plain film radiographs•CT•MRI if there is a need to evaluate neuronal involvement

Note: There is an inherent danger in using contrast enhancements. These risks include allergic reaction, shock, and death.

CTs are less expensive than MRI and are the medium of choice for head and neck trauma. CTs utilize significant doses of radiation and increase the risk of cancer.

Suggested Reading

Cramer G, Darby S (2013). Basic and clinical anatomy of the spine, spinal cord, and ANS (third edition). Elsevier Mosby.

Marchiori D (2013). Clinical imaging: with skeletal, chest and abdomen pattern differentials (third edition). Mosby.

Atlas SW. (2008). Magnetic resonance imaging of the brain and spine (forth edition). Lippincott Williams & Wilkins.

Ross JS et al. (2010). Diagnostic imaging spine (second edition). Amirsys Inc.

Anatomic Atlas of the Lumbar Spine on MRI



Anatomy

In addition to knowing the image orientation and MRI image type, it is important to have a good foundation in the anatomy of the lumbar spine as viewed on MRI. This chapter will review the lumbar anatomy as viewed in various sequences.

This sagittal T2 weighted image demonstrates typical vertebrae, intervertebral discs, and the sacrum. The light-colored disc in a T2 weighted image is indicative of a healthy well-hydrated disc. The light-colored zones in the nucleus pulposus appear brighter than the annular fibers. The vertebrae remain neutral gray in color. A normal lumbar lordosis is visualized.

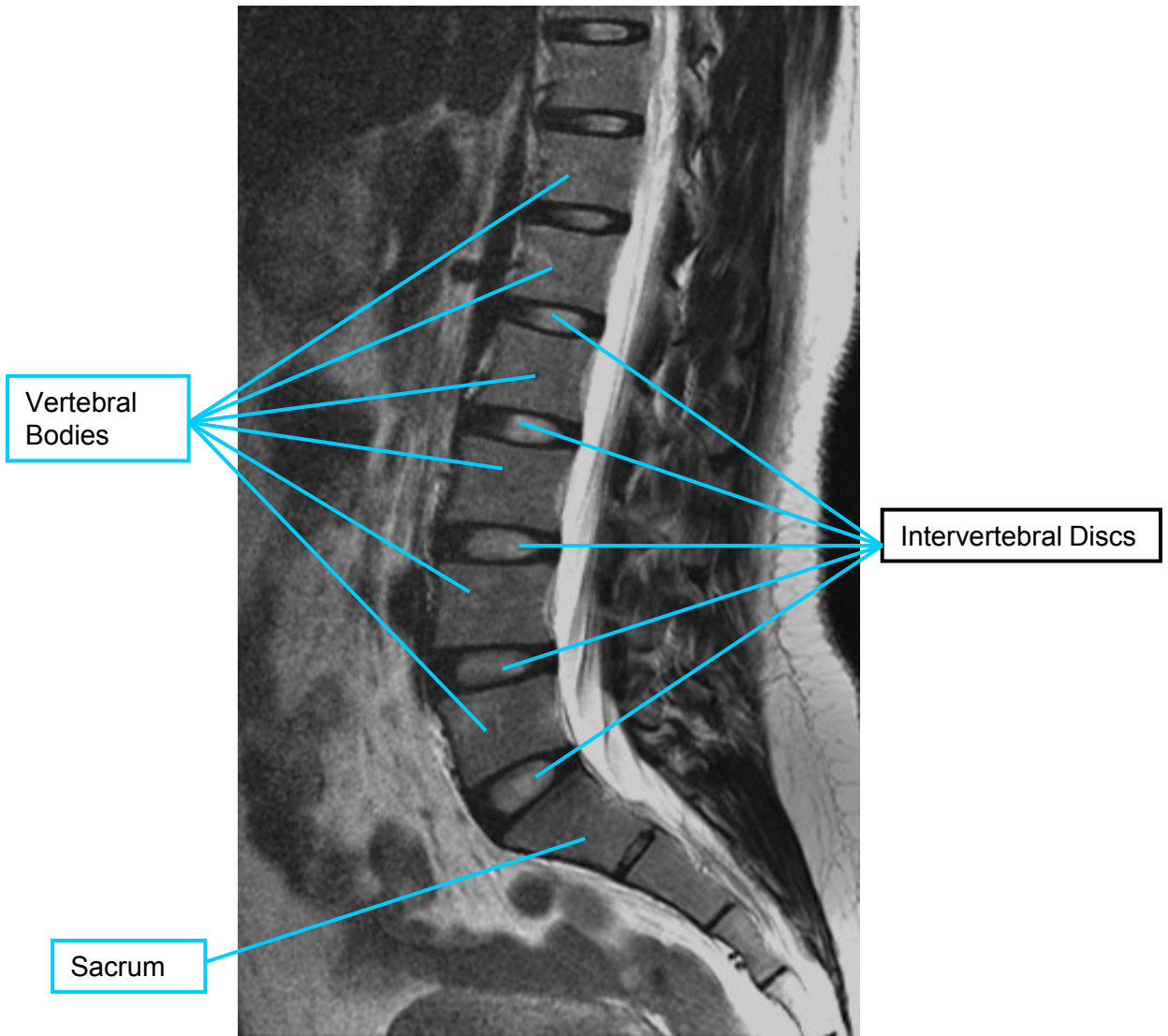


Figure 3:1

Anatomy

This image, also a T2W sagittal slice, identifies the five lumbar vertebrae and the top three sacral segments. The discs are identified by their adjoining vertebrae. The disc between L5 and S1 is called the L5-S1 disc. Sacral disc remnants are difficult to see on plain film X-rays, but are often visible on MRI. This can result in confusion when using plain films to identify structures found on MRI.

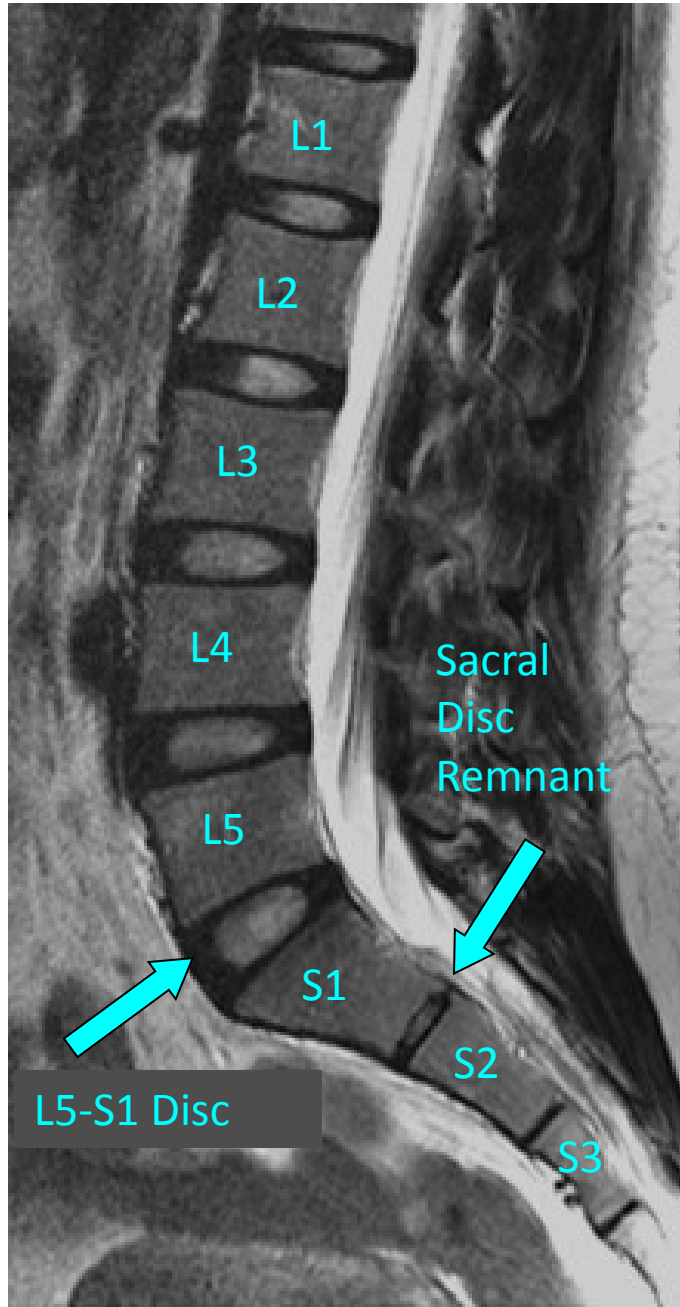


Figure 3:2.

Anatomy

Components of the intervertebral discs as viewed on a sagittal T2 weighted image. The nucleus pulposa of the L4-L5 intervertebral disc is demarcated by a red dotted line. The arrows indicate the location of the annulus fibers of the disc: the blue arrows indicate the boundaries of the posterior portion of the L2-L3 disc, and the yellow arrows identify the anterior portion of the annular fibers of L3-L4. Note on this T2 weighted image that the nucleus is lighter in color than the annular portion of the discs. This is due the increased hydration of the nucleus versus the annular fibers. As a disc ages and dehydrates, the entire disc will appear dark on a T2WI.

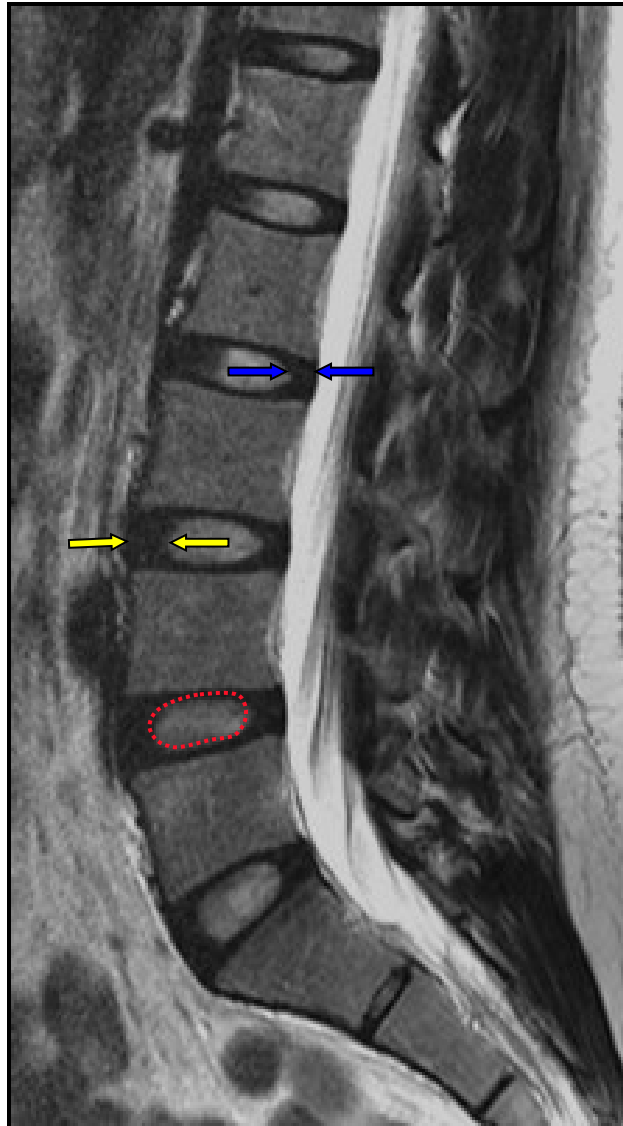
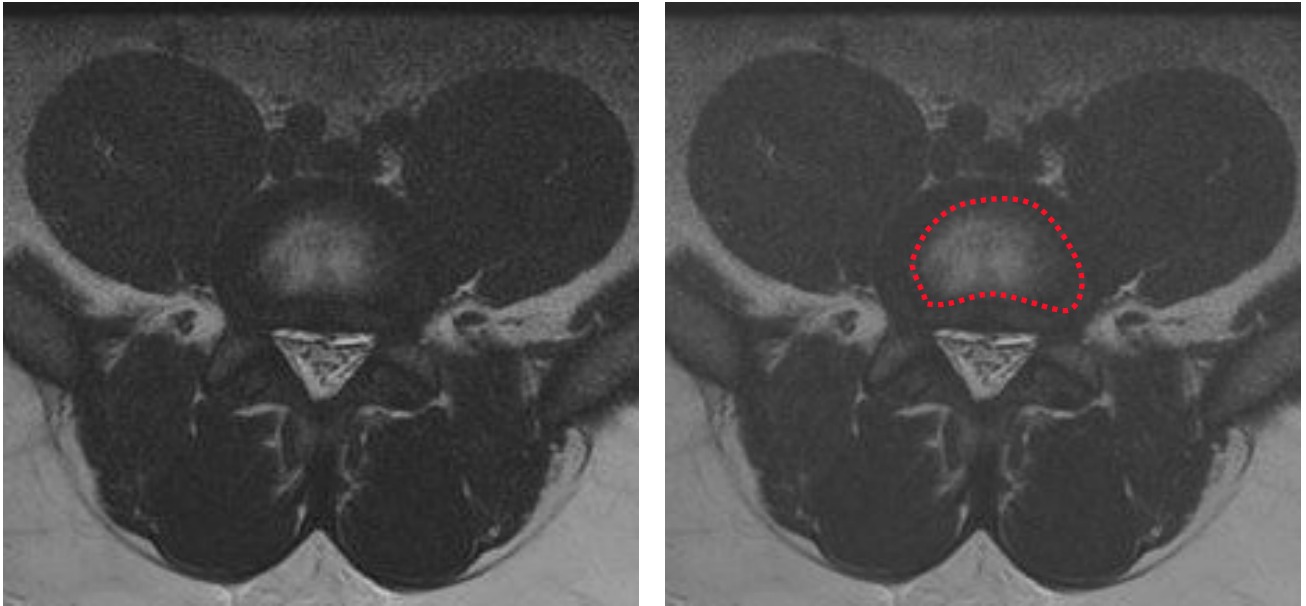


Figure 3:3.

Normal Disc Appearance



Figures 3:3 and 3:4. The appearance of a normal disc on axial T2 weighted MR. The nucleus is light in color (indicating normal fluid content), while the annular ring is dark. Figure 3:3 is the same slice as figure 3:4, but with the margins of the nucleus pulposus denoted by a red dotted line.



Figure 3:5. This sagittal image shows the level of the axial slice seen in figures 3:3 and 3:4.

The Central Canal

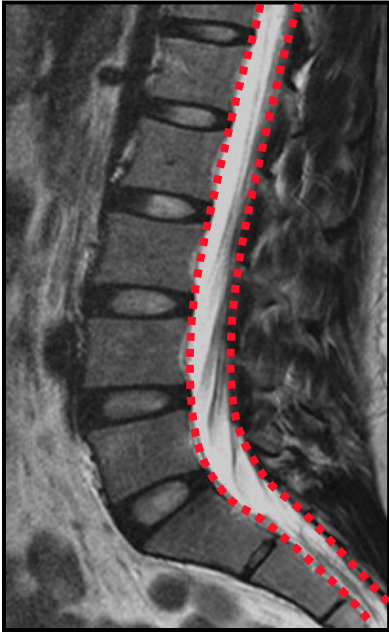


Figure 3:6.

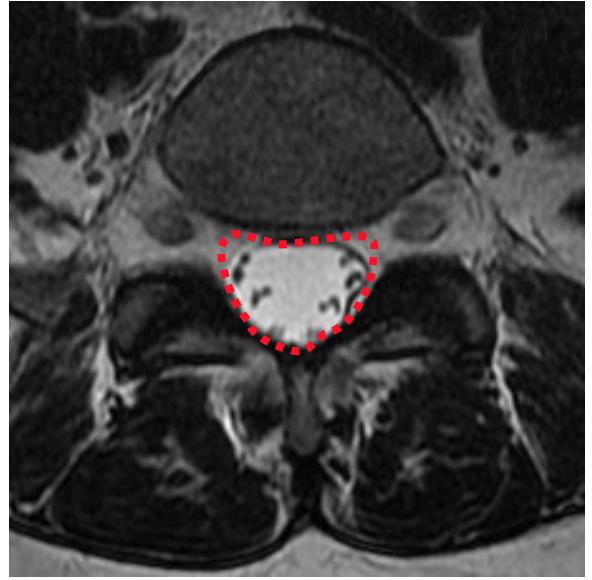


Figure 3:7.

The central canal is outlined with a red dotted line in these sagittal and axial T2 weighted images.

Anatomy of an Axial Slice Through L5

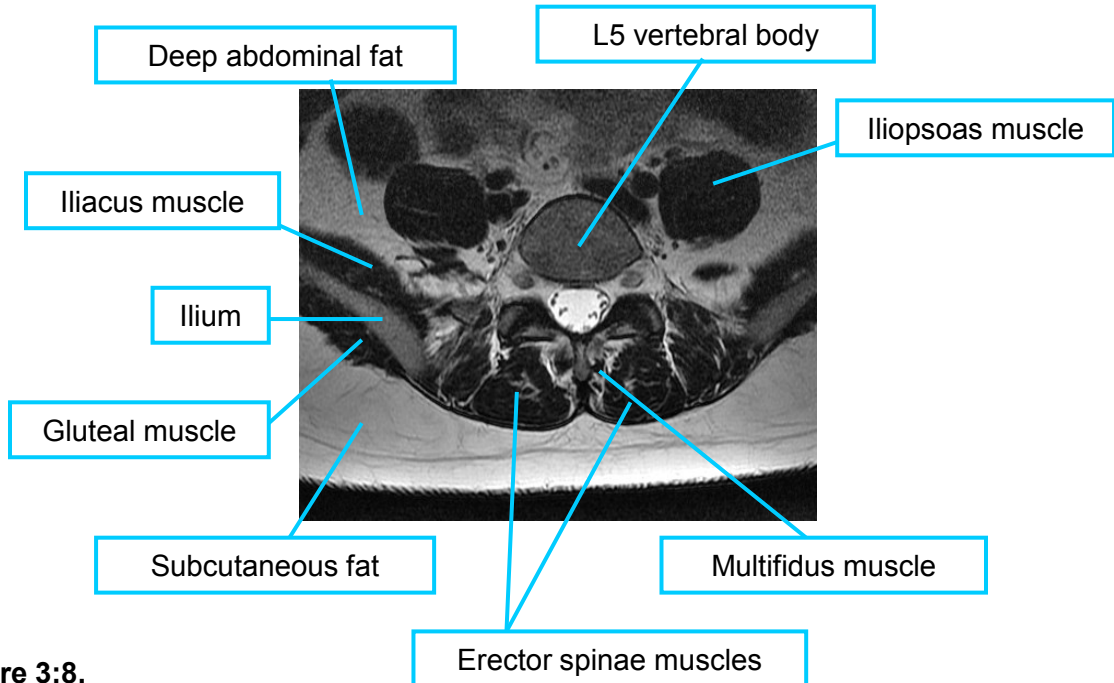


Figure 3:8.

This image, a T2W sagittal slice through the level of L5, reveals the cross-sectional anatomy of this plane. Recall that in T2 images water density is bright, fat is light-colored (but not as bright as water), air is black, muscles are dark, and bone is a neutral gray.

Expanded L5 Axial Image

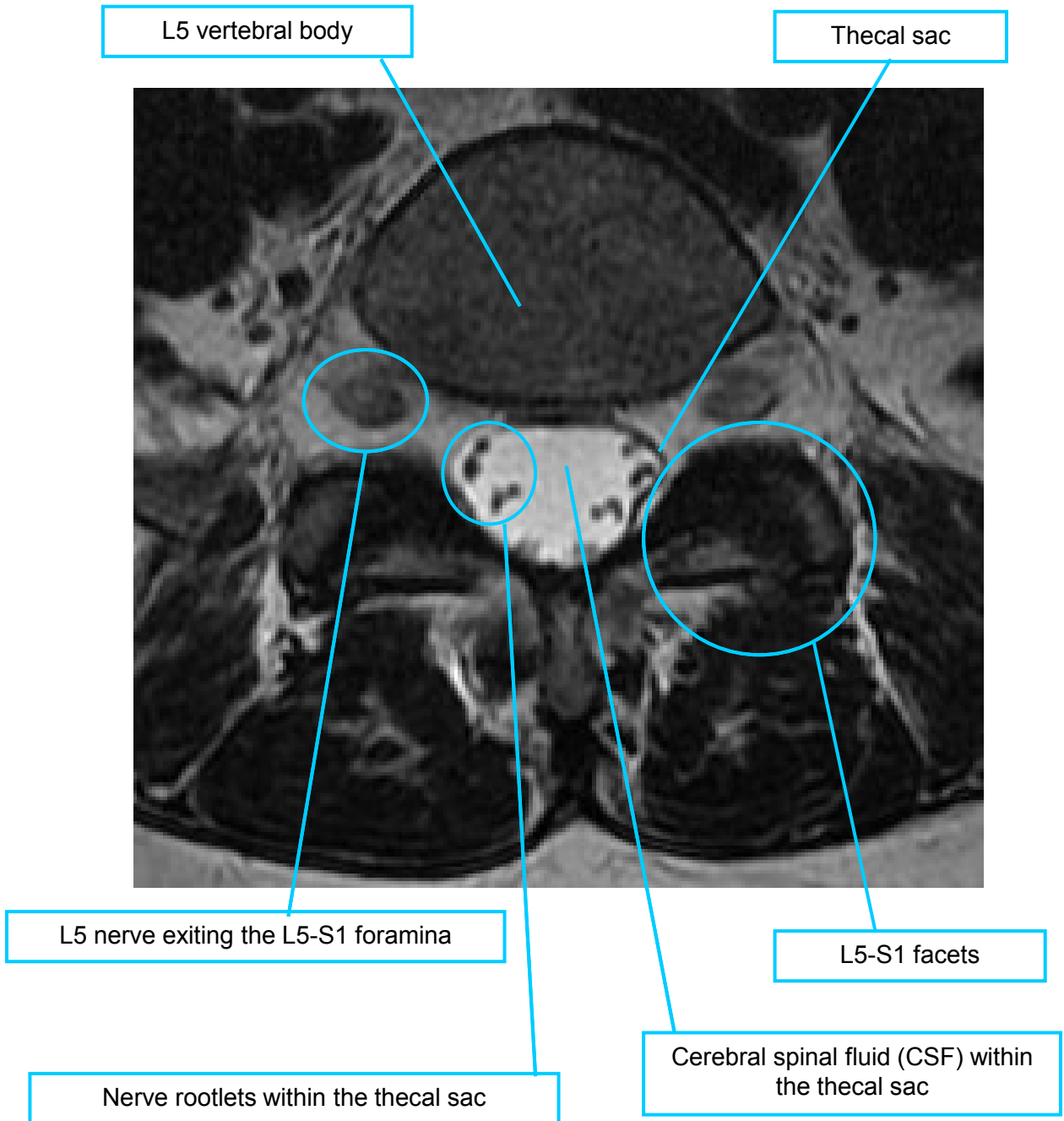


Figure 3:9.

Conus Medullaris

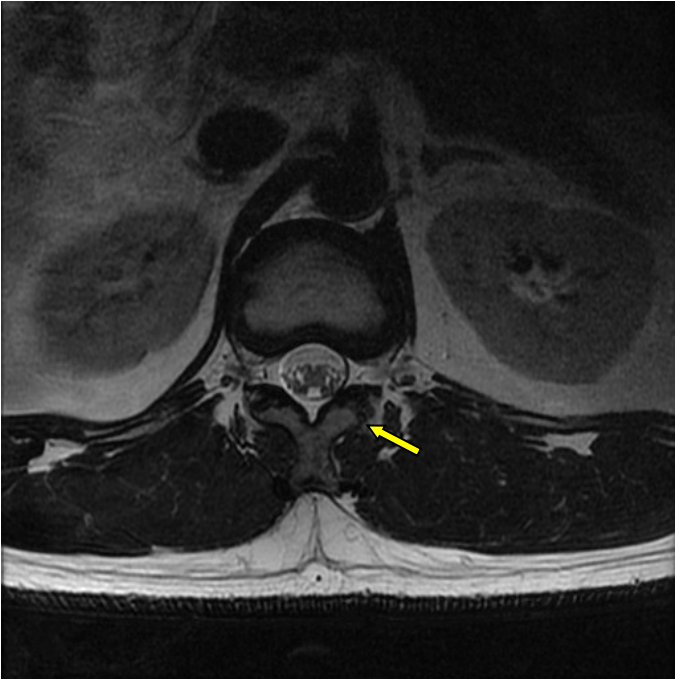


Figure 3:10. T2 weighted axial of the conus medullaris (yellow arrow).

The conus medullaris is the terminal end of the spinal cord. It typically terminates at the level of T12 or L1, but is occasionally seen terminating at L2. Though the spinal cord terminates with the conus medullaris, the spinal nerves continue inferiorly within the thecal sac in the cauda equina. These dangling nerves resemble a horse's tail, hence the Latin description *cauda equina* which literally translated is *horse's tail*.

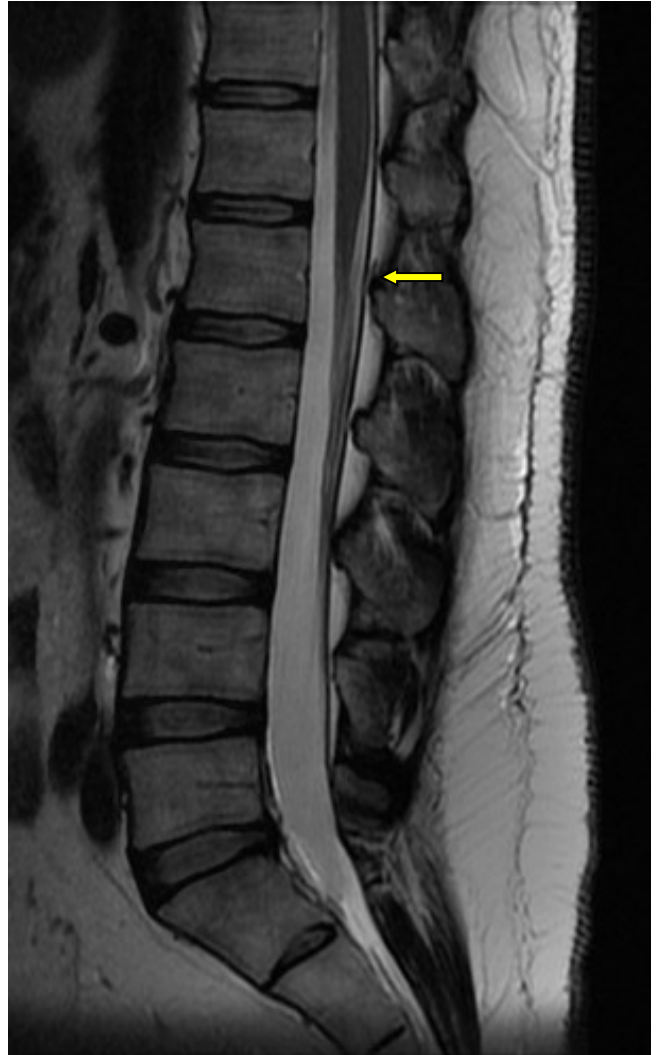


Figure 3:11. T2 weighted sagittal image of the lumbar spine showing a normal termination of the conus medullaris posterior to the vertebral body of L1 (yellow arrow).

Spinal Nerves

The exiting nerve root expands into the dorsal root ganglion as it exits the intervertebral foramina. The nerve roots are surrounded by fat from the point in which they exit the thecal sac and transverse the foramina. Within the thecal sac, nerve rootlets (identified by blue in the lower figure) are surrounded by cerebral spinal fluid (CSF) which is bright in color. These nerve rootlets are known as the cauda equina.

Figure 3:12.

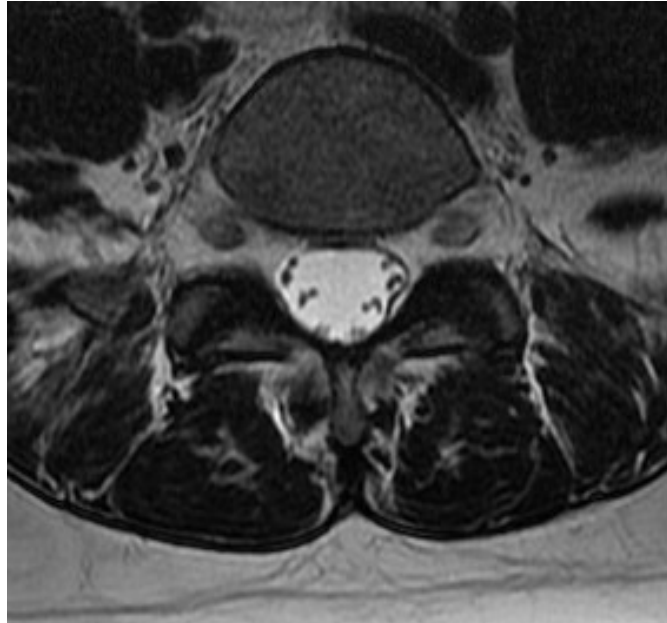
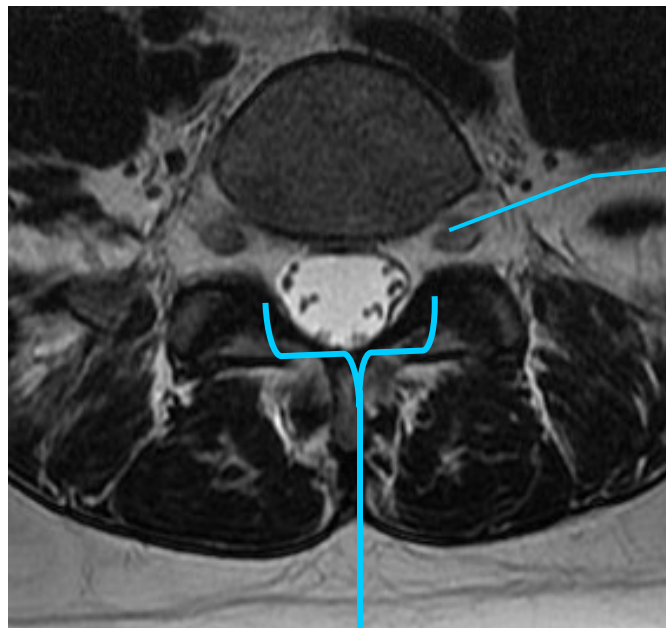


Figure 3:13.



Exiting nerve root
(the dorsal root
ganglion)

Nerve rootlets of the cauda equina

The Unique Shape of L5 on Axial Imagery

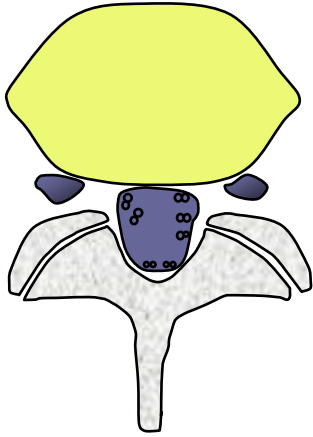


Figure 3:14.

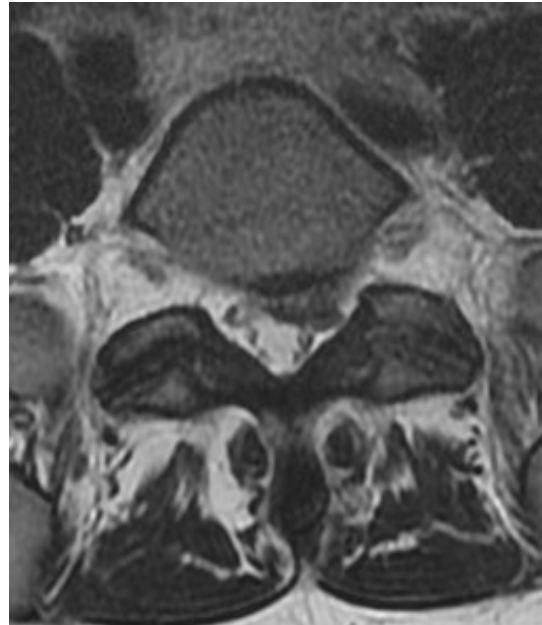


Figure 3:15.

While not an ironclad landmark, the L5 vertebra can frequently be identified by its lemon shape when viewed in an axial plane. These axial images characterize the appearance of the L5 vertebra in an axial orientation.

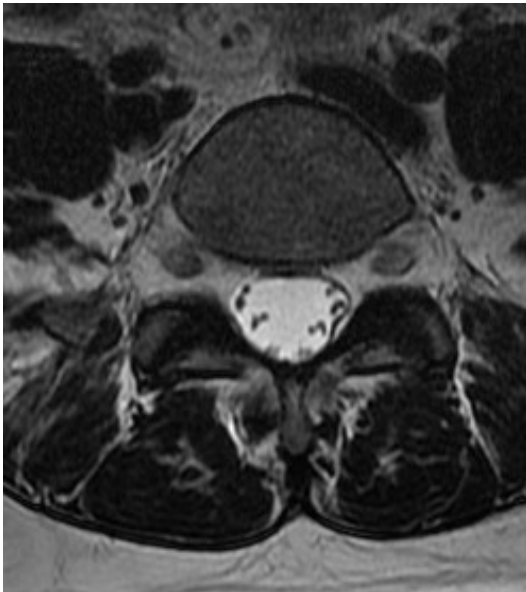


Figure 3:16.

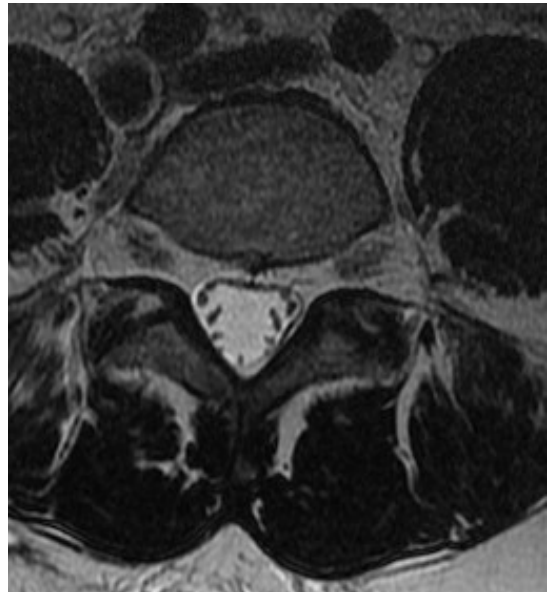


Figure 3:17.

Vertebral Anatomy

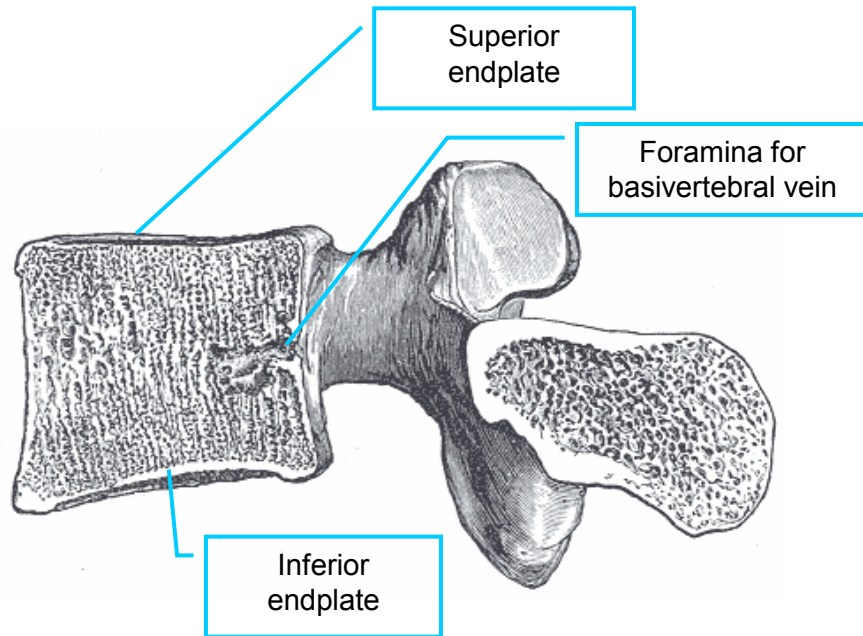


Figure 3:18. Cross section of a lumbar vertebra.

Images adapted from Henry Gray (1821–1865). *Anatomy of the Human Body*. 1918.

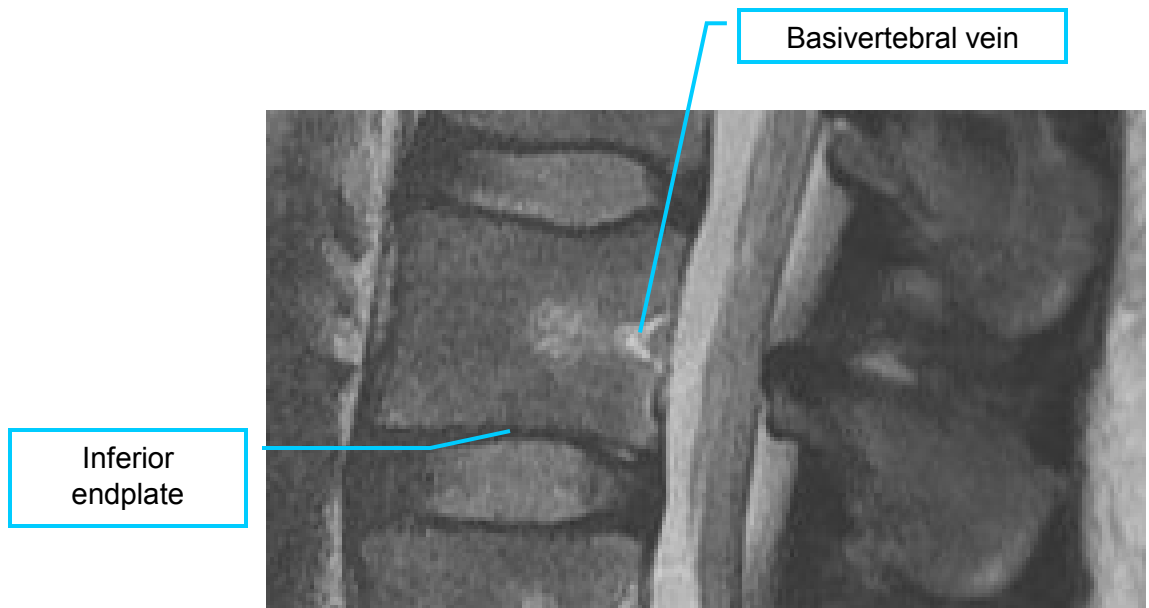


Figure 3:19. T2 sagittal of a lumbar vertebra.

Axial Image of Sacrum

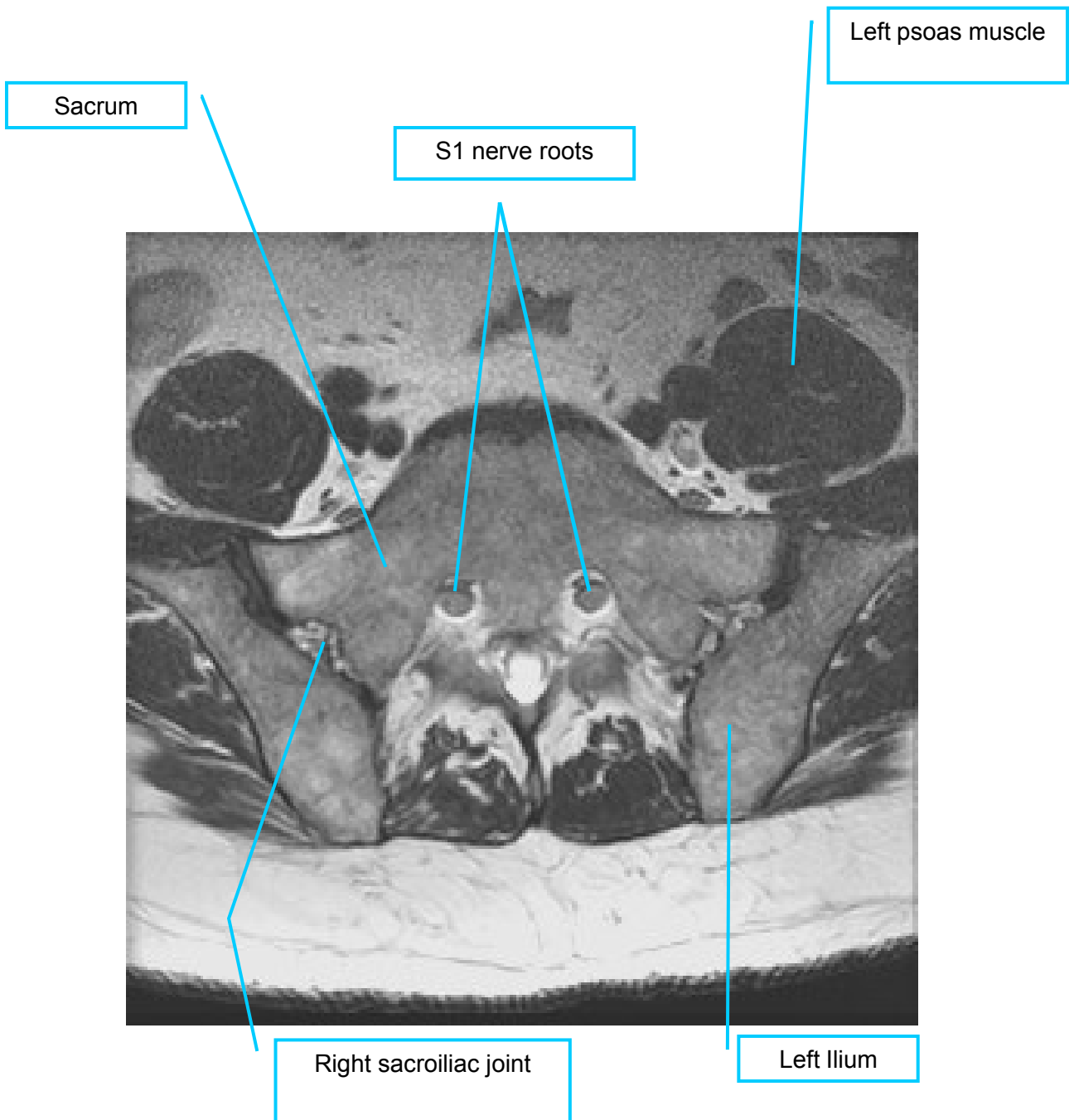


Figure 3:20. Lumbopelvic anatomy on axial imagery.

Ligamentum Flavum

There are several ligaments that stabilize and support the spine. Of those the ligamentum flavum is of particular interest to the clinician. It comprises the posterior boundary of the spinal canal and normally appears as a “V” on axial slices (red arrows). On sagittal images the ligamentum flavum is seen at the posterior of the spinal canal (yellow arrows).



Figure 3:21. Ligamentum flavum on T2 axial.



Figure 3:22. Ligamentum flavum on T2 weighted axial image.



Figure 3:23. Ligamentum flavum on T2 sagittal image.

Sagittal Lumbopelvis

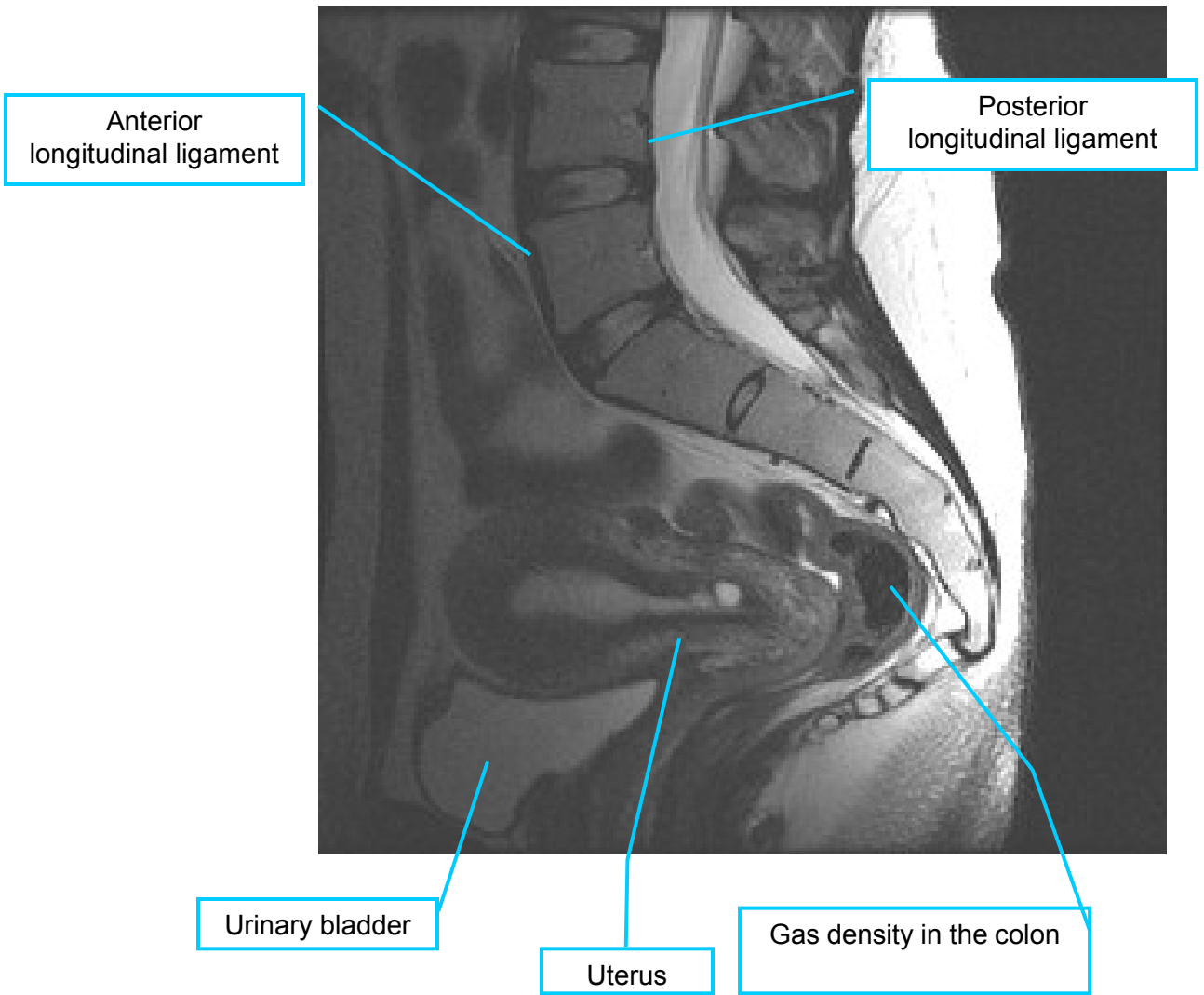
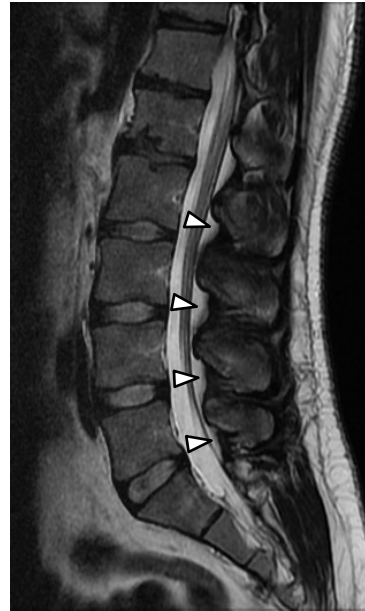
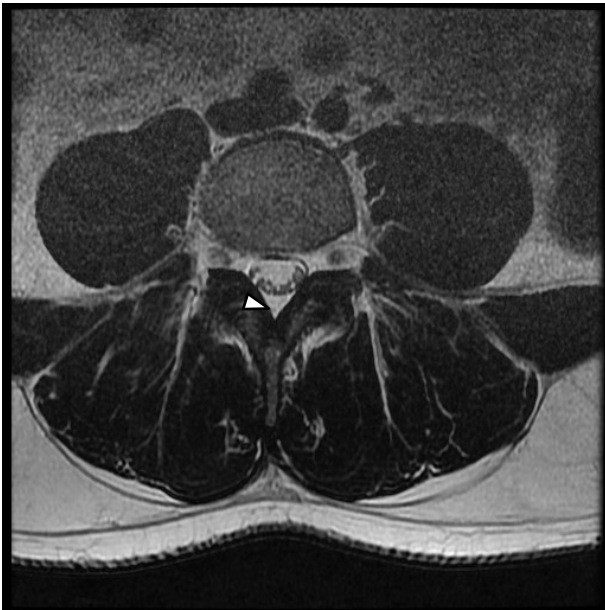


Figure 3:24. Lumbopelvic anatomy.

Normal Spinal Fat Distribution



Figures 3:25 and 3:26. Normal fat distribution within the spine. Epidural fat is located in the posterior recess of the spinal canal. The white arrows identify normal epidural fat which appears light in these T2WI.

The exiting nerve roots are surrounded by fat as it traverses the IVF. Fat is light on both T1 and T2 weighted images.

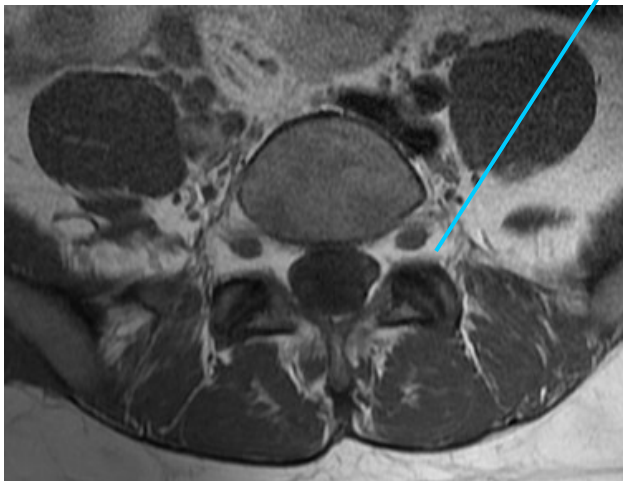


Figure 3:27. T1 weighted axial image.

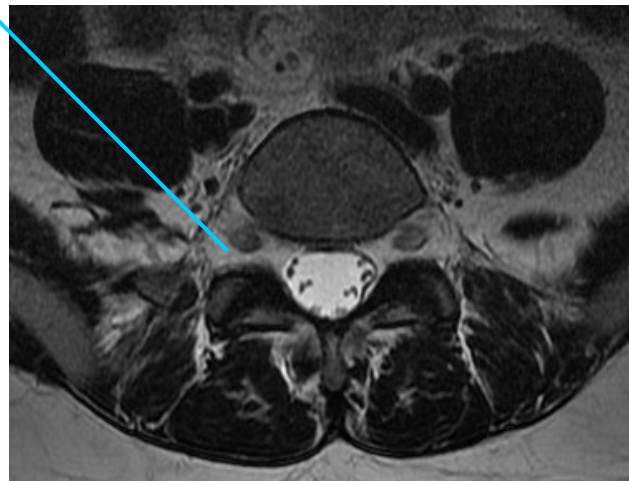


Figure 3:28. T2 weighted axial image.

The nerves are surrounded by fat as they traverse the IVF. Note the water density of the CSF is bright on T2 image and dark in the T1 image. Absence or displacement of the fatty tissue may be clinically significant.

Anatomy from a Coronal Orientation

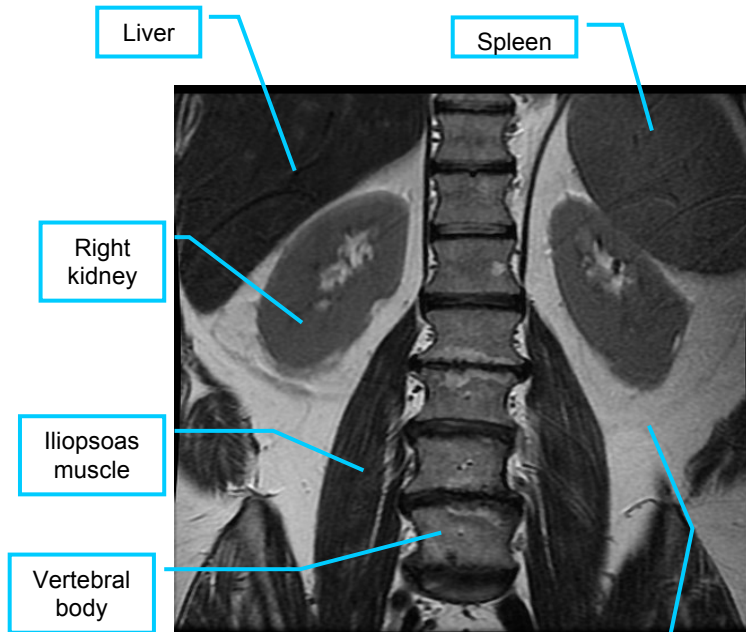
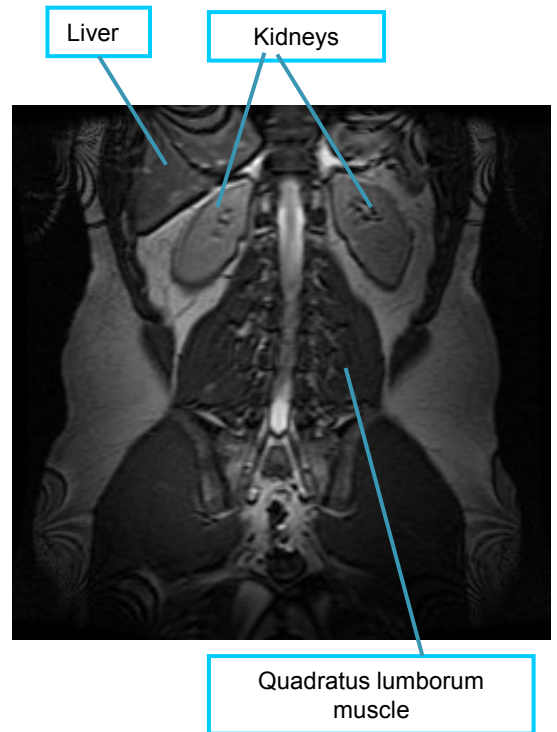


Figure 3:29. Coronal anatomy



Figures 3:30 and 3:31. Anatomy on coronal images.

Multifidus Muscles

The clinical significance of the multifidus muscles has become increasingly evident in recent years, and clinicians are looking for better ways to observe this interesting muscle. While coronal images are rarely used in most lumbar MRIs, they are useful in identifying the multifidus muscles. Note that the multifidus fibers do not run longitudinally like the erector spinae muscles (spinalis, longissimus, and iliocostalis), but rather obliquely from the lateral side of the spinous processes to the mamillary processes of the lumbar spine and the sacrum. In the lower lumbar and sacral region, the multifidi originate along the spinous processes and insert into the aponeurosis of the sacrospinalis muscle, the posterior superior iliac spine, and the posterior sacroiliac ligaments.

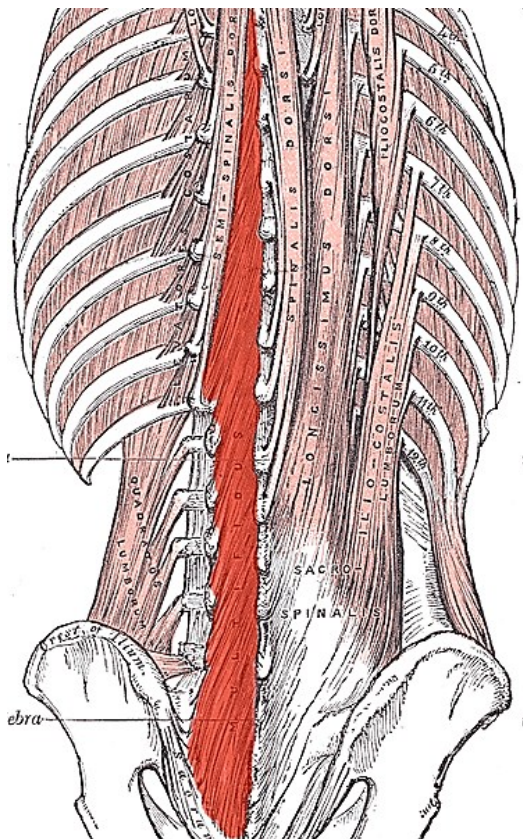


Figure 3:32. The multifidus muscles.

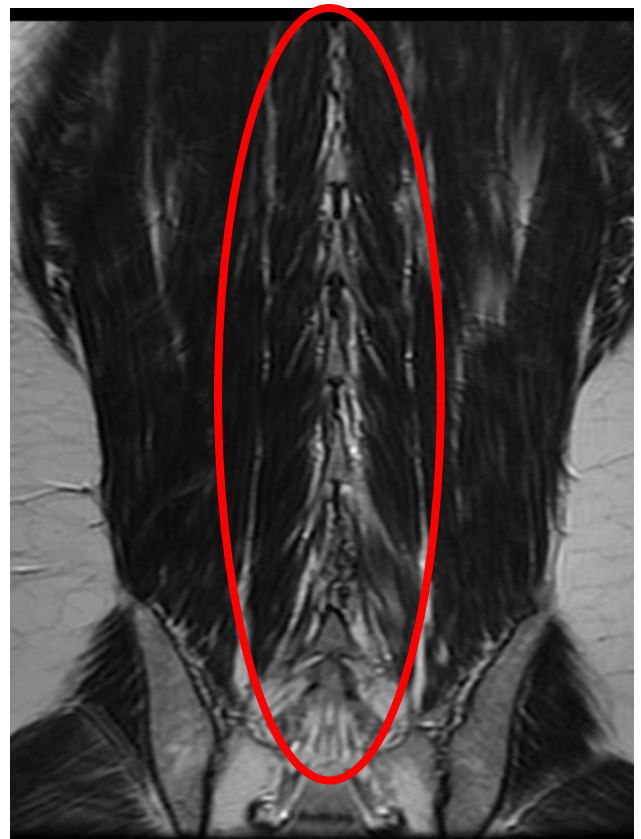


Figure 3:33. The multifidus muscles on MRI.

The illustration on the left (figure 3:32) highlights the left multifidus muscles in red. The coronal MR on the right (figure 3:33) provides a clear view of the multifidus muscles. Note the oblique orientation of the multifidus muscles. Compare them to the longitudinal orientation of the erector spinae muscles.

Image 1 adapted from Henry Gray (1821–1865). Anatomy of the Human Body. 1918.

Multifidus Muscle Characteristics

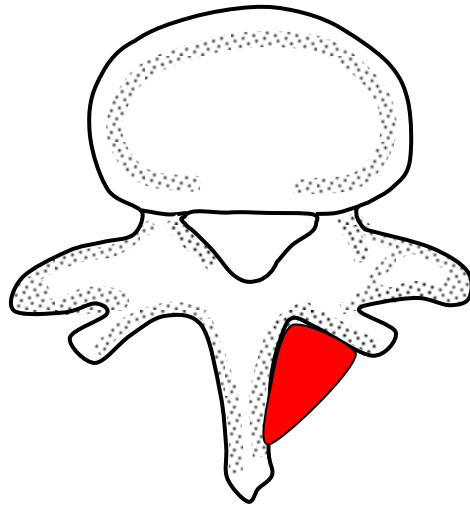


Figure 3:34. Schematic of multifidus location.

In axial imagery the multifidus lies in the laminar groove bordered by a fascial/adipose boundary. The multifidus is typically a small flat muscle and subject to atrophy and fatty infiltration. The illustration above (figure 3:34) demonstrates the location of the multifidus in red. In the axial image below (figure 3:35) the location of the multifidus is demonstrated in a T2WI within the red dotted lines.

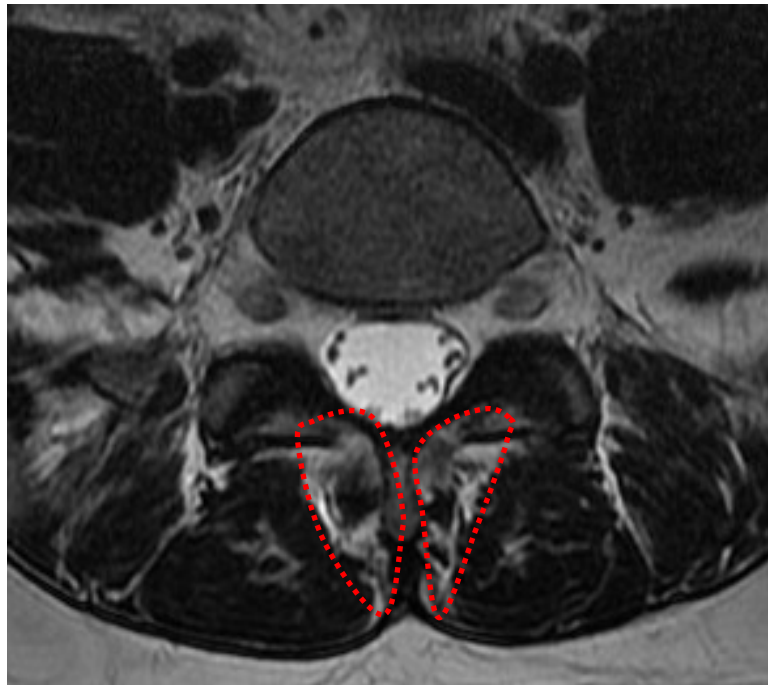


Figure 3:35. T2W axial image denoting the location of the multifidus.

The Positional Relationship between the Erector Spinae and the Multifidus

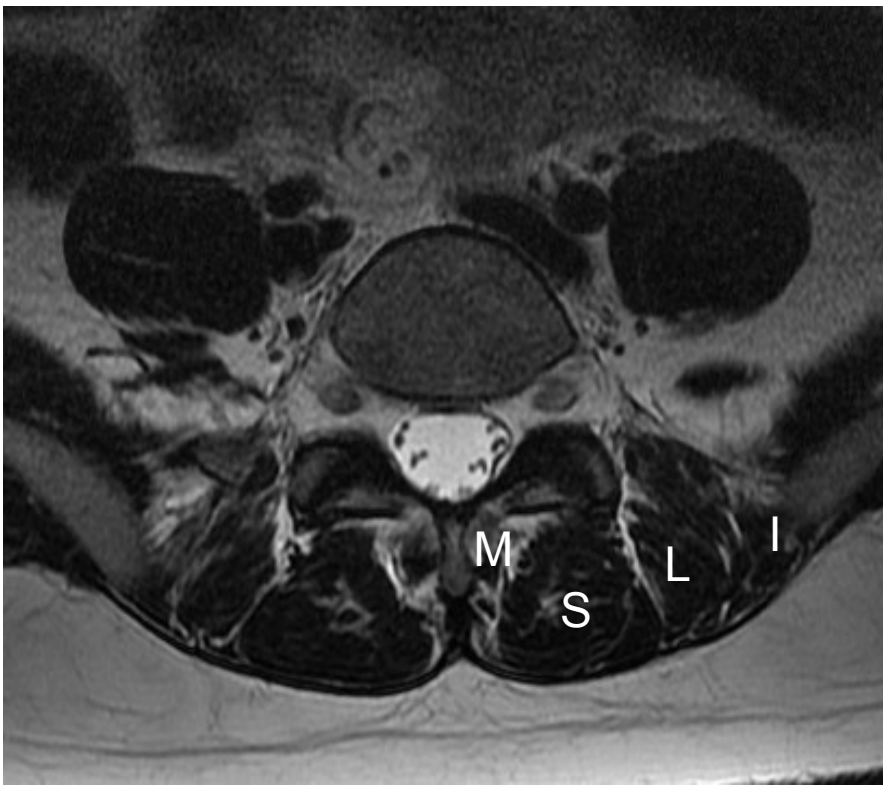


Figure 3:36. T2 weighted axial image with labeled muscles.

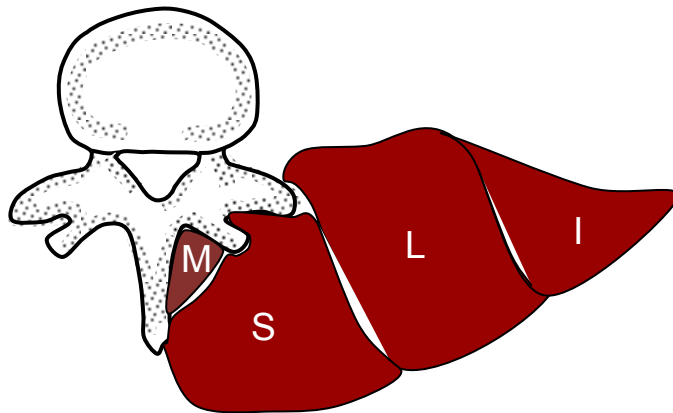


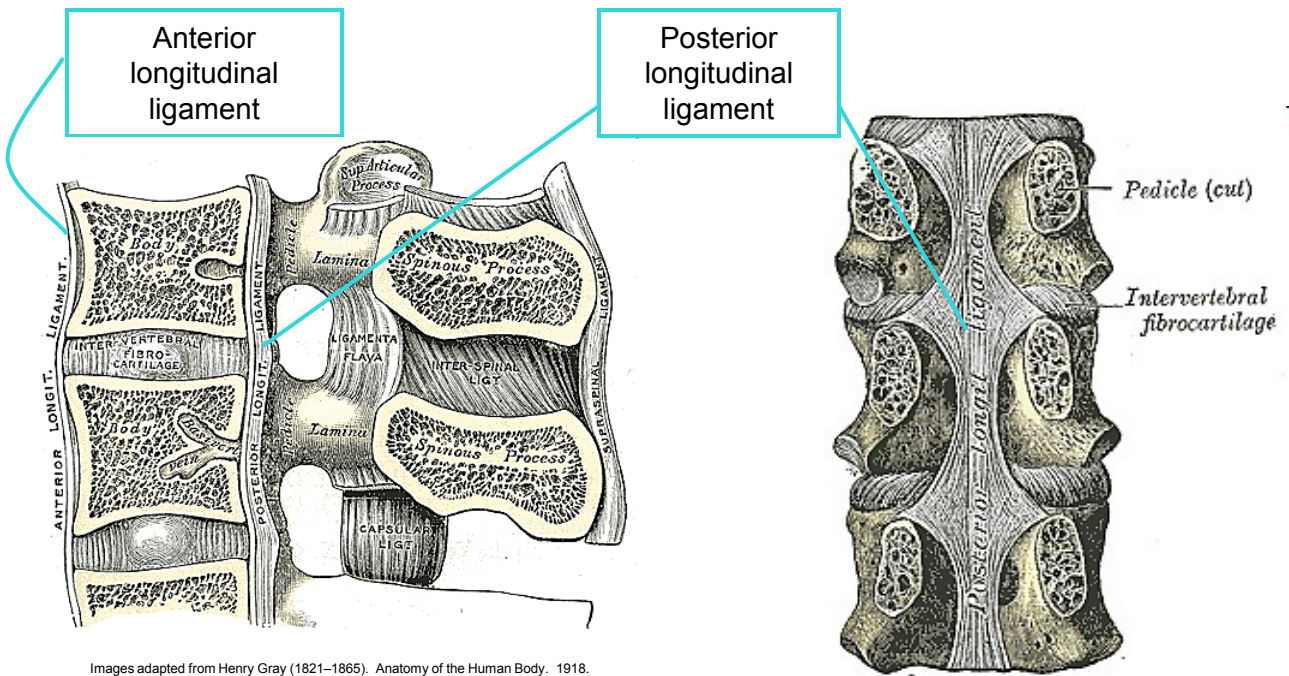
Figure 3:37. Illustration of paraspinal muscles .

The posterior muscles of the spine can be seen on axial imagery and are separated by fascial investment seen as the same intensity as adipose (figure 3:36).

The schematic (figure 3:37) identifies the location of these muscles:

M=multifidus, S=spinalis, L=longissimus, and I=iliocostalis.

The Anterior and Posterior Longitudinal Ligaments



Images adapted from Henry Gray (1821–1865). *Anatomy of the Human Body*. 1918.

Figures 3:38 and 3:39. The posterior longitudinal ligament is located within the vertebral canal and runs from the body of C2 to the sacrum. It lies posterior to the vertebral bodies and intervertebral discs. The anterior longitudinal ligament lies along the anterior of the vertebral bodies and discs. On sagittal MR these ligaments normally appear as a thin line.

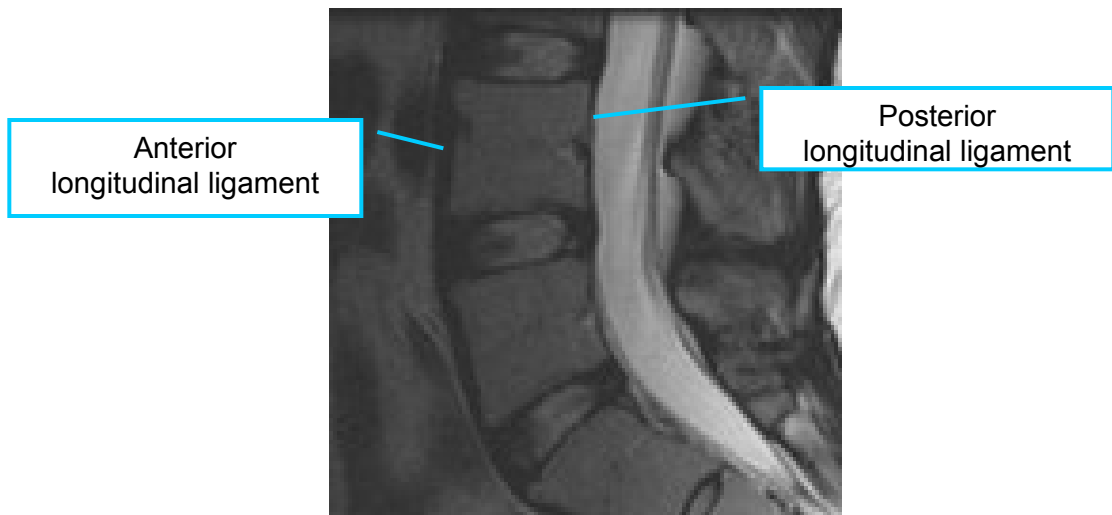


Figure 3:40. The ALL and PLL identified on a T2 weighted sagittal image.

The Great Vessels

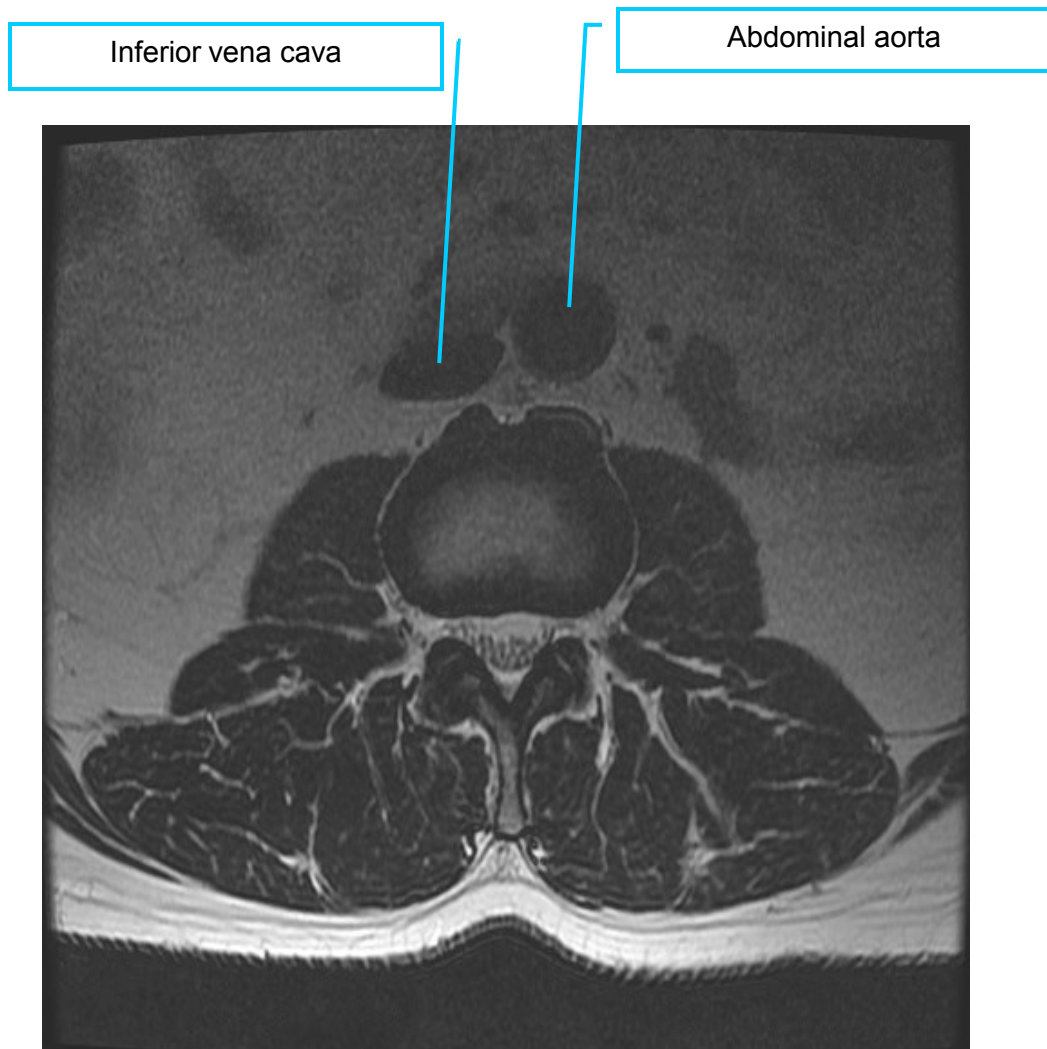


Figure 3:41. The great vessels of the abdomen.

The abdominal aorta is located on the left side of the body, (the right side of an MRI), and the inferior vena cava is on the right side of the body (the left side of an MRI). The greater pressure of the aorta helps to create a more circular inflated appearance, while the inferior vena cava has a lower hydrostatic pressure and appears less inflated.

Suggested Reading

Cramer G, Darby S (2013). Basic and clinical anatomy of the spine, spinal cord, and ANS (third edition). Elsevier Mosby.

Marchiori D (2013). Clinical imaging: with skeletal, chest and abdomen pattern differentials(third edition). Mosby.

Atlas SW. (2008). Magnetic resonance imaging of the brain and spine (forth edition). Lippincott Williams & Wilkins.

Ross JS et al. (2010). Diagnostic imaging spine (second edition). Amirsys Inc.

Standardized Anatomic Reference Descriptors



Standardized Anatomic Descriptions

“There is no more difficult art to acquire than the art of observation, and for some men it is quite as difficult to record an observation in brief and plain language.”

William Osler, Physician, 1849-1919

Every specialty has its own lexicon that has special meaning within their profession. This is fine when working within a given profession, but may confound those from another profession. The language of healthcare is always evolving and periodically contradictory and confusing. The condition known as Tarlovs cysts is slowly ceding to the more descriptive term *perineural cyst*. The term HNP (herniated nucleus pulposa) is now passé, replaced by the term herniated disc (HD). Definitions evolve and change, but dissemination of the changes lags. Periodically the various specialties join forces to identify words, diagnoses, and descriptors with multiple or conflicting definitions, and through a consensus process agree on a standardized definition. The combined task forces of the North American Spine Society, the American Society of Spine Radiology, and the American Society of Neuroradiology created a guideline for standardizing the vocabulary between the various spine specialists. They published these guidelines in the March 1, 2001 edition of *Spine*. I recommend that every spine practitioner read and apply this article. While this work proposes a guideline to standardize terms within the spine specialties, it will eventually become obsolete and will need updating too. Most of the next three chapters rely heavily on this document.

Fardon DF, Milette PC. Nomenclature and classification of lumbar disc pathology: recommendations of the combined task forces of the north American spine society, American society of spine radiology, and American society of neuroradiology. *Spine*, Volume 26(5).March 1, 2001.E93-E113

<http://www.rsna.org/radlex/committee/ASSRDiscNomenclature.pdf>

Standardized Anatomic Descriptions

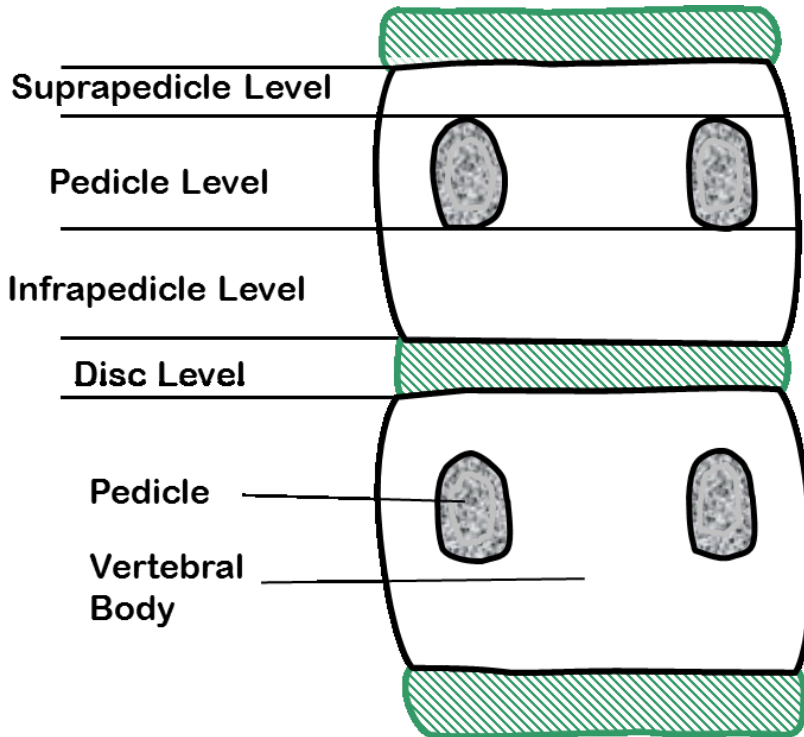


Figure 4:1. P-A view.

These schematics represent common identifying vertebral landmarks of the spine as seen on a P-A view with the posterior elements removed (figure 4:1) and on a lateral view (figure 4:2). Using these points of reference, a radiologist or spinal specialist will be able to verbalize the findings on MRI into an easy to understand written report. For example, if you were to read a report that read, “The L4-5 disc herniated posteriorly and superiorly into the infrapedicle level,” you should be able to ascertain the location of the herniation.

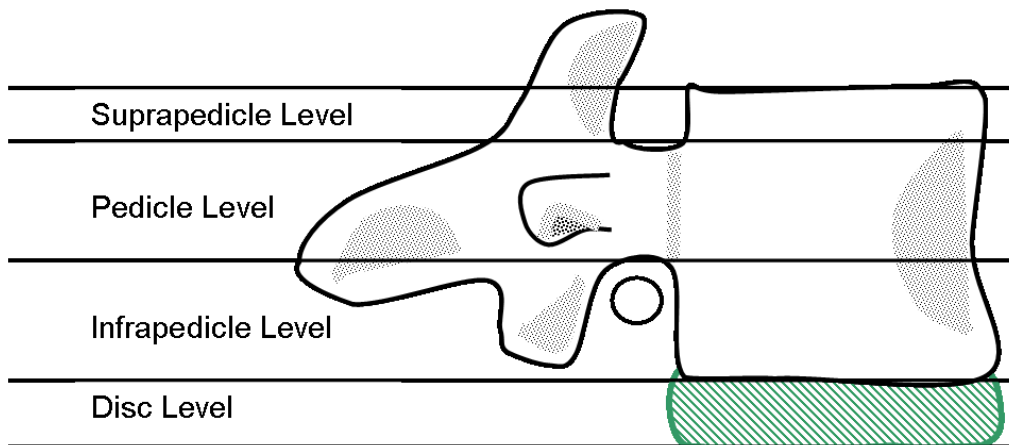


Figure 4:2. Lateral view.

Standardized Anatomic Descriptions

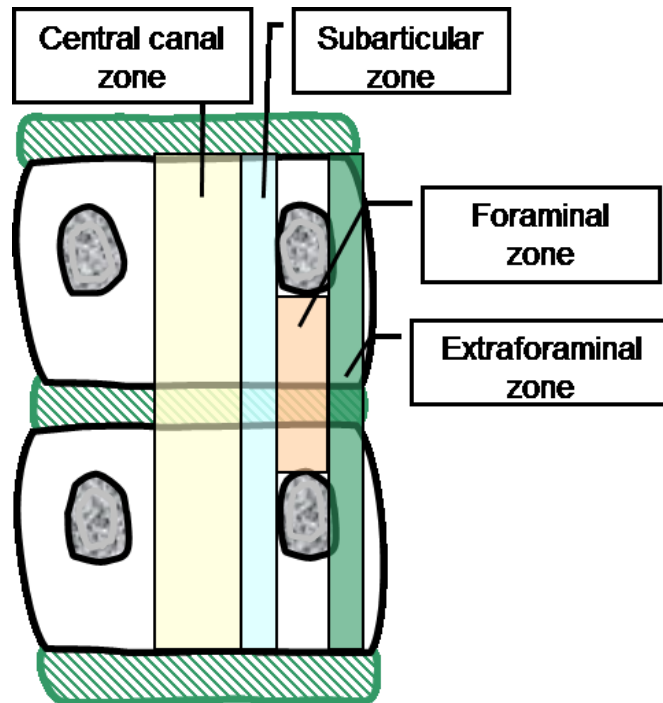


Figure 4:3.

In addition to the levels of anatomic reference, longitudinal zones are also used to describe anatomic locations in the spine. The schematic above (figure 4:3) is a posterior view of two spinal segments with the posterior elements removed. Below (figure 4:4) is a corresponding axial view of a single vertebral segment. These schematics reveal the location of the various anatomical zones: central canal zone, subarticular zone, foraminal zone, far lateral zone, and extraforaminal zone. The term paracentral is less clear-cut and is being replaced by more definitive phrases such as “right central” or “left central.” The schematic seen below represents a coronal slice through the spinal canal and the pedicles.

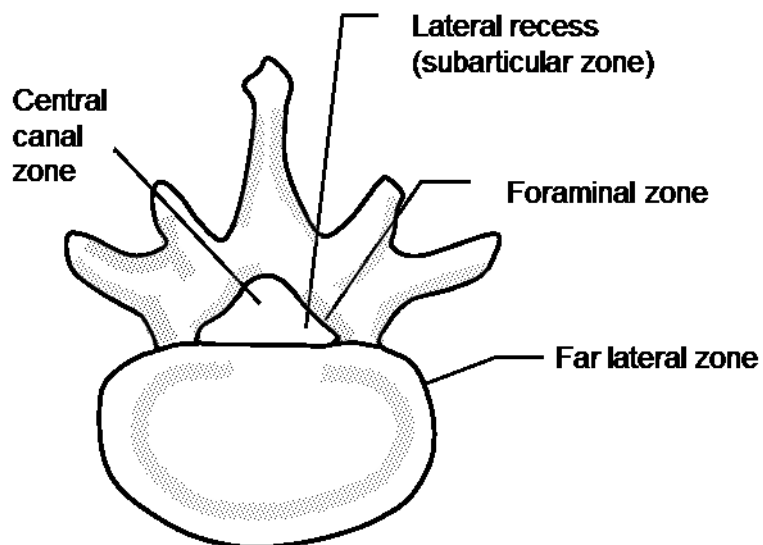


Figure 4:4.

Standardized Anatomic Descriptions

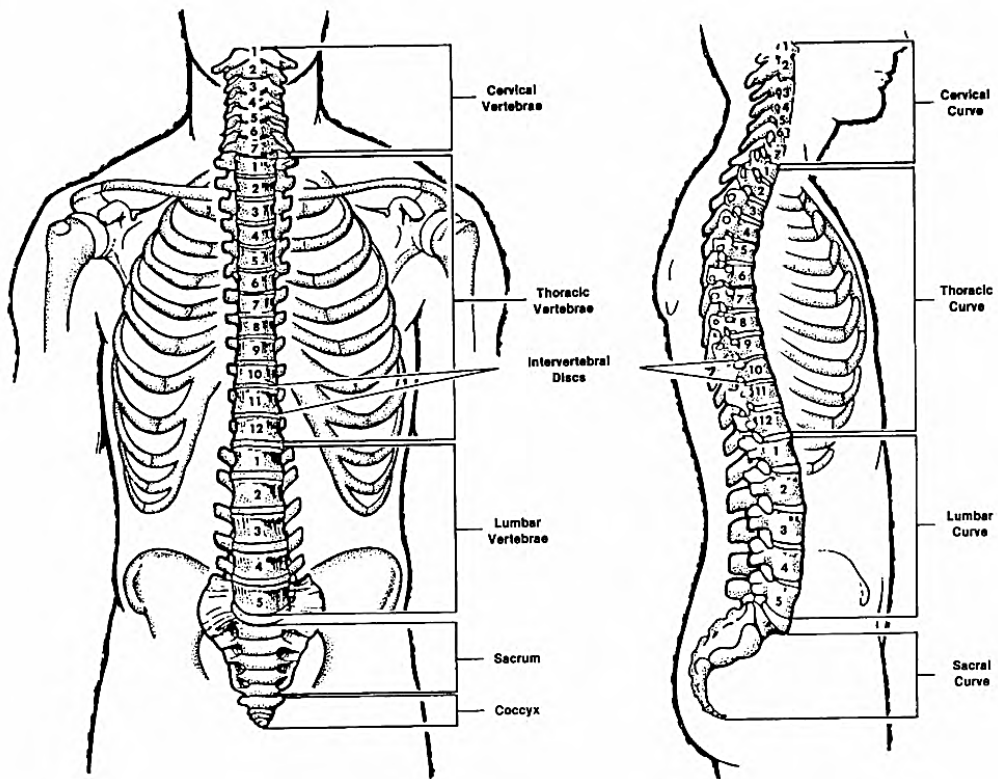


Figure 4:5. The spine.

Image from
USAMDCS
FSH, TEXAS 78234-6100
THE CENTRAL NERVOUS
SYSTEM
SUBCOURSE MD0572 EDITION 1

The spine is composed of 24 vertebrae, the sacrum, and coccyx. The segments from C2 to the sacrum have intervertebral discs. These discs are identified by the adjoining vertebrae. In the lumbar spine there are typically five discs: the L1-L2 disc, L2-L3 disc, L3-L4 disc, L4-L5 disc, and the L5-S1 disc.

While there is an L1 vertebra and nerve root, there is no L1 disc. There is a T12-L1 disc, and an L1-L2 disc. Both vertebrae must be named in the identification of the disc.

Image from
USAMDCS
FSH, TEXAS 78234-6100
THE CENTRAL NERVOUS
SYSTEM
SUBCOURSE MD0572 EDITION 1

Standardized Anatomic Descriptions

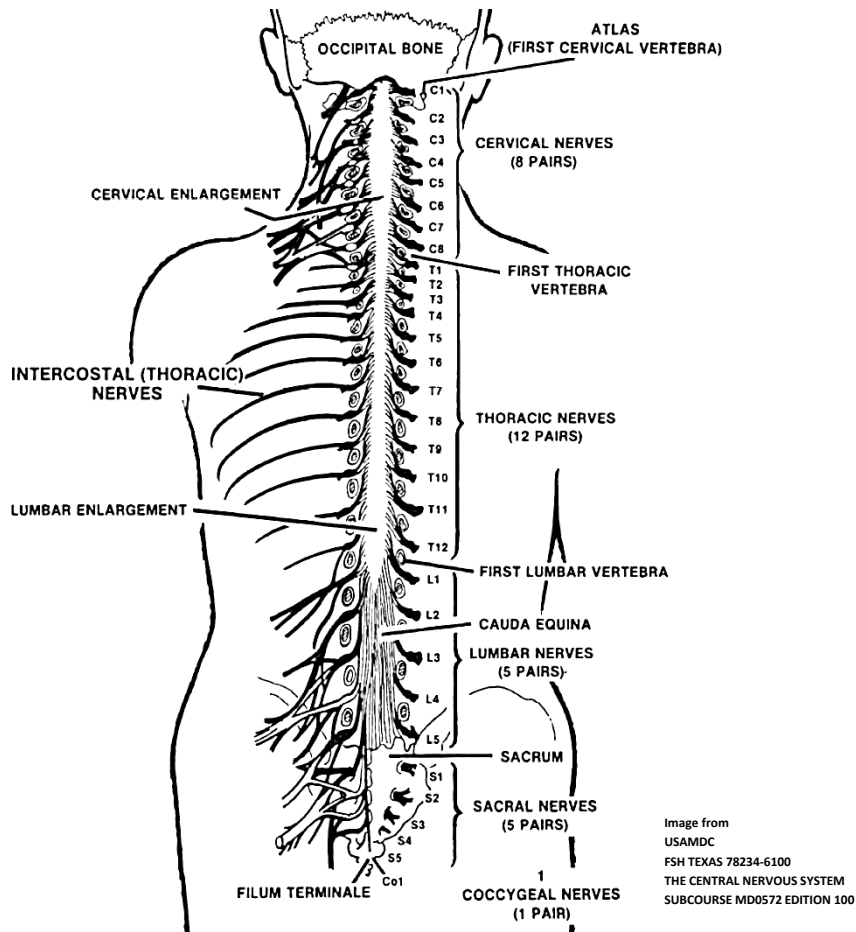


Figure 4:6.

Nerve roots are identified by the vertebral segments from which they exit the spinal column. Cervical nerve 1 (C1) exits between the occiput and the C1 vertebra and the C2 nerve root between C1-C2. The exception to this method of identification is the C8 nerve root which exits between the C7 and T1 vertebrae (there is no C8 vertebra). The sequence of nerve root identification continues from the T1 (the first thoracic) vertebra through the sacrum with the name of the nerve root being the same as the superior vertebra. The T1 nerve root exits between T1 and T2; the T2 nerve root exits between T2 and T3 and so on.

The cord is enlarged in the cervical spine (see the cervical enlargement above) and in the lower thoracic spine (called the lumbar enlargement). The spinal cord terminates at the lower portion of L1 or upper portion of the L2 vertebra. There is some anatomical variation on the level of cord termination. The termination of the cord is called the conus medullaris. From the conus medullaris, the cauda equina extends down the remainder of the spinal canal.

The filum terminale (literally meaning the terminal thread) extends from the conus medullaris of the spinal cord to the first segment of the coccyx. It is composed mainly of connective tissue.

Identifying Affected Nerve Roots

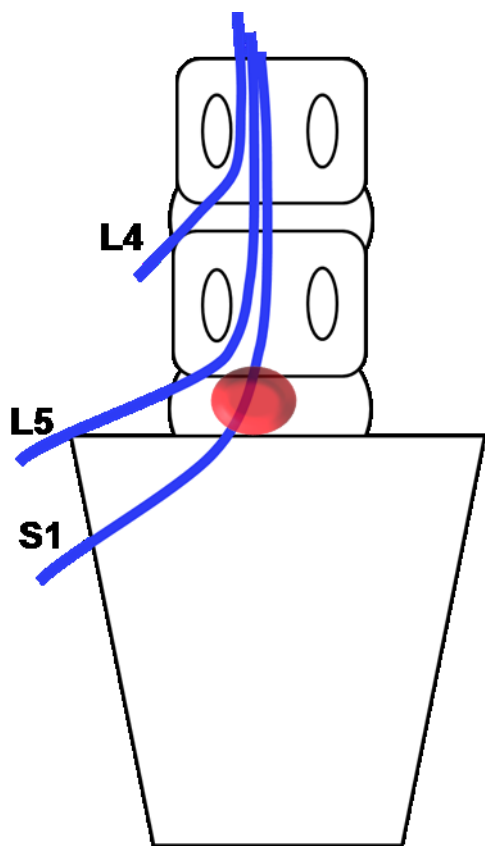


Figure 4:7. Paracentral herniation

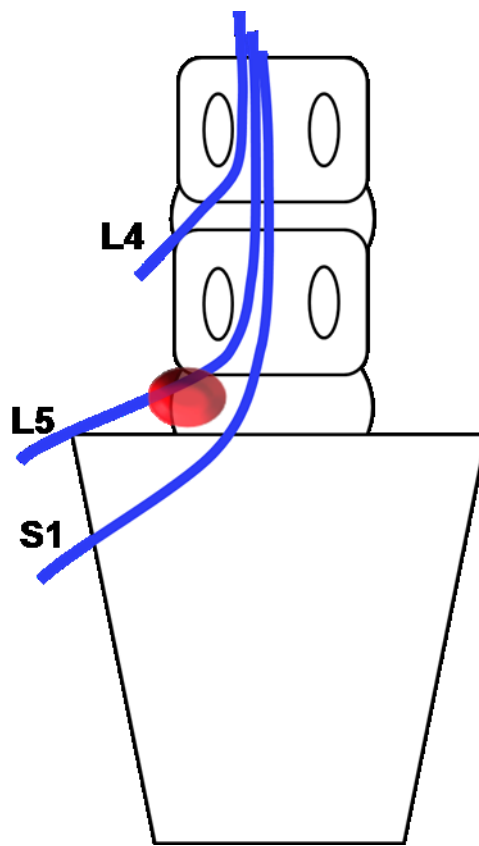


Figure 4:8. Lateral herniation

These schematics show the relationship of the lumbar nerves as they descend and exit the lumbar spine and sacrum. Note the exiting nerve roots are high and lateral as they leave the spinal canal, whereas the descending nerve roots are more central. When there is a paracentral herniation (figure 4:7), it typically affects the descending nerve root, not the exiting nerve root. To affect the exiting nerve root, the herniation usually has a foraminal or lateral component (figure 4:8).

Additionally, when there is a paracentral herniation, the nerve contacted usually has the same name as the vertebra below the herniation. A paracentral herniation of the L5-S1 disc usually affects the S1 nerve root.

Suggested Reading

Fardon DF, Milette PC. Nomenclature and classification of lumbar disc pathology: recommendations of the combined task forces of the north American spine society, American society of spine radiology, and American society of neuroradiology. Spine, Volume 26(5).March 1, 2001.E93-E113.

<http://www.rsna.org/radlex/committee/ASSRDiscNomenclature.pdf>

Cramer G, Darby S (2013). Basic and clinical anatomy of the spine, spinal cord, and ANS (third edition). Elsevier Mosby.

Marchiori D (2013). Clinical imaging: with skeletal, chest and abdomen pattern differentials(third edition). Mosby.

Atlas SW. (2008). Magnetic resonance imaging of the brain and spine (forth edition). Lippincott Williams & Wilkins.

Ross JS et al. (2010). Diagnostic imaging spine (second edition). Amirsys Inc.

Bogduk N. (2012). Clinical and radiological anatomy of the lumbar spine. Churchill Livingstone.

Classification of Lumbar Disc Derangements



Nomenclature and Classification of Lumbar Disc Lesions

Speaking the same language is foundational for optimized integrated spine care. Physicians need to have a reliable set of terms and criteria that transcend the various specialty jargon. Guided by the need to establish a standardized and universally acceptable classification system for identifying lumbar disc pathology, an interdisciplinary task force created a collective set of guidelines. Again we reference the guidelines that were presented in 2001 through the combined efforts of the North American Spine Society, American Society of Spine Radiology, and American Society of Neuroradiology. All spine practitioners are encouraged to read the original work of this task force located in Volume 26, Number 5, *Spine* 2001.

http://www.asnr.org/spine_nomenclature/discussion.shtml

Normal

The normal disc is defined as a hydrated disc that does not show signs of degeneration, loss of disc height, dehydration, bony edema, or degenerative changes.

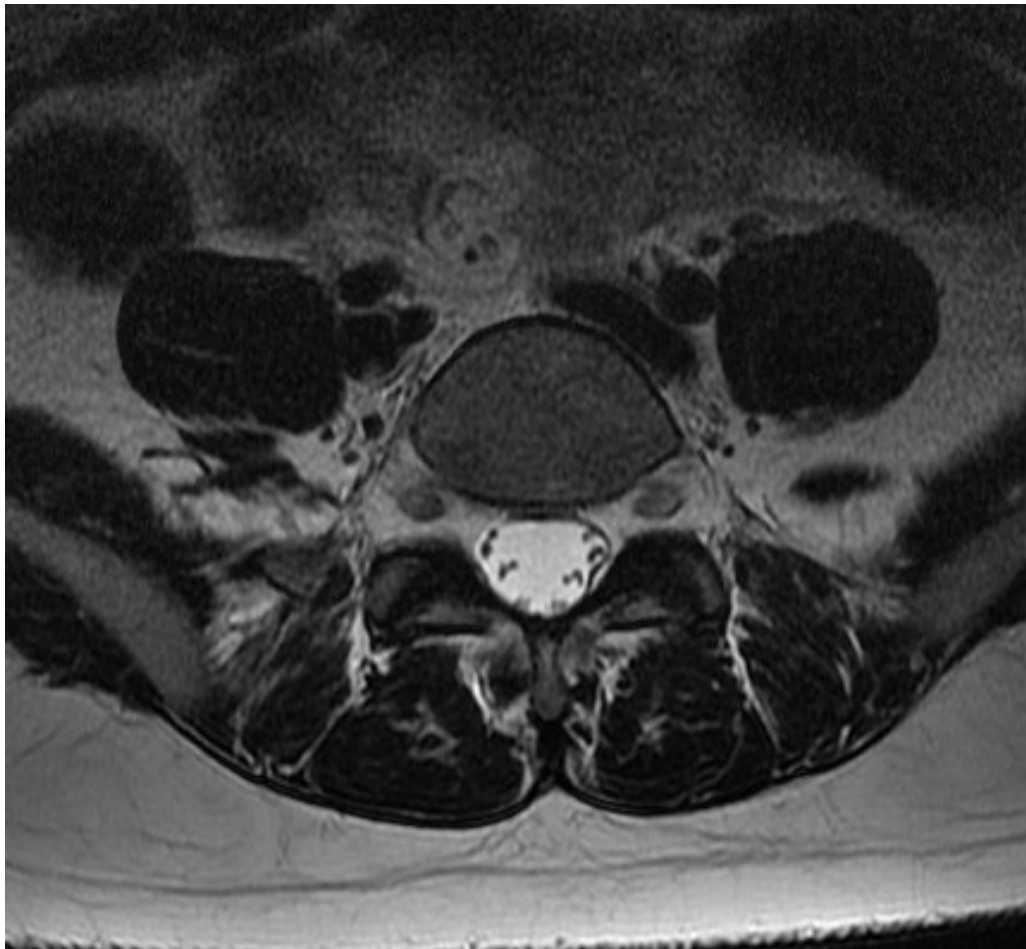


Figure 5:1. A normal axial image.

Classification of Lumbar Disc Derangements

Differentiating an *Intervertebral* Disc Herniation from an *Intravertebral* Disc Herniation

The *intervertebral* space is the region between two adjacent vertebral bodies. This space is typically occupied by the intervertebral disc. The peripheral boundaries of the intervertebral space is marked by the border of the vertebral body. An *intervertebral* herniation occurs when disc tissue migrates outside of the intervertebral boundaries.

Intravertebral herniations occur when the disc migrates into the vertebral body. This usually occurs with axial compression from trauma, excessive load bearing, or a reduction in the bony integrity of the endplate and underlying cancellous bone. Longstanding *intravertebral* herniations are usually considered a coincidental finding.

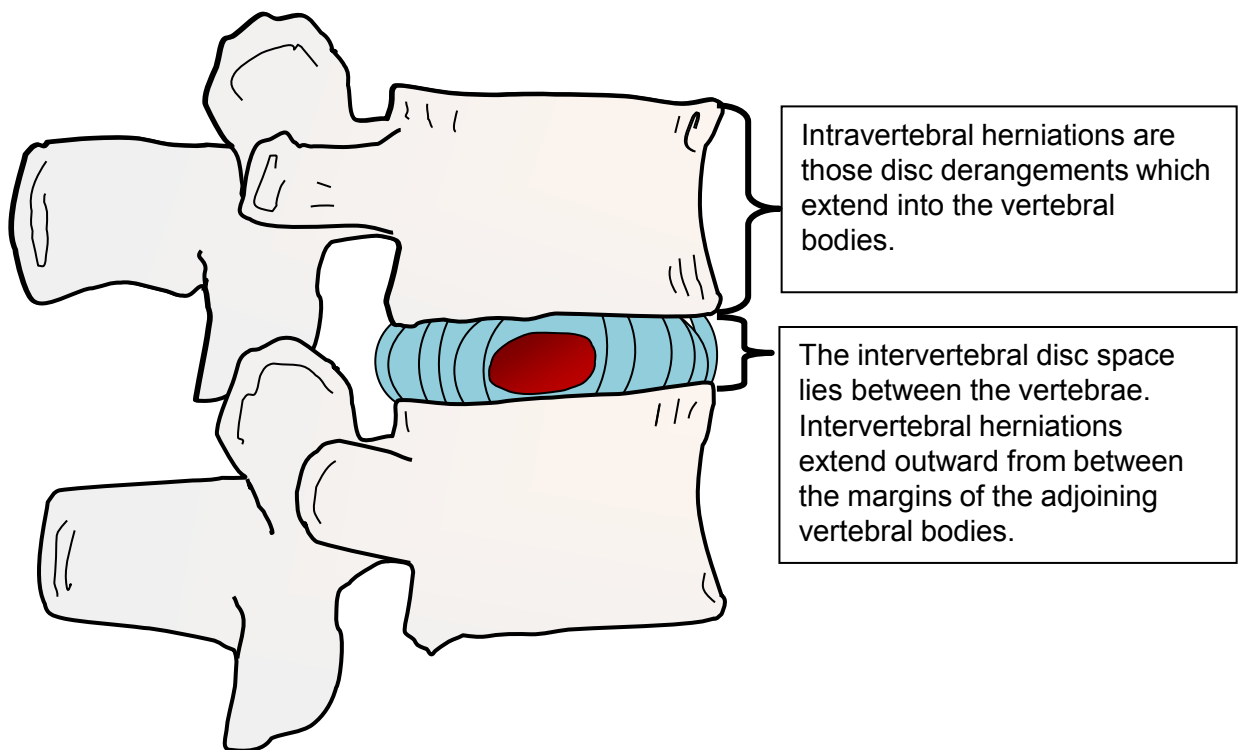


Figure 5:2. Intervertebral lumbar segments

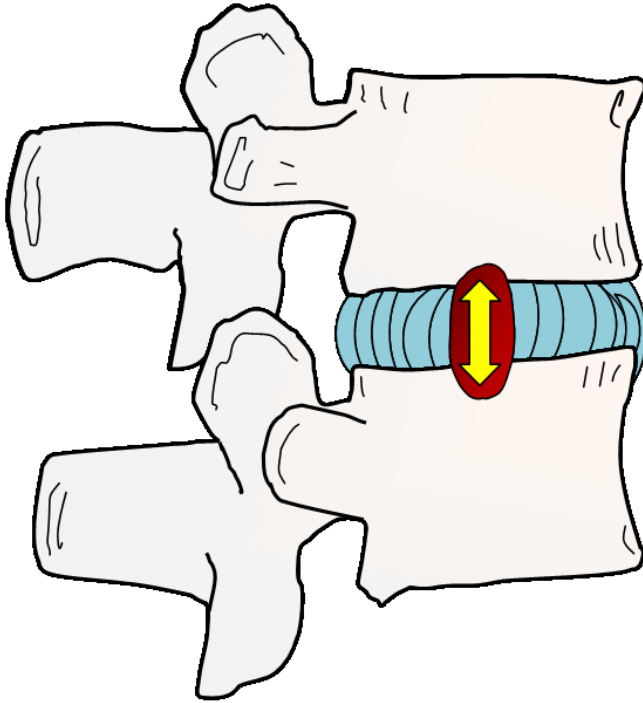


Figure 5:3. Intravertebral herniations occur when the disc breaks through the vertebral endplate of an adjoining vertebra. This schematic shows both an inferior and superior intravertebral herniation. These are commonly called Schmorl's nodes.

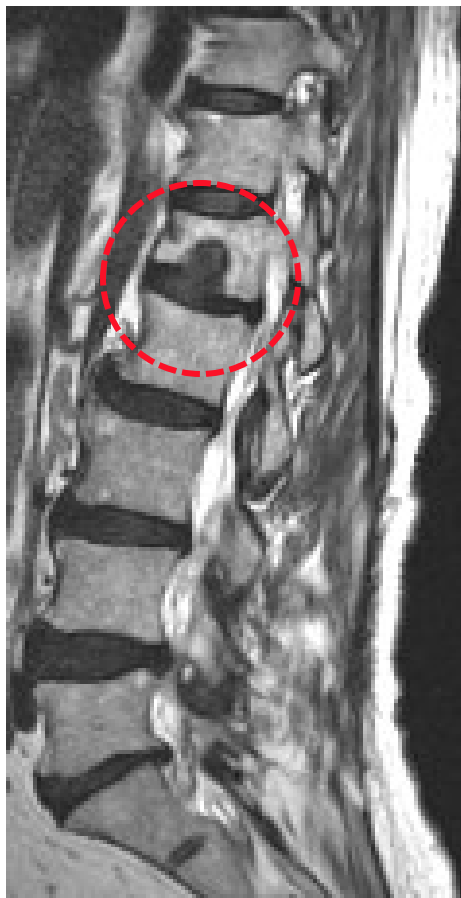


Figure 5:4. This sagittal T2 weighted image reveals a large intravertebral herniation through the inferior endplate of L1.

Axial Images

Axial schematics will be used for much of the remainder of this chapter to illustrate the characteristics of intervertebral herniations. The schematics will be based on an oval shape of the disc. This is not how the disc typically appears, but it aids in understanding the concept of classifying disc derangements.

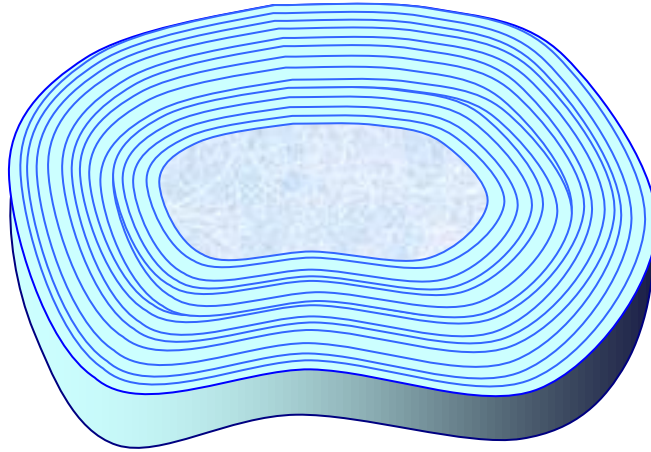


Figure 5:5. Intervertebral discs are not uniform in shape or symmetry.

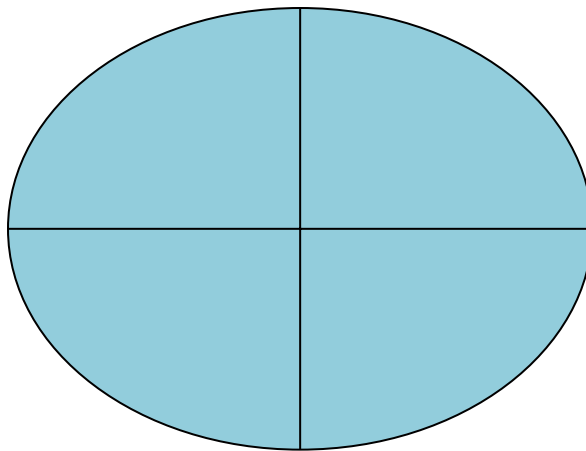


Figure 5:6. For the sake of clarity we will treat the intervertebral disc as a symmetrical oval as we describe the nomenclature of classifying disc derangements.

Classification Parameters of Intervertebral Disc Derangements

To simplify the classification of disc derangements the disc is reduced to a two dimensional oval model that is divided into quadrants. Each 90° quadrant represents 25% of the total circumference of the disc. Using axial MRI imagery and this simple guideline allows the differentiation between broad-based and focal herniations, between symmetrical and asymmetrical disc bulges, and between extrusions and protrusions of the disc.

Normal Disc

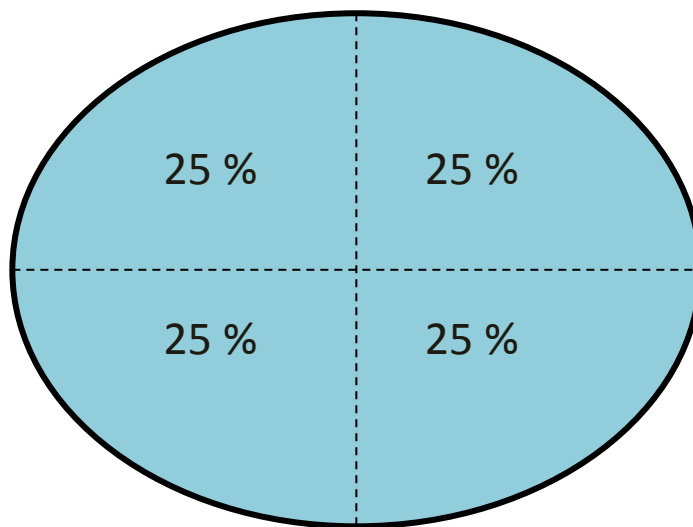


Figure 5:7. The normal disc.

Symmetrical Disc Bulge

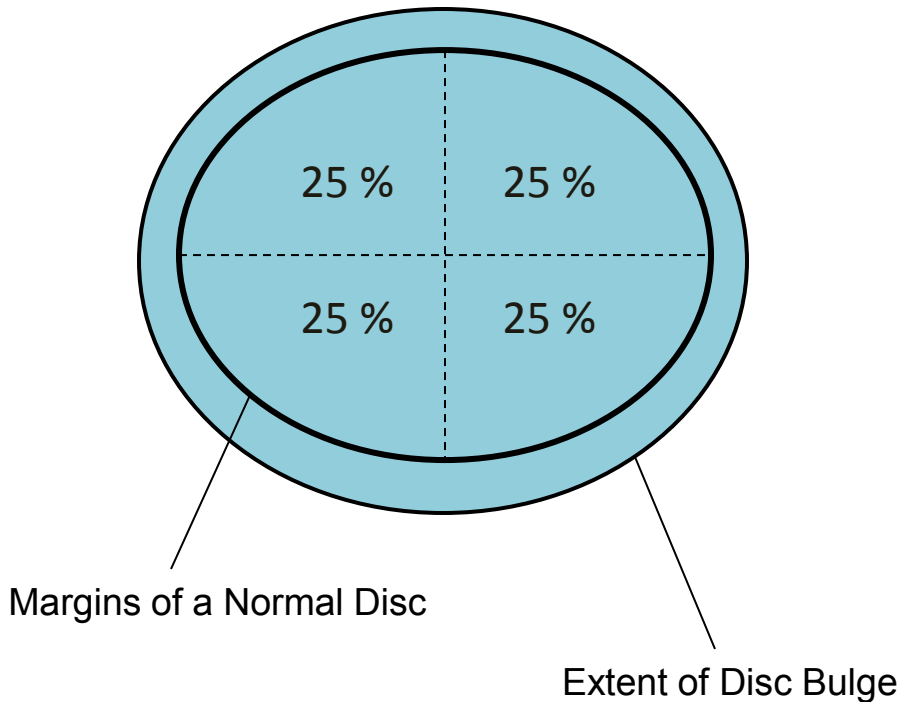


Figure 5:8. Symmetrical disc bulge.

Disc bulges are categorized as disc migration (beyond the border of the vertebral apophyses) of more than 50% (180°) of the disc circumference. Symmetrical bulging discs have a symmetrical appearance of bulging between 50 and 100 percent of the disc circumference. The above schematic depicts a symmetrical bulging disc. Disc bulges are not considered a herniation. Herniations, by contrast, are disc derangements which involve less than 50% of the circumference of the disc.

Symmetrical Disc Bulge

This axial T2 image reveals a nearly uniform disc bulge extending out in all directions. It involves 100% of the circumference of the disc. In the lower image the dotted line signifies the boundary of the vertebra, and the solid line reveals the extent of disc migration. This is a good example of a symmetrical disc bulge.

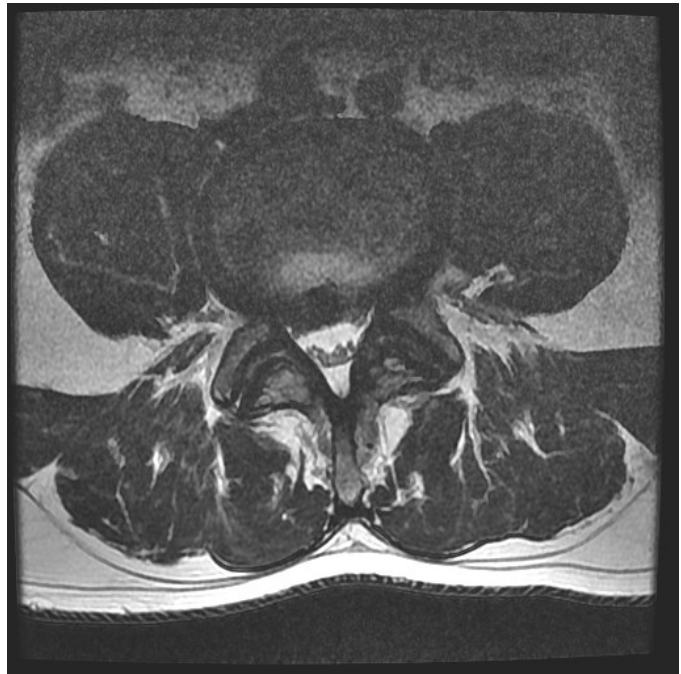


Figure 5:9. Symmetrical disc bulge on T2W axial image.

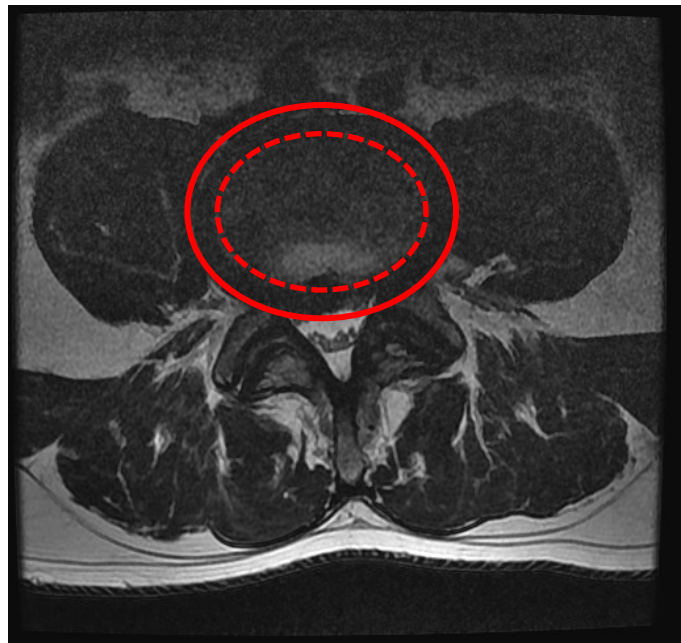


Figure 5:10. Symmetrical disc bulge. This is the same MRI slice as in figure 5:9 above, but the boundaries of the vertebral bodies are demarcated by a dotted line and the extent of the disc bulge is represented by a solid line.

Asymmetrical Disc Bulge

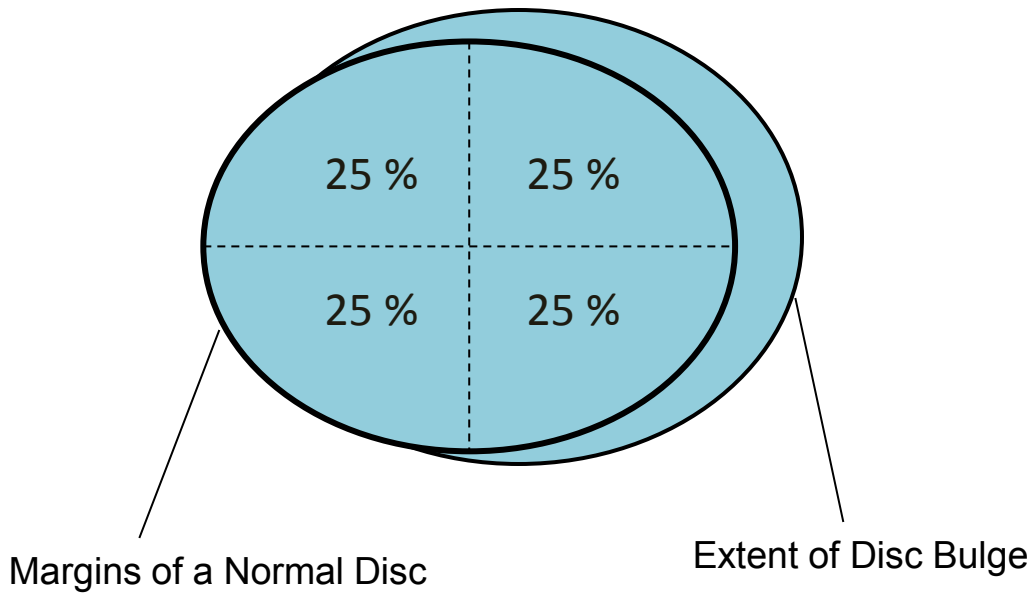


Figure 5:11. Asymmetrical disc bulge.

Asymmetrical disc bulges are categorized as disc derangements that are asymmetric, but involve outward migration of disc material of at least 50% of the disc's circumference. Asymmetrical bulging discs have an asymmetrical appearance of bulging greater than 50% of the disc's circumference. This schematic depicts an asymmetrical bulging disc.

Asymmetrical Disc Bulge

These images are of the same axial T2 slice and they reveal an asymmetric disc bulge. It is categorized as a bulge rather than a herniation since it occupies more than 50% of the circumference of the disc. In the bottom image the white arrows indicate the border of the vertebra, and the yellow arrows point to the margins of the asymmetrical disc bulge.



Figure 5:12. Asymmetrical disc bulge on a T2W axial image.

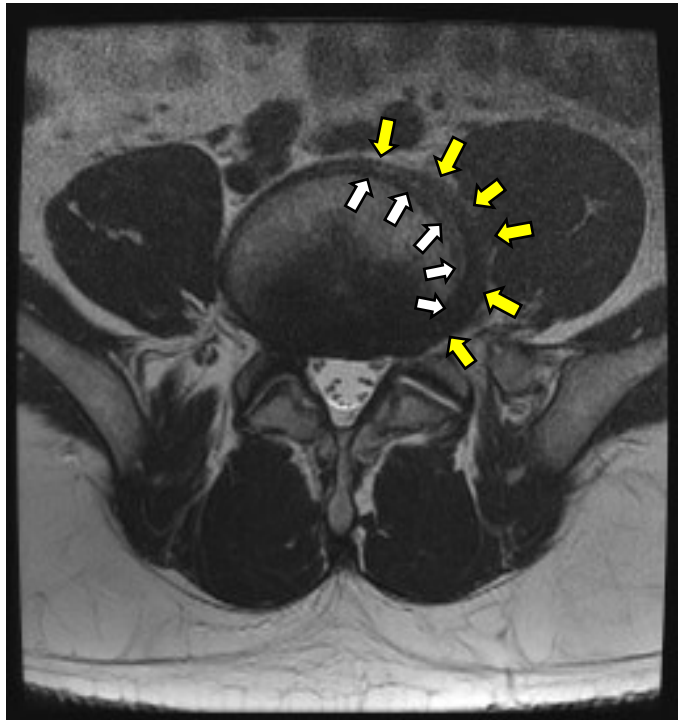


Figure 5:13. Enhanced image of an asymmetrical disc bulge on a T2W axial image. The white arrows identify the boundary of the vertebra and the yellow arrows, the boundary of the disc bulge.

Disc Herniation

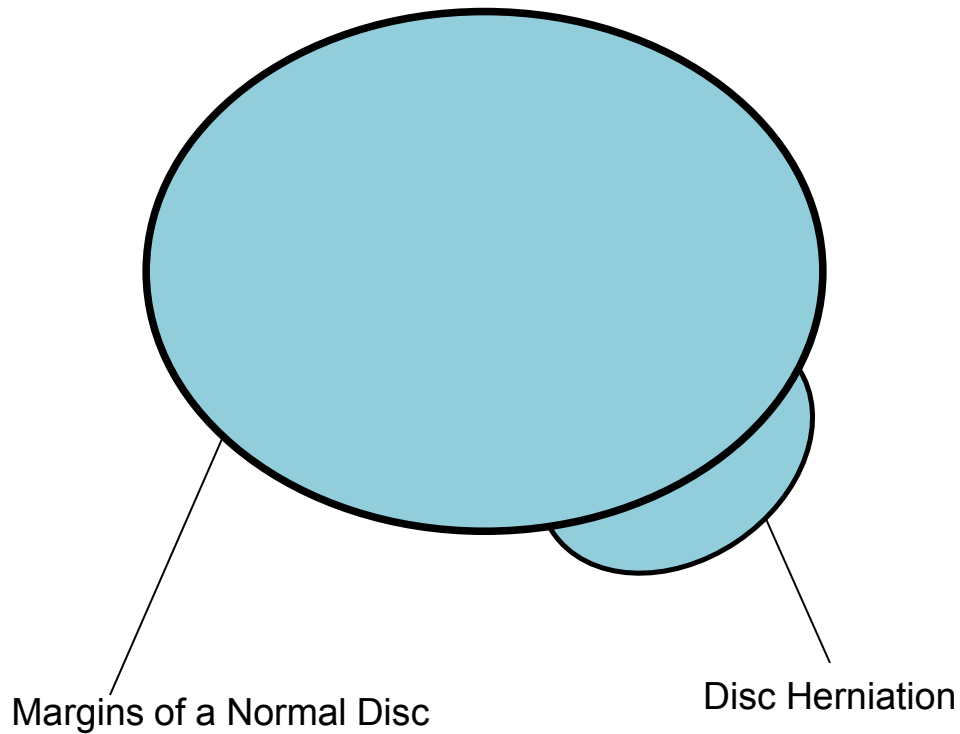


Figure 5:14. Schematic of a disc herniation.

Disc herniations are migrations of disc tissue more localized in appearance and occupying less than 50% of the disc's circumference. There are several subcategories of disc herniation.

Disc Herniation



Figure 5:15. This herniation affects less than 50% of the disc circumference, so it would be labeled a herniation rather than a bulge.

Differentiating between a Focal and a Broad-Based Disc Herniation

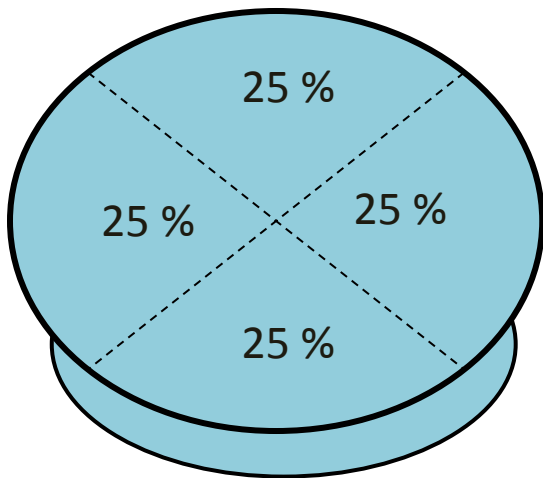


Figure 5:16. A broad-based herniation occupies 25-50% of the disc circumference.

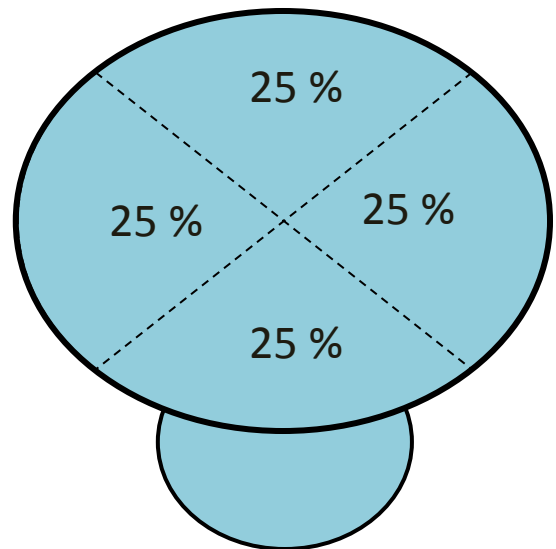


Figure 5:17. A focal disc herniation occupies less than 25% of the disc circumference. Recall that a disc bulge occupies more than 50% of a disc's circumference.

Broad-Based Disc Herniation

This broad disc herniation involves more than 25%, but less than 50% of the circumference of the disc. Thus it is classified as a broad-based disc herniation.

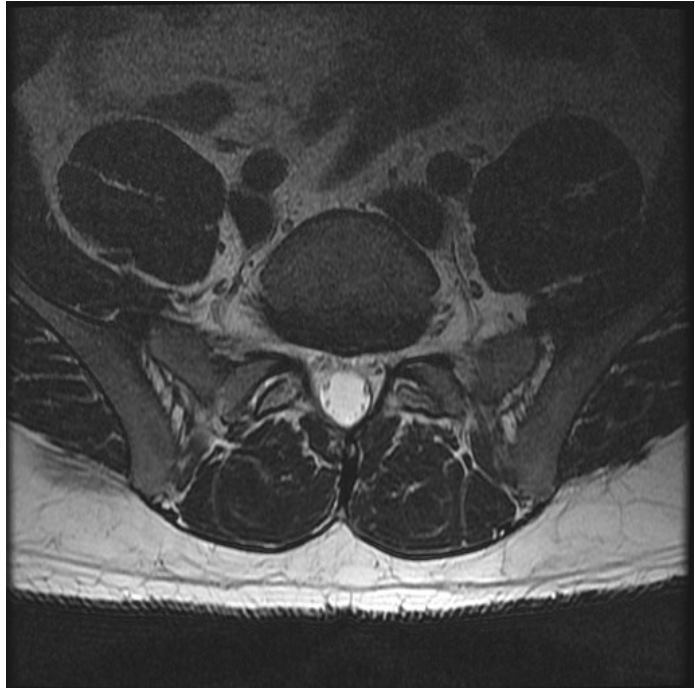


Figure 5:18. A broad-based herniation in a T2W axial image.

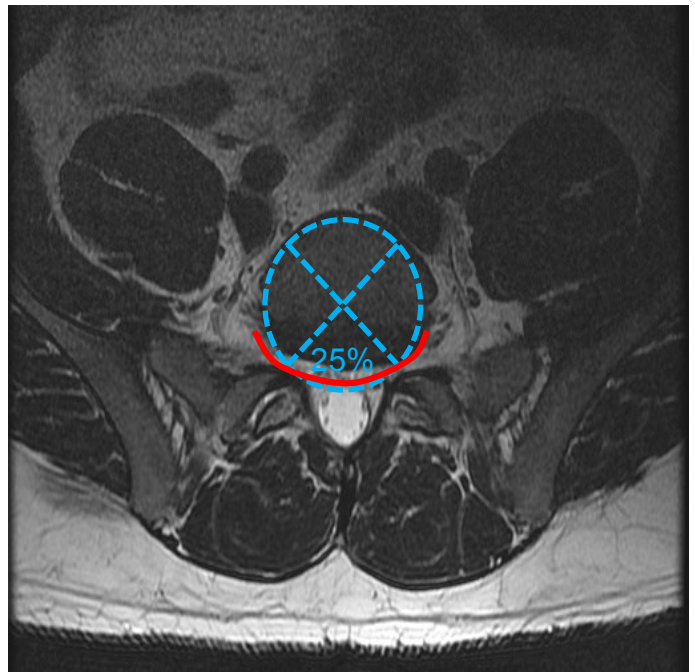


Figure 5:19. A broad-based herniation in a T2W axial image. A broad-based herniation occupies 25-50% of the disc circumference.

Focal Disc Herniation

This disc herniation clearly involves less than 25% of the circumference of the disc; so it is classified as a focal disc herniation.

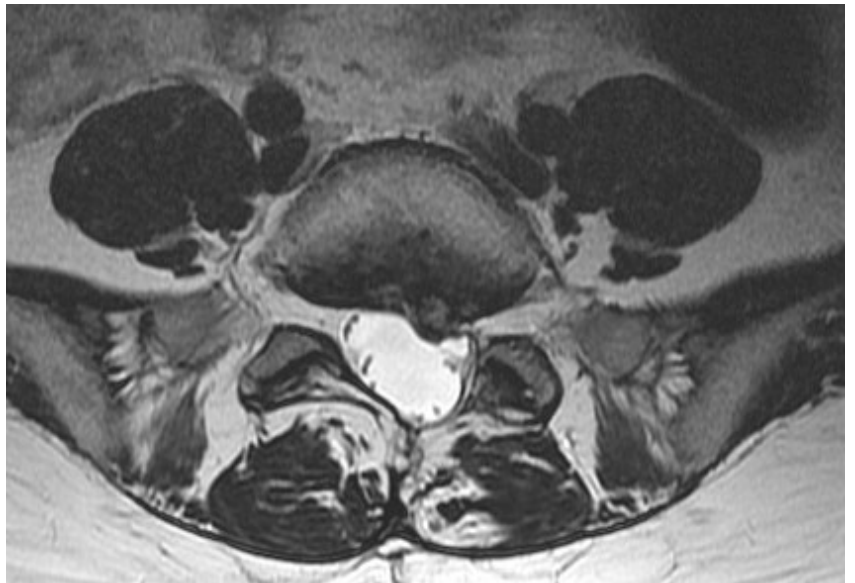


Figure 5:20. A focal herniation in a T2W axial image.

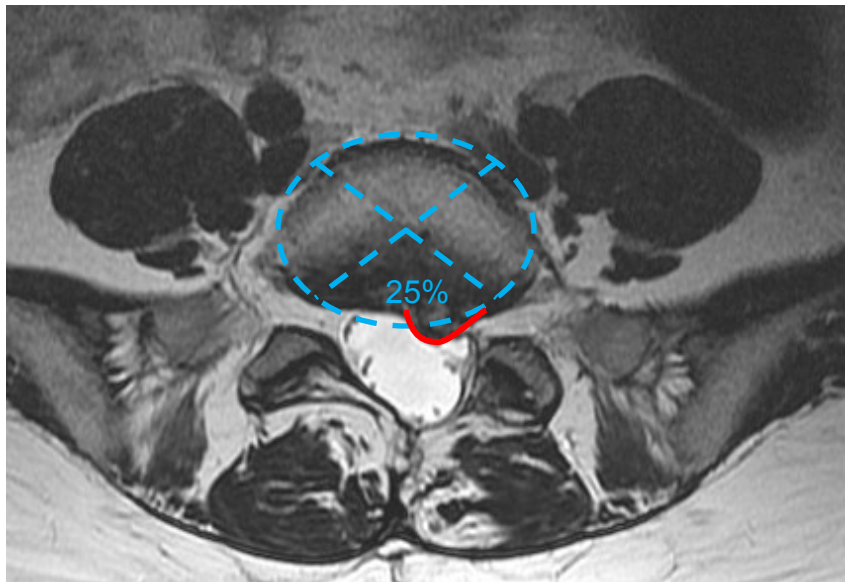
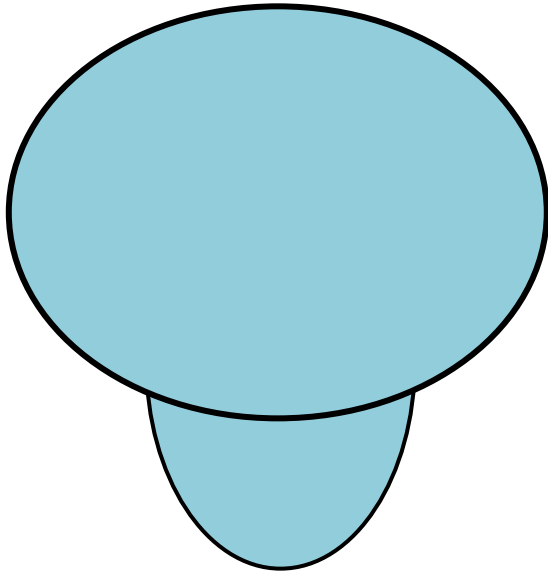


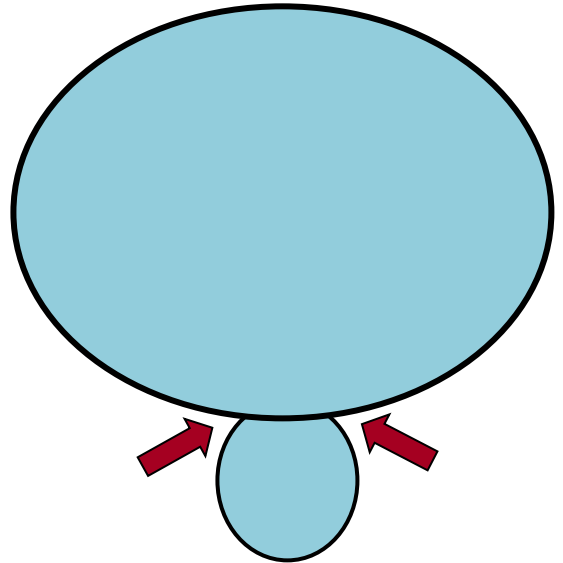
Figure 5:21. A focal herniation occupies less than 25% of the circumference of a disc.

Differentiating between a Protrusion and an Extrusion



Disc Protrusion

Figure 5:22. A disc protrusion has a base wider than its tip.



Disc Extrusion

Figure 5:23. A disc extrusion has a “waist” that is narrower than the tip.

A disc protrusion is wider at the base than it is at the tip. A disc extrusion mushrooms out so that it will have a narrowed waist at the base as indicated by the arrows.

Disc Extrusion

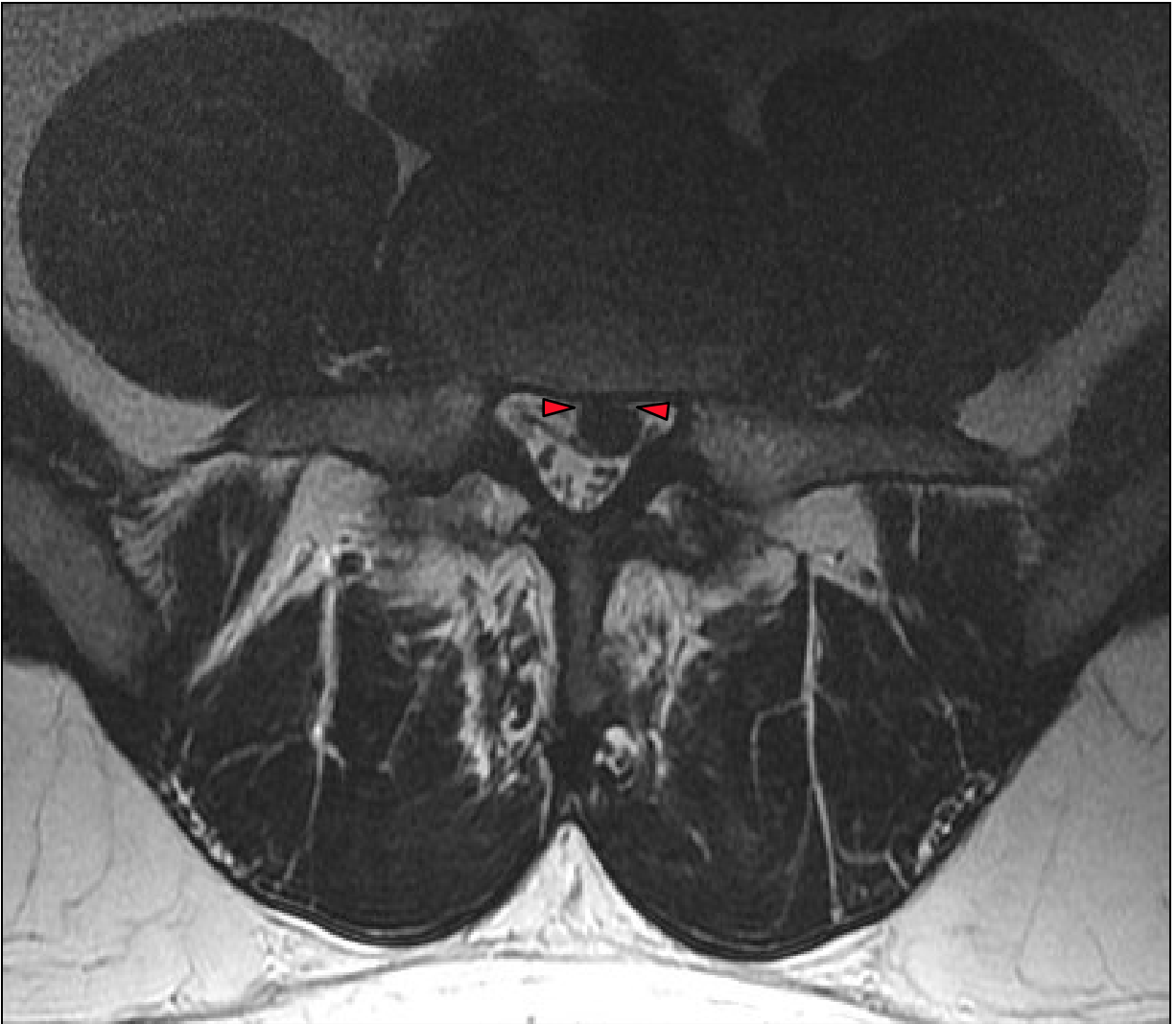


Figure 5:24. Disc extrusion with a narrowed waist (red arrows).

An extrusion is demonstrated on axial imagery by either the narrowed waist that joins the herniated portion of the disc with the rest of the disc or by the absence of a clear bridge between the herniated portion and the main body of the disc. The red arrows indicate the space between the vertebral body and the extruded disc.

Disc Extrusion

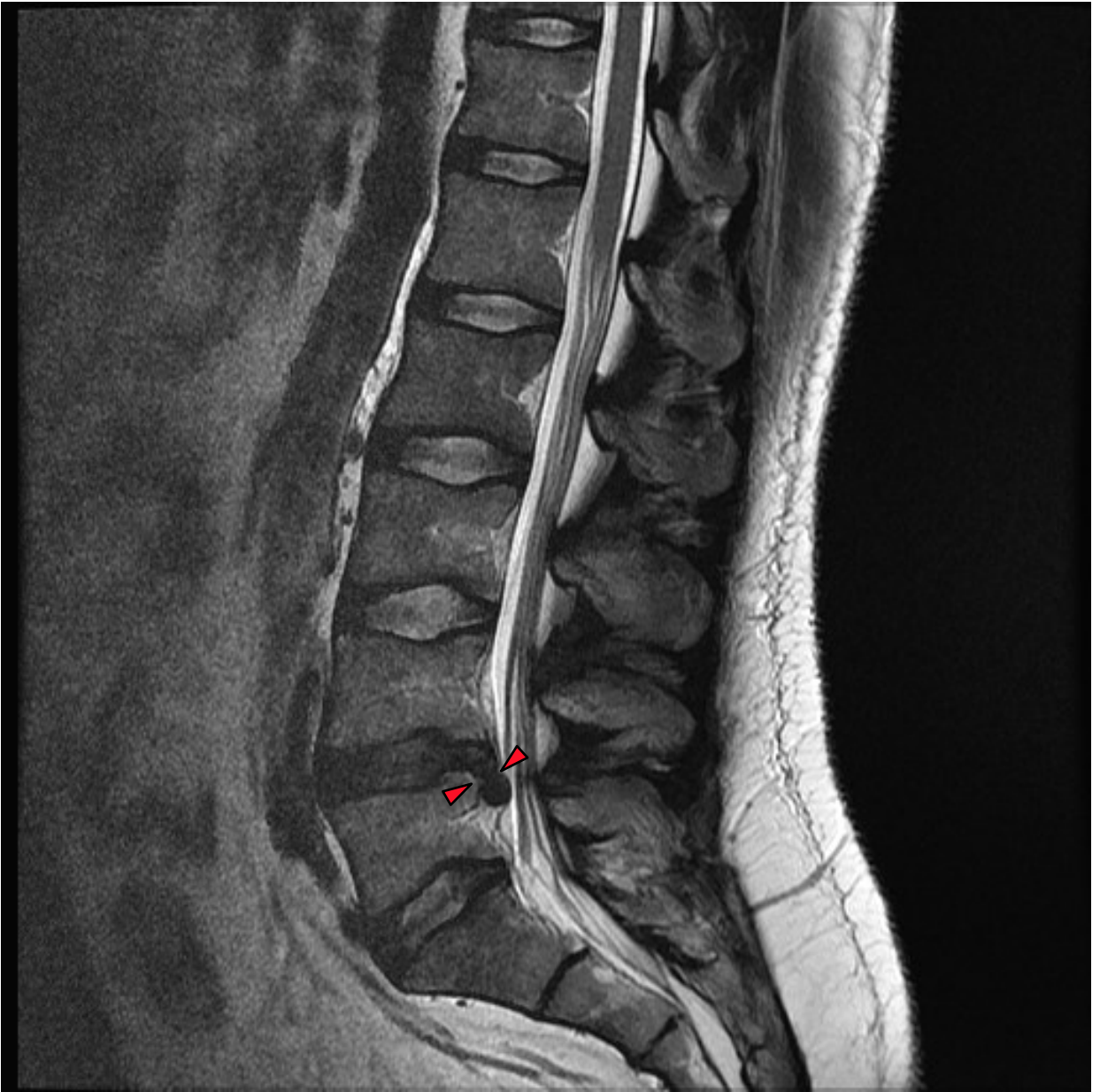
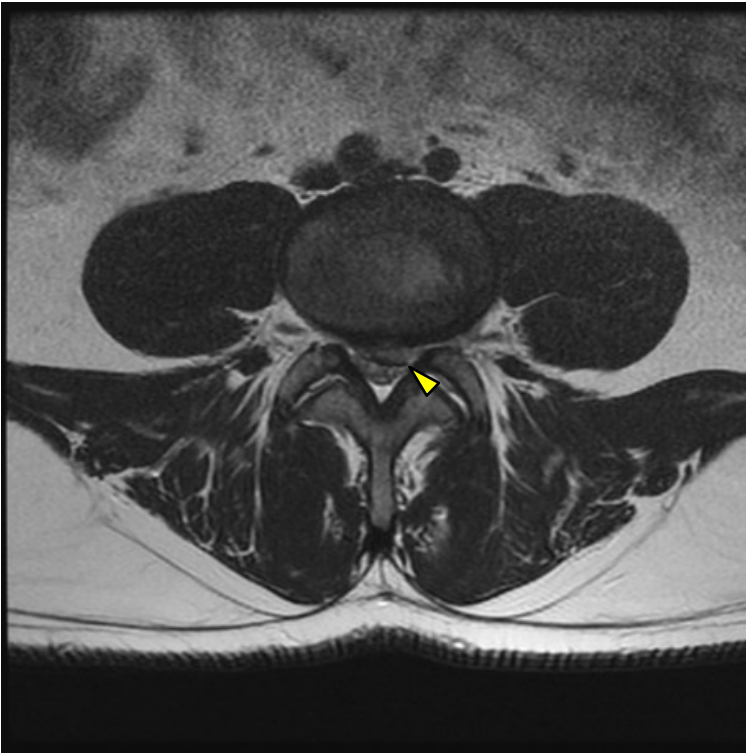


Figure 5:25. This T2 weighted sagittal image shows the characteristic waist of an extrusion.

Disc Protrusions



These T2W images depict protrusions. Note that the base of these herniations are wider than the tips, and there is no narrowed waist.

Figure 5:26. Axial image of a herniation with its base wider than its tip.

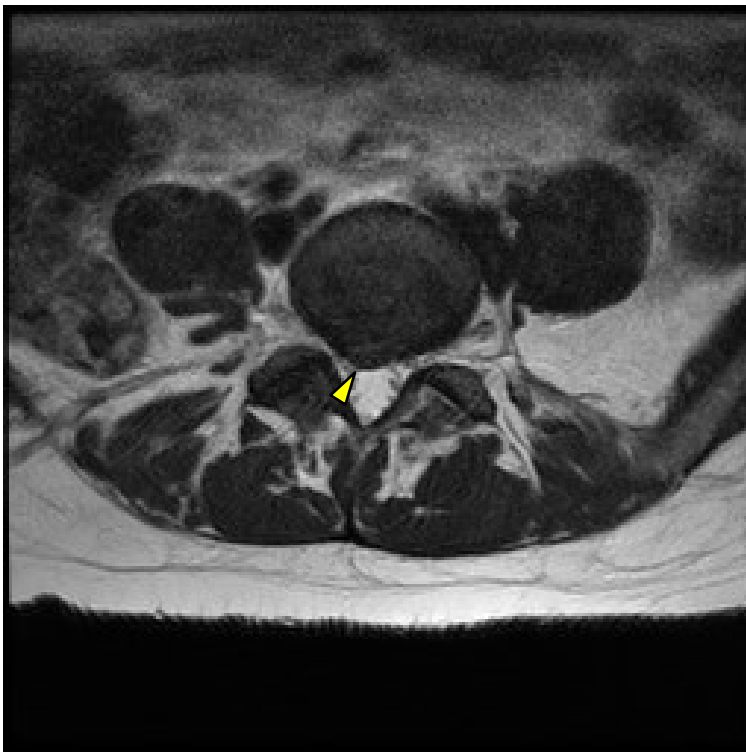


Figure 5:27. Axial image of a protruded disc.

Sagittal Views of Protrusions and Extrusions

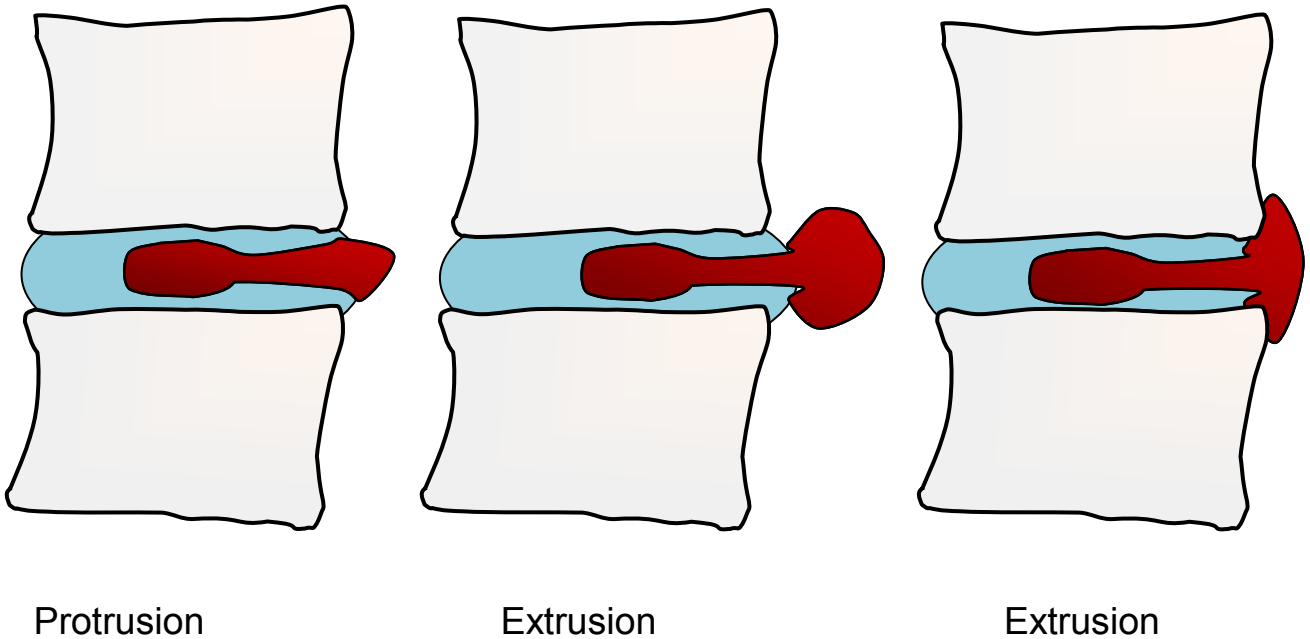


Figure 5:28. Schematics of protrusion and extrusion.

Disc extrusions can be diagnosed in either the axial or sagittal planes. A protrusion is a herniation that has a wide proximal base which narrows as it extends distally from the center of the disc. An extrusion has an expansive herniation that widens after it leaves the intervertebral space. Even if the herniation appears to have a wide base like a protrusion, it is considered an extrusion if it expands along the vertebral body to a width wider than that of the disc (see image on right). A protrusion does not exceed the cranio-caudal boundaries of the intervertebral disc.

Clarification of Extrusion versus Protrusion

To further clarify the difference between a protrusion and an extrusion, axial and sagittal images of the same disc herniation have been selected. On the axial image the disc herniation looks like a disc protrusion (the base of the herniation appears wider than the tip). However, when you view the same herniation from the sagittal orientation, you can see a narrowed waist of the disc at the point that it exits the intervertebral space, and the disc expands out. A disc extrusion is present when an expansion is visualized in either the axial or sagittal views or if a sequestered fragment is present.

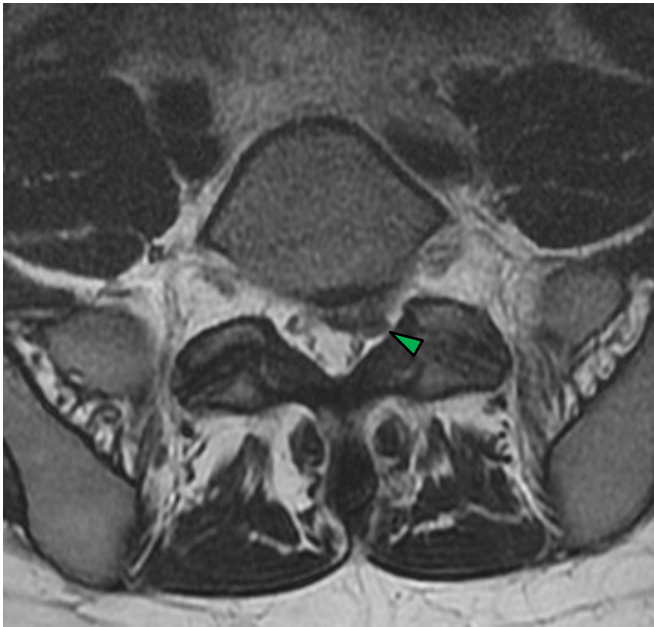


Figure 5:29. This axial image appears to be a protrusion (green arrow) as its base is wider than its tip.

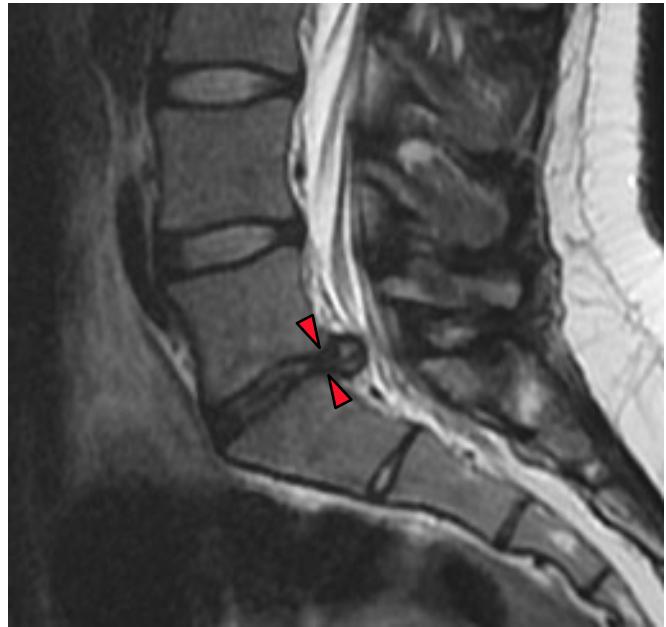


Figure 5:30. This sagittal image of the same herniation in figure 5:29 shows a narrowed waist (red arrows) making this an extrusion, regardless of its appearance on axial imagery.

Sequestered Fragment

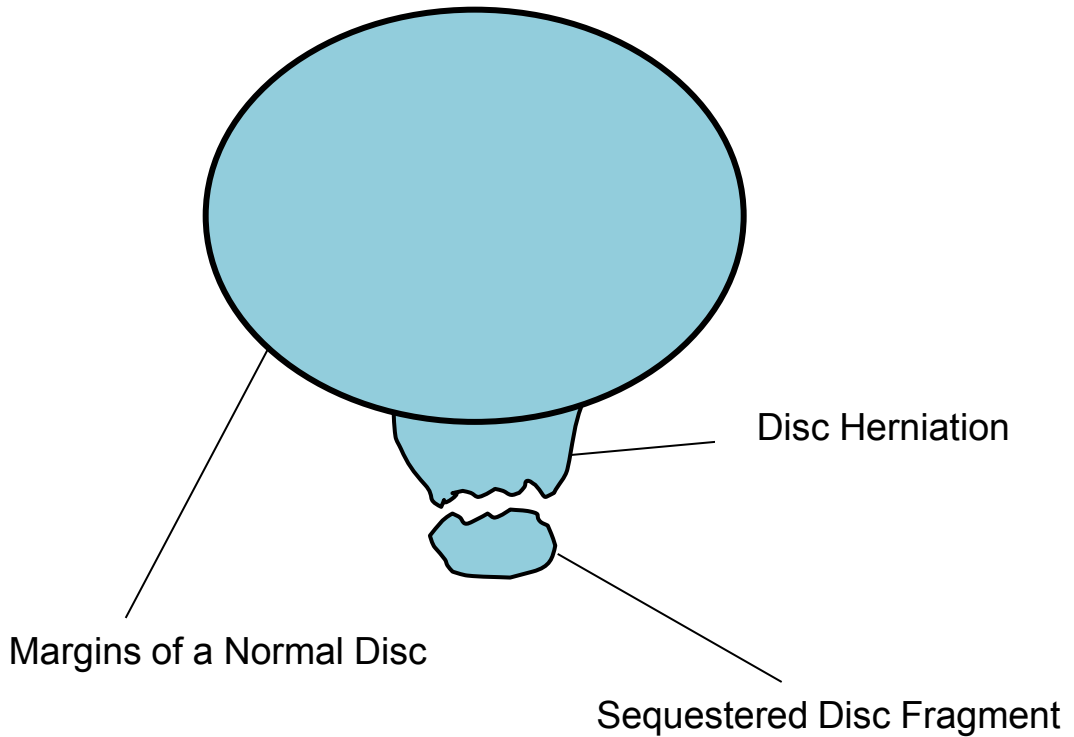


Figure 5:31. Sequestered disc fragments have broken off and are no longer contiguous with the rest of the disc.

Another category of disc extrusion is the sequestered fragment. A sequestered fragment is the designation given to a disc derangement in which a portion of the disc breaks free from the rest of the disc. Sequestered fragments can migrate from their mother discs. They are considered a category of disc extrusions. Sometimes these are referred to as “free fragments.”

Sequestered Fragment



Figure 5:32. A large sequestered disc fragment in the central canal of L5 displacing and compressing the S1 nerve root.

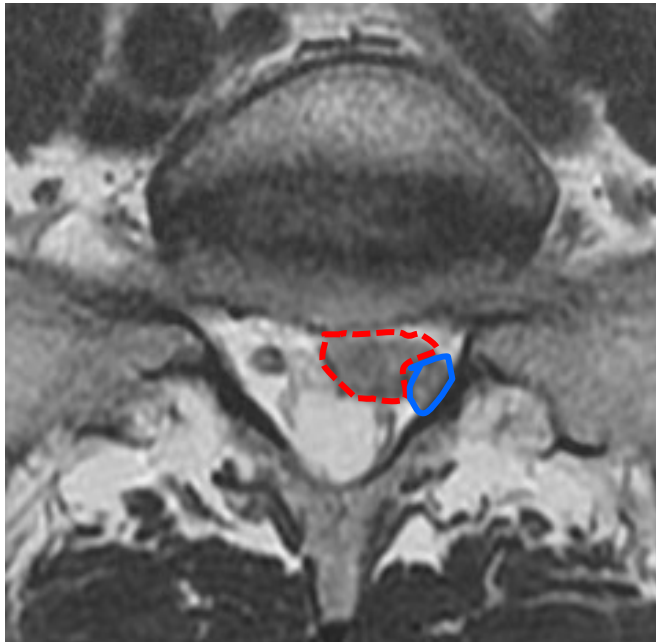
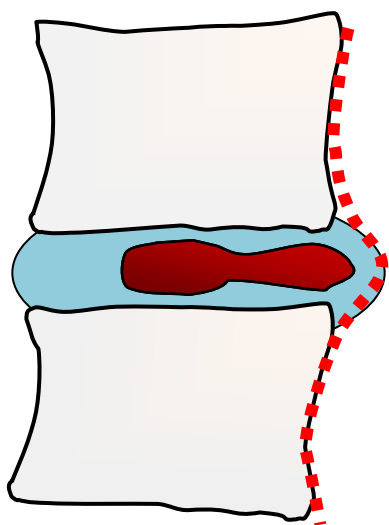


Figure 5:33. The axial image from figure 5:32 is enhanced here. The red dotted line outlines the sequestered disc fragment, and the blue line outlines the S1 nerve root..

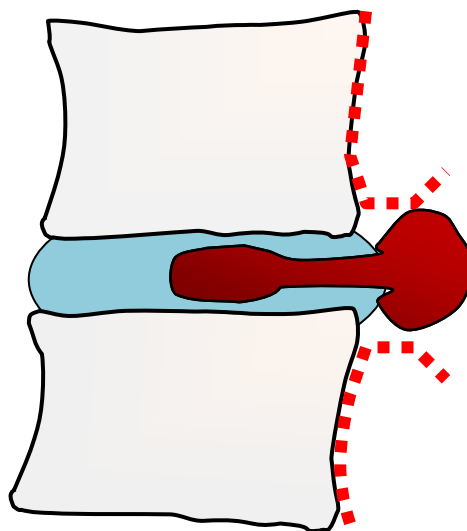
This image contains a sequestered disc fragment that displaces and compresses the left S1 nerve root. The bottom version of this MR slice highlights the sequestered disc fragment with a circumferential red dotted line around it. The compressed nerve root is identified by a solid blue line. Note the degree of swelling of the displaced left nerve root in comparison to the right nerve root.

Contained versus Non-contained Herniations

Another identifier describing disc derangements is the relationship of the derangement to the outer annulus and the posterior longitudinal ligament (PLL). The PLL lies over the posterior vertebral bodies and the posterior portion of the disc. If the PLL and the outer annulus are intact and contain the disc derangement, it may be categorized as a sub-ligamentous or contained herniation. If the disc has violated the outer annulus, it is categorized as a non-contained herniation. If the disc derangement disrupts and passes through the posterior ligaments, it has been called an extra-ligamentous herniation. The current limitations of MR often make it difficult to differentiate between ligamentous, contained, and non-contained herniations.



Sub-ligamentous and contained



Extra-ligamentous and non-contained

Figure 5:34. A sub-ligamentous herniation does not violate the integrity of the ligaments, usually the posterior longitudinal ligament (red dotted line). A contained disc derangement remains enclosed within the annulus fibers.

Figure 5:35. An extra-ligamentous herniation violates the integrity of the posterior longitudinal ligament. A non-contained disc derangement denotes disc material escaping the confines of the annulus fibers.

Normal Axial Slice

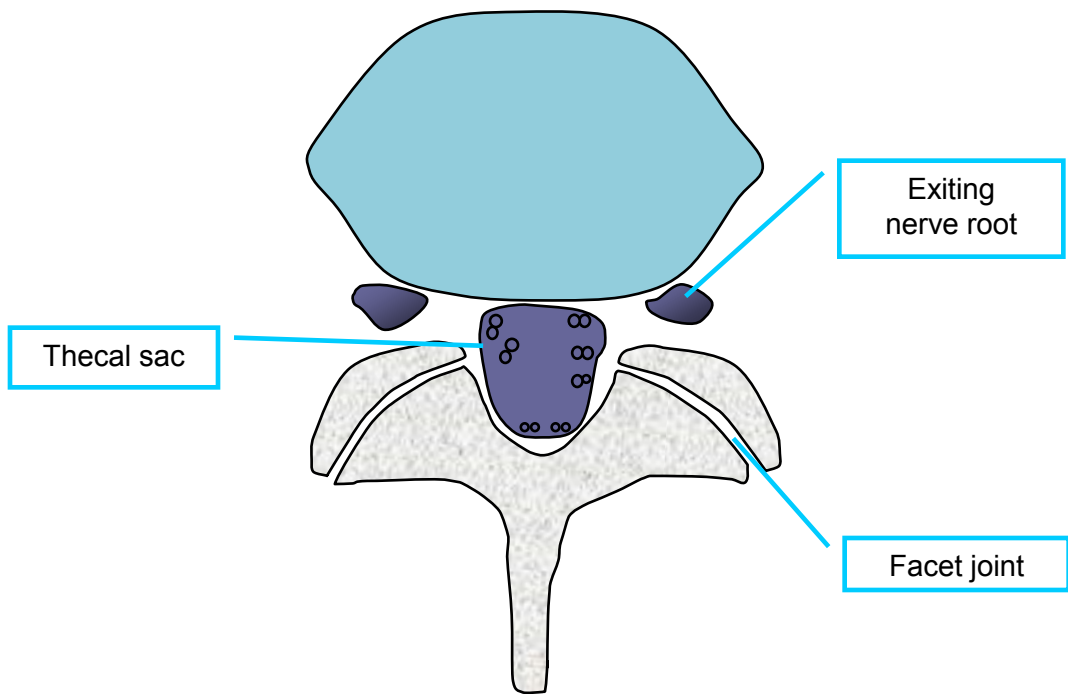


Figure 5:36. A baseline schematic of a normal axial image.

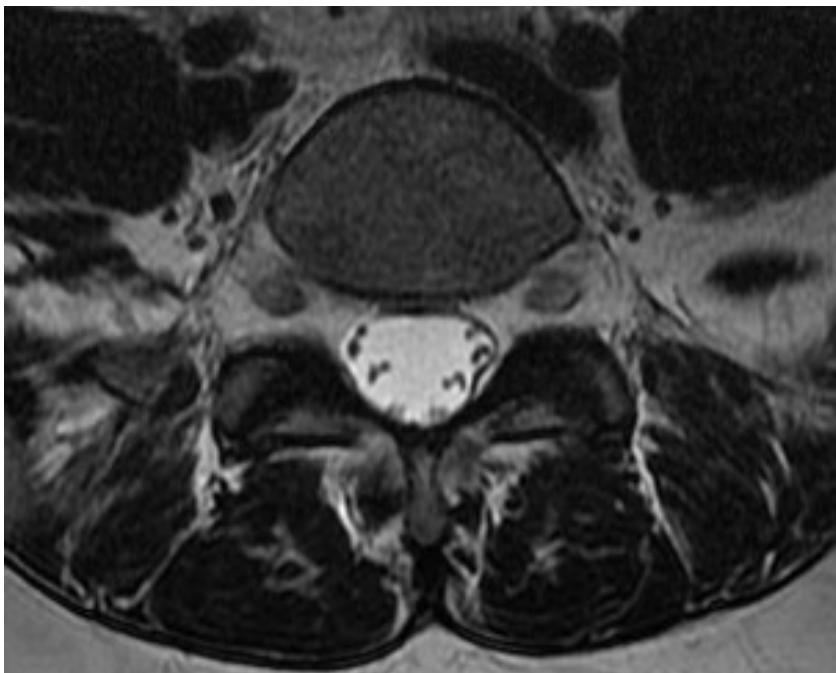


Figure 5:37. A baseline T2W axial image of a normal lumbar segment.

Central Disc Herniation

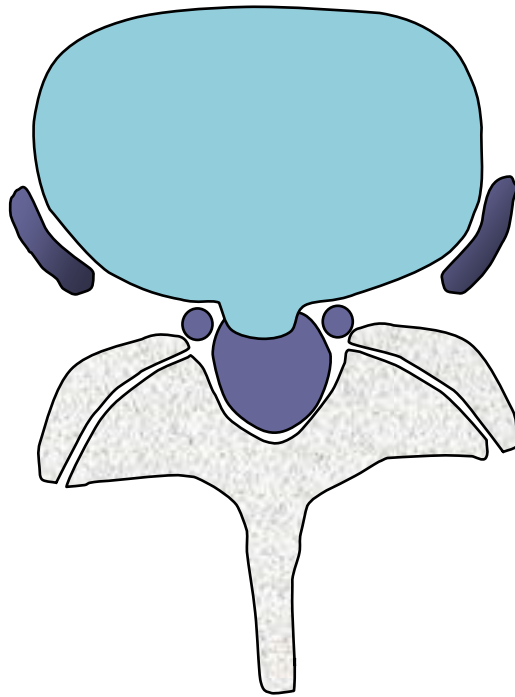


Figure 5:38. A schematic of a central disc herniation.

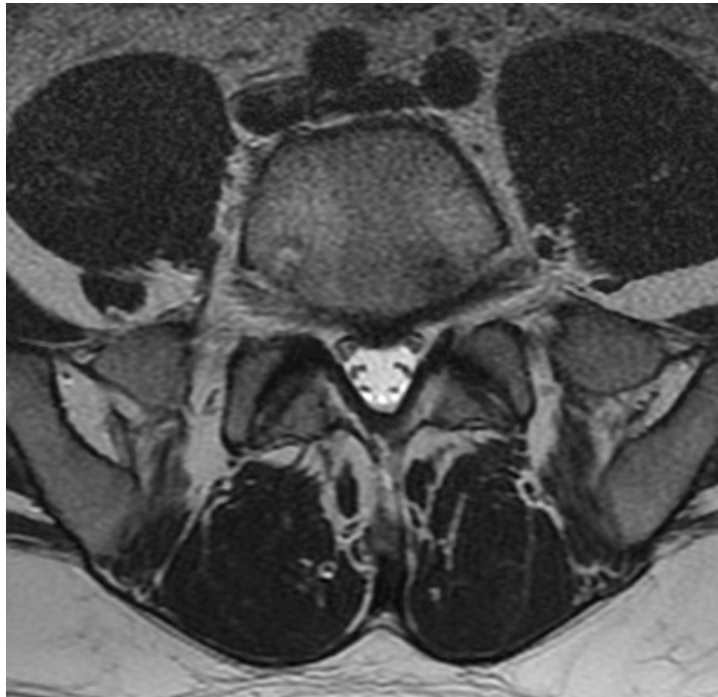


Figure 5:39. T2W axial image of a small, focal, central disc herniation.

Paracentral Disc Herniation Displacing a Nerve Root

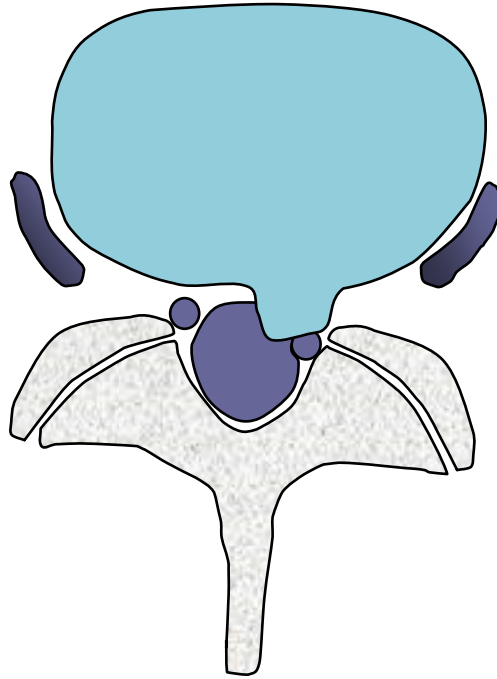


Figure 5:40. Axial schematic image of a paracentral disc herniation displacing an S1 nerve root.



Figure 5:41. Axial image of a paracentral disc herniation (green arrow) that contacts and displaces the left S1 nerve root.

Nerve Root Compression

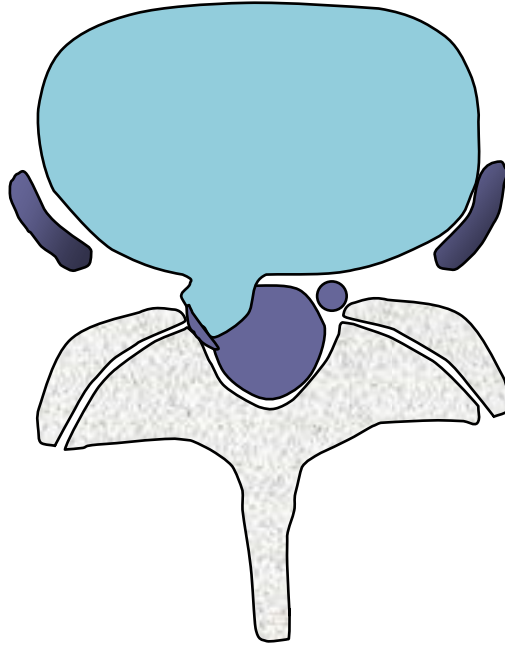


Figure 5:42. Schematic of a focal disc herniation compressing an S1 nerve root.



Figure 5:43. This axial MRI demonstrates a herniation (yellow arrow) that contacts and displaces the S1 nerve root, compressing it against the bony posterior portion of the spinal canal.

Anterior Disc Herniation

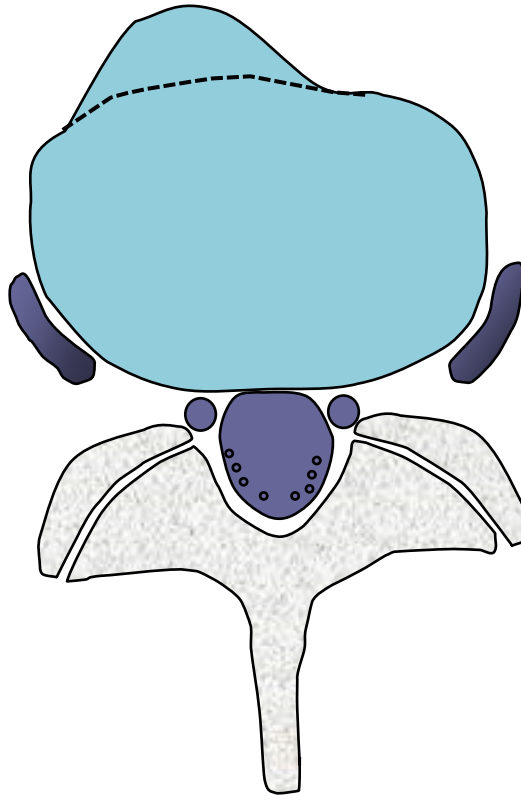


Figure 5:44. Schematic of an anterior disc herniation.



Figure 5:45. Sagittal image of a large anterior herniation (red arrow).

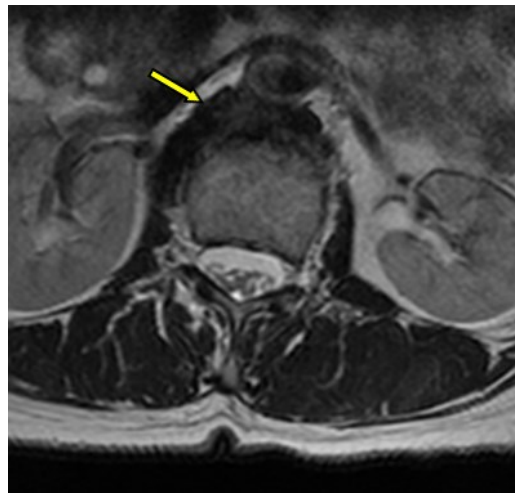


Figure 5:46. Axial image of a large anterior herniation (yellow arrow). This is the same herniation seen in figure 5:45.

Anterior disc herniations do not compromise the spinal cord, thecal sac, or nerve roots, but may be a source of pain and indicative of biomechanical failure.

Foraminal Disc Herniation

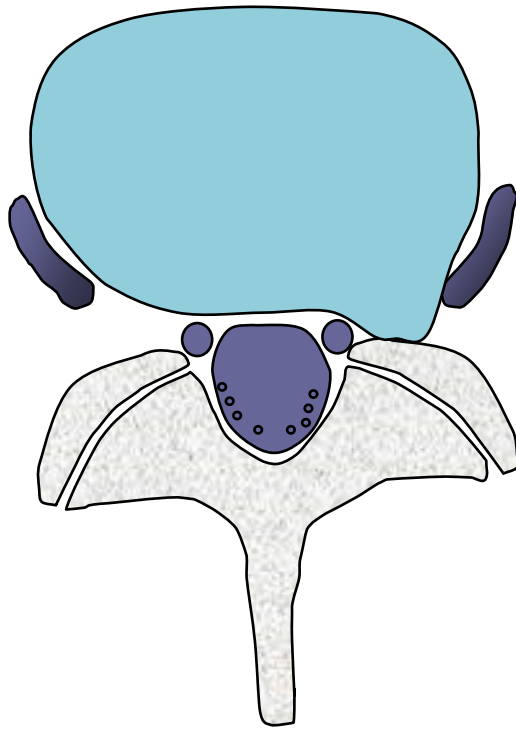


Figure 5:47. Schematic of a foraminal herniation.

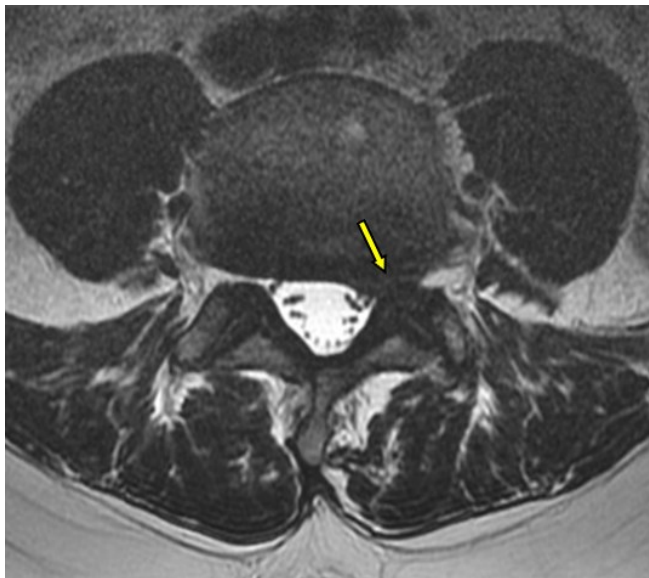


Figure 5:48. Axial image of a foraminal herniation.

Herniations into the foraminal canal can compromise the exiting nerve roots. Even a small herniation in the foraminal canal can cause significant nerve impingement.

Far Lateral Foraminal Disc Herniation

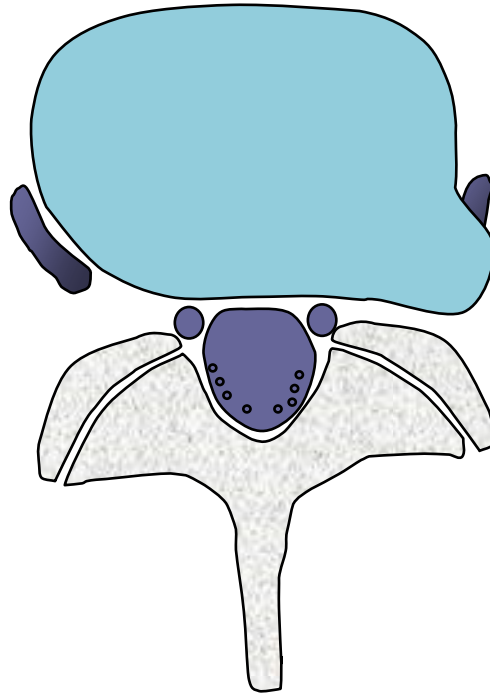


Figure 5:49. Schematic of a far lateral herniation.

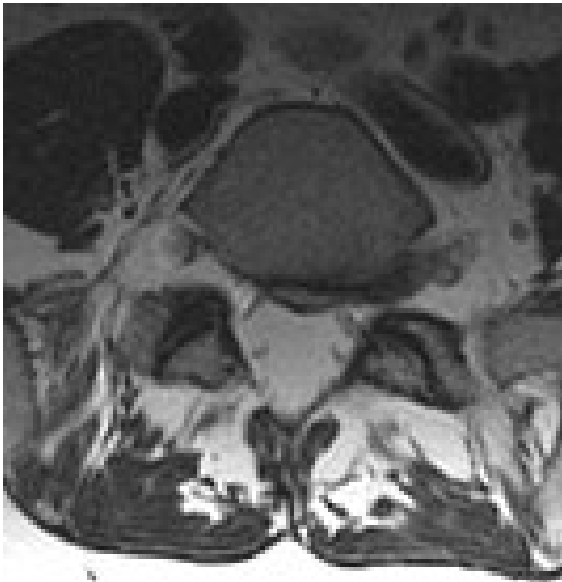


Figure 5:50. Axial image of a far lateral herniation.

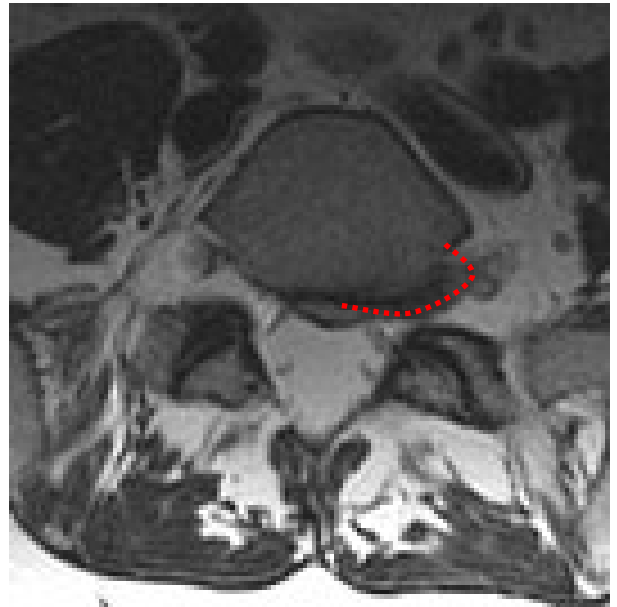


Figure 5:51. Axial image of a far lateral herniation shown outlined with a red dotted line.

Far lateral herniations may contact and affect the exiting nerve root after it leaves the intervertebral foramen. The image on the right outlines the circumference of this far lateral herniation which is visualized in both images.

Volume Descriptors

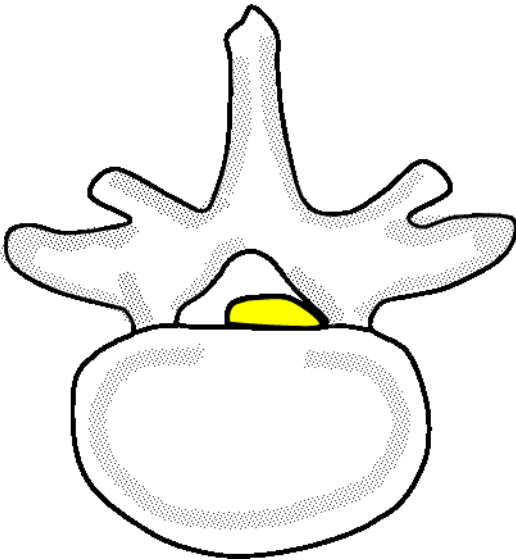


Figure 5:52. Mild herniation.

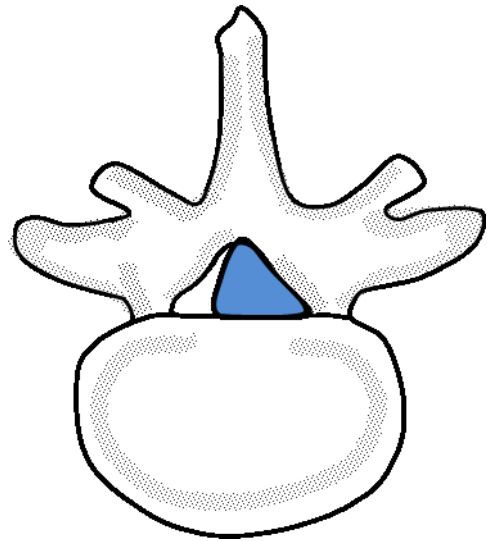


Figure 5:53. Moderate herniation.

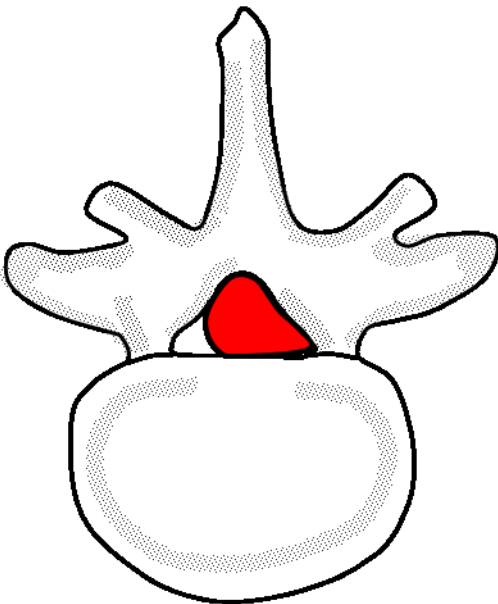


Figure 5:54. Severe herniation.

These are the volume descriptors for the amount of disc material herniated into the central canal as observed on the axial image at the slice of most severe compromise. A canal compromised less than one-third is a *mild herniation* (figure 5:52), between one-third and two-thirds is considered a *moderate herniation* (figure 5:53), and over two-thirds is a *severe herniation* (figure 5:54). This grading method can also be utilized to describe foraminal involvement.

http://www.asnr.org/spine_nomenclature/discussion.shtml

Volume Descriptors for IVF Involvement

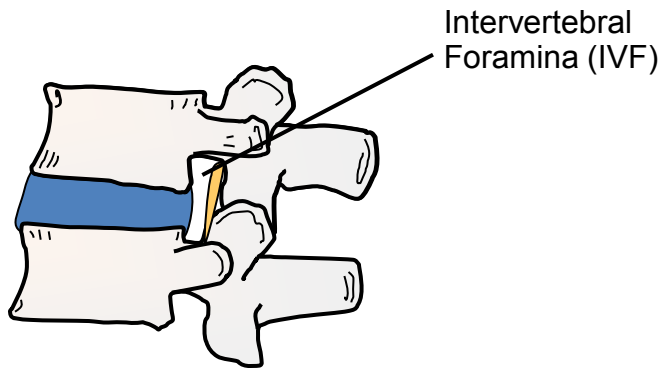


Figure 5:55. Normal/patent foramina

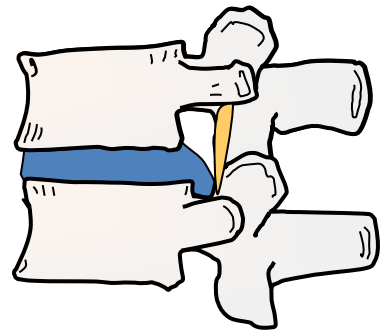


Figure 5:56. Mild foraminal occlusion

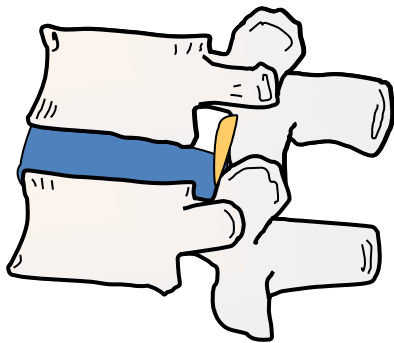


Figure 5:57. Moderate occlusion

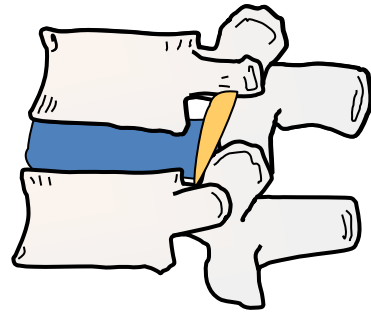


Figure 5:58. Severe IVF occlusion

The descriptors for IVF occlusion are similar to the volume descriptors used for notating the size of disc herniations. An IVF with less than one-third of the canal occluded has a *mild occlusion* (figure 5:56), an occlusion that is between one-third and two-thirds is considered *moderate* (figure 5:57), and over two-thirds is a *severe occlusion* (figure 5:58).

Suggested Reading

Fardon DF, Milette PC. Nomenclature and classification of lumbar disc pathology: recommendations of the combined task forces of the north American spine society, American society of spine radiology, and American society of neuroradiology. *Spine*, Volume 26(5). March 1, 2001. E93-E113.

http://www.asnr.org/spine_nomenclature/discussion.shtml

Cramer G, Darby S (2013). *Basic and clinical anatomy of the spine, spinal cord, and ANS* (third edition). Elsevier Mosby.

Marchiori D (2013). *Clinical imaging: with skeletal, chest and abdomen pattern differentials* (third edition). Mosby.

Classification of Annular Tears



Annular Tears

The term annular tear or annular fissure is used to categorize separation between the annular fibers, avulsion of the fibers from the vertebral body, or a tear through the fibers. A common misconception is that trauma is always indicated by a tear. Annular tears may occur from trauma or over time as part of a degenerative process. Some experts prefer the term annular fissure since it is less implicative of trauma. There are three categorizations of annular tears: radial tears, transverse tears, and concentric tears. Annular tears may be clinically significant or may be asymptomatic coincidental findings. As with many findings on MRI, just because a lesion is visible does not mean that it is clinically significant.

Radial Tears

Radial tears begin centrally and progress outward in a radial direction. Radial tears may precede the migration of the nucleus, resulting in a disc herniation.

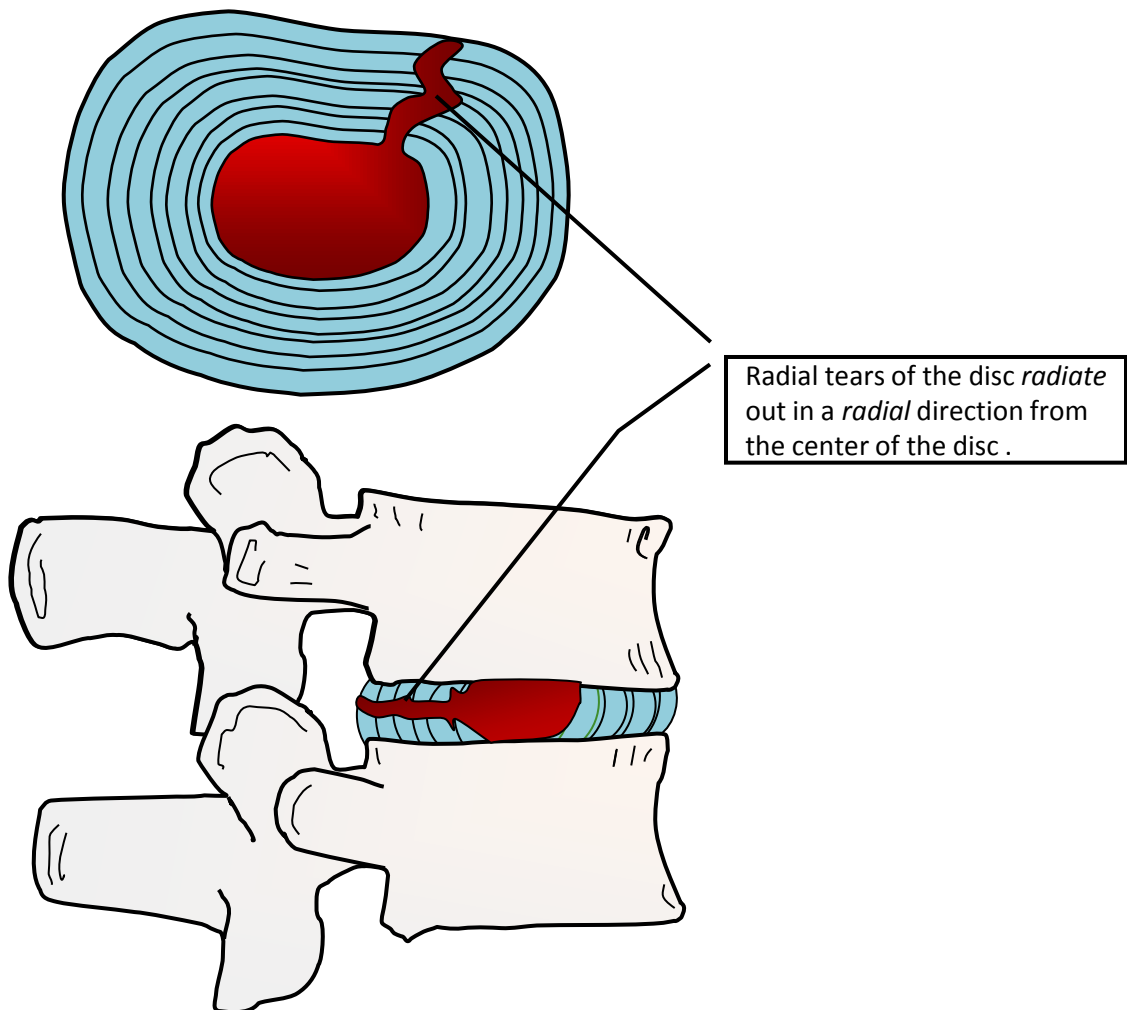
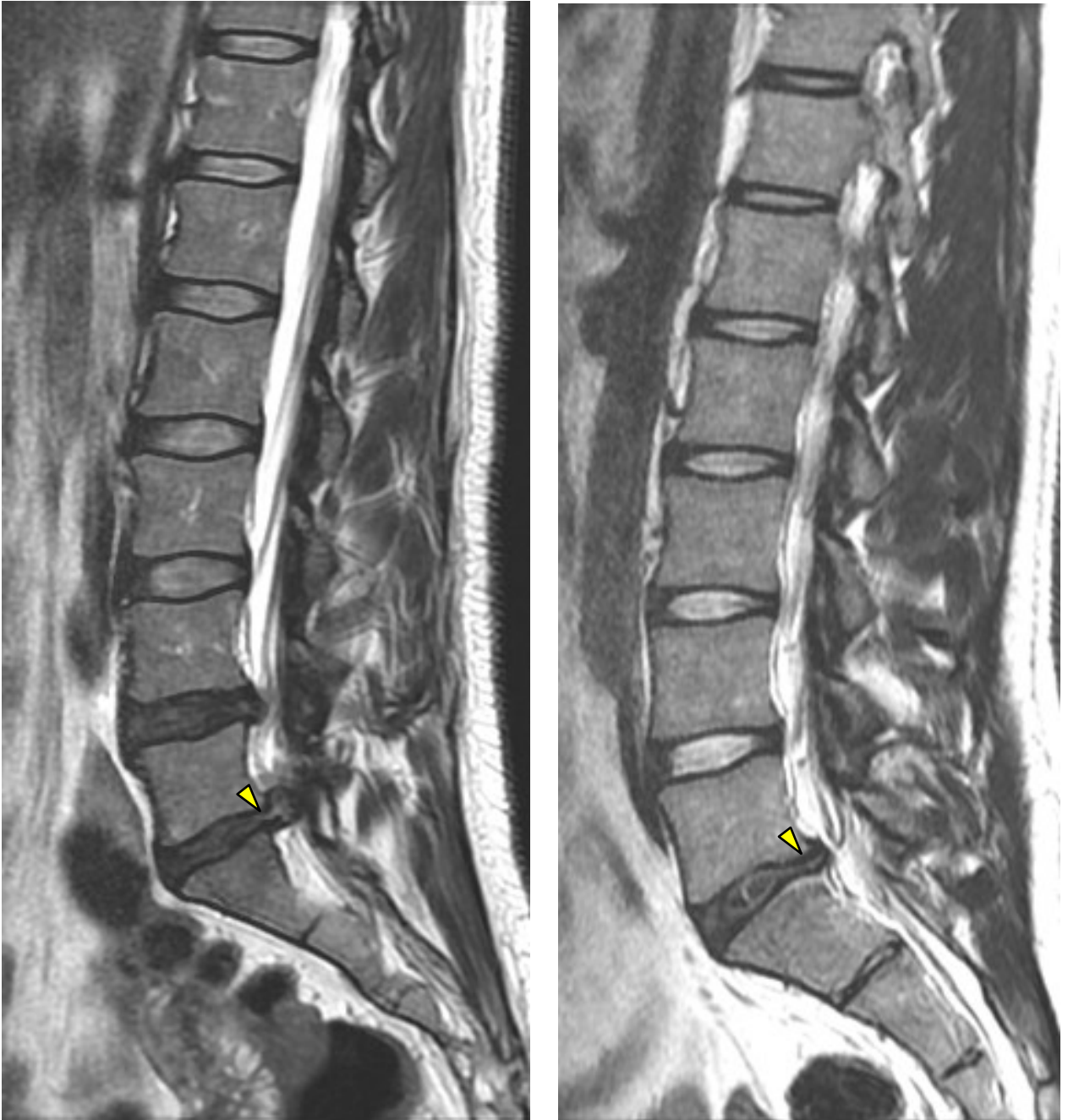


Figure 6:1. Radial disc tears.

Annular Tears



Figures 6:2 and 6:3. Radial disc tears are denoted by yellow arrows in T2W sagittal images.

Radial Tears

These two T2 sagittal images demonstrate radial tears of the annulus of the disc between L5 and the sacrum .

Transverse Tears

Transverse tears have also been called rim lesions. Transverse tears are horizontal lesions that may involve the disc tearing away from the endplate. This lesion may involve disruption of Sharpey's fibers (the matrix of connective tissue that binds the disc to the vertebral endplates) and the disc. Transverse tears appear to have a causal effect in degenerative disc disease and the formation of osteophytic spurring. They are typically small and limited to the joining of the annular attachments to the apophyseal ring—the rim of the vertebra, hence the term *rim lesion*.

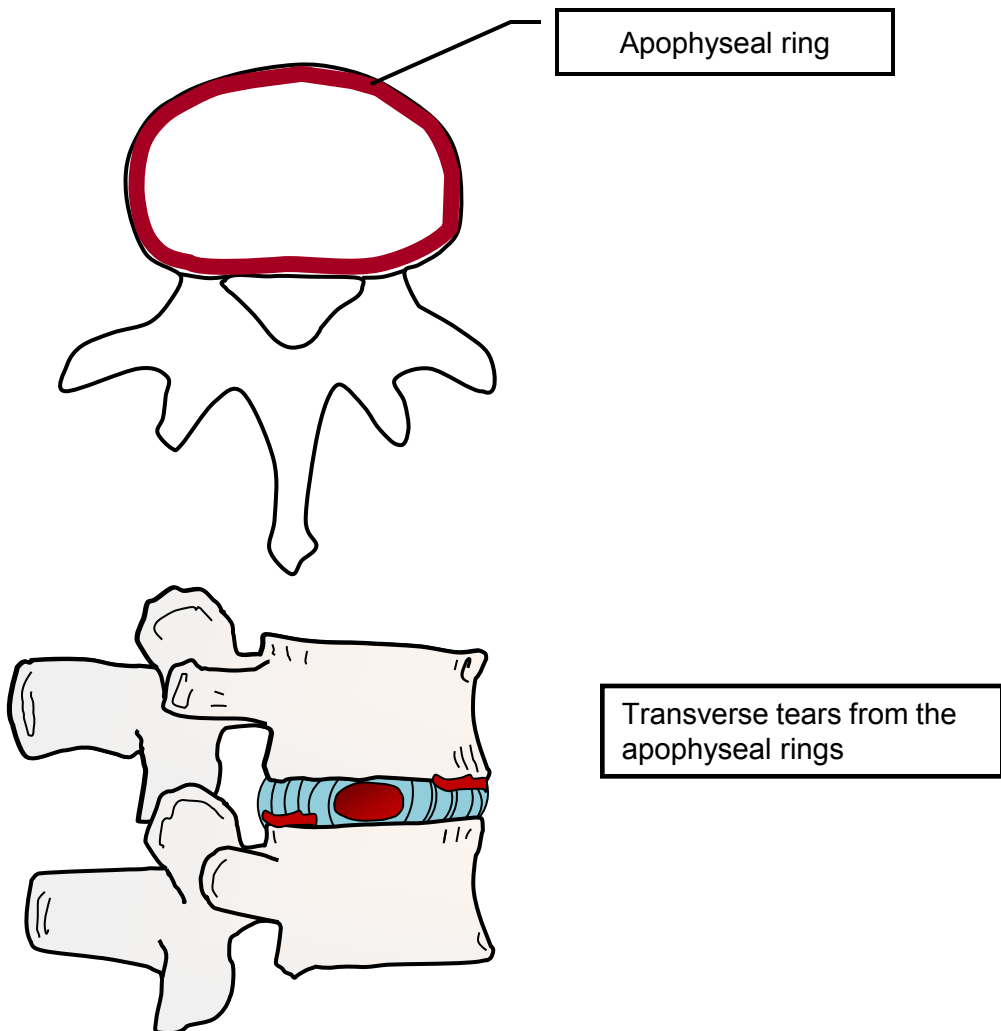
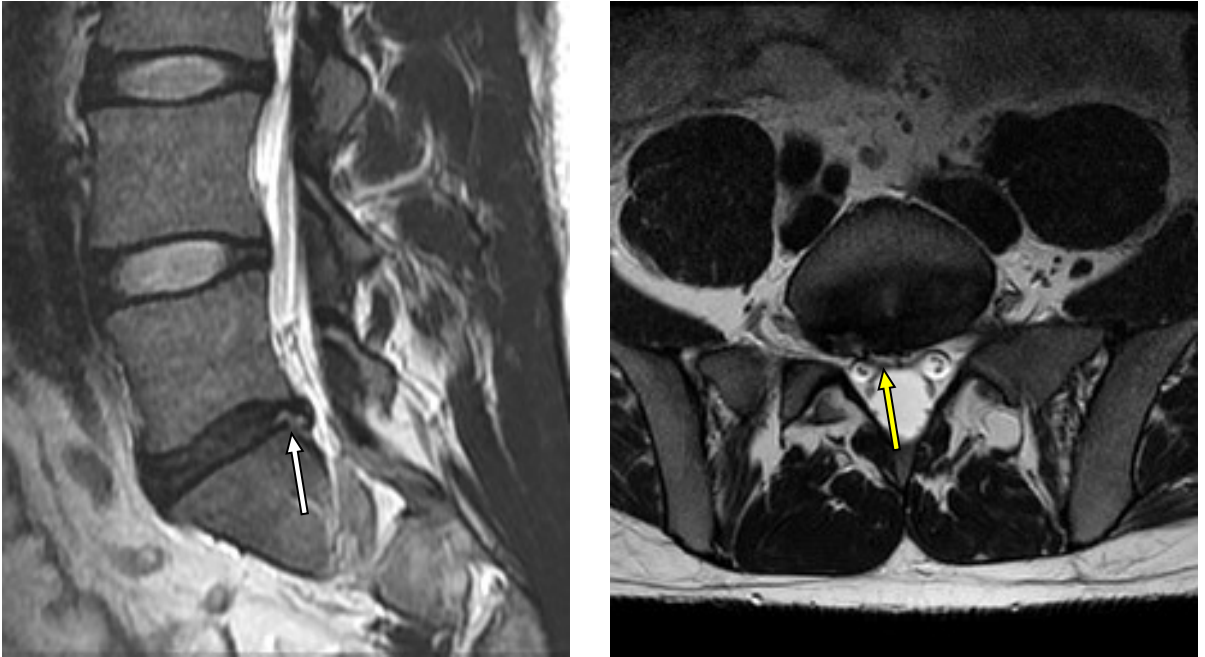


Figure 6:4. Transverse disc tears.

Transverse Tears



Figures 6:5 and 6:6. T2WI of an L5-S1 posterior transverse tear.

The two images above show a transverse annular tear from the superior endplate at the posterior margin of the sacrum. The T2 weighted images above are from the same patient. Below is an image from a different patient with a small tearing of the annulus fibers from the superior apophyseal ring of the sacrum. Annular tears are well demonstrated in T2 images and appear as high-intensity zones, thus appearing white in T2 weighted images.



Figure 6:7. Transverse disc tear.

Concentric Tears

Concentric tears are a separation of the concentric annular bands that surround the nucleus. Normally the outer third of the annulus is affected by concentric tears. Incidentally, it is the outer third of the annular fibers that are the most richly innervated and vulnerable to nociception.

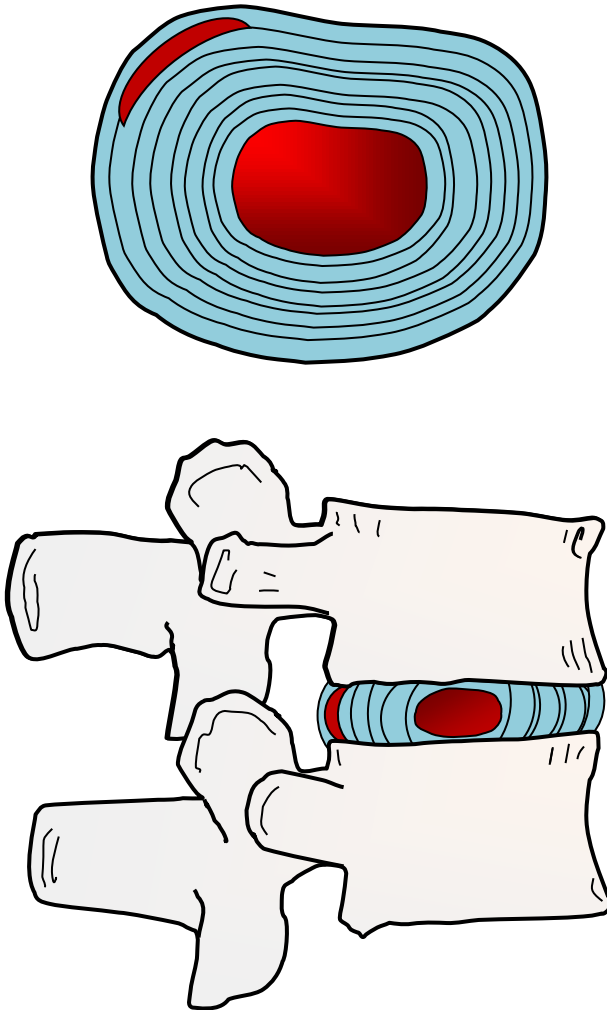


Figure 6:8. Concentric disc tear. Concentric tears separate bands of the annular rings of cartilage. They are characterized by high intensity zones (white appearance) on T2 weighted images. Most concentric tears occur in the outer portion of the disc.

Concentric Tears

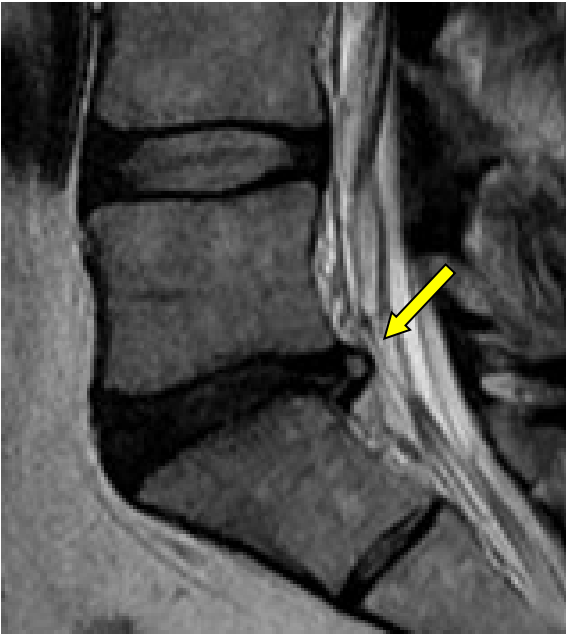


Figure 6:9. Concentric disc tear in a T2W sagittal image.

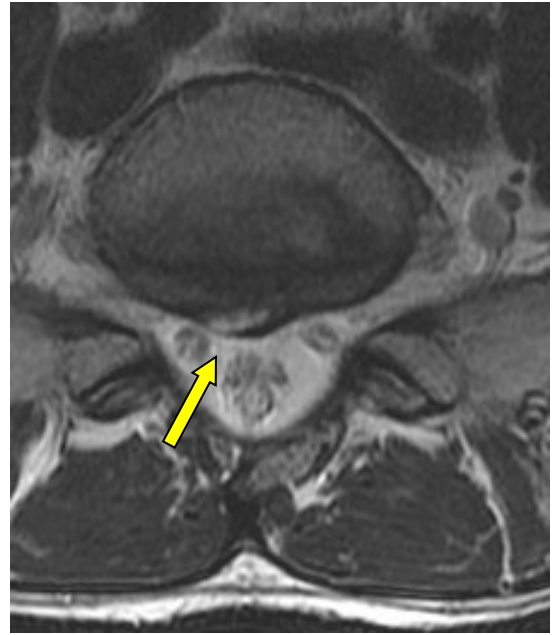


Figure 6:10. Concentric disc tear in a T2W axial image.

The T2W images above are from the same patient and show a transverse concentric tear involving the posterior portion of the L5-S1 disc. Below is an image from a different patient with a lateral concentric tear. Most concentric tears occur in the outer rings of the annulus.

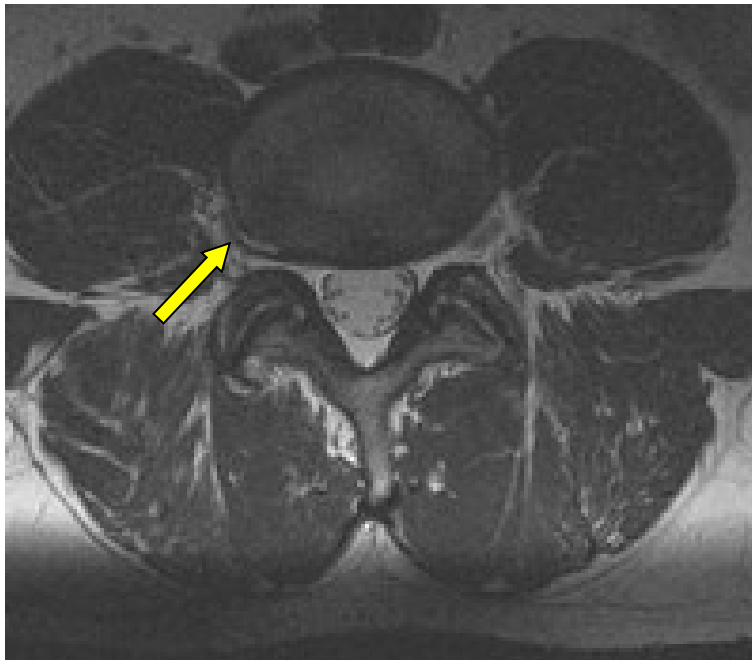


Figure 6:11. Posterior lateral concentric disc tear in a T2W axial image.

Suggested Reading

Fardon DF, Milette PC. Nomenclature and classification of lumbar disc pathology: recommendations of the combined task forces of the north American spine society, American society of spine radiology, and American society of neuroradiology. Spine, Volume 26(5).March 1, 2001.E93-E113.

<http://www.rsna.org/radlex/committee/ASSRDiscNomenclature.pdf>

Cramer G, Darby S (2013). Basic and clinical anatomy of the spine, spinal cord, and ANS (third edition). Elsevier Mosby.

Marchiori D (2013). Clinical imaging: with skeletal, chest and abdomen pattern differentials(third edition). Mosby.

Schmorl G, Junghans H, "The human spine in health & disease". New York: Grune & Stratton, 1971.

Bogduk N. (2012). Clinical and radiological anatomy of the lumbar spine. Churchill Livingstone.

Gallery of Lumbar Disc Derangements



Gallery of Lumbar Disc Derangements

This chapter is composed of a gallery of various lumbar disc derangements and will help unite the information provided in the last six chapters. As you view this pictorial essay take a moment to consider the components of each disc herniation: the vertebral level, the anatomical zone, and the type of derangement (tear, extrusion, protrusion, bulge, intravertebral herniation, and so forth). In addition to identifying the nomenclature and classification of the disc lesions, take time to familiarize yourself with the other structures in each image. Of particular interest to clinicians is the disc injury's relationship to the cord, the cauda equina, thecal sac, and nerve roots. Moreover, consider the impact of disc derangement on facets, muscles, ligaments, endplates, vertebral bodies, the canal space, epidural venous plexus, sacroiliac joints, and other anatomical structures. A disc herniation may be associated with facet effusion, multifidus atrophy, bony edema of the vertebral bodies, facetal imbrication, ligamentum flavum changes, posterior longitudinal ligament disruption, and other anatomical and functional failures.

Additionally, take time to consider the potential clinical consequences of particular disc injuries: pain distribution, orthopedic-neurologic signs, and effects on other anatomical structures. By viewing a variety of different derangements, you will begin to gain familiarity of this topic and be more competent at discerning the nuances of disc disease.

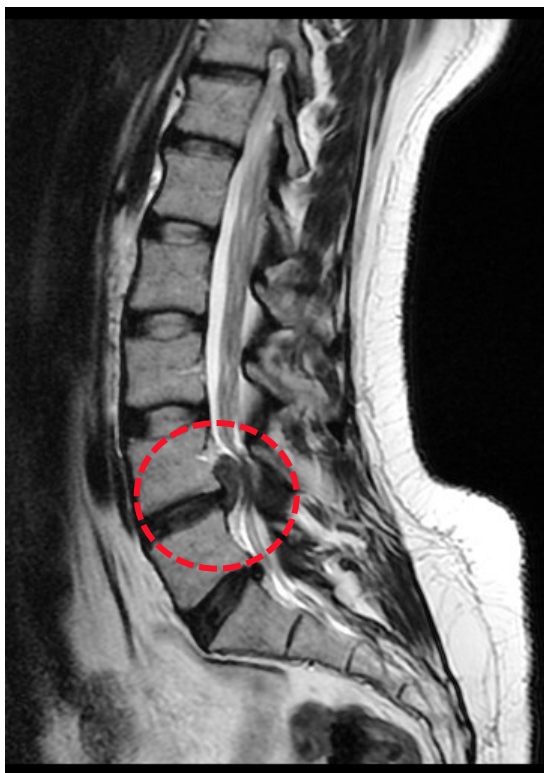


Figure 7:1. L4-L5 disc herniation with cephalad migration along the body of L4.

Comparing T1 and T2 Weighted Images of Disc Derangements

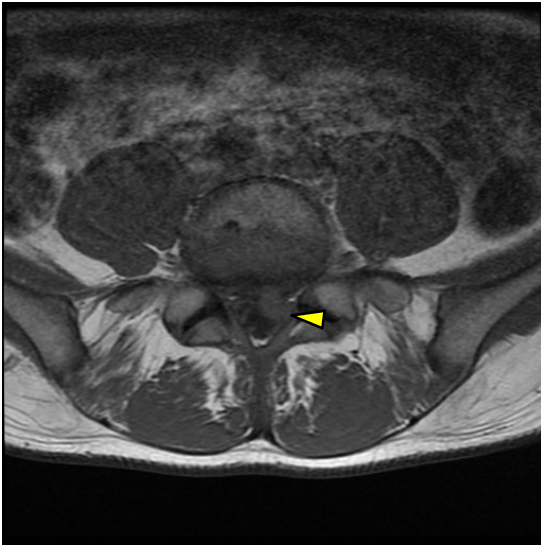


Figure 7:2. T1 axial at L4-5.

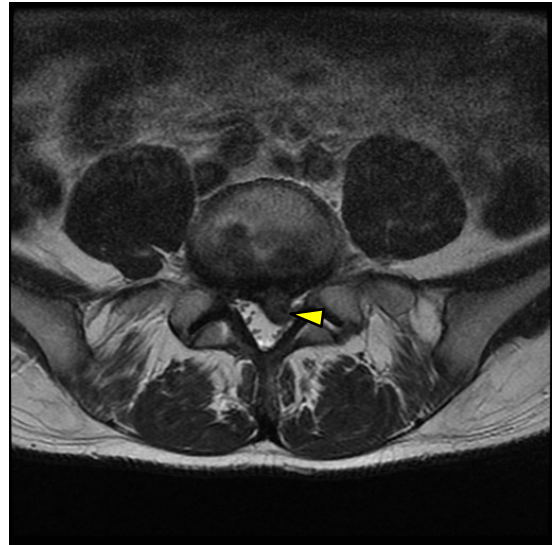


Figure 7:3. T2 axial at L4-5, the same slice as figure 7:2.



Figure 7:4. T1 sagittal of a herniation at L4-5.

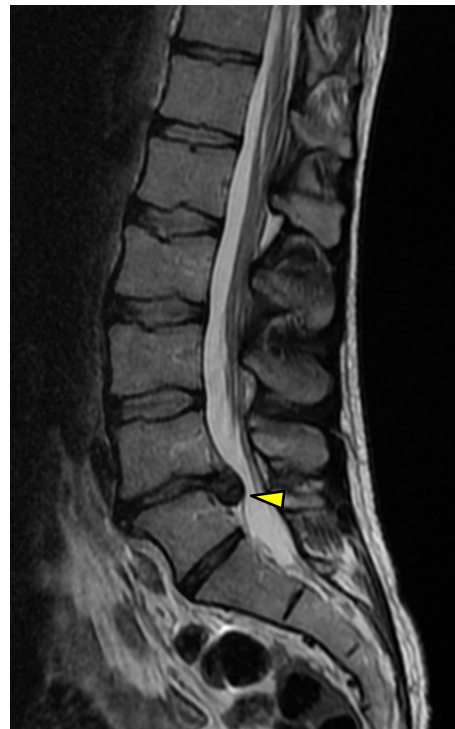


Figure 7:5. T2 sagittal of the same herniation at L4-5 in figure 7.4.

T1 images have good anatomical detail, but contrast is reduced between the disc and the cerebral spinal fluid in the thecal sac, making it more difficult to identify a disc herniation. Because of this, it is easier to view a herniation on T2 images. Most of the disc herniations in this chapter will be presented in T2 weighted format.

Caudal Sequestered Extrusion into the Sacral Canal

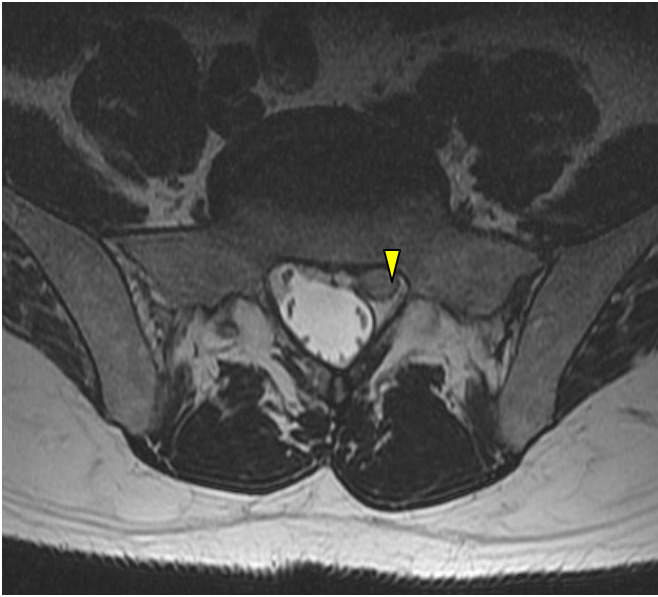


Figure 7:6. This T2 weighted axial image reveals a round circumscribed herniation (sequestered disc fragment) descending into the sacral canal and displacing the thecal sac and the S1 nerve root.



Figure 7:7. This T2 weighted sagittal image shows a light-colored sequestered disc fragment descending into the sacral canal along the body of S1.

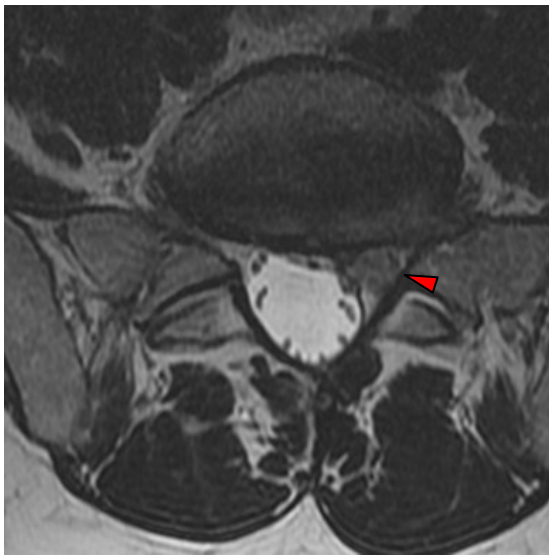


Figure 7:8. This axial image is a slice that is cephalad to the slice in figure 7:6. The sequestered fragment is clearly seen.



Figure 7:9. A sagittal T1 weighted image of a caudal herniation (green arrow) of the L5-S1 disc.

These four images show a large L5-S1 sequestered extrusion that extends caudally into the central canal of the sacrum following the left S1 nerve root and displacing the thecal sac. The light color of this extrusion is indicative of high water content.

Foraminal Herniation

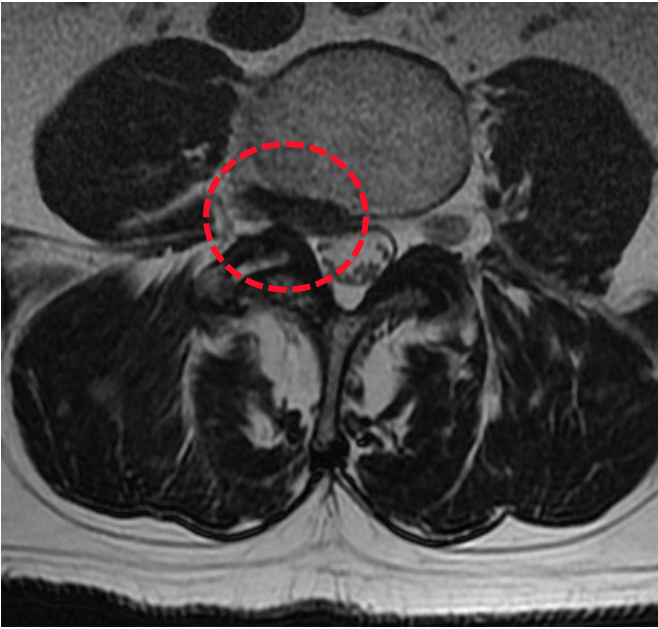


Figure 7:10. This T2 weighted axial image reveals a right foraminal herniation of the L4-5 disc.

These images reveal a foraminal herniation at L4-L5 with compression of the right L4 nerve root in a 69 year-old man. Also of note in the axial image is increased intensity within the right zygapophyseal joint and atrophy of the multifidus muscles. This focal herniation is an extrusion and extends cephalad in the IVF, contacting and compressing the exiting nerve root.



Figure 7:11. This sagittal T2 weighted image reveals a right foraminal herniation of the L4-5 disc. Note the L4-5 disc extending upward into the IVF and compressing the exiting L4 nerve root.

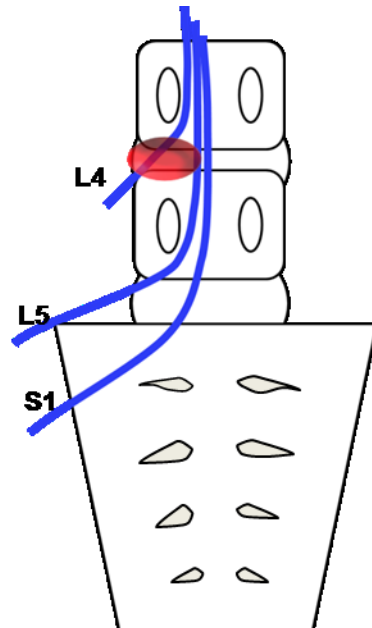


Figure 7:12. Schematic of a right-sided L4-5 foraminal herniation.

Foraminal Herniation with Zygapophyseal Effusion

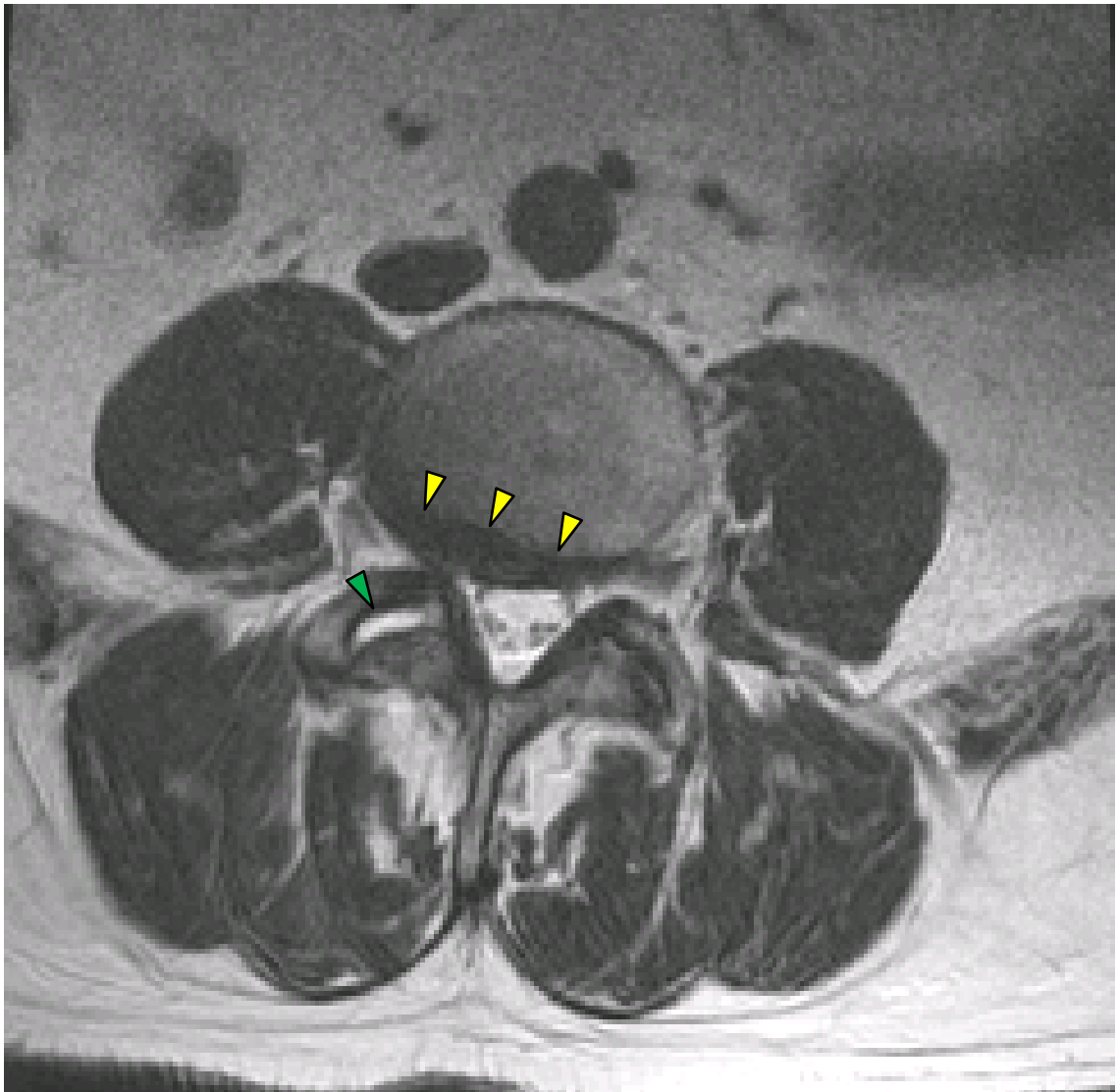


Figure 7:13. This axial image displays a broad-based disc protrusion (yellow arrows) that crosses the right IVF. Note the effusion within the right zygapophyseal joint (green arrow).

Caudal Extrusion of the L4-5 Disc



Figure 7:14. L4-L5 inferior extrusion and possible sequestration.



Figure 7:15. An axial view of the extrusion along the body of L5. Note the thecal sac displacement.

Regression of Disc Herniation

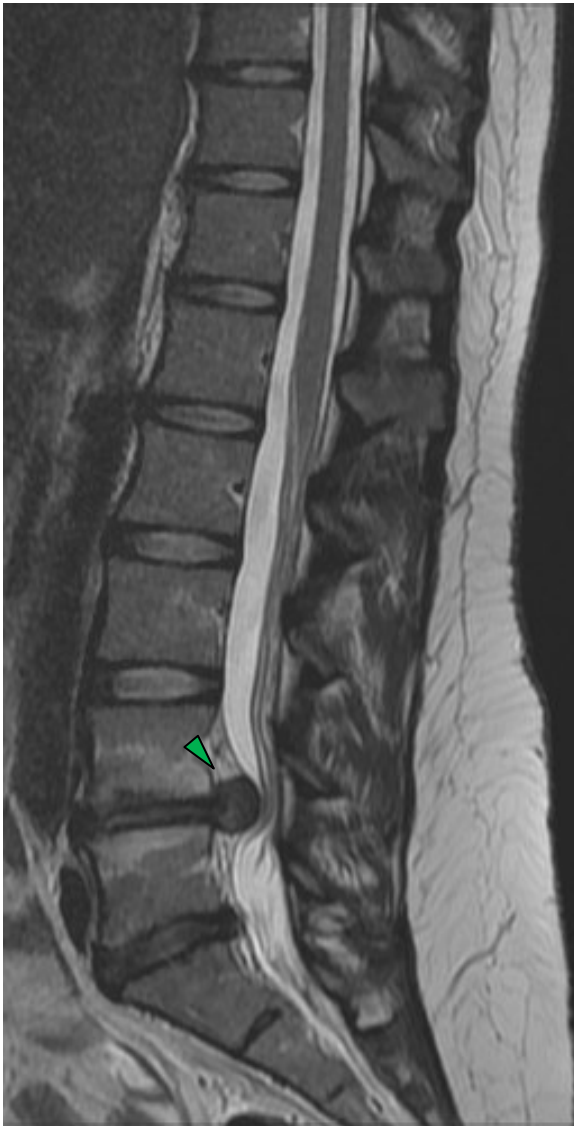


Figure 7:16. Large extrusion of the L4-5 disc.

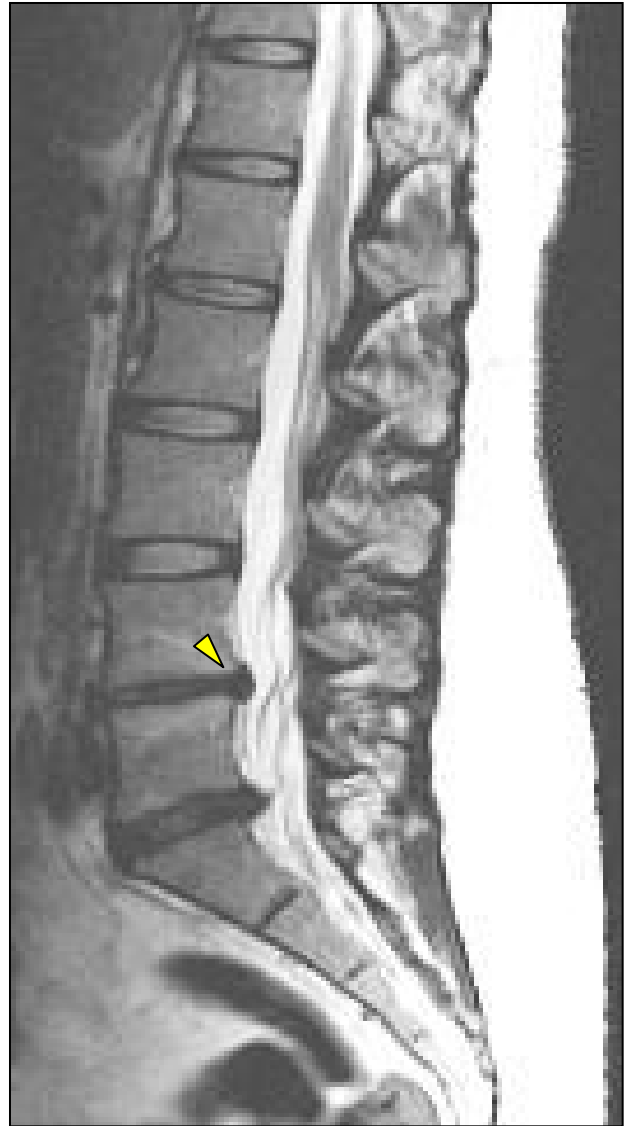


Figure 7:17. Follow-up MRI of the same patient six months later. Note the regression of the L4-5 disc herniation.

These images show the regression of a large extrusion of the L4-5 disc over a six month period of conservative care. Figure 7:16 displays a huge herniation, but a second MRI taken 6 months later, figure 7:17, reveals a significant reduction in the mass of the herniation. Note the bony edema of the adjoining vertebral bodies. Endplate disruption and bony edema of the vertebral bodies will be discussed more fully in Chapter 12. Larger herniations are more apt to regress than smaller herniations. Disc bulges tend not to regress in size. Axial images of this patient are presented on the following page.

Regression of a Disc Herniation (continued)



Figure 7:18. Large extrusion of the L4-5 disc. Note the extent of thecal sac effacement and displacement of the nerve rootlets.



Figure 7:19. Follow-up MRI of the same patient six months later. Notice the regression of the L4-5 disc herniation.

From an axial perspective figure 7:18 reveals the extent this disc extrusion occupied the central canal, subarticular zone, and foraminal zone. Figure 7:19, taken six months later, clearly demonstrates a profound reduction in the size of the herniation.

Extrusion and Post-Surgical Re-Herniation and Regression

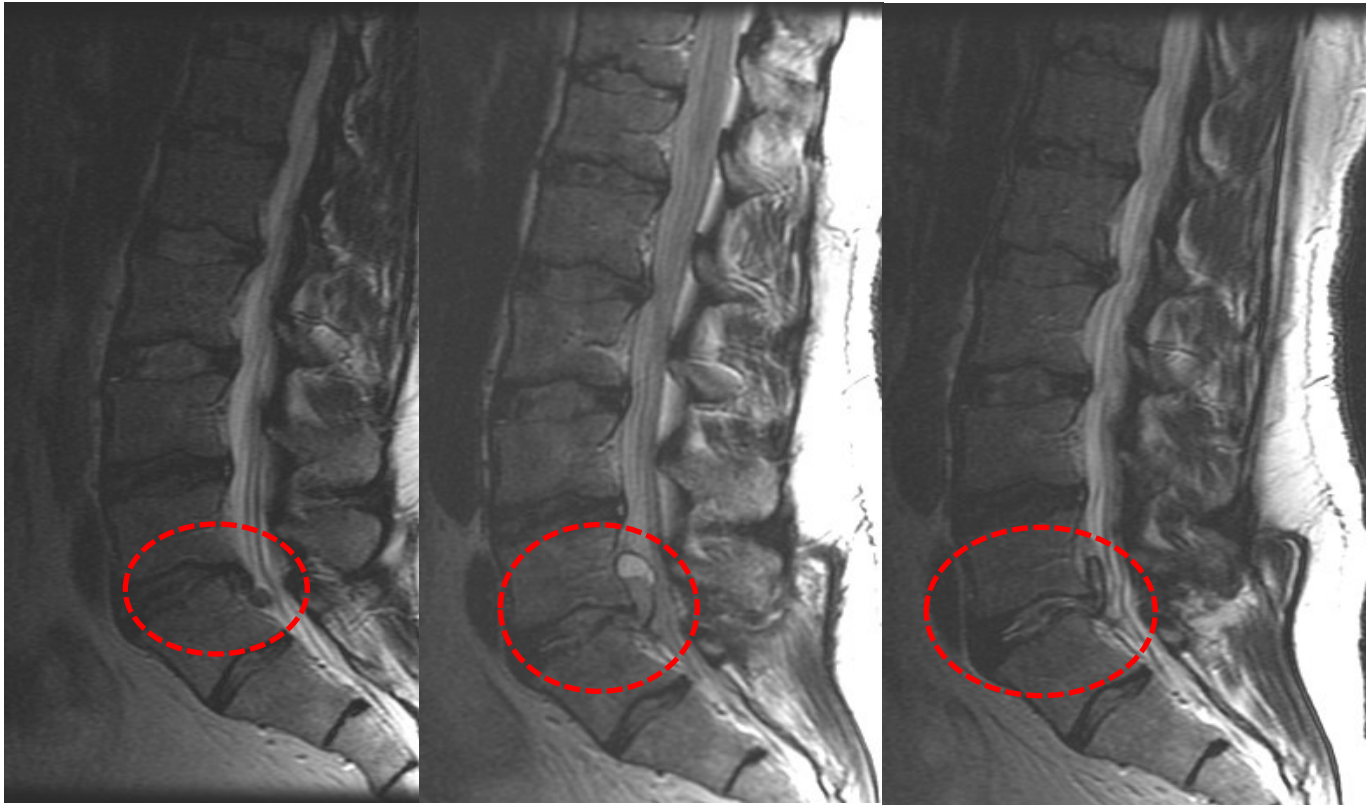


Figure 7:20. Pre-surgery.

Figure 7:21. Re-herniation two months post-discectomy.

Figure 7:22. Regression of the disc six months after the image in figure 7:21 was taken.

This sequence of images show a sequestered extrusion of the L5-S1 disc extending inferiorly into the central canal of the sacrum (figure 7:20). This patient was treated surgically with a microdiscectomy. Two months after surgery, he re-herniated the L5-S1 disc, this time with superior migration of the extruded disc along the posterior body of L5 (figure 7:21). He was treated conservatively with chiropractic care, exercise, and modified work postures. A follow-up MRI six months following the second herniation revealed what appears to be a “deflated” herniation (figure 7:22). The herniation still extends superiorly along L5, but the mass of the herniation is significantly reduced.

Focal Central Herniation



Figure 7:23. T2W sagittal image revealing a small extrusion of L5-S1.

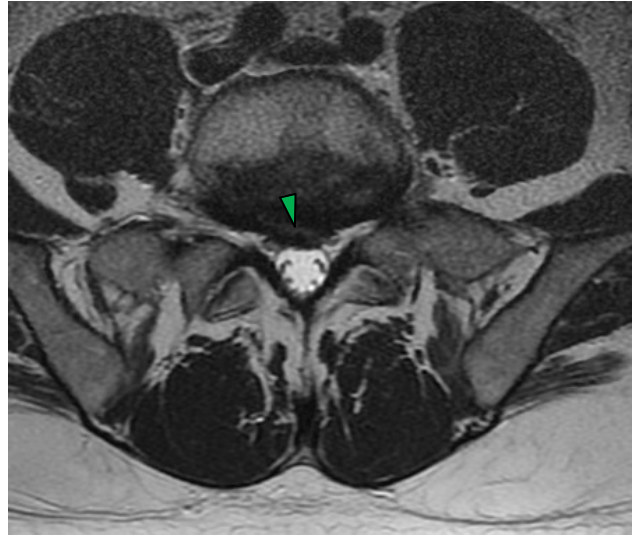


Figure 7:24. This T2W axial image of the same patient reveals a focal herniation arising from a broad-based herniation. Note the herniation is between the S1 nerve roots.

These images reveal a focal extrusion on top of a broad-based protrusion of the L5-S1 disc. The focal extrusion between the S1 nerve roots contacts both descending S1 nerve roots and effaces the thecal sac.

Herniations with Annular Tears



Figure 7:25. This T2 weighted axial image reveals a posterior concentric annular tear of the L4-5 disc.



Figure 7:26. This T2 weighted axial image reveals broad-based herniation with a posterior paracentral concentric annular tear.

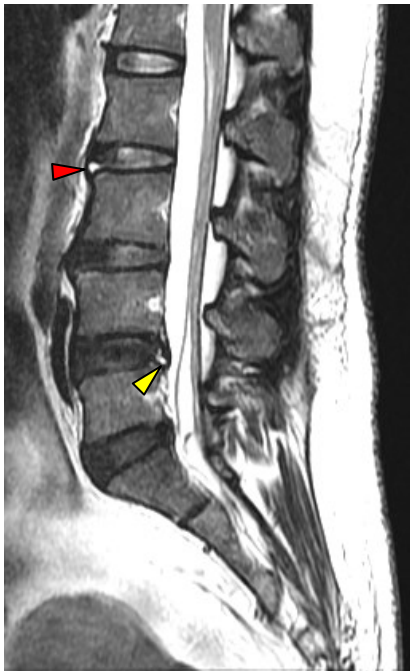


Figure 7:27. This T2 weighted sagittal image reveals a transverse annular tear of the anterior of L2-3 on the superior L3 endplate. There is also a tear along the superior endplate of L4 affecting the posterior portion of that disc.

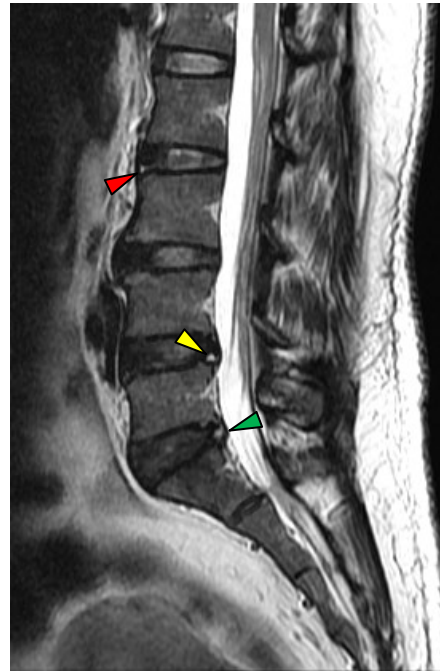


Figure 7:28. This sagittal image displays a posterior transverse tear at the superior endplate of L4 (yellow arrow), a concentric tear of the posterior L5 disc (green arrow), and a small portion of a transverse tear at the superior L3 endplate (red arrow).

Paracentral Herniation



Figure 7:29. T2W sagittal image revealing desiccation of the L4-5 and L5-S1 disc and an extrusion of the L5-S1 disc.

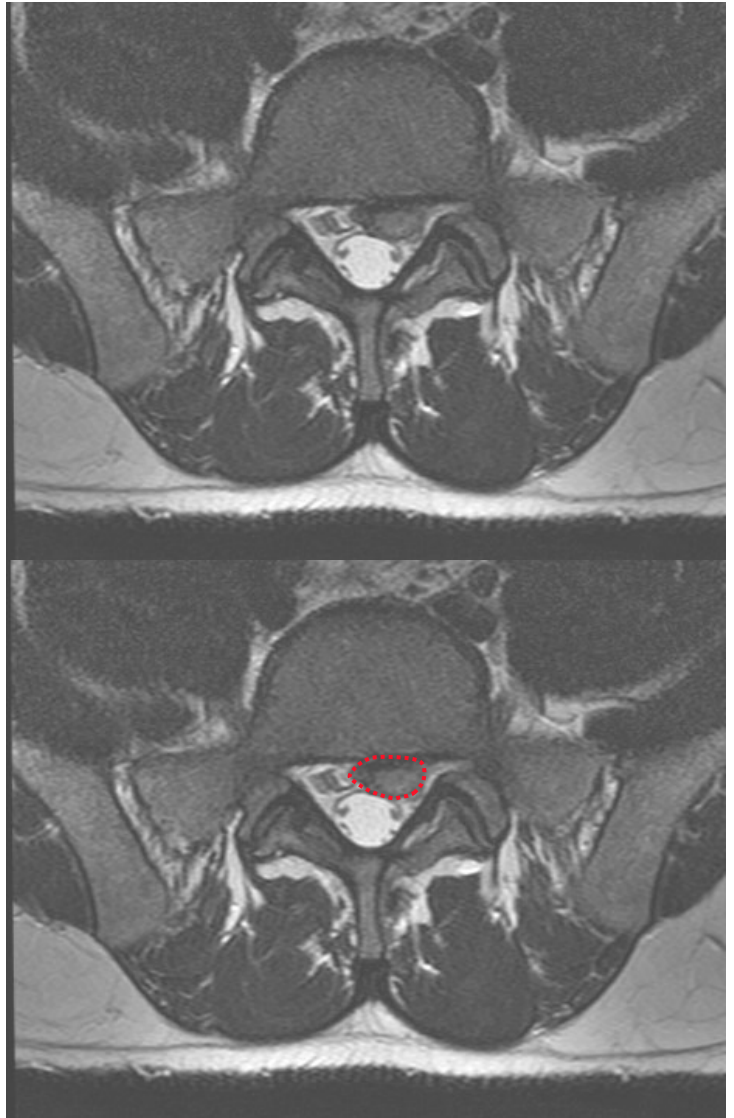


Figure 7:30. T2W axial image showing a left paracentral extrusion of the L5-S1 disc.

These T2 weighted images reveal an L5-S1 paracentral disc extrusion displacing and compressing the left S1 nerve root. Notice the levels of brightness and darkness in these images. The extruded portion of the disc is light-colored, which on a T2WI indicates a high degree of water content. In contrast, the L4-L5 disc is dark in color indicating reduced water content and desiccation.

Paracentral Extrusion

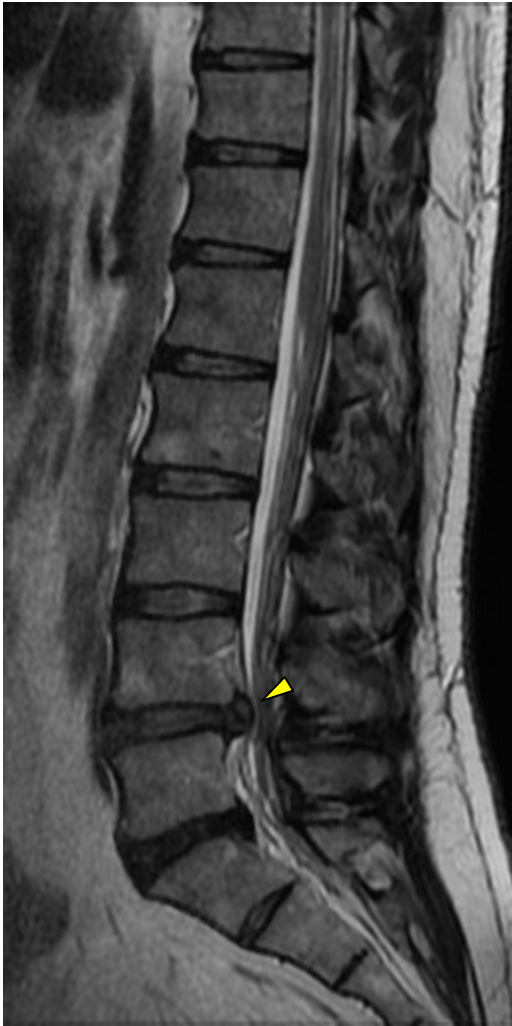


Figure 7:31. Sagittal T2 weighted image of an L4-5 extrusion.

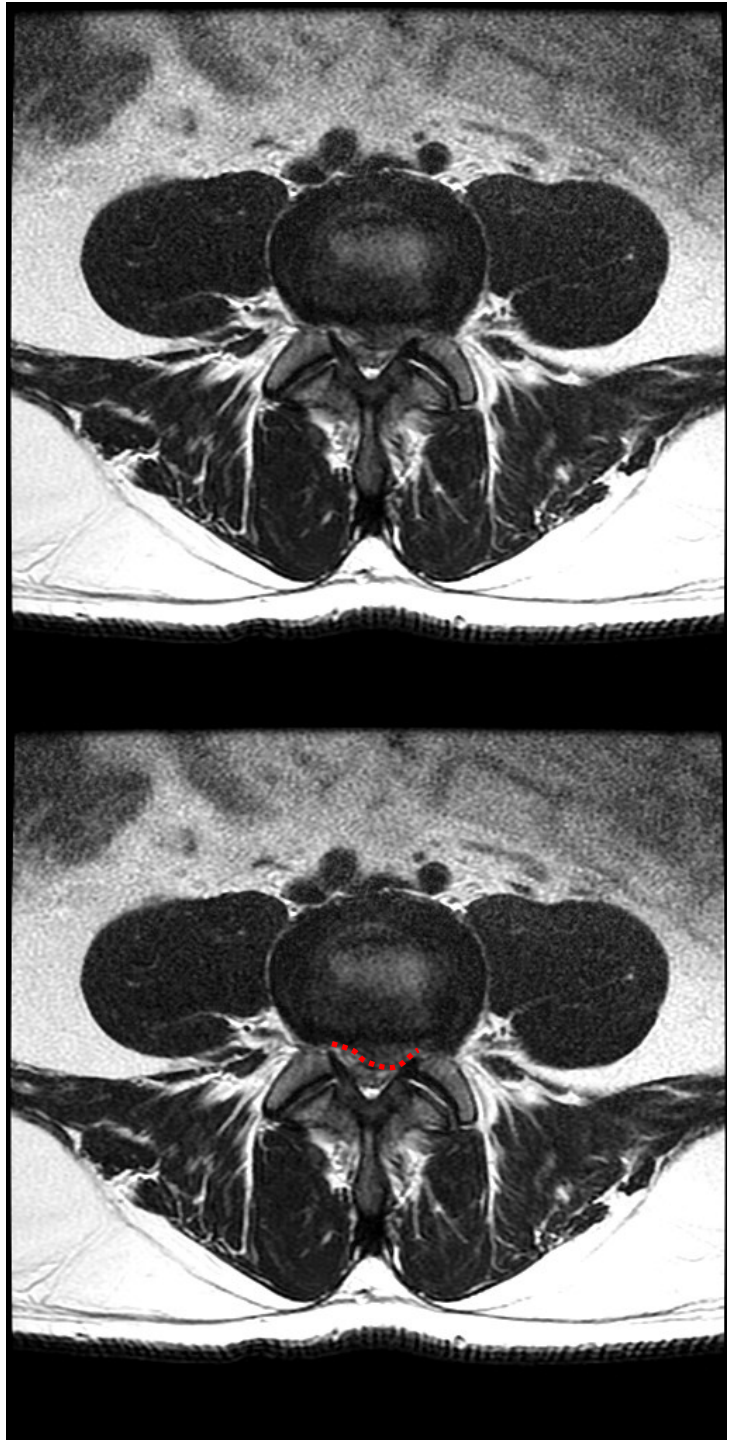


Figure 7:32. Axial T2W images of a paracentral L4-5 disc extrusion.

Broad-based Protrusion

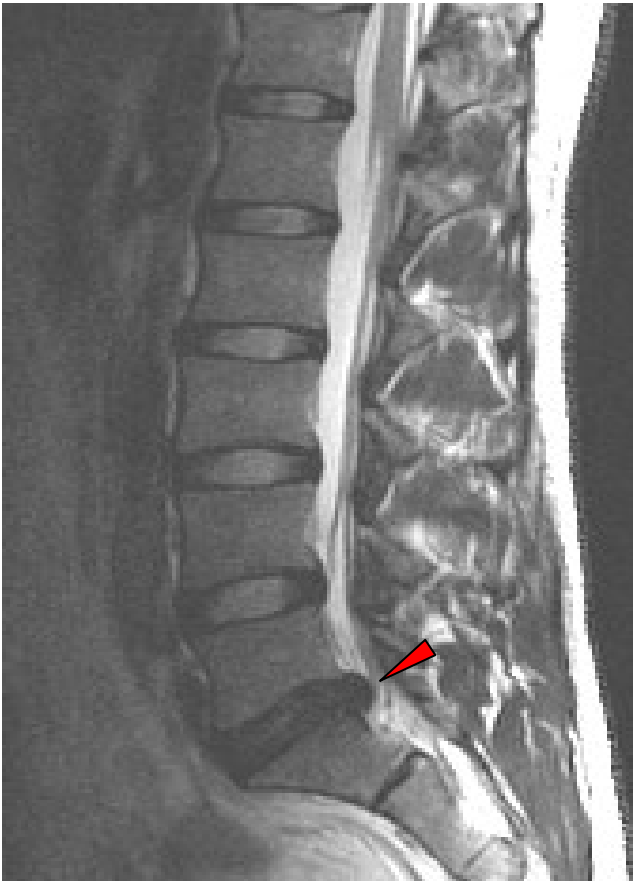


Figure 7:33. Sagittal T2 weighted image of an L4-5 protrusion.

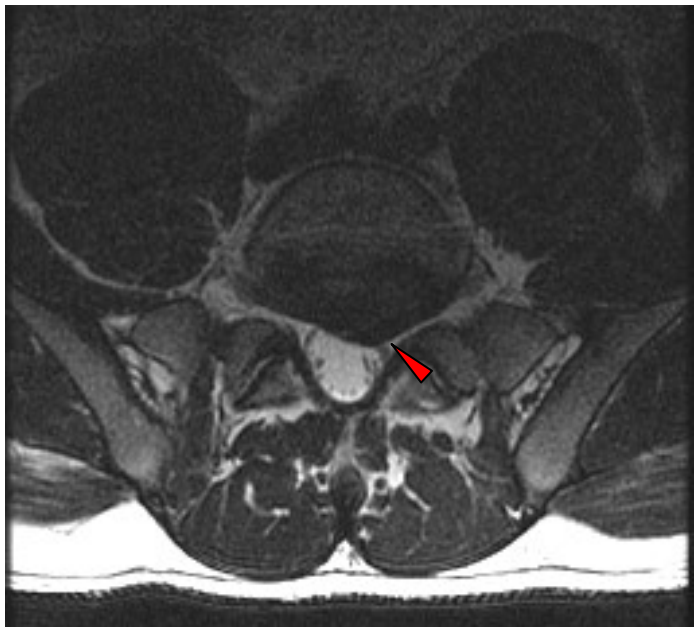


Figure 7:34. Sagittal T2 weighted image of an L4-5 extrusion.

Here we see a broad-based protrusion of the L5-S1 disc that distorts the left anterior portion of the thecal sac and narrows both IVFs. The left IVF is particularly compromised.

Paracentral Extrinsic

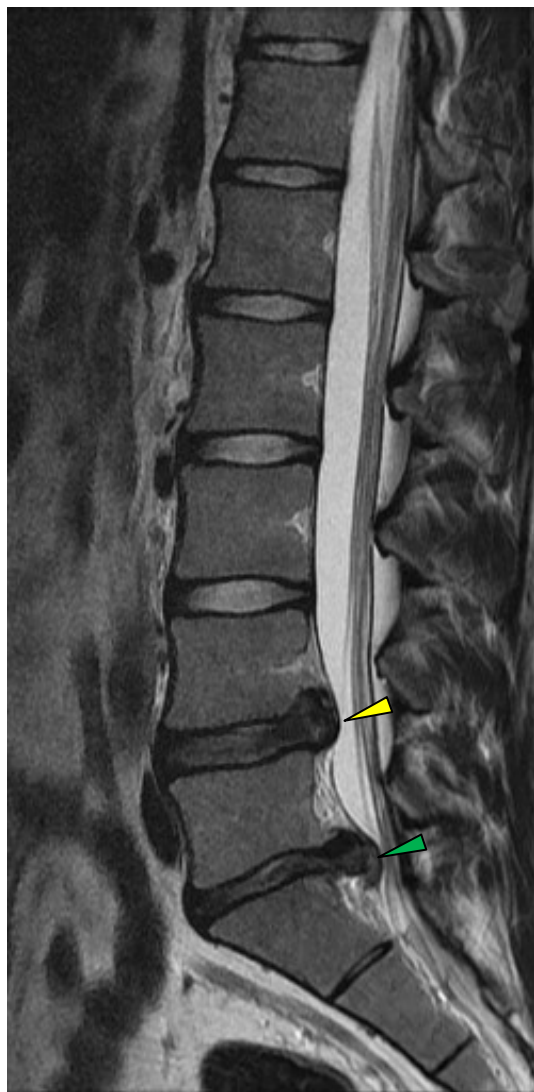


Figure 7:35. Sagittal T2 image revealing a relatively small L4-5 extrusion (yellow arrow) and a larger L5-S1 herniation (green arrow). The L5-S1 extrusion has a “hook” extending caudally from the main herniation.

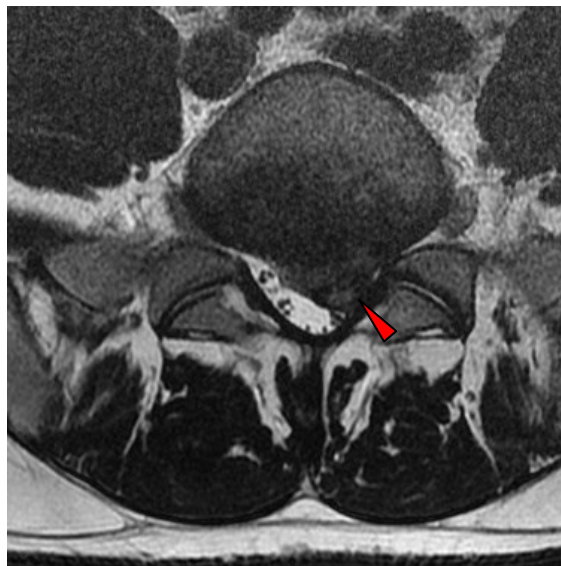


Figure 7:36. This axial represents the slice showing with the greatest herniation mass at L5-S1.

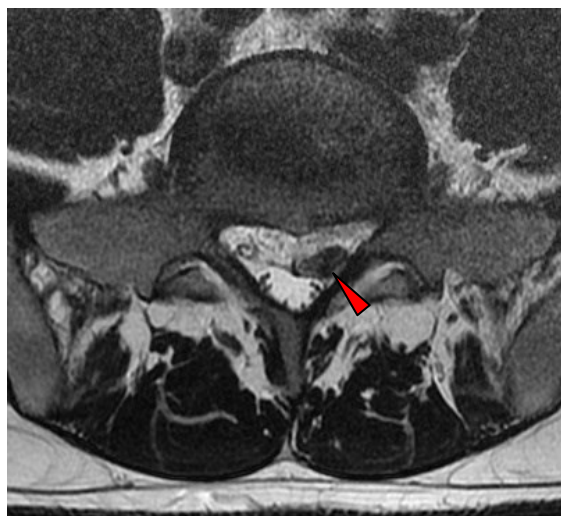


Figure 7:37. This slice shows the caudally migrated portion of the L5-S1 disc seen in figure 7:35.

These three images show a large L5-S1 herniation (a focal herniation on top of a broad-based herniation) with a portion of the disc descending caudally. This portion of the L5-S1 disc may actually be a sequestered fragment that has not displaced. In figure 7:36 the thecal sac effacement and nerve compression is worthy of note. In figure 7:37 the inferior portion of the L5-S1 disc is clearly visualized displacing the left S1 nerve. Also of note is the disc extrusion and desiccation at L4-5 seen in the T2 sagittal image.

Two Level Herniation

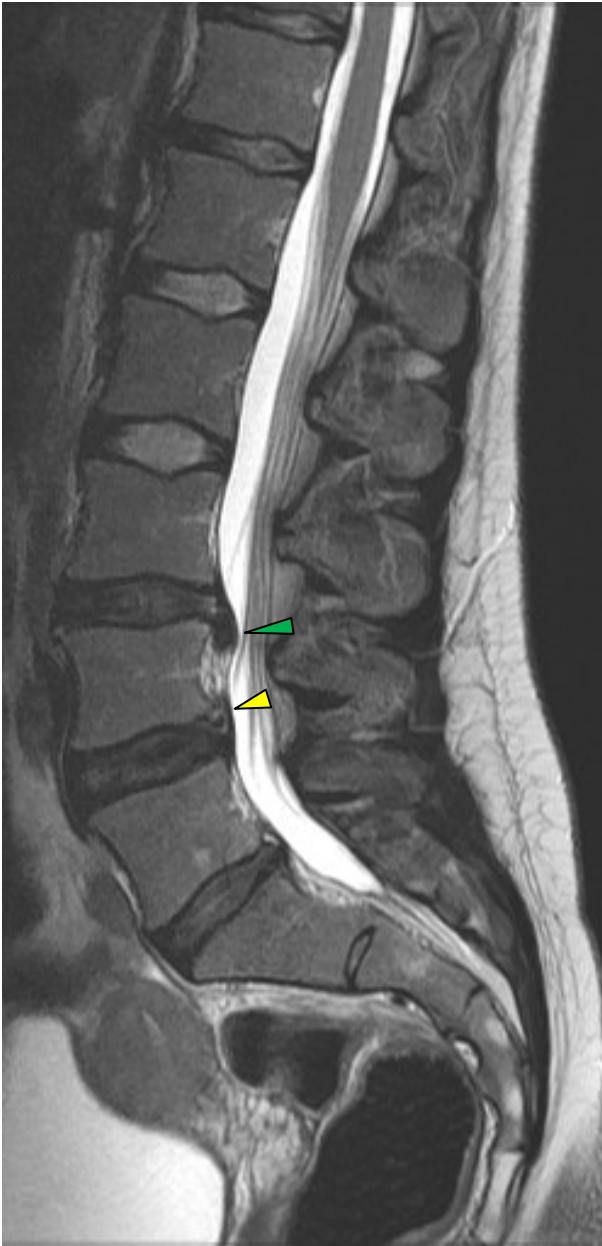


Figure 7:38. Sagittal T2 image of L3-4 (green arrow) and L4-5 (yellow arrow) extrusions.

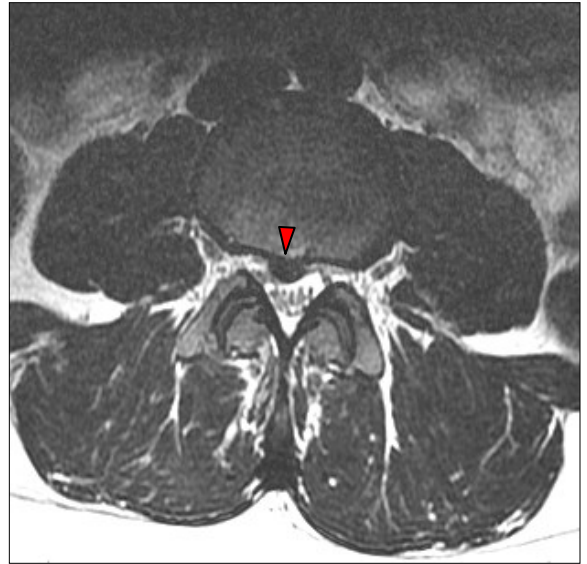


Figure 7:39. Focal paracentral extrusion at L3-4 displacing the thecal sac.



Figure 7:40. Broad-based herniation with a strong left foraminal component at L4-5.

These three images show two herniations migrating toward each other. The L3-4 herniation is seen on the sagittal image (figure 7:38) and axial image (figure 7:39). It extends inferior along the posterior body of L4. The L4-5 herniation is visualized in figure 7:38 and figure 7:40. The L4-5 herniation travels superiorly. Also notable in this series is the concentric annular disc tear affecting the posterior fibers of the L5-S1 disc.

Herniation with Nerve Root Entrapment

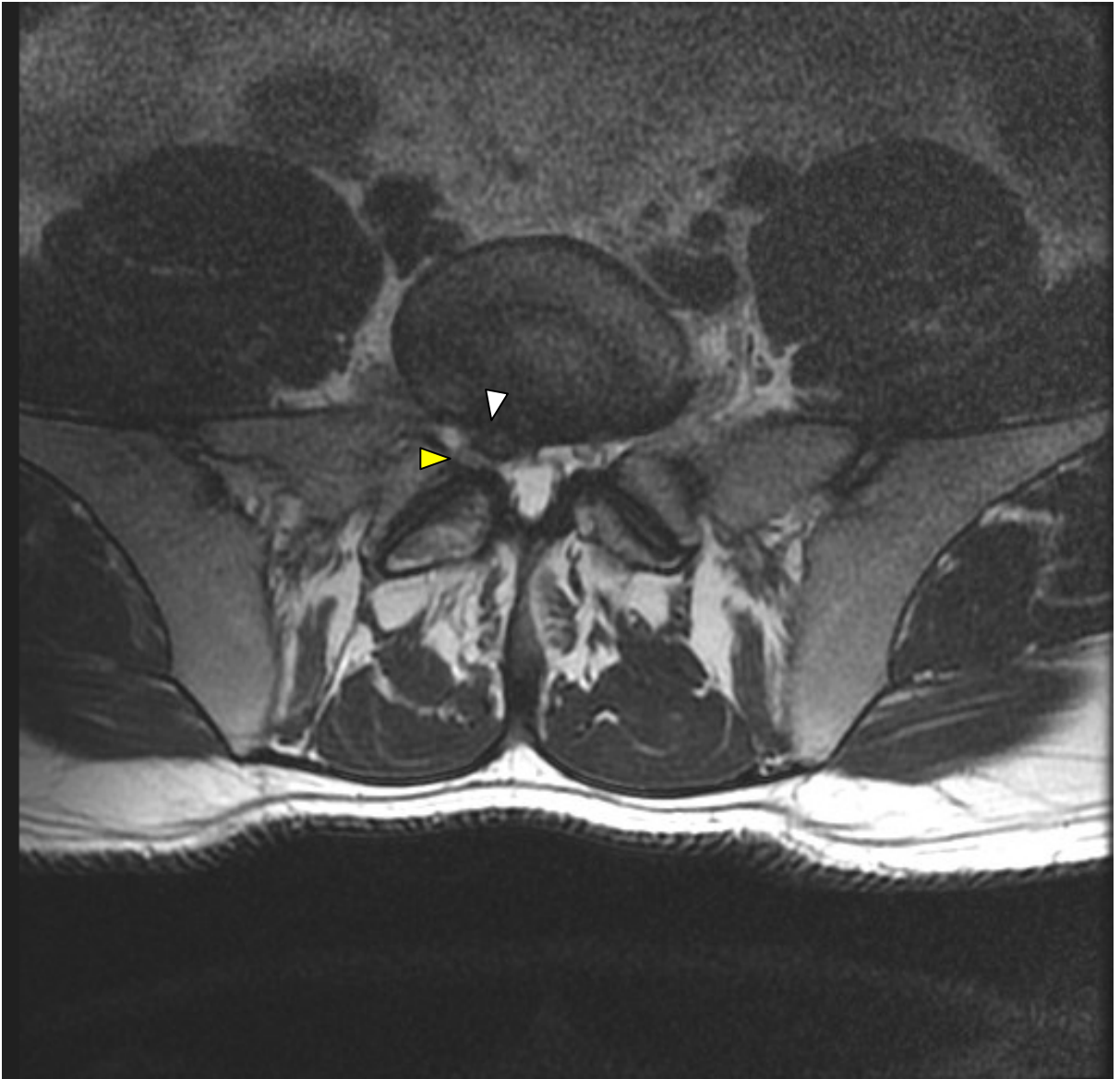


Figure 7:41. This focal foramininal zone herniation of the L5-S1 disc (white arrow) entraps and compresses the S1 nerve root (yellow arrow). Also of note in this T2W axial image is the central canal stenosis and subarticular stenosis. Ligamentum flavum hypertrophy and facet hypertrophy contribute to the stenosis.

Broad-based Extrusion

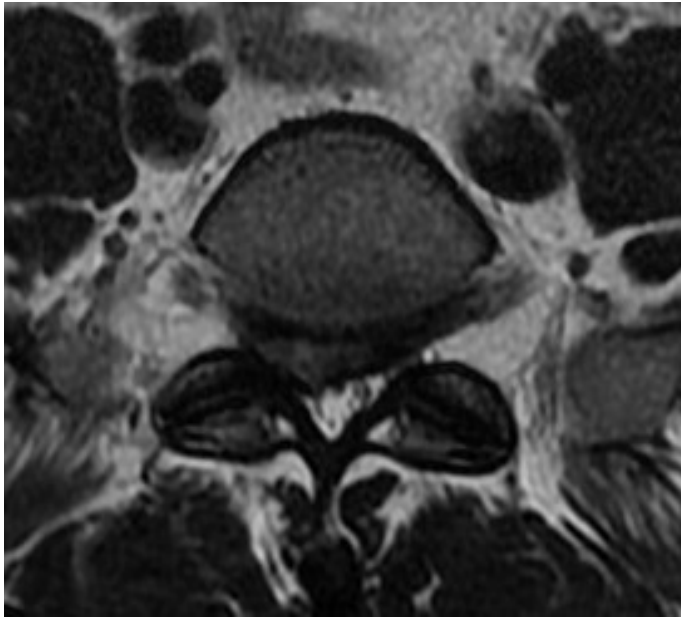


Figure 7:42. Moderate broad-based extrusion of L5-S1 extending across both foramina favoring the right.



Figure 7:43. L5-S1 extrusion and L4-L5 protrusion.



Figure 7:44. Sagittal T2WI of L4-5 and L5-S1 herniations. L5-S1 is an extrusion.

Intravertebral Herniation

Intravertebral herniations occur when the disc breaks through the vertebral endplate of an adjoining vertebra. This schematic shows both an inferior and superior intravertebral herniation. These are commonly called Schmorl's nodes.



Figure 7:45. Sagittal T2 weighted image showing an intravertebral herniation (Schmorl's node) extending superiorly into T12. Note the halo of Modic 2 (see chapter 12) changes around the lesion and affecting the L2 and L3 vertebrae.



Figure 7:46. Sagittal T2 weighted image from the same study showing another intravertebral herniation extending superiorly into L4. Note the bony edema surrounding this bony disruption.

Herniation



Figure 7:47. Sagittal T2WI showing an extrusion and degeneration of the L5-S1 disc.

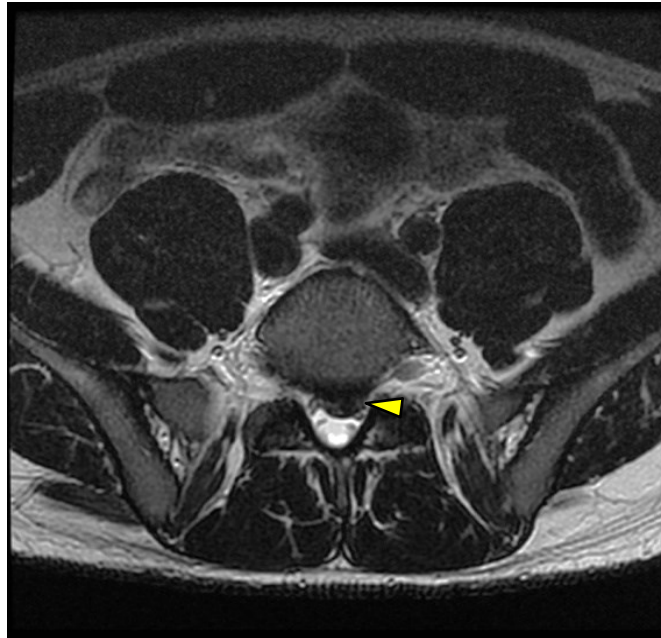


Figure 7:48. Axial T2WI of a left-sided paracentral herniation displacing the S1 nerve root and effacing the thecal sac.

Large Extrusion Projecting Inferiorly



Figure 7:49. This sagittal image shows a huge L4-5 extrusion (probably a sequestered fragment) that projects inferiorly from the L4-5 disc space along the vertebral body of L5.



Figure 7:50. This T2 weighted axial image reveals the large extrusion that occupies a great portion of the central canal posterior to the body of L5.

From the axial image this herniation would be classified as being moderately large. The sagittal view is needed to fully grasp the mass of disc material that herniated from the L4-5 disc and descended along the body of L5. This herniation resulted in a left leg foot drop, which resolved after surgery.

Sequestered Fragment



Figure 7:51. This axial image shows a sequestered fragment from the L5-S1 disc. The sequestered fragment displaces the left S1 nerve root. The left S1 nerve appears inflamed.

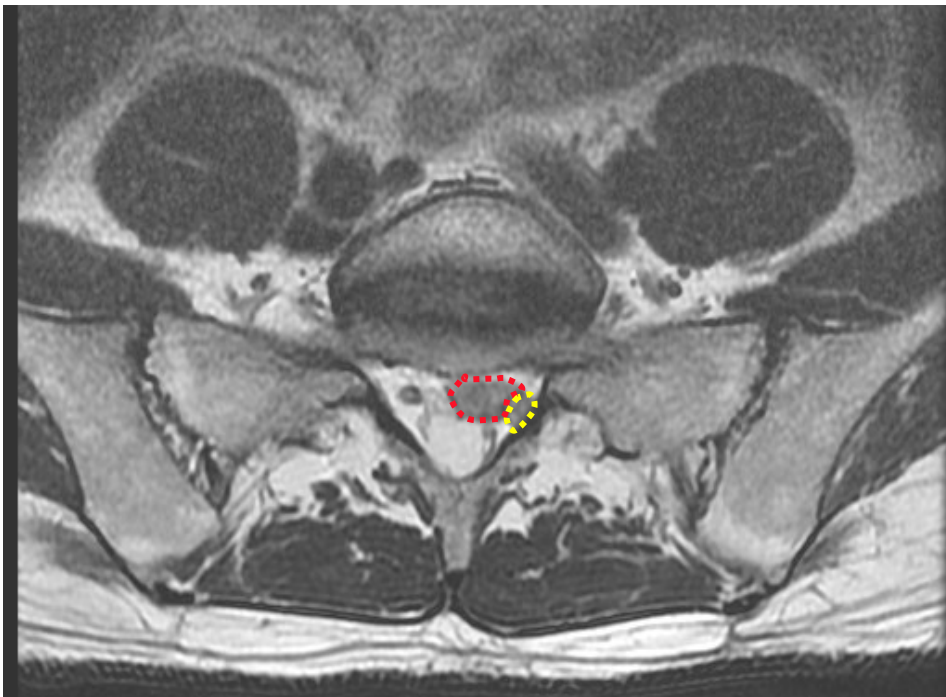


Figure 7:52. This is the same axial slice as is displayed in figure 7:52, but with demarcations. The sequestered fragment is denoted by a red dotted line, and the yellow dotted line denotes the S1 nerve root .

Re-herniation Two Weeks Post Surgery

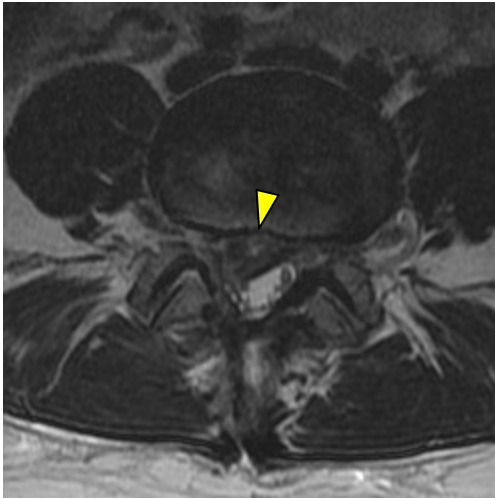


Figure 7:53. This image, taken two weeks after a discectomy, shows a large re-herniation of the L4-5 disc (the same segment and same side that had been operated on).

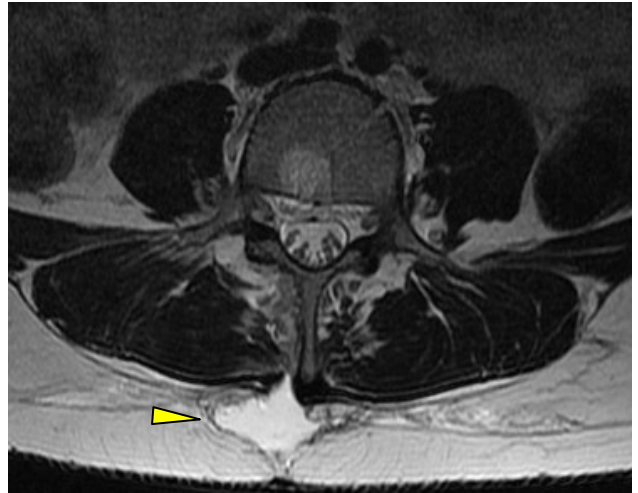


Figure 7:54. In addition to the re-herniation of L4-5, this T2 weighted image shows fluid collecting (bright on T2WI) posterior and to the right of midline.



Figure 7:55. Sagittal T2WI showing the L4-5 re-herniation (yellow arrow) and posterior fluid collection (green arrow).



Figure 7:56. Sagittal T1WI showing the L4-5 re-herniation (yellow arrow) and posterior fluid collection (green arrow).

This series of images taken two weeks following a discectomy reveals a re-herniation of the L4-L5 disc and a pseudomeningocele (see page 335, chapter 24).

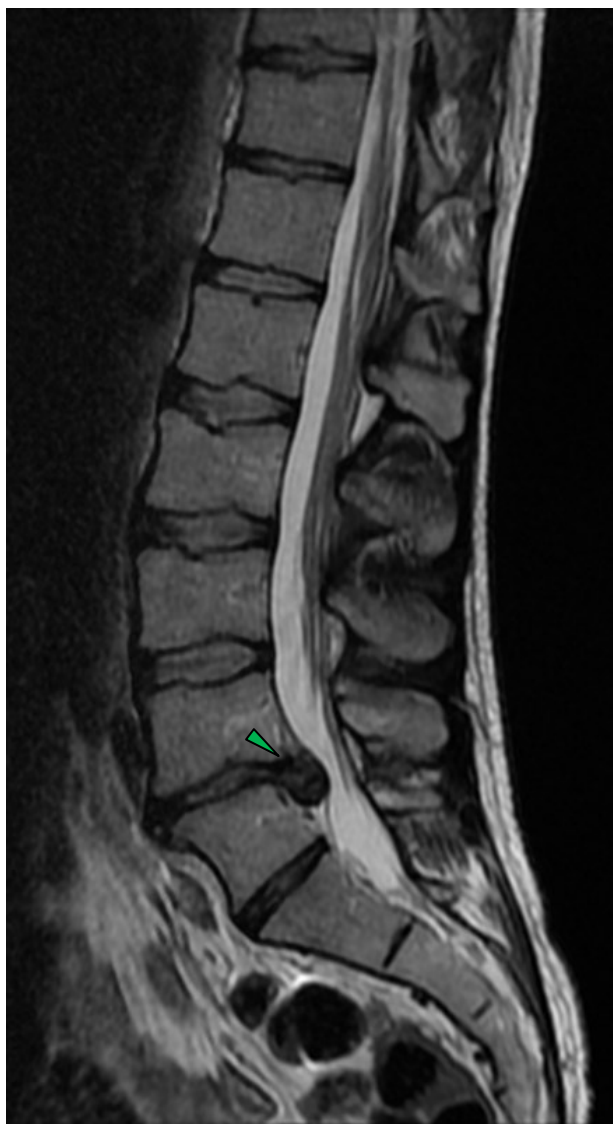
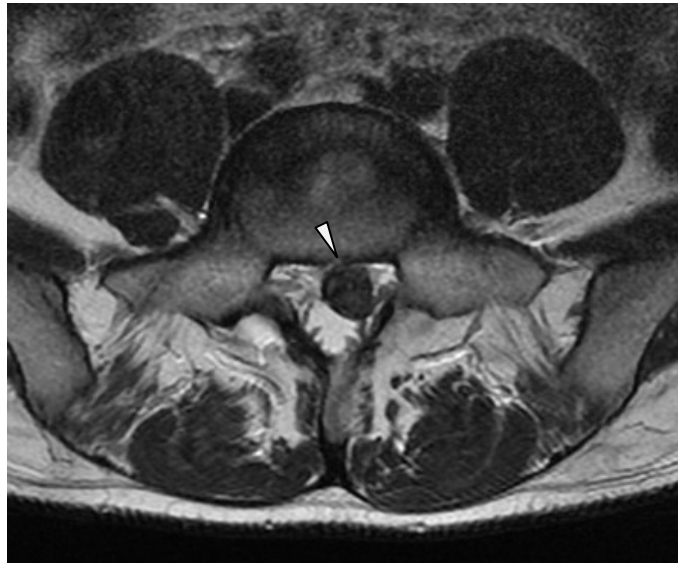


Figure 7:57. This sagittal image shows a large L4-5 extrusion that projects inferiorly from the L4-5 disc space.



Figure 7:58. This sagittal image of the same patient seen in figure 7:57 reveals significant regression of the L4-5 disc extrusion.

A series of seven images over the next three pages are taken from a patient who presented with a large herniation that regressed significantly over a five month period.



Figures 7:59 and 7:60. These axial images are from the same patient from the previous page. These images reveal two axial slices of an L4-5 herniation.



Figure 7:61. This axial slice represents the largest remnant visible of the L4-5 herniation from any image in the axial series taken five months after the series represented in figures 7:59 and 7:60.



Figure 7:62. From this axial slice, the disc derangement looks like a free-floating sequestered fragment. It represents the slice depicted by the green line in figure 7:63.



Figure 7:63. By correlating the axial images with the sagittal images, you will gain a more conceptual view of the anatomy. Here we can see that the axial slice in figure 7:62 (green arrow) captures one portion of a larger caudal extrusion, not a sequestered fragment. This concludes a seven image series.

Intravertebral Herniations



Figure 7:64. T1W sagittal image of a large intravertebral herniation through the inferior endplate of L1 into the body of L1.



Figure 7:65. T2W sagittal image of a large intravertebral herniation through the inferior endplate of L1 into the body of L1.



Figure 7:66. A different T2W sagittal slice from the same patient shows the halo of bony edema indicating that this injury is new and possibly a pain generator.

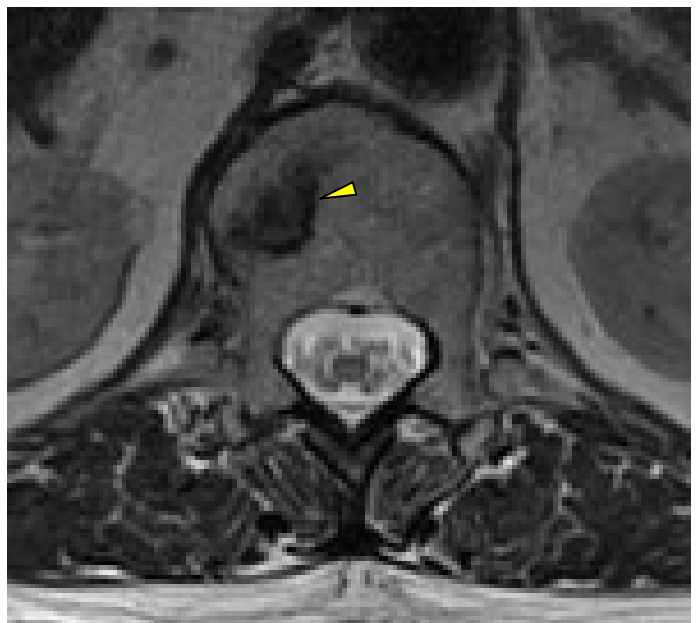


Figure 7:67. This axial T2WI image shows the disc material that has herniated into the vertebral body of L1.

Concentric Tear

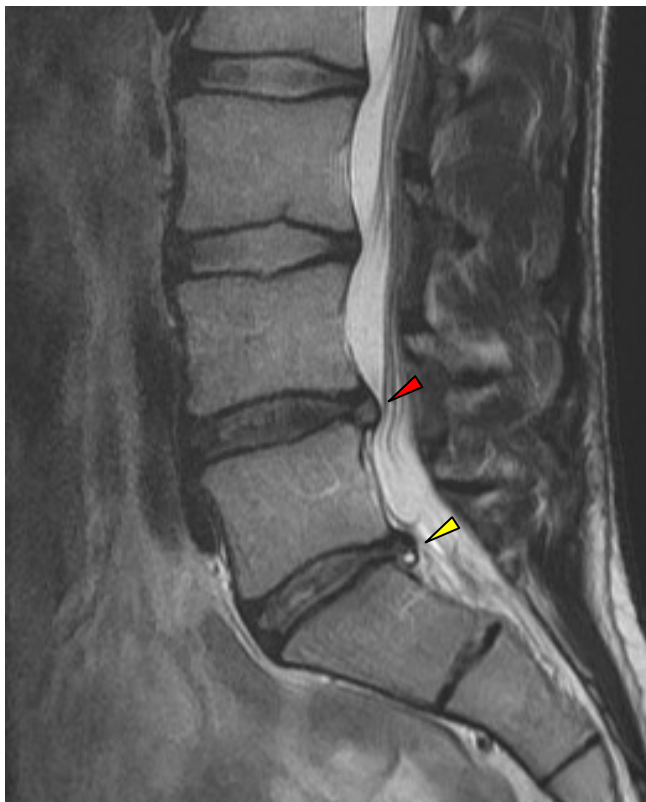


Figure 7:68. Sagittal T2WI showing an extrusion and degeneration of the L4-L5 (red arrow) and L5-S1 discs with a posterior concentric annular tear at L5-S1 (yellow arrow).



Figure 7:69. Axial T2WI of the concentric annular tear at L5-S1 (yellow arrow).

Concentric Tear

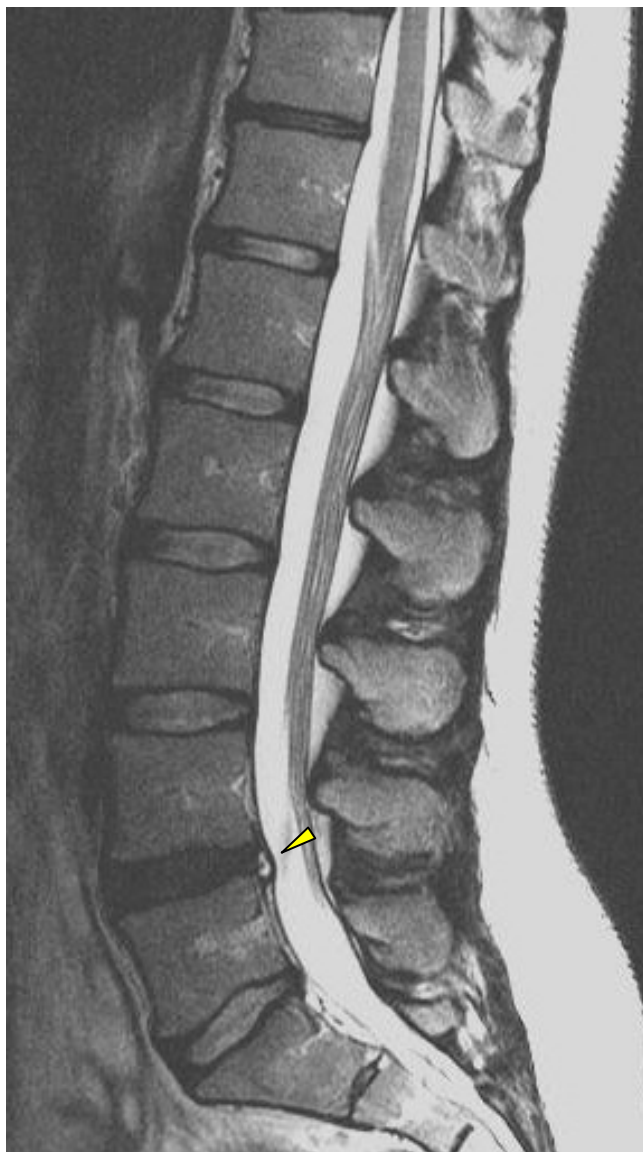


Figure 7:70. Sagittal T2WI showing a posterior concentric annular tear at L4-L5.



Figure 7:71. Sagittal T2WI showing a posterior concentric annular tear at L4-L5.

Paracentral Herniation



Figure 7:72. Sagittal T2WI showing an extrusion and degeneration at L4-L5 (yellow arrow). Desiccation is also visible at L5-S1 (green arrow).



Figure 7:73. Axial T2WI showing a left paracentral disc herniation.

Small Central Herniation

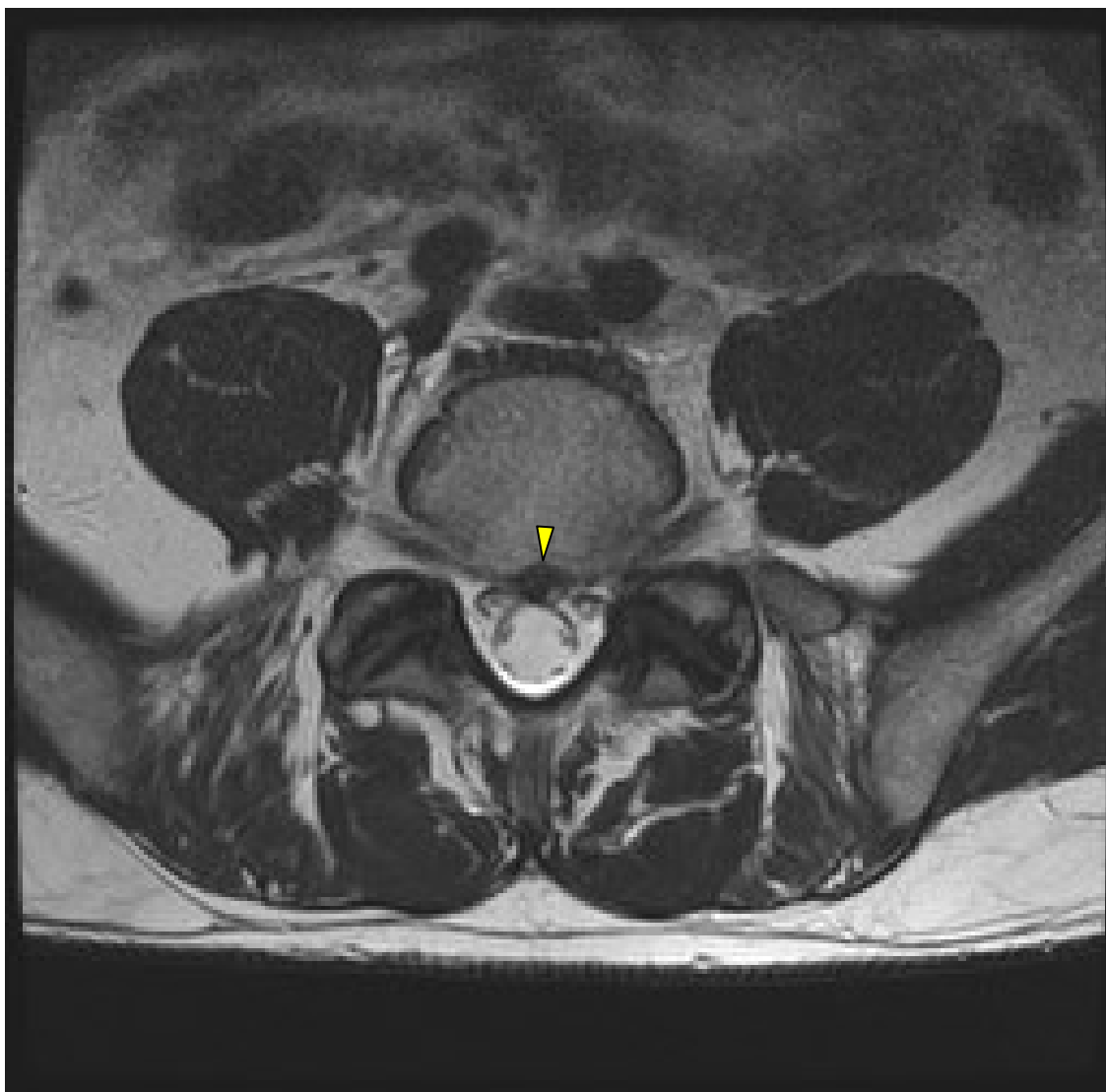


Figure 7:74. Small central herniation.

Paracentral Extrusion

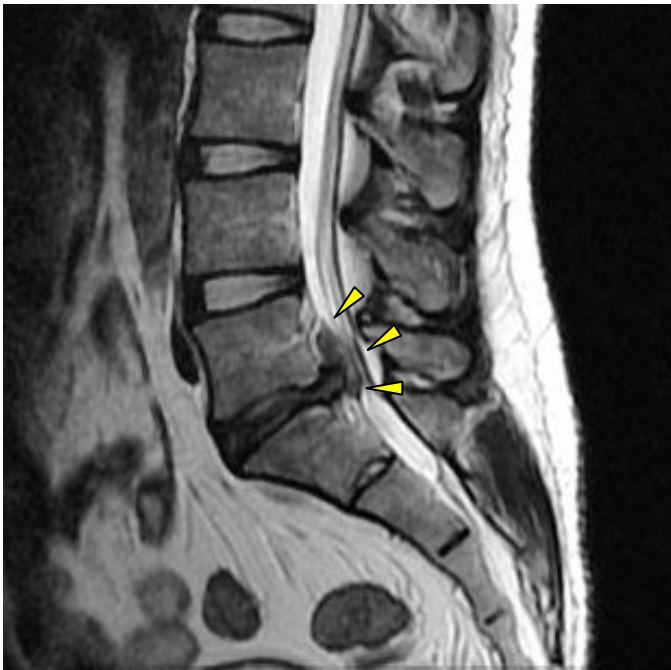


Figure 7:75. Sagittal T2WI showing an extrusion of the L5-S1 disc. A sequestered fragment sits on the extrusion like the cap of a mushroom.

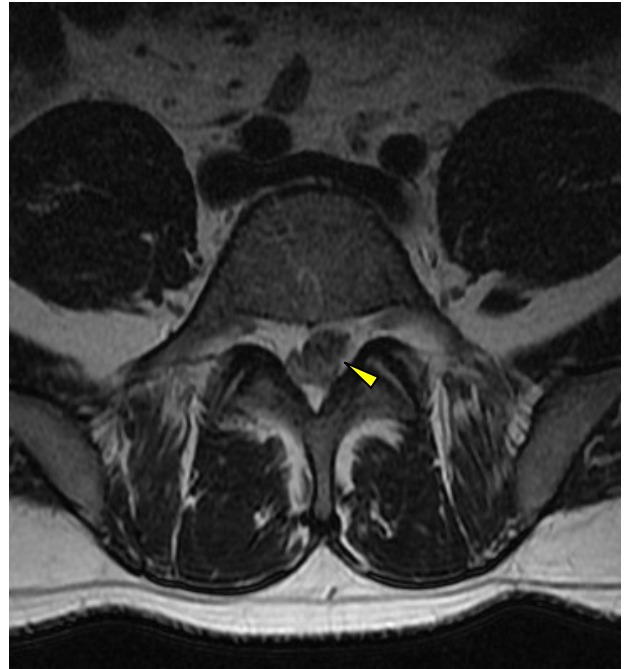


Figure 7:76. Axial T2WI showing an extrusion of the L5-S1 disc.

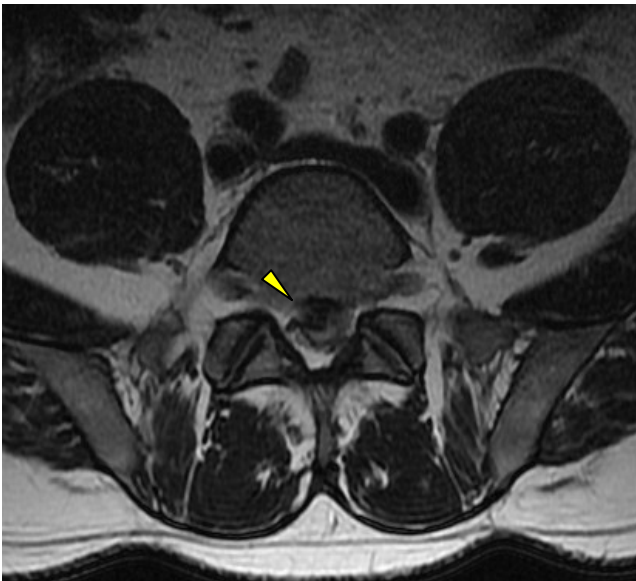


Figure 7:77. Axial T2WI showing an extrusion of the L5-S1 disc.



Figure 7:78. Axial T1WI showing an extrusion of the L5-S1 disc.

Central Extrusion



Figure 7:79. T2W sagittal image of a small L5-S1 extrusion with a concentric tear.

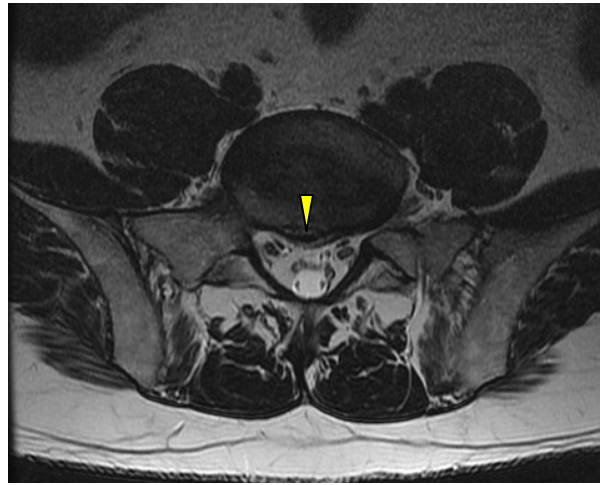


Figure 7:80. T2W axial image of the same disc derangement as seen in figure 7:79.

Paracentral Extrusion



Figure 7:81. L5-S1 extrusion, degeneration, and desiccation. The discs of the upper lumbar vertebrae are light-colored in this T2WI indicating hydration. The black disc of L5-S1 shows reduced hydration and desiccation.

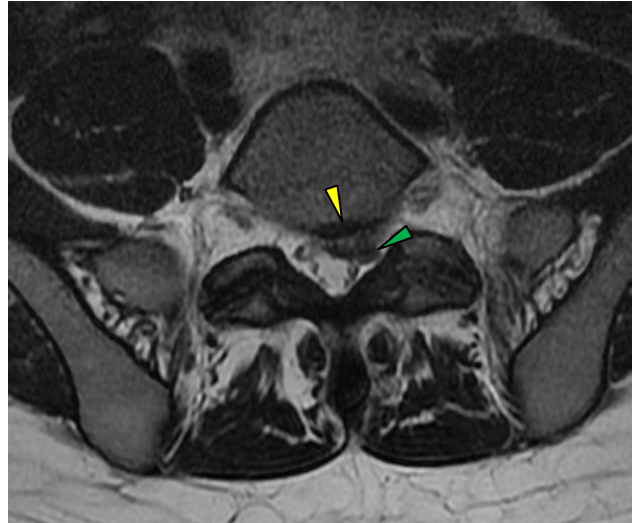


Figure 7:82. Left-sided paracentral extrusion effacing the thecal sac (yellow arrow) and displacing the left S1 nerve root (green arrow) on a T2W axial image.

Paracentral Extrusion

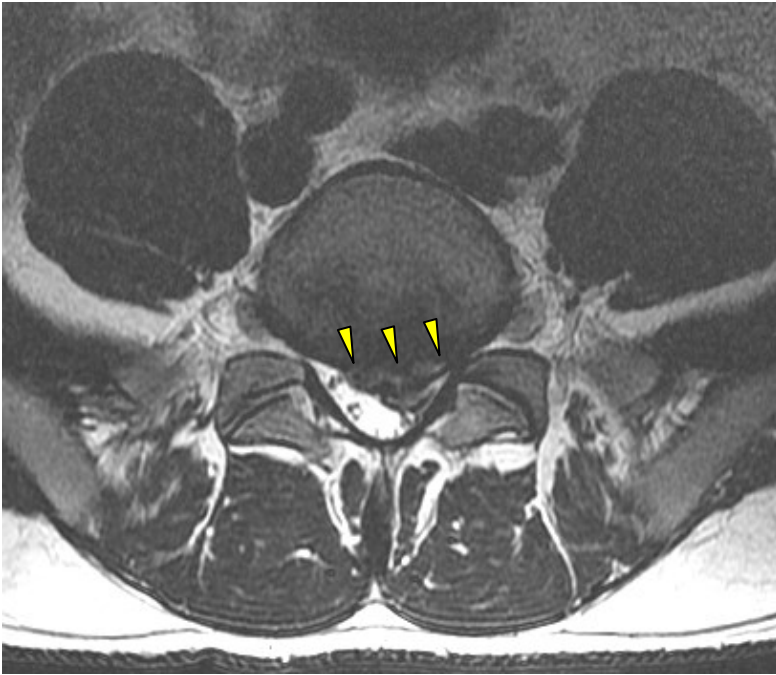


Figure 7:83. Moderate paracentral herniation on top of a broad-based herniation at L5-S1 on a T2WI.

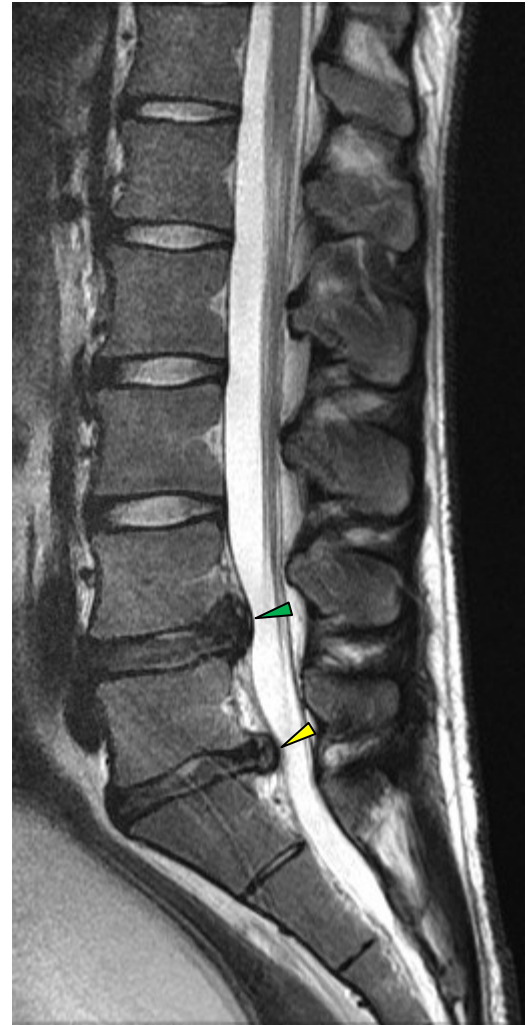


Figure 7:84. Two extrusions are visible in this sagittal image: L4-5 (green arrow) and L5-S1 (yellow arrow). The upper discs appear well hydrated, but L4-5 and L5-S1 are dark in this T2WI indicating desiccation.

Broad-based Herniation and Extrusion

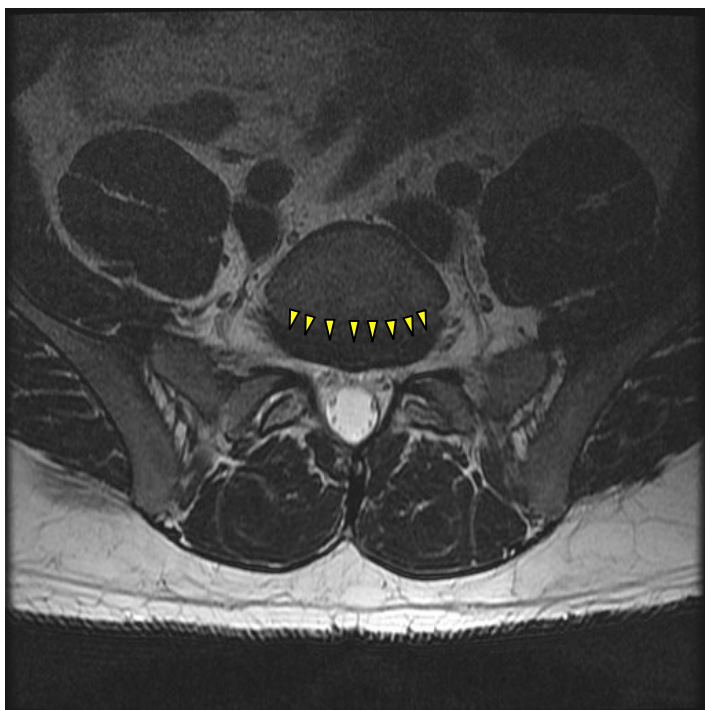


Figure 7:85. T2W axial image showing a broad-based herniation at L5-S1.



Figure 7:87. T2W sagittal image of the lumbar spine showing well-hydrated discs from L1-L5 and a cephalad migrating extrusion arising from L5-S1. Note the black disc of the L5-S1 indicative of desiccation.

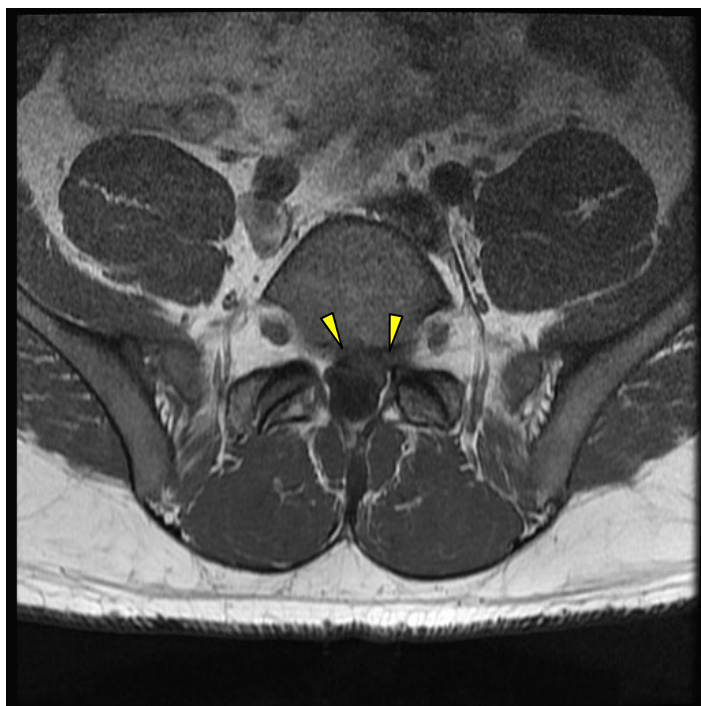


Figure 7:86. T1W image of the herniation as it extends cephalad along the body of L5.

Focal Herniation into a Large Central Canal



Figure 7:88. A degenerative disc with degenerative endplate changes at L5-S1. An extrusion exits from the L5-S1 disc into a very large central canal. Note a small hemangioma in the body of L3.



Figure 7:89. This image shows a focal disc herniation on top of a broad-based herniation. The herniation extends into a very large central canal.

Focal Extrusion Compresses and Deforms the Thecal Sac



Figure 7:90. The T2W axial image shows a focal extrusion compressing and deforming the thecal sac and its contents.



Figure 7:92. The sagittal view of this extrusion clearly shows deformation of the thecal sac at L4-5 along with disc desiccation at that level and a small perineural cyst at the level of S2. This image also demonstrates a clear view of the conus medullaris terminating at L1.

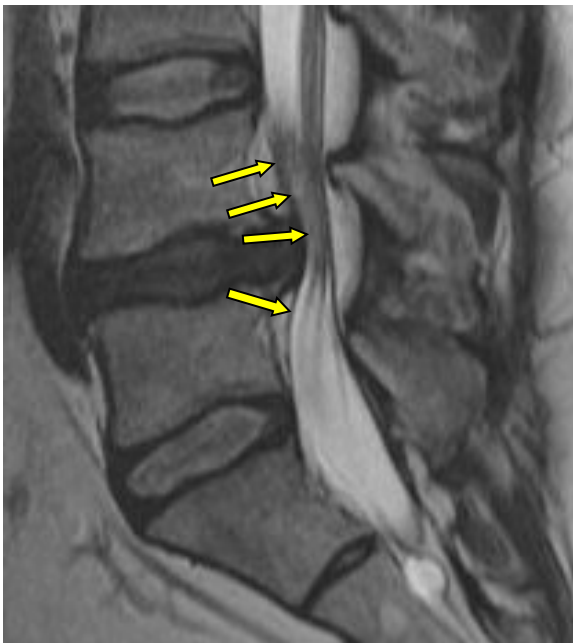


Figure 7:91. This enlargement of the sagittal slice from figure 7:92 shows the boundary of the thecal sac (yellow arrows).

Severe Herniation



Figure 7:93. A very large disc herniation at L5-S1. The mass of the herniation occupies nearly the entire central canal.



Figure 7:95. A very large disc herniation at L5-S1.

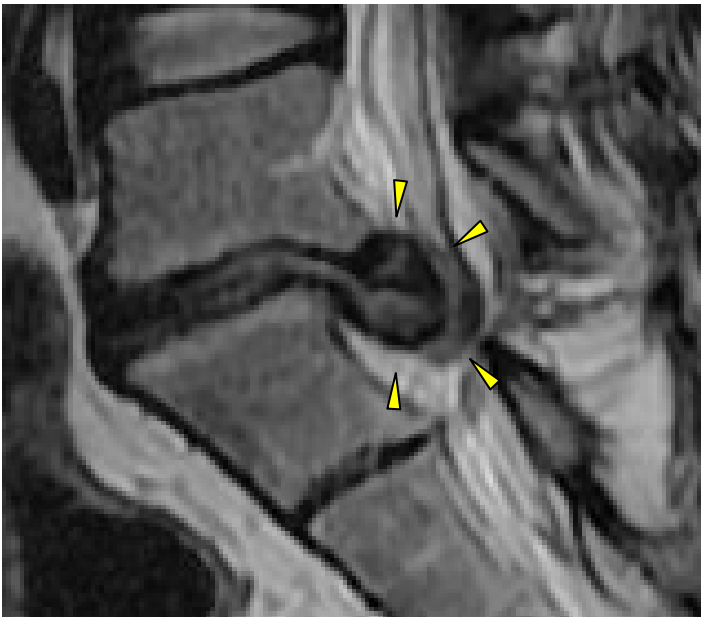


Figure 7:94. Enlarged view of the sagittal from figure 7:95.

Large Central Lumbar Herniation

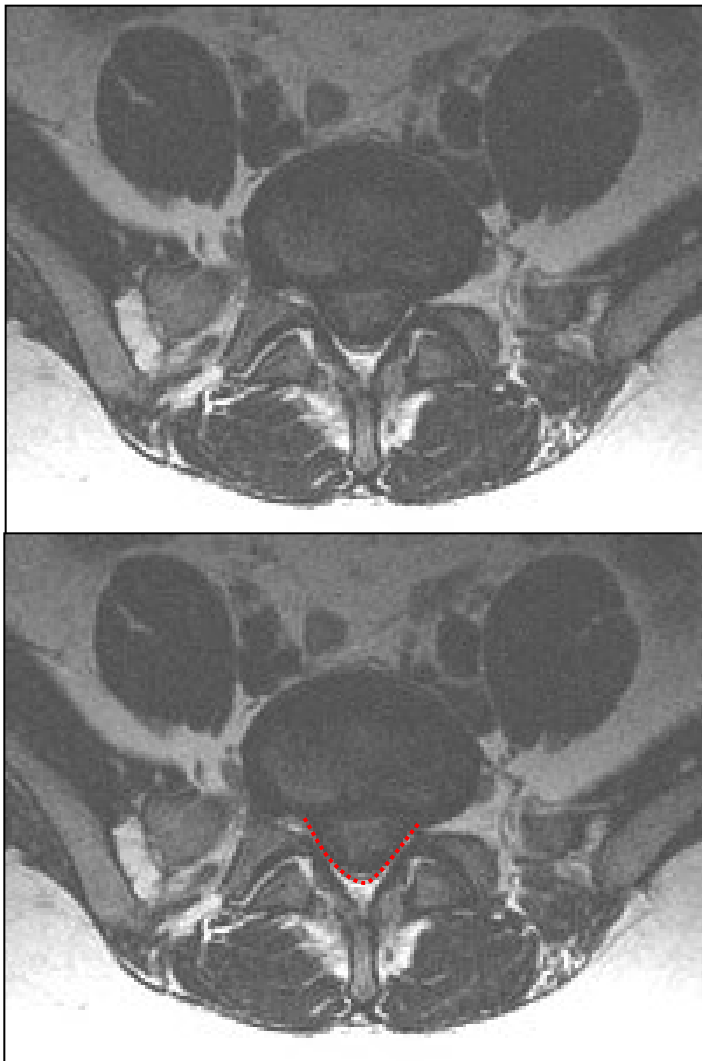


Figure 7:96. A large disc herniation at L5-S1. The mass of the herniation occupies a significant portion of the central canal.



Figure 7:97. A very large disc herniation (extrusion) at L5-S1.

Sequestered Disc Fragment Following a Hemilaminectomy



Figure 7:98. A large disc herniation at L5-S1 along the sacrum and a sequestered fragment (yellow arrow) in the central canal posterior to the body of L5. These images indicate that this patient had previously had a right hemilaminectomy at L5-S1.

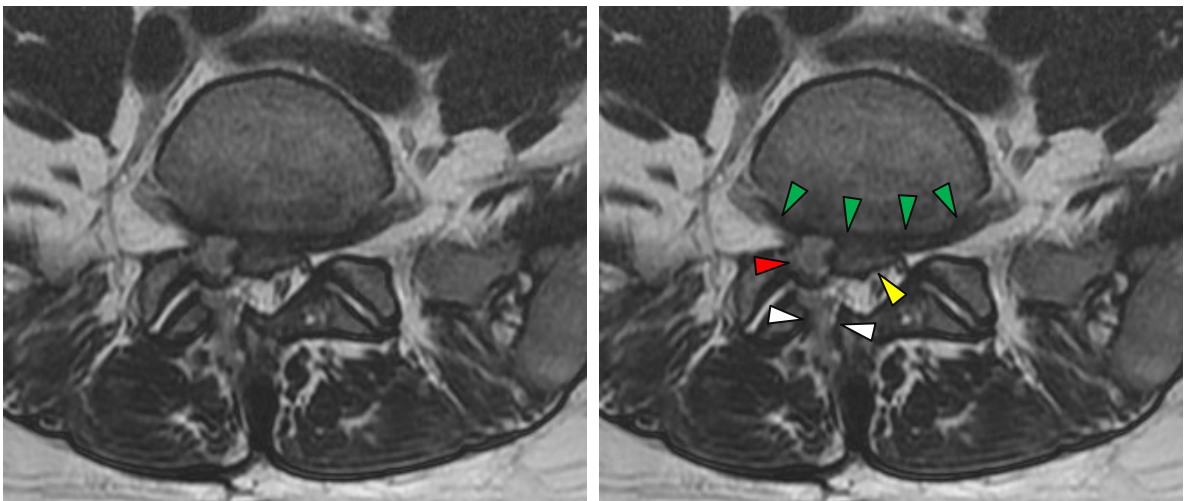


Figure 7:99. This axial image shows three distinct hues from the same disc. These hues represent the fluid content of the derangement. The broad-based disc herniation is dark (green arrows), the central portion of the herniation is neutral (yellow arrow), and the right foraminal herniation is light (red arrow). The path of the surgeon is clearly visible along the right lamina (white arrows).

Anterior Herniation

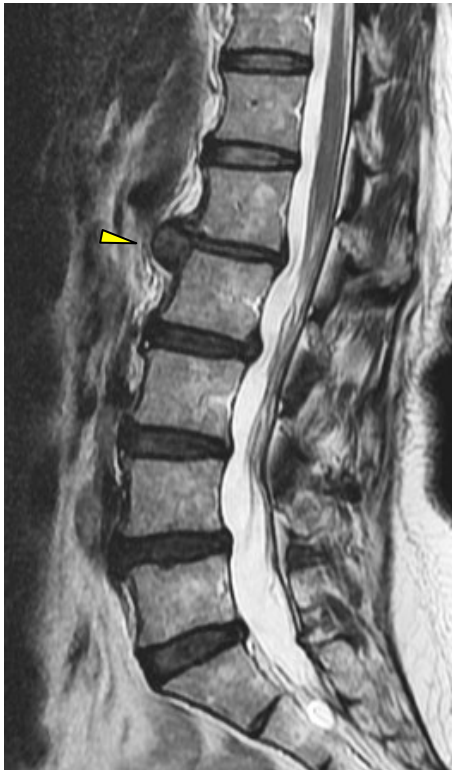


Figure 7:100. This T2W sagittal image clearly shows a large anterior herniation of L1-2.



Figure 7:101. This is a T1W sagittal image of the same anterior herniation as seen in 7:100 and 7:102.

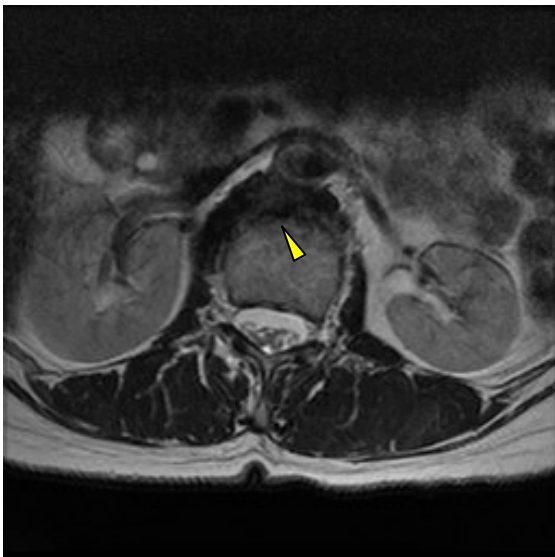


Figure 7:102. This T2W axial shows a broad anterior herniation of L1-L2 extending to the abdominal aorta.

Foraminal Herniation



Figure 7:103. The L3-4 foramina is totally occluded by this foraminal herniation.



Figure 7:104. The left L3-4 foramina is totally occluded by this dumbbell-shaped foraminal herniation.

Right Paracentral Herniation

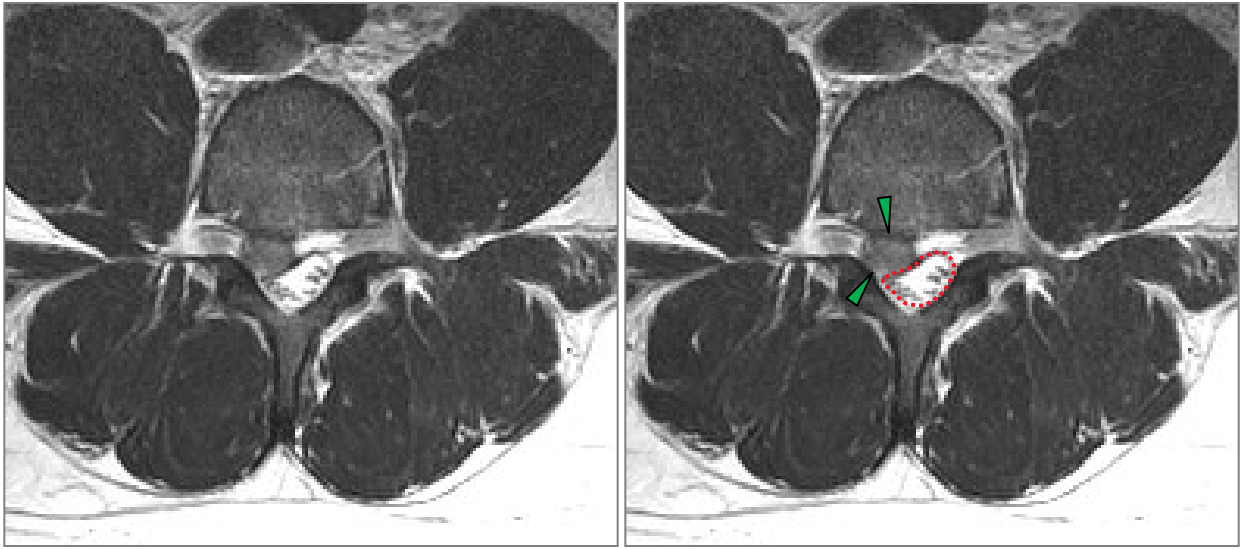


Figure 7:105. This paracentral extrusion (green arrows) deforms the thecal sac (red dotted line) and extends into the right foramina.

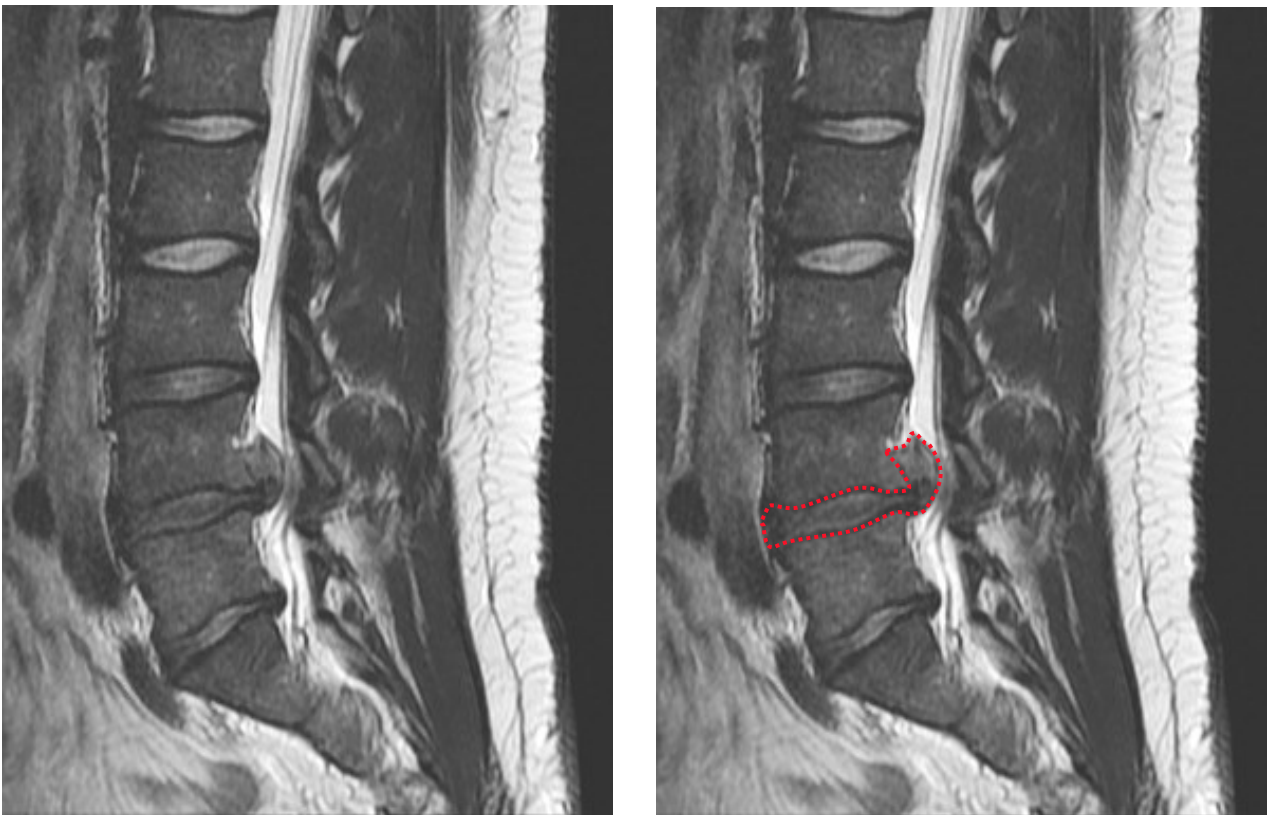


Figure 7:106. L4-5 extrusion (red dotted line) extending cephalad.

Multiple Disc Derangements

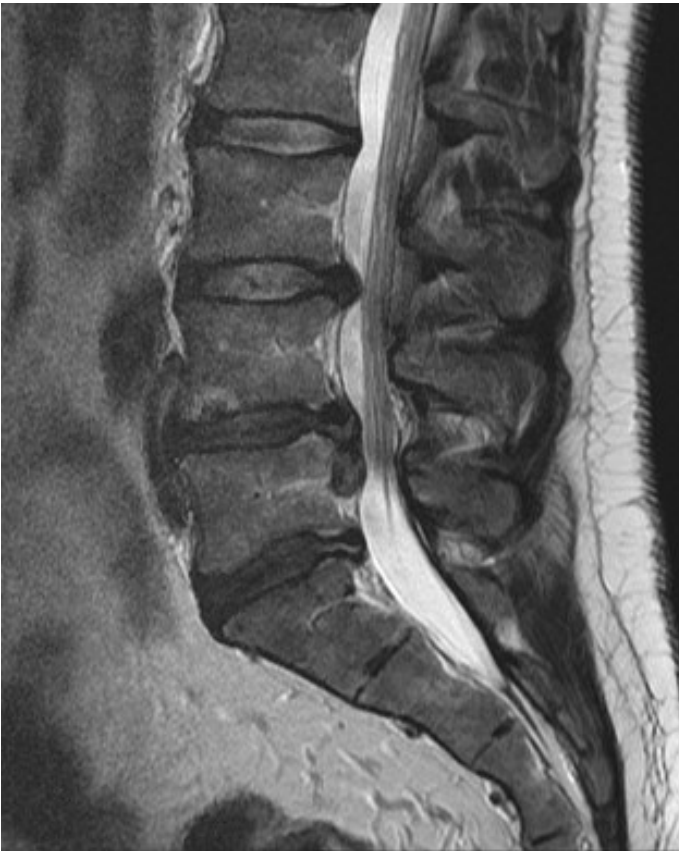


Figure 7:107. Disc derangements at L3-L4, L4-L5, and L5-S1.



Figure 7:108. Note the horizontal radial tear in the posterior L5-S1 disc (yellow arrow), and the extrusion at L4-L5 extends caudally along the posterior body (blue arrow) of L5.

Figure 7:109. L4-L5 extrusion on axial imagery (green arrow).

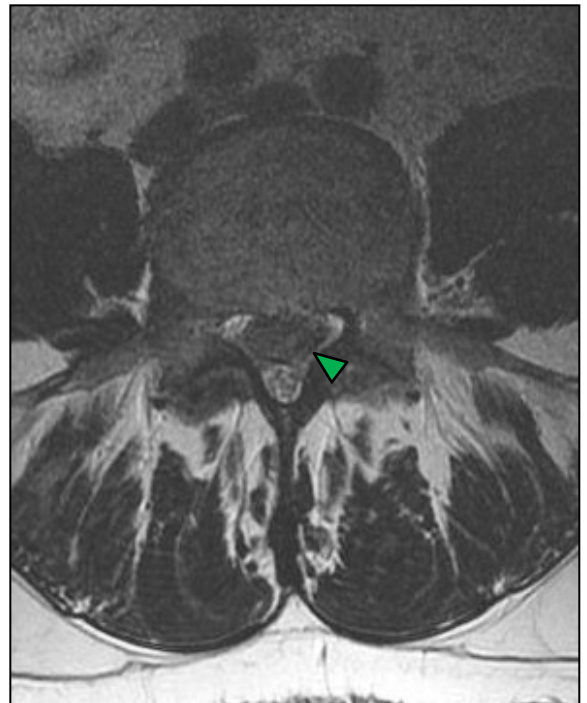




Figure 7:110. A large L4-L5 disc herniation at the site of a previous surgery. Note the large canal in this patient which extends down into the sacrum. This T2W sagittal image also reveals a post-surgical anterolisthesis of L4 on L5.

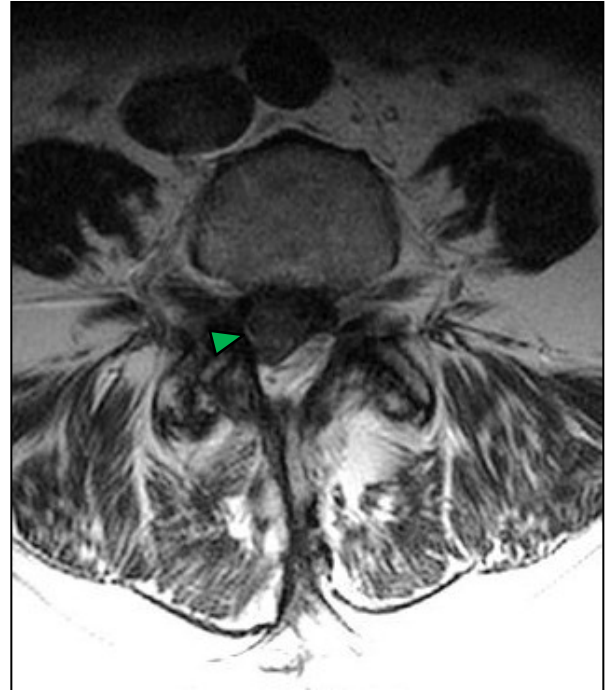


Figure 7:111. A disc herniation in an axial T2WI (green arrow). Note the fatty infiltration of the paraspinal muscles in this elderly patient.

Large Central Lumbar Herniation

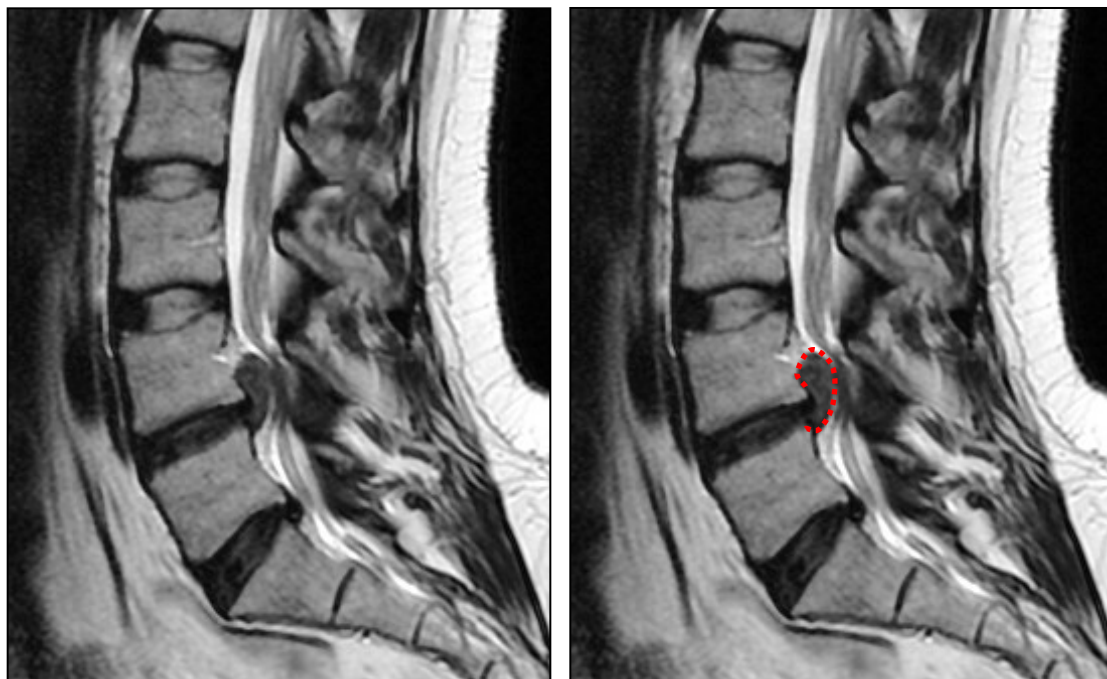


Figure 7:112. A sagittal view of a cephalad migration of an L4-L5 extrusion.

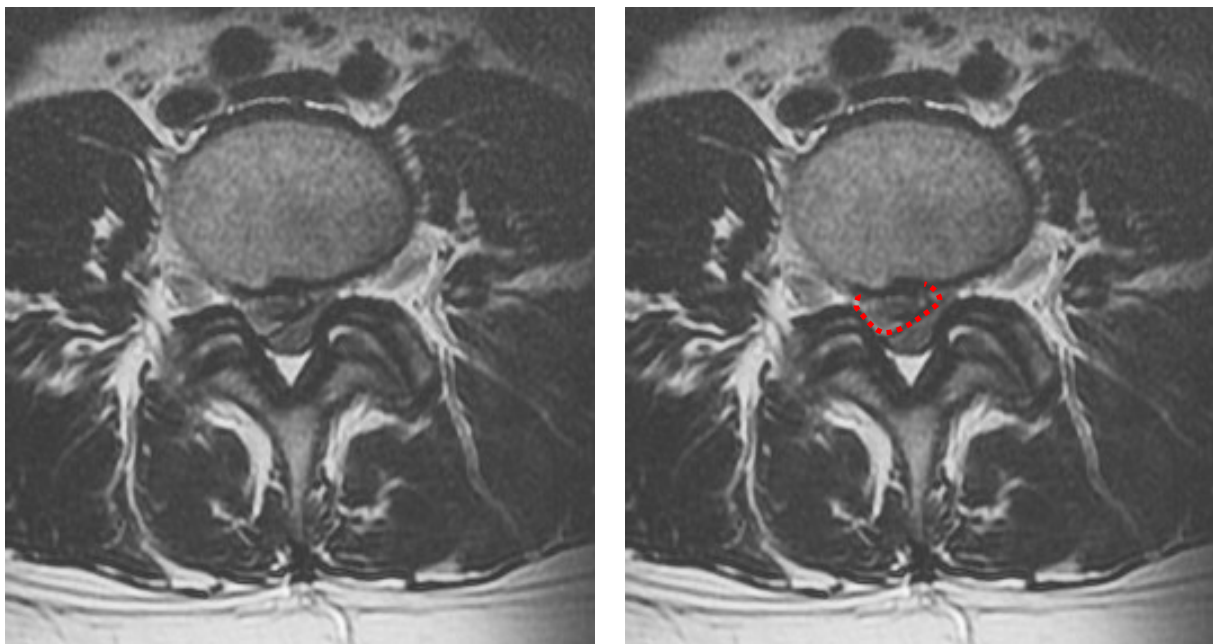


Figure 7:113. An axial view of the extrusion along L4.

Foraminal Protrusion

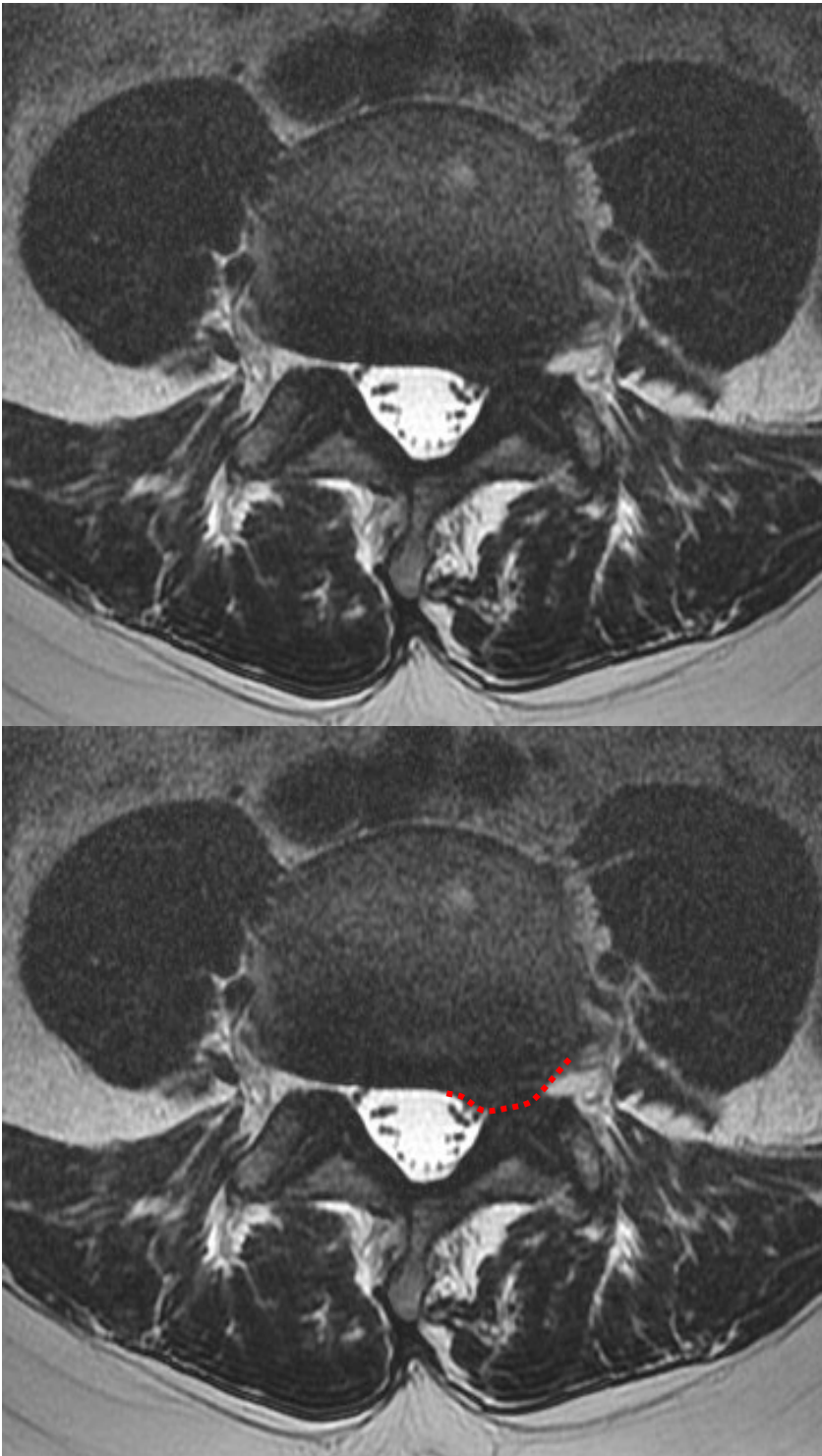


Figure 7:114. This axial (T2WI) reveals a foraminal herniation at L4-5.

Annular Tears

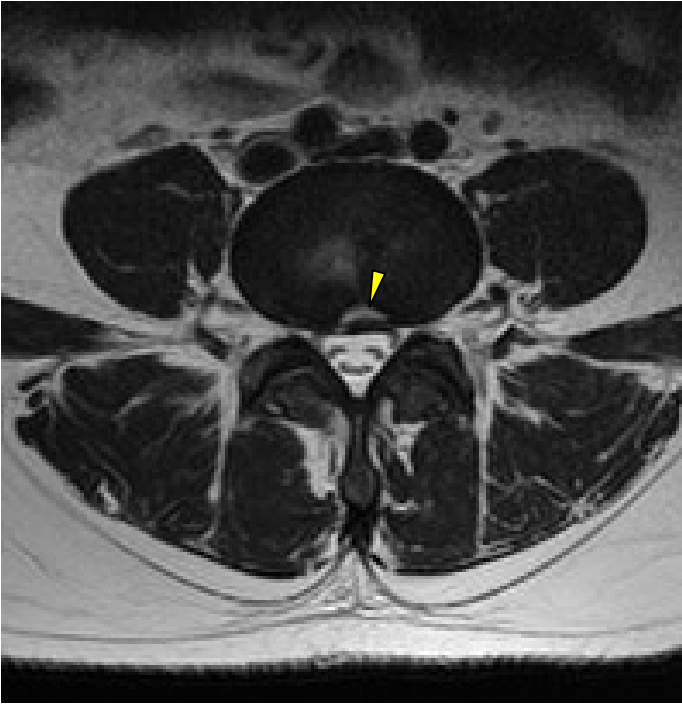


Figure 7:115. A crescent-shaped transverse tear in the posterior portion of the L4-L5 disc.

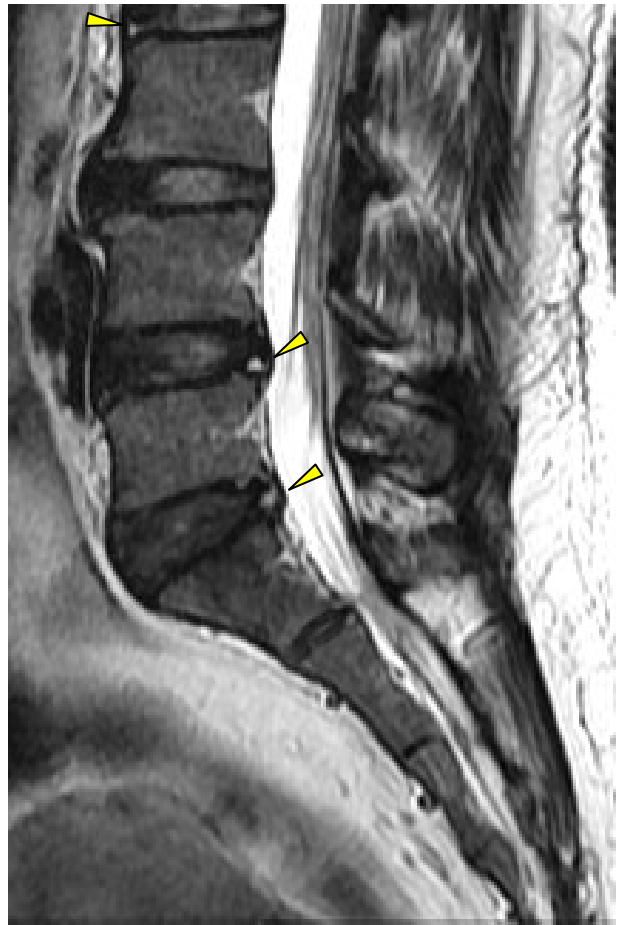


Figure 7:116. Annular tears are visible at multiple levels in this sagittal image (T2WI): a concentric tear in the posterior portion of the L5-S1 disc and transverse tears along the posterior superior endplate of L4, and the anterior superior endplate of L3.

Compressive Injuries

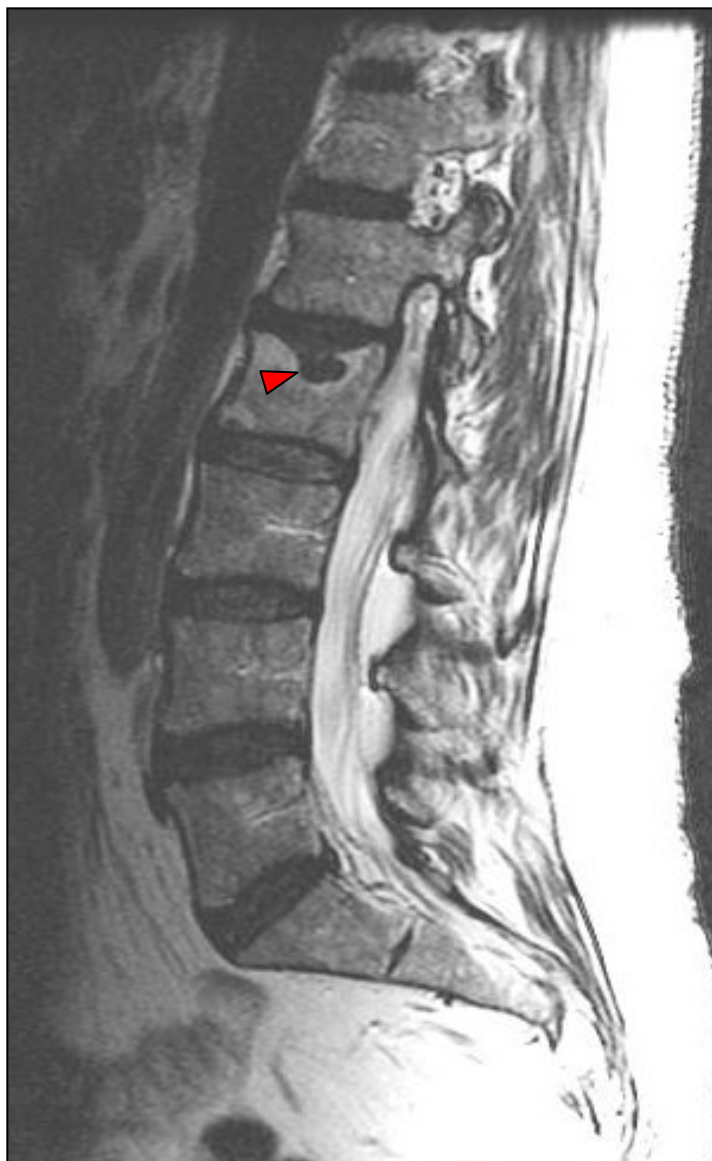


Figure 7:117. This image displays an intravertebral herniation (Schmorl's node) extending through the superior endplate of L2. This injury was symptomatic.



Figure 7:118. The compressive forces that caused the L2 intravertebral herniation visible in figure 7:117 also caused the compression fracture seen in this thoracic MRI.

Sequestered Fragment and Thecal Sac Displacement

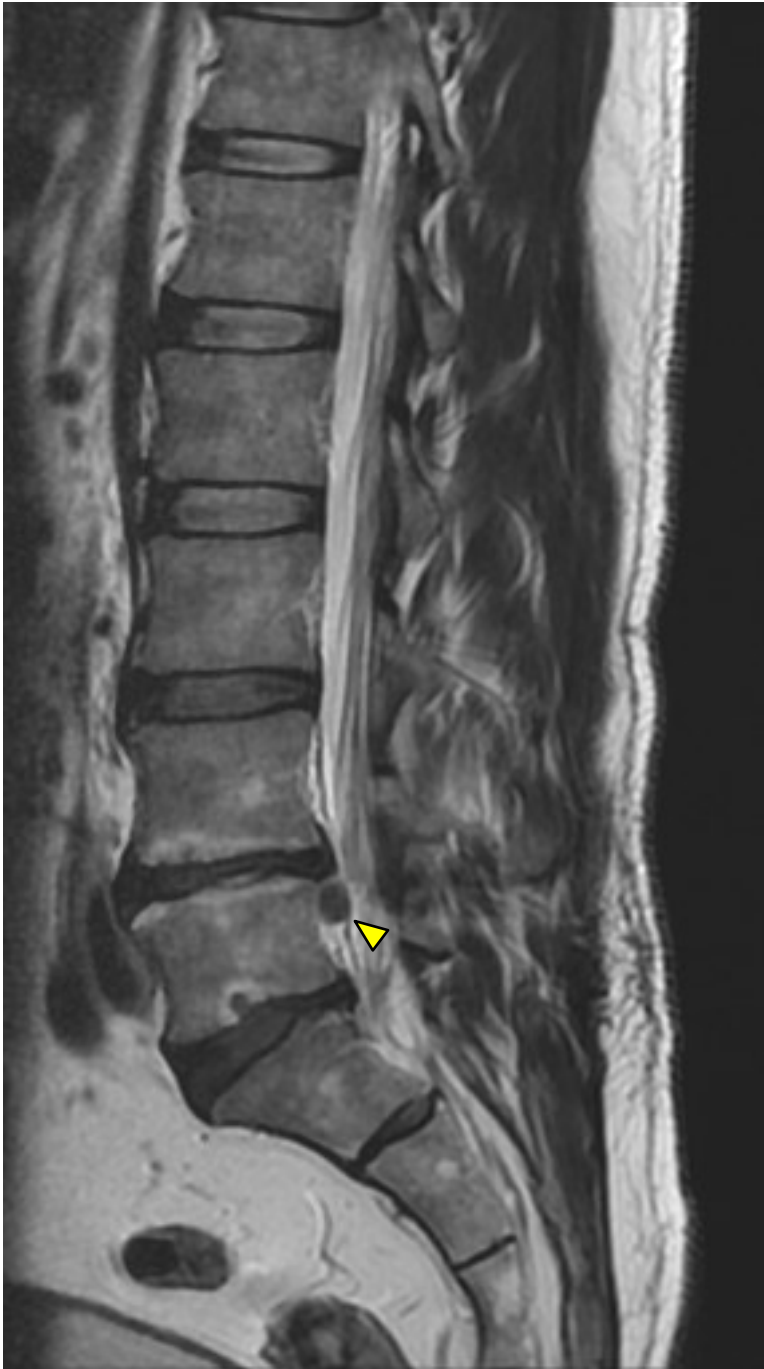


Figure 7:119. A sequestered fragment descends caudally from the L4-L5 disc (yellow arrow). Note the intravertebral herniation through the inferior endplate of L5 and the changes in the L4 and L5 endplates. These images reveal a lumbar surgery that had been performed at L4-L5.

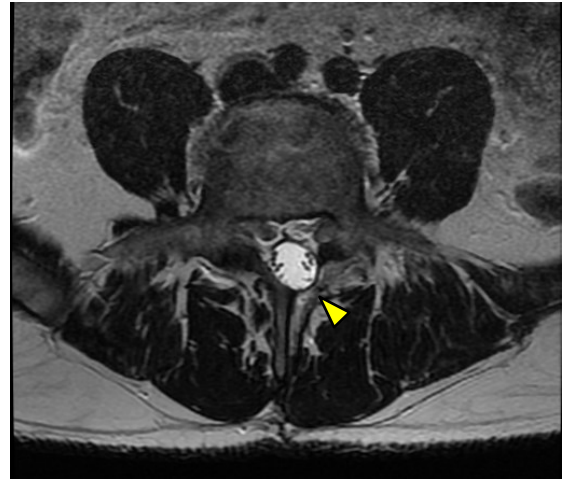


Figure 7:120. The thecal sac is displaced through a previous laminectomy in this T2 axial image (yellow arrow).



Figure 7:121. The thecal sac is displaced through a previous laminectomy in this T1 axial image (yellow arrow).

Central L5-S1 Protrusion

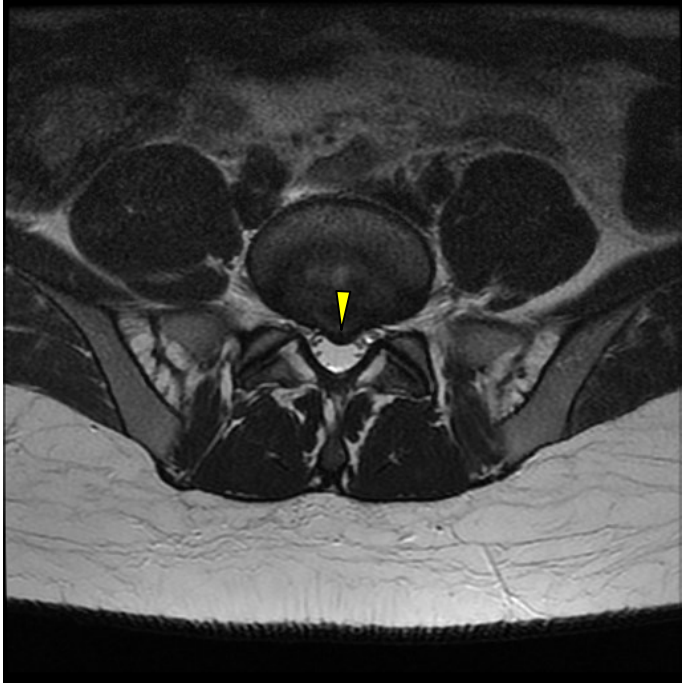


Figure 7:122. Mild Central L5-S1 protrusion.



Figure 7:123. Mild Central L5-S1 protrusion.

Suggested Reading

Fardon DF, Milette PC. Nomenclature and classification of lumbar disc pathology: recommendations of the combined task forces of the north American spine society, American society of spine radiology, and American society of neuroradiology. *Spine*, Volume 26(5). March 1, 2001. E93-E113.

<http://www.rsna.org/radlex/committee/ASSRDiscNomenclature.pdf>

Ahn SH, Ahn MW, Byun WM. Effect of the transligamentous extension of lumbar disc herniations on their regression and the clinical outcome of sciatica. *Spine*. 2000;25:475–80.

Bozzao A, Gallucci M, Masciocchi C, Aprile I, Barile A, Passariello R. Lumbar disk herniation: MR imaging assessment of natural history in patients treated without surgery. *Radiology*. 1992;185:135–41.

Delauche-Cavallier MC, Budet C, Laredo JD, Debie B, Wybier M, et al. Lumbar disc herniation. Computed tomography scan changes after conservative treatment of nerve root compression. *Spine*. 1992;17:927–33.

Komori H, Shinomiya K, Nakai O, Yamaura I, Takeda S, Furuya K. The natural history of herniated nucleus pulposus with radiculopathy. *Spine*. 1996;21:225–9.

Matsubara Y, Kato F, Mimatsu K, Kajino G, Nakamura S, Nitta H. Serial changes on MRI in lumbar disc herniations treated conservatively. *Neuroradiology*. 1995;37:378–83.

Modic MT, Ross JS, Obuchowski NA, Browning KH, Cianflocco AJ, Mazanec DJ. Contrast-enhanced MR imaging in acute lumbar radiculopathy: a pilot study of the natural history. *Radiology*. 1995;195:429–35.

Saal JA, Saal JS, Herzog RJ. The natural history of lumbar intervertebral disc extrusions treated nonoperatively. *Spine*. 1990;15:683–6.

Cribb GL, Jaffray DC, Cassar-Pullicino VN. Observations on the natural history of massive lumbar disc herniation. *J Bone Joint Surg Br*. 2007;89:782–4.

Atlas SW. (2008). *Magnetic resonance imaging of the brain and spine* (forth edition). Lippincott Williams & Wilkins.

Ross JS et al. (2010). *Diagnostic imaging spine* (second edition). Amirsys Inc.

Bogduk N. (2012). *Clinical and radiological anatomy of the lumbar spine*. Churchill Livingstone.

Spondylolysis and Spondylolisthesis

8



Types of Spondylolisthesis

Spondylolisthesis is a condition in which one vertebra slips anteriorly on the vertebra below. While five types of spondylolisthesis have been identified, this chapter will concentrate on the two most common types: degenerative and isthmic.

The various types of spondylolisthesis share the commonality of anterior vertebral slippage, but have significantly different etiologies and clinical presentations. It is important to be able to differentiate the difference and to be familiar with their radiographic presentations. This chart clarifies the main differences between the categories of spondylolisthesis:

Type of Spondylolisthesis	Pathology
Degenerative	Facetal and connective tissue degeneration leading to anterior listhesis
Isthmic	Secondary to spondylolysis of the affected pars interarticularis
Congenital	Usually from hypoplasia of the S1 facets
Traumatic	Resulting from an acute fracture that may include structures other than the pars interarticularis
Post surgical	Surgical mishaps that progress or cause a spondylolisthesis

Figure 8:1. Categories of spondylolisthesis

The most common types of spondylolisthesis encountered are degenerative and isthmic, and most of this chapter will discuss these two. However, it is important for the clinician to be aware of and familiar with the lesser known types. Thus, congenital, traumatic and post-surgical spondylolistheses will be also be touched upon, but with less detail. For these less common types of spondylolisthesis, a good working relationship between the radiologist and clinician is important for categorization.

Meyerding Classification System



Figure 8:2. Grade I spondylolisthesis of L5 on S1 viewed on a lateral plain film radiograph.

MRI is not the preferred medium for viewing and identifying a spondylolisthesis. X-ray (particularly weight bearing views) and CT are preferred to MRI for visualizing spondylolisthesis. While spondylolysis and spondylolisthesis may be diagnosed and graded on a lateral X-ray, the preferred image for identifying a spondylolysis is the oblique plain film x-ray. MRI, however, is a valuable tool for determining the effect of spondylolisthesis on the soft tissues of the spine and adjoining structures.

To categorize the degree of anterior slippage of a spondylolisthesis, the Meyerding classification system was adopted. The Meyerding scale grades a spondylolisthesis (regardless of the cause of the listhesis) on a scale of 1-4. Each number represents 25% of the superior end plate of the vertebra or sacral segment below the level of listhesis. When the posterior body of L5 slides forward up to 25% of the surface of the vertebra below, it is classified as a Grade I, at 25-50% it is a Grade II, at 50-75%, a Grade III, and at 75-100%, a Grade IV. If the vertebral body slides completely off of the segment below, it is called a spondyloptosis.

Clinical note: If a spondylolisthesis exceeds grade I (greater than 25% anterior slippage), it will have a spondylolysis. Degenerative spondylolisthesis rarely exceed 25% anterior listhesis.

Comparing Isthmic and Degenerative Spondylolisthesis

An isthmic spondylolisthesis is characterized by pars interarticularis defect or stress fracture (spondylolysis) that essentially splits the vertebra into two pieces.

In the degenerative variety of spondylolisthesis, the posterior elements of the vertebral segments degenerate to the point in which they cannot prevent anterior listhesis (slippage). This results in an anterior listhesis of the entire vertebral body along with the posterior elements of the vertebra.

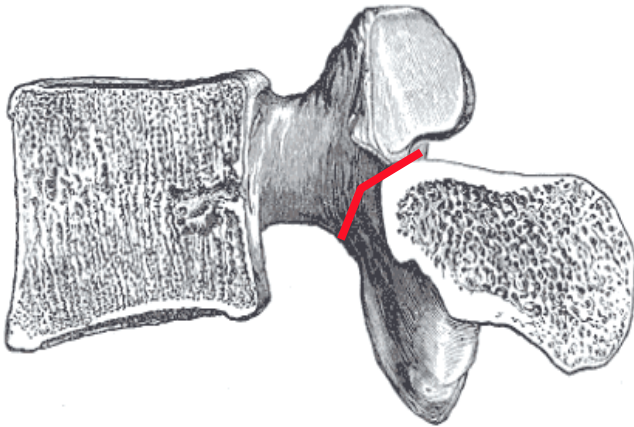


Figure 8:3. Isthmic spondylolisthesis occurs after a bony insult occurs. A stress fracture (though this terminology has been disputed) of the pars interarticularis, also known as a spondylolysis, occurs as a result of repeated stresses or microtrauma.

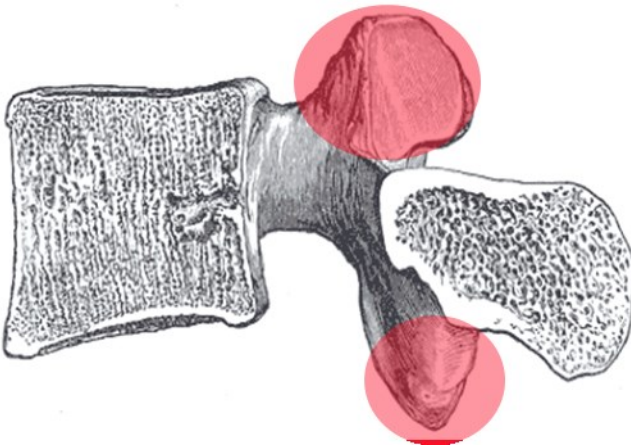


Figure 8:4. Degenerative spondylolisthesis is by far more common in the general population (though less common in younger populations). Degenerative spondylolisthesis occurs over time, secondary to degenerative changes of the facet joints, discs, and subsequent ligament laxity.

Images adapted from Henry Gray (1821–1865). *Anatomy of the Human Body*. 1918.

Characteristics of a Spondylolisthesis in Sagittal Images

In addition to the primary radiographic findings of a pars interarticularis defect and anterior listhesis of the vertebral body, there are secondary findings characteristic of spondylolisthesis.

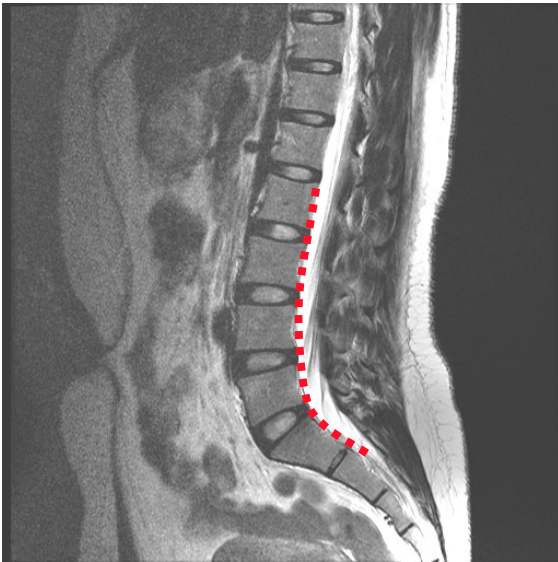


Figure 8:5. A normal spine will have a continuous uninterrupted alignment of the vertebral segments

Figure 8:5 shows a normal spine without anterior listhesis. The red dotted line traces the posterior longitudinal ligament and posterior vertebral bodies revealing a normal lumbar lordosis.

Bilateral pars interarticularis spondylolysis literally breaks the vertebra into two pieces. When a spondylolysis progresses to a spondylolisthesis, it is common for the vertebral body to travel anterior and the posterior elements to list posterior (figure 8:6). In contrast, a degenerative spondylolisthesis will have the entire vertebra travel anterior (figure 8:7).

While an isthmic spondylolisthesis may expand the central canal, a degenerative spondylolisthesis will frequently contribute to a stenosis of the central canal. This concept is expanded upon on the following page.

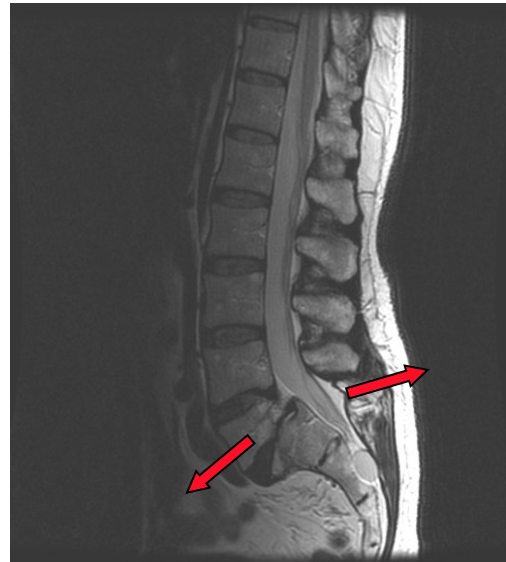


Figure 8:6. An isthmic spondylolisthesis may have a separation of the two segments of the vertebra. These segments may migrate in opposite directions (red arrows).

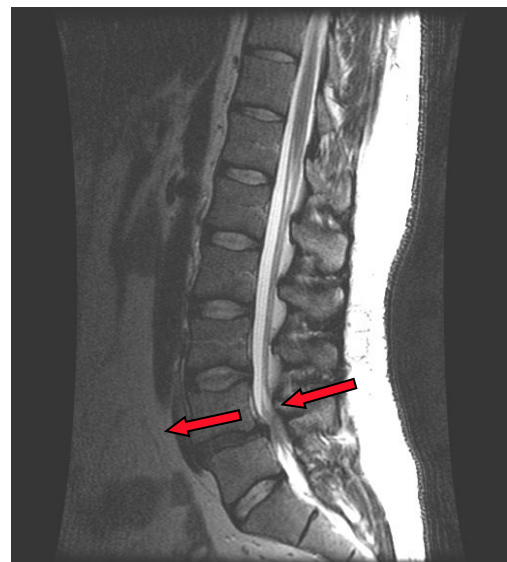


Figure 8:7. Degenerative spondylolisthesis has the entire vertebra moving anterior as a unit. Degenerative spondylolisthesis will not progress past 25%.

Conceptualizing the Effects of Spondylolisthesis on the Central Canal

Figure 8:8. This schematic shows the thecal sac descending through the spinal canal in a normal manner.

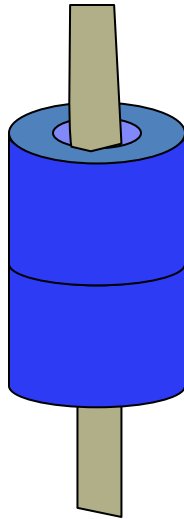


Figure 8:9. When a degenerative spondylolisthesis occurs, the thecal sac is distorted as it follows the snaking central canal.

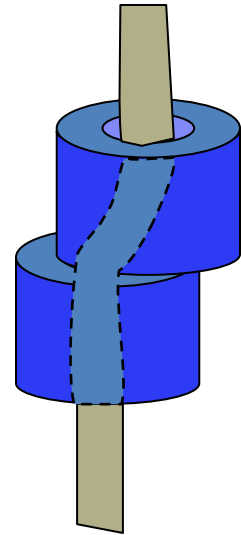


Figure 8:10. In degenerative spondylolisthesis the vertebral arch is preserved causing a canal narrowing as the alignment of the canal is compromised. This is often compounded by the stenotic effects of degeneration and ligamentum flavum hypertrophy. Degenerative spondylolisthesis is often associated with a clinical presentation characteristic of central canal stenosis. This image depicts the compromised alignment of the two adjoining vertebra from above. The canal appears narrowed when viewed from above.

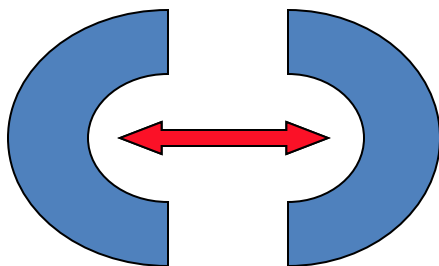
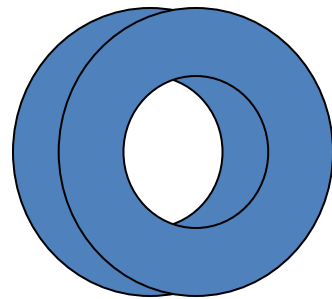


Figure 8:11. When a bilateral spondylolysis is present, the vertebral arch is not preserved. The two components of the vertebra may open causing a widening of the canal.

These images are an attempt to simplify the understanding of the effects of degenerative and isthmic spondylolisthesis on the central canal of the spine. Simply put, degenerative spondylolisthesis generally results in central canal stenosis, and isthmic spondylolisthesis expands the central canal at the level of the lysis.

Characteristics of a Spondylolisthesis in Axial Images

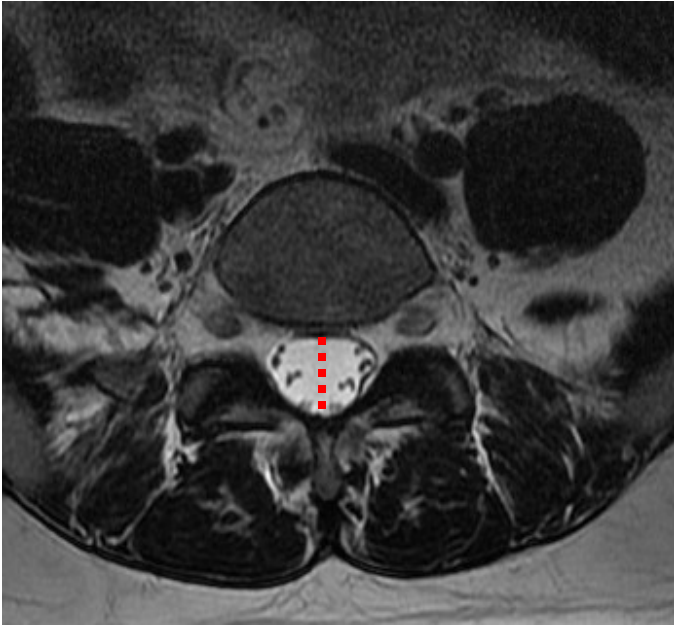


Figure 8:12. Normal size central canal.

The central canal of the lumbar spine is typically oval shaped (figure 8:12). In an isthmic spondylolisthesis with a defect of the pars interarticularis, the body of the vertebra moves anterior while the posterior arch migrates posterior. This elongates the canal into an anomalous appearance (figure 8:13). Note the gap between the posterior vertebral body and the anterior thecal sac in figure 8:13.

Degenerative spondylolisthesis, by contrast, is frequently characterized by a reduction in canal size (figure 8:14). Axial imagery can aid in identifying the type of spondylolisthesis and its effects on other structures.

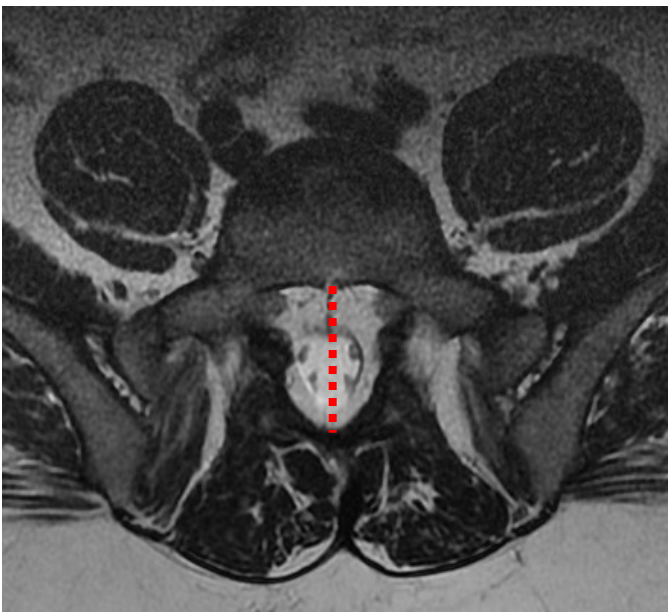


Figure 8:13. Elongated central canal. This finding is characteristic of an isthmic spondylolisthesis.

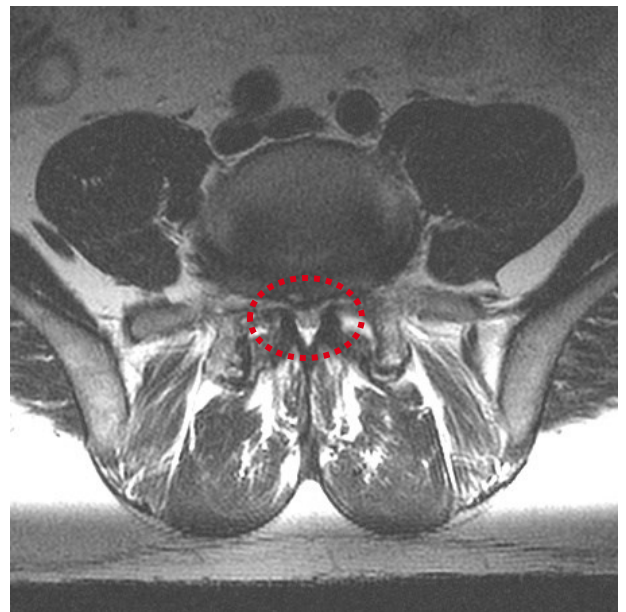


Figure 8:14. Stenotic central canal. This finding is characteristic of a degenerative spondylolisthesis.

These T2W MRIs correlate axial images with sagittal images. These images clearly show the central canal stenosis associated with degenerative spondylolisthesis (figures 8:15 and 8:16). This stands in stark contrast to the isthmic spondylolisthesis which is characterized by the elongated canal visualized on the axial image (figures 8:17 and 18).

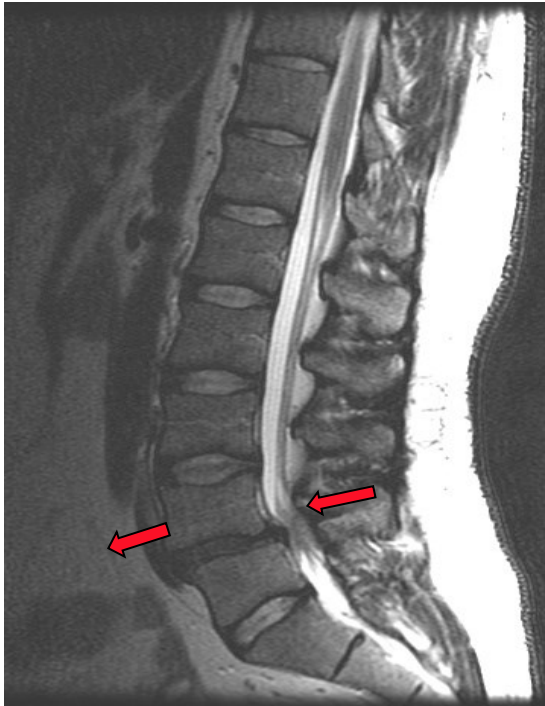


Figure 8:15. Sagittal image of a degenerative spondylolisthesis of L4 on L5. The entire vertebra has slipped forward.

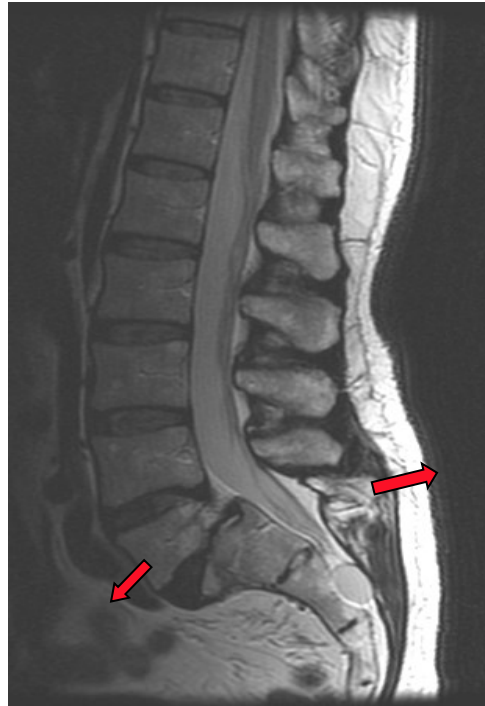


Figure 8:16. Sagittal image of an isthmic spondylolisthesis of L5 on the sacrum. The anterior and posterior elements travel in opposite directions.

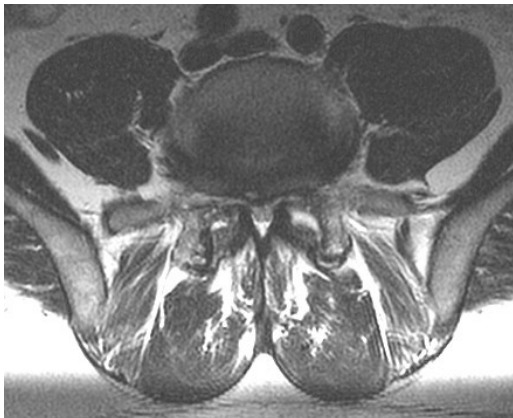


Figure 8:17. Axial image of degenerative spondylolisthesis with severe central canal stenosis and facetal effusion.



Figure 8:18. This axial image of an isthmic spondylolisthesis reveals an elongated central canal as the vertebral elements migrate away from each other.

Spondylolysis, Facetal Effusion, and a Resulting Synovial Cyst

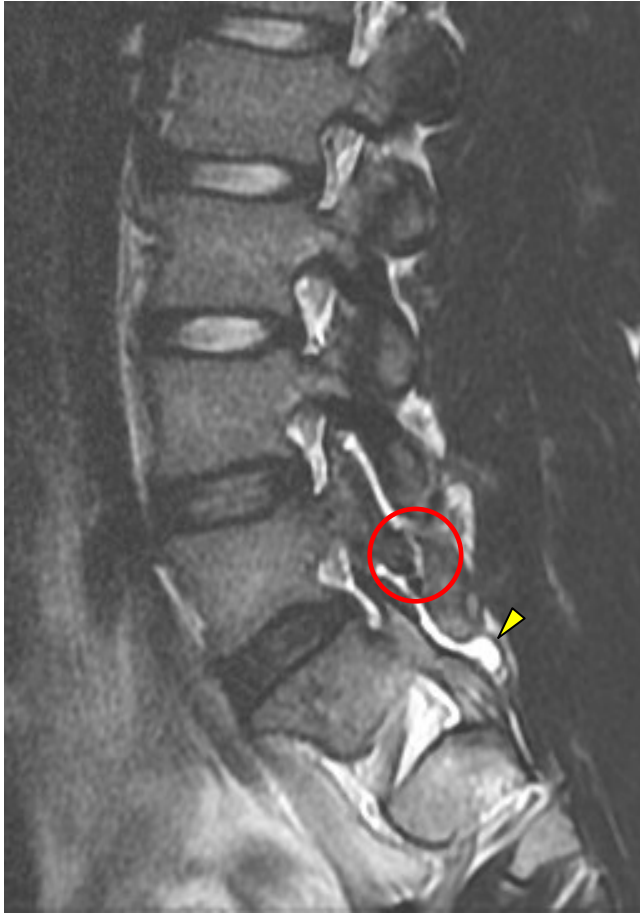


Figure 8:19. A spondylolysis is visualized (with the red circle) in this T2W sagittal. A synovial cyst arises from the facet of L5-S1 (yellow arrow).



Figure 8:20. The same image as figure 9:19 without denotations.

This T2W image of a football lineman shows facetral effusion (hyperintense on T2) at L4-5, L5-S1 with a synovial cyst extending posteriorly and caudally from the L5-S1 facet (yellow arrow). The pars defect is identified with the red circle. The image on the right is the same image without the markers. These findings correlate with his symptoms and history of pain and traumatic lumbar extensions while playing football. Facet effusion can be an indicator of reduced segmental stability in degenerative spondylolisthesis.

Wedging of a Vertebral Body Secondary to Isthmic Spondylolisthesis

Finding a wedged lumbar vertebra, particularly at L5, is associated with spondylolisthesis secondary to spondylolysis. While it is not fully understood if this finding predisposes the vertebra to lysis or if it occurs as a result of lysis and listhesis, experts are leaning toward the thought that this trapezoid deformation occurs over time after the spondylolysis and listhesis occur.

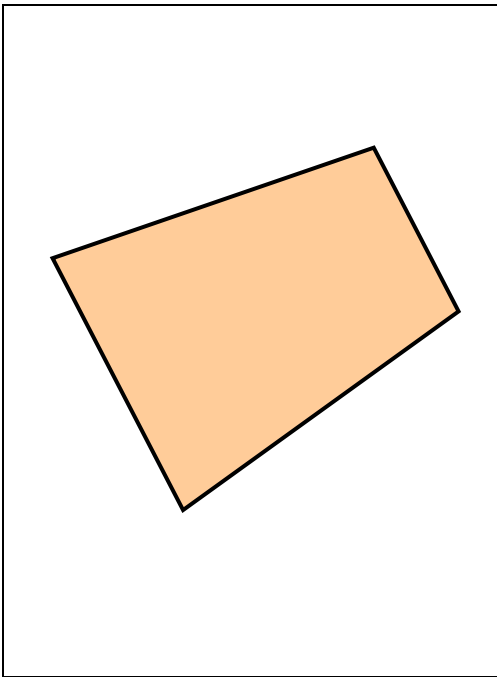


Figure 8:21. Trapezoid shape.



Figure 8:22. The vertebra affected by the lysis has a tendency to take on a trapezoid shape. This phenomenon is not pathognomonic for an isthmic spondylolisthesis, but is a point of reference that may alert the clinician to a spondylolisthesis.

Characteristics of the IVF in Spondylolisthesis

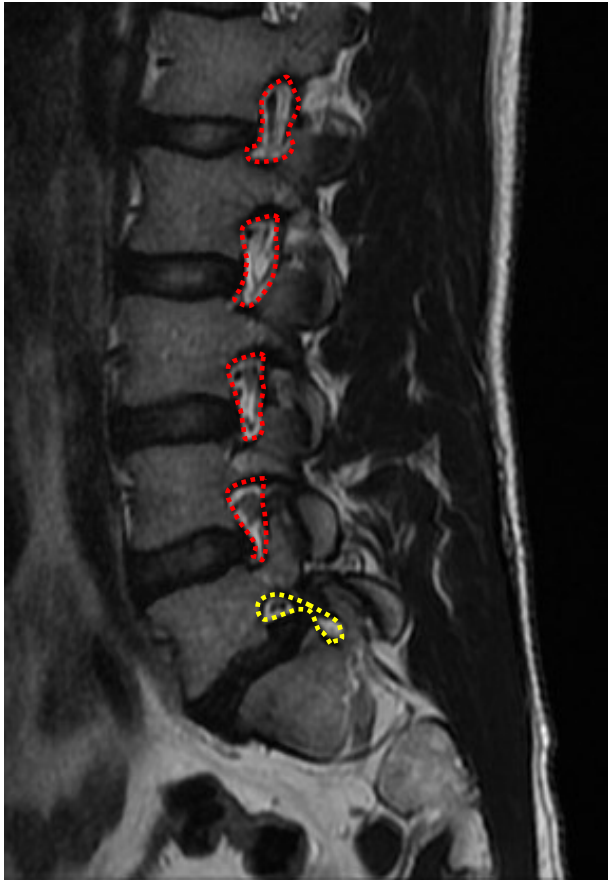


Figure 8:23. The shapes of the lumbar foramina are outlined by dotted lines. The red dotted lines show the normal peanut shaped foramina of the IVFs from L1-L5. The yellow dotted line shows the abnormal shape of the IVF as found in an isthmic spondylolisthesis.

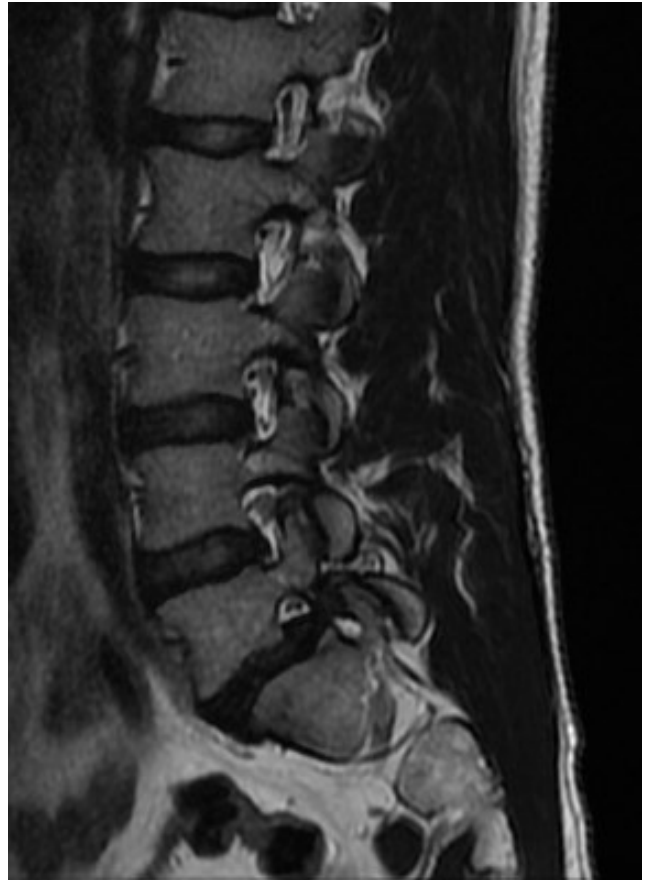
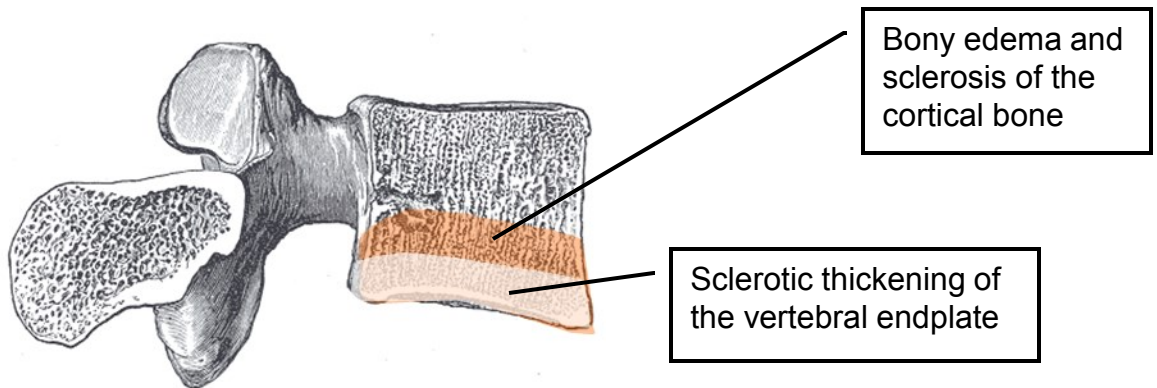


Figure 8:24. The same T2W sagittal image as figure 8:23 without the markers.

The normal outline of an intervertebral foramina (IVF) tends to be shaped like a peanut. Note the shape of the upper IVFs outlined in red in figure 8:23. In contrast, the L5-S1 IVF, outlined in yellow is contorted due to the anterior slippage of L5. This contortion is representative of a reduction in the size of the IVF resulting in foraminal stenosis. Figure 8:24 shows the same T2W sagittal image without the lines.

Bony Edema Secondary to Spondylolisthesis

Inflammatory and degenerative changes to the endplates and adjoining bone of the vertebra frequently accompany spondylolisthesis. These secondary degenerative changes are visible on MRI. The changes are named after the well-published radiologist Michael T. Modic. Figure 8:25 is a schematic revealing the appearance of Modic degenerative changes on MRI.



Henry Gray (1821–1865). *Anatomy of the Human Body*. 1918.

Figure 8:25. Modic schematic .

Bony edema, disc degeneration, and sclerotic changes to the vertebral endplates secondary to spondylolisthesis are clearly visible in figures 8:26 and 27.



Figure 8:26. T1W sagittal image.



Figure 8:27. T2W sagittal image.

Pars Defect



Figure 8:28. Bony edema of the pars interarticularis (yellow arrows) is visible on this T2 weighted axial image indicating a probable isthmic spondylolisthesis.

This T1W axial image reveals evidence of a pars defect. MRI reveals bony edema and soft tissue changes, but does not reveal discrete injury to bone. X-ray and CT are preferred for viewing bony injuries.

Characteristics of Spondylolisthesis

These images reveal what the anterior lip of L5 looks like on axial imagery (figure 8:29) as it extends past the margins of the sacrum. Figure 8:30 is a selected sagittal image of this patient. The blue line in figure 8:31 shows the level of the slice that was used to create figure 8:29. Incidentally the sagittal images display a perineural cyst affecting the S2 nerve root.



Figure 8:29. This axial image shows a “Napoleon hat sign.”



Figure 8:30. T2W sagittal supine image of the spondylolisthesis from figure 9:29.

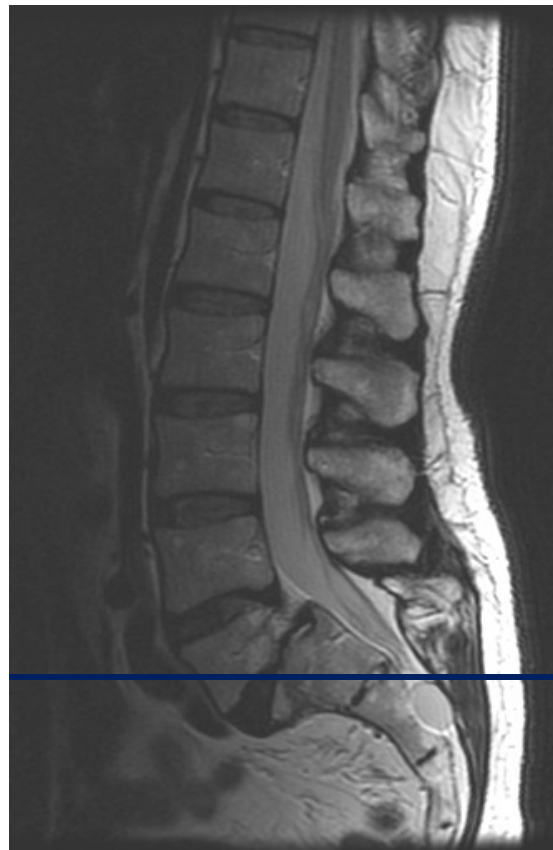


Figure 8:31. This image shows the level of the slice taken to make the image in figure 9:29.

Double Set of Zygapophyseal Joints

This axial image (figure 8:32) shows two sets of zygapophyseal (facet) joints. This unusual looking image is almost bizarre in appearance. By analyzing the sagittal views (figure 8:33) we can see that the L4-5 and L5-S1 facets are approximated by the anterolisthesis of L5 on S1. The red line across the sagittal image of figure 8:34 shows the MRI slice that was used to produce the axial image which is visualized in figure 8:32. By following the red line we can clearly see how the facets of L4-5 and L5-S1 could appear on the same axial slice.

This finding underscores the importance of comparing sagittal views with axial views to gain a complete perspective of the lumbar spine.



Figure 8:32. Axial image of an L5 isthmic spondylolisthesis. This unusual image shows four zygapophyseal joints.

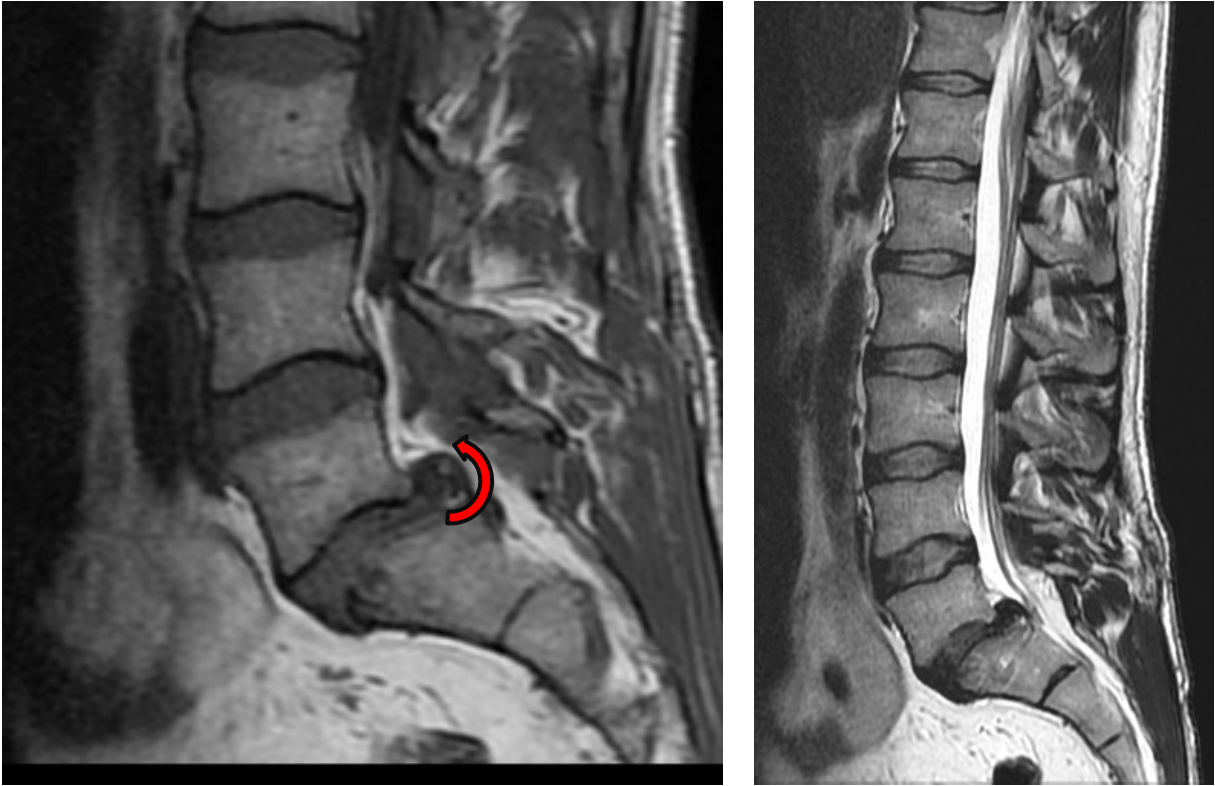


Figure 8:33. T2WI of L5 on S1 isthmic spondylolisthesis.



Figure 8:34. The red line shows the level of axial imagery that would show four zygapophyseal joints in one axial image (figure 8:32).

Disc Roll-up



Figures 8:35 and 8:36. L5-S1 spondylolisthesis with disc roll-up.

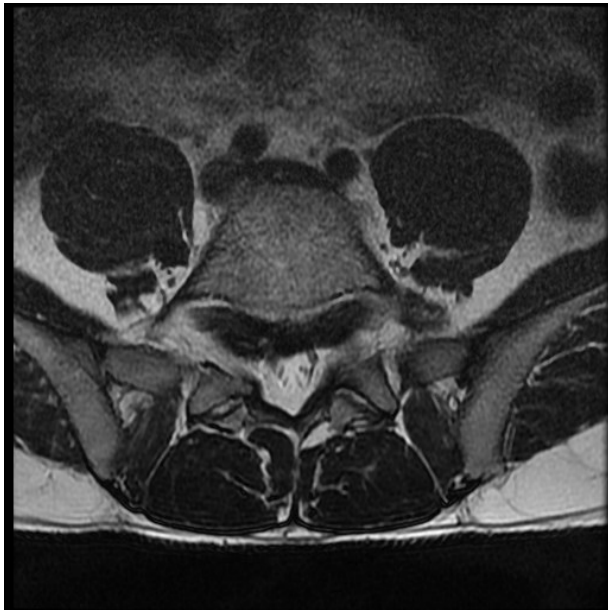


Figure 8:37. Axial T2WI of the spondylolisthesis disc roll-up shown on figures 8:35 and 8:36.

Another common finding in isthmic spondylolisthesis is the “rolling up” or “peeling” of the disc below the listhesis and less commonly “rolling down” of the disc above the spondylolisthesis. This disc migration can contribute to or cause a stenosis of the IVF. Some radiologists call this rolling up a “pseudo-bulge.”

Disc Roll-up

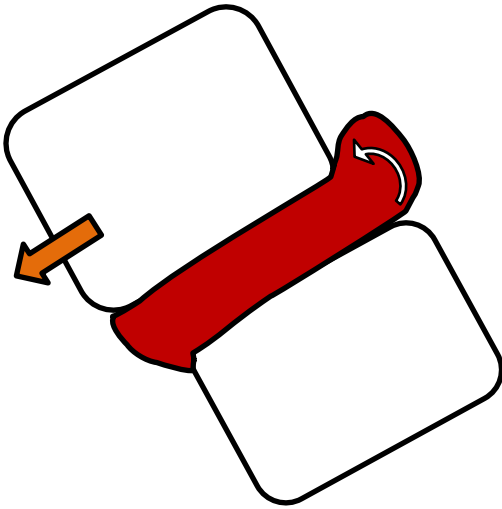


Figure 8:38 and 8:39. The disc roll-up phenomenon that occurs with a spondylolisthesis has unique characteristics on MRI. The disc tends to stay anchored to the lower segment, but will no longer stay in alignment with the vertebra that is listing forward.

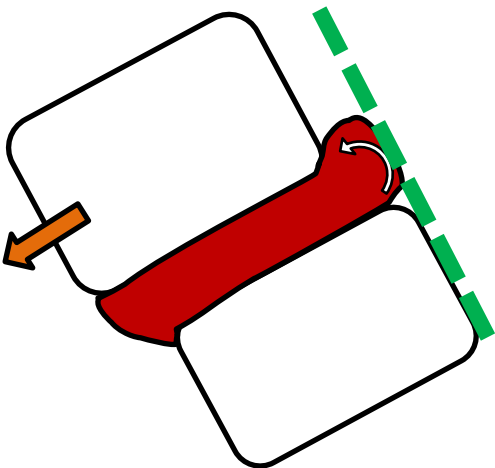


Figure 8:40 and 8:41. In sagittal imagery of a spondylolisthesis, a line drawn along the posterior body of the lower segment typically shows the disc to be in line with the inferior segment.

Disc Roll-up

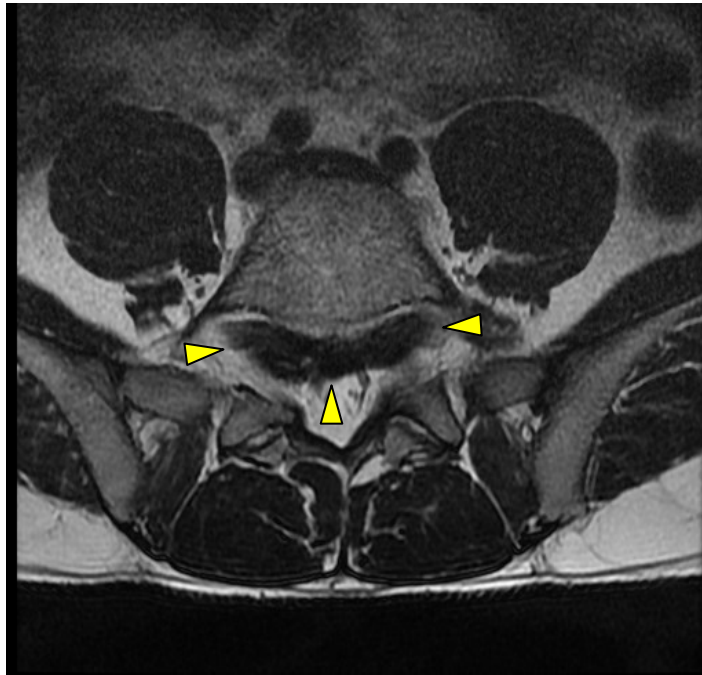


Figure 8:42. On axial imagery of a spondylolisthesis, it is not uncommon for the appearance of a pseudo-bulge or pseudo-disc herniation to be seen. Here is a pseudo-disc herniation of the L5-S1 disc.

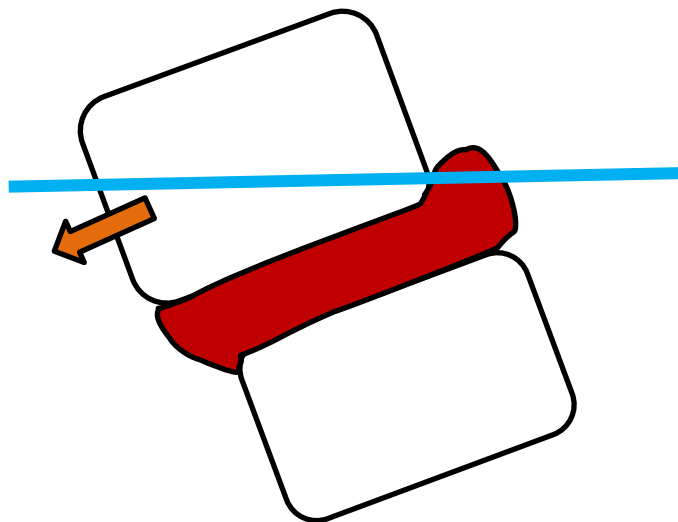


Figure 8:43. The phenomenon of a pseudo-bulge or pseudo-disc herniation occurs when the axial image slice (blue line in the schematic) contains the rolled up portion of the disc along with vertebra listing forward. By integrating axial and sagittal views, the clinician can more fully understand what occurs to the disc in a patient with spondylolisthesis.

Disc Roll-up and Roll-down



Figure 8:44. Sagittal PD FSE



Figure 8:45. Sagittal T1WI



Figure 8:46. Sagittal T2WI



Figure 8:47. Off-center sagittal T2WI slice from the same patient.

This series shows not only the L5-S1 disc rolling up, but the L4-L5 disc rolling down following an L5 anterolisthesis.

Secondary Characteristics of Isthmic Spondylolisthesis

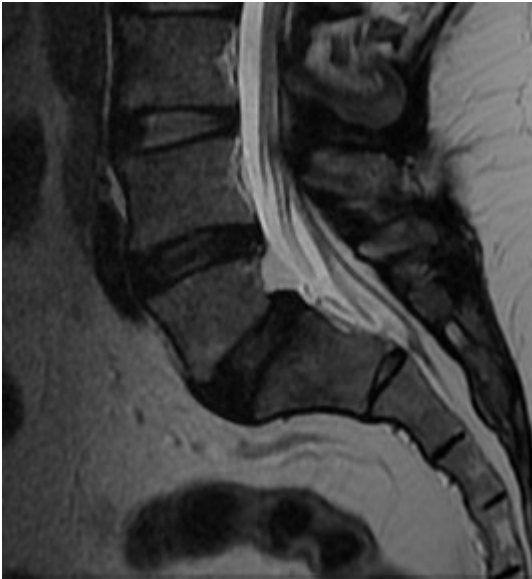


Figure 8:48 Sagittal T2WI reveals a trapezoid shaped L5 and an L5 anterolisthesis.

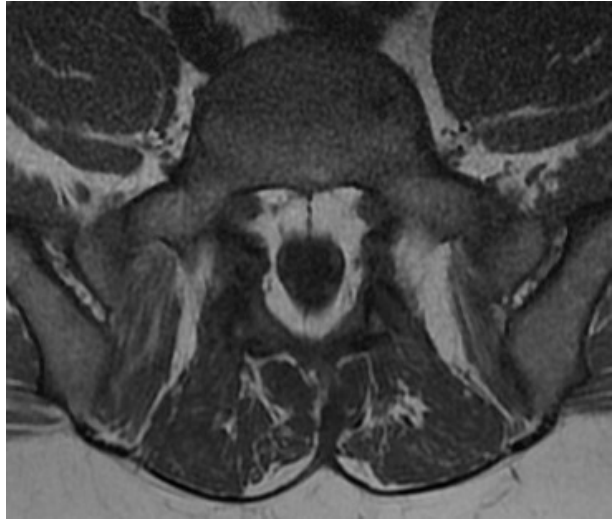


Figure 8:49. Axial T1WI. Note the elongated central canal.

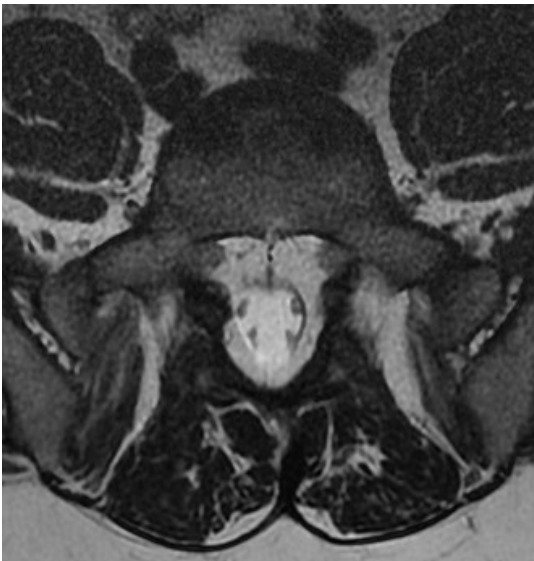


Figure 8:50. Axial T2WI revealing an expansion of the central canal.

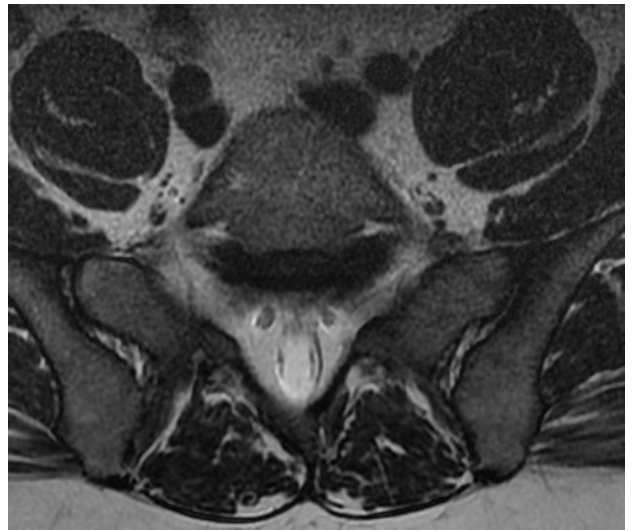


Figure 8:51. Axial T2WI showing the migration of the L5-S1 disc as it “rolls up” behind the body of L5.

These images of an isthmic spondylolisthesis reveal enlargement of the central canal, anterolisthesis, a trapezoid shaped L5, and a “roll-up” of the adjoining intervertebral discs.

Isthmic Spondylolisthesis with Synovial Cysts

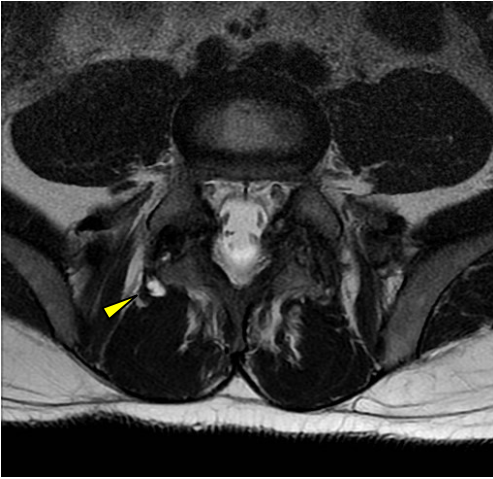


Figure 8:52. Axial T2W image of an isthmic spondylolisthesis show a synovial cyst arising from the inferior portion of the right L5-S1 facet .

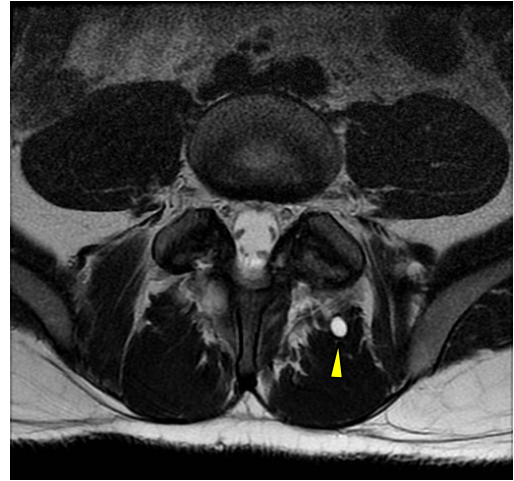
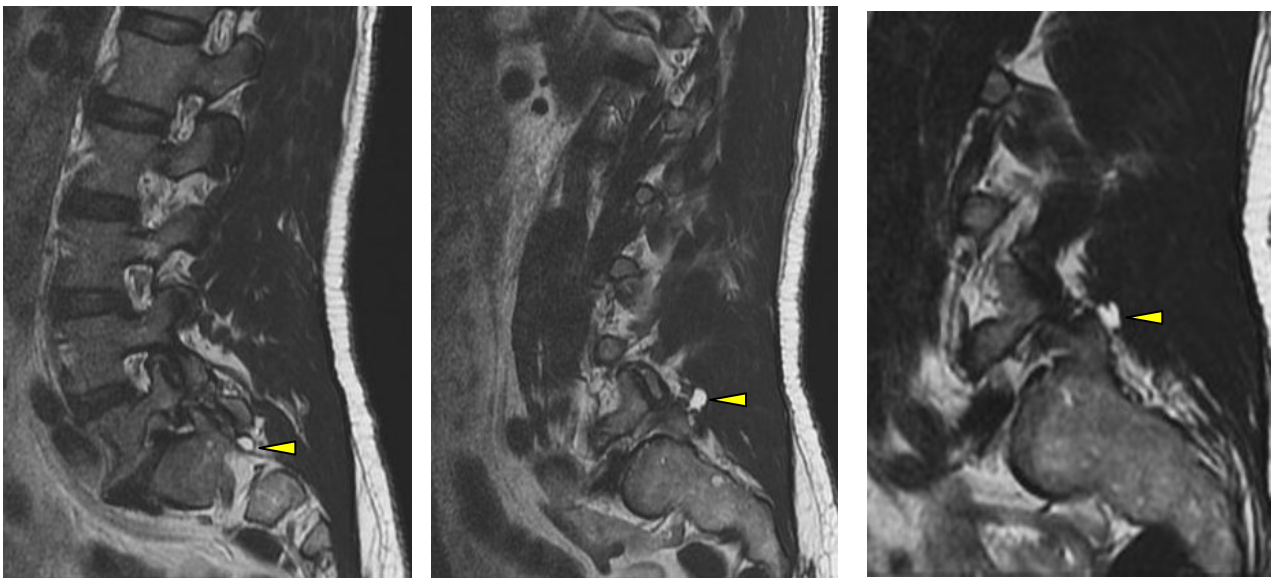


Figure 8:53. This axial T2W image of the same patient shows another synovial cyst arising from the right L5-S1 facet.



Figures 8:54-56. These sagittal T2 weighted images show three synovial cysts arising from the facets adjoining an L5 on S1 spondylolisthesis.

A spondylolisthesis can place stress on facets and cause effusion. The excessive fluid production (effusion) can result in a ballooning of the facet joint's capsule creating synovial cysts. When synovial cysts project posteriorly, they usually do not require intervention. However, if the synovial cyst projects into the central canal, intervention may be indicated. These images are all of the same patient whose L4-L5-S1 facets produced multiple synovial cysts projecting posteriorly.

Degenerative Spondylolisthesis

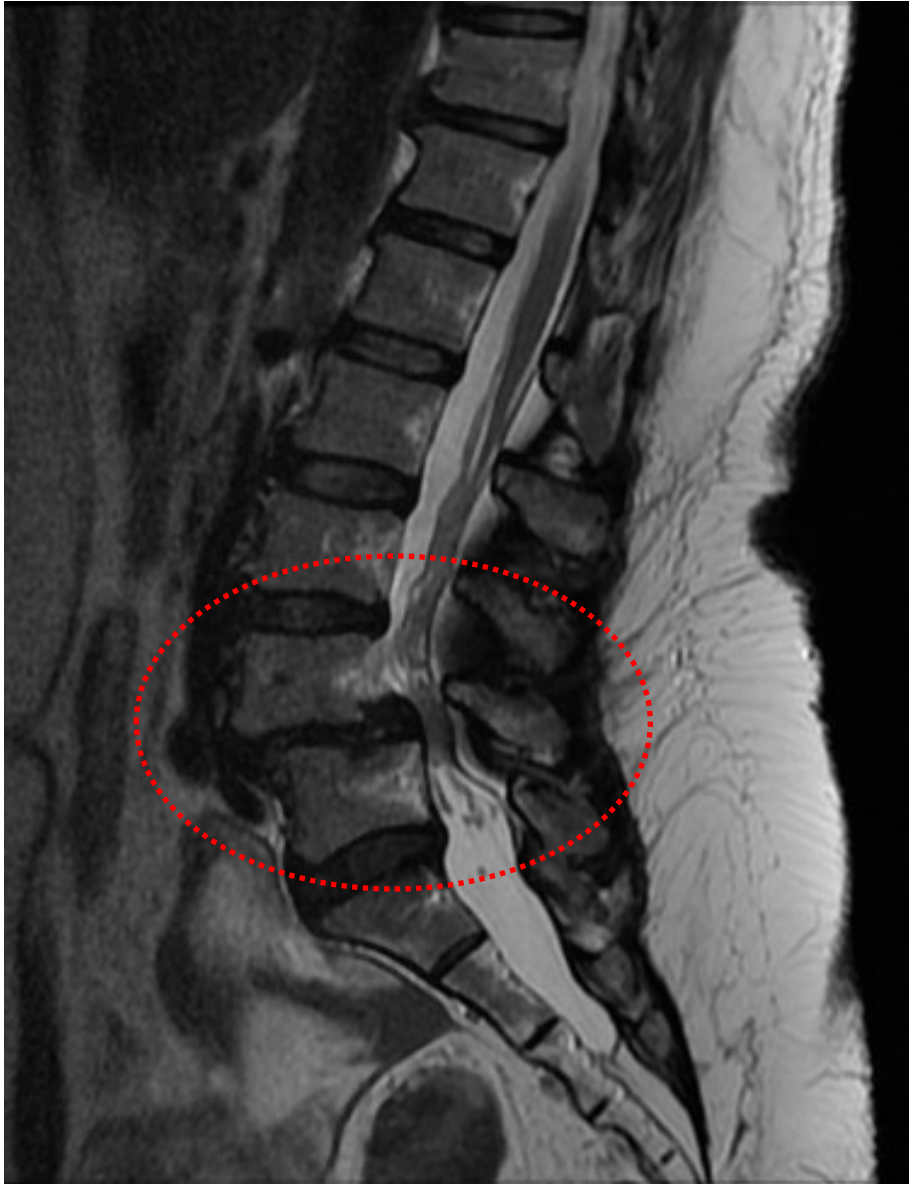


Figure 8:57. Degenerative spondylolisthesis of L4 on L5.

Degenerative spondylolistheses can also manifest this rolling up of the disc. Given the degeneration of the disc, anterolisthesis, facet hypertrophy, and ligamentous buckling and thickening, this phenomenon could be particularly contributory to creating central canal and foraminal stenosis.

Degenerative Spondylolisthesis



Figure 8:58. T2 weighted sagittal image of a degenerative spondylolisthesis.



Figure 8:59. A STIR sagittal image of the same patient.

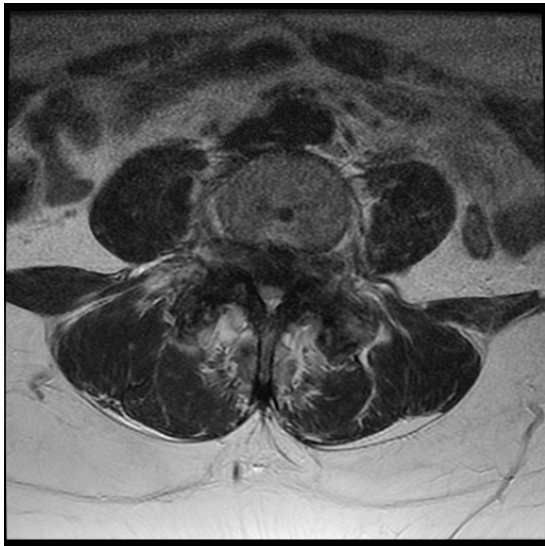


Figure 8:60. Erosion of facets and disc roll-up on a T2W axial image.

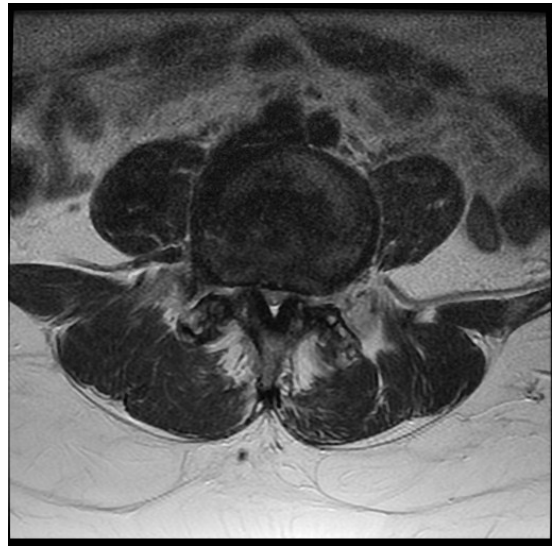


Figure 8:61. Central canal stenosis.

In this case the facets of L4-5 eroded and degenerated to such an extent that they could no longer function to restrain the anterior listhesis of L4 on L5. Though these images show severe anterior listhesis, it should be noted that this patient was lying on her back while the MRIs were taken. The following page has weight bearing flexion and extension views. Weight bearing plain films or upright MRIs are preferred methods of viewing the degree of listhesis (versus supine MRI images).

Degenerative Spondylolisthesis

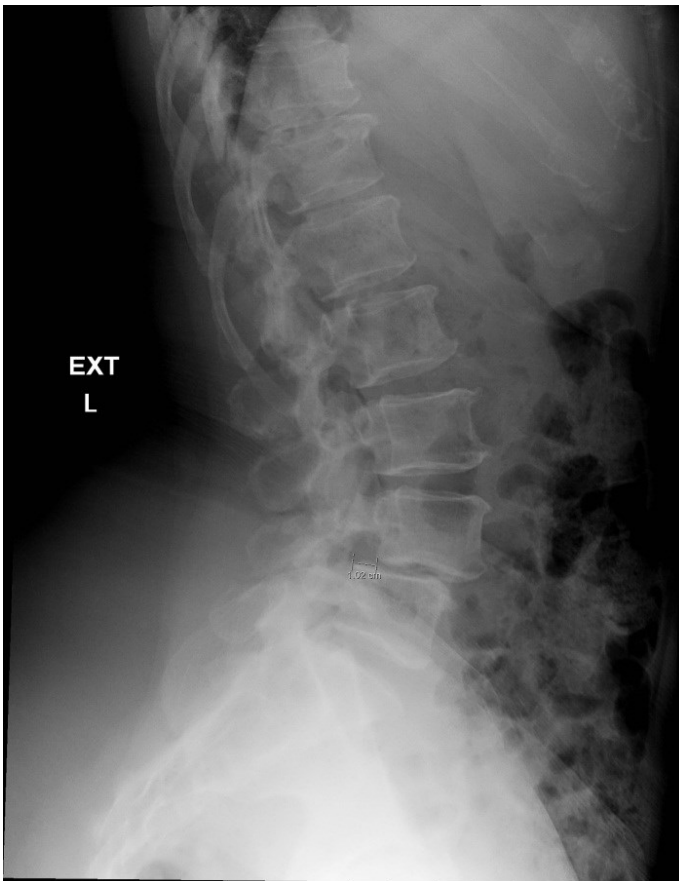


Figure 8:62. Plain film upright radiograph of the lumbar spine in extension.

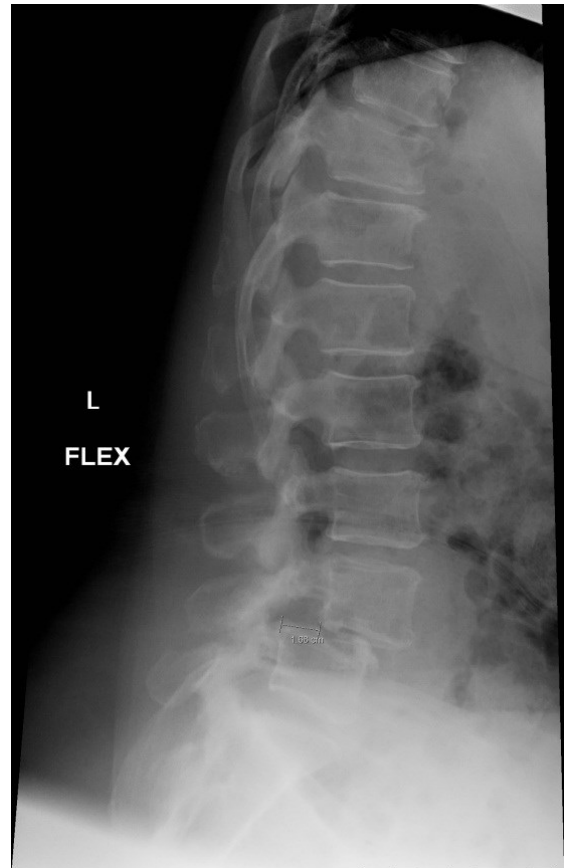


Figure 8:63. Plain film upright radiograph of the lumbar spine in flexion.

Recumbent lumbar MRI may reveal some of the effects of spondylolisthesis, but it is not the preferred medium for accessing degrees of listhesis or stability. Plain film radiographs taken standing upright, standing in extension, and standing in flexion are preferred over recumbent MRI for determining degrees of listhesis and stability. Upright and functional MRI are also valuable assessment tools.

Degenerative Spondylolisthesis



Figures 8:64 and 8:65. These two sagittal images display the characteristics that are common in degenerative spondylolisthesis. The image on the left presents facet degeneration of the L4 facets. The image on the right shows anterolisthesis, disc degeneration, disc rolling at the level of listhesis, and stenosis. Note that the posterior vertebral elements of L4 have maintained a normal relationship with the vertebral body; they have not come apart as is seen in most cases of listhesis secondary to spondylolysis.

Post-Surgical Re-Herniation and Spondylolisthesis



Figure 8:66. Post-surgical spondylolisthesis of L5 and re-herniation of the L4-L5 disc on a T2W sagittal image.



Figure 8:67. Post-surgical spondylolisthesis of L5 and re-herniation of the L4-L5 disc on a T2W axial image.

Upright, Functional, and Dynamic MRIs and Spondylolisthesis

One of the criticisms directed at using standard MRIs for evaluating spondylolisthesis is that the patient is lying supine during the MRI. Lying supine will allow a mobile segment to settle into a lower state of displacement. One study of 510 patients with lower back pain revealed that supine MRI missed 18.1% of spondylolisthesis cases that were observed in dynamic (flexion) MRIs. As more upright and functional MRI units are made available, this diagnostic medium may replace the neutral/supine MRI for visualizing functional and anatomical disruptions of the lumbar spine.



Figure 8:68. T2W sagittal image taken while lying recumbent in a conventional MR tube. (Image provided by FONAR Corporation and used with permission.)



Figure 8:69. The same patient from figure 8:68 was re-imaged in an upright MRI. This image clearly reveals an anterior listhesis of L3 on L4 that was not visible on the recumbent MRI. (Image provided by FONAR Corporation and used with permission.)

Isthmic Spondylolisthesis with IVF Occlusion

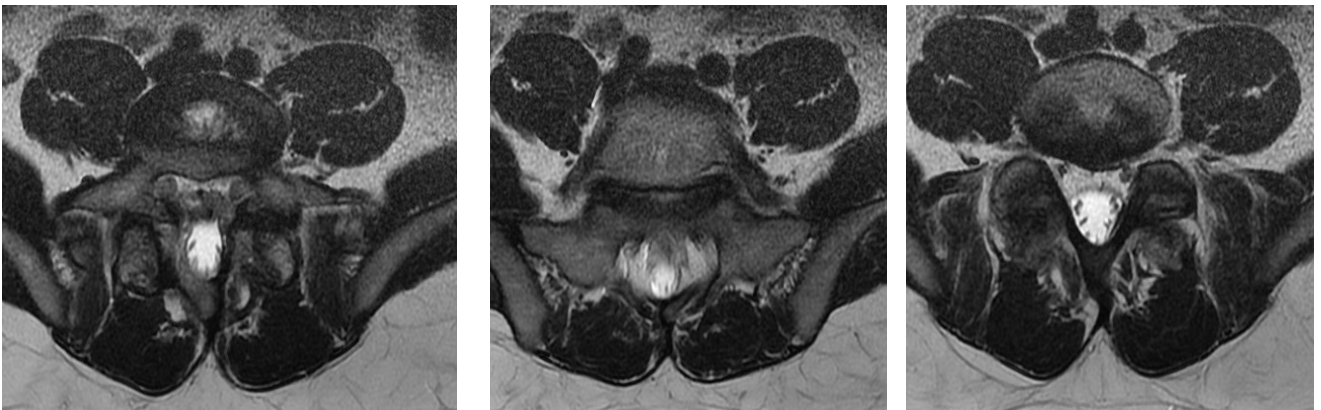


Figure 8:70. Plain film radiograph.



Figure 8:71. T2 weighted sagittal showing significant disc rolling of the L4-5 and L5-S1 discs.

This case presents an isthmic spondylolisthesis in a patient with transitional anomalies of the lumbosacral anatomy. Of particular interest is the amount of disc roll-up of the L5-S1 disc and disc roll-down of the L4-L5 disc. The L5-S1 intervertebral foramina is almost completely occluded.



Figures 8:72, 73, and 74. T2W axial revealing transitional anomalies of the lumbosacral anatomy.

Isthmic Spondylolisthesis with IVF Occlusion



Figure 8:75. Disc rolling at mid-central canal.



Figure 8:76. L5-S1 intervertebral foramina occlusion.

These T2 weighted sagittal images show the significant disc rolling above and below the L5 vertebra. Figures 8:76 and 8:77 demonstrate severe IVF occlusion of the L5-S1 IVF from the listhesis and the L5-S1 disc.

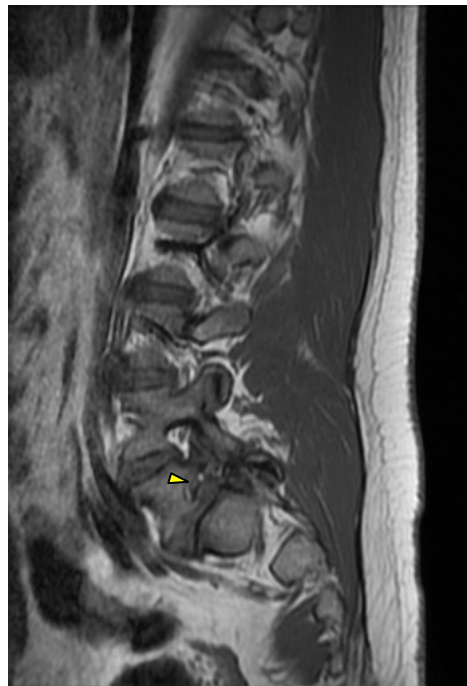


Figure 8:77. L5-S1 intervertebral foramina occlusion.

Suggested Reading

Antoniades SB, Hammerberg, KW, DeWald, RL. Sagittal plane configuration of the sacrum in spondylolisthesis. Spine: 1 May 2000. Volume 25, Issue 9, pp 1085-1091.

Lattig F, Fekete Truncal flexion, Grob D, Kleinstuck FS, Jeszensky D, Mannion AF. Lumbar facet joint effusion in MRI: a sign of instability in degenerative spondylolisthesis? Eur Spine Journal. 2012 Feb; 21 (2):276-81. Epub 2011 Sep 20.

Meyerding HW: Spondylolisthesis. Surg Gynecol Obstet 54:371-377, 1932.

McPhee B: Spondylolisthesis and spondylolysis, in Youmans JR (ed): Neurological Surgery: A Comprehensive Reference Guide to the Diagnosis and Management of Neurosurgical Problems, ed 3. Philadelphia: WB Saunders, 1990, Vol 4, pp 2749-2784.

Sim GPG, Vertebral contour in spondylolisthesis. British Journal of Radiology (1973) 46, 250-254 .

<http://bjr.birjournals.org/cgi/content/abstract/46/544/250>

Cramer G, Darby S (2013). Basic and clinical anatomy of the spine, spinal cord, and ANS (third edition). Elsevier Mosby.

Marchiori D (2013). Clinical imaging: with skeletal, chest and abdomen pattern differentials (third edition). Mosby.

Atlas SW. (2008). Magnetic resonance imaging of the brain and spine (forth edition). Lippincott Williams & Wilkins.

Ross JS et al. (2010). Diagnostic imaging spine (second edition). Amirsys Inc.

Spondylosis

9



Spondylosis

Spondylosis is a term that literally interpreted from Latin means *condition of the spine*. It refers to degenerative osteoarthritis of the spine. It is a broad, vague term that covers many findings. For that reason it has more value in radiology reports than in clinical diagnosis. Spondylosis is common and frequently present in patients without symptoms. It is characterized by hypertrophic osteophytic changes, desiccation of the discs, loss of disc height, ligamentous instability, facet hypertrophy, facet imbrication, and bony remodeling. This series of images shows a moderately severe spondylitic lumbar spine. The dark disc spaces in these T2WI indicate a loss of hydration (desiccation) of these discs. Disc bulges, hypertrophic facets, and thickening of the ligamentum flavum all contribute to stenosis of the central canal, lateral recess, and the foramina.



Figures 9:1 and 9:2. T2W sagittal images of moderately severe spondylosis of the lumbar spine.

IVF Encroachment



Figure 9:3. T2 weighted sagittal image revealing IVF encroachment of the L3-4, L4-5, and L5-S1 segments.



Figure 9:4. Another T2 weighted sagittal image revealing IVF encroachment of the L4-5 and L5-S1 segments.

Spondylosis can result in intervertebral foraminal (IVF) encroachment/stenosis. These two sagittal images show occlusion of lumbar IVFs resulting from degenerative osteophytes.

Spondylosis



Figure 9:5. Degeneration of intervertebral discs can cause slackening of the spinal ligaments which can lead to degenerative spondylolisthesis. Note the anterolisthesis of L3 and L4 and the retrolisthesis of L2.



Figure 9:6. The body responds to slackened ligaments by producing osteophytes as seen particularly at the level of L4 and L5.

Spondylosis

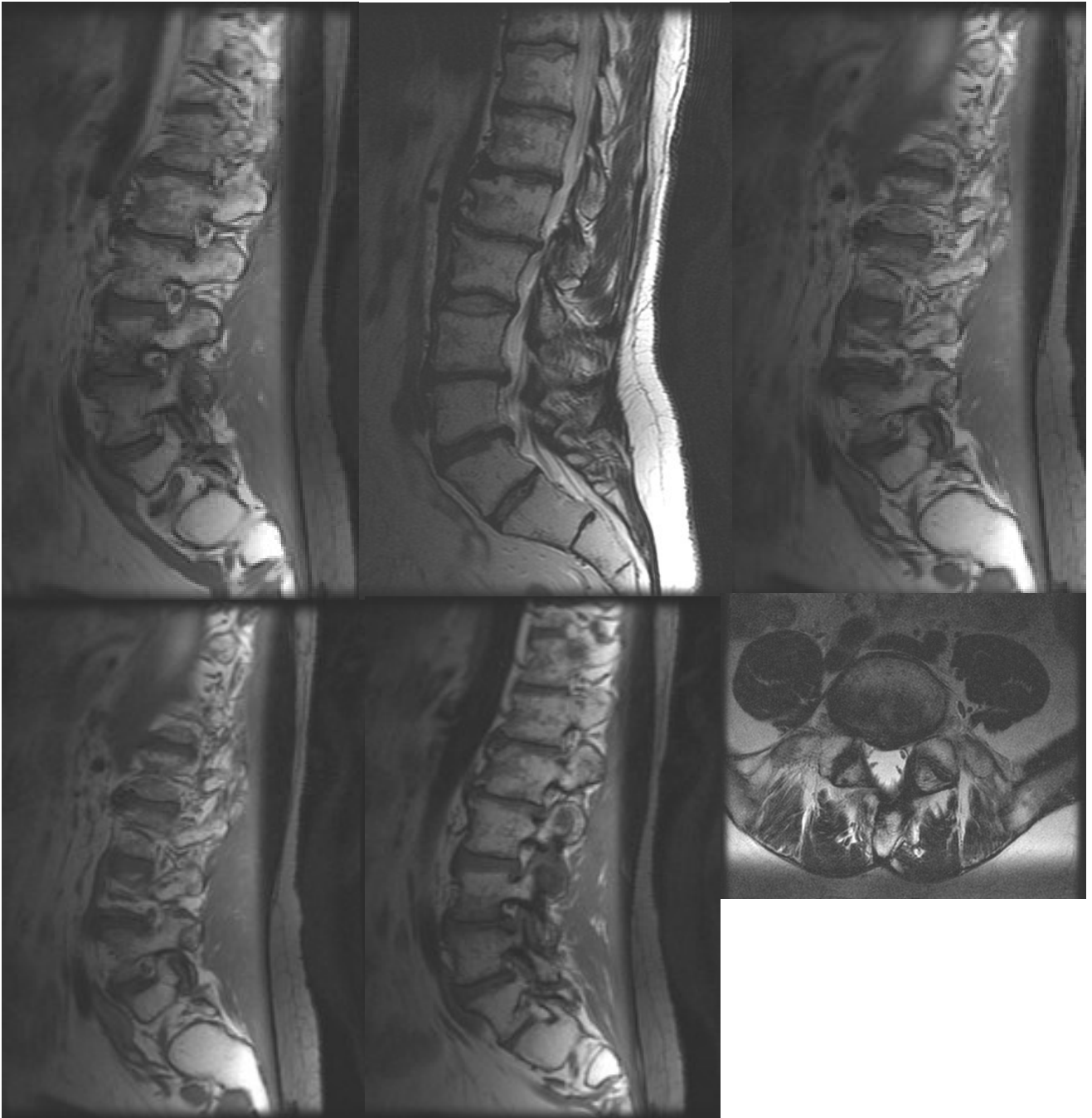


Figure 9:7. Multiple levels of degeneration and disc bulges. L4 has a degenerative spondylolisthesis.



Figure 9:8. Hypertrophic changes of the vertebral bodies and facets.

Spondylosis



Figures 9:9-14. Premature degenerative changes in a thirty-eight year-old athletic man. Note the endplate changes, fatty infiltration of bone, the disc degeneration, IVF encroachment, and osteophytic spurring.

Suggested Reading

Heithoff KB, Gundy CR, Burton CV, Winter RB, Juvenile discogenic disease. Spine. 1994 Feb 1;19 930 335-40.

Resnick D, Niwayama G, Guerra J et-al. Spinal vacuum phenomena: anatomical study and review. Radiology. 1981;139 (2): 341-8.

Resnick D, Kransdorf MJ (2005). Bone and joint imaging. W B Saunders Co.

Cramer G, Darby S (2013). Basic and clinical anatomy of the spine, spinal cord, and ANS (third edition). Elsevier Mosby.

Marchiori D (2013). Clinical imaging: with skeletal, chest and abdomen pattern differentials(third edition). Mosby.

Central Canal Stenosis

10



Central Canal Stenosis

To fully understand what a central canal stenosis is, we need to understand what the central canal is and what is normal. The central canal is the protective conduit that protects the spinal cord and (from L1-L2 caudally) the cauda equina. The bony arch of the central canal usually does not change size. Stenosis usually occurs at the levels of the intervertebral disc where the disc bulges. Facet hypertrophy and ligament thickening can combine to narrow the central canal. The length of the pedicles is important for maintaining adequate canal size. Pedicles can be congenitally short or asymmetrical in length, contributing to stenosis.

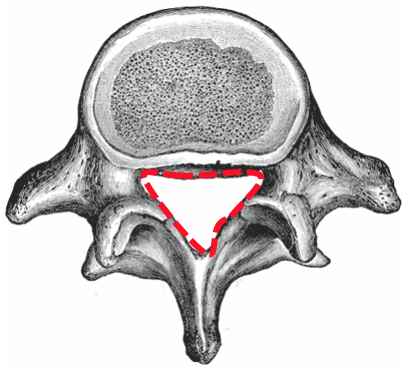


Figure 10:1. The posterior border of the vertebral body along with the arch of the pedicles and lamina comprise the bony portion of this protective conduit. The central canal is outlined with a red dotted line.

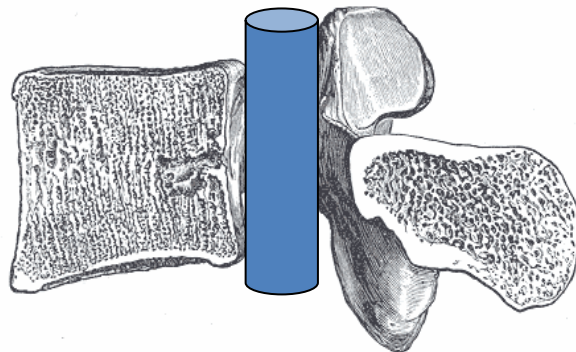


Figure 10:2. A transection of a vertebral segment showing the canal's position within the vertebra.



Figure 10:3. A T2 weighted axial revealing a widely patent central canal at L5.

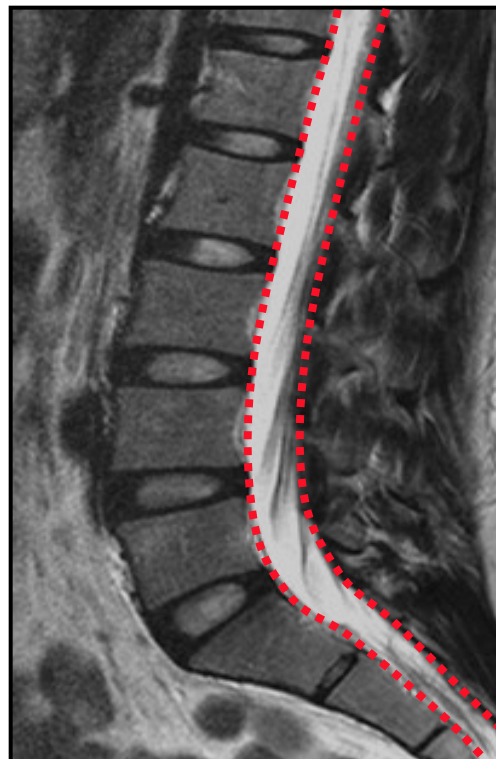


Figure 10:4. A T2 weighted sagittal image of a patent central canal traveling the length of the lumbar spine.

Central Canal Stenosis

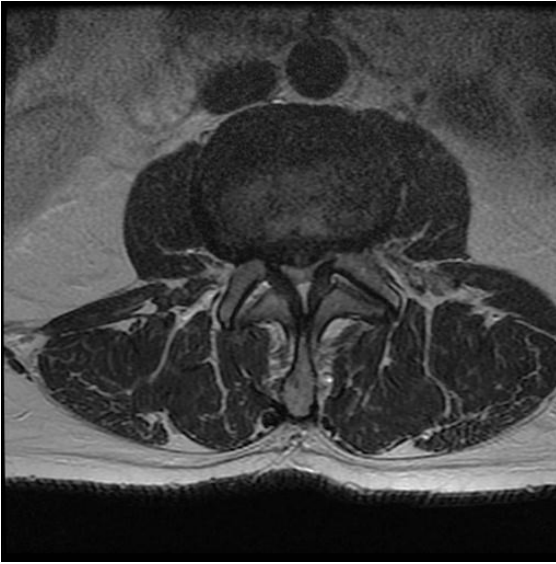


Figure 10:5. Stenosis at the L2-3 disc space. Note the congenitally narrowed canal, ligamentum flavum hypertrophy, and facet hypertrophy.



Figure 10:6. Even in patients with central canal stenosis, the canal is usually patent at the middle of the vertebral body.



Figure 10:7. Note that stenosis typically occurs at the vertebral interspace where a disc bulge, ligamentum flavum hypertrophy, and facet hypertrophy combine to narrow the central canal. Note the canal narrowing at L1-L2, L2-L3, and L3-L4.

In patients with stenosis the entire canal is usually not stenotic. Only the intervertebral region where the combination of disc, facet hypertrophy, and ligamentum flavum hypertrophy or enfolding combine to narrow the central canal. This can be compounded by a degenerative spondylolisthesis.

Central Canal Stenosis

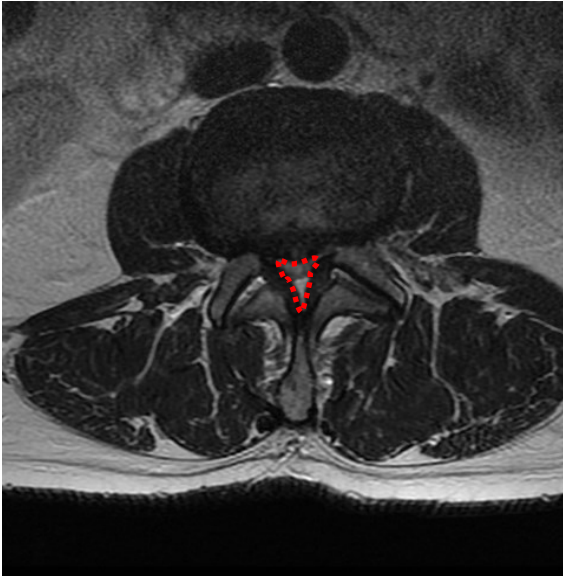


Figure 10:8 and 10:9. Sagittal T2WI revealing a stenosis at the L2-L3 section of the canal and a herniation at L5-S1.

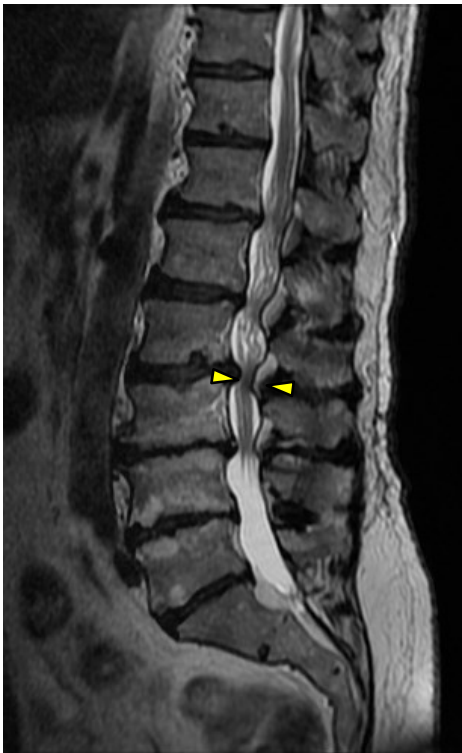


Figure 10:10 and 10:11. Sagittal T2WI displays a stenosis at the L2-L3 level of the canal.

These images expose a lumbar stenosis at L2-L3 arising from a congenitally narrow canal, ligamentum flavum hypertrophy, an L2-L3 disc bulge, and facet hypertrophy.

Central Canal Stenosis



Figure 10:12. Normal lumbar central canal. This T2 weighted axial image clearly demonstrates a patent central canal.

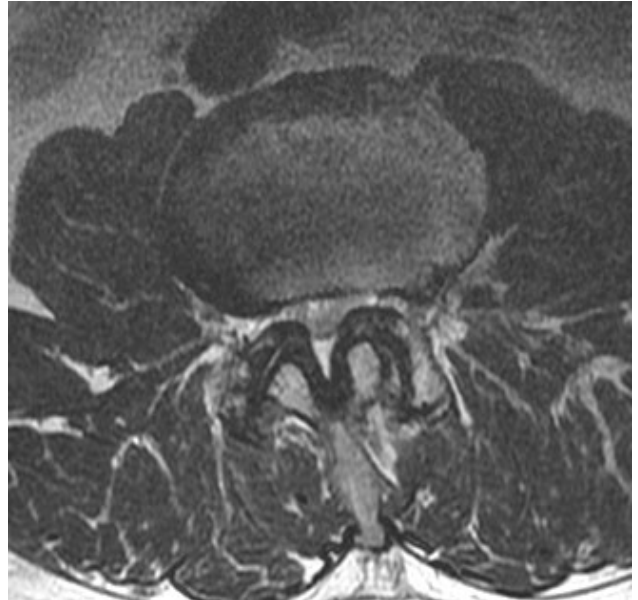


Figure 10:13. Lumbar stenosis of the central canal and lateral recesses secondary to facet hypertrophy and ligamentum flavum hypertrophy.

Spondylosis may result in degenerative stenosis. The combination of decreased disc height, enfolding and thickening of spinal ligaments, and bony hypertrophy contribute to this slowly progressing condition. The image on the left (figure 10:12) shows a widely patent central canal, lateral recesses (subarticular zone), and intervertebral foramina. The exiting nerve roots are suspended in a supple cradle of fat.

The image on the right (figure 10:13) reveals a moderately severe stenosis that affects the central canal, lateral recesses, and foramina. The point at which a narrowing of the canal becomes a stenosis is imprecise and is usually left to the interpretation of the radiologist.

Central Canal Stenosis



Figure 10:14. This T2W sagittal image shows an L4-5 central canal stenosis that is caused by the convergence of a disc bulge, disc degeneration, degenerative spondylolisthesis of L4 on L5, ligamentum flavum hypertrophy, and facet hypertrophy.

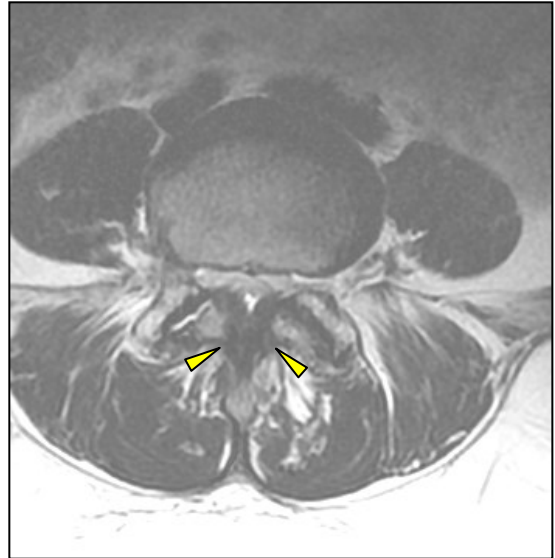


Figure 10:15. This T2W axial image shows significant ligamentum flavum hypertrophy and facet hypertrophy from degeneration.

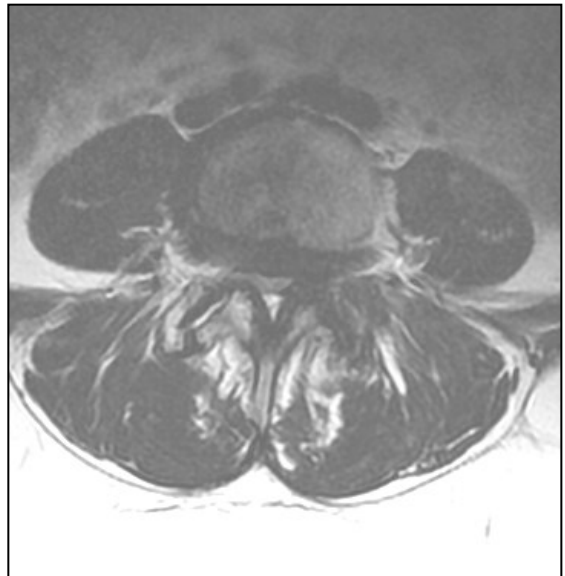


Figure 10:16. Disc bulging at L4-L5 compounds the narrowing effects of the hypertrophic changes of the ligamentum flavum and the zygapophyseal joints.

A Case of Complicated Central Canal Stenosis

This case represents a “sampler pack” of comorbid conditions that contribute to this central canal stenosis. This case compiles ligamentum flavum hypertrophy, a synovial cyst, degenerative spondylolisthesis, disc bulging, facet hypertrophy, and epidural lipomatosis to narrow the central canal. Figures 10:17 to 10:25 are all images taken from the same case.



Figure 10:17. This T2W sagittal image reveals a stenosis of the central canal caused by an accumulation of various factors. This image reveals a degenerative spondylolisthesis, ligamentum flavum hypertrophy, facet hypertrophy, an L4-L5 disc bulge, and a large synovial cyst at L4-L5.

A Case of Complicated Central Canal Stenosis (continued)



Figure 10:18. A facet that is inflamed and effused (white arrow) can give rise to a synovial cyst (red arrow). This synovial cyst occupies a significant portion of the central canal.

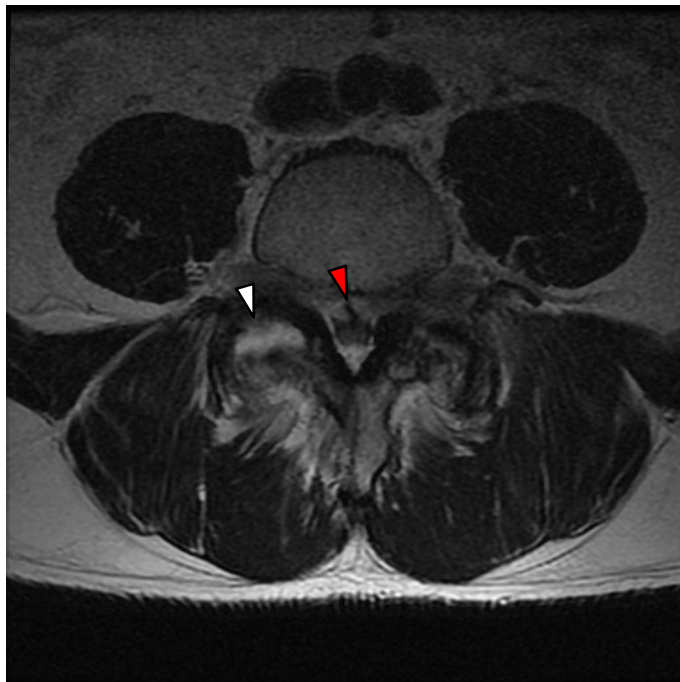


Figure 10:19. Facetal effusion denoted by the white arrow and spinal epidural lipomatosis denoted by the red arrow.

A Case of Complicated Central Canal Stenosis (continued)



Figure 10:20. Consolidation of the thecal sac with no visible stenosis .

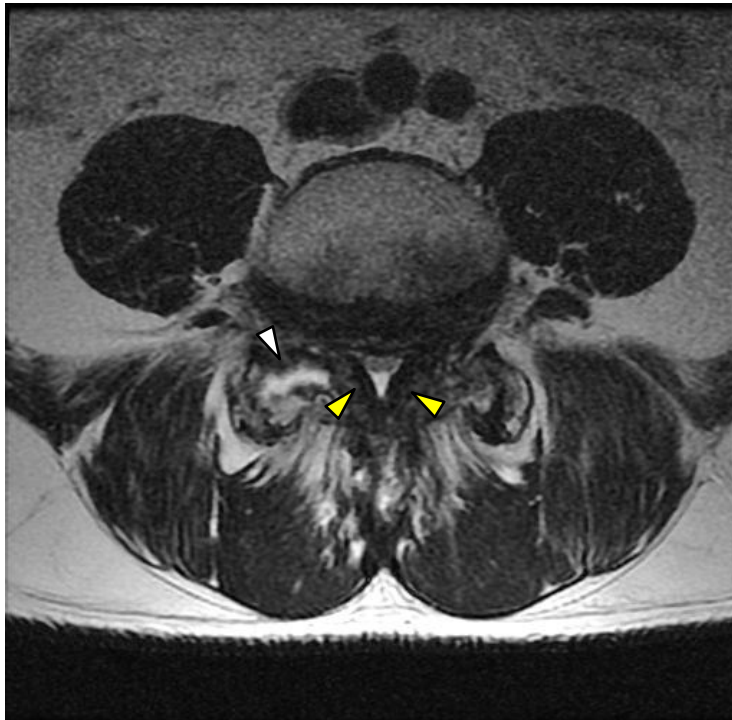


Figure: 10:21 Central canal stenosis from facet hypertrophy, ligamentum flavum hypertrophy (yellow arrows), and a disc bulge. The white arrow points to a facet effusion.

A Case of Complicated Central Canal Stenosis (continued)



Figure 10:22. T2WI showing spinal epidural lipomatosis (excessive fat deposition) encroaching into the central canal.

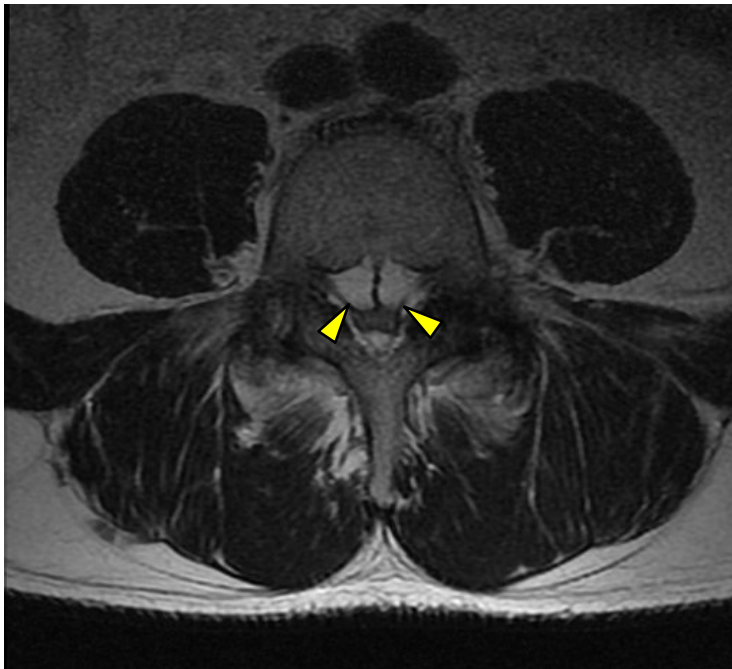


Figure 10:23. The adjoining axial slice reveals even more encroachment/central canal stenosis. Additional fat posteriorly contributes to the canal narrowing.

A Case of Complicated Central Canal Stenosis (continued)



Figure 10:24. T2W sagittal image. The yellow arrow points to a synovial cyst that contributes to central canal narrowing.

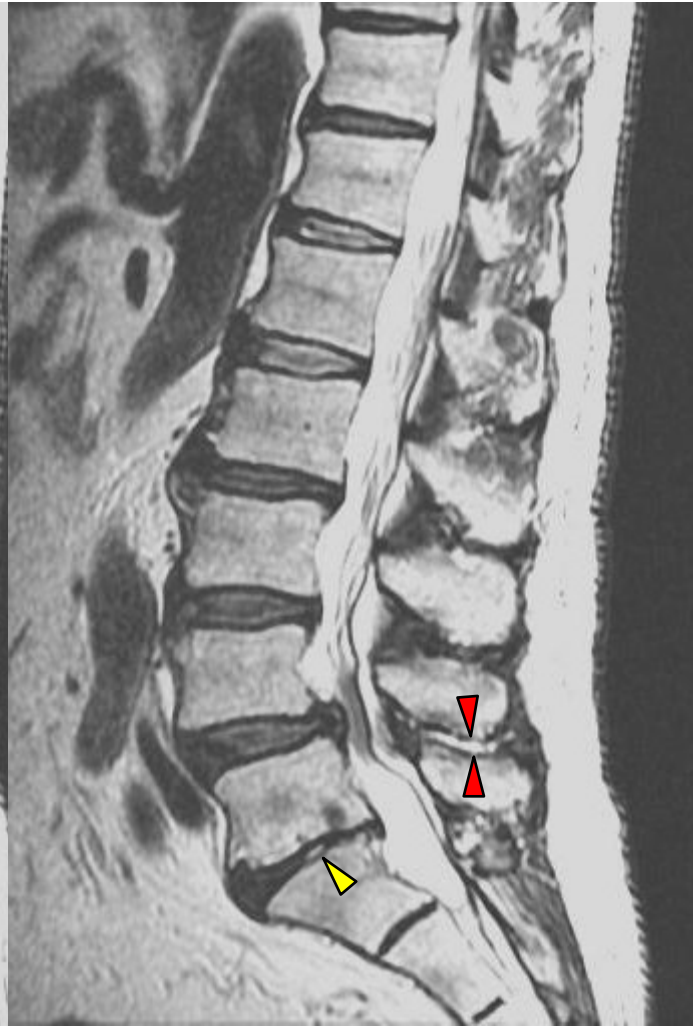


Figure 10:25. The yellow arrow points to a high intensity zone (white on T2WI), probably depicting an annular tear. The red arrows point to increased fluid (effusion) in the interspinous bursa.

Narrowed Central Canal from Enfolding of the Ligamentum Flavum

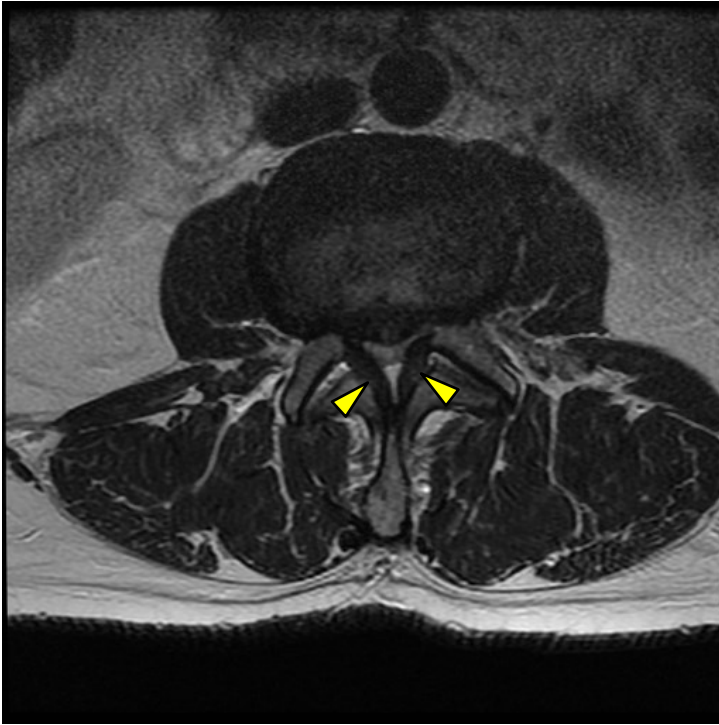


Figure 10:26. Redundant ligamentum flavum combines with a disc bulge and facet hypertrophy to create a central canal stenosis visible in this T2 weighted axial image of the L2-L3 interspace. Associate this image with the sagittal image in figure 10:27.

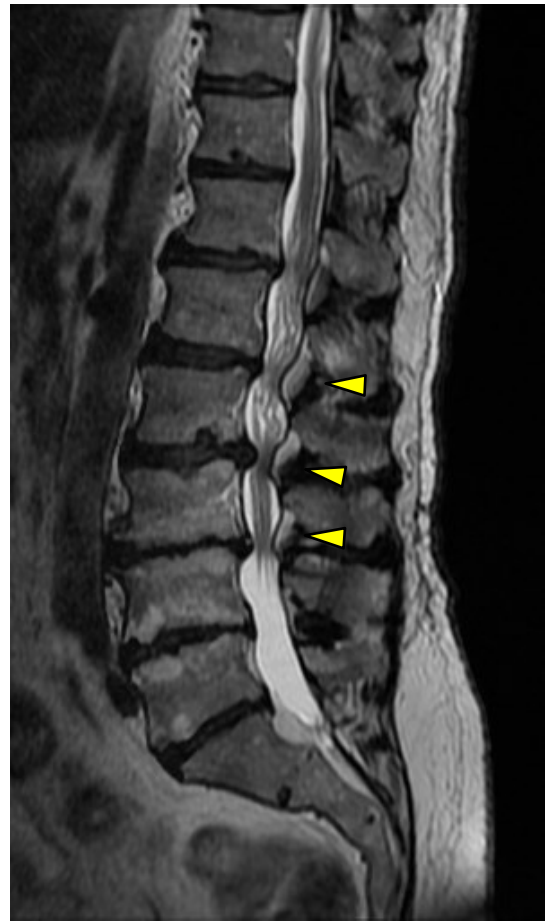


Figure 10:27. Redundant ligamentum flavum in T2 weighted sagittal image. Note the stenosis at L2-L3 and L3-L4.

A developmentally narrowed central canal, usually attributed to congenitally short pedicles, predisposes a spine to develop a central canal stenosis as normal age-related degeneration contributes to a narrowing of the canal. These age-related changes include ligamentum flavum enfolding (redundant ligamentum flavum) and hypertrophy, facet hypertrophy, and disc bulges.

Congenitally Narrowed Central Canal

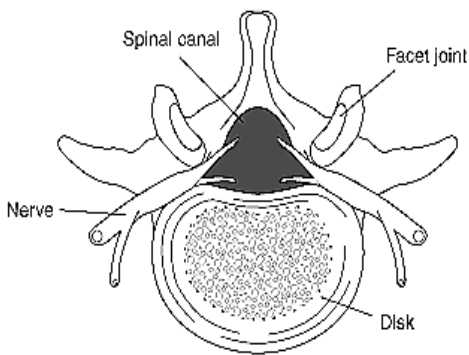


Figure 10:28. Normal lumbar central canal.

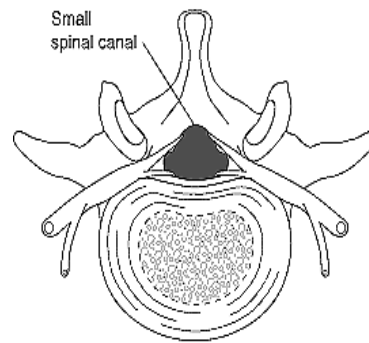


Figure 10:29. A congenitally small canal.

A developmentally narrowed central canal tends to produce stenosis symptoms earlier and with a more profound clinical presentation than a more patent canal. A congenital canal tends to have a more rapid onset of stenosis with less spinal degeneration. The difference between a congenitally narrowed canal and a stenosis is that a stenosis refers to a focal narrowing of the canal, whereas a congenitally narrowed canal is the generalized narrowing of the canal. Shortened pedicles are frequently blamed for congenital narrowing of the canal.

Clinically, patients with congenital stenosis will report with multiple levels of stenosis, and they present with symptoms at a younger age.

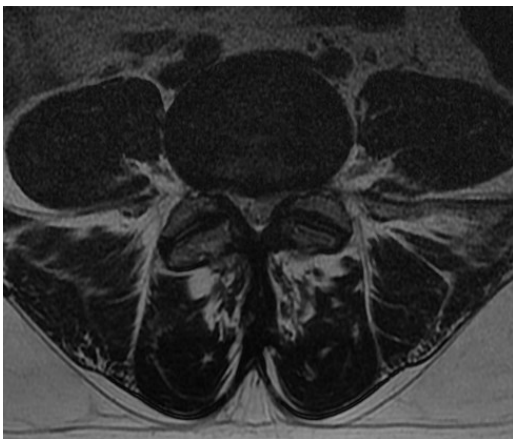


Figure 10:30. A congenitally narrowed central canal in a 32 year-old female. Her stenosis is compounded by space occupying hypertrophy of the facets.



Figure 10:31. A congenitally narrowed central canal in a 23 year-old male.

Figures 10:28, and 10:29 are copyright free images acquired through U.S. Department of Health and Human Services Public Health Service National Institutes of Health National Institute of Arthritis and Musculoskeletal and Skin Diseases NIH Publication No. 05-5282 September 2005.

Stenosis



Figure 10:32. Normal lumbar central canal. This T2 weighted axial image clearly shows a patent central canal.



Figure 10:33. A congenitally narrowed central canal in a 32 year-old female. Her stenosis is magnified by space occupying hypertrophy of the facets.

These two images show a contrast in central canal size. The image in figure 10:32 shows a widely patent central canal with ample room for the spinal nerves of the cauda equina. In stark contrast is the image in figure 10:33; it has a tight canal that has little room to spare for the contents of the thecal sac.

Suggested Reading

Clark K. Significance of the small lumbar spinal canal: cauda equina compression syndromes due to spondylosis. 2. Clinical and surgical significance. J Neurosurg 1969 Nov;31 (5):495-8.

Cramer G, Darby S (2013). Basic and clinical anatomy of the spine, spinal cord, and ANS (third edition). Elsevier Mosby.

Marchiori D (2013). Clinical imaging: with skeletal, chest and abdomen pattern differentials(third edition). Mosby.

Atlas SW. (2008). Magnetic resonance imaging of the brain and spine (forth edition). Lippincott Williams & Wilkins.

Ross JS et al. (2010). Diagnostic imaging spine (second edition). Amirsys Inc.

Bogduk N. (2012). Clinical and radiological anatomy of the lumbar spine. Churchill Livingstone.

Fractures

11



Lumbar Fracture

Identifying the bony extent of spinal fractures is best done with computed tomography (CT), though initial screening is frequently performed with plain film radiology. MRI is a good adjunct to CT and plain film radiographs.

MRI has the advantage of clearly identifying soft tissue integrity or damage. It can also provide insight into the degree of bony edema and the formation of epidural hematomas.

When a spine fractures, fragments of bone may be pushed backwards into the spinal canal or cord. This is known as retropulsion. The retropulsion of bony fragments into the canal and possibly even into the cord is a great concern in compression fractures of the spine. Retropulsion is most clearly seen on CT, but the effect of a retropulsed fragment on soft tissues such as the cord is more evident in an MRI.

The next few pages will present a gallery of images revealing common presentations of vertebral fractures.

Compression Fracture



Figure 11:1. Compression fracture in a 91 year-old man seen on a T2W sagittal image.

Compression fractures occur in healthy individuals who experience a traumatic event or more commonly after petite trauma in osteoporotic patients, as seen in this MRI of a 91 year-old male. Back pain is the most common symptom associated with compression fractures. Structurally an increased spinal kyphosis frequently occurs. Compression fractures usually result in loss of height. The pain of a stable compression fracture usually abates in 8-12 weeks.

Compression Fracture



Figure 11:2. Stable compression fracture of L1 with no retropulsion of bone posteriorly. Endplate disruptions, intravertebral herniations (AKA Schmorl's nodes) and Modic changes within the cancellous bone (AKA trabecular or spongy bone) of the L1 vertebra.

Contortion of the Aorta Secondary to Compression Fractures



Figure 11:3. Multiple level compression fractures. The reduction in spinal column height of these fractures resulted in a buckling of the aorta.

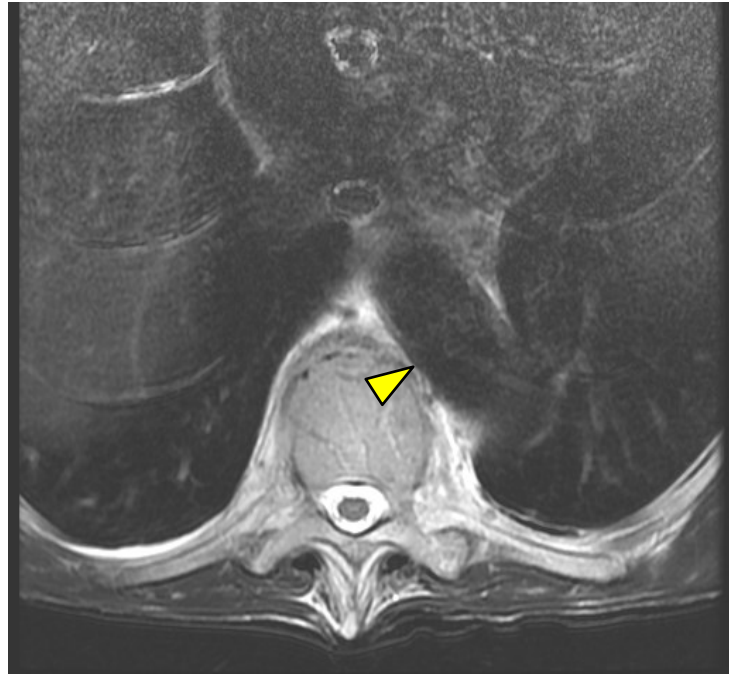
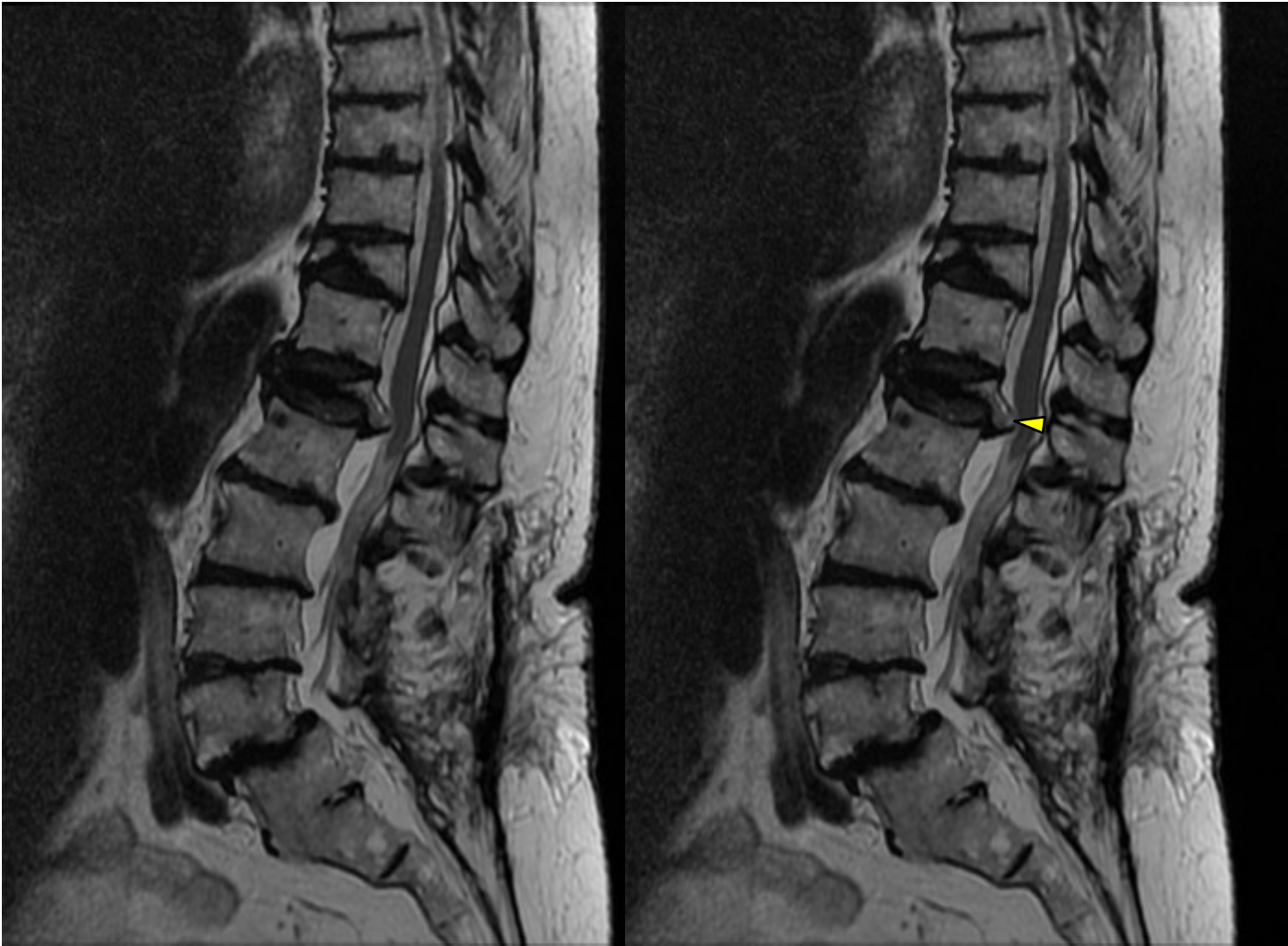


Figure 11:4. Buckling of the aorta (yellow arrow) seen in axial.

The loss of height attributed to compression fractures can lead to crowding of internal structures. In this case of multiple fractures, the aorta is forced into a torturous contorted path, the lungs and heart have lost chest space, and the bone fragments have migrated posteriorly into the central spinal canal.

Compression Fractures and Retropulsion



Figures 11:5 and 11:6. Retropulsion of bony fragments of T12 compression fracture.

This image reveals a number of significant findings: compression fractures, post-surgical changes, spondylolisthesis, endplate disruption, fusion, spondylosis, disc derangements and degeneration, and cord effacement. While most compression fractures are stable and do not endanger the spinal cord, this patient has a significant posterior displacement (retropulsion) of bony fragments at T12. The fragments of T12 efface and displace the thecal sac and the cord. This spine is not stable.

Burst Fracture



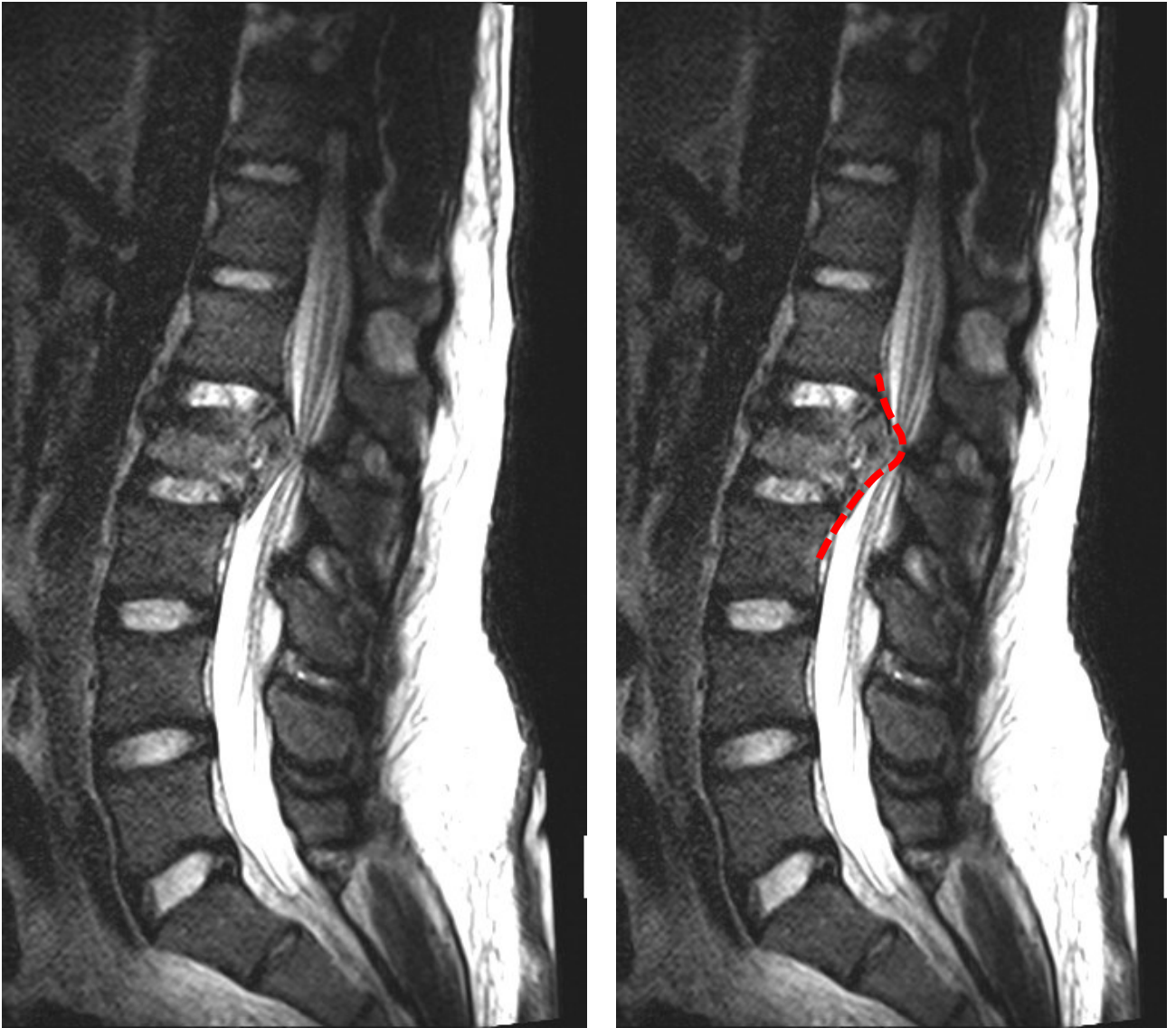
Figure 11:7. Burst fracture of L3 visualized on a sagittal CT.



Figure 11:8. T2 weighted sagittal MR image of an L3 burst fracture. Note the integrity of the spinal canal is preserved.

Burst fractures or compression fractures in healthy non-osteoporotic patients are usually the result of significant trauma. This patient experienced significant compressive forces that caused an L3 burst fracture.

Burst Fracture



Figures 11:9. Acute compression fracture of L2 with intrusion into the central canal.

Burst Fracture



Figures 11:10 and 11:11. Axial image of the compression fracture of L2 with bony retropulsion into the central canal and cauda equina.



Figure 11:12. Coronal view of L2 fracture.

Compression Fracture



Figure 11:13. STIR (short inversion-time inversion recovery) sagittal image. Notice how bright the body of L2 appears. This is due to edema (fluid) at that level. The brightness of the fracture at L2 also indicates it is recent.

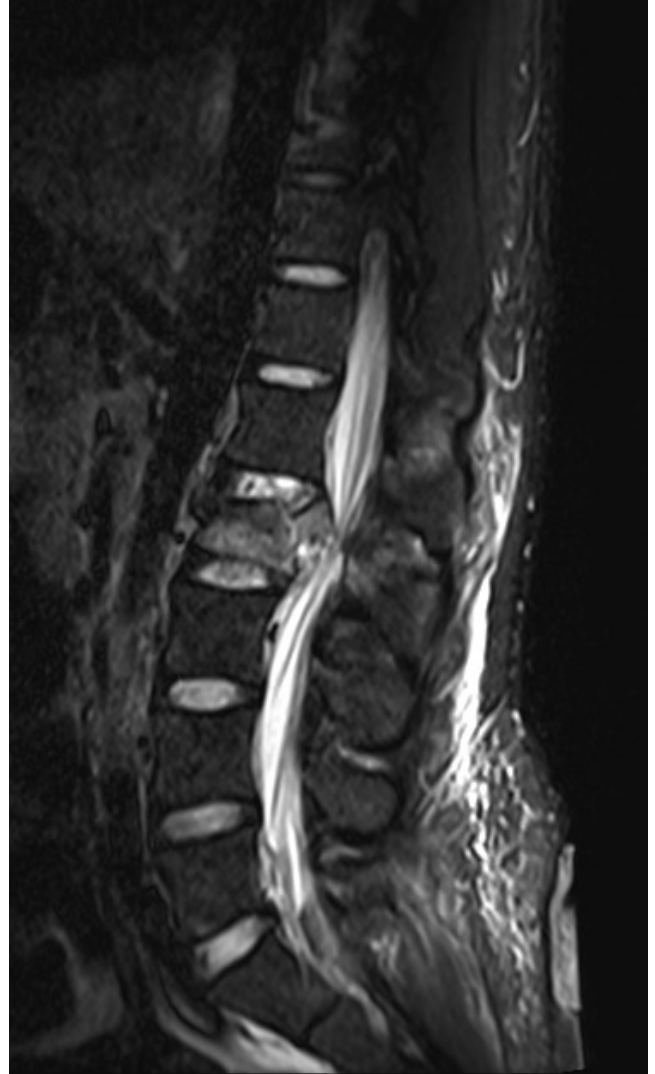
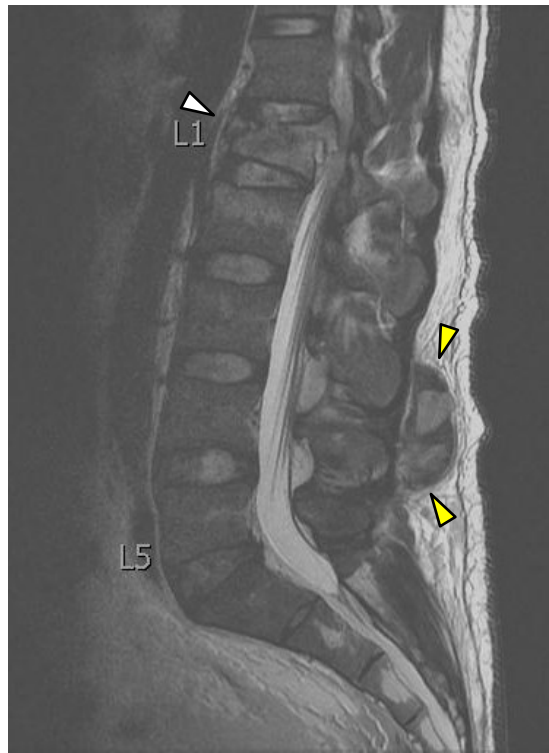
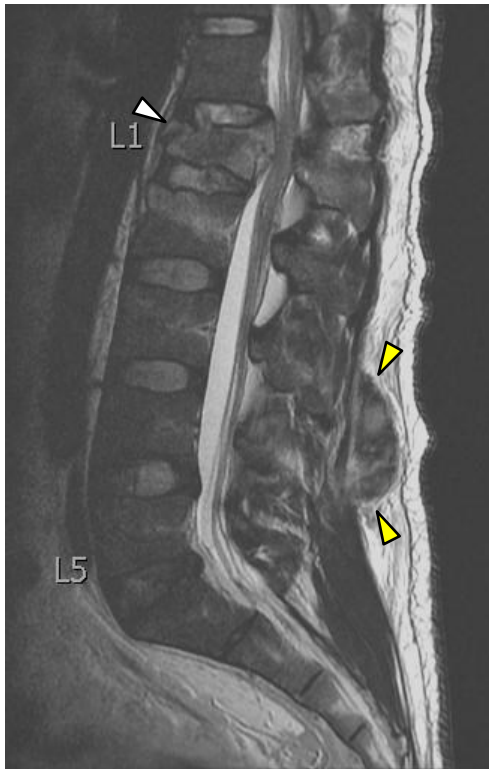


Figure 11:14. Another STIR sagittal slice of the same patient. This image shows the extent of the retropulsion into the central canal.

Burst Fracture



Figures 11:15 and 11:16. Traumatic burst fracture of L1 (white arrow) with a compression fracture. Note the bony edema in L1 and L2 and the hematoma posterior to the spinous processes of L3 and L4 (yellow arrows). Also, take note of the retropulsion of the posterior vertebral body of L1.

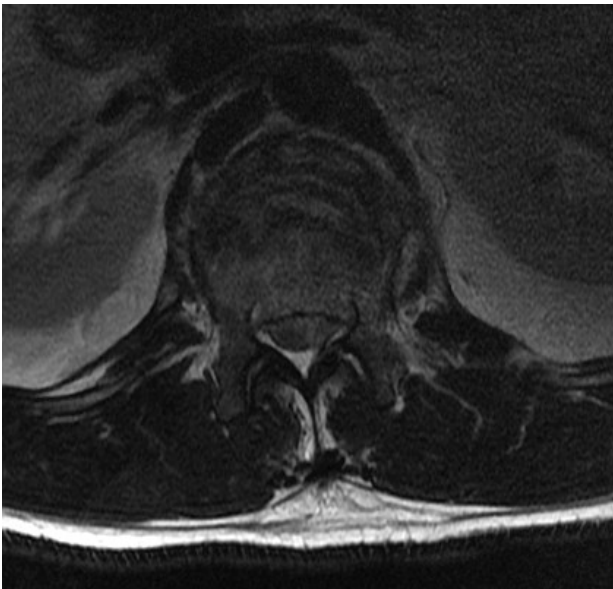


Figure 11:17. T2W axial image of the L1 fracture. Note the significant central canal stenosis resulting from the retropulsion of bone posteriorly.

Suggested Reading

Lee IS, Kim HJ, Lee JS et-al. Dural tears in spinal burst fractures: predictable MR imaging findings. *AJNR Am J Neuroradiol.* 2009;30 (1): 142-6.

Atlas SW, Regenbogen V, Rogers LF et-al. The radiographic characterization of burst fractures of the spine. *AJR Am J Roentgenol.* 1986;147 (3): 575-82.

Shuman WP, Rogers JV, Sickler ME et-al. Thoracolumbar burst fractures: CT dimensions of the spinal canal relative to postsurgical improvement. *AJR Am J Roentgenol.* 1985;145 (2): 337-41.

Marchiori D (2013). *Clinical imaging: with skeletal, chest and abdomen pattern differentials*(third edition). Mosby.

Schoenfeld AJ, Dinicola NJ, Ehrler DM, Koerber A, Paxos M, Shorten SD, Bowers J, Jackson E, Smith MJ. Retrospective review of biopsy results following percutaneous fixation of vertebral compression fractures. *Injury.* 2008 Mar;39(3):327-33. Epub 2007 Sep 18.

Lavelle W, Carl A, Lavelle ED, Khaleel MA. Vertebroplasty and kyphoplasty. *Anesthesiol Clin.* 2007 Dec;25(4):913-28.

Atlas SW. (2008). *Magnetic resonance imaging of the brain and spine* (forth edition). Lippincott Williams & Wilkins.

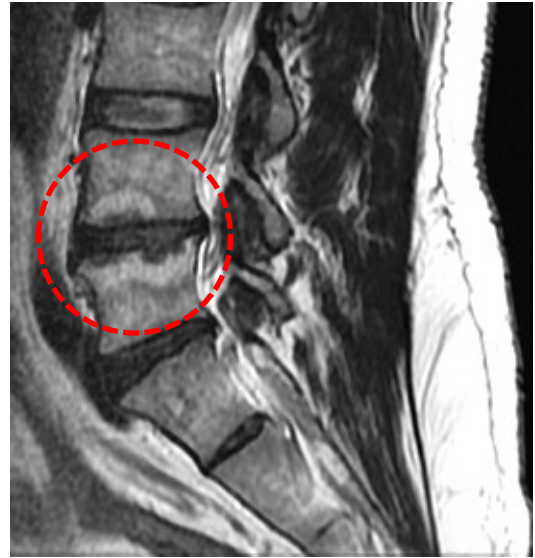
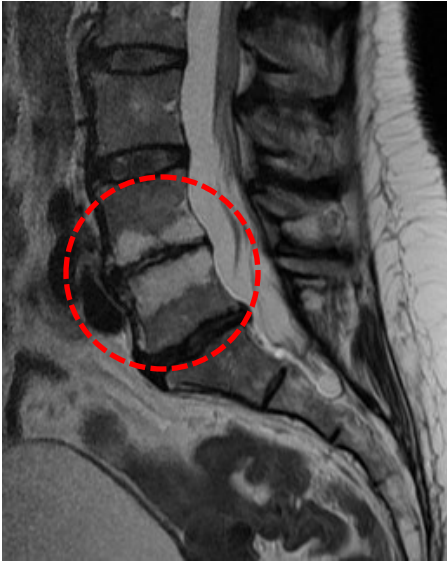
Ross JS et al. (2010). *Diagnostic imaging spine* (second edition). Amirsys Inc.

Bogduk N. (2012). *Clinical and radiological anatomy of the lumbar spine.* Churchill Livingstone.

Modic Changes on MRI: Vertebral Body Marrow Morphology



Modic Changes



Figures 12:1 and 12:2. Reactionary changes to the endplates and bony marrow are called Modic changes. Notice the bright areas of the vertebral bodies circled in red .

Vertebral body edema is a common finding on MR imagery, but it is frequently absent from radiographic reports. This may be due to the radiologist considering it clinically irrelevant. However, the more practical consideration is that every finding on MR cannot be recorded, and most practitioners do not want excessive details. Most practitioners want to know if there is a need for surgical referral or a referral to an oncologist: (Is there neurological defect? Is there a neoplasm?) Degenerative changes like bony edema may seem like unimportant background noise to the busy clinician. However, recent studies have found that vertebral marrow edema is clinically significant and can be progressive.

Michael T. Modic, MD, identified and published his findings on vertebral bony marrow changes in the journal *Radiology* in 1988. Since that time these findings and his grading criteria have born his name. Modic changes represent MR observations of vertebral marrow and endplate changes. These changes have been linked to trauma, disc disruption, and degeneration. More studies are currently underway to identify the clinical significance of this finding and to fully understand its progression.

The vertebral body has an outer barrier of cortical bone that is particularly dense at the vertebral endplates. Within this tough outer shell lies the subcortical marrow cavity. This cancellous bone is less dense and is porous. It is normal for this porous bone to contain marrow. The T1 and T2 weighted images will reflect the presence of normal marrow with a supportive bony matrix. When edema is present in the marrow, it is characterized by an influx of water content: T1 weighted images show loss of signal (hypointense signal in the marrow), while T2 weighted images will demonstrate an increased (hyperintense) signal.

Modic Classifications on MRI

Modic Classifications	T1WI	T2WI
Type 1 Bone marrow edema and swelling	Hypointense	Hyperintense
Type 2 Associated with ischemic conversion of normal marrow to yellow fatty marrow	Hyperintense	Isointense or mildly hyperintense
Type 3 Believed to be representative of subchondral bone sclerosis	Hypointense	Hypointense

Figure 12:3. This chart categorizes the types of Modic changes seen on MRI.

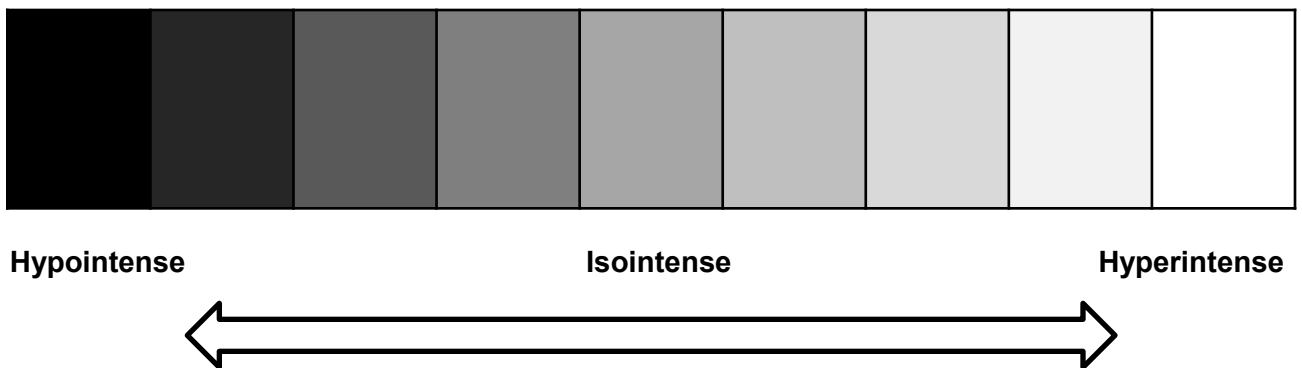
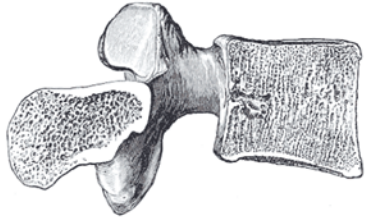
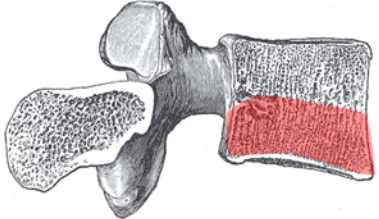
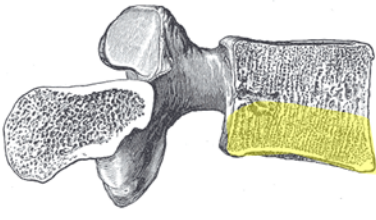
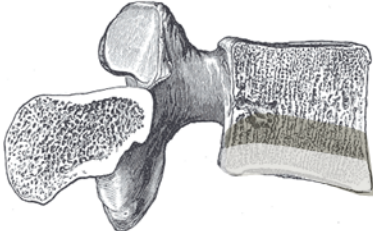


Figure 12:4. Shades of gray. Interpreting findings on MRI is not always black or white. When we use terms like hypointense or hyperintense, we are not saying that the image will be black or white, but will tend toward darkness or lightness on a grayscale continuum.

Bone Morphology and Modic Classifications

Evidence emerging indicates there is a progressive nature to Modic changes. The bony edema of type I Modic changes may progress to type II, and type II may progress to type III.

Figure 12:5. Characteristics of Bone Morphology in Vertebral Bodies	
<p>Normal bone is spongy and uniform in appearance. The vertebral endplates are a thin dense margin of bone.</p>	 <p style="text-align: center;">Normal</p>
<p>Bony edema has been connected with acute endplate or disc disruption. This edema is visible on MRI and is classified as Type 1 Modic change. It has been associated with pain and inflammation.</p>	 <p style="text-align: center;">Type 1 Modic Changes</p>
<p>Type 2 Modic changes are indicative of yellow fatty infiltration into cortical bone following bony ischemia. Type 2 Modic changes may progress from type 1 Modic changes.</p>	 <p style="text-align: center;">Type 2 Modic Changes</p>
<p>Type 3 changes are categorized by sclerotic changes of subchondral bone and thickening of the endplates. In time, thickened endplates will reduce nutrient and fluid movement into adjoining discs. This will contribute to reduced fluid content within the adjoining disc and subsequent degenerative disc disease.</p>	 <p style="text-align: center;">Type 3 Modic Changes</p>

Type 1 Modic Characteristics

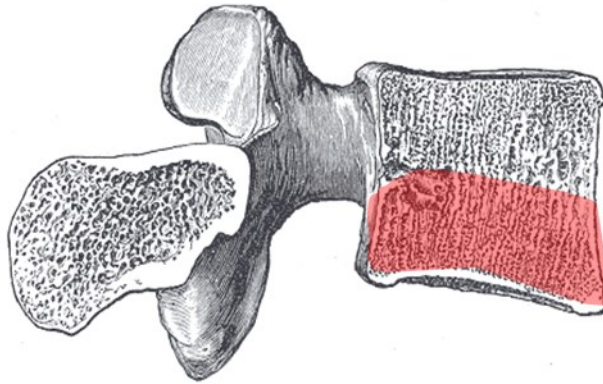


Image adapted from Henry Gray (1821–1865). *Anatomy of the Human Body*. 1918.

Figures 12:6. Bony edema extending into the spongy subcortical bone.

The high water content of inflammation and edema is evident in type 1 Modic changes. Type 1 changes are manifested as hypointense (dark) on T1 and hyperintense on T2 weighted images.



Figure 12:7. T1 weighted sagittal image revealing type 1 Modic changes. Fluid (bony edema) is dark on T1.



Figure 12:8. T2 weighted sagittal image revealing type 1 Modic changes. The edema is light on T2WI.

Type 2 Modic Characteristics

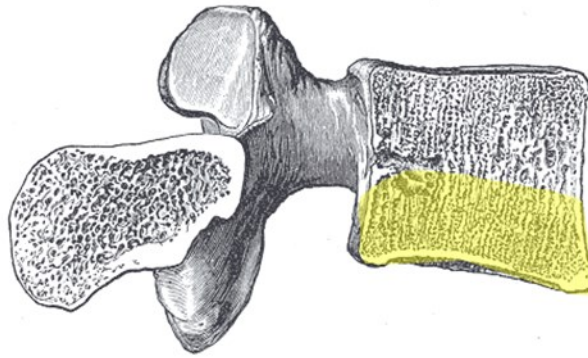


Image adapted from Henry Gray (1821–1865). *Anatomy of the Human Body*. 1918.

Figure 12:9. Fatty infiltration extending into the spongy subcortical bone.

On T1 images, the fatty infiltration of Type 2 Modic changes will appear hyperintense, and on T2 weighted images, they will appear hyperintense or isointense.



Figure 12:10. T1 weighted sagittal lumbar image showing hyperintense signals arising from the adjoining vertebral bodies and endplates of L5 and S1.



Figure 12:11. T2 weighted sagittal lumbar image showing isointense or mildly hyperintense signal from the adjoining L5 and S1 vertebral bodies and endplates.

Type 3 Modic Characteristics

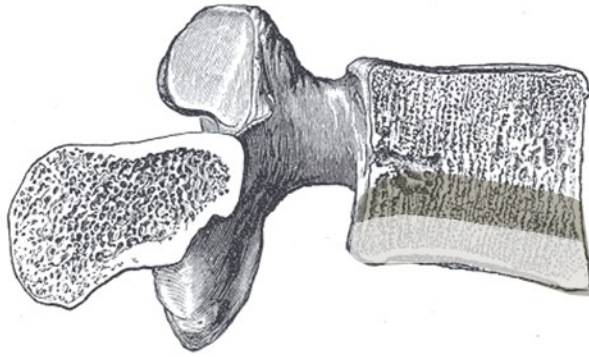


Image adapted from Henry Gray (1821–1865). *Anatomy of the Human Body*. 1918.

Figure 12:12. Sclerotic changes of the cortical bone and thickening of the vertebral endplates.

T1 and T2 weighted MRI will manifest type 3 Modic changes with decreased signal or hypointensity. These findings can typically be correlated with sclerosis on plain film x-ray. The images below demonstrate type 3 Modic changes in a patient with degenerative disc disease of L5-S1 following an old discectomy.



Figure 12:13. T1 weighted sagittal lumbar image showing hypointensity of the inferior L5 and superior S1 vertebral bodies and endplates.



Figure 12:14. T2 weighted sagittal lumbar image showing hypointensity of the inferior L5 and superior S1 vertebral bodies and endplates.

Type 3 Modic Characteristics

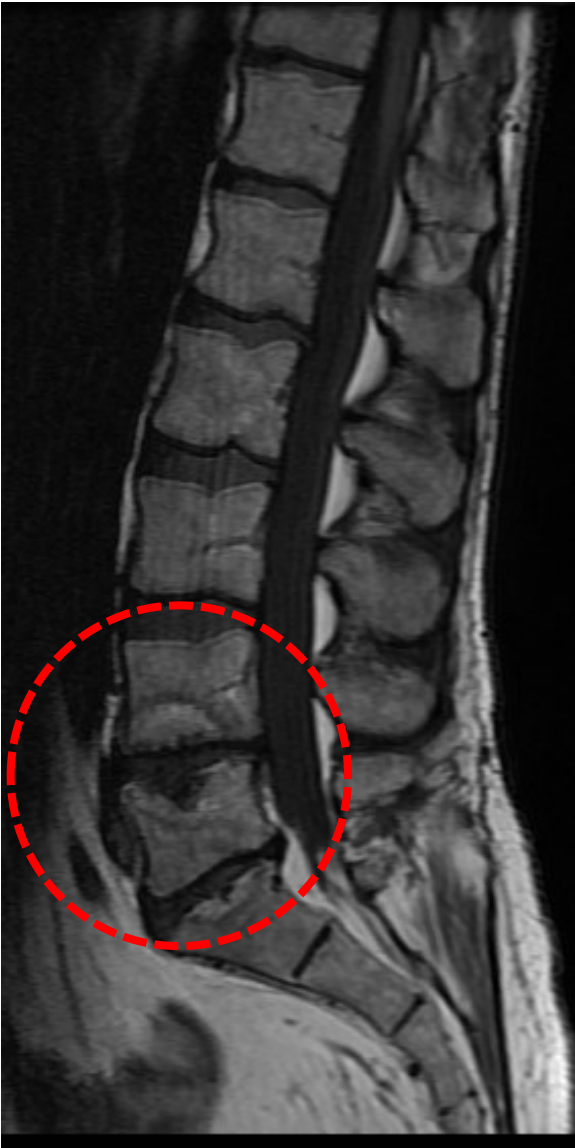


Figure 12:15. T1 weighted sagittal lumbar image showing hypointensity of the inferior L4 and superior L5 vertebral bodies and endplates.

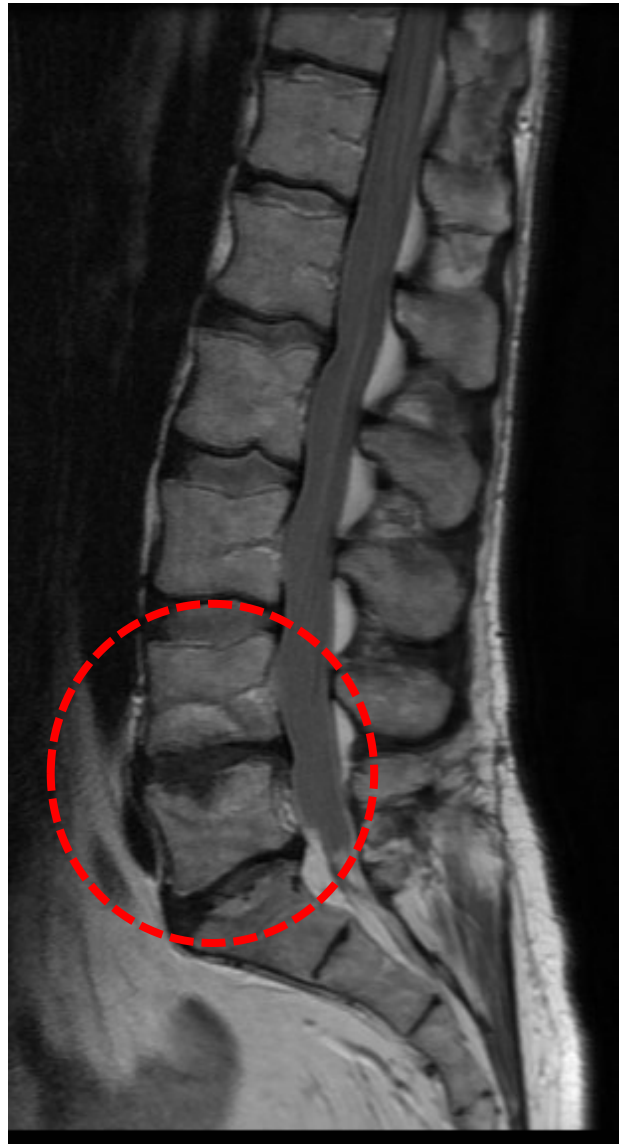


Figure 12:16. T2 weighted sagittal lumbar image showing hypointensity of the inferior L4 and superior L5 vertebral bodies and endplates.

These MRIs show a superior endplate fracture of L5 and the resulting Modic changes. They show a similar gray appearance of the reactionary changes which indicates these are type 3 Modic changes.

Reactionary Changes to an Acute Intravertebral Herniation

These T2 weighted MRIs show the reactionary halo of bony edema Modic 1 changes, following an acute injury. This patient had retired from her sedentary lifestyle as an executive in her mid-fifties and purchased a farm. While performing heavy lifting on her new farm she felt and heard a pop in her back that was accompanied by pain. An MRI revealed a Schmorl's node (intravertebral disc herniation) extending into the inferior endplate and vertebral body of L3. These images also clearly show bony edema surrounding the fracture and even affecting the superior endplate of L4.

Modic changes can help differentiate new injuries from old. Newer injuries are more likely to have reactionary bony edema (Modic 1 changes).



Figure 12:17. This T2 weighted sagittal lumbar image was taken seven years prior to the intravertebral herniation.

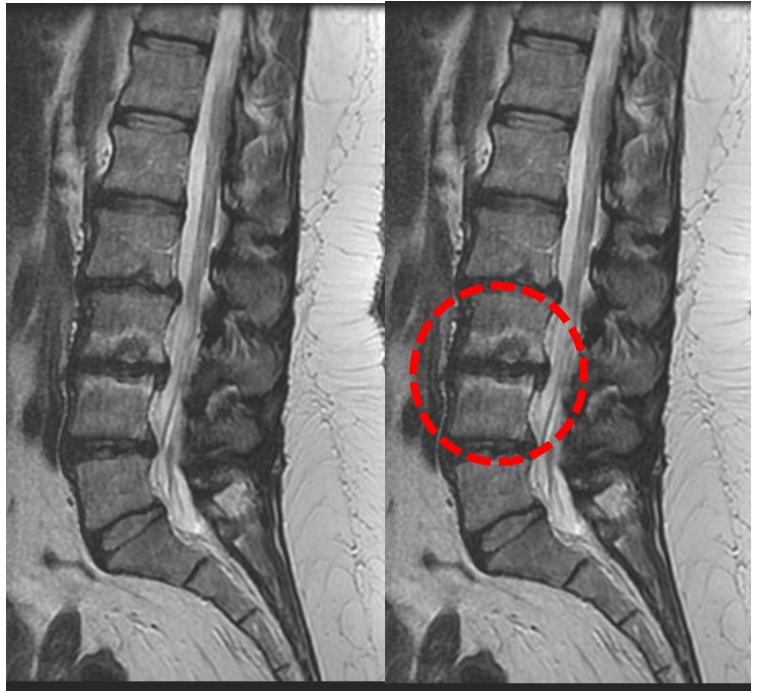


Figure 12:18 and 12:19. These T2 weighted sagittal lumbar images show both the intravertebral herniation and reactionary Modic 1 changes.

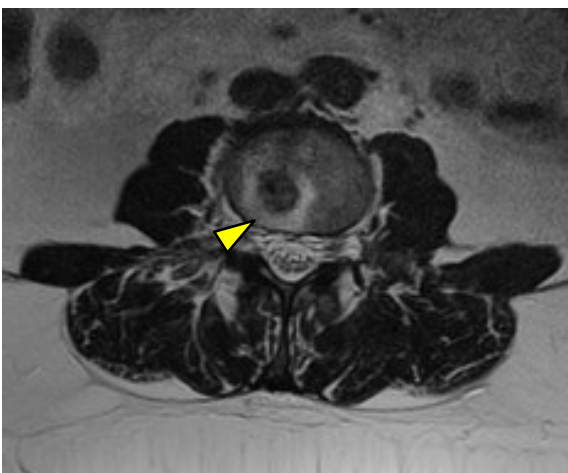


Figure 12:20. This T2 weighted axial lumbar image shows both the clear margins of the intravertebral herniation (yellow arrow) and the hyperintense reactionary Modic 1 changes encircling the injury.

Suggested Reading

de Roos A, Kressel H, Spritzer C, et al. MR imaging of marrow changes adjacent to end plates in degenerative lumbar disk disease. *AJR Am J Roentgenol* 1987;149:531–34.

Braithwaite I, White J, Saifuddin A, et al. Vertebral end-plate (Modic) changes on lumbar spine MRI: correlation with pain reproduction at lumbar discography. *Eur Spine J* 1998;7:363–68.

Modic MT, Steinberg PM, Ross JS, et al. Degenerative disc disease: Assessment of changes in vertebral body marrow with MR imaging. *Radiology*, 1988;166:193-9.

Modic MT, Masaryk TJ, Ross JS, et al. Imaging of degenerative disk disease. *Radiology* 1988;168:177–86.

Modic MT, Ross JS. Lumbar degenerative disk disease. *Radiology*. 2007 Oct;245 (1): 43-61.

Karchevsky M, Schweitzer ME, Carrino JA, et al. Reactive endplate marrow changes: a systematic morphologic and epidemiologic evaluation. *Skeletal Radiol* 2005;34:125–29.

Kjaer P, Korsholm L, Bendix T, et al. Modic changes and their associations with clinical findings. *Eur Spine J* 2006;15:1312–19.

Kuisma M, Karppinen J, Niinimäki J, et al. A three-year follow-up of lumbar spine endplate (Modic) changes. *Spine* 2006;31:1714–18.

Rahme R, Mousa R. The Modic Vertebral Endplate and Marrow Changes: Pathologic Significance and Relation to Low Back Pain and Segmental Instability of the Lumbar Spine. *AJNR Am J Neuroradiol* 29:838–42 _ May 2008 _ www.ajnr.org

<http://www.ajnr.org/content/29/5/838.full>

Atlas SW. (2008). *Magnetic resonance imaging of the brain and spine* (forth edition). Lippincott Williams & Wilkins.

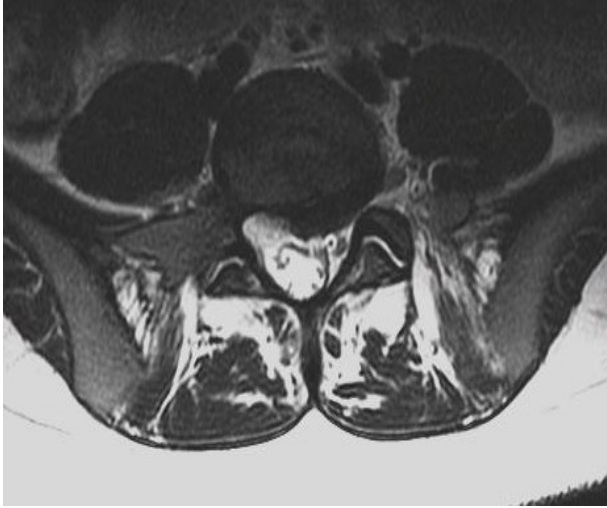
Ross JS et al. (2010). *Diagnostic imaging spine* (second edition). Amirsys Inc.

Lumbar Facets

13



Facet Contours and Orientation

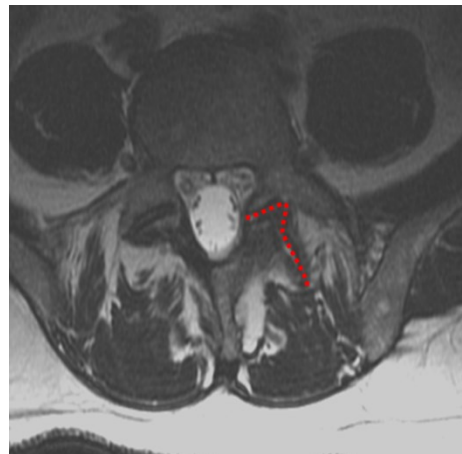


Figures 13:1 and 13:2. These T2W axial images display asymmetrical facets and S-shaped joint lines.

Facet anomalies are rarely reported on MRI reports. Usually the only ink the facets receive are about degenerative changes or severe disruptions. But manual practitioners would benefit from knowing more about the facets.

For this reason it is especially important for clinicians to be comfortable looking at facets and analyzing them. This chapter will introduce the clinician to facet orientation, effusion, anomalies, and hypertrophy, as well as synovial cysts arising from facets and other clinically significant aspects of the lumbar facets .

Lumbar facet effusion has been identified as a sign of instability in degenerative spondylolisthesis. These axial images show anomalous facets.



Figures 13:3 and 13:4. This image reveals asymmetrical facets with the left facet having both coronal and sagittal components.

Anatomical Variants: Wrap Around Facet

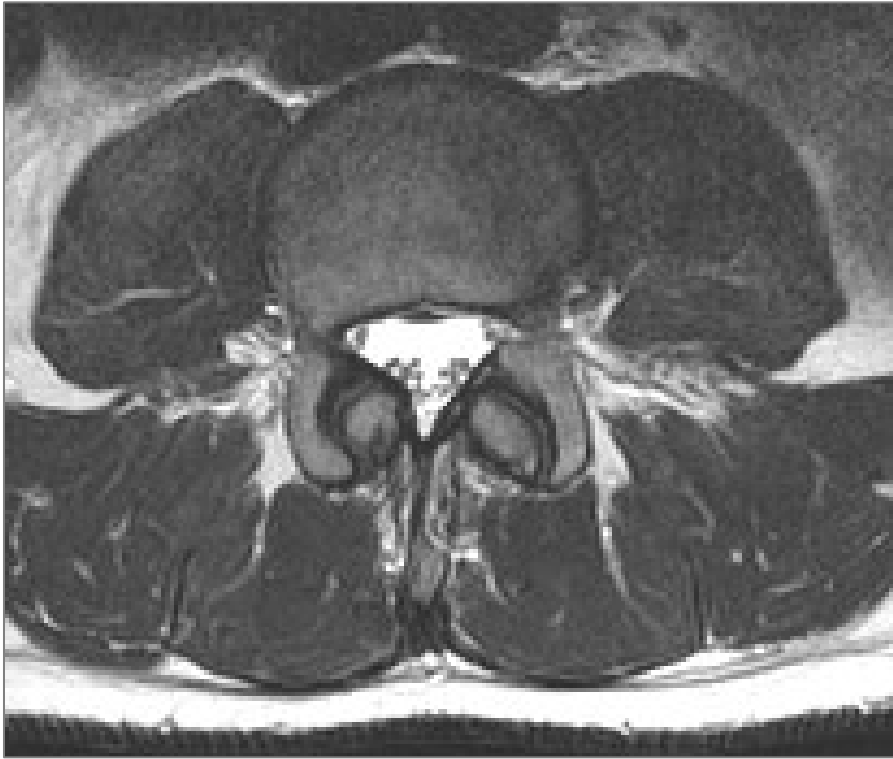


Figure 13:5. This T2W axial image reveals facets that are circular in orientation.

Anatomists typically classify vertebral facets as being either coronal or sagittal in orientation. Occasionally a vertebra will have asymmetrical facets with one oriented coronal and the other oriented sagittal. But there can be other anatomical variants that may or may not be clinically significant. Here we see facets that are circular in configuration. It is conceivable that this configuration could affect interarticular motion and spinal function.

Certainly a manual practitioner would be interested in knowing the configuration of the facet joints (also known as zygapophyseal joints).



Figure 13:6. This schematic overlays the facets and highlights the extent of the circular shape of this intervertebral unit.

Asymmetrical Facets



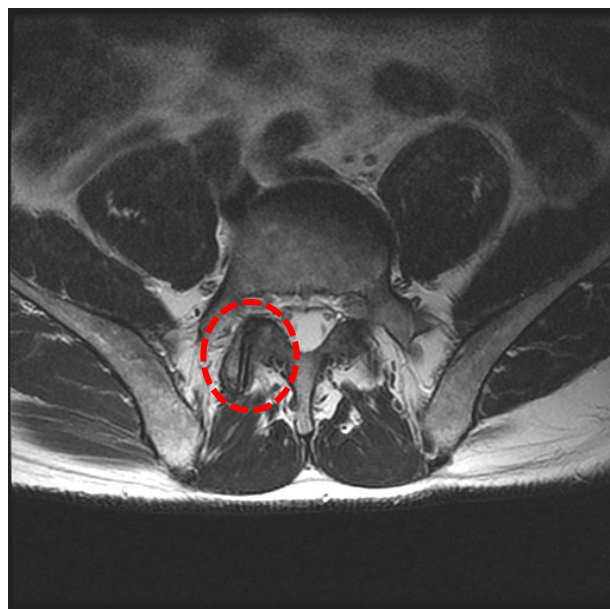
Figure 13:7 Asymmetry of the L5-S1 facets revealed on axial CT.



Figure 13:8. Second axial image of patient with facet asymmetry.

These are CT axial images revealing asymmetry of the L5-S1 facets. The left facets (seen on the right of this image) are sagittal, while the right are coronal.

Variations in Facet Anatomy

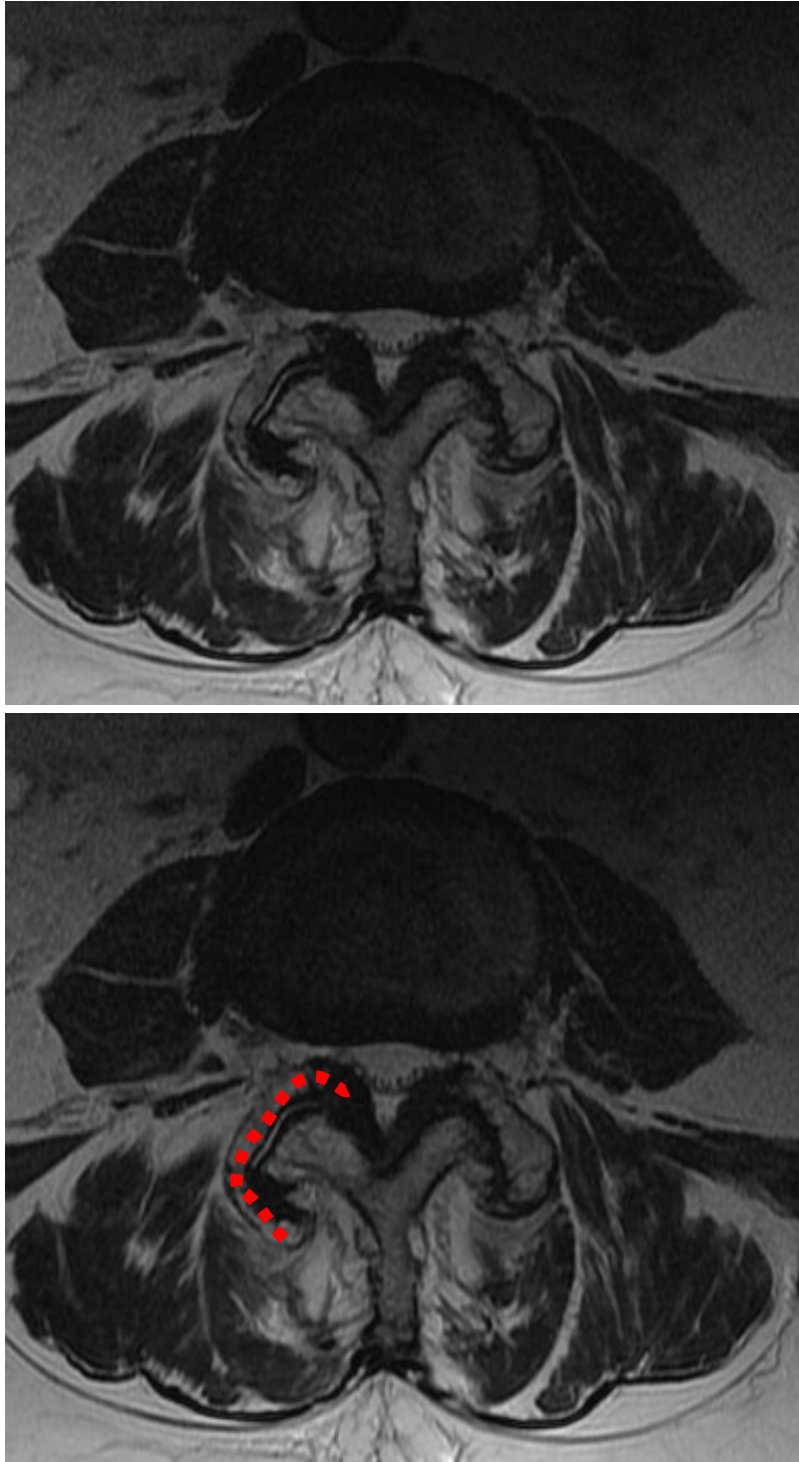


Figures 13:9 and 13:10. Axial T2WI of atypical facet joint anatomy.



Figures 13:11 and 13:12. Axial T2WI of atypical facet joint anatomy.

Hypertrophic Facets



Figures 13:13 and 13:14. Facet hypertrophy that wraps around the articulating facet and limits joint motion.

Synovial Cyst Arising from Facet Effusion

These images show degenerative and asymmetrical facets contributing to a central canal stenosis. The left L4-5 facet (seen on the right of the axial images) shows the white sign of effusion. This effusion gives rise to the synovial cyst that extends into the central canal.



Figures 13:15 and 13:16. These T2W axial images show asymmetry of the facets, effusion, which is seen as white fluid within the left facet (red arrow), and a synovial cyst bubbling out from the facet capsule to occupy space within the central canal (yellow arrow).

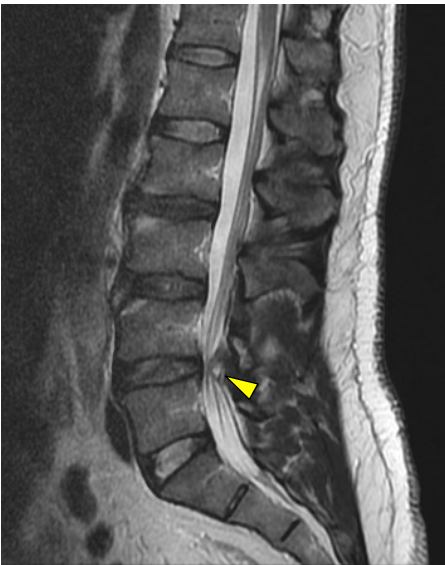


Figure 13:17. Synovial cyst in sagittal T2 is seen contributing to spinal stenosis (yellow arrow).



Figure 13:18. The synovial cyst and joint effusion is less distinct in this T1 axial image.

Facetal Effusion

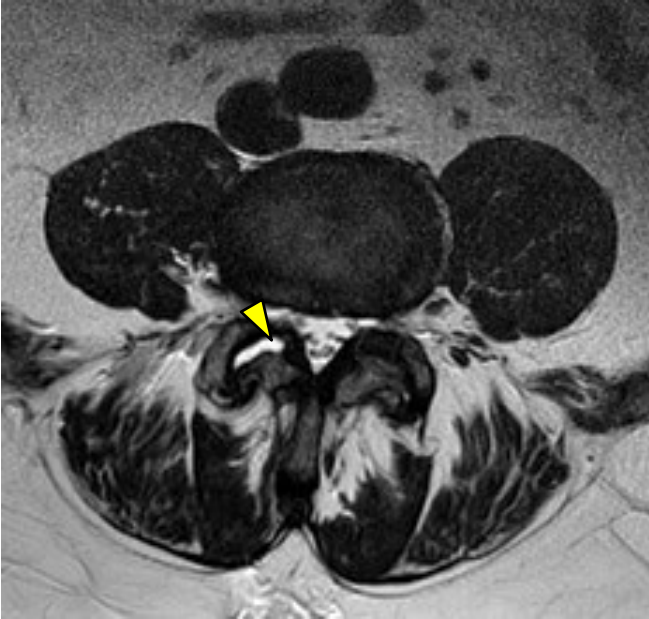


Figure 13:19. This T2W axial image clearly reveals effusion of the right facet joints.

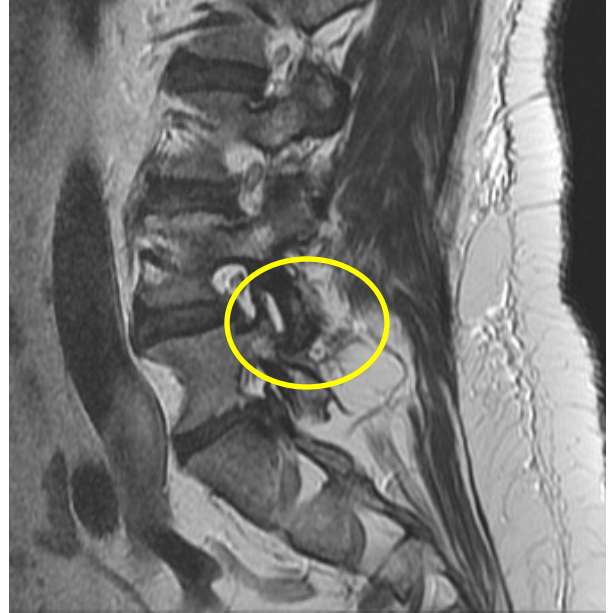


Figure 13:20. This T2W axial image reveals effusion of the L4-5 facet.

Facet joint effusion is characterized by increased swelling and fluid accumulation within the facet joint and has been correlated with back pain. Synovial cysts of the spine arise from facets burdened with swelling and fluid accumulation. As the fluid accumulates, the synovium of the facet may balloon out forming a synovial cyst. These cysts may or may not be symptomatic. Spinal synovial cysts are more likely to cause symptoms if they occupy space in the spinal canal or IVFs.

The presence of lumbar facet joint effusion is more prevalent in patients with lumbar instability. This finding is clinically significant.

Facetal Effusion



Figures 13:21 and 13:22 clearly show a significant degree of effusion of the L4-L5 facets. The axial of normal facets in Figure 13:23 is provided to show the difference between normal and inflamed zygapophyseal joints.

Figure 13:21. Facet effusion at L4-L5 in a sagittal T2 weighted image. Take note of the shape and size of the IVF at this level compared to IVFs at other levels seen in this image. Facet effusion can cause IVF encroachment.

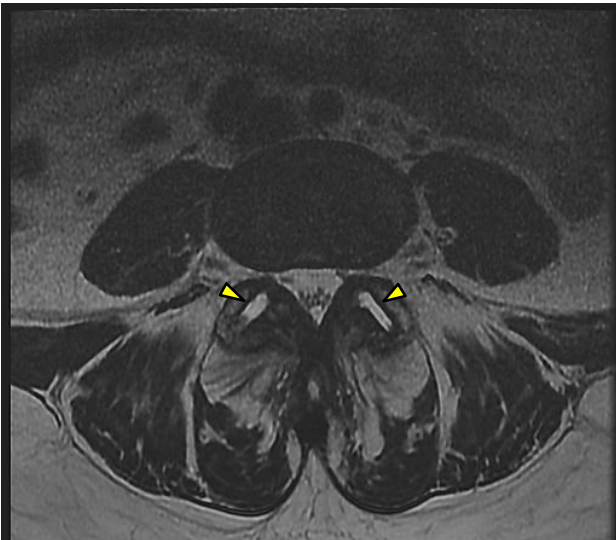


Figure 13:22. Bilateral zygapophyseal joint effusion in a T2 weighted axial image.

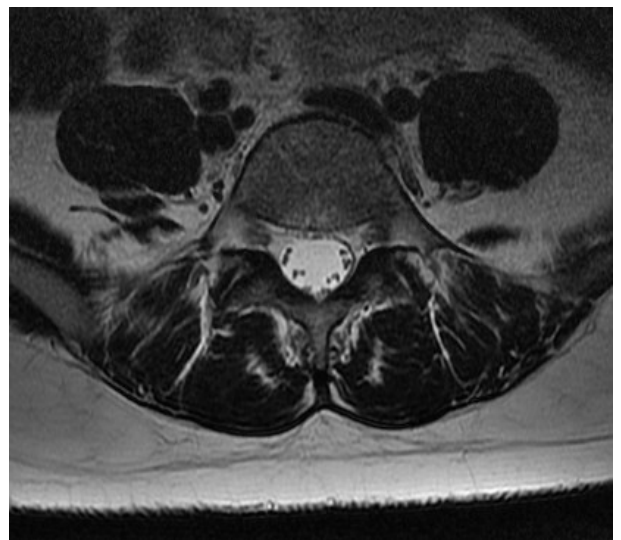


Figure 13:23. Normal facets in a T2W axial.

Synovial Cyst

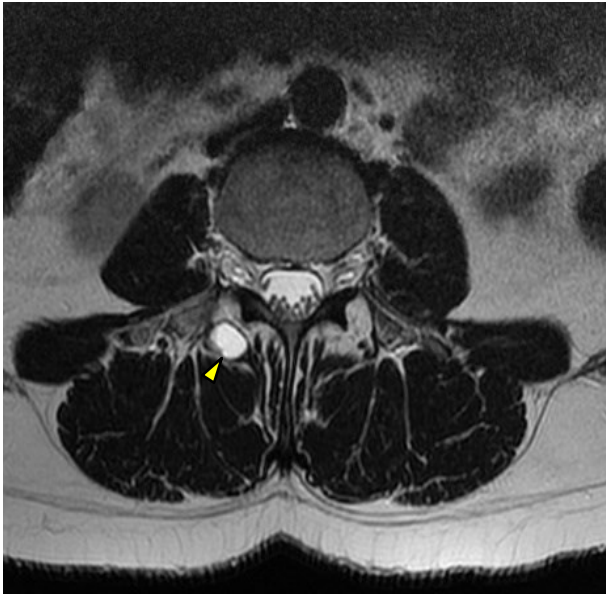


Figure 13:24. This T2W axial reveals a synovial cyst (yellow arrow) that projects posteriorly from the right zygapophyseal joint. Note the high intensity (white in this T2WI) of the synovial cyst.



Figure 13:25. This T1W axial reveals a synovial cyst (yellow arrow). While difficult to differentiate from muscle in T1 images, comparing T1 and T2 can differentiate water from fat densities.



Figure 13:26. This T2W sagittal image reveals a synovial cyst (yellow arrow).



Figure 13:27. This T1W sagittal image reveals a synovial cyst (yellow arrow).

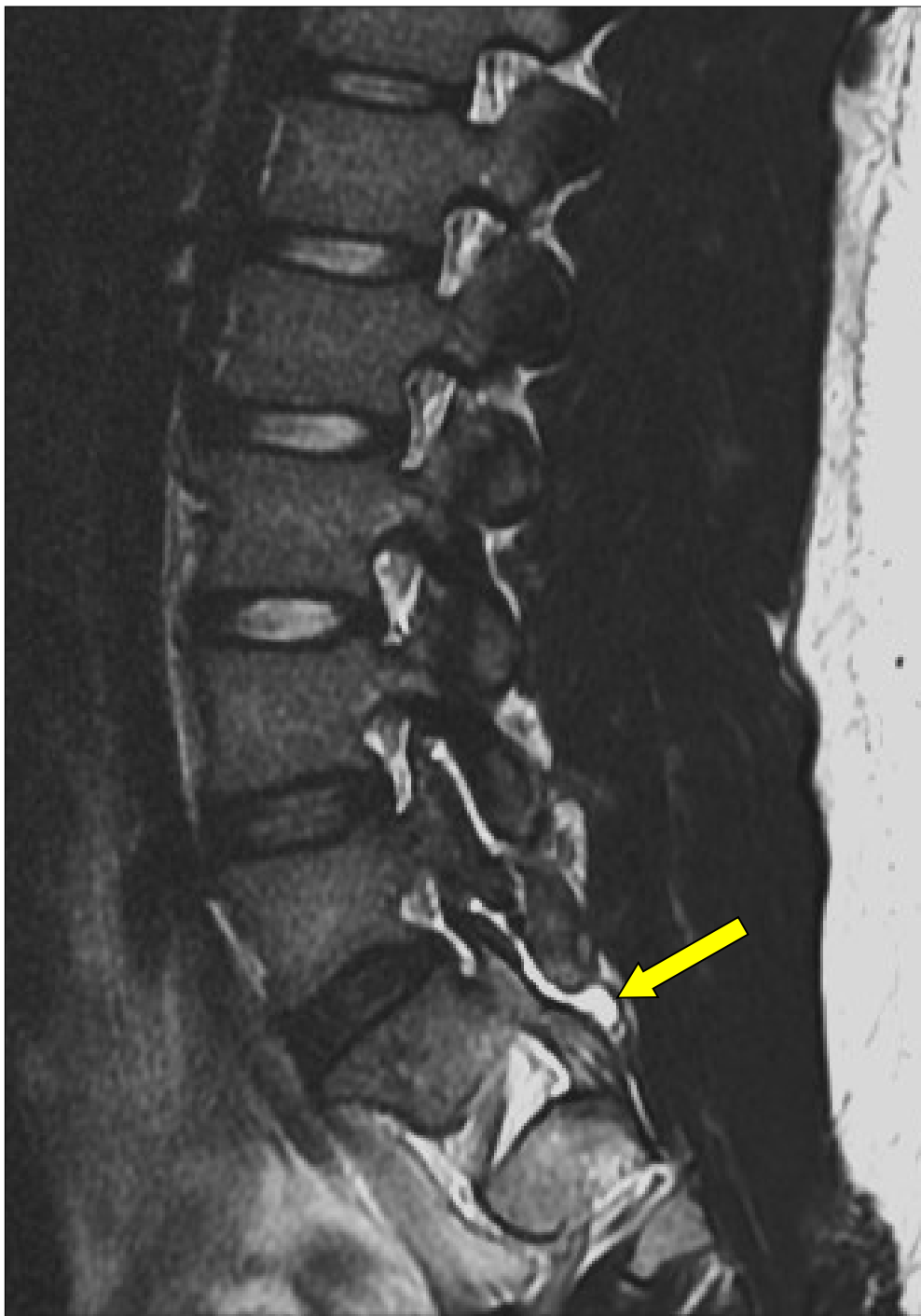


Figure 13:28. This image shows effusion of the L4-5 and L5-S1 facets along with a pars defect of the L5 pars. The L5-S1 facet effusion extends beyond the margins of the facet joint as it balloons out into a posterior synovial cyst (yellow arrow).

Synovial Cyst Protruding into the Central Canal and IVF

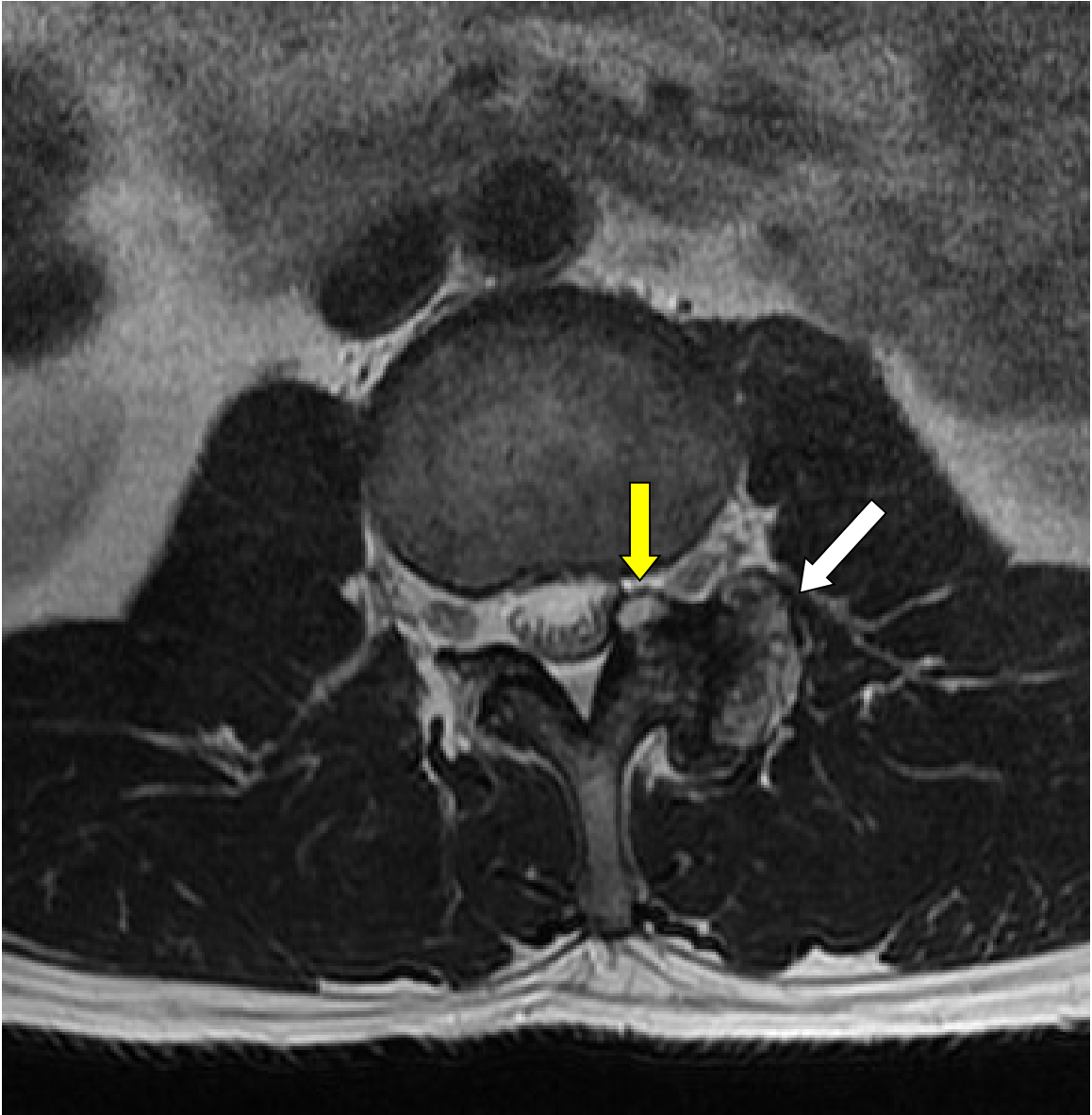


Figure 13:29. This T2W axial image reveals a synovial cyst (yellow arrow) that projects anterior from the left facet joint. The cyst abuts and displaces a portion of the thecal sac. This synovial cyst arises from a hypertrophic and degenerative left facet joint (white arrow).

Facet Effusion

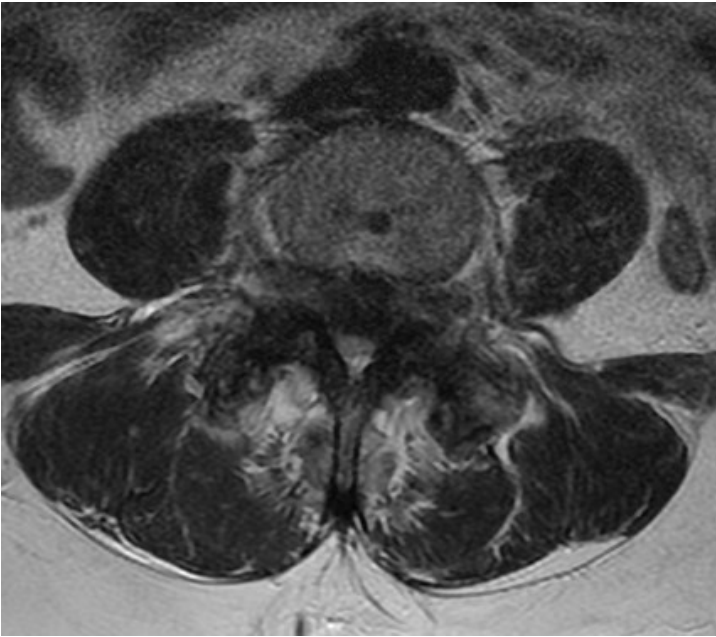


Figure 13:30. Effusion of the L4-L5 facet seen on T2W sagittal image.



Figure 13:31. A T2W axial of the same patient. The facet joint is so filled with fluid that it is significantly gapped.

Facet Erosion and Degenerative Spondylolisthesis



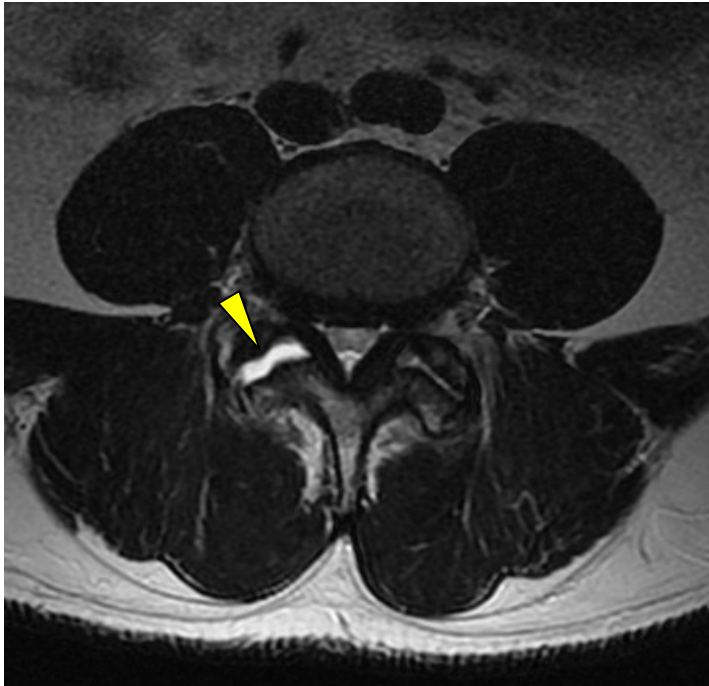
One of the functions of the facet joints is to prevent the anterior displacement of one vertebra on another. With severe facet degeneration and erosion, the restraining function of the facets is negated. Without the restraint of the facets, a vertebra will migrate anterior, resulting in a degenerative spondylolisthesis. These images show severely degenerated L4-L5 facets and the subsequent degenerative spondylolisthesis of L4 on L5.

Figure 13:32. A T2W axial showing severe degeneration and erosion of the facet joints.



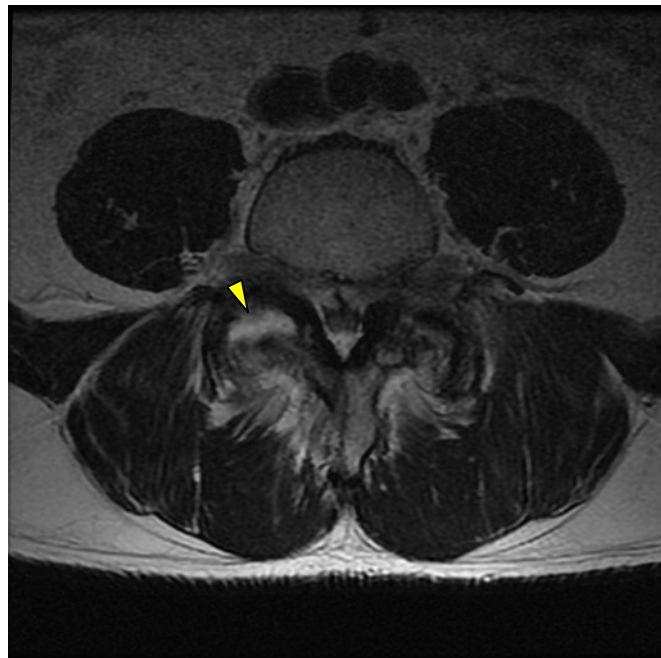
Figure 13:33. A T2W sagittal image revealing a degenerative spondylolisthesis that resulted from facet erosion.

Facetal Effusion



Figures 13:34-36. These images show axial and sagittal T2W images with an L4-L5 left facet joint effusion.

Effusion and Synovial Cysts



Figures 13:37 and 13:38. Severe facet joint erosion and effusion of the L4-L5 facet seen on T2W axial image (yellow arrow). This case is further complicated by a broad disc bulge, ligamentum flavum hypertrophy, and a synovial cyst in the central canal (figure13:39).

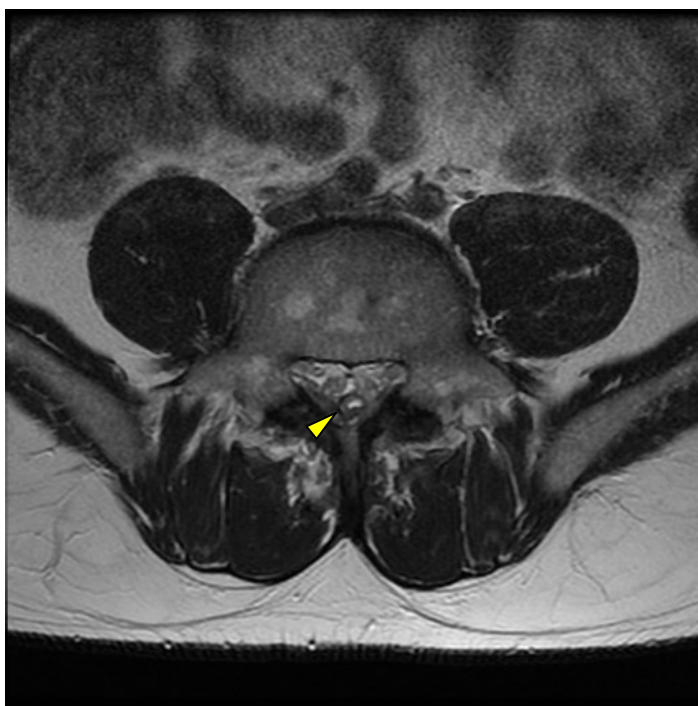
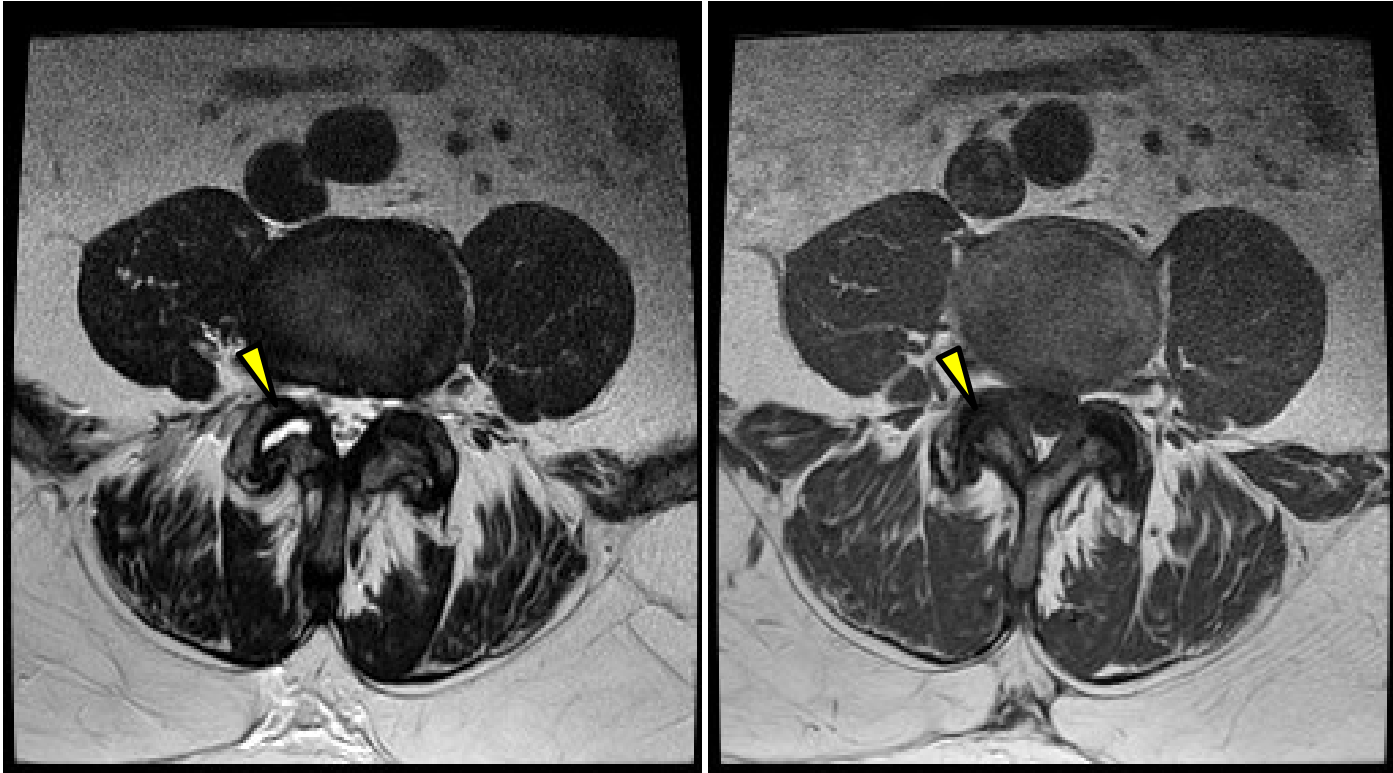


Figure 13:39. A synovial cyst within the central canal can be clinically significant (T2W axial image).

Facet Joint Effusion



Figures 13:40 and 13:41. Facet joint effusion of L4-L5 seen on an axial T2WI on the left and T1WI on the right.



Figure 13:42. Bilateral facet joint effusion as seen on a T2W axial.

Weight Bearing Facets

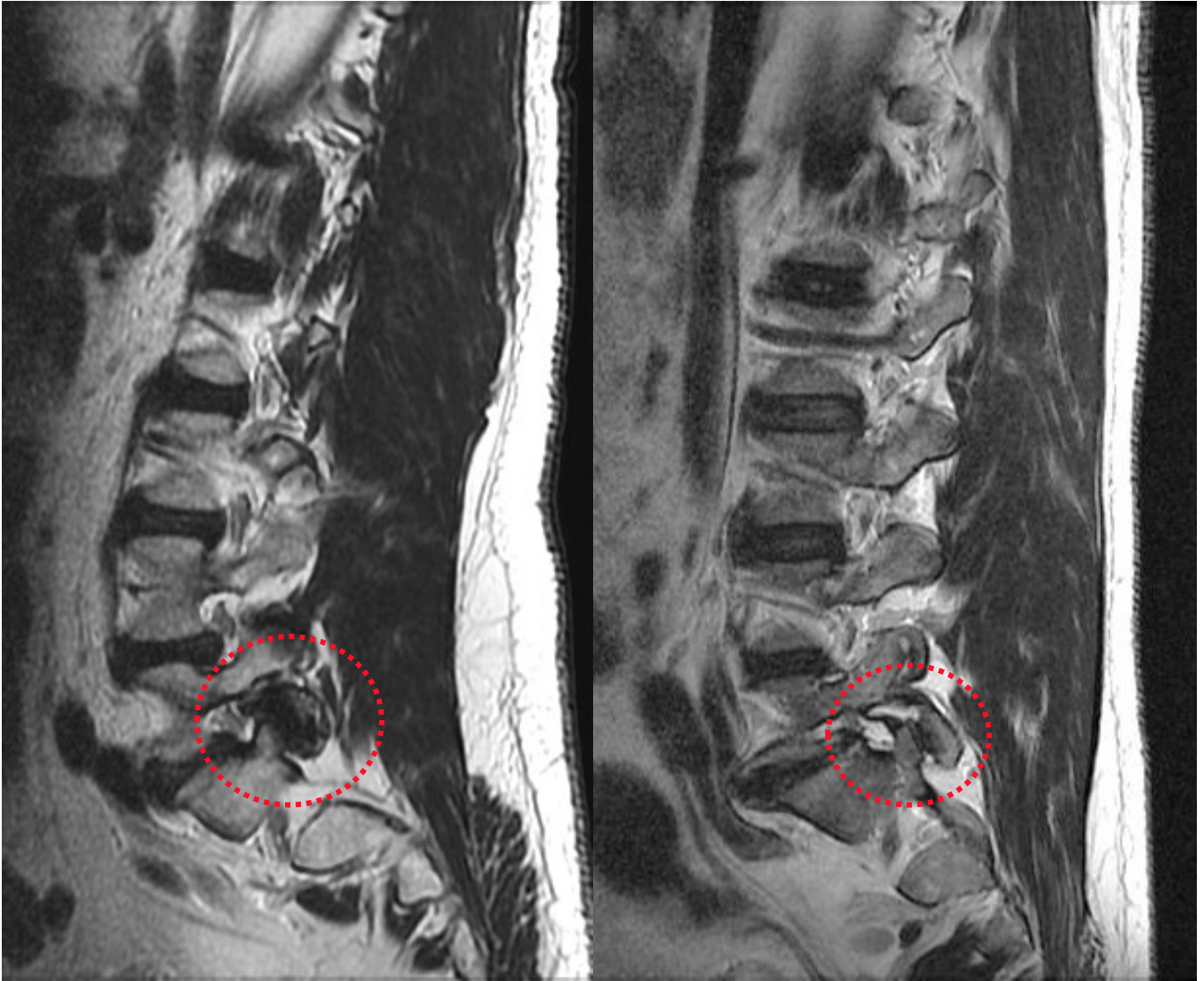


Figure 13:43. This T2W sagittal image shows severe L5-S1 facet degenerative changes. This patient's anatomy appears to cause the L5-S1 facets to bear much of the axial compressive force placed on the spine.

Figure 13:44. Another "pillar" facet resulting in facet degeneration and facet joint effusion.

When facets project up from the sacrum like a pillar, they bear the weight of axial compression. This leads to early degenerative changes and frustration in responding to treatment.

Suggested Reading

Lattig F, Fekete TF, Grob D, Kleinstück FS, Jeszenszky D, Mannion AF. Lumbar facet joint effusion in MRI: a sign of instability in degenerative spondylolisthesis? *Eur Spine J*. 2012 Feb;21(2):276-81. doi: 10.1007/s00586-011-1993-1. Epub 2011 Sep 20.

Venkatanarasimha N, Suresh SP. *AJR Teaching File: An Uncommon Cause of Spinal Canal Stenosis*. *AJR* 2009;193:S56–S58 0361–803X/09/1933–S56 © American Roentgen Ray Society. *SPINE* Volume 32, Number 14, pp 1555–1560.

Rihn JA, Lee JY, Khan M, Ulibarri JA, Tannoury C, Donaldson WF, Kang JD. Does Lumbar Facet Fluid Detected on Magnetic Resonance Imaging Correlate With Radiographic Instability in Patients With Degenerative Lumbar Disease?

Caterini R, Mancini F, Bisicchia S, Maglione P, Farsetti P The correlation between exaggerated fluid in lumbar facet joints and degenerative spondylolisthesis: prospective study of 52 patients. *J Orthop Traumatol*. 2011 June; 12(2): 87–91.

Berven S, Tay BB, Colman W, Hu SS. The lumbar zygapophyseal (facet) joints: a role in the pathogenesis of spinal pain syndromes and degenerative spondylolisthesis. *Semin Neurol*. 2002 Jun;22(2):187-96.

Pal GP, Routal RV. Mechanism of change in the orientation of the articular process of the zygapophyseal joint at the thoracolumbar junction. *J Anat*. 1999 Aug;195 (Pt 2):199-209.

Lakadamyali H, Tarhan NC, Ergun, TC, et al. STIR Sequence for Depiction of Degenerative Changes in Posterior Stabilizing Elements in Patients with Lower Back Pain *Am. J. Roentgenol*. 2008 191: 973-979 *Am. J.*

Cramer G, Darby S (2013). *Basic and clinical anatomy of the spine, spinal cord, and ANS* (third edition). Elsevier Mosby.

Marchiori D (2013). *Clinical imaging: with skeletal, chest and abdomen pattern differentials*(third edition). Mosby.

Atlas SW. (2008). *Magnetic resonance imaging of the brain and spine* (forth edition). Lippincott Williams & Wilkins.

Ross JS et al. (2010). *Diagnostic imaging spine* (second edition). Amirsys Inc.

Bogduk N. (2012). *Clinical and radiological anatomy of the lumbar spine*. Churchill Livingstone.

Vertebral Hemangiomas

14



Hemangiomas

Hemangiomas are the most common benign neoplasm of the spine. Hemangiomas are composed of dilated blood vessels that displace or erode bone. This disruption causes the remaining trabeculae to thicken. That thickening gives the vertebra a corduroy appearance on plain film radiographs.

Being able to discern the difference between malignant neoplasms and predominantly benign findings such as hemangiomas is a valuable skill. Hemangiomas are common, so common that it is easy to become complacent and flippantly identify all intravertebral findings as hemangiomas. Being familiar with common incidental findings will add confidence to the provider and help in identifying what is not normal. Keep in mind that it is the clinician reviewing MRs with patients (versus the radiologist) who will be confronted with a startled patient gawking at a large scary-looking hemangioma during a report of findings.

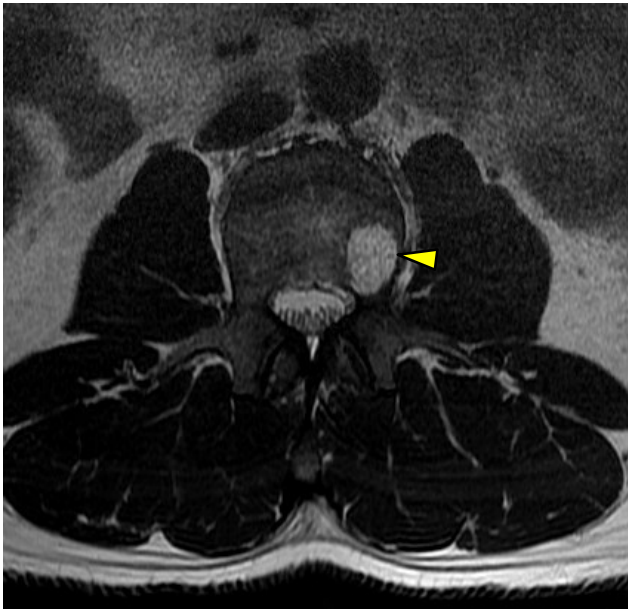


Figure 14:1. Axial T2WI with a hemangioma in the L3 vertebral body.



Figure 14:2. Sagittal T2WI with a hemangioma in the L3 vertebral body.

Hemangioma in the Vertebral Body of L4

Spinal hemangiomas are common. Because of this, most clinicians dismiss them without a second thought, and in the vast majority of hemangiomas this would be acceptable. Hemangiomas are benign, asymptomatic, and slow growing with no known tendency to become malignant. Spinal hemangiomas are composed of a proliferation of vascular tissue. This proliferation of vascular tissue can displace bone and in some cases create a risk for compression fractures.

Occasionally other conditions are mistaken for hemangiomas. The differential diagnosis list for hemangiomas includes metastatic cancer, Paget's disease, lymphoma, prominent basivertebral veins (a normal anatomical variant), and multiple myeloma.

Treatment of a hemangioma is rare. Observation is the most common management of this finding.



Figure 14:3. Sagittal T1WI with a hemangioma in the body of L4.



Figure 14:4. Sagittal T1WI with a hemangioma within the vertebral body of L4.

Differentiating between Vertebral Body Metastasis and a Hemangioma

Any discussion about the differentiation between benign and cancerous lesions on MRI should occur over the safety net provided by radiologists. Hemangiomas are a common benign finding on lumbar MRI and are usually incidental and asymptomatic. Upon first viewing of a large hemangioma on MR, a clinician may be taken back by the appearance of this impressive looking lesion. Having confidence in the differentiation of these two findings will expedite appropriate progression of care.

Lesion Type	T1	T2	T2 with Fat suppression
Hemangioma	Bright	Bright	Dark
Metastasis	Dark	Bright	Bright



Figure 14:5. This T1WI shows a bright hemangioma within the anterior body of L4.



Figure 14:6. Metastasis is seen at two levels, L1 and L4, in this T1WI. Note the darkness of the entire vertebral body of L4 in this T1WI.

Prominent Basivertebral Veins

Along with hemangiomas and other common inconsequential findings seen on MRI are vascular foramina. Some images tend to have more pronounced variations of this normal anatomical finding. Prominent basivertebral veins are normal variants that may draw attention from an untrained eye.



Figure 14:7. Prominent appearance of the basivertebral veins at every level in this T2W sagittal image. This is a normal anatomical finding.

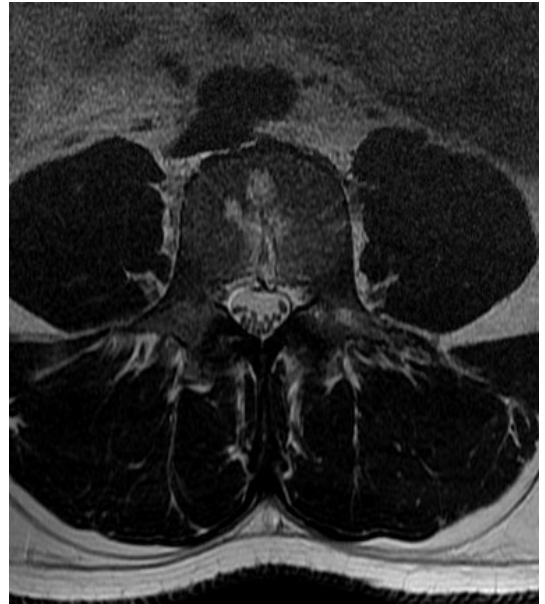


Figure 14:8. Normal vascular variant of the basivertebral vein on a T2W axial image.



Figure 14:9. This is the same MRI level as seen in figure 14:8, but in a T1W axial image.

Suggested Reading

Aksu G, Fayda M, Saynak M, Karadeniz A. Spinal cord compression due to vertebral hemangioma. *Orthopedics*. Feb 2008. Vol 31. Issue 2.

Marchiori D (2013). *Clinical imaging: with skeletal, chest and abdomen pattern differentials*(third edition). Mosby.

Hwang PM. Vertebral abnormality in a patient with suspected malignancy *Proc (Bayl Univ Med Cent)*. 2002 July; 15(3): 325–326.

Conjoined Nerve Roots

15



Conjoined Nerve Roots

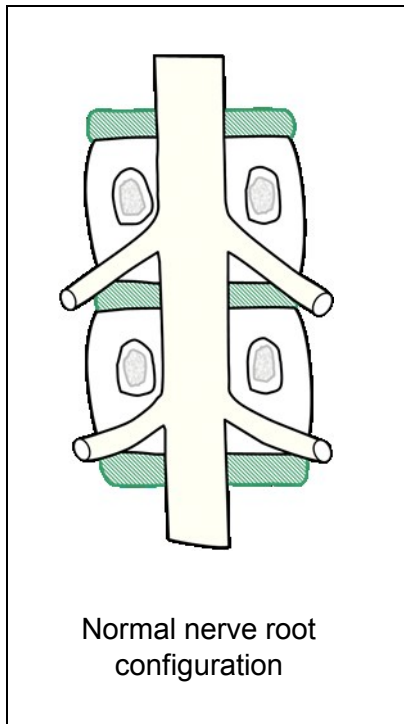


Figure 15:1.

Identifying conjoined nerve roots can be difficult for even skilled radiologists, but since they are periodically left out of radiology reports it is important that spine practitioners learn how to identify the location and clinical significance of conjoined nerves. Anchoring or tethering the nerve roots or the cord into a position of lesion is one of the most disturbing aspects of a conjoined nerve root. Though most conjoined nerve roots will not be symptomatic, symptoms may develop if the conjoined nerve tethers a nerve root into the path of a herniation, stenosis, or other compressive lesion.

The nerve roots normally exit the intervertebral foramina in the upper 1/3 of the foramina. If a conjoined nerve tethers a nerve root so that it exits the lower portion of the foramina, it will be much more susceptible to the pressure of a disc herniation, facet hypertrophy, or foraminal stenosis. This can create a clinically significant complex for manual practitioners, surgeons, therapists, and pain practitioners. While conceptualizing conjoined nerve roots is best done in coronal orientation, like in the schematics pictured, coronal images are rarely available in MRI studies. Therefore, relying on clues from axial and sagittal images is the best way to identify this anatomical anomaly.

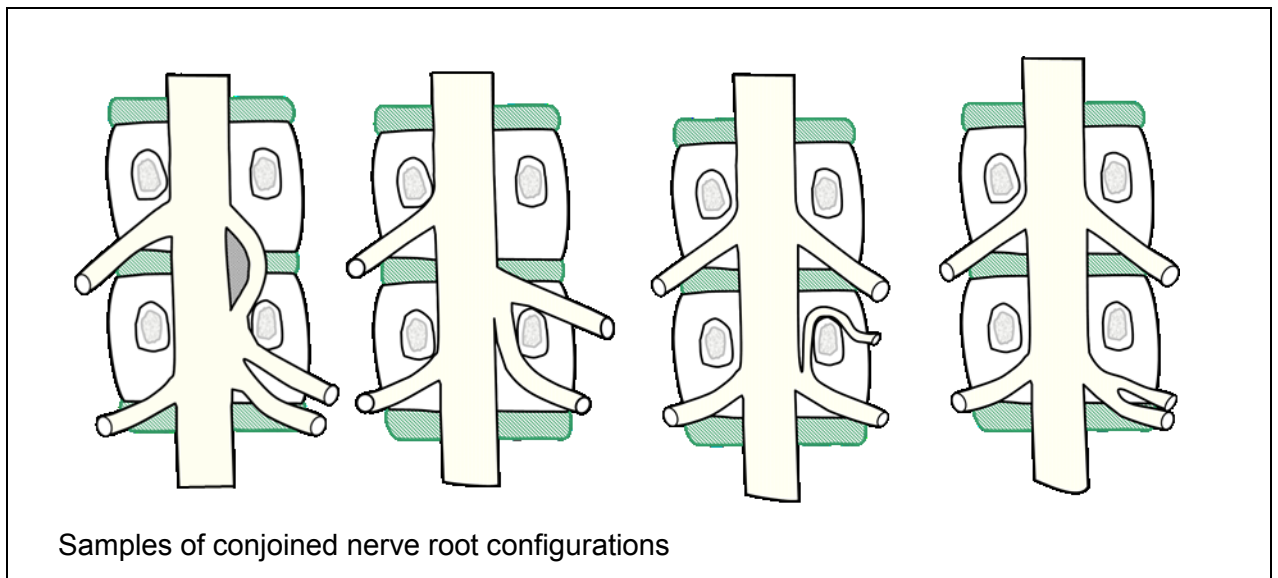


Figure 15:2.

Identifying Conjoined Nerve Roots on MRI

Asymmetry in the exiting nerve rootlets is an indication of possible conjoined nerve roots. The nerve rootlets should appear to travel in symmetrical pairs. The left and right side of the thecal sac should roughly mirror each other. Figure 15:3 shows a group of several rootlets grouped together on the left side of the central canal (circled in red). Figure 15:4 is a schematic of the axial image seen in figure 15:3.

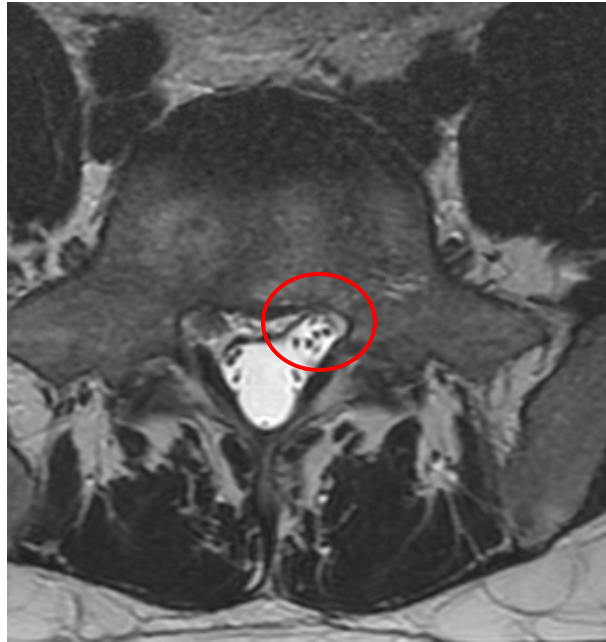


Figure 15:3. T2W axial image showing asymmetry of the exiting nerve rootlets.

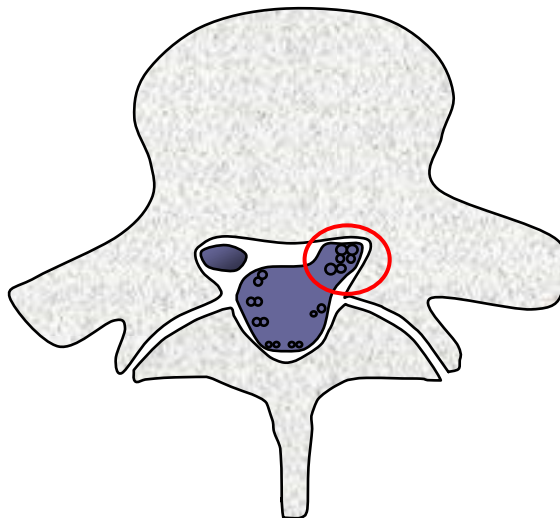


Figure 15:4. Schematic of the axial slice seen in Figure 15:3.

Identifying Conjoined Nerve Roots on MRI

This T2W axial image reveals two nerves traveling in the same anterior sacral foramina. Nerves sharing the same foramina is an indicator of conjoined nerve roots.

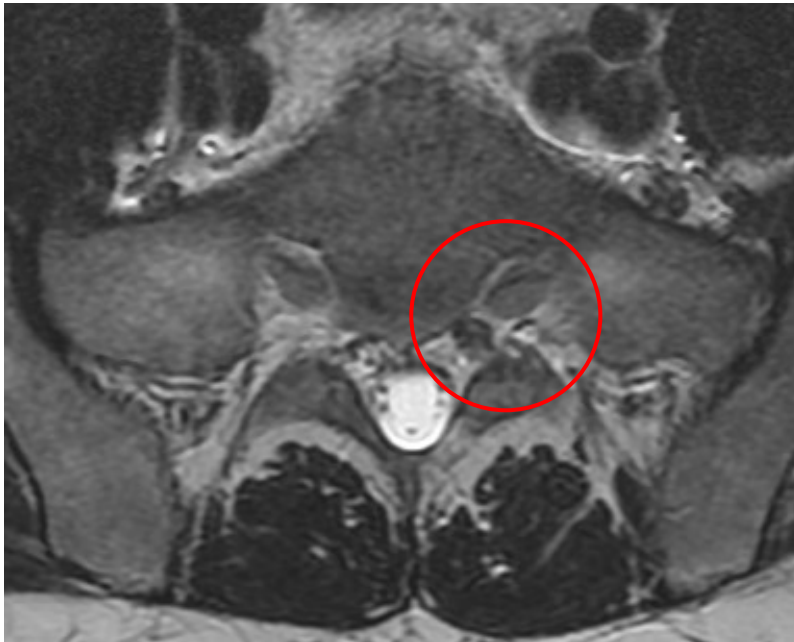


Figure 15:5. T2W axial image showing two nerves sharing the same anterior sacral foramina (red circle).

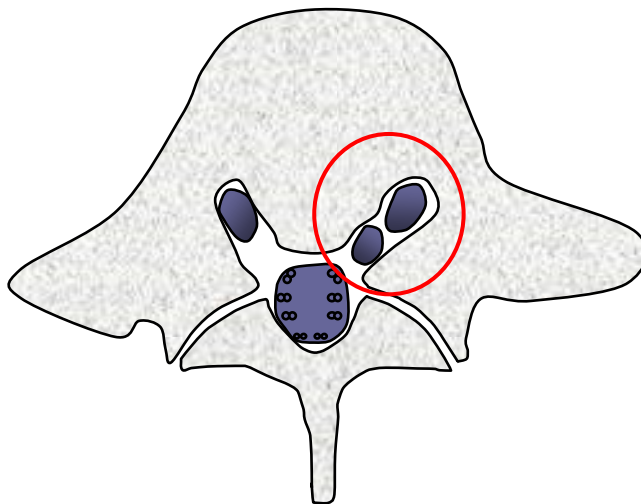
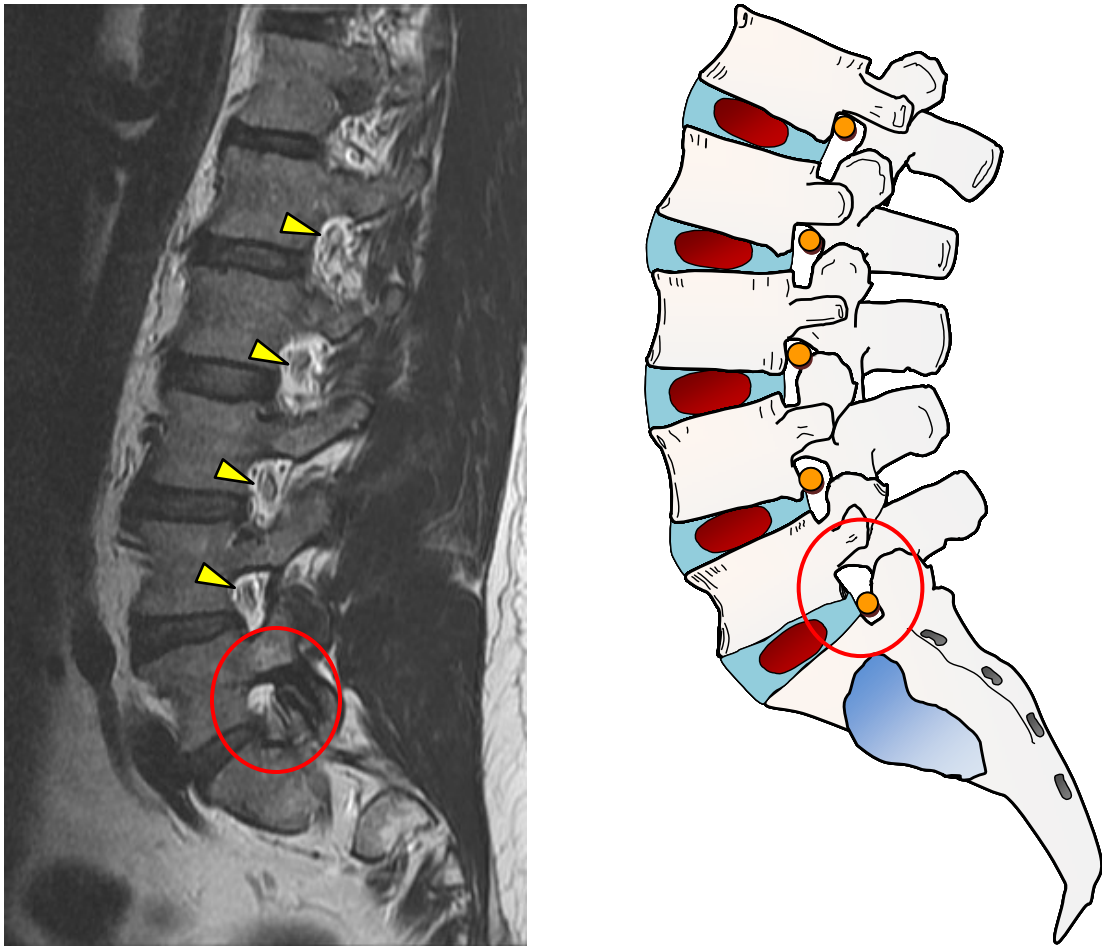


Figure 15:6. Schematic of the axial image of the sacrum shown in figure 15:5.

Identifying Conjoined Nerve Roots on MRI

Nerve roots normally exit through the upper portion of the lumbar foramina. Suspect a conjoined nerve root if the nerve is located in the lower 1/3 of an IVF as seen in both the sagittal MRI on the left and the schematic on the right at L5-S1. After identifying a nerve exiting low in the IVF in a sagittal view, analyze the axial images for evidence of anomaly.



Figures 15:7 and 15:8. T2W sagittal image and schematic showing an anchoring of the L5 nerve root in the lower portion of the L5-S1 foramina (red circle). Note that all of the other nerve roots exit through the upper 1/3 of the lumbar intervertebral foramina (yellow arrows).

Identifying Conjoined Nerve Roots on MRI

Normally a nerve root exits the IVF above the level of the disc, in the upper 1/3 of the IVF. This location prevents the nerve from being too vulnerable to compression from disc bulges, herniations and degenerative hypertrophy. Conjoined nerve roots can anchor the nerve root in the lower 1/3 of the IVF. This increases their likelihood of compromise and injury.

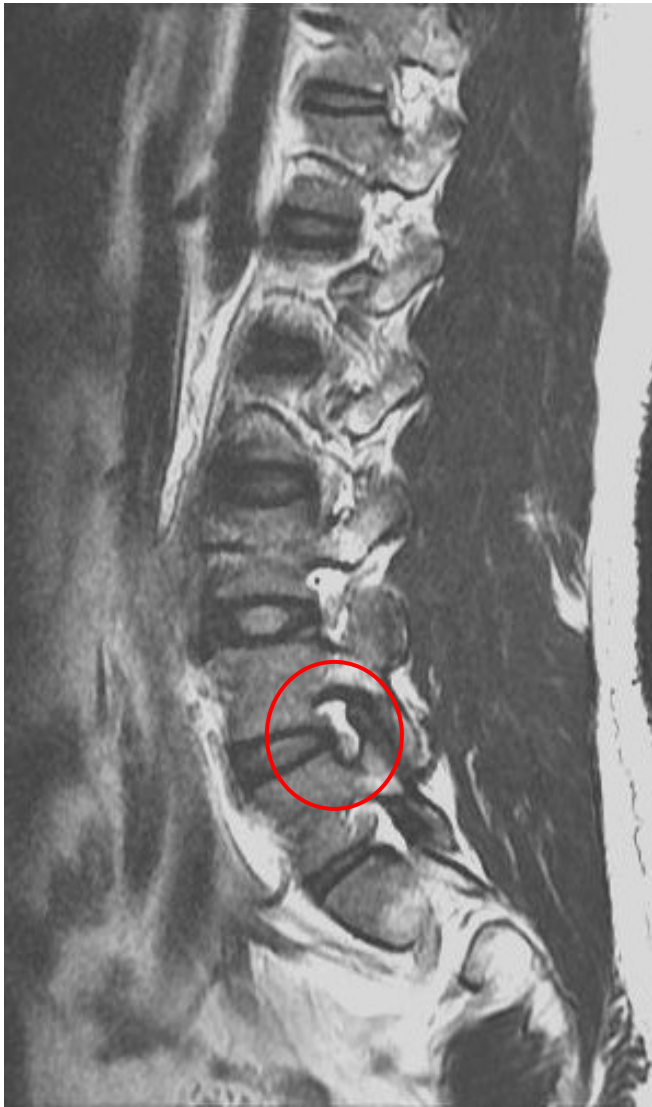


Figure 15:9. T2W sagittal image showing the right L4 nerve exiting at the bottom of the L4-L5 IVF. The L3 nerve is also lower than normal.

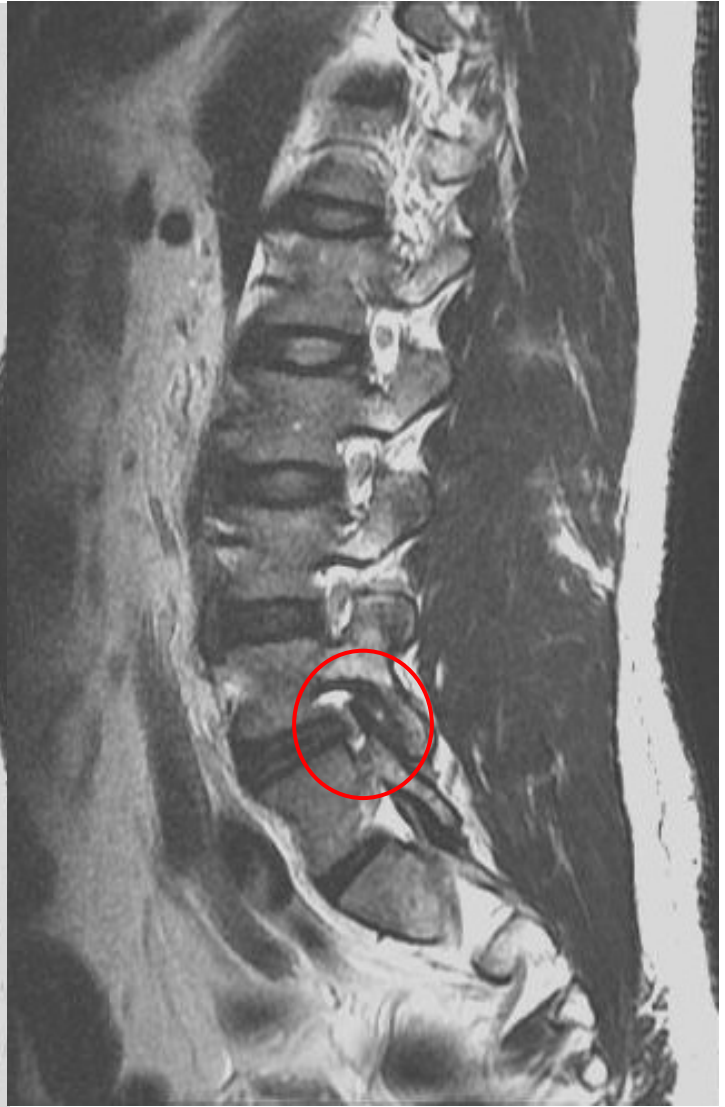


Figure 15:10. This T2W sagittal image of the same patient shows a foraminal disc protrusion entrapping the left L4 nerve root in the L4-L5 IVF.

Identifying Conjoined Nerve Roots on MRI

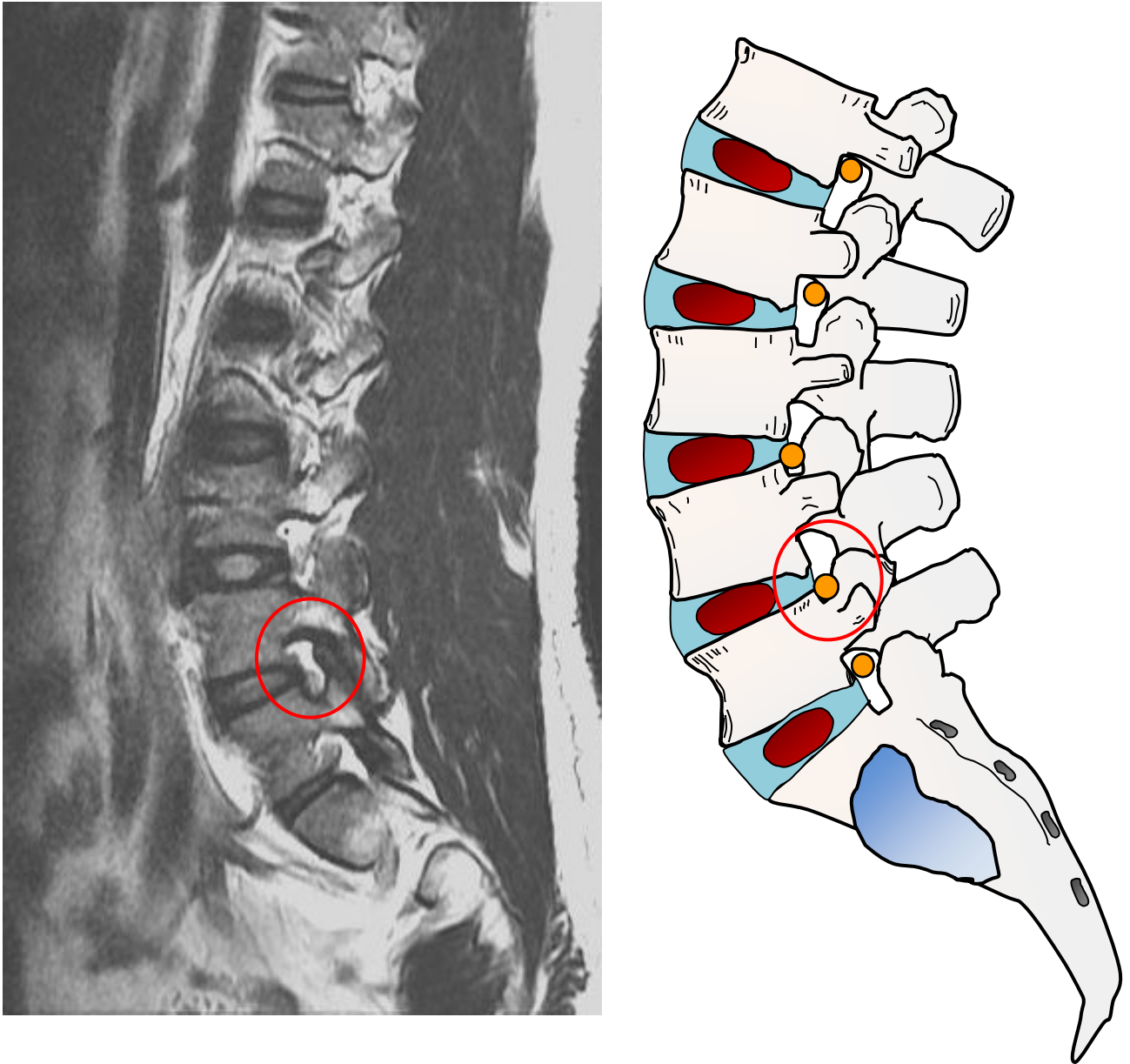
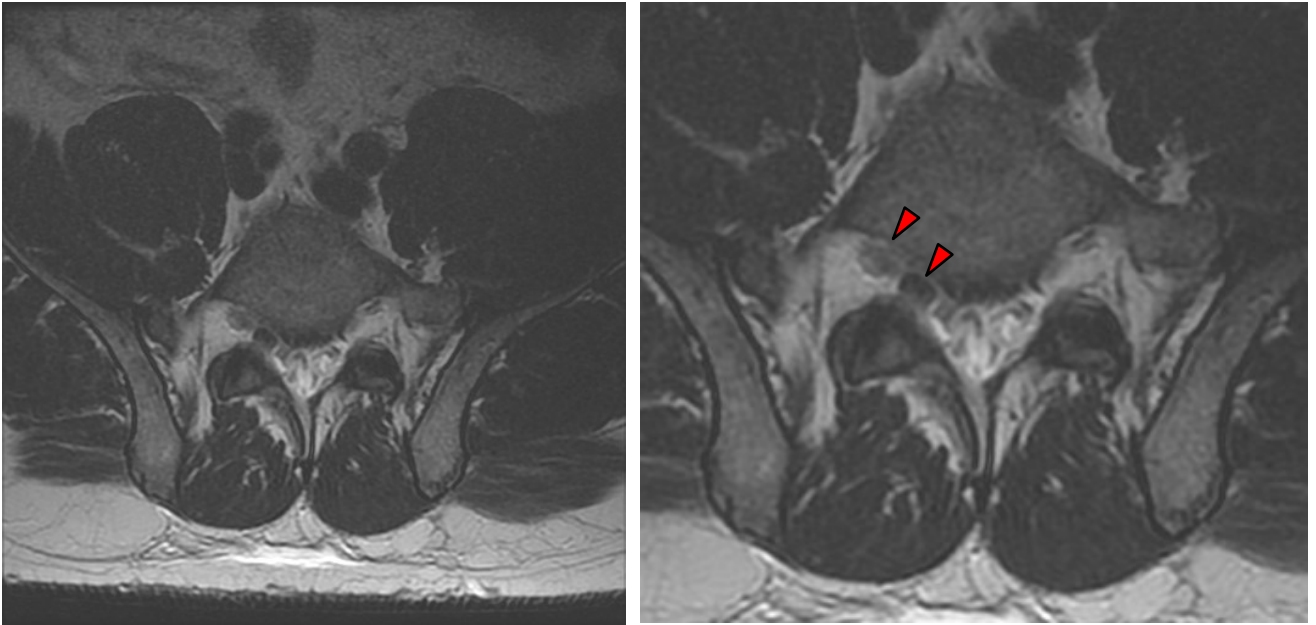


Figure 15:11. T2W sagittal image and schematic showing an anchoring of the L4 nerve root in the lower portion of the L4-L5 foramina.

Identifying Conjoined Nerve Roots on MRI



Figures 15:12 and 15:13. These axial T2W images show two nerve roots exiting the same foramina. This is highly suggestive of conjoined nerve roots.

MRI is certainly the most accurate and non-invasive diagnostic method for identifying conjoined nerve roots. Conjoined nerve roots can pose significant clinical concerns and complications. The occurrence rate in cadaver studies is approximately 8%. Clinically the reporting rate is much lower. This condition is hard to diagnose and frequently is missed by radiologists and clinicians.

L5 and S1 are the most common segments associated with this condition. There also seems to be an increased rate of conjoined nerve roots in patients with other vertebral malformations. These conditions include spina bifida, spondylolisthesis, and other posterior vertebral defects.

Suggested Reading

Scuderi GJ, Vaccaro AR, BrusovanikGV, Kwon BK, BertaSC. Conjoined lumbar nerve roots: A frequently underappreciated congenital abnormality. *Journal of Spinal Disorders & Techniques*: April 2004 - Volume 17 - Issue 2 - pp 86-93.

Böttcher J, Petrovitch A, Sörös P, Malich A, Hussein S, Kaiser WA. Conjoined lumbosacral nerve roots: current aspects of diagnosis. *European Spine Journal*. March 2004, Volume 13, Issue 2, pp 147-15.

Lotan R, Al-Rashdi A, Yee A, Finkelstein J. Clinical features of conjoined lumbosacral nerve roots versus lumbar intervertebral disc herniations *Eur Spine J*. 2010 July; 19(7): 1094–1098.

Neidre A, Macnab I. Anomalies of the lumbosacral nerve roots. Review of 16 cases and classification. *Spine*. 1983;8 (3): 294-9.

Song SJ, Lee JW, Choi JY et-al. Imaging features suggestive of a conjoined nerve root on routine axial MRI. *Skeletal Radiol*. 2008;37 (2): 133-8.

Mccormick CC. Developmental asymmetry of roots of the cauda equina at metrizamide myelography: report of seven cases with a review of the literature. *Clin Radiol*. 1982;33 (4): 427-34.

Classification of Spinal Cord Tumors and Masses by Location



Space Occupying Lesions, Tumors, and Masses

The identification, diagnosis, and classification of tumors and masses is best left to the experts: radiologists. Having said that, all MSK practitioners should have a basic understanding of the characteristics of space occupying lesions (SOL) and how they affect the surrounding structures.

The location descriptors in this chapter describe SOL location in relation to the spinal cord, cauda equina, and thecal sac. Spinal cord lesions fall into one of three categories: extradural, extramedullary, and intramedullary. Extradural lesions are spinal lesions found in the spine, but outside of the thecal sac. Intradural extramedullary lesions are found within the thecal sac, but outside of the spinal cord. Intramedullary lesions are found within the cord.

Extradural Lesions	Extramedullary Lesions	Intramedullary Lesions
<ul style="list-style-type: none">•Disc herniation•Metastasis to the vertebra•Synovial cyst•Hematoma•Abscess•Schwannoma*•Neurofibroma*	<ul style="list-style-type: none">•Schwannoma*•Neurofibroma*	<ul style="list-style-type: none">•Ependymoma•Astrocytoma•Hemangioblastoma•Syrinx•Demyelinating disease•Myelitis

*Schwannomas and neurofibromas can be found intradurally and extramedullary. They are not intramedullary lesions.

Location Classification of Spinal Tumors and Masses

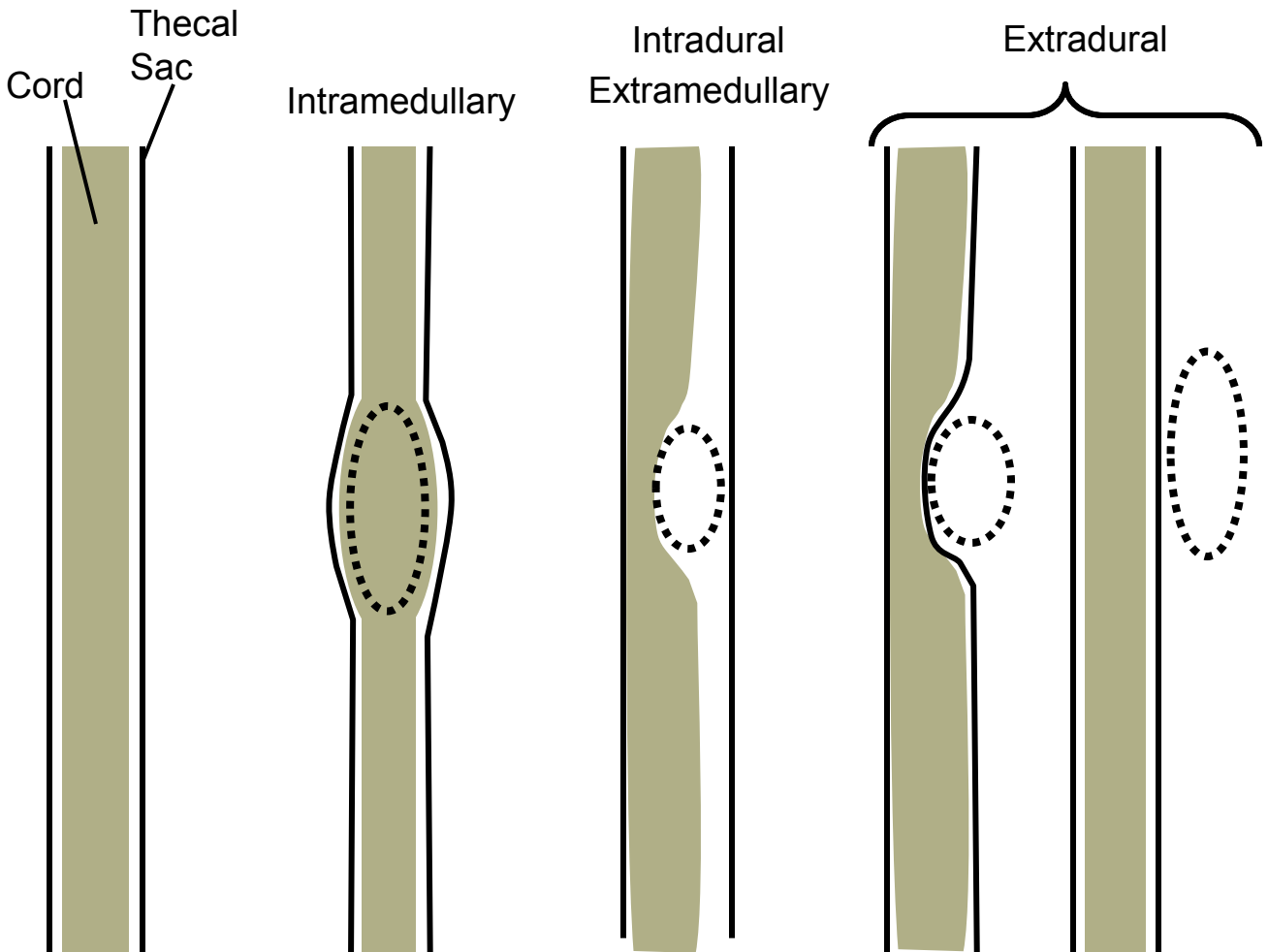


Figure 16:1. Space occupying lesions of the spine are categorized by their location and relationship to the thecal sac and to the spinal cord.

Space occupying lesions of the spine are categorized by their location and relationship to the thecal sac and to the spinal cord. Is the lesion within or outside of the cord? Is it in or outside of the thecal sac? Is the lesion inside the thecal sac, but outside of the cord. These are the location identifiers for space occupying lesions of the spine. Lesions within the cord are called intramedullary lesions, cysts, or tumors. Lesions within the dura mata (the membrane of the thecal sac) are intradural lesions. Those located outside the dura mata are called extradural lesions, masses, cysts or tumors. Since the cord terminates high in the lumbar spine, there will be few truly intramedullary lesions. We can see expansive lesions in the conus medullaris and the filum terminale as well as in the caudal equina.

Intramedullary Tumors

Intramedullary

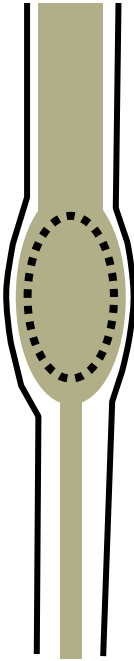


Figure 16:2.

Ependymomas are an example of an intramedullary tumor. They are usually slow growing benign tumors arising from the epithelial lining of the spinal cord's central canal. These images show an expansive ependymoma within the filum terminale.

Ependymomas are the most common primary tumors of the spinal cord. As in this case they most frequently occur in the lower portion of the spinal cord or in the filum terminale.

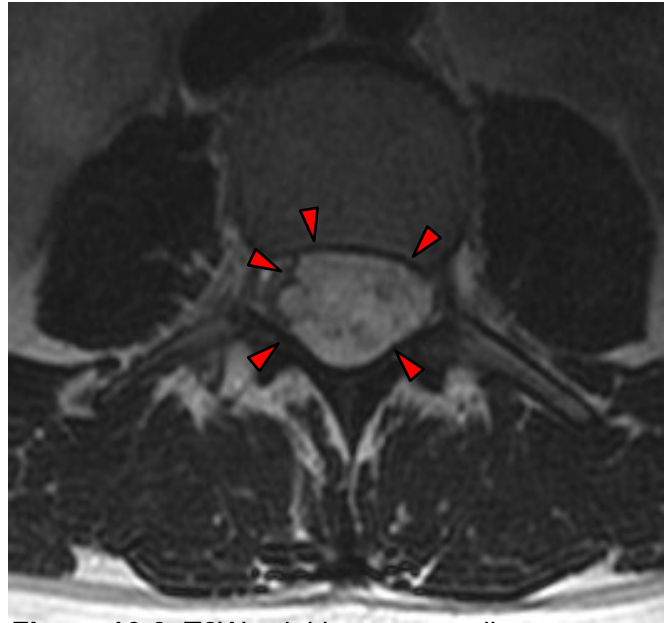


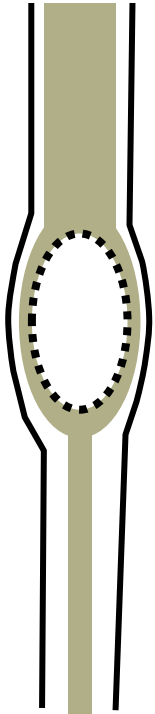
Figure 16:3. T2W axial image revealing an ependymoma filling most of the central canal.



Figure 16:4. T2W sagittal image revealing an ependymoma arising from the filum terminale.

Intramedullary Tumors and Masses

Intramedullary



These images display a conus medullaris cyst. This lesion is considered an intramedullary cyst. The use of FIESTA (Fast Imaging Employing Steady sTate Acquisition) imagery helps to clearly visualize cystic lesions of this type.

Figure 16:5.

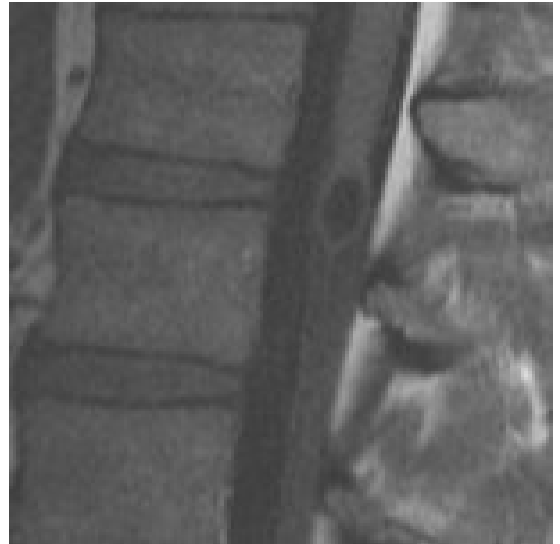


Figure 16:6. Sagittal T1 weighted image showing the conus medullaris cyst as a dark void.

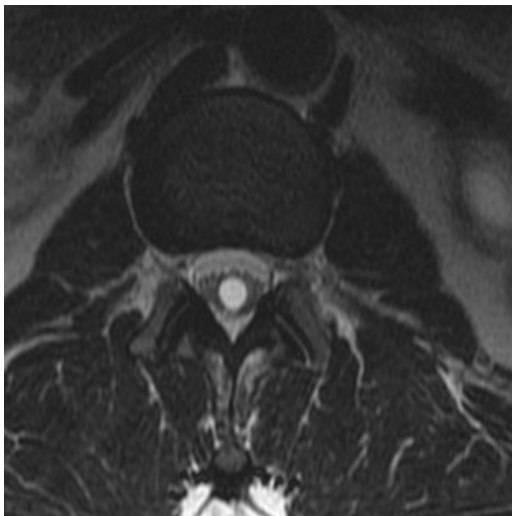


Figure 16:7. Axial FIESTA images revealing a conus medullaris cyst.

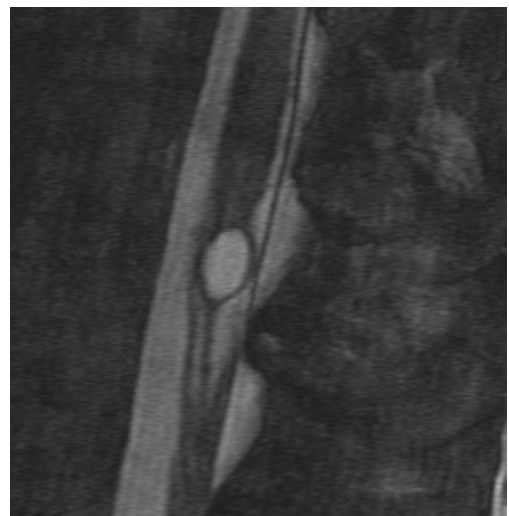


Figure 16:8. Sagittal FIESTA image revealing a conus medullaris cyst.

Intramedullary Tumors and Masses: Syrx

Intramedullary



Figure 16:9.

Cavities within the spinal cord can have a significant clinical impact. The term syrinx is used to describe a fluid-filled cyst within the central canal of the spinal cord. The CSF-filled cyst can expand outward, compressing and damaging nerves. These are rarely seen in the lumbar spine, so a thoracic example is used here.



Figure 16:10. Syrinx in a thoracic spine T2W sagittal image.



Figure 16:11. A T2W axial image shows the expansiveness of this syrinx.

Intradural/Extramedullary Tumors and Masses: Lipoma

Intradural
Extramedullary



Figure 16:12

An intradural lipoma has the potential to create significant adverse effects. This space occupying lesion is an intradural extramedullary mass which has the potential to anchor the cord and cause severe neurological impediment.



Figure 16:13. Axial T2 weighted image showing a lipoma in the thecal sac.



Figure 16:14. Sagittal T1 weighted image showing a large lipoma (yellow arrow) within the thecal sac.

Extradural Tumors and Masses

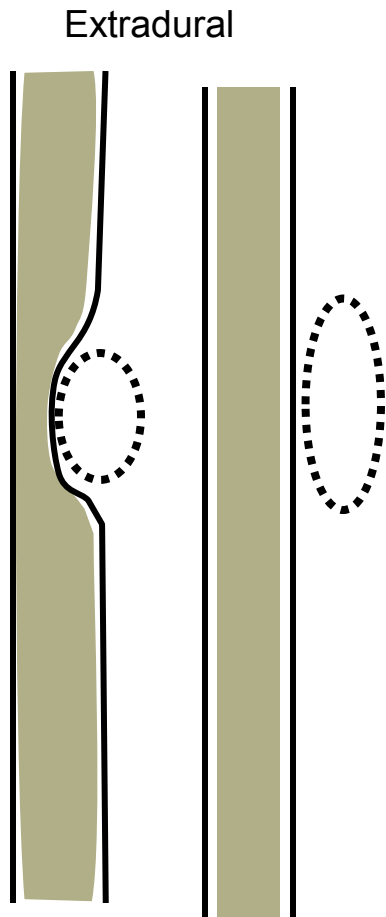


Figure 16:15.

An extradural lesion is located outside of both the dura and the cord. It may or may not compress or efface the thecal sac or cord.



Figure 16:16. This image displays an extradural mass effacing the thecal sac.

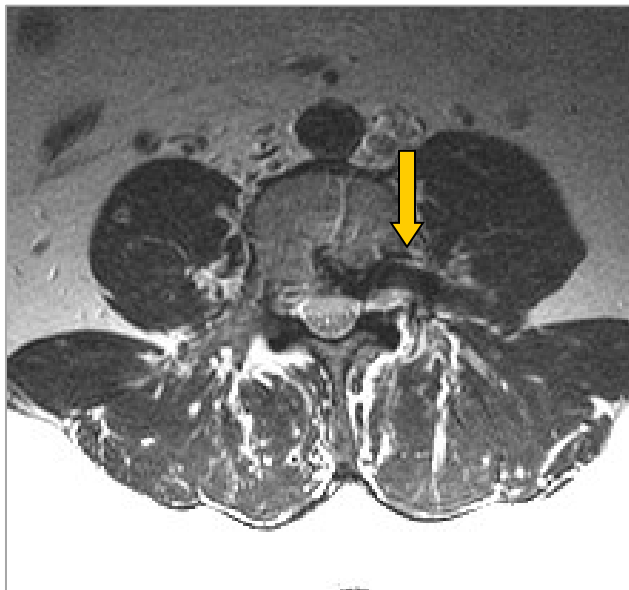


Figure 16:17. This vascular anomaly of the intervertebral vein is an extradural lesion.

Extradural Tumors and Masses

Extradural

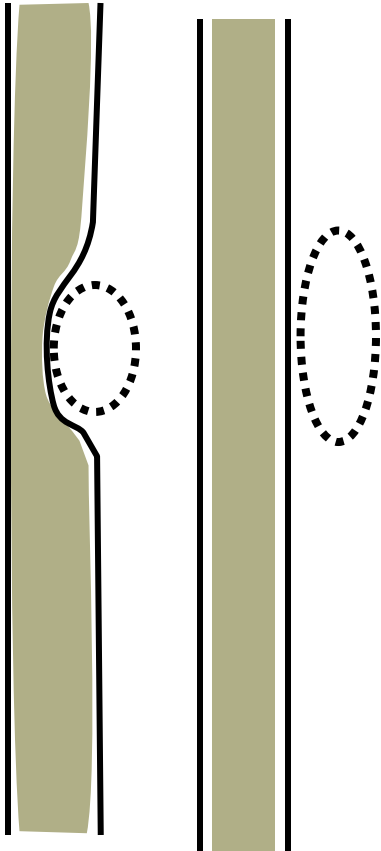


Figure 16:18.

An extradural lesion is located outside of both the dura and the cord. It may or may not compress or efface the thecal sac or cord.



Figure 16:19. A schwannoma enhanced with gadolinium. This schwannoma is an example of an extradural lesion.

Suggested Reading

Börm W, Gleixner M, Klasen J. Spinal tumors in coexisting degenerative spine disease--A differential diagnostic problem. *Eur Spine J* 2004;13:633-8.

El-Mahdy W, Kane PJ, Powell MP, Crockard HA. Spinal intradural tumours: Part I--Extramedullary. *Br J Neurosurg* 1999;13:550-7.

Grimm S, Chamberlain MC. Adult primary spinal cord tumors. *Expert Rev Neurother* 2009;9:1487-95.

Hogen Esch RI, Staal MJ. Tumors of the cauda equina: The importance of an early diagnosis. *Clin Neurol Neurosurg* 1988;90:343-8.

Yuh EL, Barkovich AJ, Gupta N. Imaging of ependymomas: MRI and CT. *Childs Nerv Syst.* 2009 October; 25(10): 1203–1213.

Lee RR. MR imaging of intradural tumors of the cervical spine. *Magn Reson Imaging Clin N Am* 2000;8:529-40.

Wu JS, Hochman MG. Soft-tissue tumors and tumorlike lesions: a systematic imaging approach. November 2009 *Radiology*, 253, 297-316.

Atlas SW. (2008). *Magnetic resonance imaging of the brain and spine* (forth edition). Lippincott Williams & Wilkins.

Ross JS et al. (2010). *Diagnostic imaging spine* (second edition). Amirsys Inc.

Bogduk N. (2012). *Clinical and radiological anatomy of the lumbar spine*. Churchill Livingstone.

Perineural (Tarlovs) Cysts

17



Perineural (Tarlovs) Cysts

Perineural cysts (aka Tarlov cysts, Tarlovs cysts, and Tarlov's cysts) are fluid-filled meningeal dilations of the posterior nerve root sheath, usually at the dorsal root ganglion. They are commonly viewed in the sacrum but can also be observed in the lumbar, thoracic, and cervical spine. Dr. Isadore Tarlov first described the presence of perineural cysts in 1931 while studying the histology of the filum terminale at Royal Victoria Hospital in Montreal. Since then, this finding has borne his name. Despite its identification 70 years ago, scant scientific knowledge is available about this condition. Studies have shown perineural cysts to be present in 4.6-9% of the population. Although they are usually considered a coincidental finding on MRI and predominantly asymptomatic, some authors have reported perineural cysts to be symptomatic up to 20% of the time (1% of the total population, 20% of those with perineural cysts) and could pose a challenge to both the patient and the clinician.

Radiography

The advent of advanced diagnostic imagery such as MRI and CT has resulted in more frequent reports of perineural cysts. However, it is rare for any diagnostic imaging procedure to be ordered for the sake of identifying a perineural cyst. Perineural cysts are commonly found on MRIs taken for other diagnostic purposes.

On MRI, perineural cysts are typically seen as well-circumscribed and ovoid in shape. They tend to exist as singularities and less often in clusters. T2 weighted MRI is the preferred medium to view perineural cysts. In T2 weighted MRI, water density appears white; in T1 weighted MRI, water density structures appear black and may be more difficult for the less experienced eye to visualize. Perineural cysts can also be made visible with computer tomography (CT), particularly when intrathecal contrast enhancement is used. CT with enhancement is used to determine the degree of communication between the perineural cysts and the thecal sac. Bony erosion caused by perineural cysts can be identified on plain film radiographs, but this is not the preferred medium for viewing this phenomenon.

What is a Perineural (Tarlovs) Cyst?

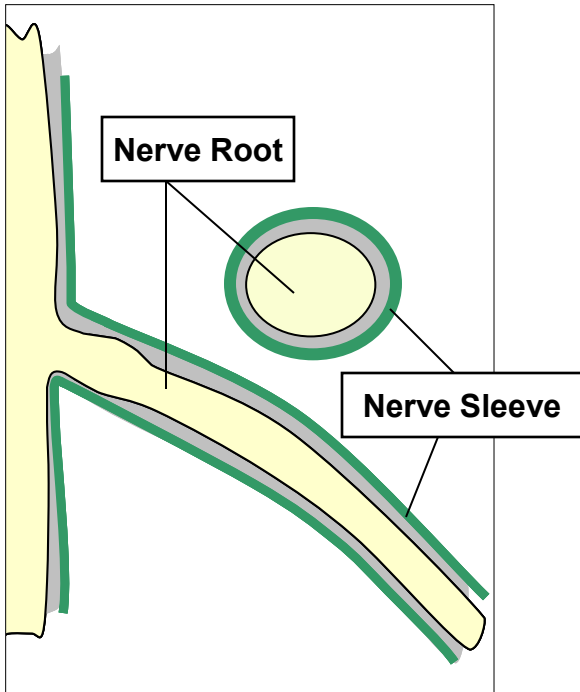


Figure 17:1. Schematic of the normal nerve root .

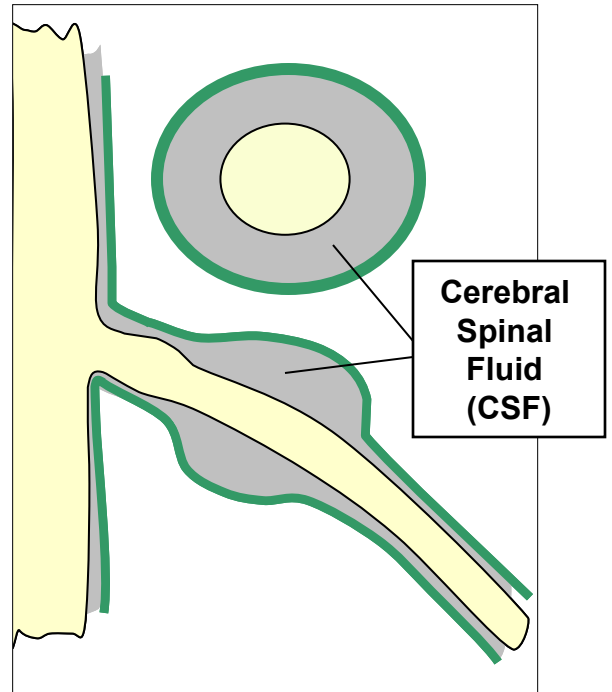


Figure 17:2. Dilation of the nerve sleeve filling with CSF.

Perineural cysts are fluid-filled meningeal dilations of the posterior nerve root sheath, usually at the dorsal root ganglion. These schematics illustrate the normal relationship of the dural sleeve and the nerves.



Figure 17:3. This image of the sacrum shows eight perineural cysts clustered together like a cluster of grapes.

Characteristics of Perineural Cysts on MRI

This sequence of images demonstrates the characteristics of two large perineural cysts affecting the dural sleeves of the S2 nerve roots. Note the high intensity of the perineural dilation of the cysts in T2 and the low intensity of the cysts on T1. These images also reveal significant bony erosion of the sacrum which weakens the integrity of the sacrum.

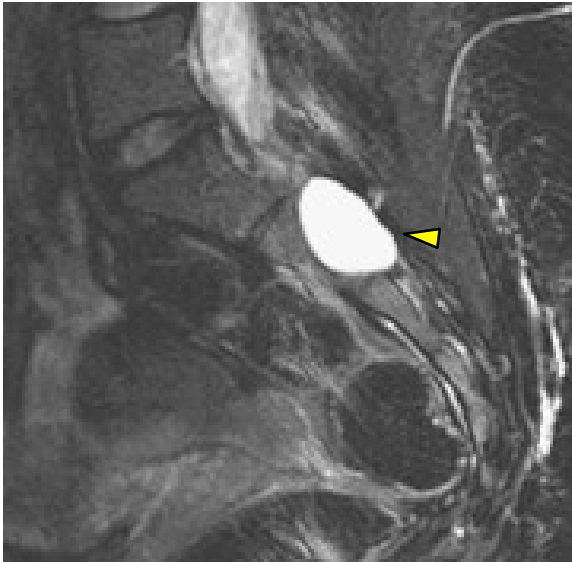


Figure 17:4. Large ovoid perineural cysts affecting the sleeve of the S2 nerve root on fat-suppressed T2 weighted image.

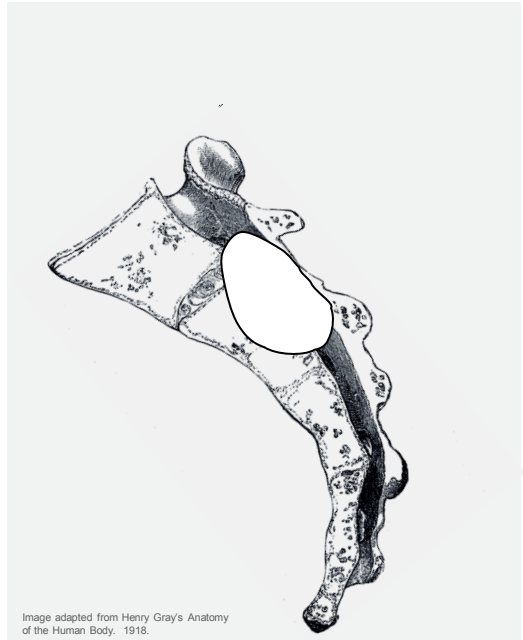


Figure 17:5. Schematic of the cyst.

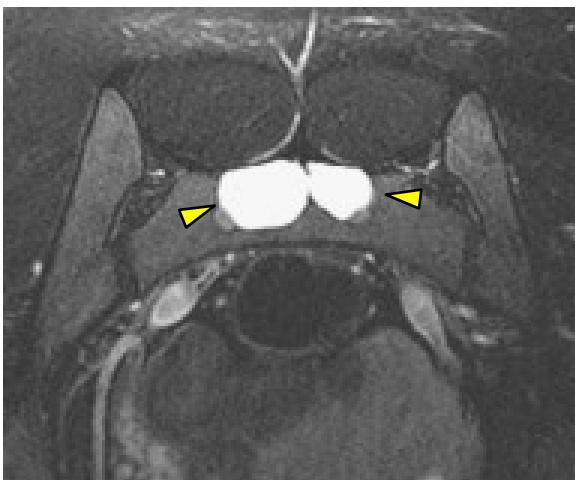


Figure 17:6. Axial fat-suppressed T2 weighted image demonstrating two large perineural cysts in the sacrum.

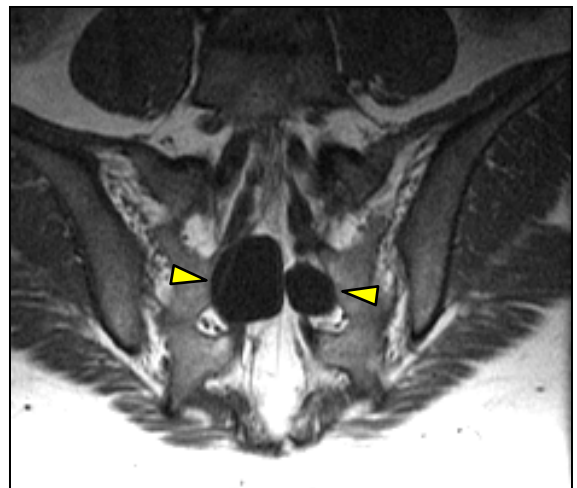


Figure 17:7. T1 image of perineural cysts. Fat is hyper-intense while the perineural cysts are hypointense (black).

Multiple Cysts of the Perineural Tissues

Perineural cysts may be seen in clusters. They all appear like a cluster of grapes or like bubbles. Multiple cysts may be seen at every level of the spine, but are most common in the sacrum.



Figure 17:8. T2 weighted sagittal image revealing multiple expansive perineural cysts causing erosion of the sacrum.



Figure 17:9. T1 weighted sagittal version of the same sagittal slice.

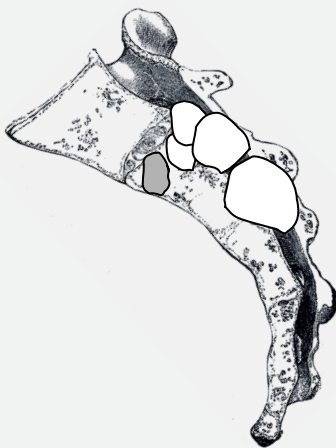


Image adapted from Henry Gray's Anatomy of the Human Body. 1918.

Figures 17:10 and 17:11. These illustrations demonstrate the relationship of this expansive cluster of cysts (left) and a normal cross-section of sacrum (right).

Typical Presentation of Perineural Cysts

The previous two pages presented perineural cysts that were noteworthy due to their size or number. This page will demonstrate the typical presentation of a perineural cyst. Typically they are solitary, seen in the sacrum and affecting the S2 (or less likely the S1) nerve roots. They are ovoid in shape and well defined.



Figure 17:12. T1 weighted sagittal image.

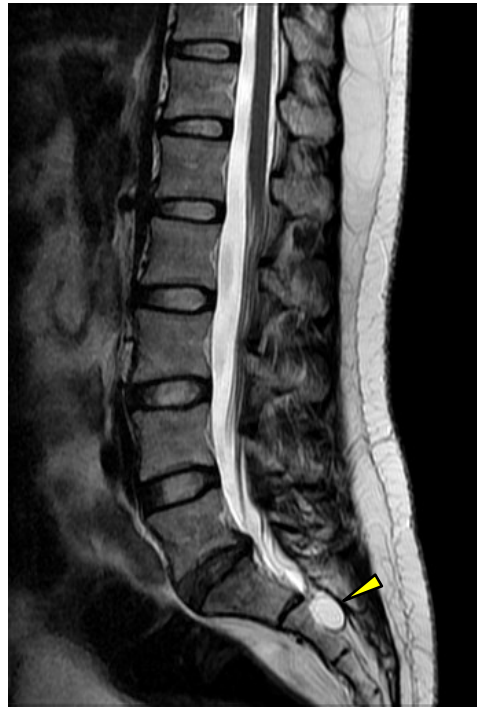


Figure 17:13. T2 weighted sagittal image.

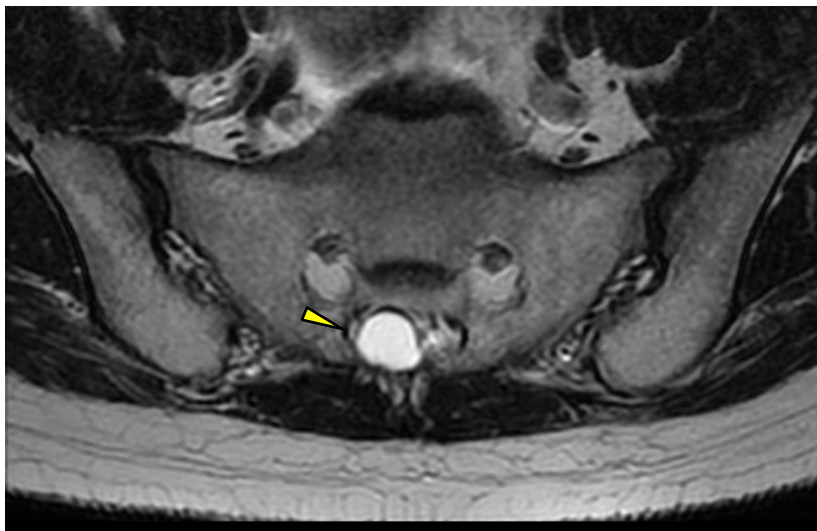


Figure 17:14. T2 weighted axial image.

Large Perineural Cyst Displacing the Thecal Sac

These images display a large perineural cyst which displaces the thecal sac at the level of L2-3.



Figure 17:15. Sagittal T1W image.



Figure 17:16. Sagittal T2W image.

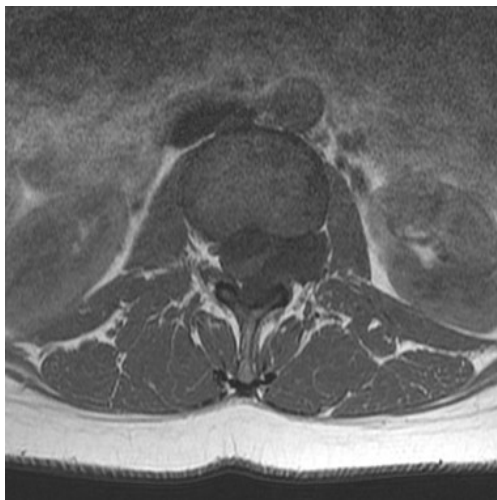


Figure 17:17. T1W axial image.

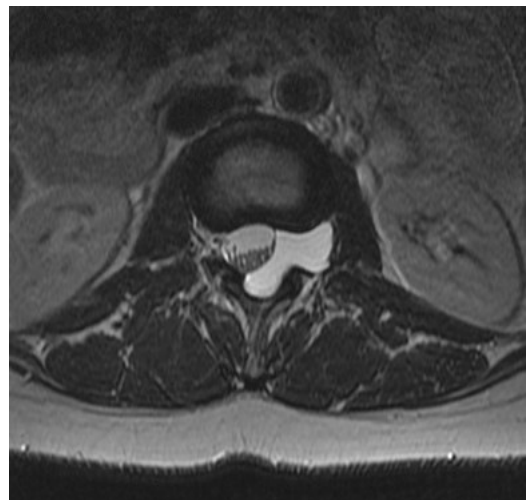


Figure 17:18. T2W axial image.

Suggested Reading

Langdown AJ, Grundy JR, Birch NC. The clinical relevance of Tarlov cysts. *J Spinal Disord Tech.* 2005;18:29–33.

Paulsen RD, Call GA, Murtagh FR. Prevalence and percutaneous drainage of cysts of the sacral nerve root sheath (Tarlov cysts) *AJNR Am J Neuroradiol.* 1994;15:293–297. discussion 298-299.

Seaman WB, Furlow LT. The myelographic appearance of sacral cysts. *J Neurosurg* 1956;13:88-94.

Paulsen RD, et al. Prevalence and percutaneous drainage of cysts of the sacral nerve root sheath (Tarlov cysts). *AJNR* 1994; 15:293,297.

Mummaneni PV, et al. Microsurgical treatment of symptomatic sacral Tarlov cysts. *Neurosurgery* 2000; 47:74-79.

Bartels RH, van Overbeeke JJ. Lumbar cerebrospinal fluid drainage for symptomatic sacral nerve root cysts: an adjuvant diagnostic procedure and/or alternative treatment? Technical case report. *Neurosurgery* 1997; 40:861-865.

Patel MR, et al. Percutaneous fibrin glue therapy of meningeal cysts of the sacral spine. *AJR* 1997; 168:367-370.

Voyadzis JM, e. Tarlov cysts: a study of 10 cases with review of the literature. *J Neurosurg (Spine 1)* 2001;95:25-32.

Wu JS, Hochman MG. Soft-tissue tumors and tumorlike lesions: a systematic imaging approach. November 2009 *Radiology*, 253, 297-316.

Tarlov IM. Perineural cysts of the spinal nerve roots. *Arch Neural Psychiatry.* 1938;40:1067–74.

Prashad B, Jain AK, Dhammi IK. Tarlov cyst: Case report and review of literature *Indian J Orthop.* 2007 Oct-Dec; 41(4): 401–403.

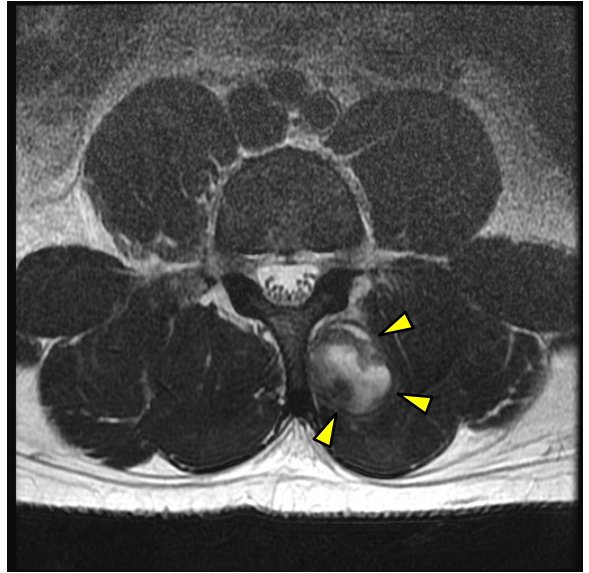
Hematomas

18



Paraspinal Hematoma

Trauma in the form of a blow, fall, or tearing of tissue can result in bleeding into the soft tissues. Patients with increased bleeding tendencies may have hematomas without noting trauma. This internal bleeding can result in the formation of a space occupying pocket of blood, a hematoma. These images show a hematoma that appeared nine days prior in the left paraspinal L3-4 region. Note the heterogenic appearance that is particularly evident in the T2 weighted images.



Figures 18:1 and 18:2. T2W axial image showing a hematoma in the left (right side in these images) paraspinal muscles.

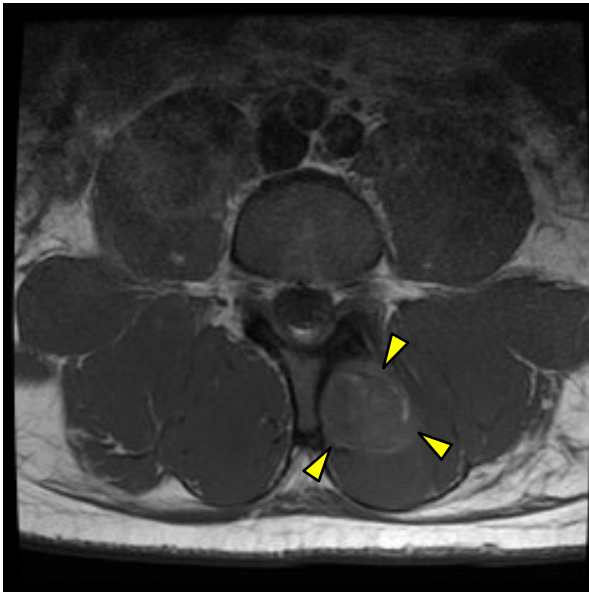


Figure 18:3. T1W axial image showing a hematoma in the left paraspinal muscles.

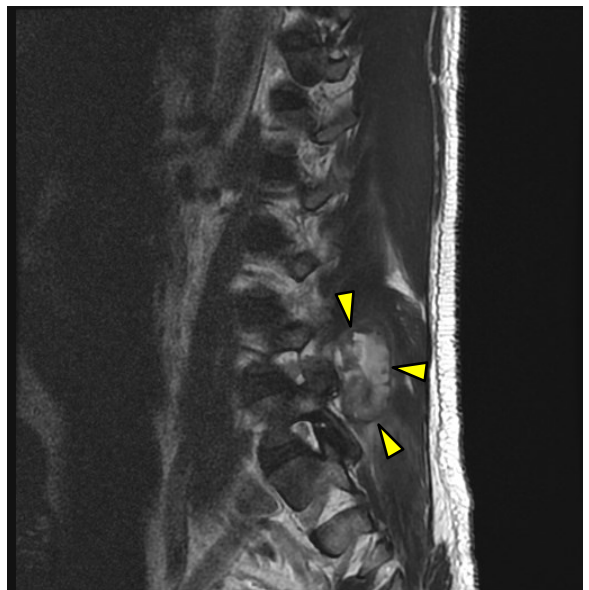


Figure 18:4. T2W sagittal image showing a hematoma in the paraspinal muscles.

Paraspinal Hematoma

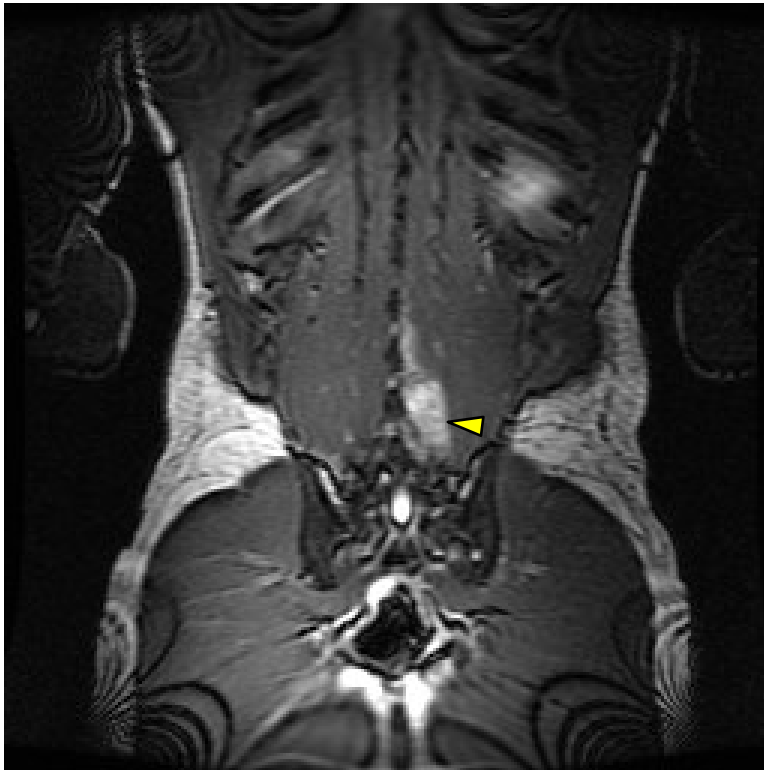


Figure 18:5. Coronal image showing the hematoma in the left multifidus.

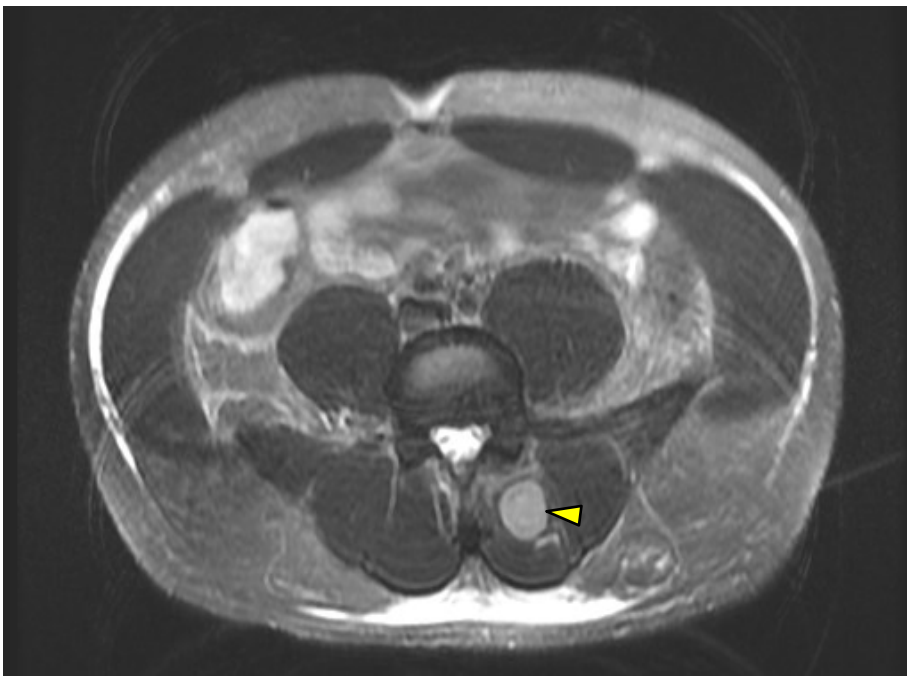


Figure 18:6. T2 fat-saturated axial image showing the hematoma in the left paraspinal muscles.

Right Iliacus Hematoma

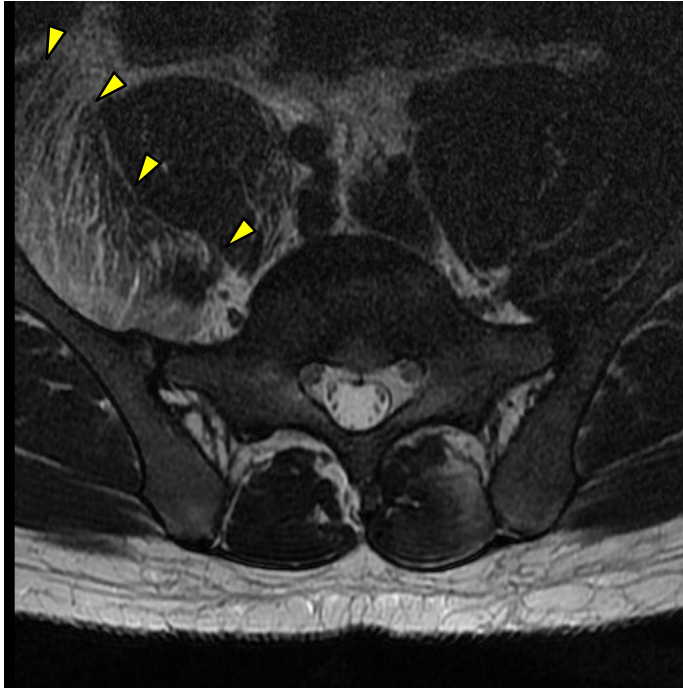


Figure 18:7. T2 weighted image showing the hematoma in the right iliacus designated by yellow arrows.

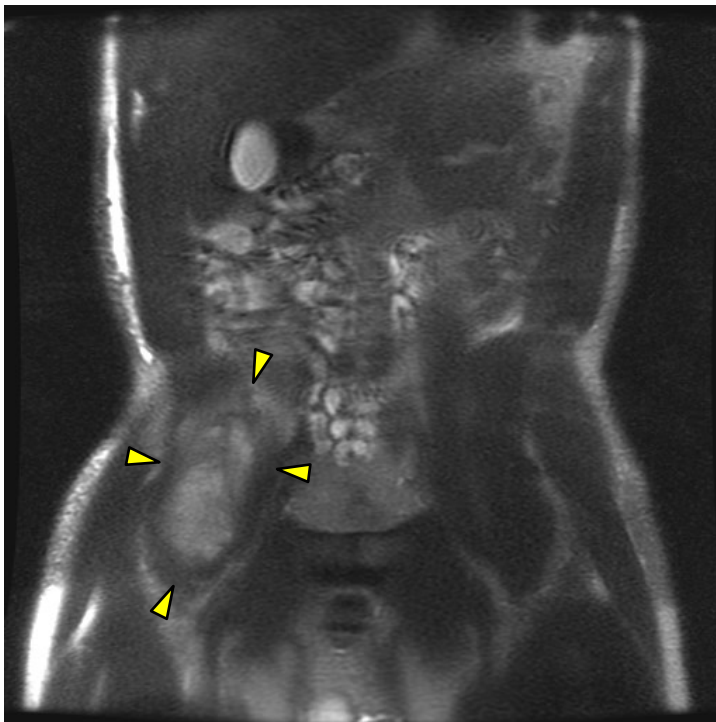


Figure 18:8. Coronal image showing the hematoma in the right iliacus (yellow arrows).

Hematoma

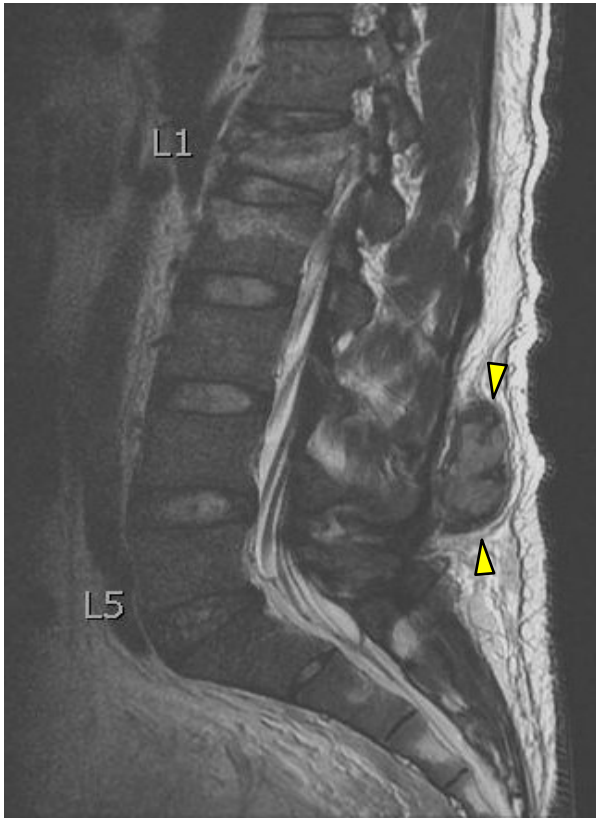


Figure 18:9. Post-traumatic hematoma posterior to L4. Note the compression fracture of L1.

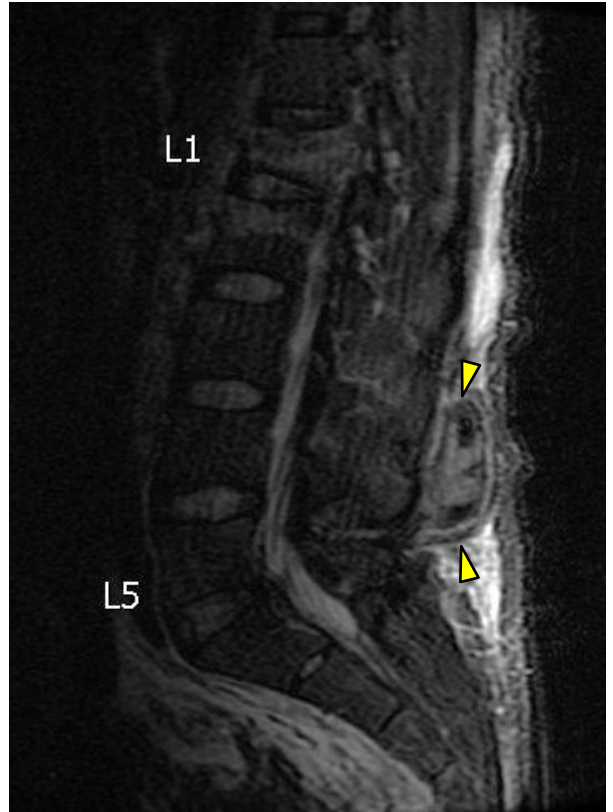


Figure 18:10. Post-traumatic hematoma posterior to L4.

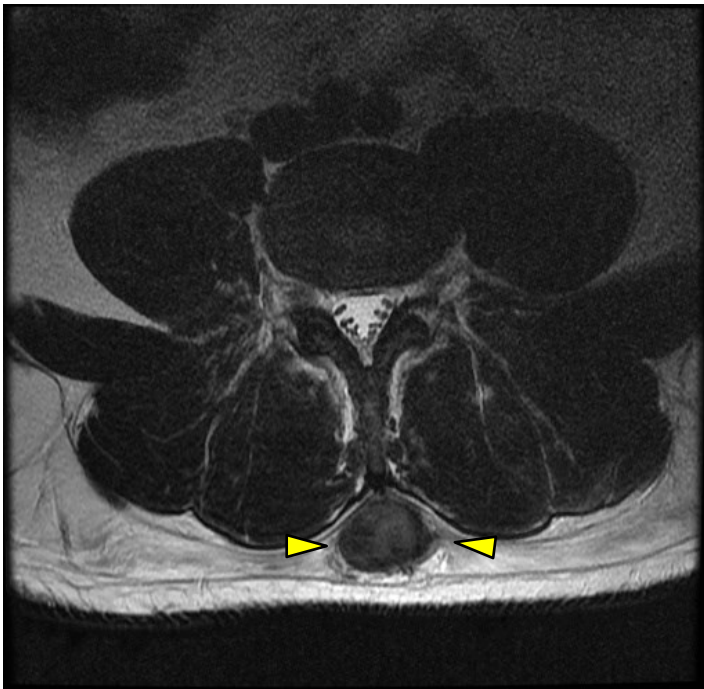


Figure 18:11. Post-traumatic hematoma posterior to L4.

Suggested Reading

Wu JS, Hochman MG. Soft-tissue tumors and tumor like lesions: a systematic imaging approach. November 2009 *Radiology*, 253, 297-316.

Lee YS, Kwon ST, Kim JO, Choi ES. Serial MR imaging of intramuscular hematoma: experimental study in a rat model with the pathologic correlation. *Korean J Radiol.* 2011 Jan-Feb; 12(1): 66–77.

Cramer G, Darby S (2013). *Basic and clinical anatomy of the spine, spinal cord, and ANS* (third edition). Elsevier Mosby.

Marchiori D (2013). *Clinical imaging: with skeletal, chest and abdomen pattern differentials* (third edition). Mosby.

Metastasis

19



Metastasis

It cannot be overstated that clinicians should always have MRIs read by a board certified radiologist. It is assumed that this book is not adequate instruction in itself for diagnosing neoplasms. Always consult with your radiologist when there is a history of cancer or when cancer is suspected.

If you believe that your radiologist may have missed a neoplasm, contact the radiologist and discuss the images. Have the image identifiers available to share with the radiologist.



Figure 19:1. T1 weighted sagittal image of vertebral body metastasis at L1 and L4.

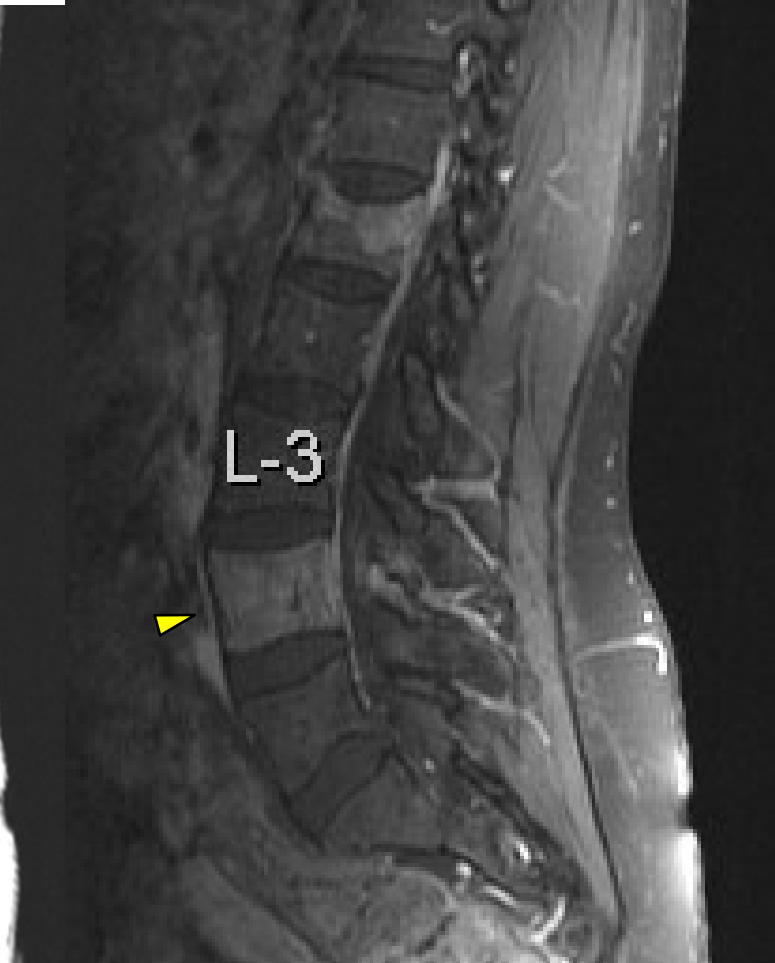


Figure 19:2. This sagittal T1 fat sat image was taken after the administration of gadolinium. Note how the appearance of the metastatic disease is heightened by the enhancing agent.

Metastases



Figures 19:3 and 19:4. T2W sagittal images of the lumbar spine show diffuse metastases and bony disruption.

Neoplasms of the spine can arise as primary lesions from the spine or can metastasize from another region of the body. The most common sites that cancer has metastasized to the spine from includes the lungs, prostate, and breasts. If one tumor is found, it is termed *metastasis*; if multiple tumors are found it is referred to as *metastases*. When cancer spreads to the spine, the vertebrae become brittle. This often leads to compression fractures.

Characteristics of Metastases on Lumbar MR



Figure 19:5. T1 weighted sagittal image revealing diffuse metastases of the lumbar spine .



Figure 19:6. T2 weighted sagittal image.

	T1	T2	T2 with Fat suppression
Metastases	Dark	Bright	Bright

Figure 19:7. Characteristics of metastases on T1,T2, and T2 with fat suppression.

Differentiating Fat in Bones from Bony Metastases



Figure 19:8. Fatty infiltration into the vertebral bodies in this T2WI.



Figure 19:9. Metastases into the vertebral bodies on a T2WI.

Fatty infiltration into bone can have a heterogeneous mottled appearance that may appear to look like metastases, and metastases may appear to the clinician like fatty infiltration. On MRI comparing T1, T2, and fat suppressed images will help to distinguish fat infiltration from neoplasms (see figure 19:10). It is important to always defer to a trained radiologist for the identification of pathology.

Differentiating Fat from Bony Metastases			
	T1	T2	T2 with fat suppression
Fat	Bright	Bright	Dark
Metastases	Dark	Bright	Bright

Figure 19:10. Characteristics of fat and bony metastases on MRI.

Characteristics of Metastases on Lumbar MR

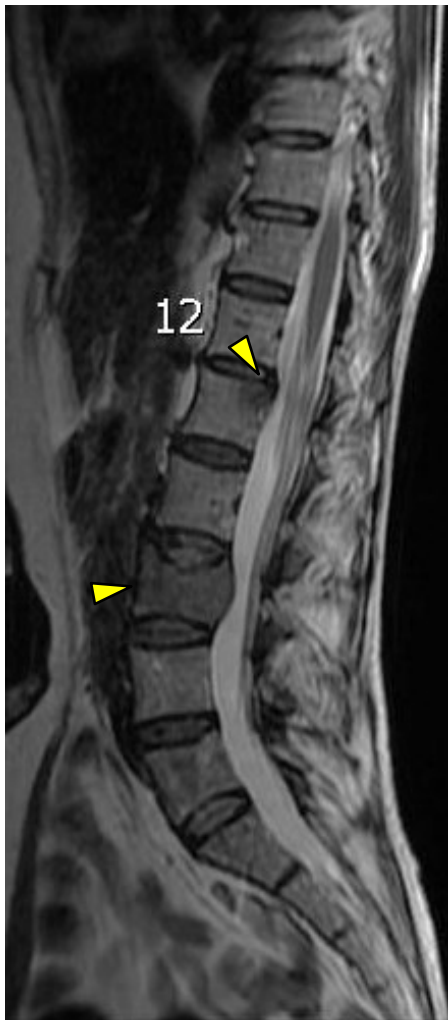


Figure 19:11. Metastases of thyroid cancer to the vertebral bodies of L1 and L3 is visible on this sagittal T2 image.

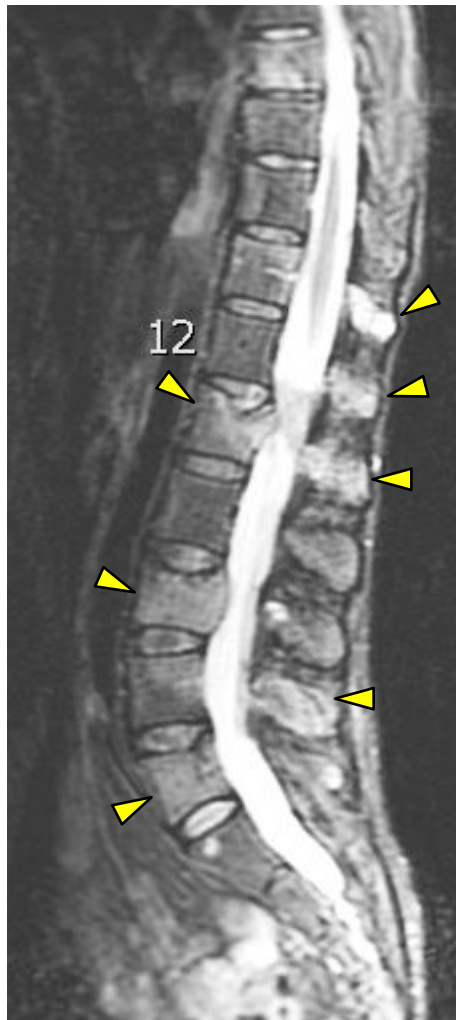


Figure 19:12. By selecting the proper MRI enhancements the cancer becomes more evident. This T2 image with fat suppression helps to reveal additional metastases.

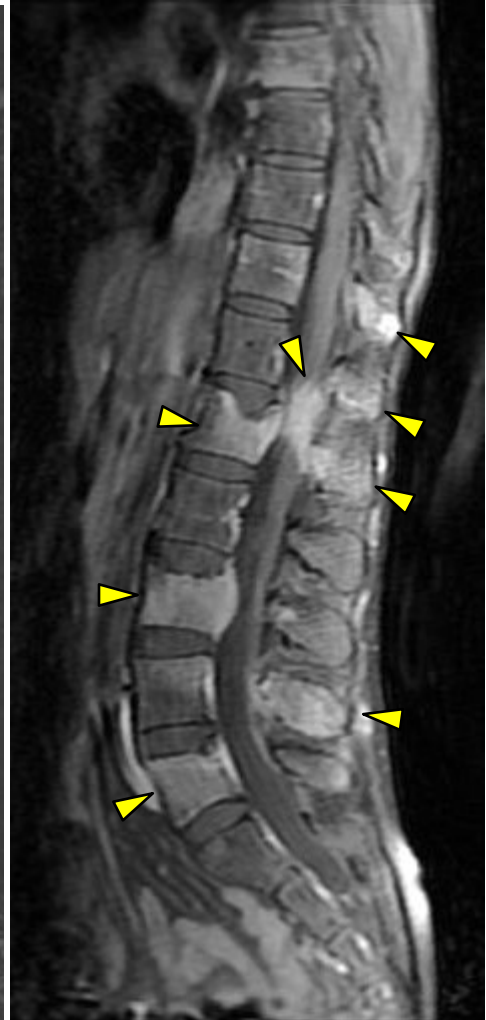


Figure 19:13. This T1 fat sat image with gadolinium enhancement further illuminates the extent of the metastases.

When cancer is suspected, it is a good idea to communicate with a radiologist to ensure that the most appropriate studies are requested. Certain MRI studies are very effective at illuminating metastases. Compare these three images and the impact that the various image types have on visualizing the cancer.

Characteristics of Metastases on Lumbar MR

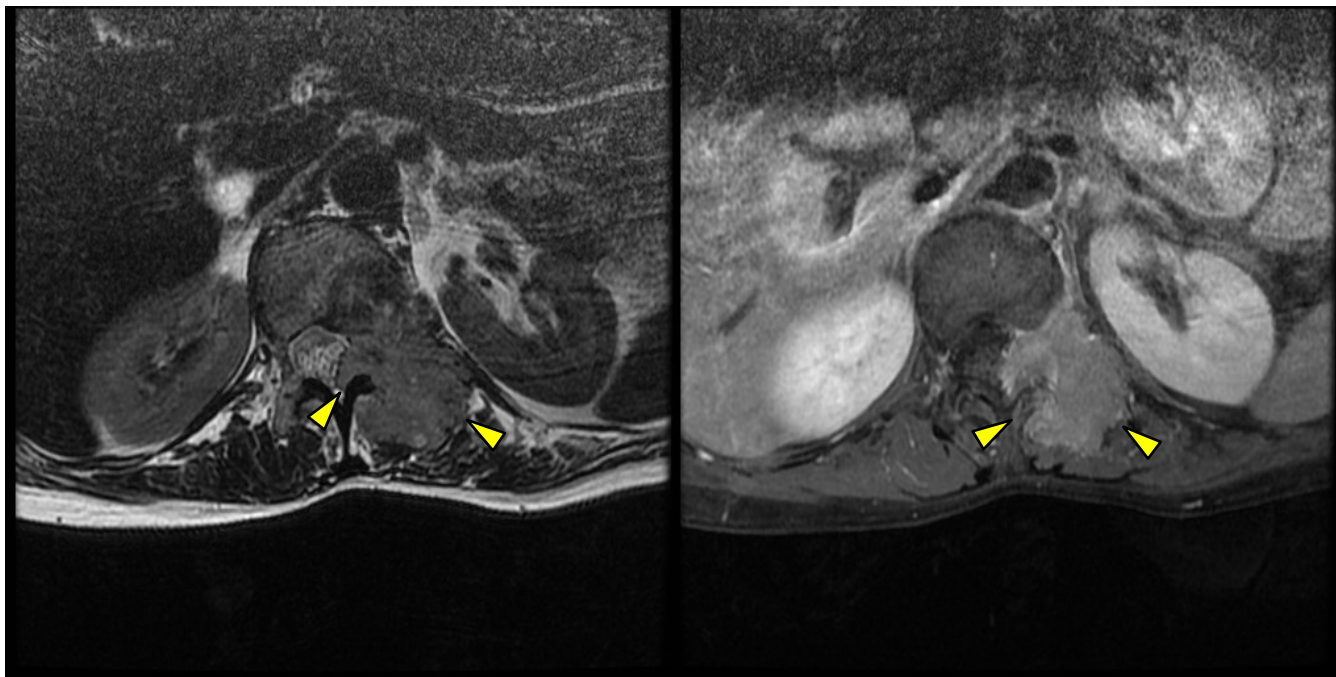


Figure 19:14. Metastasis of thyroid cancer to L1. This large mass is visible on T2WI.

Figure 19:15. Metastasis of thyroid cancer to L1. This T1 fat sat image with gadolinium enhancement brings out the details of this metastasis.

Suggested Reading

Wu JS, Hochman MG. Soft-tissue tumors and tumorlike lesions: a systematic imaging approach. November 2009 *Radiology*, 253, 297-316.

Guise TA, Mohammad KS, Clines G et-al. Basic mechanisms responsible for osteolytic and osteoblastic bone metastases. *Clin. Cancer Res.* 2006;12 (20 Pt 2): 6213s-6216s.

Sebastian PR, Fisher M, Smith TW et-al. Intramedullary spinal cord metastasis. *Surg Neurol.* 1981;16 (5): 336-9.

Beall DP, Googe DJ, Emery RL et-al. Extramedullary intradural spinal tumors: a pictorial review. *Curr Probl Diagn Radiol.* 36 (5): 185-98.

Kalayci M, Cağavi F, Gül S et-al. Intramedullary spinal cord metastases: diagnosis and treatment - an illustrated review. *Acta Neurochir (Wien).* 2004;146 (12): 1347-54.

Marchiori D (2013). *Clinical imaging: with skeletal, chest and abdomen pattern differentials* (third edition). Mosby.

Atlas SW. (2008). *Magnetic resonance imaging of the brain and spine* (forth edition). Lippincott Williams & Wilkins.

Ross JS et al. (2010). *Diagnostic imaging spine* (second edition). Amirsys Inc.

Tumors: Schwannomas and Ependymomas

20



Schwannoma

Schwannomas are benign nerve sheath tumors that are composed entirely of Schwann cells. Since these tumors are benign, the major clinical impact arises from compression of other tissues, particularly nerve tissue. Schwann cells are supportive of nerves and encompass the axons. Schwannomas are extramedullary (outside the spinal cord) neoplasms. These tend to arise in middle-aged adults with a male to female prominence of 3:1 and may present with symptoms similar to those of herniated discs.

On MRI schwannomas are typically hypointense on T1 weighted images and hyperintense and heterogeneous on T2 weighted images. Schwannomas are enhanced with gadolinium.

The following two pages show the characteristics of a schwannoma in various MRI orientations and image types.

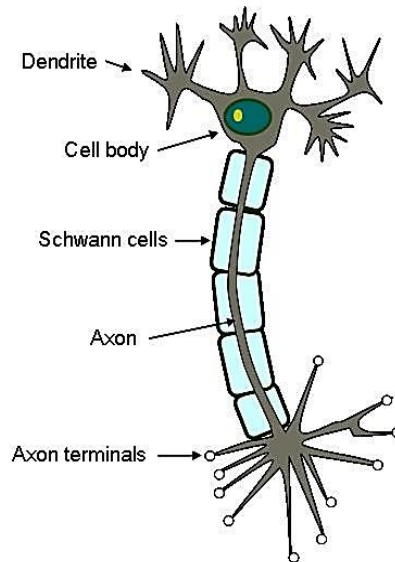


Figure 20:1. Schematic of a Schwann cell.

Schwannoma Extending through the IVF and into the Iliopsoas Muscle

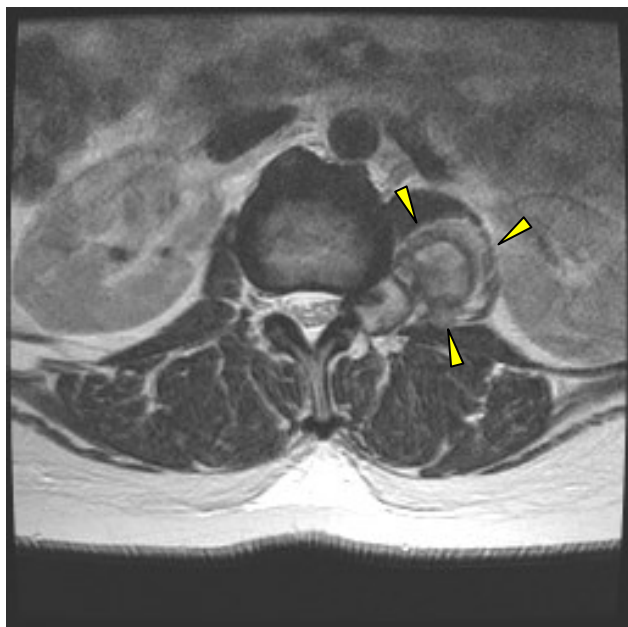


Figure 20:2. T2 weighted axial image showing heterogeneous expansion of a schwannoma into the left psoas.

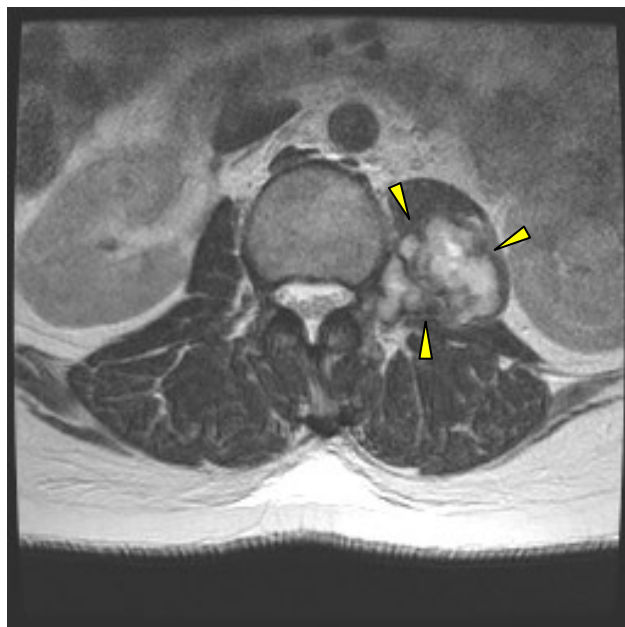


Figure 20:3. Another T2 weighted axial image showing heterogeneous expansion of a schwannoma into the left psoas.

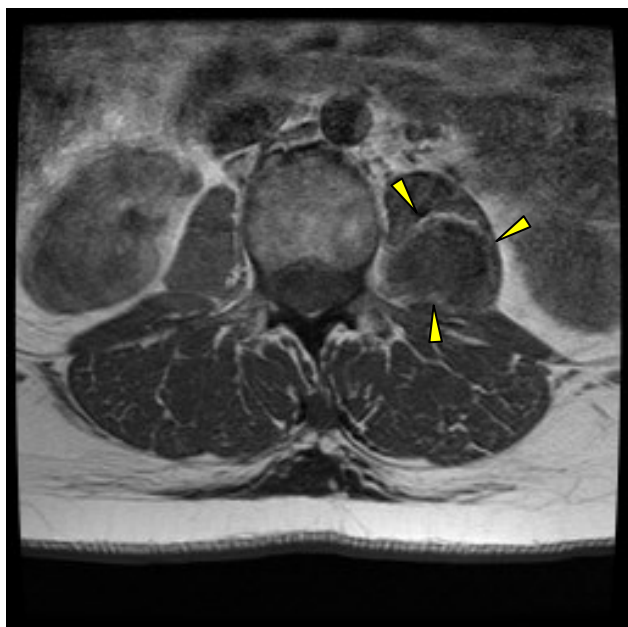


Figure 20:4. T1 weighted axial image. The Schwannoma is dark in color.

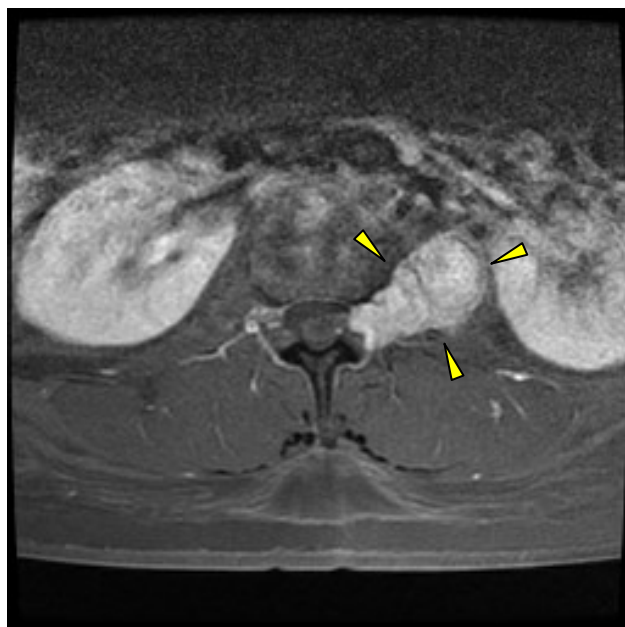


Figure 20:5. T1 weighted axial image with gadolinium enhancement. The fat is suppressed, but the kidneys and the schwannoma shine bright.

Schwannoma Protruding through the Iliopsoas Muscle



Figure 20:6. Proton density sagittal image of a schwannoma protruding through the iliopsoas muscle.



Figure 20:7. Post-gadolinium T1 weighted sagittal image of a schwannoma protruding through the iliopsoas muscle. Note the high intensity of the tumor and the kidney.



Figure 20:8. T2 weighted sagittal image of a schwannoma.



Figure 20:9. T1 weighted sagittal image of a schwannoma.

Myxopapillary Ependymoma

An ependymoma is an intramedullary tumor that arises from the ependyma (glial tissue found in the central nervous system). Ependymomas are the most common type of primary neoplasms in the spinal cord and filum terminale (figures 20:10 and 11). The diagnosis of spinal cord tumors is best left to the neuroradiologists. On finding an ependymoma, a neurosurgical referral is appropriate.

These tumors arise mainly in the conus medullaris and filum terminale. Clinically they often present in young adults, males more prevalent than females, and with a long history of lower back pain. They are slow growing tumors.

This condition is treated surgically and, if indicated, with radiation therapy.

MRI studies should include images with and without enhancement (gadolinium). They typically are isointense on T1, hyperintense (light) on T2, and are enhanced with contrast.

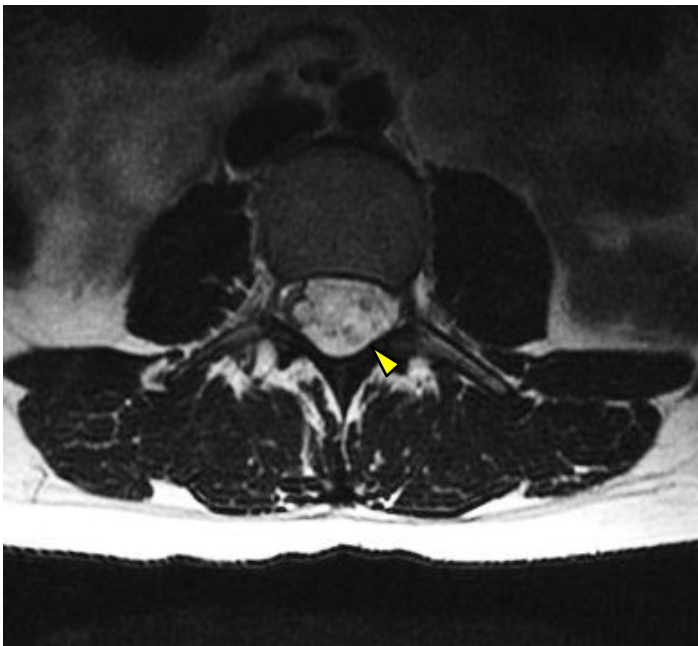


Figure 20:10. T2 axial image of a myxopapillary ependymoma of the filum terminale.



Figure 20:11. T2 weighted sagittal image.

Suggested Reading

David P. Friedman et.al, Intradural schwannomas of the spine: MR findings with emphasis on contrast-enhancement characteristics , 158:1347-1350, June 1992.

Taher El Gammali et.al, MR Myelography: Imaging Findings, AJR 1995;164:173-177. J Neuroradiol. 2005 Jan;32(1):42-9.

De Verdelhan O, Haegelen C, Carsin-Nicol B, Riffaud L, Amlashi SF, Brassier G, Carsin M, Morandi X. Service de Neuroradiologie, Fédération d'Imagerie Médicale.

López J, Diaz DR, Medina YC, et al. Schwannoma intramedular cervical. Arch Neurocién 2004;9:55-8.

Slooff JL, Kernohan JW, MacCarty CS. Primary intramedullary tumors of the spinal cord and filum terminale. 1964.

Wu JS, Hochman MG. Soft-tissue tumors and tumorlike lesions: a systematic imaging approach. November 2009 Radiology, 253, 297-316.

Inflammatory Joint Disease

21



Inflammatory Joint Disease

Inflammatory changes in the spine can result from infection, rheumatologic conditions, autoimmune disease, trauma, chronic irritation, or iatrogenic insult. While this section will show a few signs of spinal inflammation, the chapter on Modic changes is another resource for identifying bony edema.

Even though an entire chapter of this book is dedicated to vertebral body and endplate inflammation and degenerative changes (see chapter 12), we need to include bony edema within this discussion of inflammatory disease.

The high water content of inflammation and edema is evident in type 1 Modic changes. Type 1 changes are manifested as hypointense (dark) on T1 and hyperintense on T2 weighted images. This is indicative of an acute reactionary process.



Figure 21:1. T1 weighted sagittal image revealing type 1 Modic changes. Fluid (bony edema) is dark on T1.



Figure 21:2. T2 weighted sagittal image revealing type 1 Modic changes. The edema is light on T2WI.

Bony edema can be caused by infection, fracture, disc injury, or from a number of other sources. It can be the first sign of a more serious condition. Type 1 Modic changes usually indicate an active inflammatory process is going on. Understanding the characteristics of Modic changes will help the clinician to know whether the condition is actively inflamed (Modic 1 changes) or has reacted to the insult in a more chronic manner (Modic 2 and Modic 3 changes).

Psoriatic Arthritis of the Sacroiliac Joint



Figure 21:3. T1 weighted axial image of the sacrum and sacroiliacs with fat saturation after receiving a contrast enhancement injection.

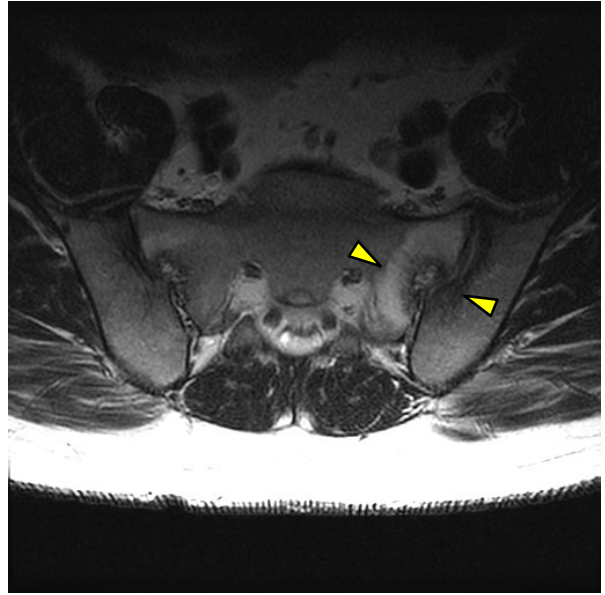


Figure 21:4. T2 axial demonstrating bony edema and erosion of the sacral joint surface and bone.

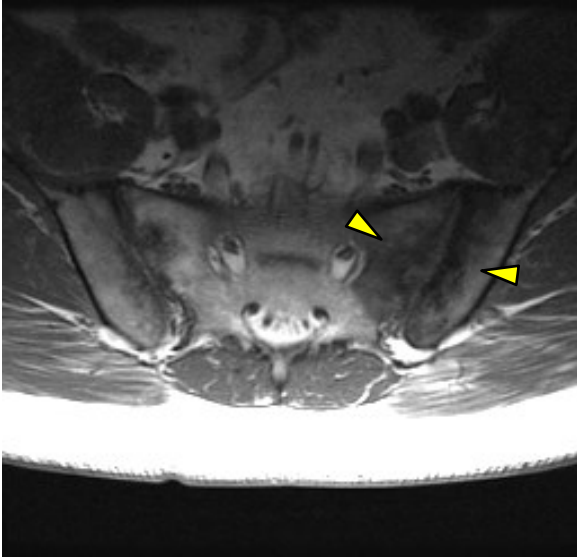


Figure 21:5. T1 weighted axial image of the sacrum and sacroiliacs. Note the bony edema which appears dark in this T1WI.

Bony edema, synovitis, joint effusion, and joint and bone erosion are characteristics of psoriatic arthritis that can be seen on MRI. These MRI features are shared with rheumatoid arthritis and other inflammatory joint and infectious diseases. Differentiating between various inflammatory and infectious joint diseases requires a comprehensive clinical, laboratory, and radiographic approach. Given the dangers and aggressiveness of joint infections, aggressive and emergent measures should be employed when infection is suspected.

Pyogenic Spondylitis and Discitis

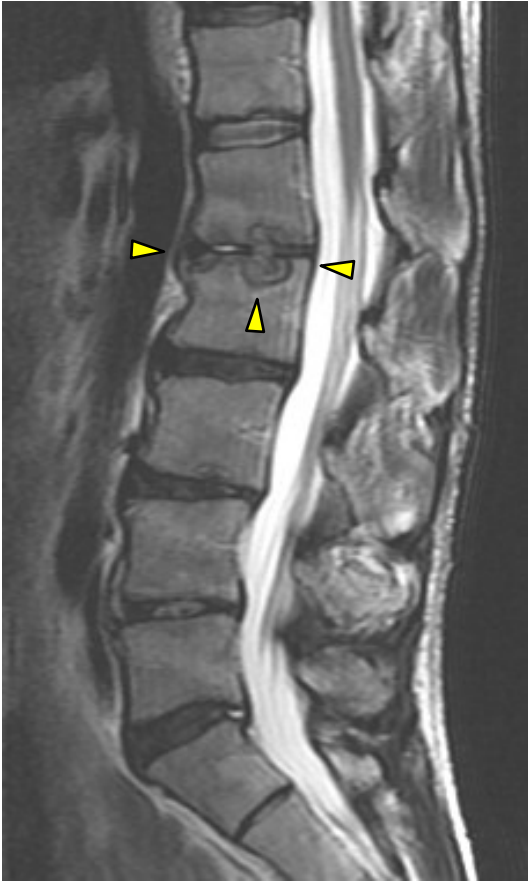


Figure 21:6. T2 weighted sagittal image of a staphylococcus aureus infection of L1, L2, and the L1-2 disc. Note the marrow changes along with endplate and disc disruption.



Figure 21:7. CT sagittal of the same patient revealing loss of disc height and bony erosion of the endplates and vertebral bodies of L1 and L2.

Identifying infections of the lumbar spine requires the knowledge of symptoms, clinical presentation, lab findings, and radiology. Staphylococcus aureus is the most common organism involved in pyogenic spondylitis and discitis, but other organisms may also cause infections of the spine. The T2 weighted sagittal MR image (figure 21:6) shows destruction of the affected vertebrae, L1 and L2, along with the L1-2 disc, and erosion of the vertebral endplates and vertebral bodies. The halo of a high intensity signal extends well into the vertebral bodies. The CT (figure 21:7) reveals bony and disc destruction associated with infectious spondylitis and discitis. Bone and disc destruction are the hallmarks of pyogenic spondylitis and discitis. This diagnosis is a medical emergency and requires prompt and aggressive medical treatment.

Plain film spinal radiology will not display evidence of disc or bony infection until 7 to 10 days have passed from the onset of symptoms. Clinical presentation includes fever, chills, elevated ESR, and leukocytosis. Patients at risk for discitis and infectious spondylitis include immune depressed patients, trauma, recent surgery or dental work, and patients with systemic infections.

Facet Effusion



Figure 21:8. Effusion of the L4-L5 facet seen on T2W sagittal image.

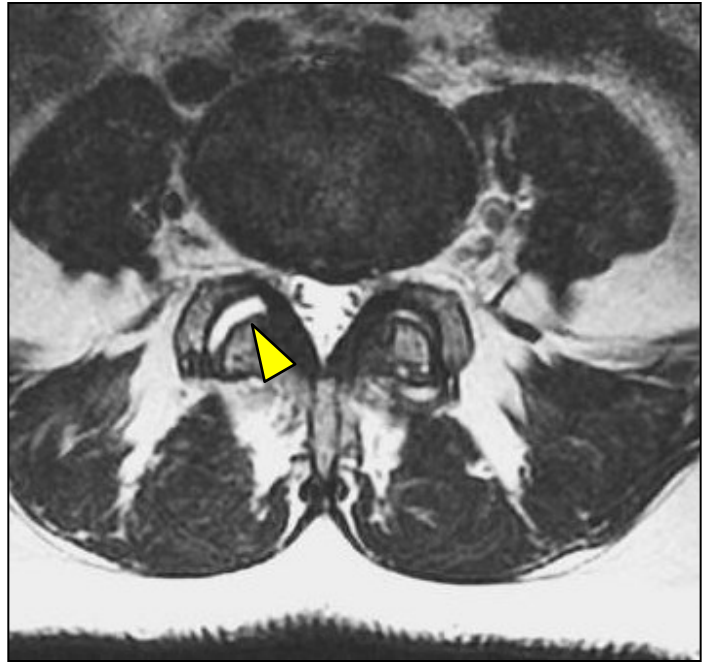


Figure 21.9. A T2W axial of the same patient. The facet joint is so filled with fluid that the joint is significantly gapped.

Fluid in a joint is indicative of inflammation. When facet effusion is present, it can be caused by mechanical irritation or by an inflammatory process or disease. This can result from a rheumatologic condition, trauma, infection, or disease.

Suggested Reading

Marchiori D (2013). *Clinical imaging: with skeletal, chest and abdomen pattern differentials*(third edition). Mosby.

McQueen F, Lassere M, Østergaard M. Magnetic resonance imaging in psoriatic arthritis: a review of the literature. *Arthritis Res Ther.* 2006;8:207. doi: 10.1186/ar1934.

Atlas SW. (2008). *Magnetic resonance imaging of the brain and spine* (forth edition). Lippincott Williams & Wilkins.

Ross JS et al. (2010). *Diagnostic imaging spine* (second edition). Amirsys Inc.

Fat

22



Fat

Recognizing fat and its characteristics is an essential skill set for anyone interested in reading MRI. The characteristics of fat on T1 and T2 weighted images was discussed in detail in a previous chapter. This chapter will highlight fat as a space-occupying lesion, discussing the appearance of fatty lesions such as lipomas, fatty filum terminale, tethered cord, fatty infiltration into bones, and epidural lipomatosis.

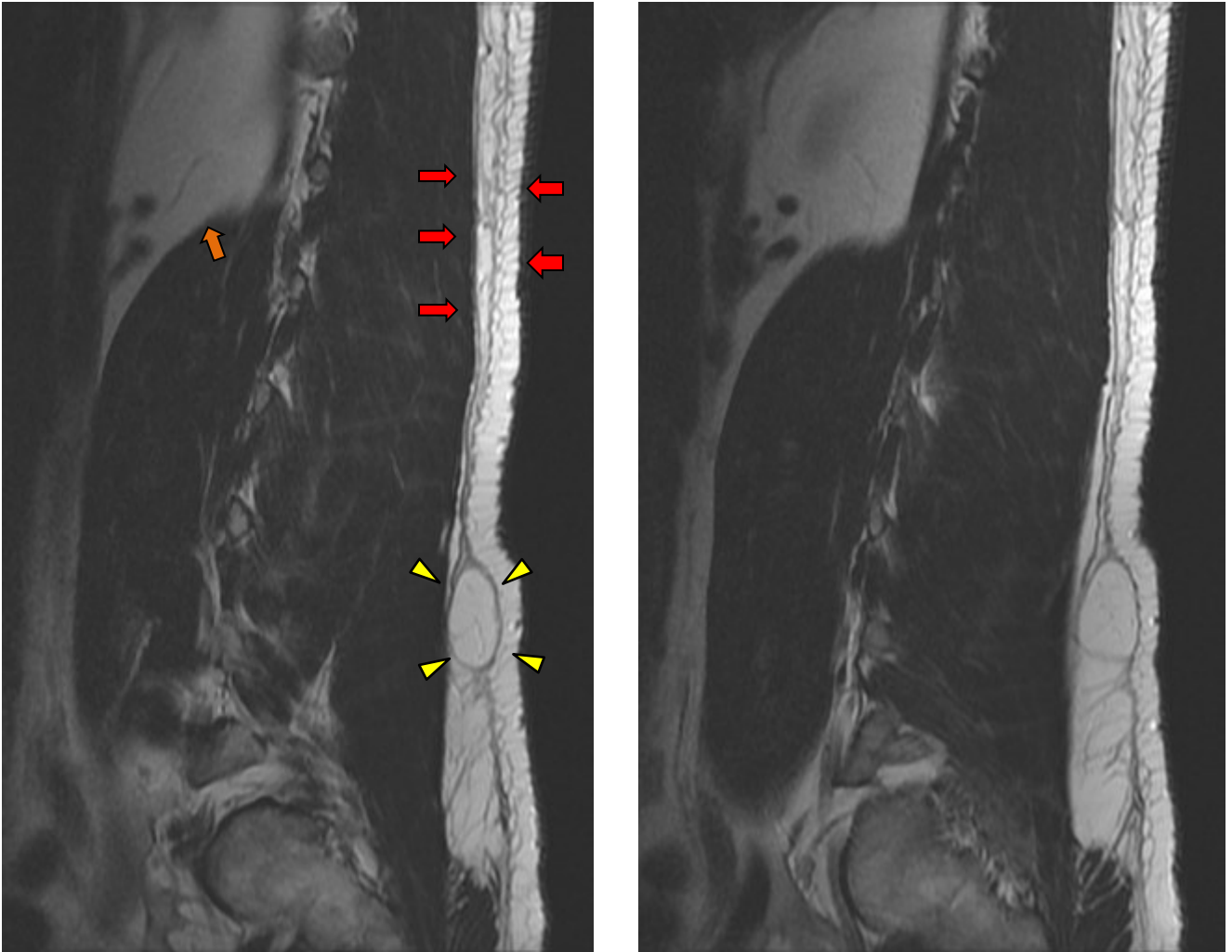
Fat is common, so we need to be able to identify fatty tissue and distinguish it from other tissues. We also need to know when a fatty lesion is potentially dangerous. Lipomas are common and benign and usually just an incidental finding on physical or radiographic examination. However, they can produce profound symptoms if they are contained within the spinal canal.



Figure 22:1. This large lipoma was removed from a forearm due to its compression of the median nerve. Published with permission from Sebastian E Valbuena, Greg A O'Toole and Eric Roulot through Creative Commons.

Sebastian E Valbuena, Greg A O'Toole and Eric Roulot: *Compression of the median nerve in the proximal forearm by a giant lipoma: A case report.* In: *Journal of Brachial Plexus and Peripheral Nerve Injury* 2008, 3:17 doi:10.1186/1749-7221-3-17 (Open Access Article, published under cc-by-2.0)

Lipoma



Figures 22:2 and 22:3. These T2W sagittal images are slices taken lateral of midline and show the investment of a fairly large lipoma (yellow arrows). This lipoma was easily palpated and had the consistency of a rubbery mass. The subcutaneous fat and its network of supporting vessels can be seen between the red arrows. The orange arrow points toward the deep visceral fat that surrounds the internal organs.

Lipomas are a common benign neoplasm. Periodically their size, location, or number will be a source of alarm to patients. Normally they are found in or around other fatty tissues. Use known fatty structures as a point of reference for comparison of intensity and structure. If it is the same color and consistency of other fatty structures, it is probably fat.

Lipoma

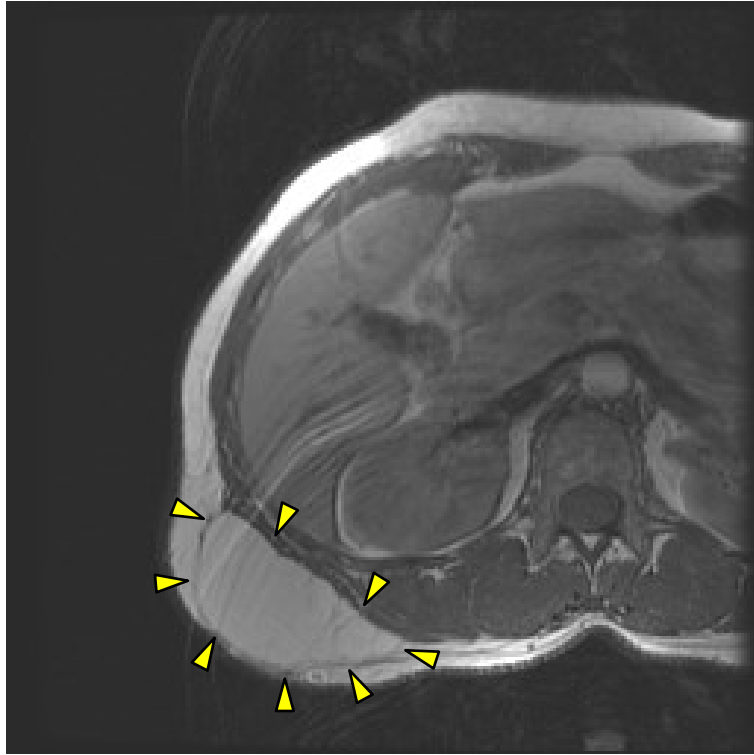


Figure 22:4. A large subcutaneous lipoma (yellow arrows) at the level of the right kidney.

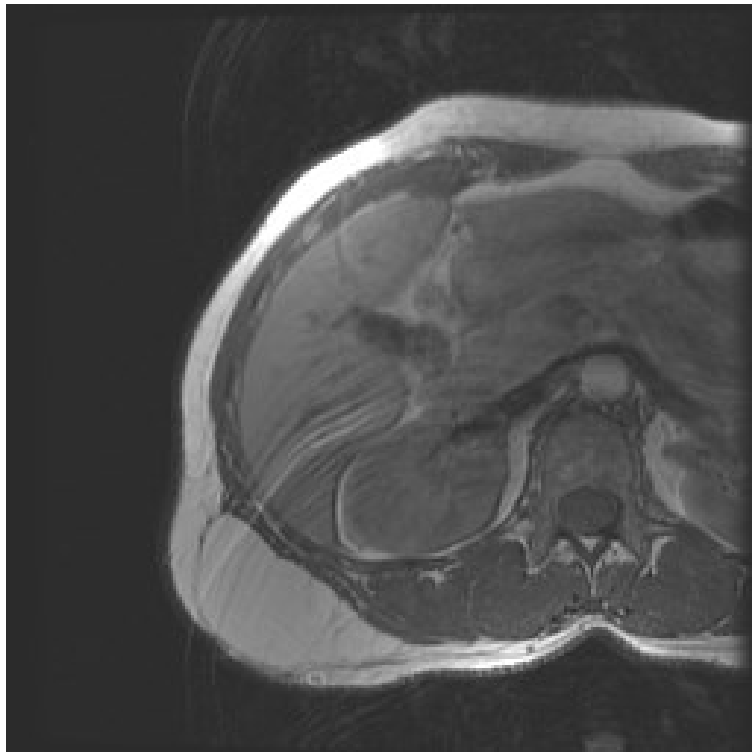


Figure 22:5. The large lipoma from figure 22:4 without the arrows.

Lipoma



Figure 22:6. T1 weighted sagittal image of the thoracic spine revealing a paraspinal lipoma.



Figure 22:7. T1 weighted axial image of the thoracic spine revealing a paraspinal lipoma.

Lipomas are benign fatty tumors that are typically of little clinical consequence. An MSK provider will see thousands of lipomas in a career. Clinically, they are typically pain-free encapsulated nodules of fat. Finding a tumor can cause a patient with a lipoma significant anxiety, and it is important that clinicians are able to dispel the patient's fears. Having a lipoma is not an indication to order an MRI, unless its size and location cause significant symptoms or impairment.

These images show a paraspinal lipoma in T1 weighted views. Note how the lipoma is invested in the subcutaneous fascia and how circumscribed it appears. Lipomas may be quite large and still be asymptomatic. Patients may request to have lipomas removed for cosmetic purposes. .

Lipoma in the Paraspinal Muscles

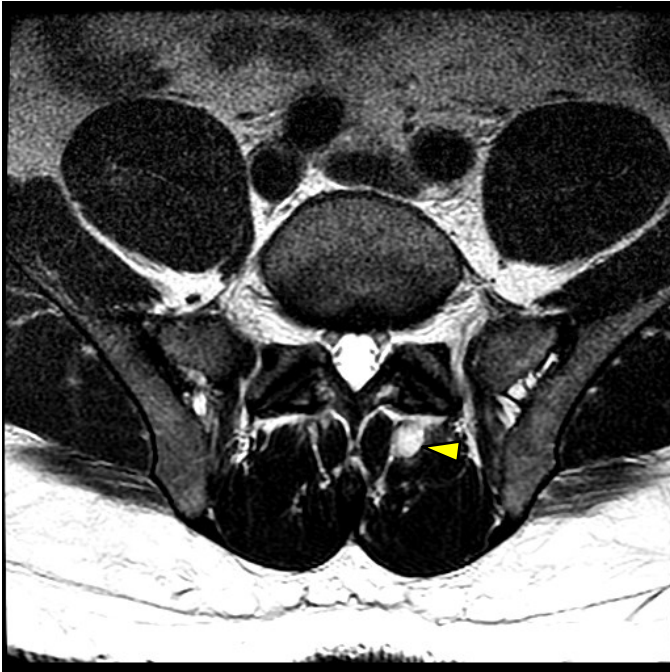


Figure 22:8. T2 weighted axial image of a paraspinal lipoma.

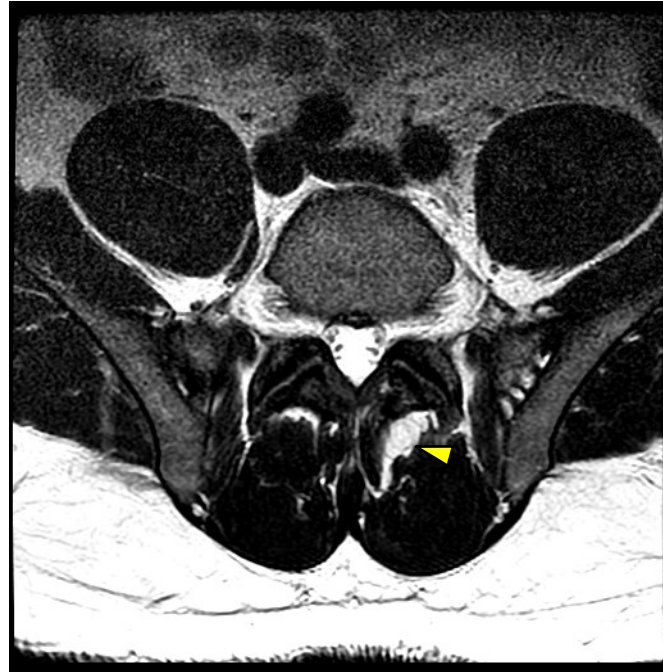


Figure 22:9. T2 weighted axial image.

Lipomas are rarely considered clinically significant unless they place pressure on adjoining tissue. As the name indicates, lipomas are tumors of fatty material. These benign tumors are the most common type of soft tissue tumor. To identify a lipoma on MRI it is best to compare T1, T2, and when possible, fat-saturated images. The images on this page reveal a lipoma that is located deep below the paraspinal muscles. Because lipomas are composed of fat, they will be hyperintense on both T1 and T2 weighted imagery and hypointense on fat-suppressed imagery.

It is important to be able to differentiate between this benign lesion and other more ominous lesions.

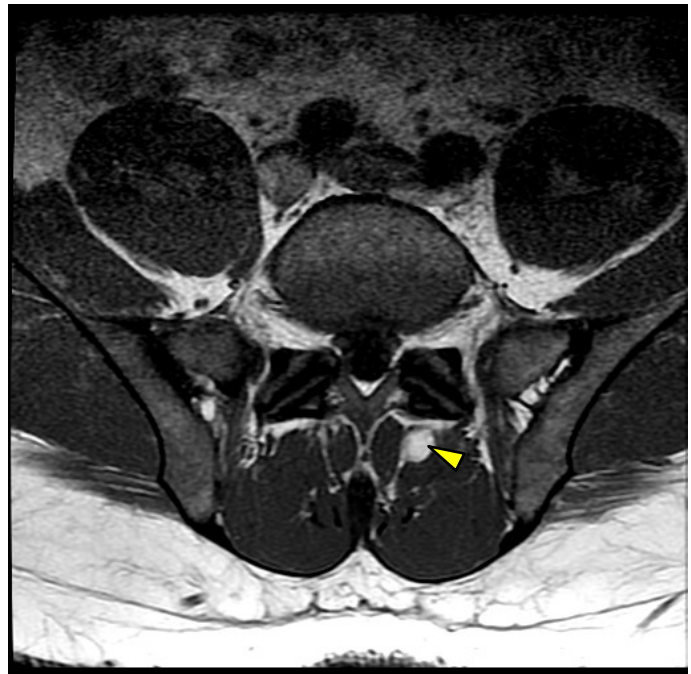


Figure 22:10. T1 weighted axial image. Note the tone of this lipoma is consistent with the subcutaneous and visceral fat.

Lipoma of the Filum Terminale

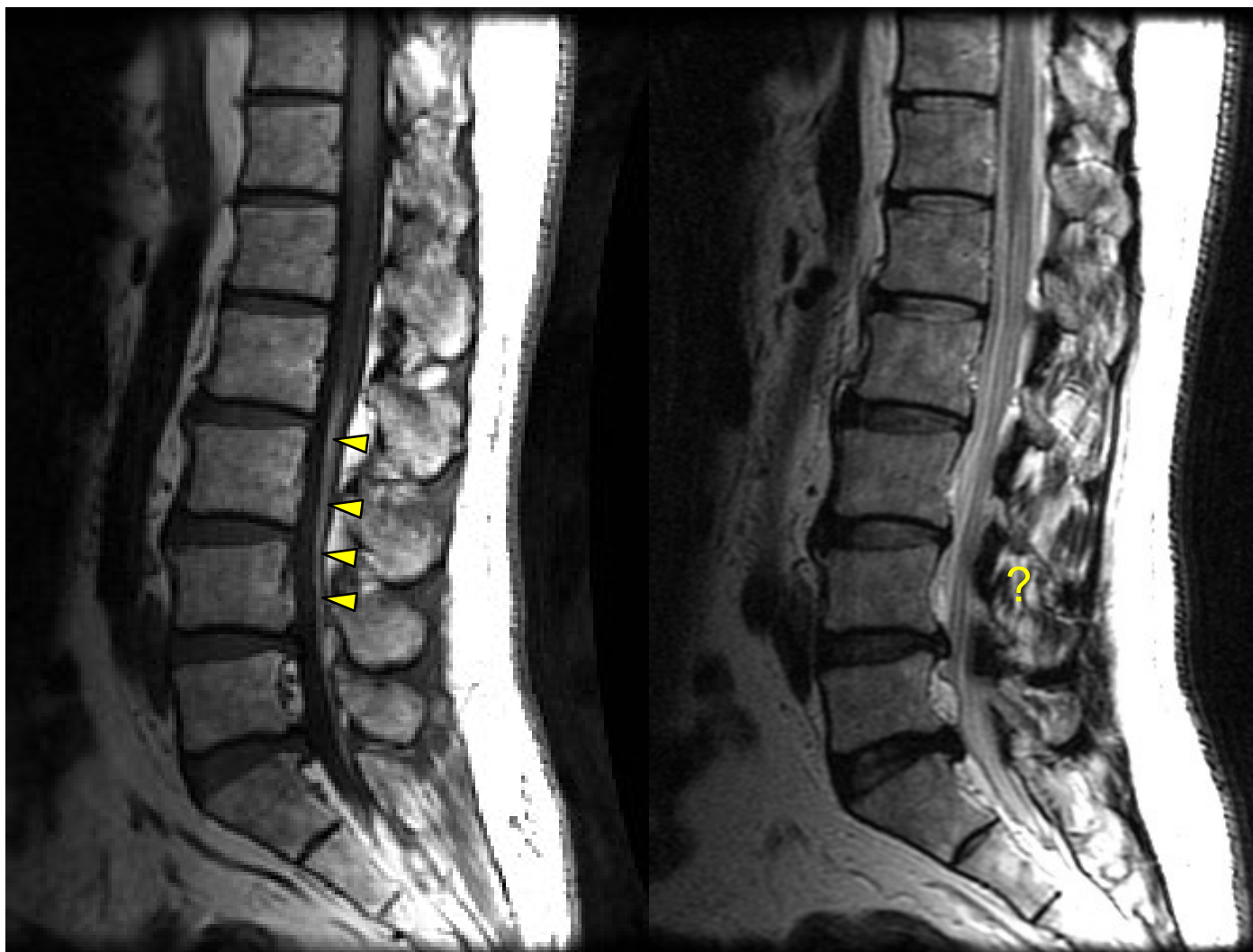


Figure 22:11. This T1W sagittal image shows the fatty filum terminale as hyperintense.

Figure 22:12. The fatty filum terminale is more difficult to distinguish on this T2WI.

A fatty filum terminale is usually an incidental finding on MRI. However, when the lipoma is large, it can cause a tethered cord syndrome that disrupts bladder and lower extremity function. There is some evidence that even a small fatty terminale can contribute to clinically significant conditions under the right circumstances. The characteristics of a fatty filum terminale on MRI are as follows: T1- hyperintense (bright); T2- hyperintense; Fat Saturation- saturated; Gadolinium- not enhanced.

Lipoma of the Filum Terminale

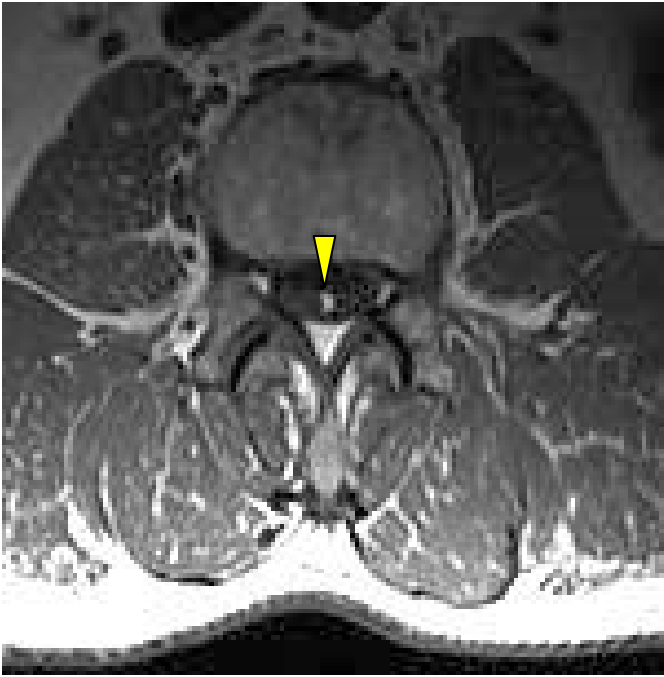


Figure 22:13. This T1W axial image clearly shows the fatty filum terminale as a hyperintense white dot in the dark thecal sac.



Figure 22:14. This T2W axial image shows the fatty filum terminale as a hyperintense white dot in the thecal sac.

Figure 22:15. MRI Characteristics of a Lipoma of the Filum Terminale

T1	T2	Fat Saturation	Gadolinium Enhancement
Bright (hyperintense)	Bright (hyperintense)	Saturated	Not Enhanced

T2 with Fat Saturation

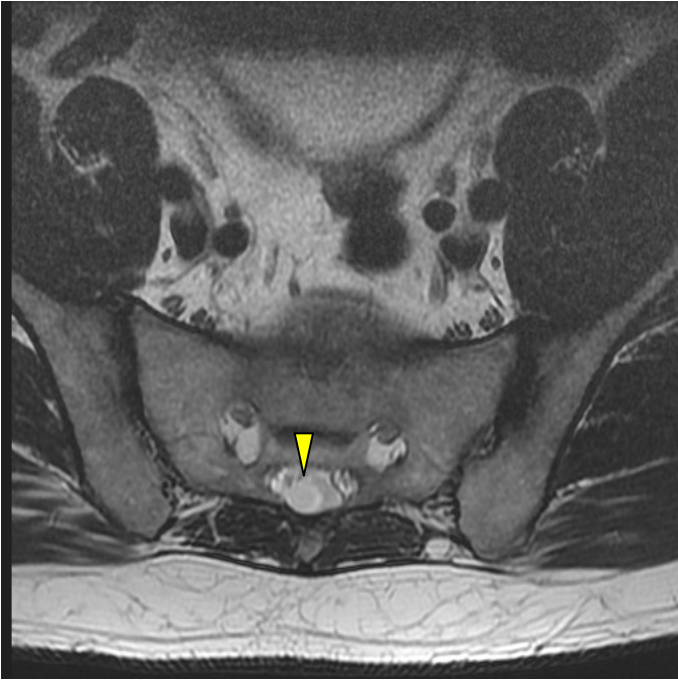


Figure 22:16. T2 weighted axial image.



Figure 22:17. T2 weighted fat saturated axial image.

By comparing normal T2 images and T2 fat-saturated images, the clinician can differentiate fatty structures from water density structures. In figure 22:16 a structure appears suspicious for a large lipoma within the thecal sac of the sacrum. Large lipomas in the sacrum can cause tethered cord syndrome, so it is important to be able to differentiate lipomas from other lesions.

By suppression of the fat signal, we can differentiate water densities from fat densities. Comparing these images, the lesion that is visible in figure 22:16 does not darken with fat suppression in figure 22:17. Therefore, we can accept that this is a water density lesion, most likely a perineural cyst.

While contemplating the composition of various structures, compare the composition of known structures with that of the unknown. Look at known fat, water, and gas densities. Is your unknown structure consistent with any of these densities? In these images we can see that the questionable structure is similar to the water density seen in the urinary bladder. It is a water density.

Tethered Cord

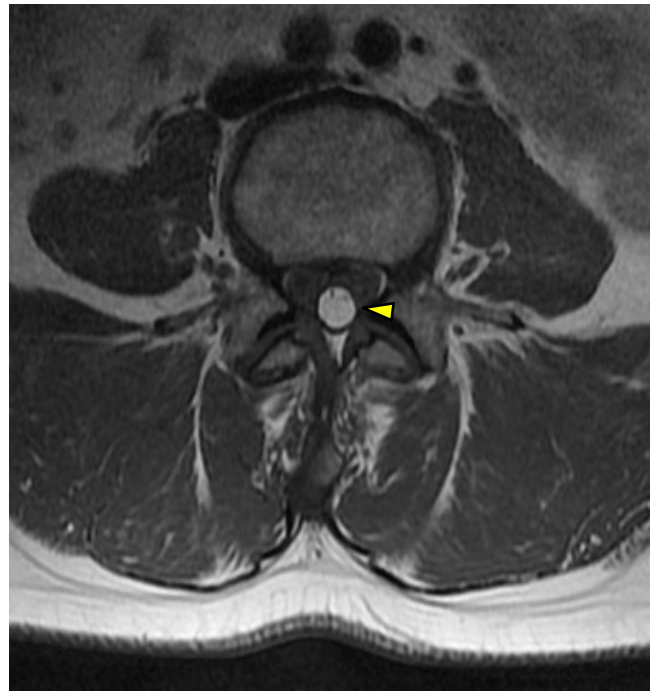
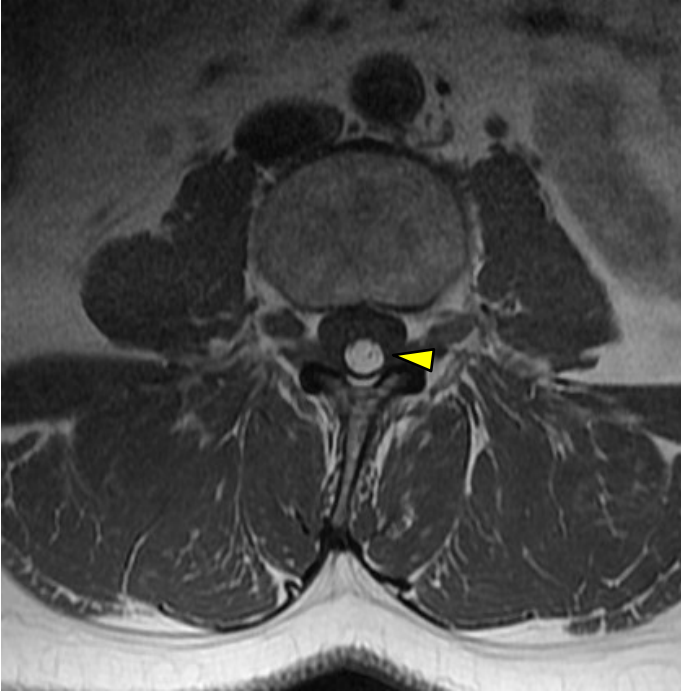


Figure 22:18 and 22:19. These T1 weighted axials reveal a large lipoma within the thecal sac. Note that the CSF is dark in T1 weighted images. This is useful in differentiating fluid-filled cysts from lipomas. Lipomas of this size frequently result in tethered cords as discussed in the previous chapter.



Figure 22:20. This T2 weighted axial image reveals a large lipoma within the thecal sac.

Tethered Cord (continued)

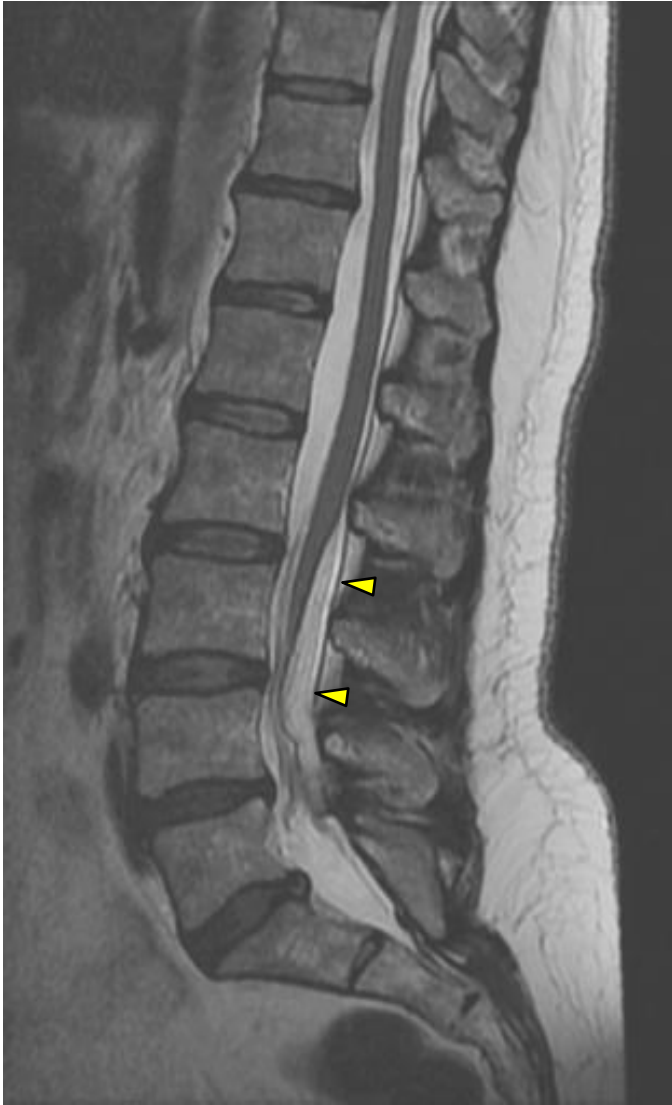


Figure 22:21. This T2 weighted sagittal image reveals a large lipoma within the thecal sac. This lipoma is an intradural extramedullary space occupying lesion.



Figure 22:22. This fat-suppressed T2 weighted image is useful to clarify that this space-occupying lesion is indeed a fat density. In fat-suppressed T2 weighted images, water densities are bright, and fat densities are suppressed (dark).

Lipomas of the filum terminale can become so enlarged that they anchor the cord and create a tethered cord. Tethered cords can cause severe neurological damage.

Fatty Infiltration into Bone

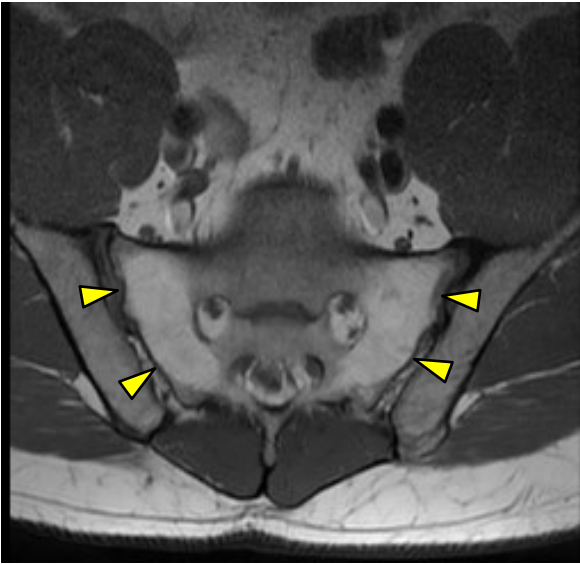


Figure 22:23. T1 weighted axial image showing fatty infiltration into the sacrum.



Figure 22:24. T1 weighted sagittal image with fatty infiltration into the sacrum.

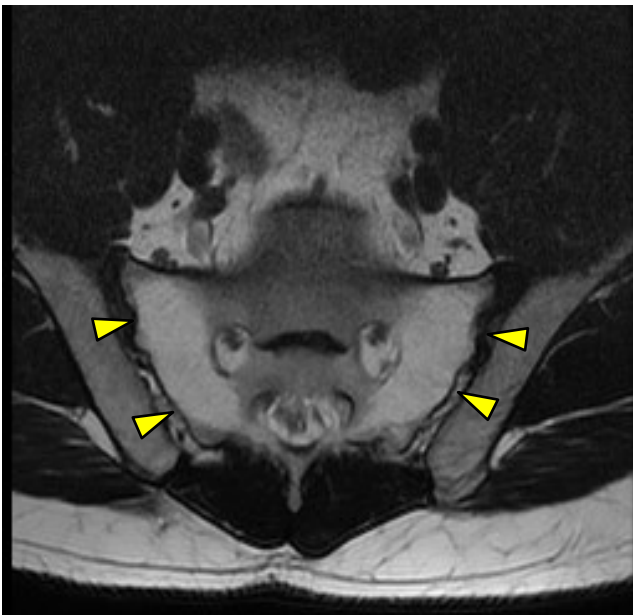


Figure 22:25. T2 weighted axial image with fatty infiltration into the sacrum.

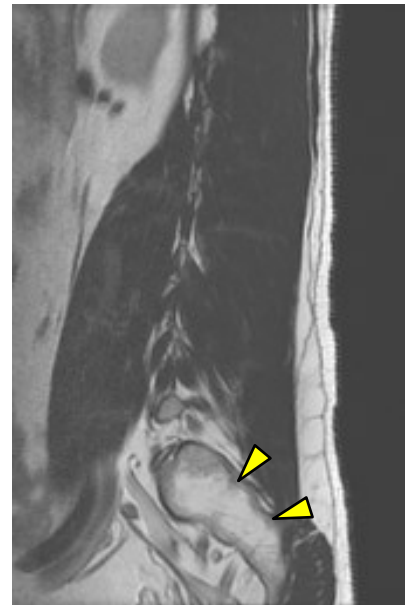


Figure 22:26. T2 weighted sagittal image with fatty infiltration into the sacrum.

Fatty infiltration into the bone is a common benign finding on MR. These images show fatty infiltration into the sacrum of a 41 year-old male. In addition to naturally occurring fatty infiltration into bone, it may be sequelae of radiation exposure or treatment. Fatty replacement of the normal marrow may also be part of degenerative changes (see chapter 12 on Modic Changes).

Spinal Epidural Lipomatosis



Figure 22:27. T2 weighted axial with epidural fat deposits denoted by yellow arrows.



Figure 22:28. T1 weighted axial image.

Epidural lipomatosis of the spine (excessive fat deposition in the spinal canal) has been attributed to steroid therapy, endocrinopathy, and inconclusively to obesity. Idiopathic spinal epidural lipomatosis is rare, but has been documented. Spinal epidural lipomatosis can cause back pain, nerve root impingement, and cord compression. These images demonstrate excessive fat deposition posterior to the vertebral bodies and anterior to the spinal canal. Increasing obesity in the developed world may contribute to an increase in the occurrence of this condition, but the increase in the prevalence of MRIs has also been sited as a cause for increased diagnosis of this condition.

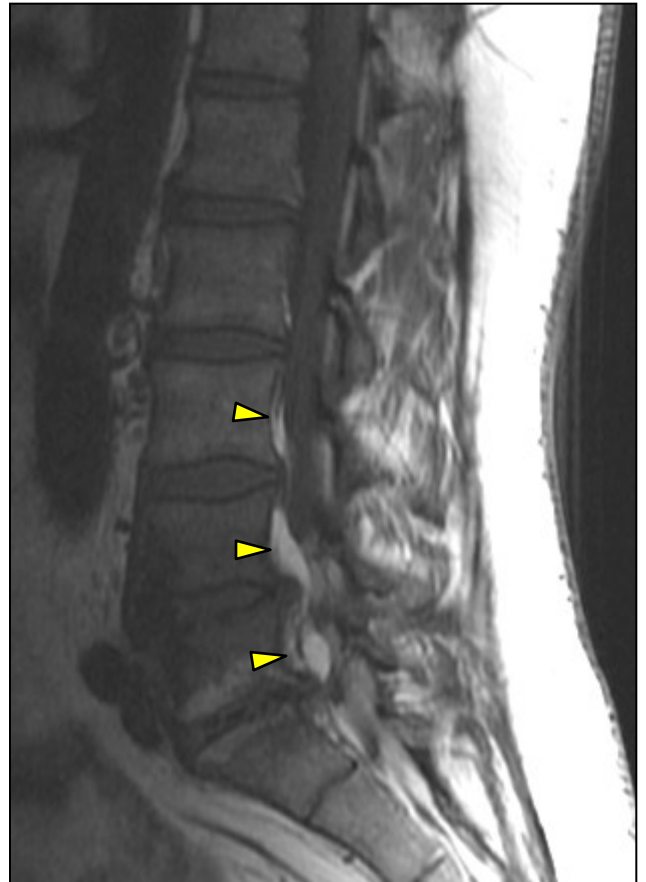


Figure 22:29. T1 weighted sagittal image of the same patient from figures 22:27 and 22:28. The arrows point out the presence of excessive fat in the anterior canal.

Spinal Epidural Lipomatosis (continued)



Figure 22:30. T2 weighted axial with epidural fat indenting the thecal sac.

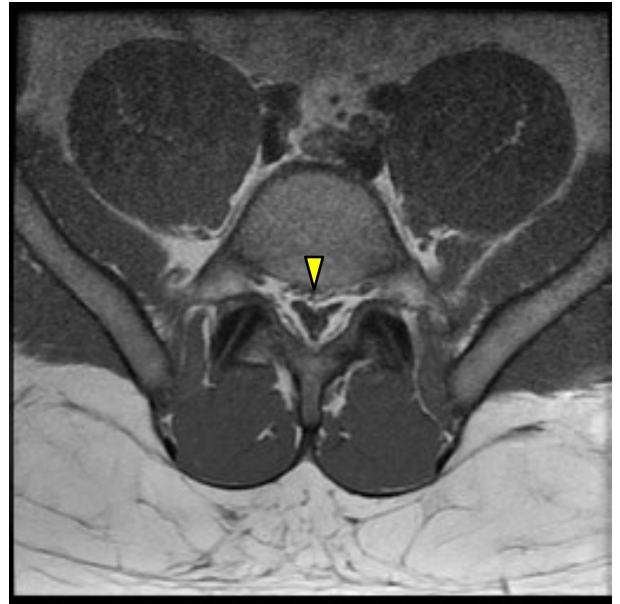


Figure 22:31. T1 weighted axial revealing the "Y" sign of thecal sac compression associated with epidural lipomatosis.

Epidural lipomatosis has been attributed to various compression findings on MRI including the "Y" sign (figure 22:31). This is caused by the compression of the thecal sac into a trifold shape of three lobes that looks much like a "Y" (Kuhn).

Epidural Lipomatosis



Figure 22:32. T1 weighted axial image showing a significant encroachment of the central canal by of epidural lipomatosis.



Figure 22:33. T1 weighted sagittal image showing a significant encroachment of the central canal by of epidural lipomatosis.

Epidural Lipomatosis

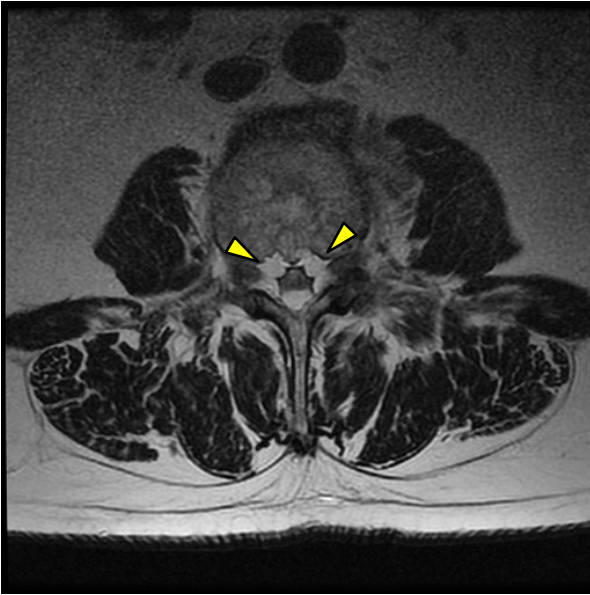


Figure 22:34. T1 weighted axial image showing a significant encroachment of the central canal by epidural lipomatosis.

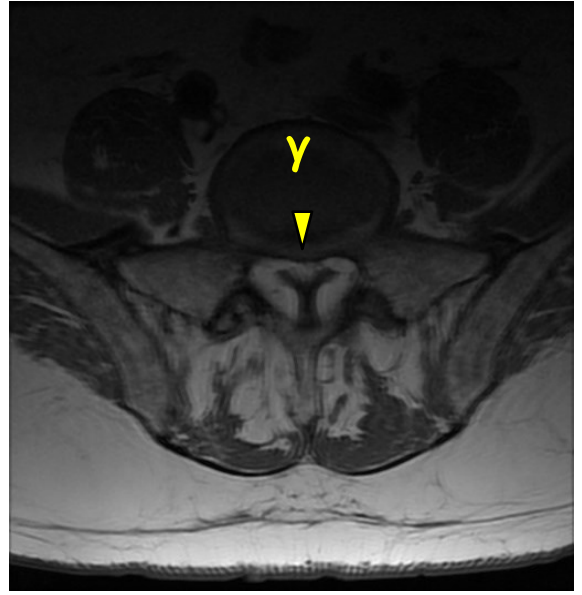


Figure 22:35. T1 weighted axial image showing the "Y" phenomenon that is indicative of epidural lipomatosis.



Figure 22:36. T2 weighted sagittal image showing a significant encroachment of the central canal with diffuse epidural lipomatosis.

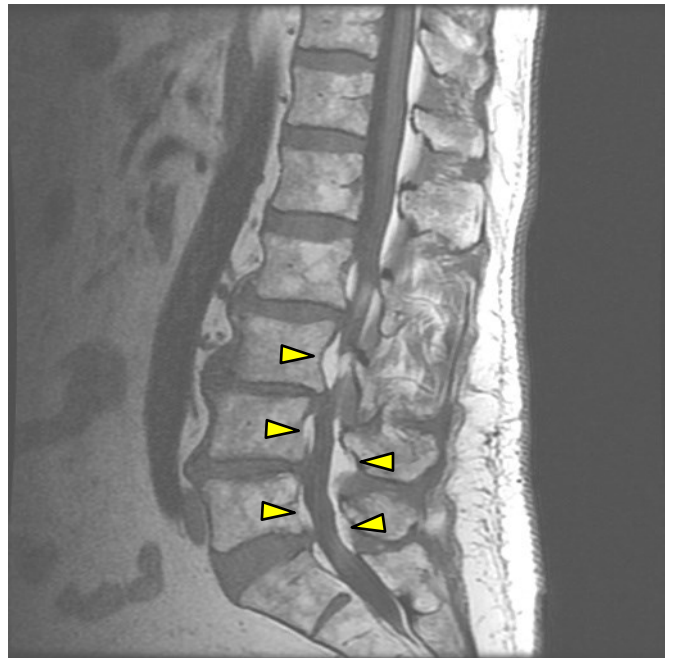


Figure 22:37. T1 weighted sagittal image showing a significant encroachment of the central canal from epidural lipomatosis which is particularly evident by comparing water densities and fat densities in T1.

Fatty Replacement of Muscle

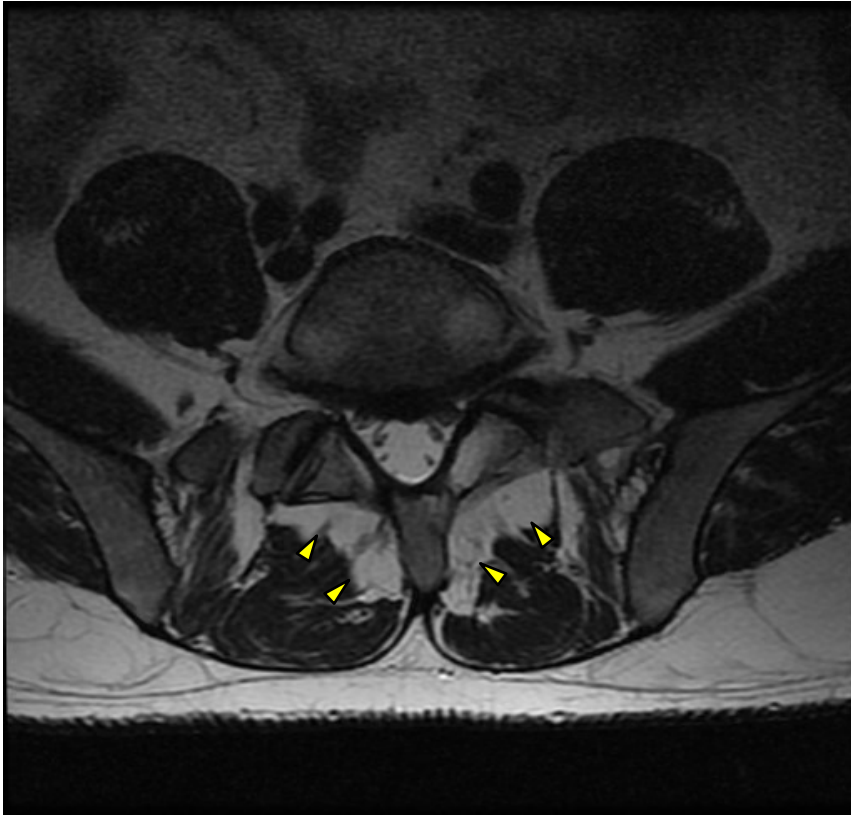


Figure 22:38. T1 weighted axial image showing fatty replacement of the multifidus muscles.

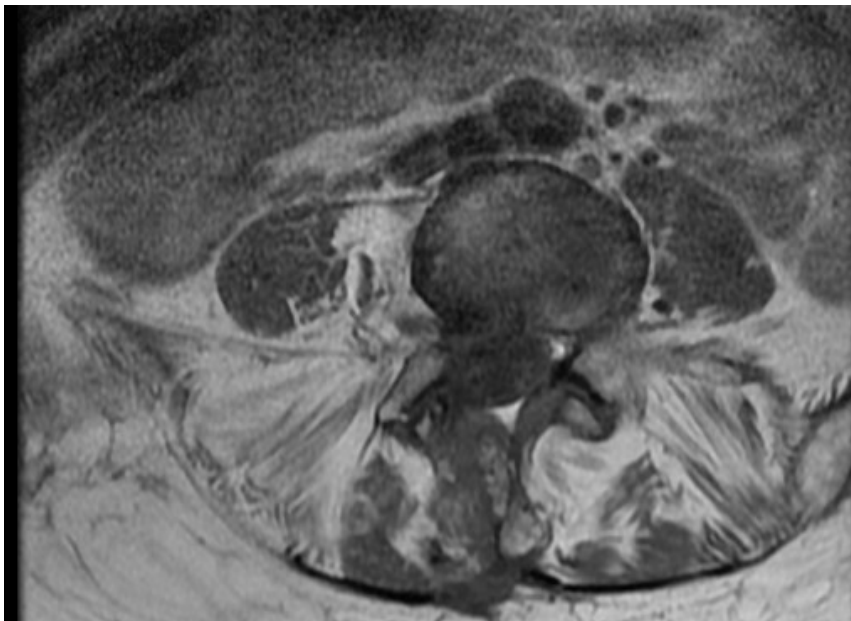
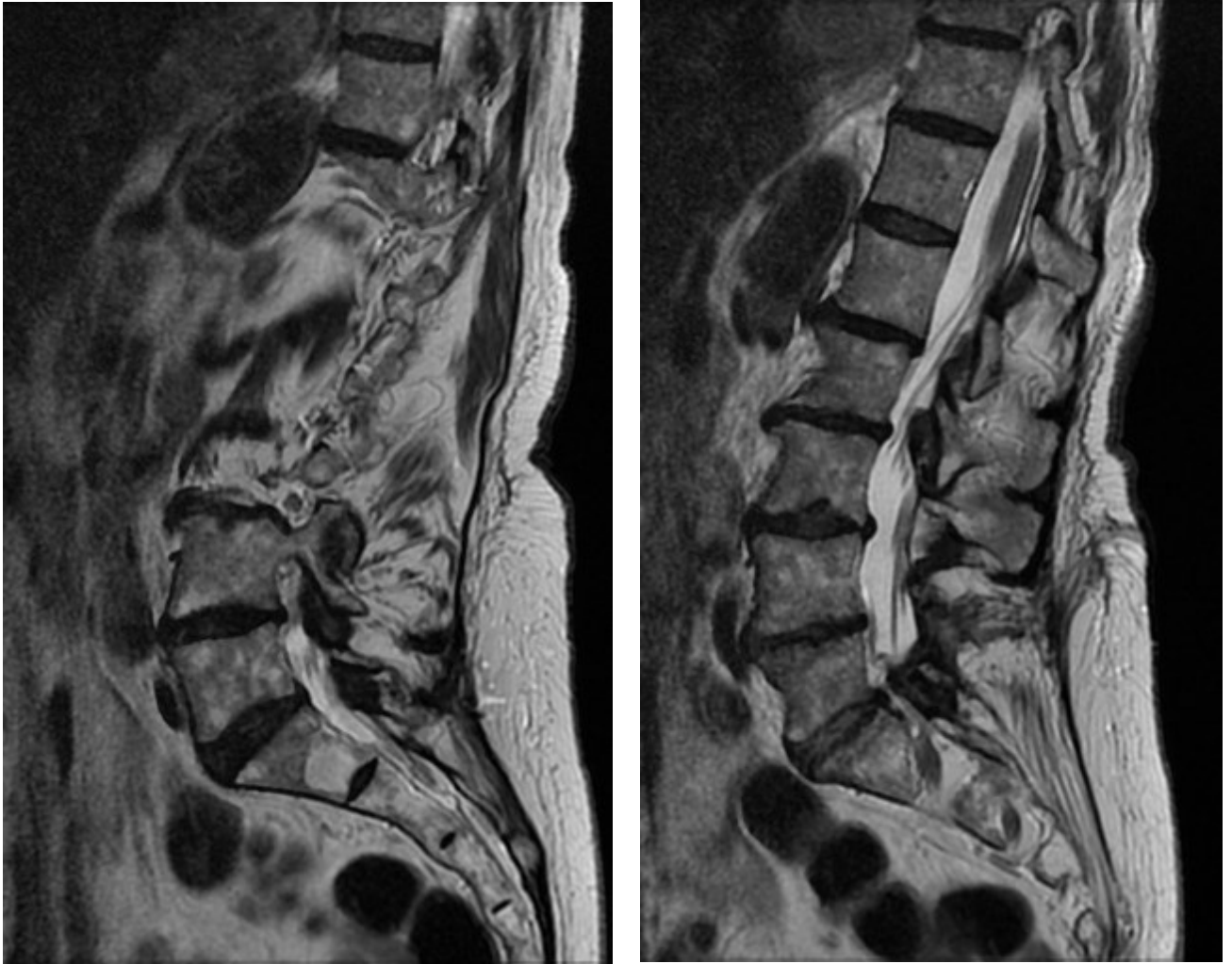


Figure 22:39. T1 weighted axial image showing extensive fatty replacement of the paraspinal muscles in an 80 year-old man.

Fat in Bones



Figures 22:40 and 22:41. The mottled appearance of fatty infiltration into the vertebral bodies is clearly visible in these T2W sagittal images.

Fatty infiltration into the vertebral bodies is a common finding on MRI, especially with age. These T2 weighted sagittal images reveal the botchy appearance of fat within the trabecular bone (spongy bone). Compare areas of known fat with the consistency of suspected fat in the spine. Matching the T1 and T2 images will also be beneficial in determining if the light-colored infiltration is fat or some other substance.

Differentiating Fat in Bones from Bony Metastases



Figure 22:42. Fatty infiltration into the vertebral bodies in this T2WI.



Figure 22:43. Metastases into the vertebral bodies on a T2WI.

Fatty infiltration into bone can have a heterogeneous mottled appearance that may appear like metastases, and metastases may remind the clinician of fatty infiltration. On MRI comparing T1, T2, and fat-suppressed images will help to distinguish fat infiltration from neoplasms (see figure 22:44). It is important to always defer to a trained radiologist for the identification of pathology.

Differentiating Fat from Bony Metastases			
	T1	T2	T2 with fat suppression
Fat	Bright	Bright	Dark
Metastases	Dark	Bright	Bright

Figure 22:44. Characteristics of fat and bony metastases on MRI.

Suggested Reading

T. Iizuka: Fatty Filum Terminale on MRI. *The Internet Journal of Spine Surgery*. 2007 Volume 3 Number 1.

Lisai P, Doria C, Crissantu L, Meloni GB, Conti M, Achene A. Cauda equina syndrome secondary to idiopathic spinal epidural lipomatosis. *Spine* 2001;26:307-309.

Haddad SF, Hitchon PW, Godersky JC. Idiopathic and glucocorticoid-induced spinal epidural lipomatosis. *J Neurosurg* 1991;74:38-42.

Kuhn MJ, Youseff HT, Swan TL, Swenson LC. Lumbar epidural lipomatosis: The "Y" sign of thecal sac compression. *Comput Med Imaging Graph* 1994;18:367-372.

Kumar K, Nath RK, Nair CPV, Tchang SP. Symptomatic epidural lipomatosis secondary to obesity. *J Neurosurg* 1996;85:348-350.

Kurt E, Bakker-Niezen SH. Neurogenic claudication by epidural lipomatosis: a case report and review of literature. *Clinical Neurol Neurosurg* 1995;97:354-357.

Alicioglu B, Sarac A, Tokuc B. Does abdominal obesity cause increase in the amount of epidural fat? *Eur Spine J*. 2008 October; 17(10): 1324–1328.

Pinkhardt EH, Sperfeld AD. Is spinal epidural lipomatosis an MRI-based diagnosis with clinical implications? A retrospective analysis. *Acta Neurologica Scandinavica*. June 2008 Volume 117, Issue 6, pages 409–414.

Hadar H, Gadoth N, Heifetz M. Fatty Replacement of Lower Paraspinal Muscles: Normal and Neuromuscular Disorders. *AJR* 141: 895-898, November 1983.

Wu JS, Hochman MG. Soft-tissue tumors and tumorlike lesions: a systematic imaging approach. November 2009 *Radiology*, 253, 297-316.

Resnick D, Kransdorf MJ. *Bone and joint imaging*. W B Saunders Co. (2005).

Robertson SC et al. Idiopathic spinal epidural lipomatosis. *Neurosurgery*. 1997 Jul;41(1):68-74; discussion 74-5.

Selmi F et al. Idiopathic spinal extradural lipomatosis in a non-obese otherwise healthy man, *Br J Neurosurg*. 1994;8(3):355-8.

Atlas SW. (2008). *Magnetic resonance imaging of the brain and spine* (forth edition). Lippincott Williams & Wilkins.

Ross JS et al. (2010). *Diagnostic imaging spine* (second edition). Amirsys Inc.

Gadolinium Enhancement

23



Gadolinium

Gadolinium is a contrast medium used commonly in the study of organs and disease. MRI with gadolinium enhancement has some value in the examination of certain musculoskeletal conditions. Gadolinium is administered to the patient through an IV injection. It is a paramagnetic compound that has an increased intensity (brightness) on T1W images.

Gadolinium has an affinity for vascular tissue so it is used to differentiate between vascular and avascular structures. A tumor that is vascular will enhance with gadolinium, but a hematoma will not. Scar tissue, which is initially vascular granulation tissue, will enhance with gadolinium, but intervertebral disc material typically will not.

Gadolinium is relatively safe when compared to other contrast media, which may be why it is the most commonly used medium of enhancement. However, it does carry some risk.

Indications for Using Gadolinium

1. Previous spine surgery. Gadolinium will help differentiate between (avascular) disc material and fibrosis which is vascular. The disc material will not enhance, so it can be differentiated from scar tissue.
2. Differentiating between a solid and a cystic mass. A fluid-filled cystic lesion will not enhance, but a vascular mass will.
3. Determining if a tumor is vascular or avascular. A lipoma will not enhance, but a sarcoma will.
4. Gadolinium use is preferred when ruling out either a primary tumor or metastatic disease.
5. Osteomyelitis
6. Abscess
7. Bone cyst
8. History of cancer

Risks to Using Gadolinium

1. Allergic reaction
2. Kidney damage. Gadolinium is ultimately filtered through the kidneys. For this reason it is recommended that those with renal disease not use gadolinium.
3. Patients with nephrogenic systemic fibromatosis (NSF) should avoid gadolinium.
4. Pregnancy. Gadolinium is contraindicated during pregnancy.
5. Breast feeding mothers should discontinue breast feeding until the gadolinium has passed from their system.

Clinical note: When in doubt about using gadolinium or any contrast media, consult your radiologist.

Gadolinium Enhancement

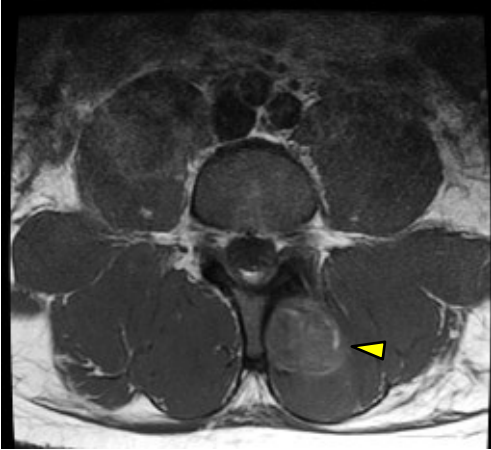


Figure 23:1. T1W axial image of a left-sided paraspinal hematoma.

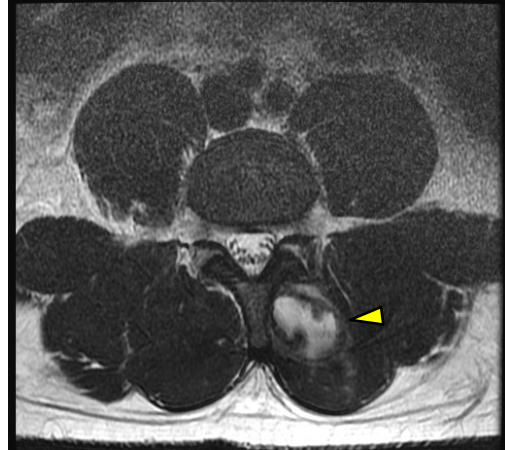


Figure 23:2. T2W axial image of a left-sided paraspinal hematoma.



Figure 23:3. T1W axial image of a schwannoma extending into the left iliopsoas muscle.



Figure 23:4. Schwannoma that extends from the IVF into the left iliopsoas muscle in this T2 axial image.

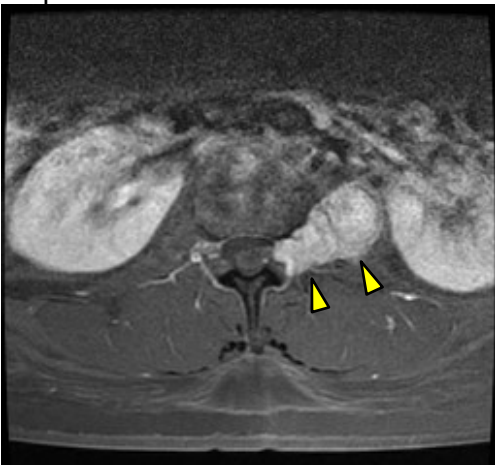
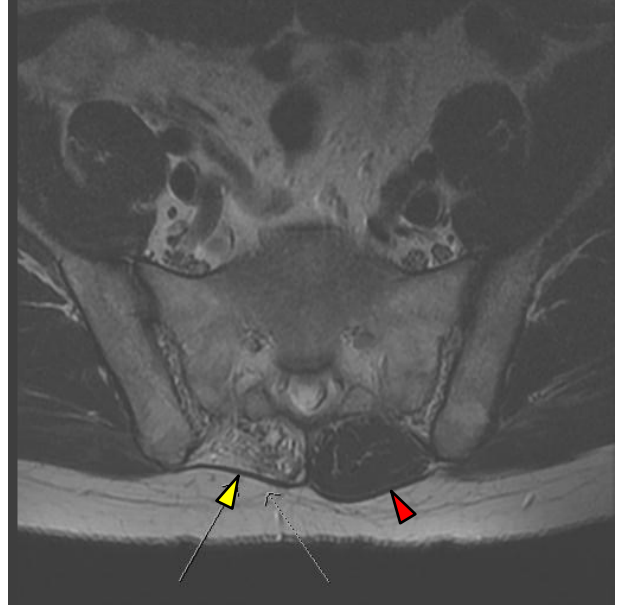
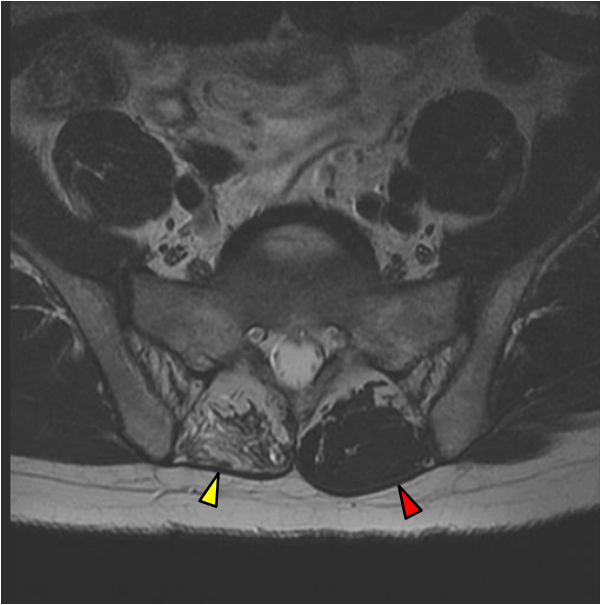


Figure 23:5. Gadolinium enhances the visualization of the Schwannoma in this fat-suppressed T1 axial.

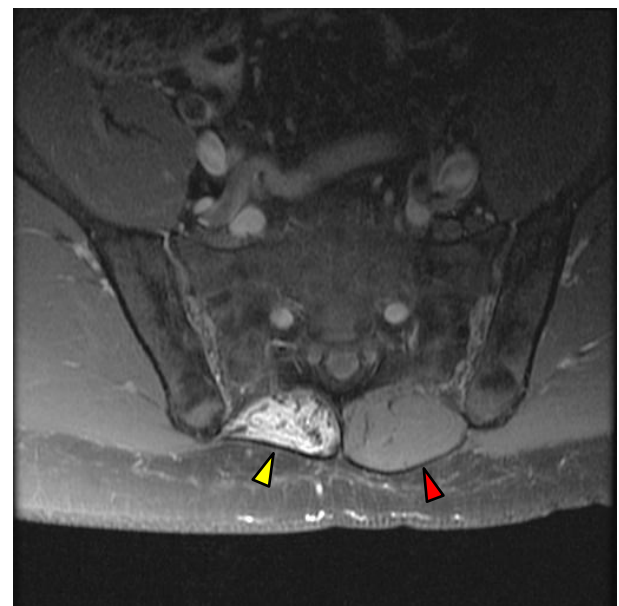
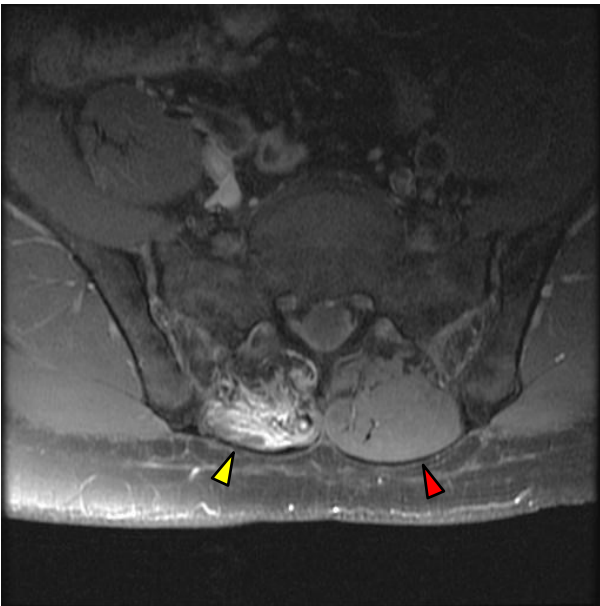
These images demonstrate two different lesions that look similar on MRI. Figures 23:1 and 23:2 display a hematoma in the left paraspinal muscles. Figures 23:3 and 23:4 are images of a schwannoma penetrating the left iliopsoas muscle. Notice the lesions are both hypointense in the T1 axials and then hyperintense and heterogeneous in the T2 images. If you only had these MRI images available, you might be at a disadvantage in differentiating these two very different lesions. The use of gadolinium enhancement (figure 23:5) aids in identifying the schwannoma.

Gadolinium Enhancement

Scar tissue is enhanced by gadolinium. The images on these two pages show a patient with surgical decompression surgery of the lumbar spine. Compare the pre- and post-gadolinium images. The images below clearly show the affinity that gadolinium has for scar tissue. This patient has significant post-surgical scarring in the right paraspinal muscles.



Figures 23:6 and 23:7. These axial images show an isointense signal in the right paravertebral muscles (yellow arrow) which could represent fatty infiltration or scar tissue. The red arrow points to the left paraspinal muscles which are normal.



Figures 23:8 and 23:9. These axial images were taken after the administration of gadolinium. The hyperintense signal in the right paravertebral muscles (yellow arrow) indicates gadolinium uptake into vascular tissue indicating this is scar tissue. The red arrow points to the normal left paraspinal muscles.

Gadolinium Enhancement



Figure 23:10. T2 weighted sagittal image of a post-surgical lumbar spine.



Figure 23:11. Post-gadolinium T1 fat sat sagittal of the same patient. Note the enhancement of the discs (green arrows) indicating increased vascularity and scarring in the discs. Also note the posterior paraspinal enhancement (within the red circle) indicating post-surgical scarring.

Gadolinium aids in determining the content of a space-occupying lesion. After lumbar discectomy, non-contrasted MRI (figure 23:10) showed space-occupying lesions that appeared to be re-herniations of the discs at L3-L4 and L4-L5. The administration of gadolinium (figure 23:11) revealed enhancement consistent with the vascularity associated with scar tissue. Gadolinium can help differentiate between disc material and post-surgical scarring. In this case there is significant scarring.

Gadolinium Enhancement

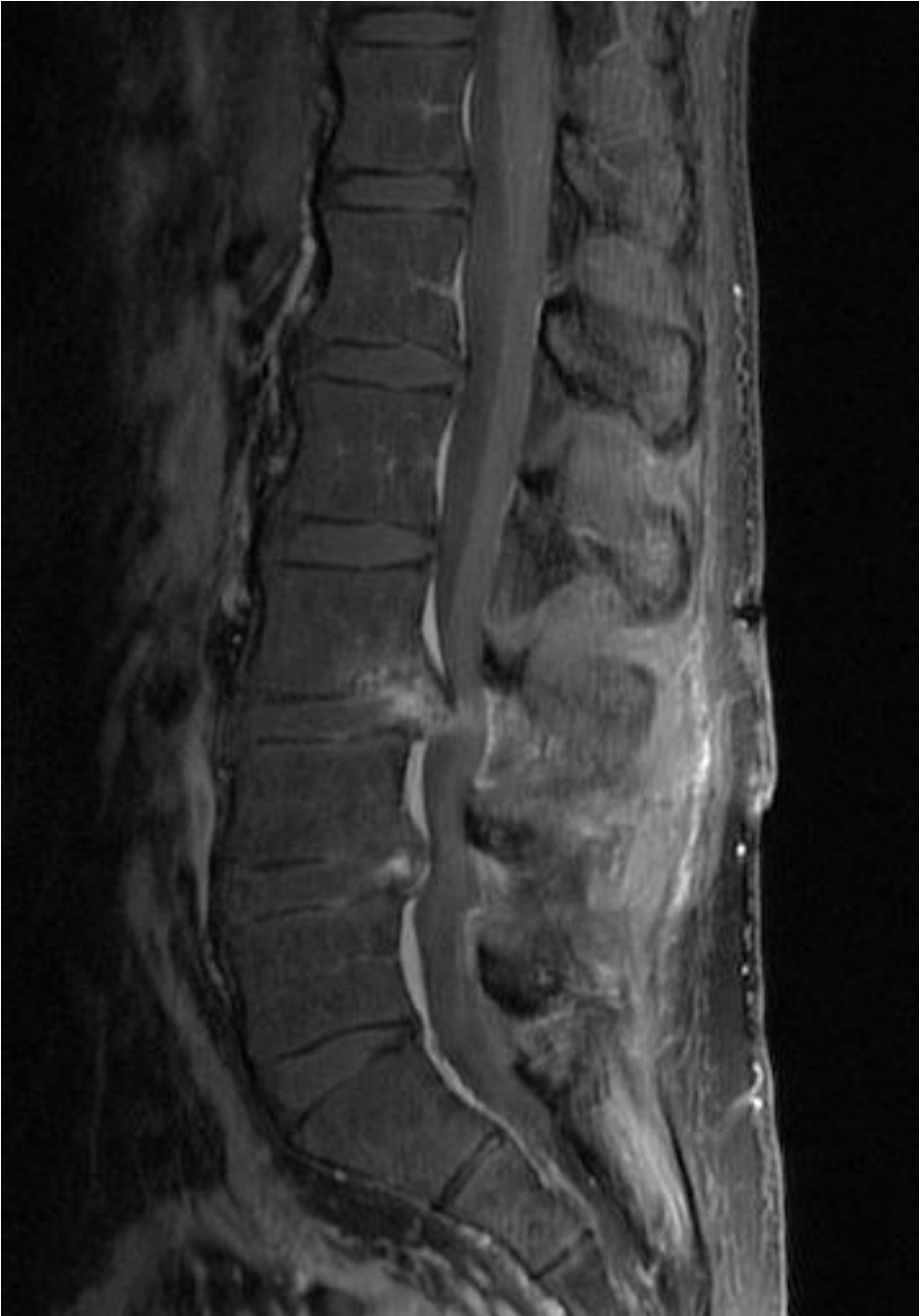


Figure 23:12. Post-gad T1 FS (the same slice as seen on figure 23:11, but without the identifying markers) showing increased enhancement of the posterior discs of L3-L4 and L4-L5.

Suggested Reading

Geraldes C, Laurent S. Classification and basic properties of contrast agents for magnetic resonance imaging. *Contrast Media & Molecular Imaging* 4(1): 1–23. doi:10.1002/cmml.265. PMID 19156706.

Murphy KJ, Brunberg JA, Cohan RH. (1 October 1996). Adverse reactions to gadolinium contrast media: A review of 36 cases. *AJR Am J Roentgenol* 167 (4): 847–9. doi:10.2214/ajr.167.4.8819369. PMID 8819369.

Penfield, Jeffrey G; Reilly, Robert F (2007). What nephrologists need to know about gadolinium. *Nature Clinical Practice Nephrology* 3 (12): 654–68. doi:10.1038/ncpneph0660. PMID 18033225.

<http://www.ismrm.org/special/EMEA2.pdf>

Grobner, T. (2005). Gadolinium - a specific trigger for the development of nephrogenic fibrosing dermopathy and nephrogenic systemic fibrosis?. *Nephrology Dialysis Transplantation* 21 (4): 1104–8. doi:10.1093/ndt/gfk062. PMID 16431890.

Marckmann, P; Skov, L, Rossen, K, Dupont, A, Damholt, MB, Heaf, JG, Thomsen, HS (2006). Nephrogenic systemic fibrosis: suspected causative role of gadodiamide used for contrast-enhanced magnetic resonance imaging. *Journal of the American Society of Nephrology* 17 (9): 2359–62. doi:10.1681/ASN.2006060601. PMID 16885403.

Centers for Disease Control and Prevention (CDC) (2007). Nephrogenic fibrosing dermopathy associated with exposure to gadolinium-containing contrast agents--St. Louis, Missouri, 2002-2006. *MMWR. Morbidity and mortality weekly report* 56 (7): 137–41. PMID 17318112.

Broome DR, Girguis MS, Baron PW, Cottrell AC et al. Gadodiamide-associated nephrogenic systemic fibrosis: why radiologists should be concerned. *AJR Am. J. Roentgenol.* 2007 Feb; 188 (2): 586-92.

Wu JS, Hochman MG. Soft-tissue tumors and tumorlike lesions: a systematic imaging approach. November 2009 *Radiology*, 253, 297-316.

Atlas SW. (2008). *Magnetic resonance imaging of the brain and spine* (forth edition). Lippincott Williams & Wilkins.

Ross JS et al. (2010). *Diagnostic imaging spine* (second edition). Amirsys Inc.

Post-Surgical Findings

24



Post-Surgical Findings

Surgery alters the anatomy and integrity of the spine. Some post-surgical findings are particularly important and will require clinical intervention. This chapter will uncover some of the common findings seen in the post-surgical spine: pseudomeningoceles, paraspinal scarring and adhesions, post-surgical cystic lesions, laminectomy, and surgical implants.

Hemilaminectomy

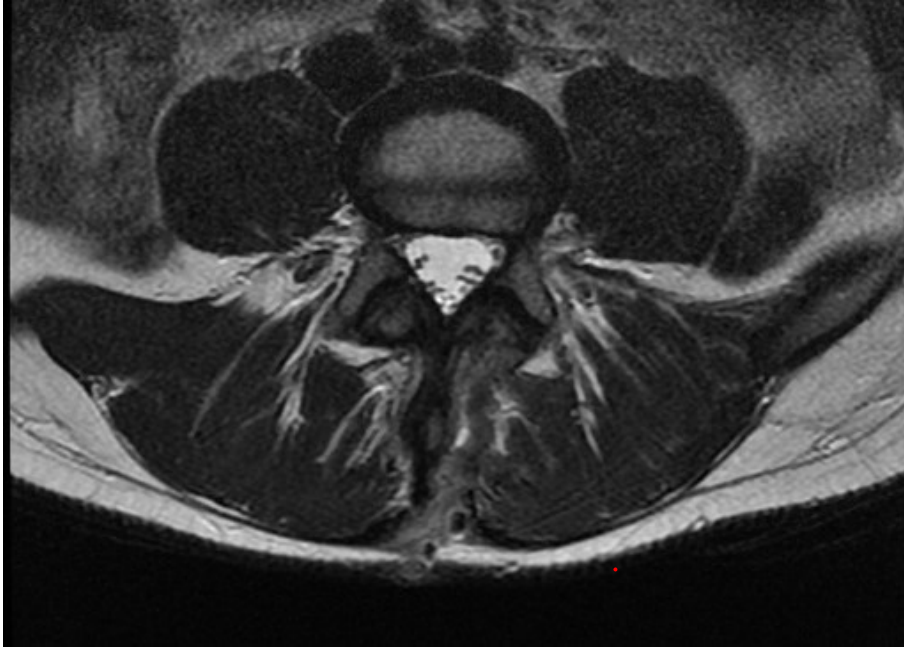


Figure 24:1. This T2W axial image shows a healing scar from a hemilaminectomy.

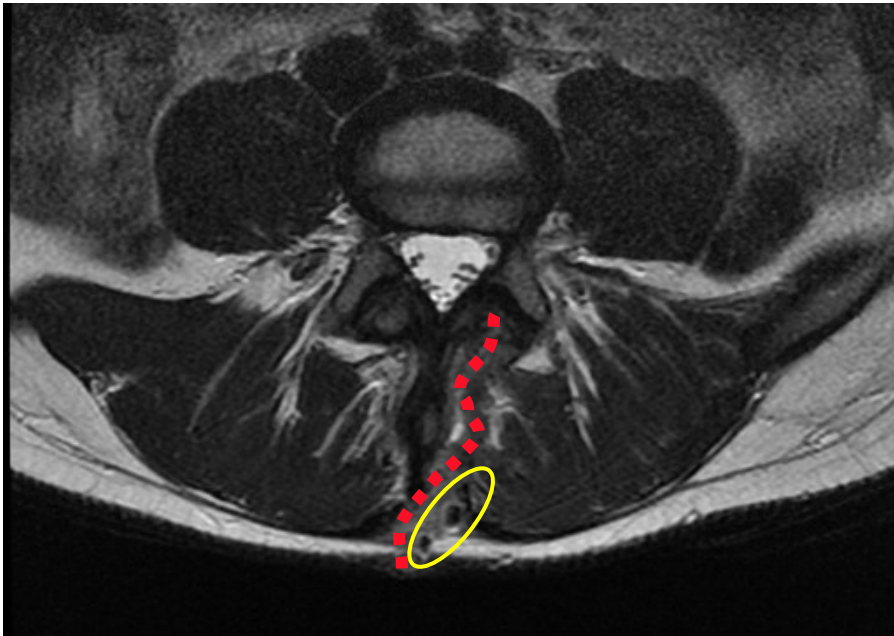
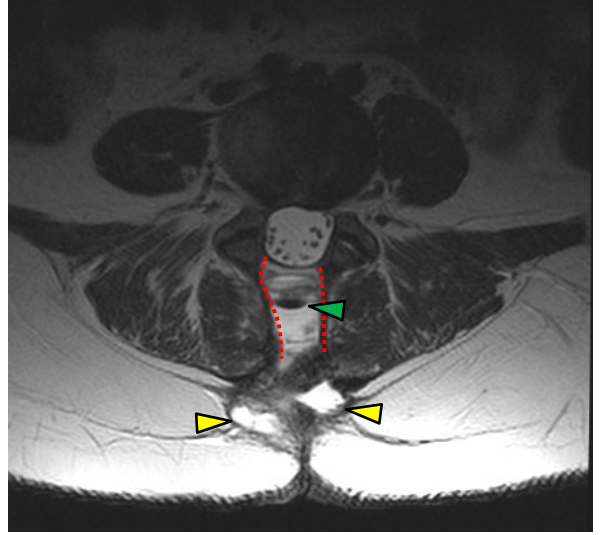
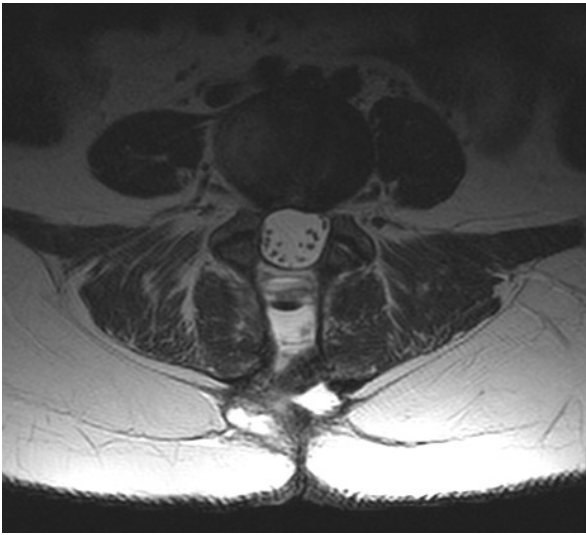
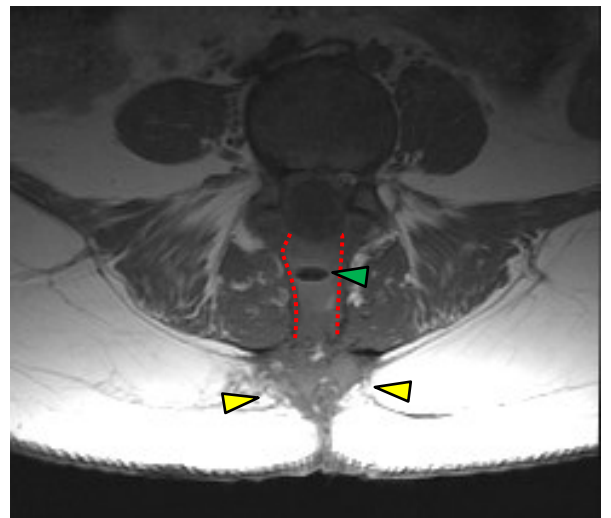
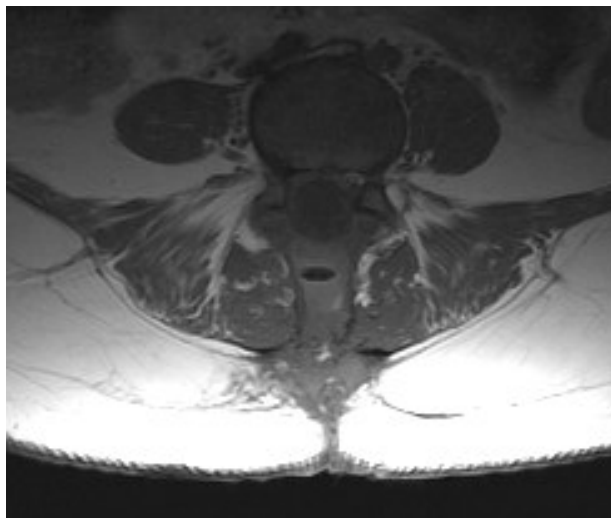


Figure 24:2. This image is the same slice as figure 24:1 with the surgical path shown by a red dashed line. The yellow oval shape contains three cystic lesions along the surgical path.

Laminectomy



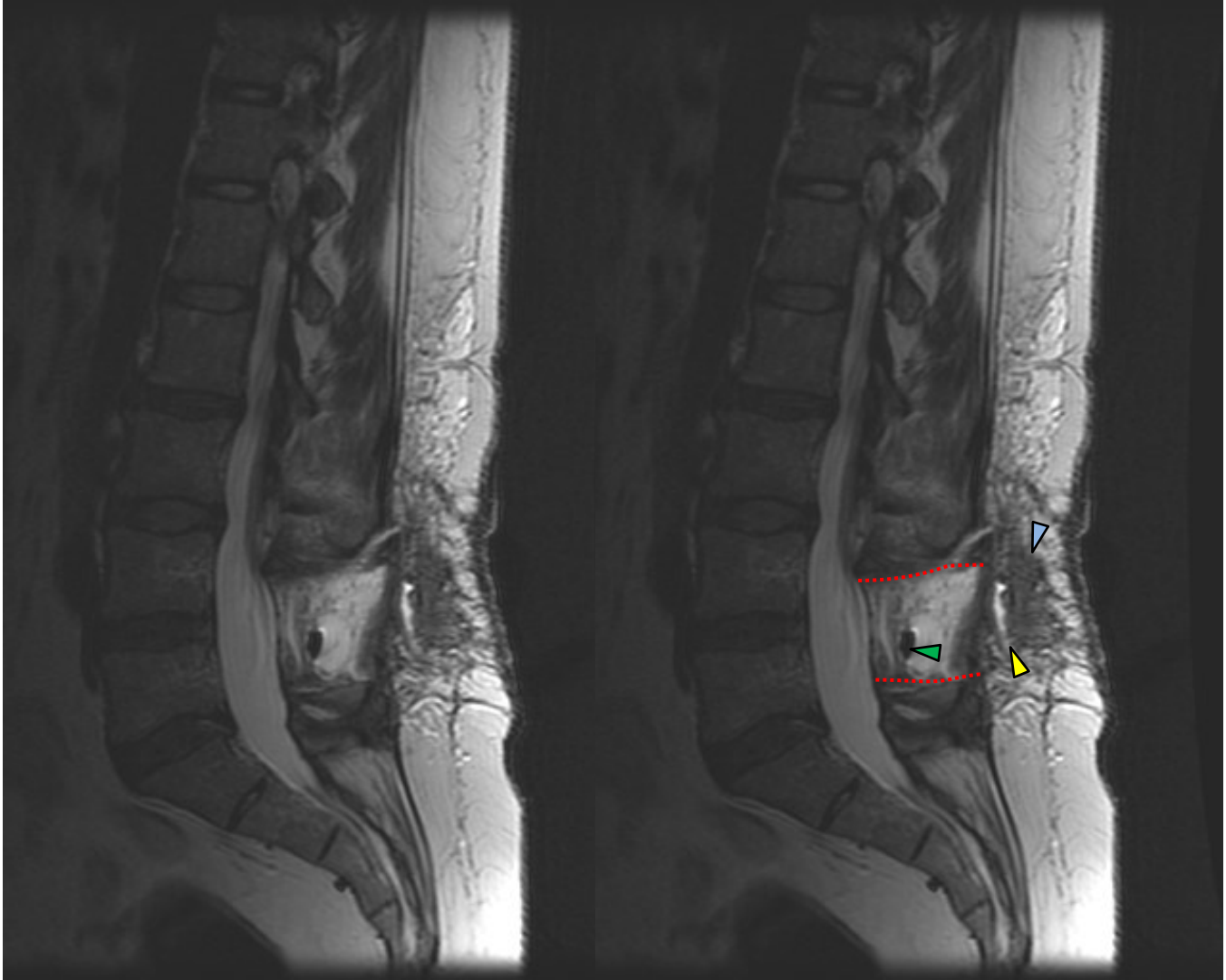
Figures 24:3 and 23:4. T2W axial image. Note the pocket of gas posterior to the thecal sac (green arrow) and the light-colored fluid-filled pockets (yellow arrows). The gap left by the laminectomy is defined by the red dotted lines.



Figures 24:5 and 24:6. T1W axial image. Note the pocket of gas posterior to the thecal sac (green arrow) and the light-colored fluid-filled pockets (yellow arrows). The gap left by the laminectomy is defined by the red dotted lines.

These images show several radiographic images following an L5 laminectomy. The path of the surgeon is visible in all three images along with a gas pocket posterior to L5 that is dark in both T1 and T2 weighted images. Fluid-filled pockets are also seen posterior to L5. These pockets are dark on T1 weighted images and light on T2 weighted images.

Laminectomy



Figures 24:7 and 24:8. This is a T2W sagittal image of an L5 laminectomy. Note the path of the surgeon through the subcutaneous fat (blue arrow), the absence of the L5 lamina and spinous process (between the red dotted lines), and the air pocket in the void where the L5 spinous process had been (green arrow).

This image is a sagittal that corresponds to the axials seen on page 333.

Pseudomeningocele

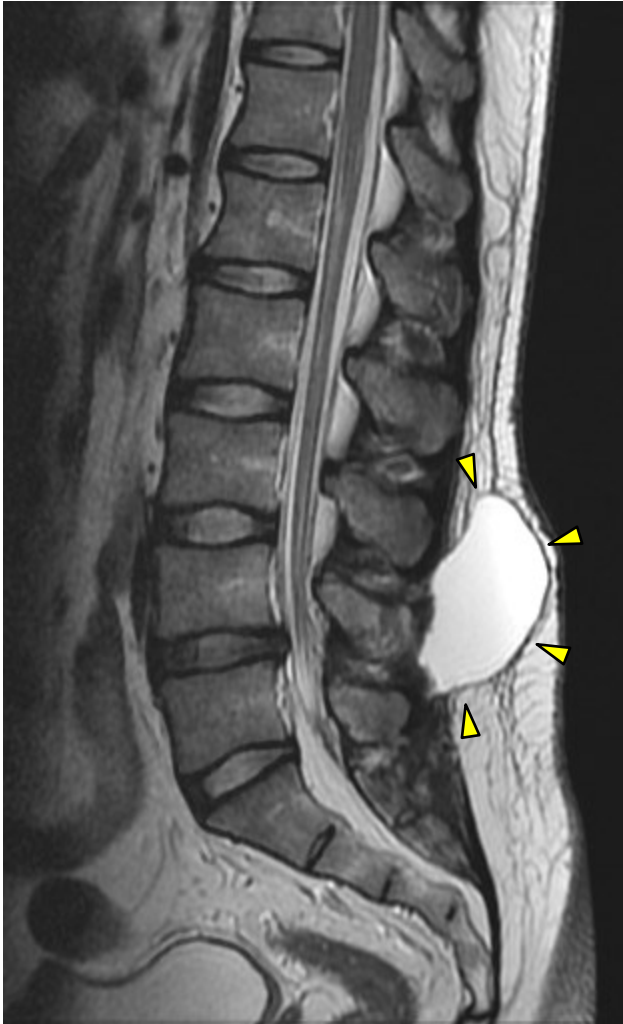


Figure 24:9. This T2W sagittal image clearly reveals a post-surgical pseudomeningocele. Note the white-colored pouch of fluid posterior to L4.

A postoperative pseudomeningocele is a complication of spine surgery. This unintended complication is essentially a pouch of cerebrospinal fluid (CSF) that has leaked into the paraspinal tissues. It appears cyst-like on MRI.



Figure 24:10. T2W axial image.

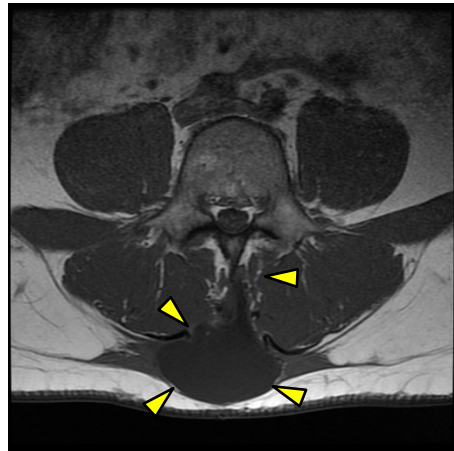


Figure 24:11. T1W axial image.

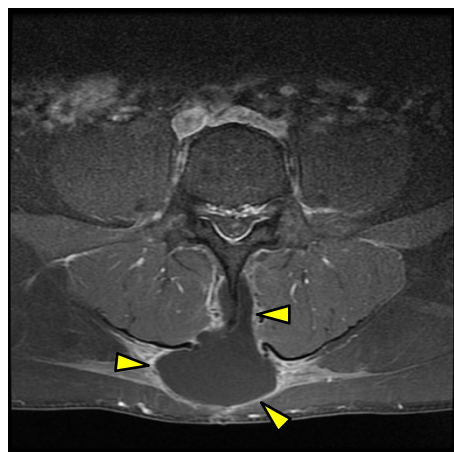


Figure 24:12. T1 fat-saturated image.

Meningoceles and Pseudomeningoceles

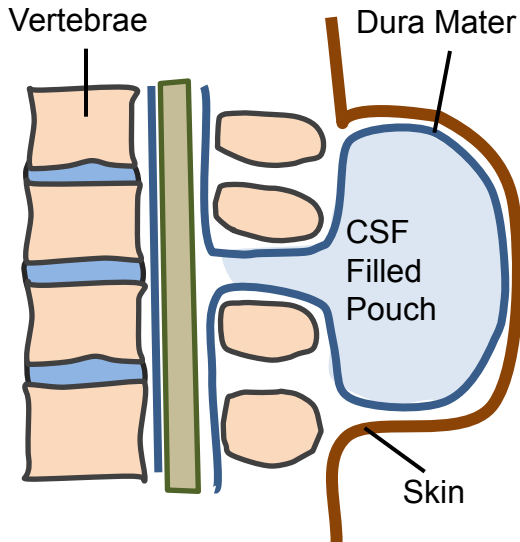


Figure 24:13. Schematic of a meningocele. A fluid-filled ballooning of the dura mater. Meningoceles are commonly associated with spina bifida deformations.

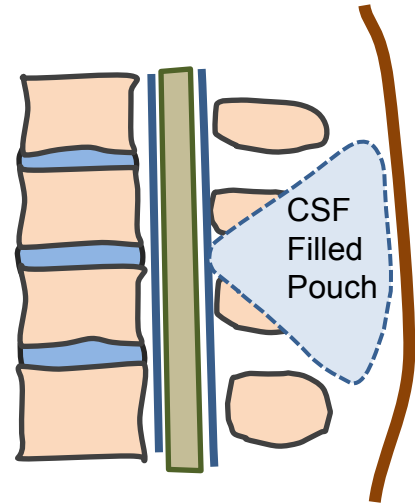


Figure 24:14. A pseudomeningocele may look somewhat like a meningocele on MRI, though it is not retained within the meninges. It is contained within the surrounding soft tissues.



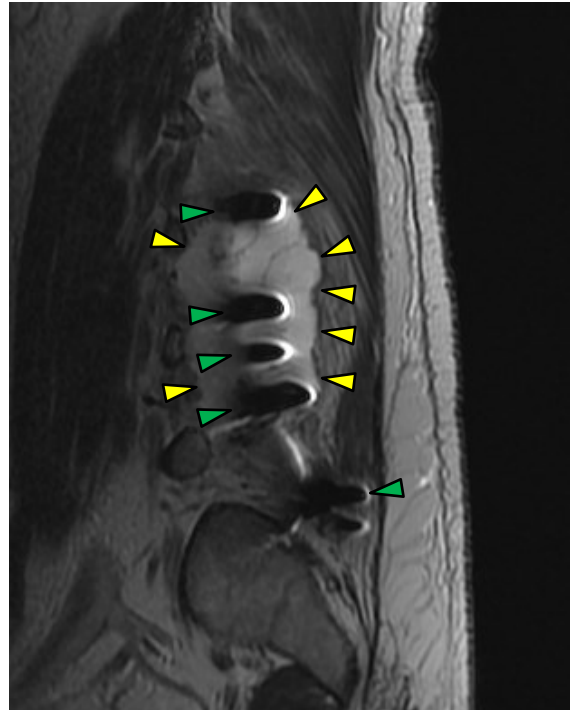
Figure 24:15. A post-surgical pseudomeningocele observed in a sagittal T2 weighted image of the lumbar spine.

A meningocele is a cyst-like collection of cerebral spinal fluid (CSF) in a pouch contained within the meninges and the dura mater. A meningocele is frequently associated with spina bifida. Meningoceles may be related to severe neurological complications.

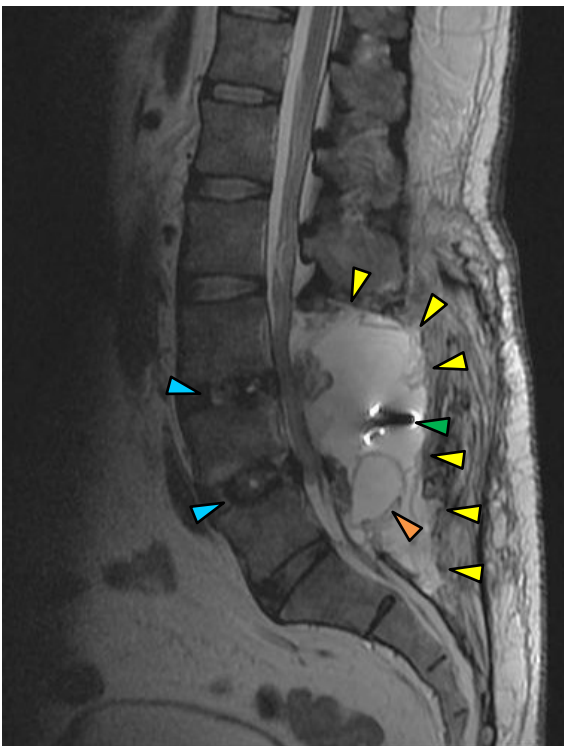
Pseudomeningoceles are abnormal accumulations of CSF in the tissues surrounding the spine or brain. Pseudomeningoceles are not contained within the dura mater. Pseudomeningoceles may appear following surgery or injury that has resulted in a CSF leak. The leaking CSF deforms surrounding soft tissues to create its own fluid-filled cavity that may resemble a meningocele in appearance, hence the name pseudomeningocele.

Seromas are pockets of serous fluid which may weep from tissues following surgery. Seromas lack the red blood cells seen in hematomas.

Post-Fusion Pseudomeningocele



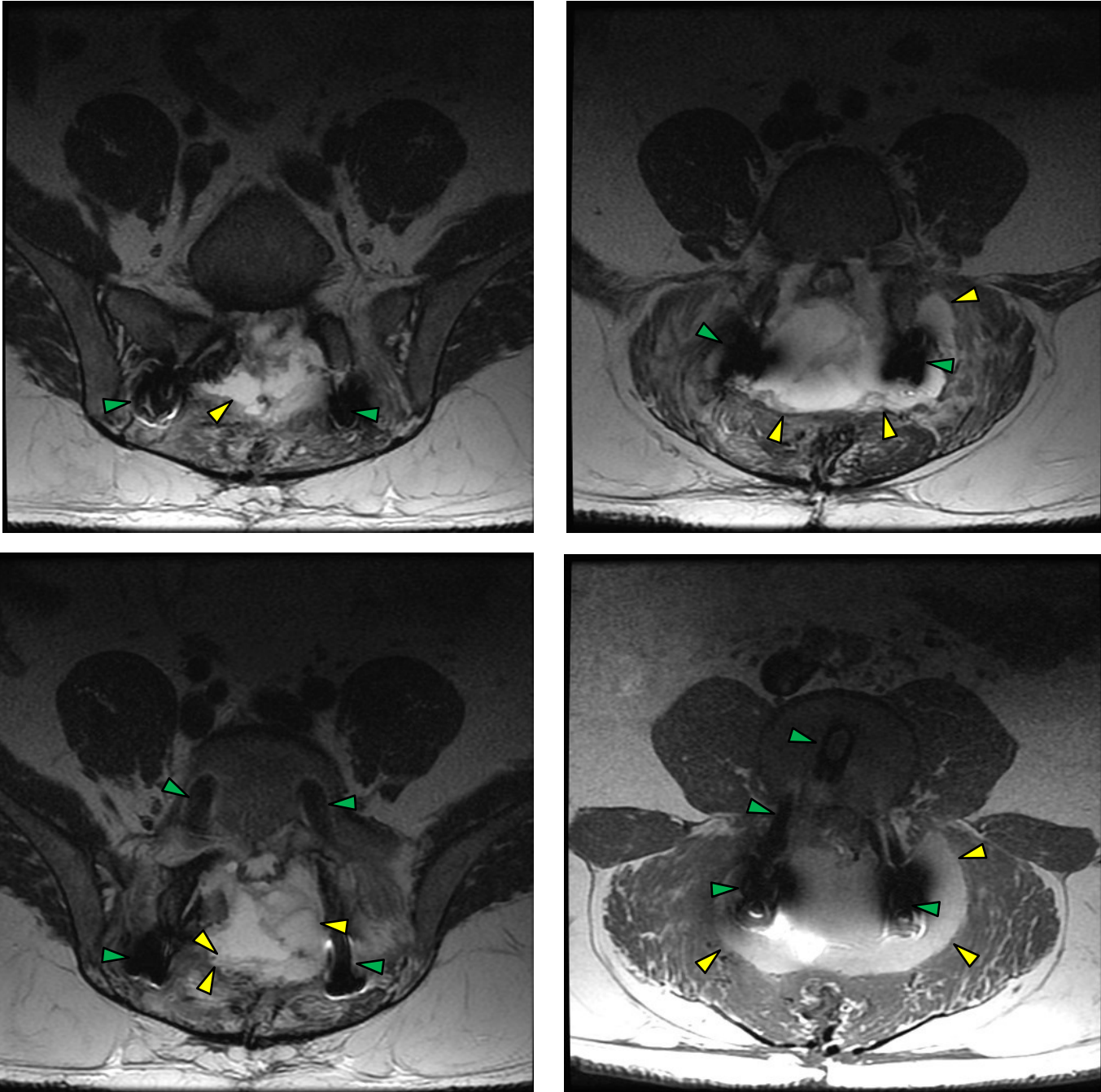
Figures 24:16 and 24:17. These T2W sagittal images show a post-fusion pseudomeningocele with its margins identified by the yellow pointers. The surgical screws appear as black voids and are identified by the green pointers.



These T2 weighted sagittal images show evidence of orthopedic fixation appliances and evidence of fluid collections in the gap left by a laminectomy. In figure 24:18 we can see intradiscal devices (bone graft material) and a large pseudomeningocele posterior to the thecal sac. Note the displacement of the paravertebral muscles posteriorly by the expansion of the pseudomeningocele.

Figure 24:18. This image shows another sac of fluid within the pseudomeningocele (orange pointer), as well as the intervertebral placement of cadaverous bone to stimulate fusion (blue pointers). The outer margins of the pseudomeningocele is denoted by the yellow pointers.

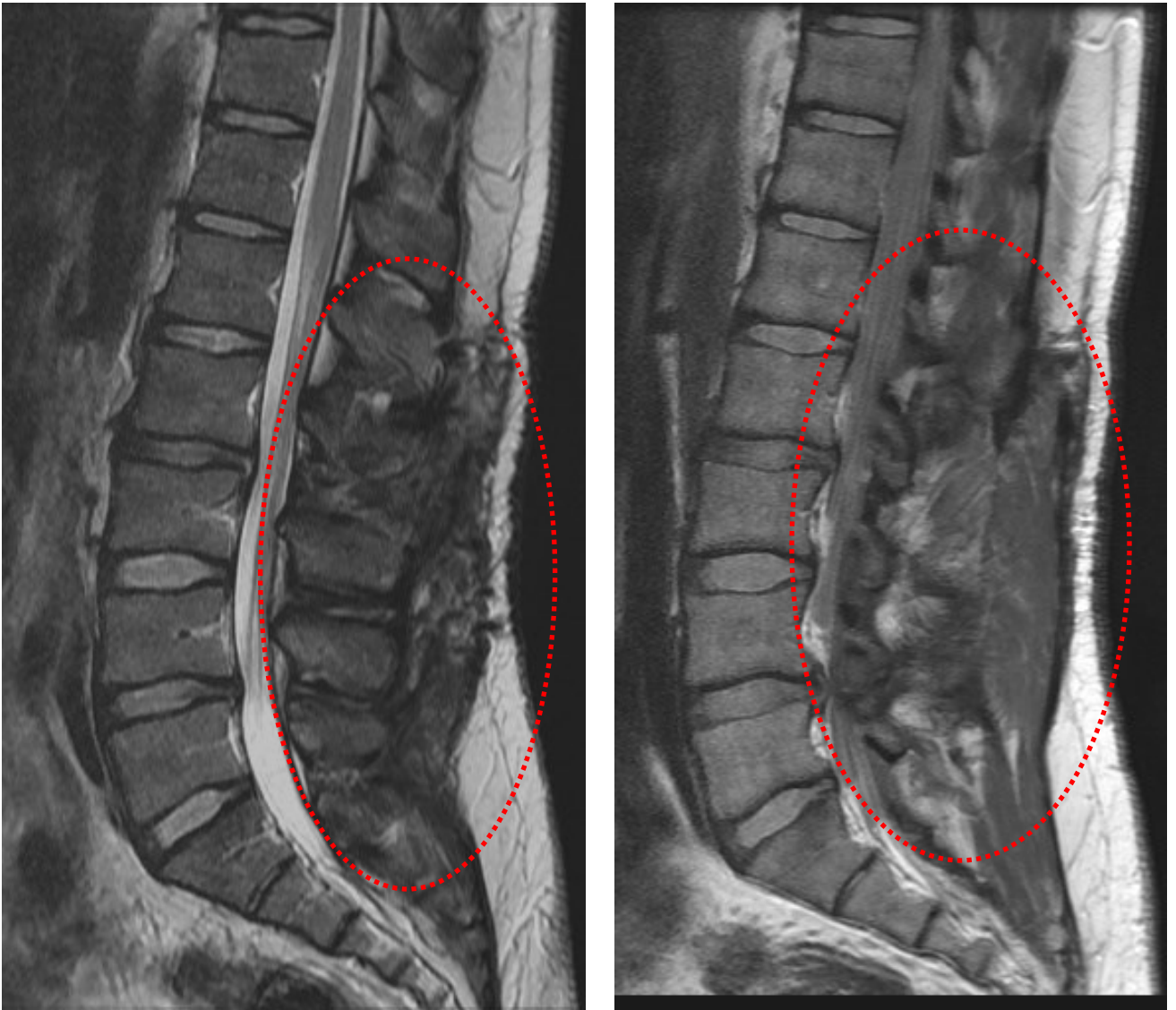
Post-Fusion Pseudomeningocele (continued)



Figures 24:19-22. T2W axial images following surgical fusion surgery. The yellow arrows point to a heterogeneous collection of fluids, probably a seroma with residual blood products. The green arrows point to the metal screws that secure the vertebra and allow fusion to take place.

A seroma is a space-occupying pocket of serous fluid that can develop after surgery when serous fluid weeps out.

Five Level Hemilaminectomy Discectomy



Figures 24:23 and 24:24. These T2W sagittal images are of a 45 year-old man who had lumbar surgery five years prior. The surgery included five levels of hemilaminectomy and discectomy. Note the extent of scar tissue in the soft tissues.

Post Hemilaminectomy

These images show the third disc extrusion of the L5-S1 disc. This herniation occurred after two previous discectomies. This is not an uncommon occurrence. According to investigators, re-herniation after surgery happens 9-25% of the time.



Figure 24:25. T2W sagittal image of a large extrusion at L5-S1.



Figure 24:26. Another T2W sagittal image of the same extrusion at L5-S1. This image shows the extent of foraminal occlusion of the left L5-S1 IVF by the extrusion.

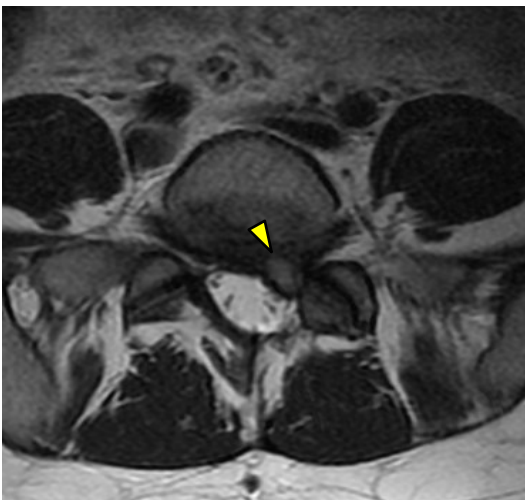


Figure 24:27. This T2W axial image shows a focal extrusion superimposed on a broad-based herniation. This extrusion is affecting the left IVF of L5-S1.

Right Hemilaminectomy Two Months Post-Surgery

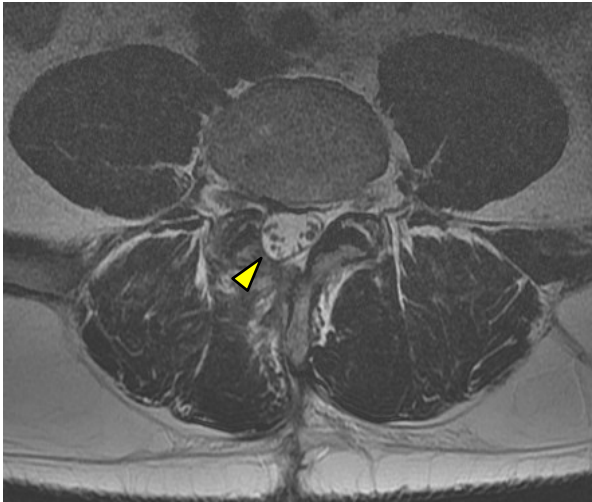


Figure 24:28. T2W axial image of the thecal sac displaced through the opening in the lamina which was created by the right hemilaminectomy. Note the oblong shape of the thecal sac.

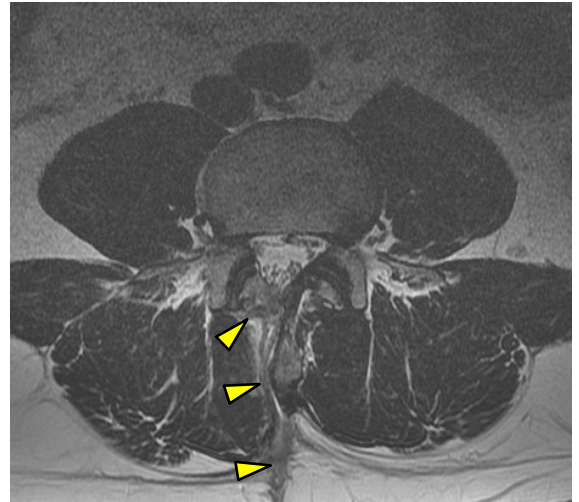
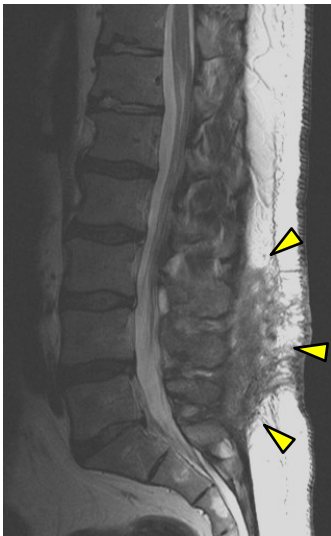


Figure 24:29. T2W axial image showing the path of the surgeon on this patient two months after a hemilaminectomy.



Figures 24:30 and 24:31. T2W sagittal images showing post-surgical changes in this post-hemilaminectomy at two months.

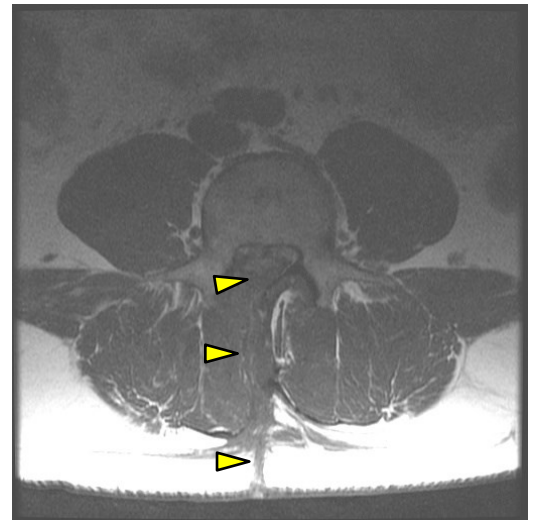


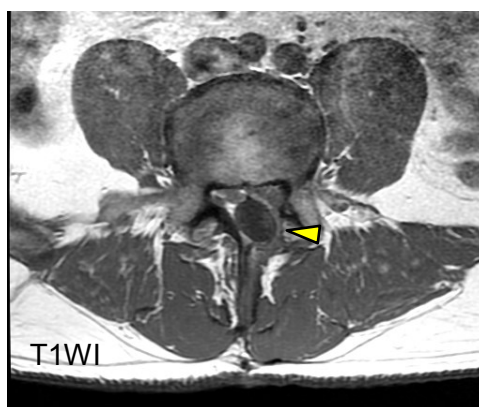
Figure 24:32 T1W axial image showing the path of the surgeon on this patient two months after a hemilaminectomy.

This series of images shows the MRI findings of a lumbar spine two months after a right hemilaminectomy. The path of the surgeon is clearly visible in all of the images. The axial images show the thecal sac being displaced into the gap in the posterior right arch by the hemilaminectomy.

Displacement of the Thecal Sac through a Hemilaminectomy



Figures 24:33 and 24:34. T2W and T1W sagittal images show post-surgical re-herniation, and sequestered fragmentation arising from the L4-L5 disc.



Figures 24:35 and 24:36. These images reveal partial displacement of the thecal sac through the hemilaminectomy (yellow pointer). Note the oblong appearance of thecal sac.

This series of images shows the MRI findings of a lumbar spine after a left hemilaminectomy. The path of the surgeon is less visible on these images than those of the previous page. The axial images show the thecal sac being displaced into the gap in the posterior arch left by the hemilaminectomy. The sagittal images reveal a sequestered disc fragment from an extrusion at L4-5.

Pre- and Post-Surgical Images of an Ependymoma

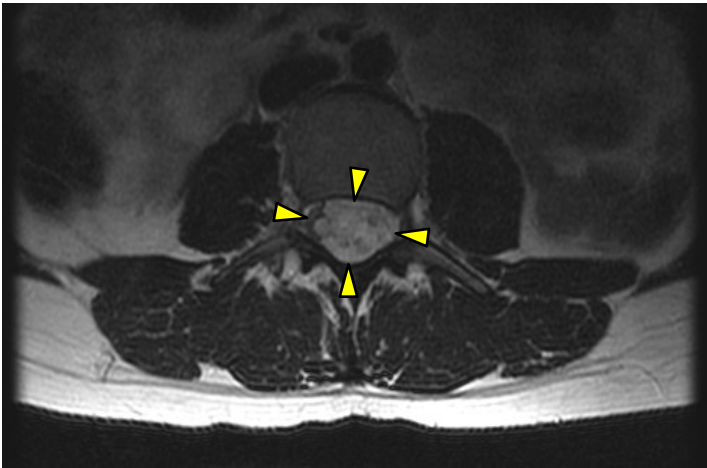


Figure 24:37. T2W axial image of an ependymoma.

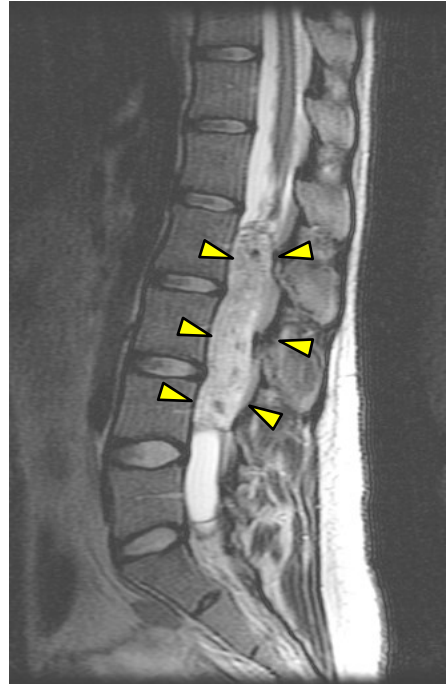


Figure 24:39. T2W sagittal image of a large ependymoma in the central canal from L2-L4.



Figure 24:38. T2W axial image of diffuse ill-defined, disrupted, post-surgical changes.

This series of images shows the MRI findings of a lumbar spine after a large ependymoma was removed from L2-L4. This tedious surgery caused significant disruption of the paraspinal muscles and posterior elements of the spine.



Figure 24:40. Post-surgical T2W sagittal image showing extensive post-surgical changes following the removal of the ependymoma.

Re-herniation of L4-5 Two Weeks after a Discectomy

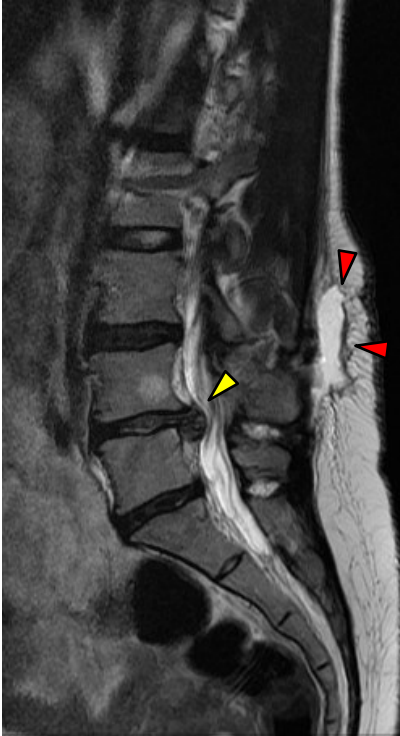


Figure 24:41. T2W sagittal image of a large L4-L5 extrusion (yellow arrow). Note the pocket of fluid posterior to the spinous processes of L3 and L4 (red arrows).



Figure 24:42. T1W sagittal image of a large L4-L5 extrusion (yellow arrow). Note the pocket of fluid posterior to the spinous processes of L3 and L4 (red arrows).

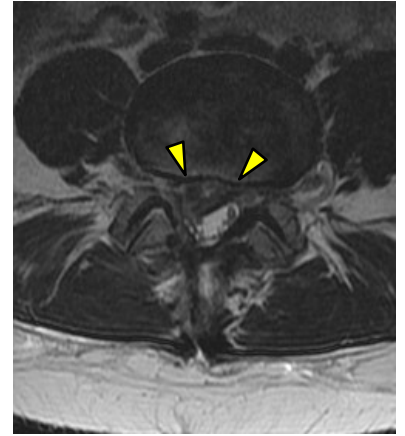


Figure 24:43. This T2W axial image shows the re-herniation (extrusion) of the L4-5 disc.

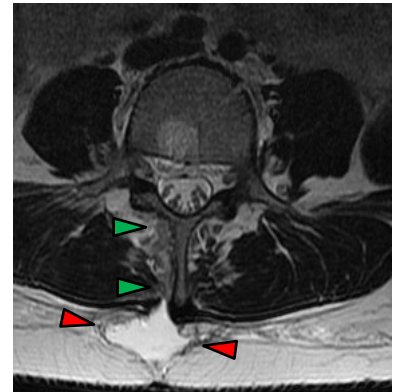
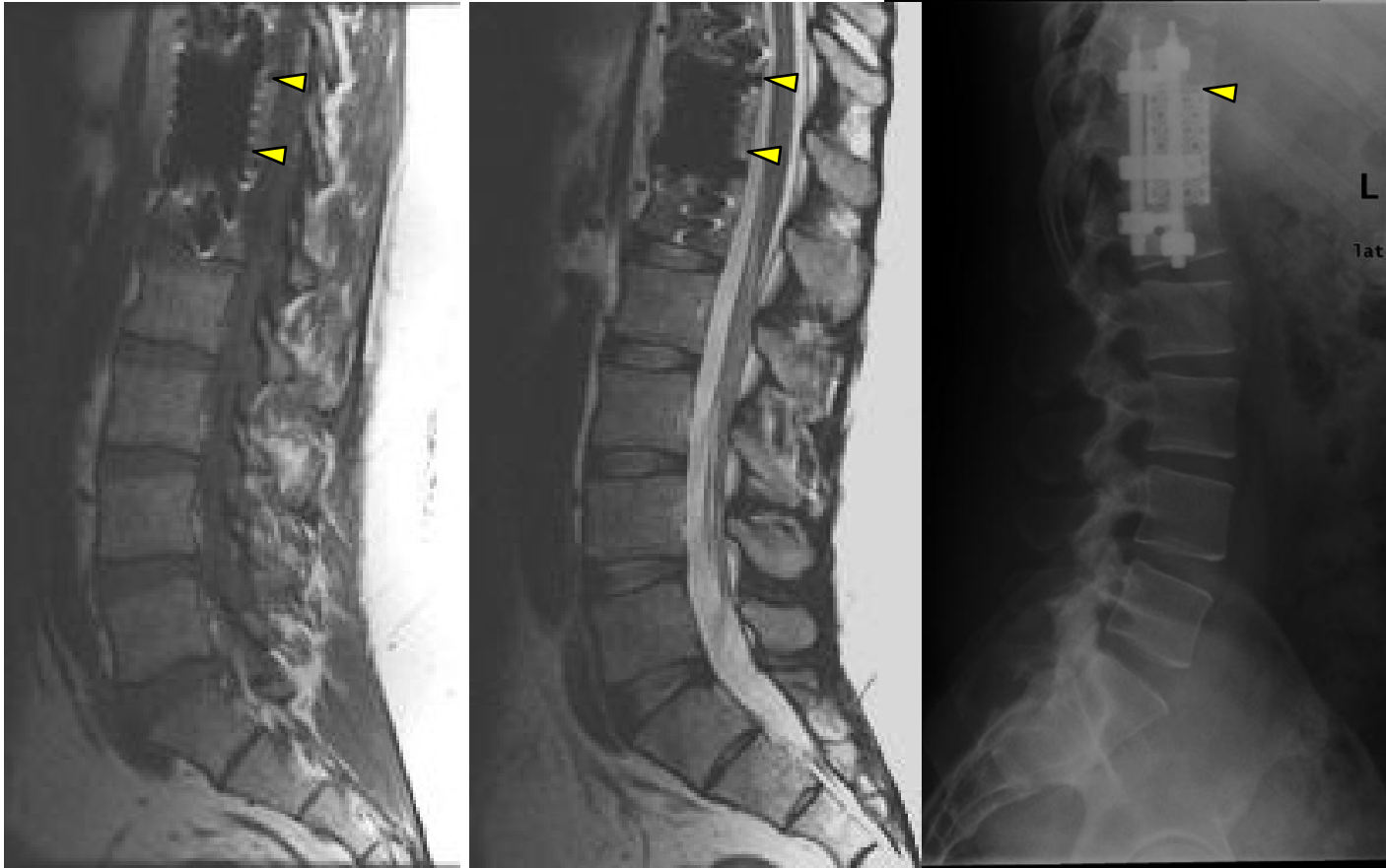


Figure 24:44. This T2W axial image reveals the path of the surgeon (green arrows) and fluid accumulation in the paraspinal soft tissues (red arrows).

This series of images show the MRI findings of a lumbar spine two weeks following a right discectomy. These images display a large paracentral re-herniation that occurred at the site of the previous surgery. *Re-herniations* at the site of surgery occur between 9-25%.

Fracture with Surgical Implant



Figures 24:45 and 24:46. T2W sagittal image of a surgical implantation of titanium hardware that was used to stabilize a fracture of T12.

Figure 24:47. Plain film radiograph of the same implant that is represented in figures 24:45 and 24:46.

Because titanium is not a ferrous metal, titanium implants will only minimally impact the quality of MR images. Ferrous implants are prone to be influenced by the strong magnet of the MRI and can create patient hazards as well as negatively influence the quality of the MR image. Since titanium is not magnetic, it is not affected by the strong magnet of the MRI and will appear as a void in the image.

Suggested Reading

Hu R, et al. A Population based study of reoperations after back surgery. *Spine* 1997;22:2265-2271.

Malter A., et al. 5-Year reoperation rates after different types of lumbar surgery. *Spine* 1998;23:814-820.

Atlas S., et al. Surgical and nonsurgical management of sciatica secondary to lumbar disc herniation: five-year outcomes from the Maine lumbar spine study. *Spine* 2001;26:1179-1187.

Osterman H., et al. Risk of multiple reoperations after lumbar discectomy: a population based study. *Spine* 2003;28:621-627.

Atlas et. al. Long-term outcomes of surgical and nonsurgical management of sciatica to a lumbar herniation: 10 year results from the Maine lumbar spine study. *Spine* 2005;30:927-935.

Wu JS, Hochman MG. Soft-tissue tumors and tumorlike lesions: a systematic imaging approach. November 2009 *Radiology*, 253, 297-316.

Arachnoiditis and Arachnoid Cysts



Arachnoiditis

Misunderstood and underreported, arachnoiditis can result from routine medical procedures and leave patients permanently incapacitated. Arachnoiditis is a neuropathic malady that affects the arachnoid layer of the meninges. A more severe type of arachnoiditis is adhesive arachnoiditis. Adhesive arachnoiditis results in scarring and adhesions within the meninges. Additionally, it compresses the nerve rootlets within the thecal sac and can cause nerves to adhere to one another. While described as a rare condition, it has become evident to me that there is no clear tracking method for this disease and many cases may go undiagnosed. Since many doctors are not familiar with this condition, it may be mistaken for other conditions such as disc extrusions, cauda equina syndrome, failed back surgery, or multiple sclerosis.

Refractory pain is the predominant symptom of arachnoiditis. Other symptoms include urinary and bowel dysfunction, sexual dysfunction, numbness, tingling, loss of mobility, headaches, fatigue, and extremity pain and weakness. Since there is no consistent pattern of symptoms for this malady, a correct diagnosis may be difficult.

Treatment of arachnoiditis is difficult and frequently focused on pain reduction. Spinal procedures (epidural injections, intrathecal injections, and surgery) may cause or worsen this condition, so they are typically avoided. Medical management is often limited to protracted use of opiates, antidepressants, steroids, and other treatments intended to minimize pain. Since the degree of symptoms may vary in severity, some patients with arachnoiditis may live relatively normal lives and can be managed with interdisciplinary care: medical care, chiropractic, psychology, and physical therapy. While none of these professions can claim to cure or even help every case of arachnoiditis, any treatment that is safe and may control the symptoms should be considered.

Causes

Three causes have been identified to induce arachnoiditis: Chemicals, trauma, and infection.

Ironically most cases of arachnoiditis are attributed to iatrogenic causes. The chemicals used in spinal injections are the leading iatrogenic cause of this condition. The trauma of a lumbar puncture, spinal surgery, and injury can also cause arachnoiditis. The chronic trauma of spinal stenosis and disc derangement has also been cited to cause arachnoiditis.

Infection is another cause of arachnoiditis. Meningitis (viral, fungal, or bacterial) can result in arachnoiditis.

Arachnoiditis

Radiographic findings

While plain film radiographs will not contribute to the diagnosis of arachnoiditis, magnetic resonance images can reveal characteristic findings of arachnoiditis. On MRI, compression or adhesion of nerve rootlets of the cauda equina may be visualized. The nerve rootlets of the cauda equina will frequently be clumped in the anterior portion of the thecal sac in patients with adhesive arachnoiditis rather than in their normal location which is more posterior.

As epidural steroid injections and percutaneous spinal procedures become more routine and widely used, we can expect to see a rising number of these patients entering our offices.

Arachnoiditis

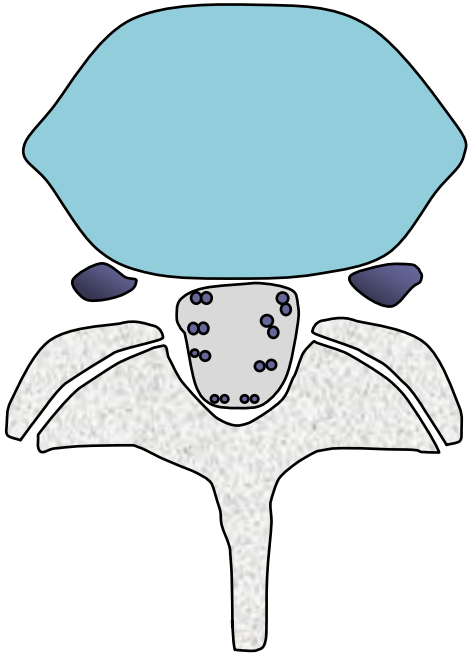


Figure 25:1. A schematic axial image of a normal lumbar segment. Note the wide distribution of the nerve rootlets within the thecal sac.

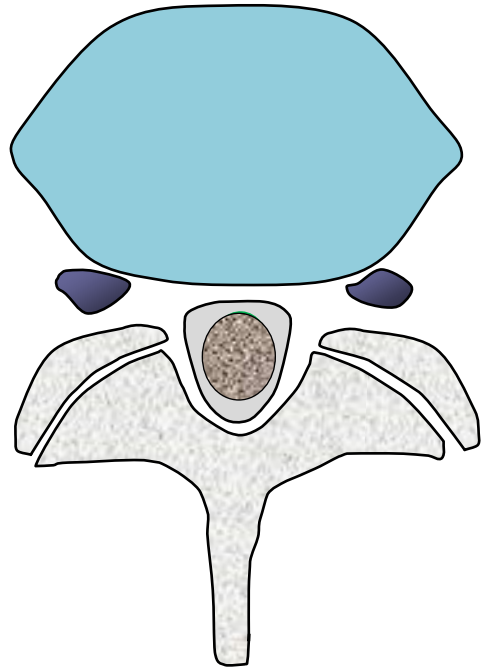


Figure 25:2. This schematic depicts a patient with arachnoiditis. The nerve rootlets are adhered together in a blurred mass.

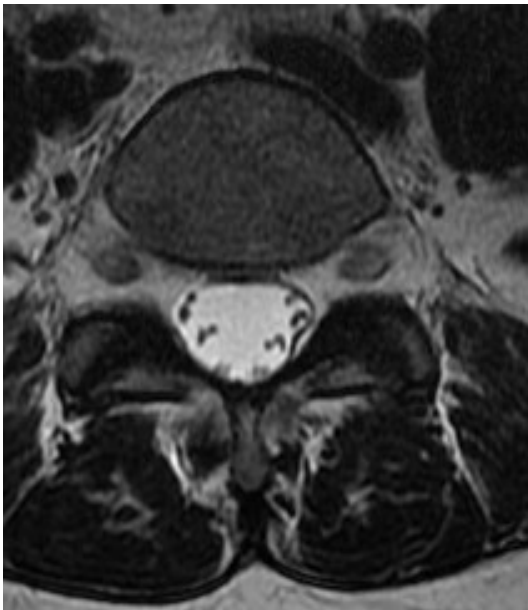


Figure 25:3. A T2W axial image of a normal lumbar segment with divergent nerve rootlets.



Figure 25:4. A T2W axial image of a patient with adhesive arachnoiditis. Note the clumping together of the nerve rootlets of the cauda equina.

Arachnoiditis

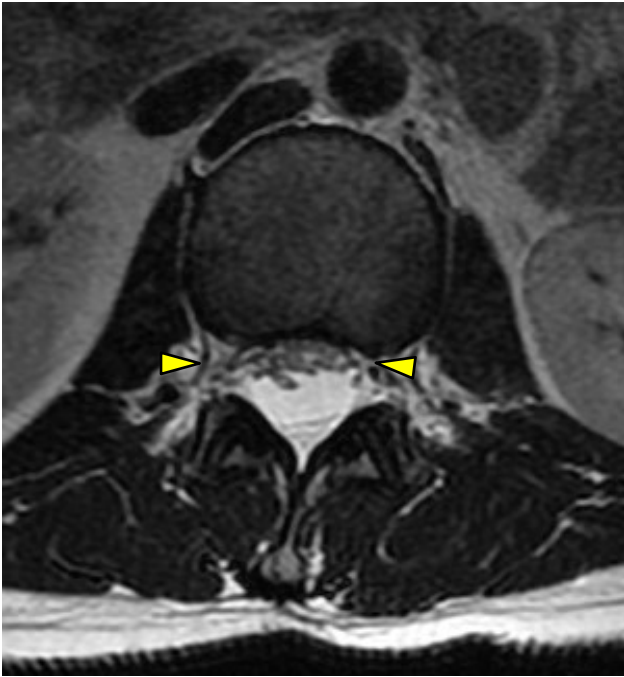


Figure 25:5. Anterior clumping of the nerve rootlets of the cauda equina (yellow arrows) is indicative of arachnoiditis. This image is a slice from the upper lumbar spine.

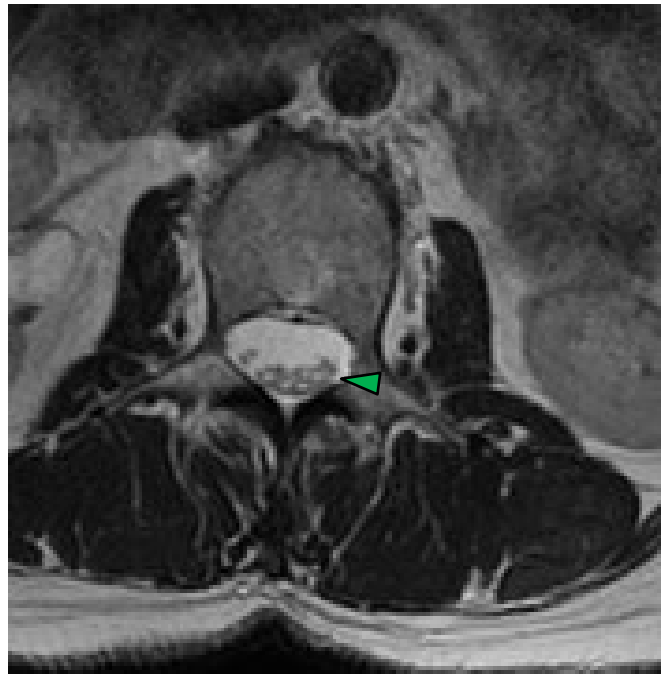


Figure 25:6. Normal. This image displays the normal distribution of nerve rootlets in the upper lumbar spine. They are normally found in the posterior portion of the thecal sac in the upper lumbar spine and migrate anteriorly as they descend.



Figure 25:7. Normal. This image displays the normal spreading and anterior migration of the nerve rootlets in the lower lumbar spine.

These images contrast the anterior clumping together of the nerve rootlets of the cauda equina (figure 25:5) as seen in arachnoiditis with the normal anatomy of the upper lumbar spine (figure 25:6) and lower lumbar spine (figure 25:7).

Arachnoiditis

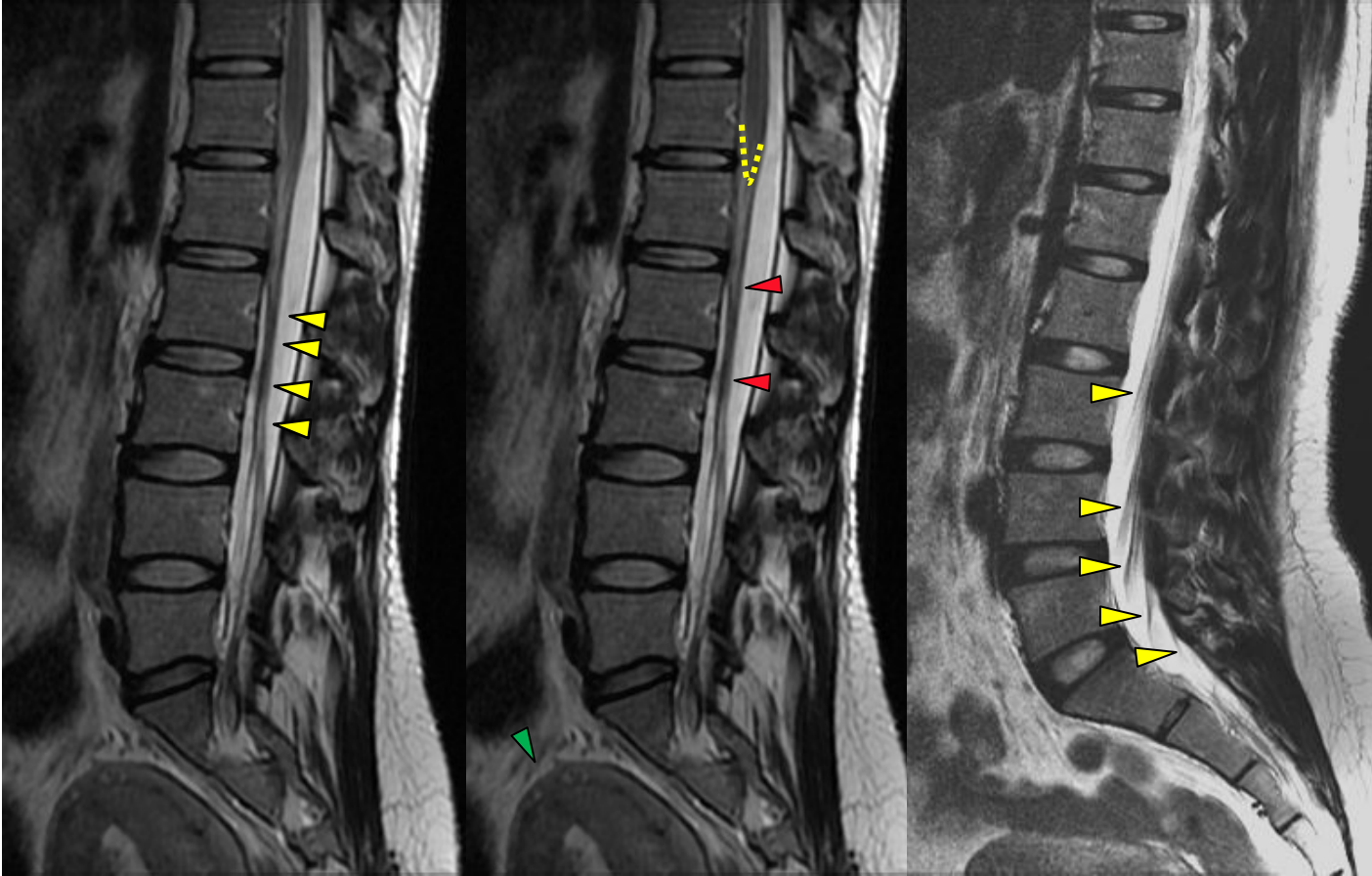


Figure 25:8. T2 weighted sagittal image of a patient with arachnoiditis. This patient's arachnoiditis began with an epidural injection intended to reduce the pain of childbirth.

Figure 25:9. This image is a duplication of figure 25:8. The yellow dotted line outlines the conus medullaris and the red arrows point to the cauda equina clumped together in the anterior portion of the spinal canal. The green arrow points to the enlarged post-partum uterus.

Figure 25:10. Normal. This T2 weighted sagittal image shows the normal appearance of the cauda equina on MR. The yellow arrows point to the nerve rootlets of the cauda equina. Note the nerve rootlets are normally found in the posterior portion of the central canal and migrate inferior and anterior before exiting the intervertebral foramina.

This series of sagittal images shows the anterior clumping of the cauda equina that is characteristic of arachnoiditis. The significance of the enlarged post-partum uterus is that this patient's arachnoiditis arose after receiving epidural anesthesia for childbirth.

Arachnoiditis

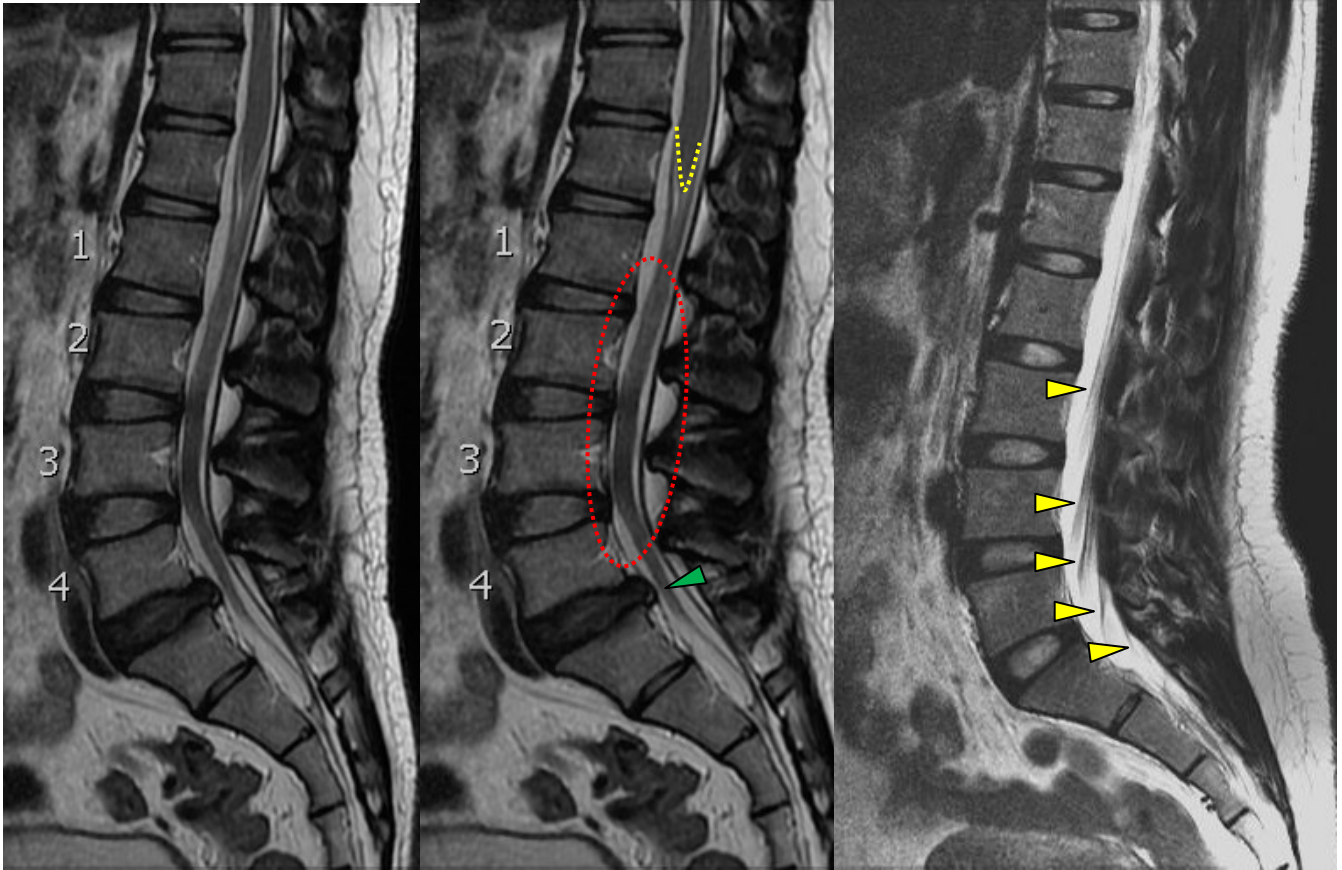


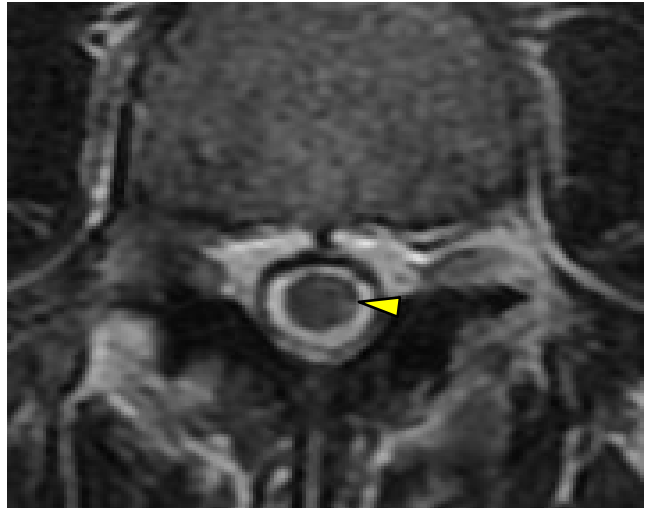
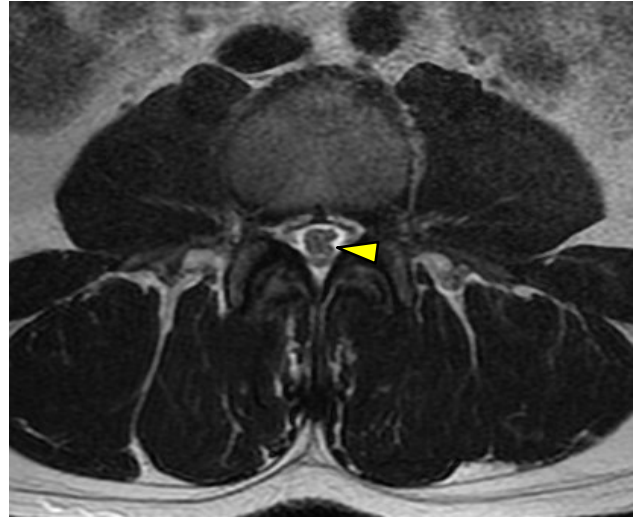
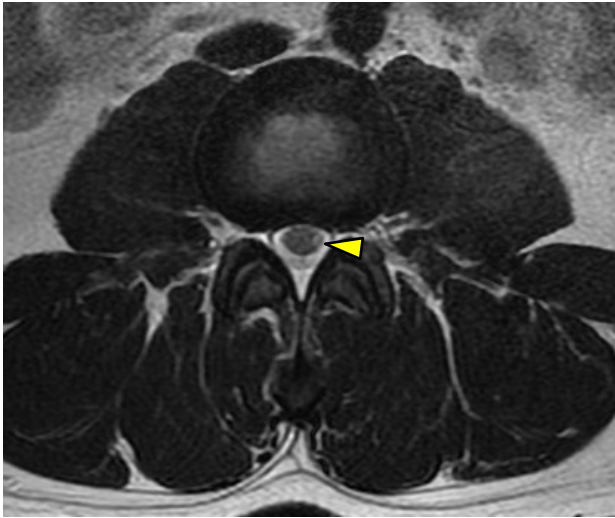
Figure 25:11. T2 weighted sagittal image of a patient with arachnoiditis.

Figure 25:12. A duplication of of 25:11. The yellow dotted line outlines the conus medullaris, the red circle encloses a section of the cauda equina that is adhered together into one large clump, and the green arrow points to an L5-S1 disc herniation with a concentric annular tear.

Figure 25:13. Normal. This T2 weighted sagittal image shows the normal appearance of the cauda equina on MR. The yellow arrows point to the wispy nerve rootlets of the cauda equina. Note they are separate and not clumped together.

This series of sagittal images compares the appearance of a patient with adhesive arachnoiditis (figures 25:11 and 25:12) and a normal lumbar spine (figure 25:13). Figures 25:11 and 25:12 show the clumped together presentation of the cauda equina. In comparison the nerve rootlets of the cauda equina in figure 25:13 are wispy and separate.

Arachnoiditis



Figures 25:14-17. Adhesive arachnoiditis. This series of axial T2 weighted images shows the characteristic adhesive clumping of nerve rootlets of the cauda equina.

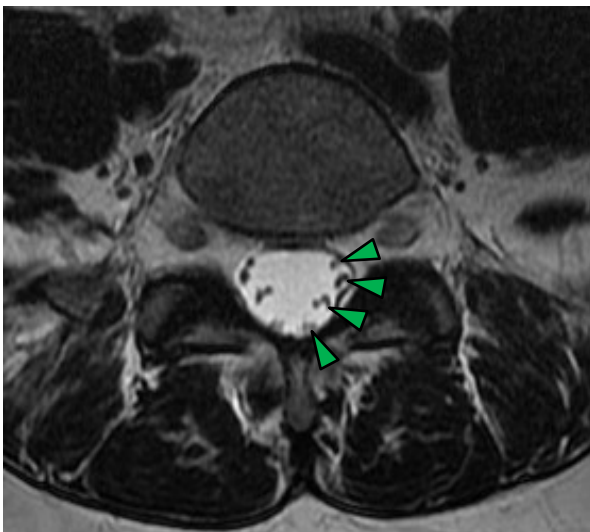


Figure 25:18. Normal. For reference and comparison, this T2W axial displays the normal dispersed nerve rootlets of the cauda equina (green arrows).

Spinal Arachnoid Cysts

Arachnoid cysts are uncommon findings in the spine. They are usually asymptomatic and discovered incidentally. Arachnoid cysts are filled with cerebral spinal fluid contained within arachnoid tissue. Though usually asymptomatic, arachnoid cysts can be clinically significant and cause harm, including neurological compromise (paresis, numbness, bowel /bladder dysfunction, etc.). They are normally congenital, but can be a result of trauma or surgery. The use of gadolinium is helpful to differentiate arachnoid cysts from tumors.

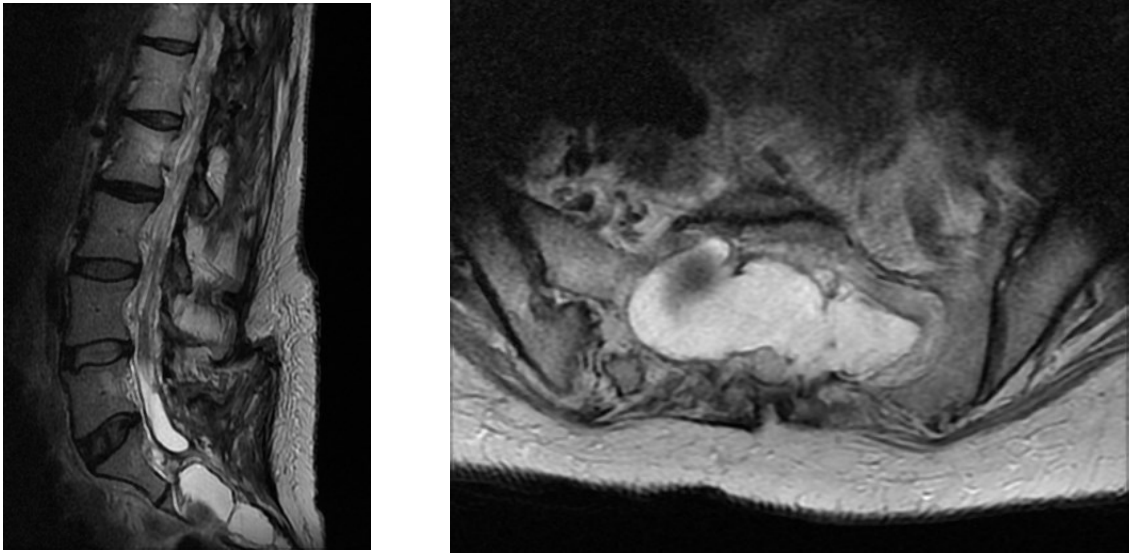


Figure 25:19 and 25:20. These T2 weighted images show a hyperintense expansive lesion in the lower lumbar spine and in the sacrum.

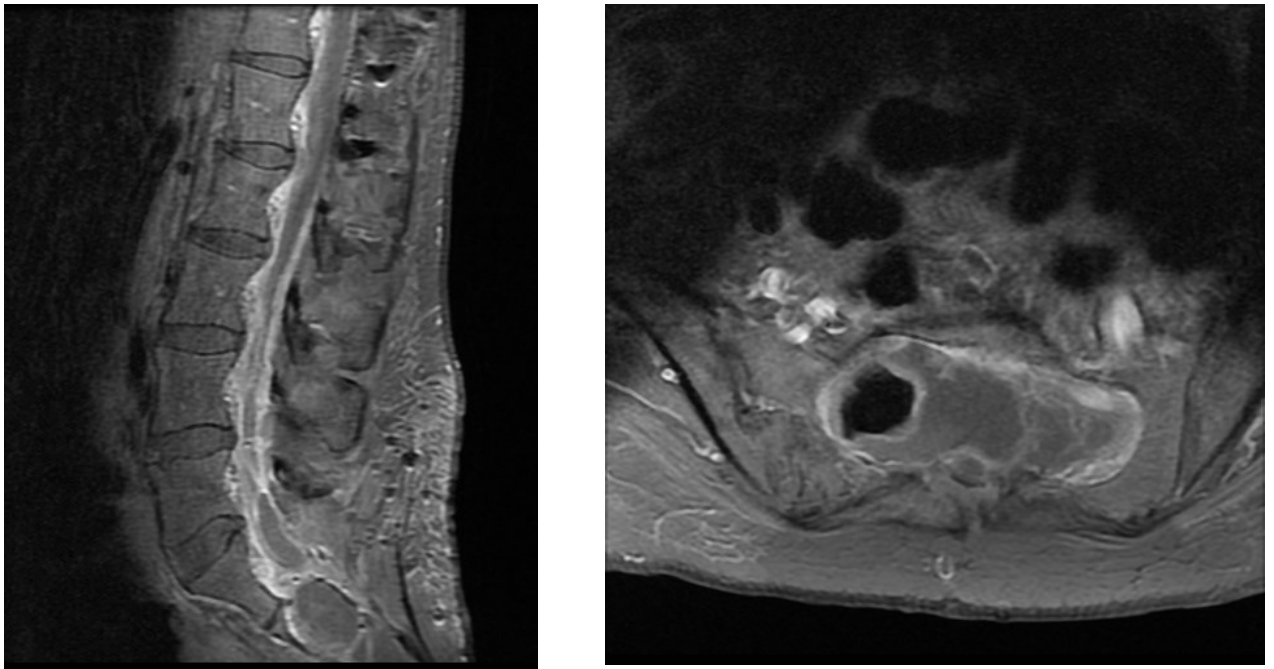


Figure 25:21 and 25:22. In these T1 fat sat images with gadolinium, the lesion did not enhance. This ensured that it was not a vascular lesion like a tumor.

Suggested Reading

Aldrete JA. Clinical Diagnosis. In: Arachnoiditis: the silent epidemic, JA Aldrete (ed.) Futuremed. Denver. 2000. pp 201-220.

Ribeiro C, Reis FC. Adhesive lumbar arachnoiditis. Acta Med Port. 1998 Jan;11(1):59-65.

Delamarter RB, Ross JS, Masaryk TJ, Modic MT, Bohlman HH. Diagnosis of lumbar arachnoiditis by magnetic resonance imaging. Spine (Phila Pa 1976). 1990 Apr;15(4):304-10.

Struffert T, Brill G, Reith W. Lumbar arachnoiditis as differential chronic spinal symptoms diagnosis]. Radiology. 2001 Nov;41(11):987-92.

Etchepare F, Roche B, Rozenberg S, Dion E, Bourgeois P, Fautrel B. Post-lumbar puncture arachnoiditis. The need for directed questioning. Joint Bone Spine. 2005 Mar;72(2):180-2.

DA Nelson, WM Landau. Intraspinal steroids: history, efficacy, accidentally, and controversy with review of United States Food & Drug Administration Reports. Neurosurgery/Psychiatry Review,2001

Moreira, Navarro et.al. Clinical and histological effects of the intrathecal administration of MPA (Depo-Medrol) in dogs-animal trial. 2010 Pain Physician.

Wu JS, Hochman MG. Soft-tissue tumors and tumorlike lesions: a systematic imaging approach. November 2009 Radiology, 253, 297-316.

Lolge S, Chawla A, Shah J et-al. MRI of spinal intradural arachnoid cyst formation following tuberculous meningitis. Br J Radiol. 2004;77 (920): 681-4.

Hamamcioglu MK, Kilincer C, Hicdonmez T et-al. Giant cervicothoracic extradural arachnoid cyst: case report. Eur Spine J. 2006;15 Suppl 5 : 595-8.

Brant WE, Helms CA. Fundamentals of Diagnostic Radiology. Lippincott Williams & Wilkins. (2007).

Atlas SW. (2008). Magnetic resonance imaging of the brain and spine (forth edition). Lippincott Williams & Wilkins.

Ross JS et al. (2010). Diagnostic imaging spine (second edition). Amirsys Inc.

Bogduk N. (2012). Clinical and radiological anatomy of the lumbar spine. Churchill Livingstone.

Incidental Visceral Findings

26



Incidental Visceral Findings

Lumbar MRIs will reveal much more than just musculoskeletal and nerve findings. Incidental findings of all sorts will invariably present, from congenital anomalies and anatomical variants, to cysts and pathology. This chapter is a limited collection of some of the more common incidental findings that will be seen on lumbar MRI. Some of these findings may not even warrant mention in a radiologist's report. However, it is conceivable that some of these findings may be clinically significant, even if the radiologist chooses not to mention them.

While we do not want to identify every incidental finding as being clinically significant, we need to know what is common and asymptomatic and what is common and potentially clinically significant.

Enteric Cyst

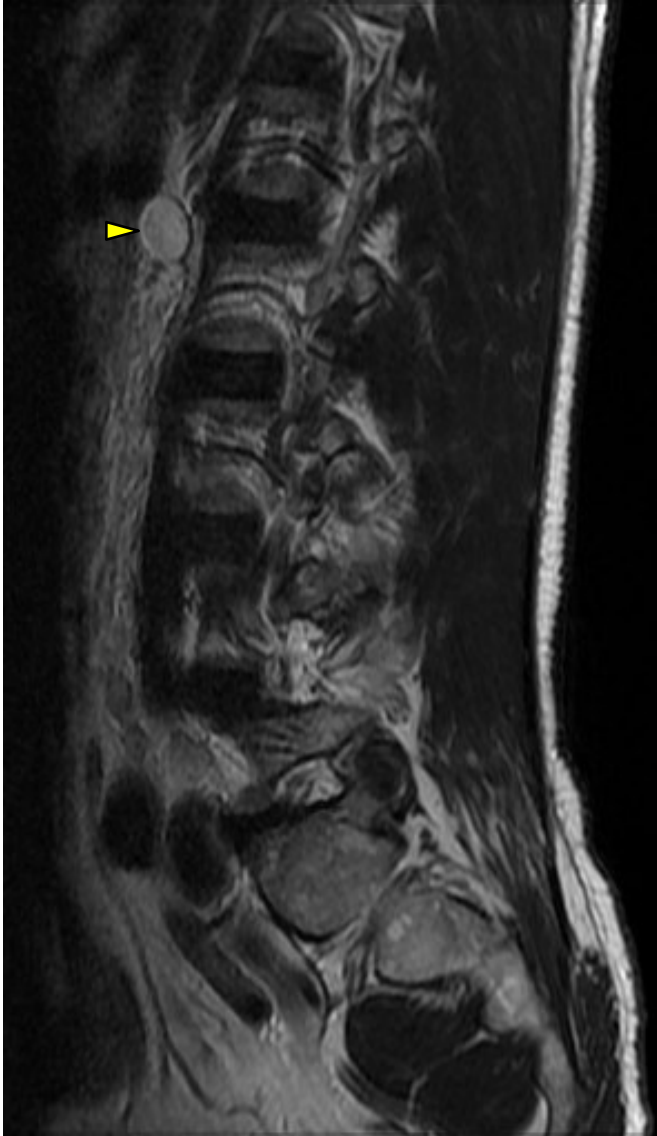


Figure 26:1. T2 weighted sagittal image of the lumbar spine shows a small benign enteric cyst.

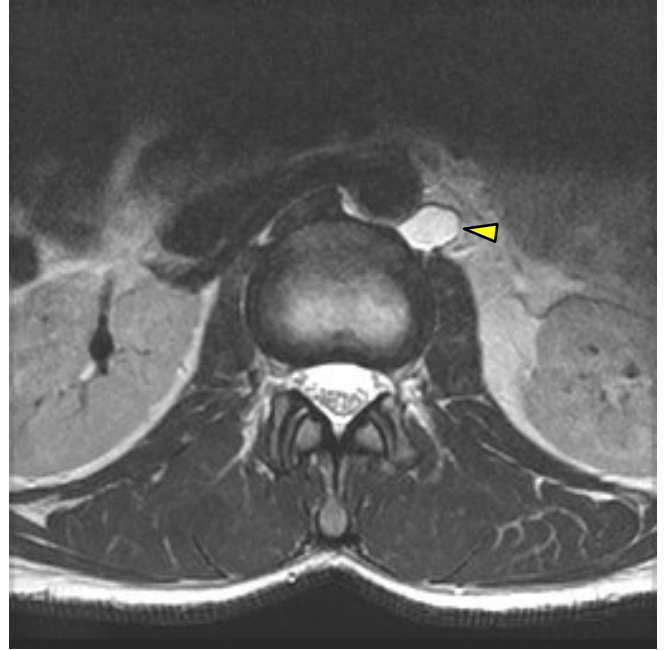


Figure 26:2. T2 weighted axial image of the lumbar spine shows a small benign enteric cyst. This finding is of limited concern save for the fact the cyst abuts the abdominal aorta.

Enteric cysts are usually benign. They are pockets of fluid created by an anomalous membranous sac and typically lined with epithelium.

Simple Renal Cyst

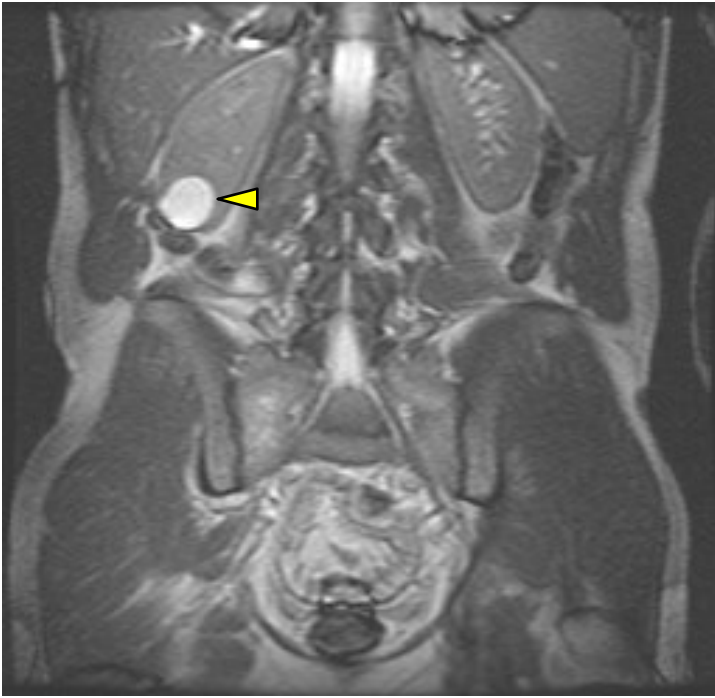


Figure 26:3. Simple renal cyst in the inferior right kidney is visible in this coronal view.

Simple renal cysts are fluid-filled cysts that may be caused by blocked renal ducts. This benign finding is present in more than 50% of those over the age of 50 and are increasingly common with age. Simple renal cysts display the characteristic water densities on MRI, hypointense in T1WI and hyperintense in T2WI. Simple cysts are considered a coincidental finding and normally do not require intervention.

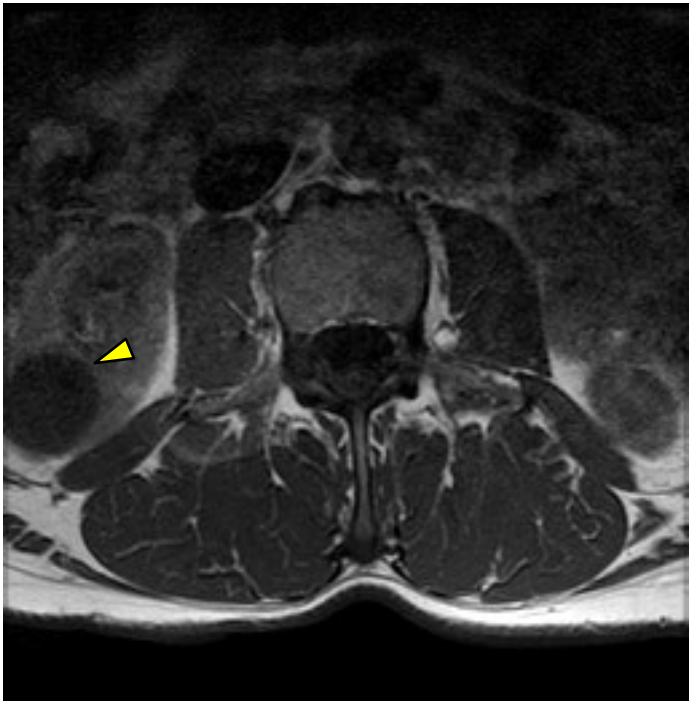


Figure 26:4. Simple renal cyst in the inferior right kidney is visible in this axial T1 image.

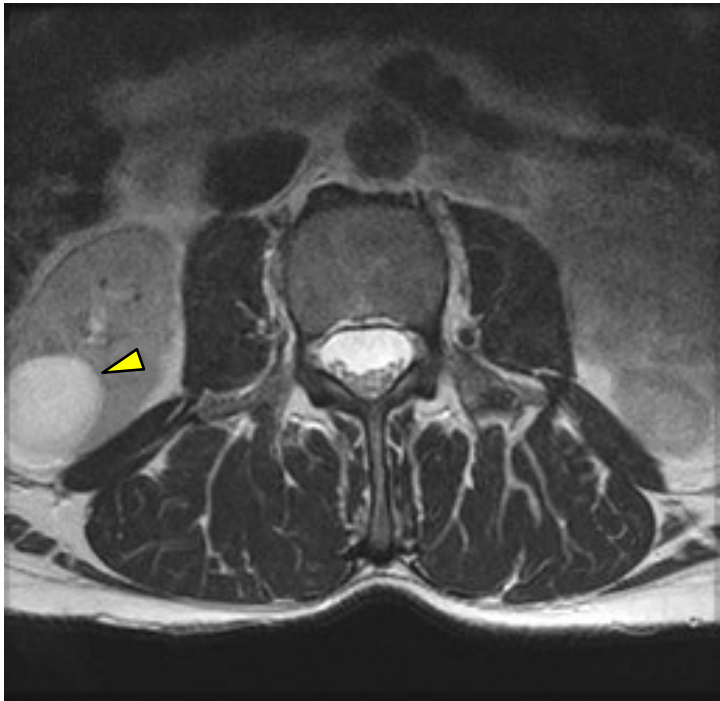


Figure 26:5. T2 weighted axial image of a large solitary simple renal cyst.

Multiple Renal Cysts



Figure 26:6. Coronal image of multiple large renal cysts.

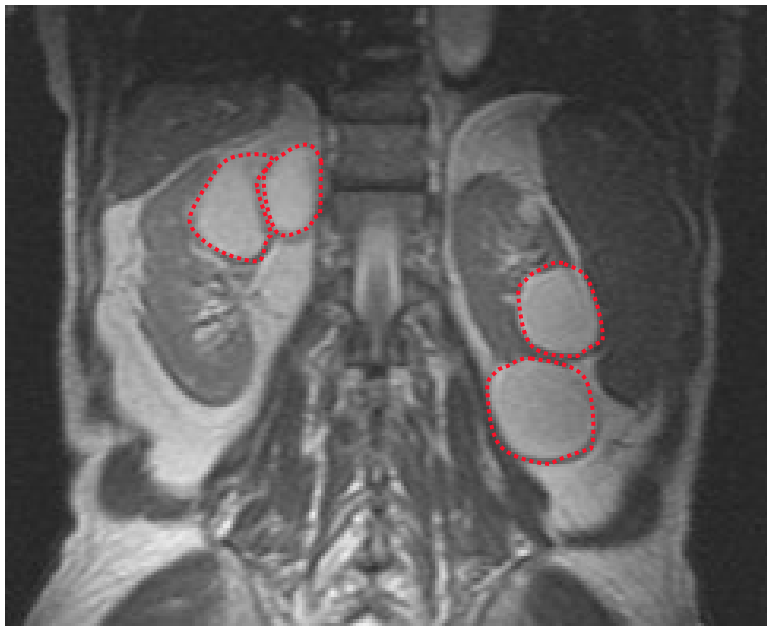


Figure 26:7. Cysts outlined with red dashed lines.

Huge Renal Cysts

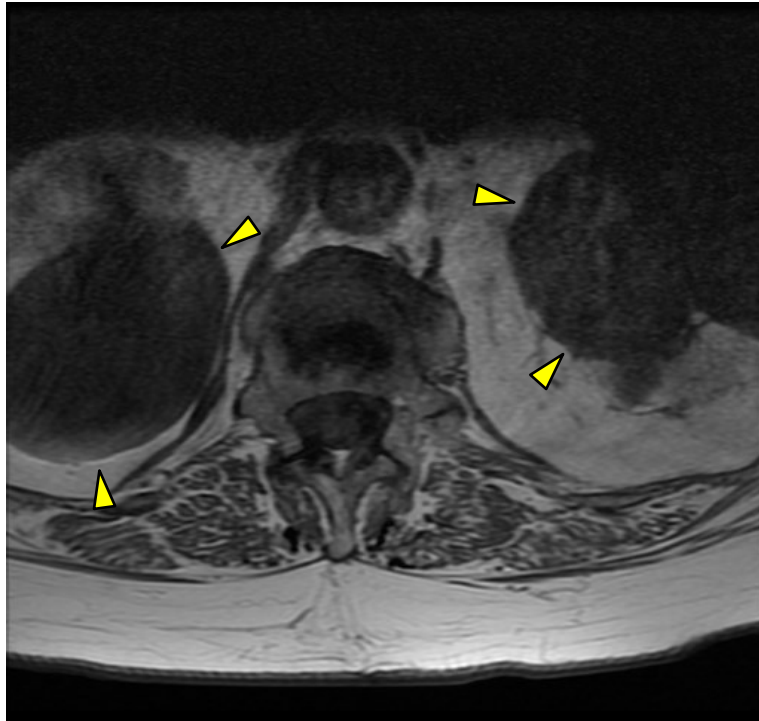


Figure 26:8. T1 weighted axial of large multiple renal cysts bilaterally. The fluid in the cysts appears dark in color.

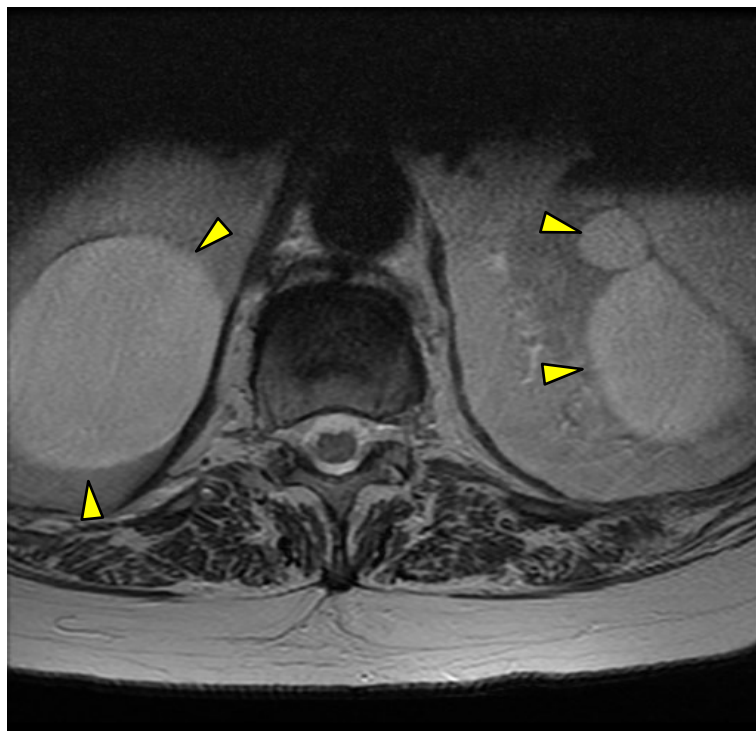


Figure 26:9. T2 weighted axial of large multiple renal cysts bilaterally. The fluid content is light in T2.

Hypertrophic Heterogeneous Uterus

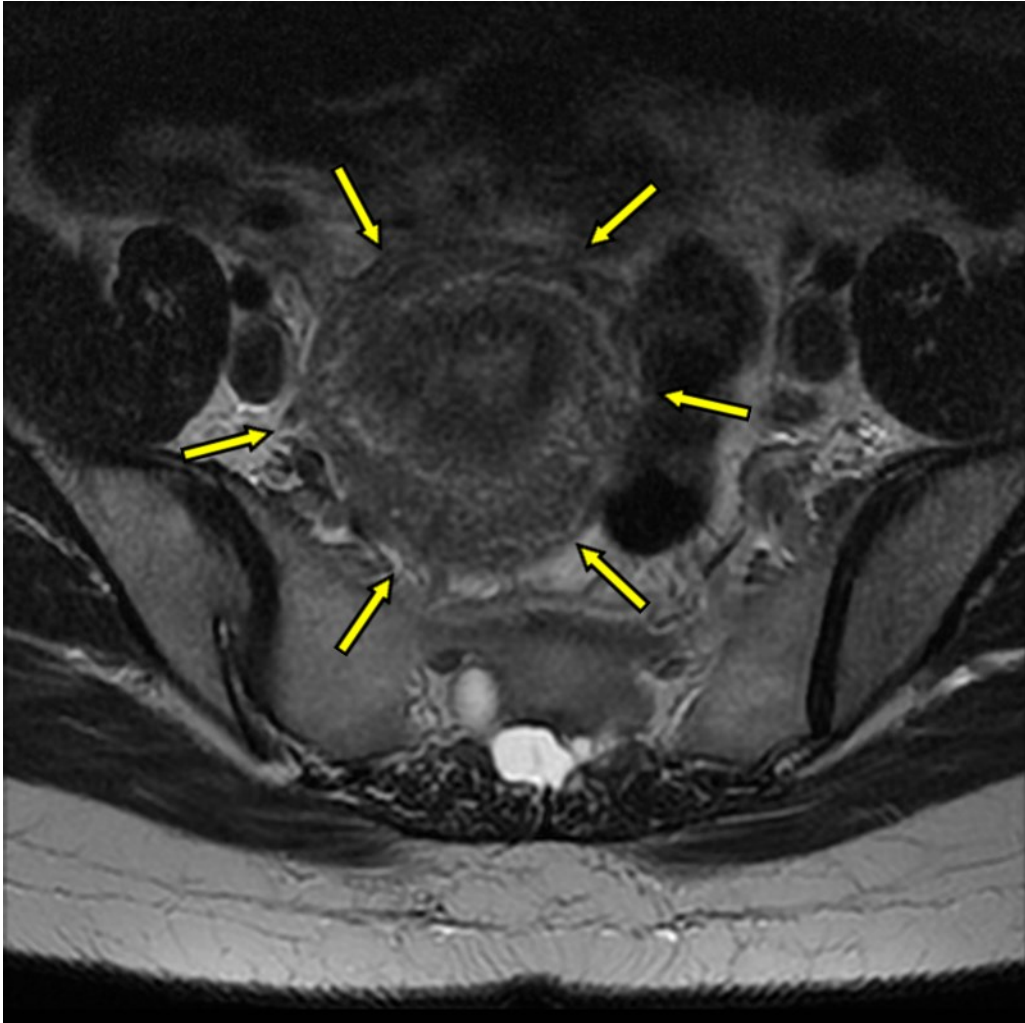


Figure 26:10. This image reveals an enlarged heterogeneous uterus which was a coincidental finding on this T2 weighted axial image from a lumbar spine MRI. This finding was not associated with any symptoms.

Hypertrophic Postpartum Uterus

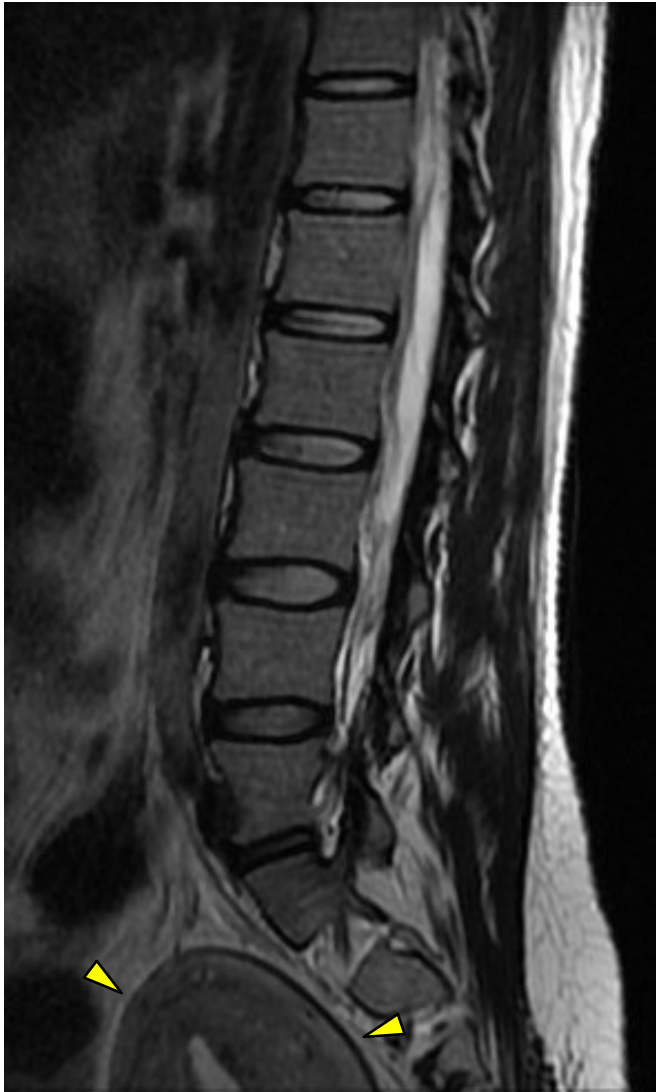


Figure 26:11. T2 weighted sagittal image of a patient with a postpartum hypertrophic uterus.

This series of images shows the coincidental finding of an enlarged (hypertrophic) uterus in a patient who had just delivered a child. This is a normal variant in postpartum women.

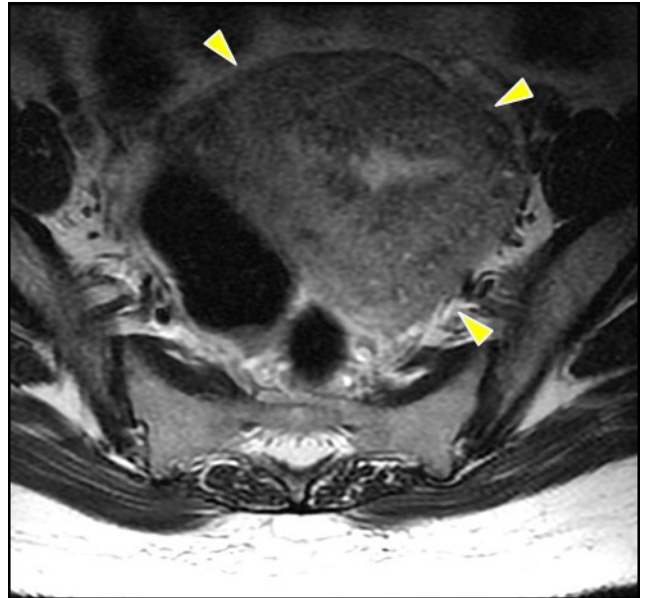


Figure 26:12. T2 weighted axial image of a patient with a postpartum hypertrophic uterus.

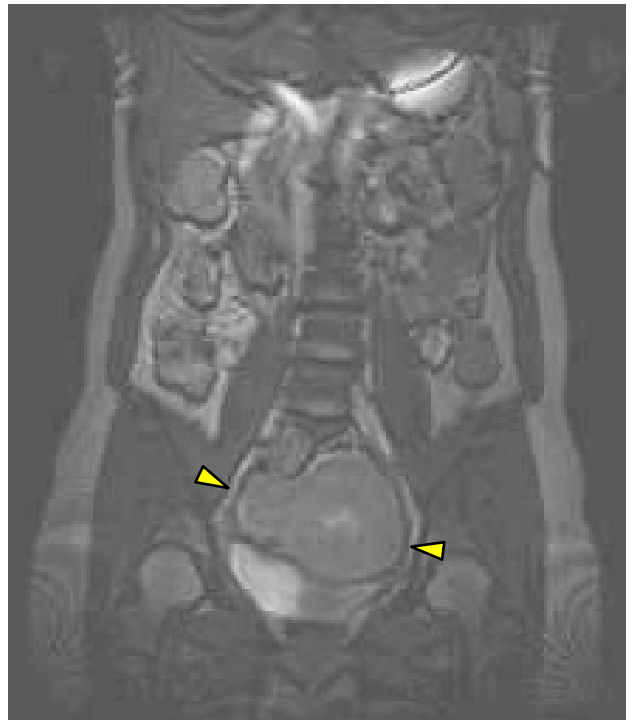


Figure 26:13. Coronal image of a patient with a postpartum hypertrophic uterus.

Large Adnexal Hemorrhagic Cyst

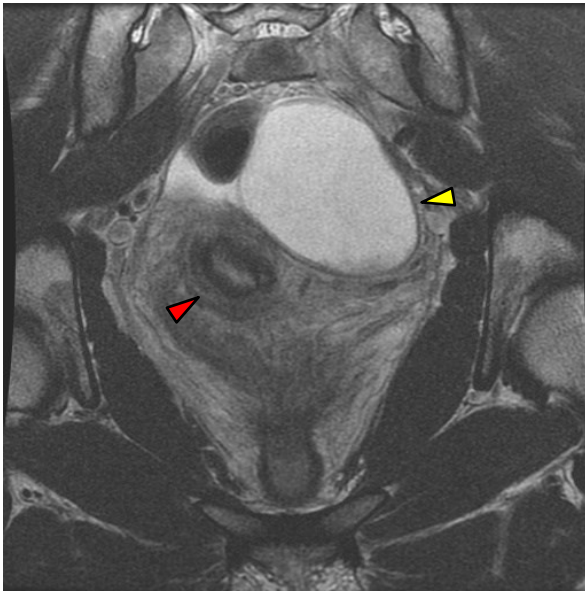


Figure 26:14. T2 weighted axial image of a 5.6 by 4.7 cm ovarian cyst (yellow arrow). Also a uterine fibroid is visible in the right uterine fundus (red arrow).

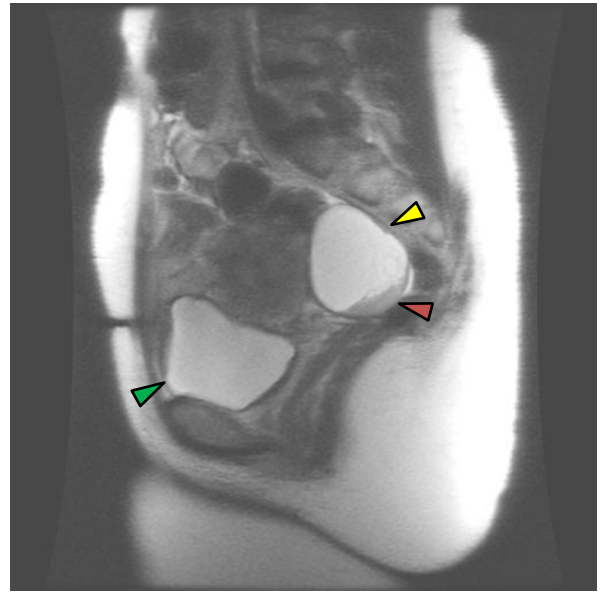


Figure 26:15. T2 weighted sagittal image. The green arrow points to the urinary bladder, the yellow to an ovarian cyst, and the red to the darker region of the cyst that contains blood components.

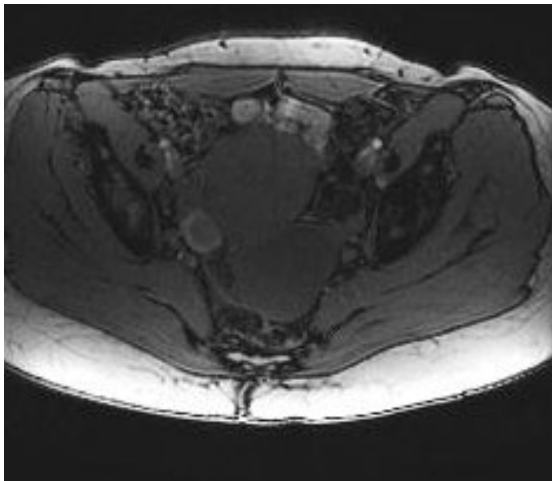


Figure 26:16. T1 weighted axial image.

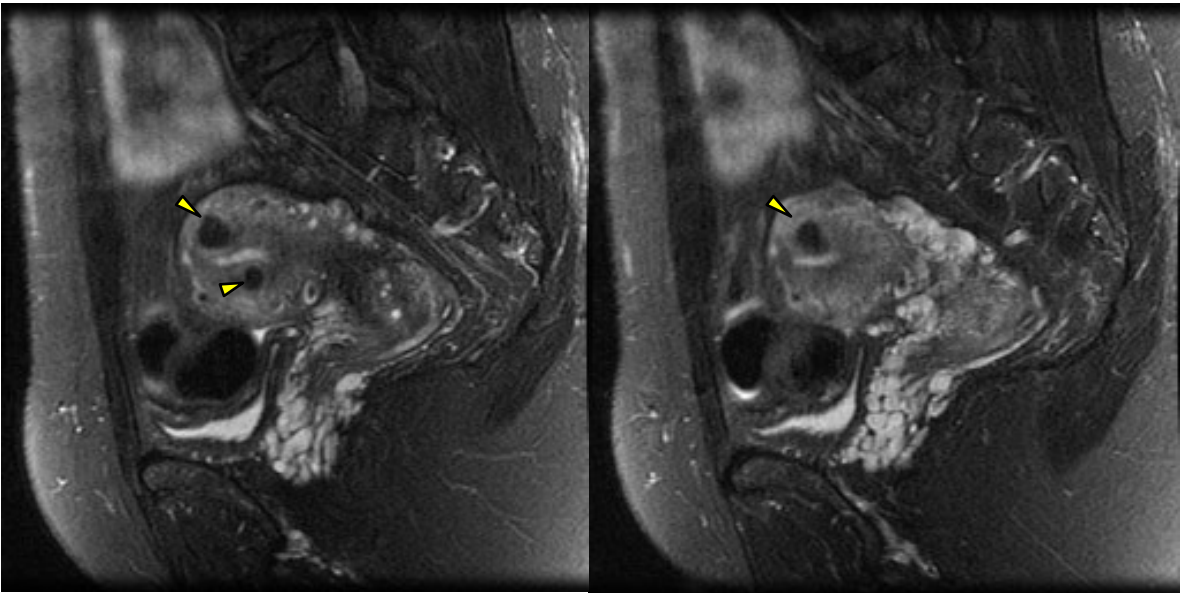


Figure 26:17. Coronal image revealing a left-sided adnexal cyst.

The adnexal region of the pelvis is the anatomy adjacent to a woman's uterus. The adnexal region is composed of the ovaries, fallopian tubes, supporting ligaments and tissues, bowel, and blood vessels. A large cyst can place pressure on the bladder or rectum causing secondary symptoms.

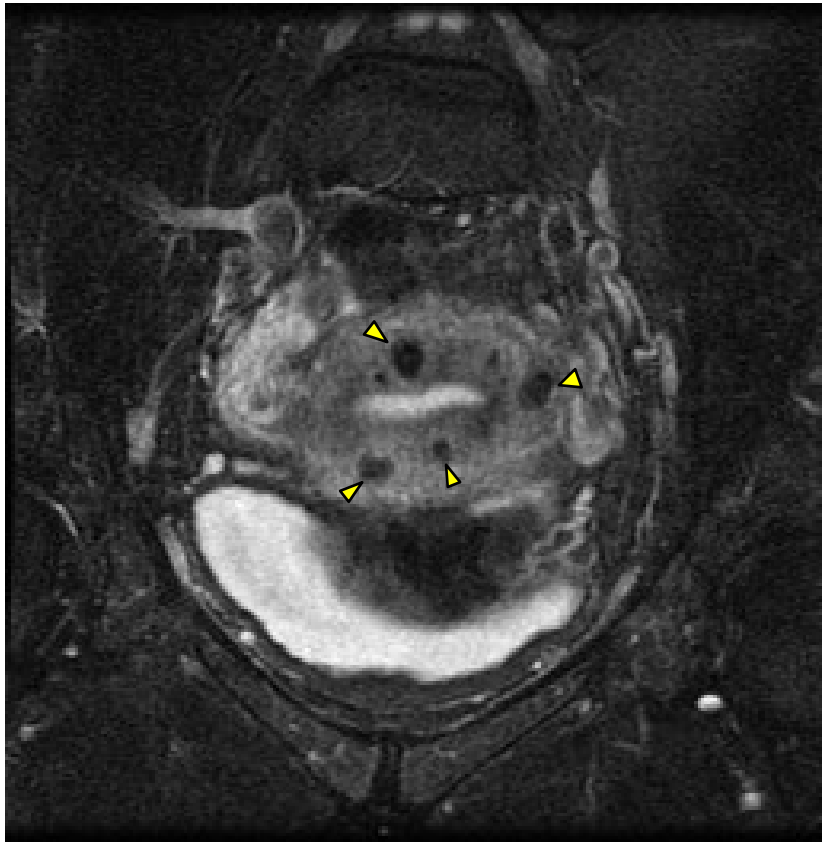
The term *adnexal cyst* is a fairly nondescript term that does not identify the exact structures involved, the size, or severity of the lesion. The adnexal cyst seen here is most likely an ovarian cyst.

Uterine Fibroids



Figures 26:18 and 26:19. Fat-suppressed T2 weighted sagittal image of a patient with multiple uterine fibroids (also known as leiomyomas or myomas).

Figure 26:20. Fat-suppressed T2 weighted axial image of a patient with multiple uterine fibroids.



Uterine Fibroids

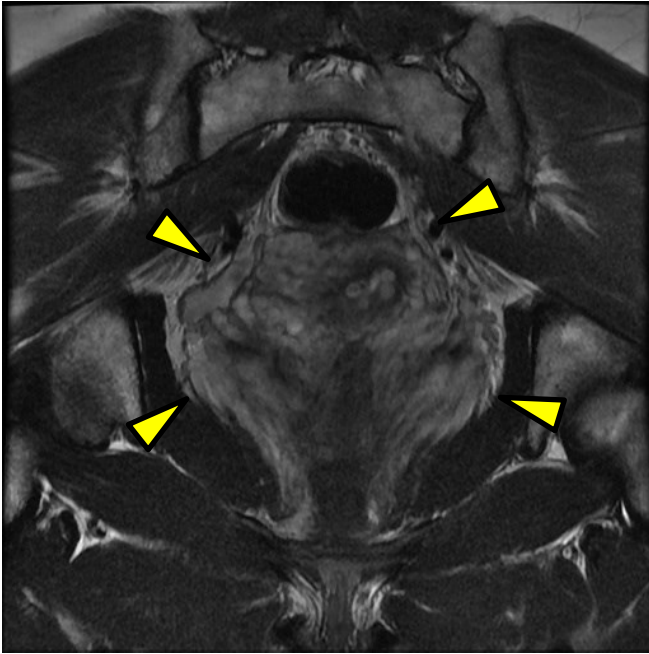


Figure 26:21. Enlarged uterus with diffuse multiple fibroids and fibrosis.

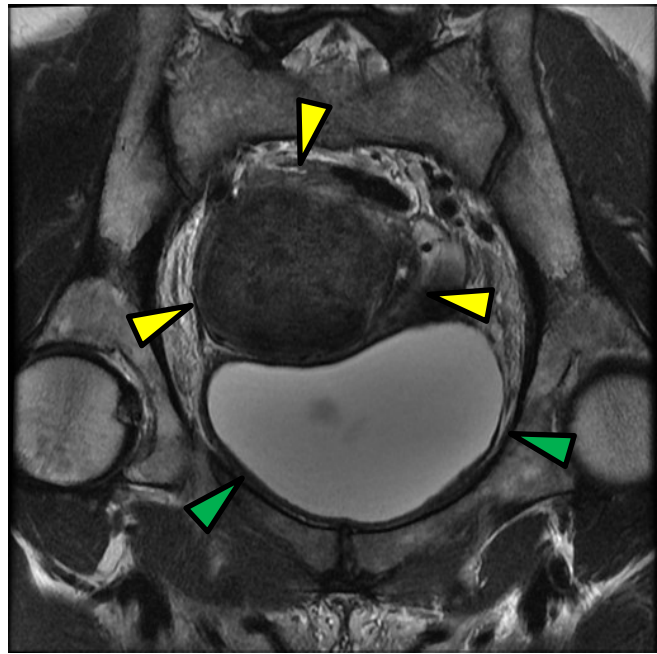
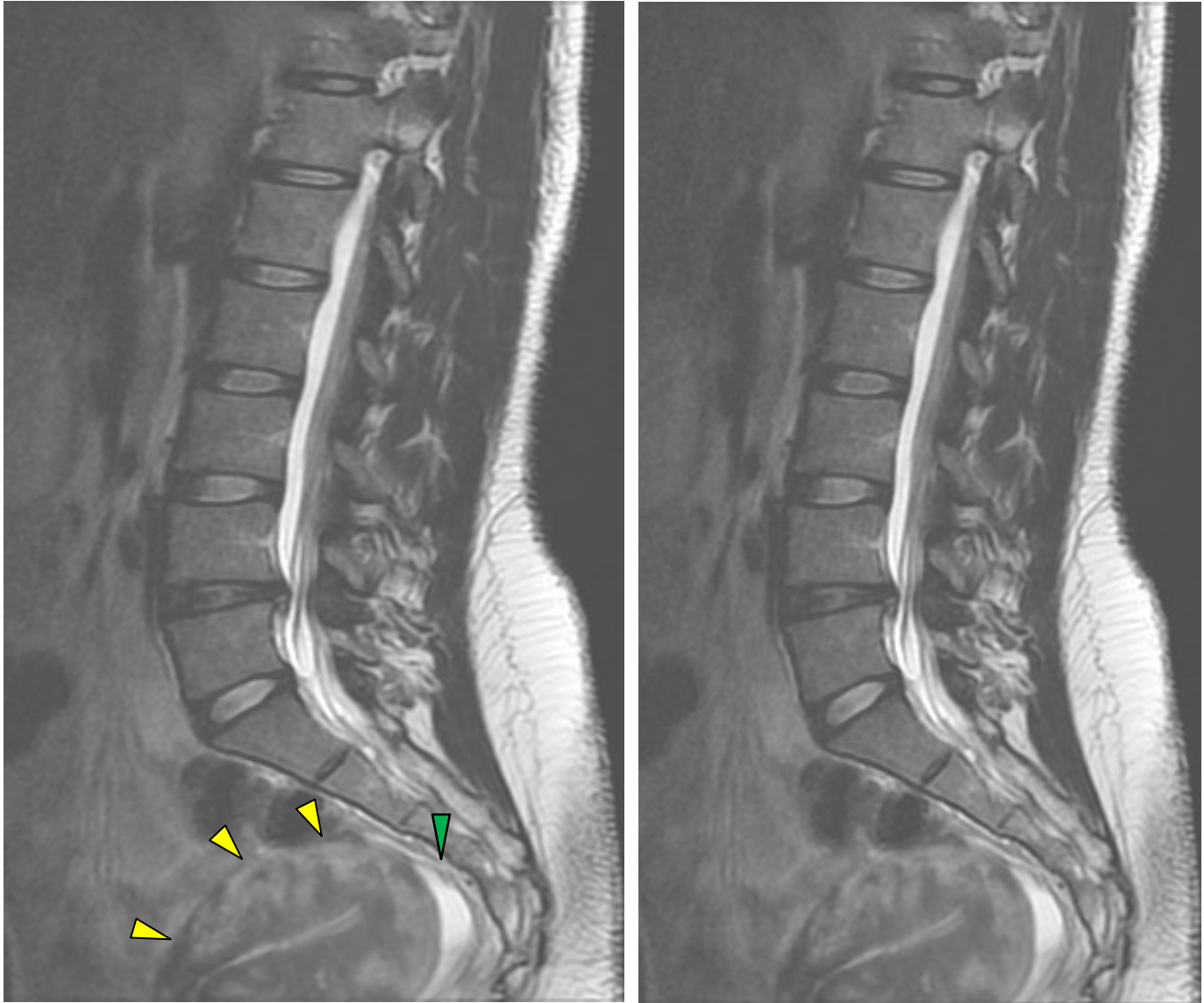


Figure 26:22. In addition to the diffuse fibrosis of the uterus and multiple fibroids, this patient had a large uterine fibroid (yellow arrows). The green arrows point to the urinary bladder.

Heterogeneous Uterus



Figures 26:23 and 26:24. In addition to the L4-L5 disc extrusion, this patient also has an enlarged heterogeneous uterus (yellow arrows) and fluid collection in the posterior cul-de-sac of the pelvis.

Hemorrhagic Ovarian Cyst



Figure 26:25. Coronal image revealing the bright color of a left-sided ovarian cyst.

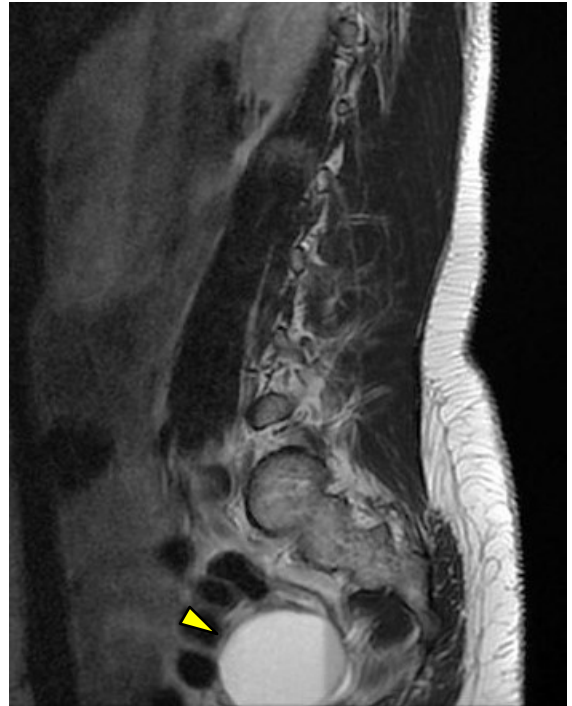


Figure 26:26. Sagittal T2 weighted image showing a large hemorrhagic ovarian cyst.

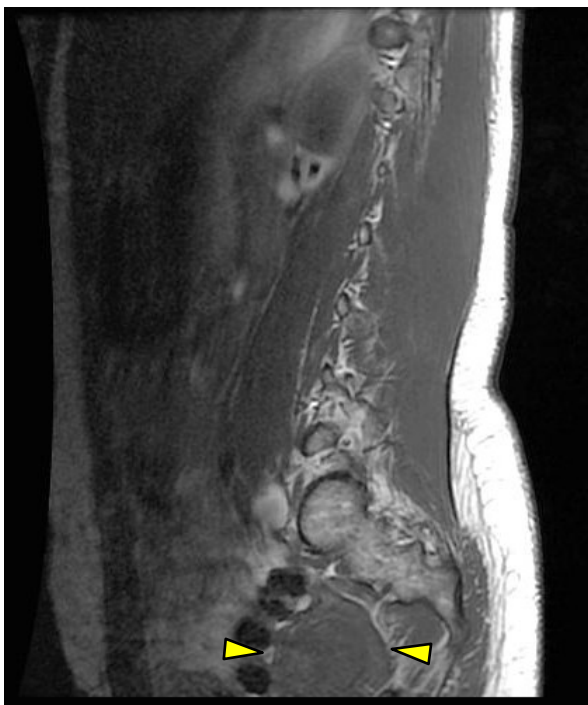


Figure 26:27. Sagittal T1 weighted image.

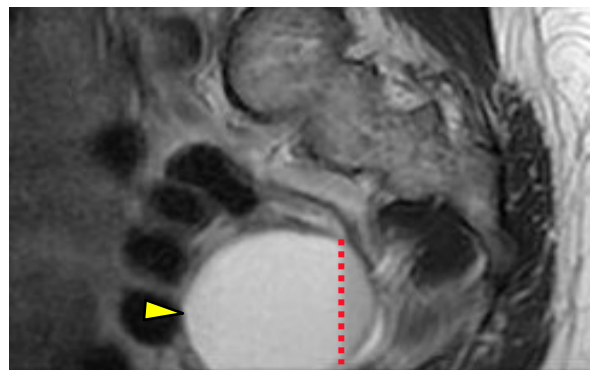


Figure 26:28. Sagittal T2 weighted image of the hemorrhagic ovarian cyst seen in figure 26:26 With red dotted line denoting the fluid line.

A hemorrhagic cyst occurs when a benign fluid-filled cyst fills with blood following the rupture of a small blood vessel in the ovary. Note the fluid line in figure 26:28. This denotes a separation of the types of fluids in the cyst: cystic fluid versus blood. The line is vertical because the patient is lying on her back for the MRI.

Ovarian Cysts



Figure 26:29. Coronal image of fluid in the posterior cul-de-sac of the pelvis.

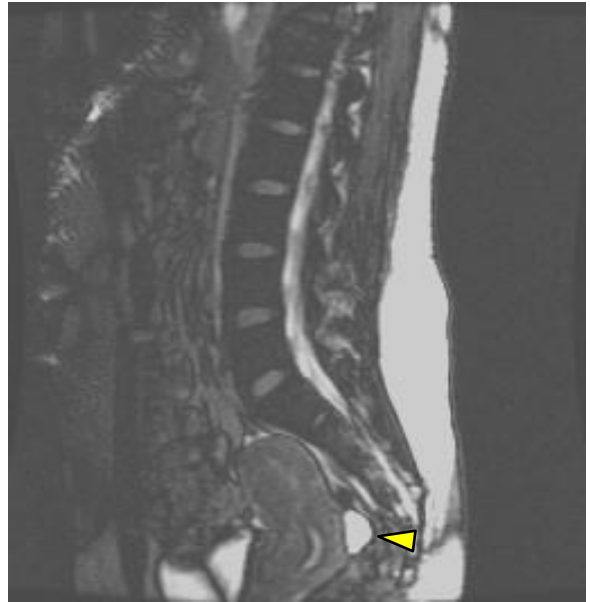


Figure 26:30. T2 weighted sagittal image reveals free fluid in the posterior cul-de-sac of the pelvis indicated by the yellow arrow.

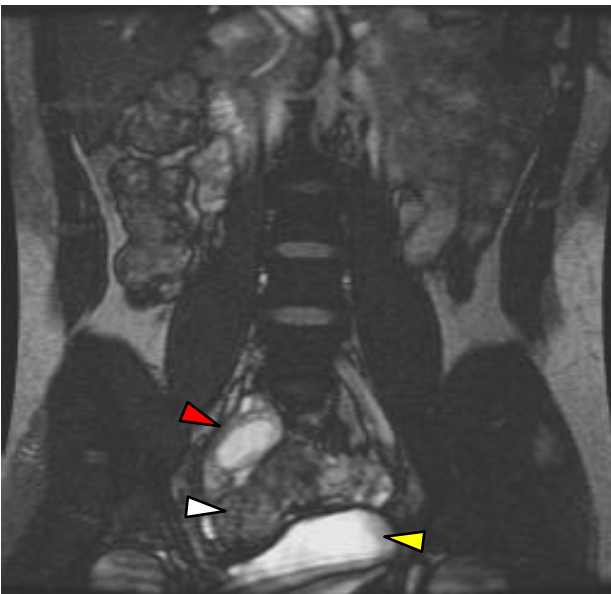


Figure 26:31. Coronal image of a right ovarian follicle (red arrow). Note the heavily laden colon (white arrow) lying upon and effacing the urinary bladder (yellow arrow).

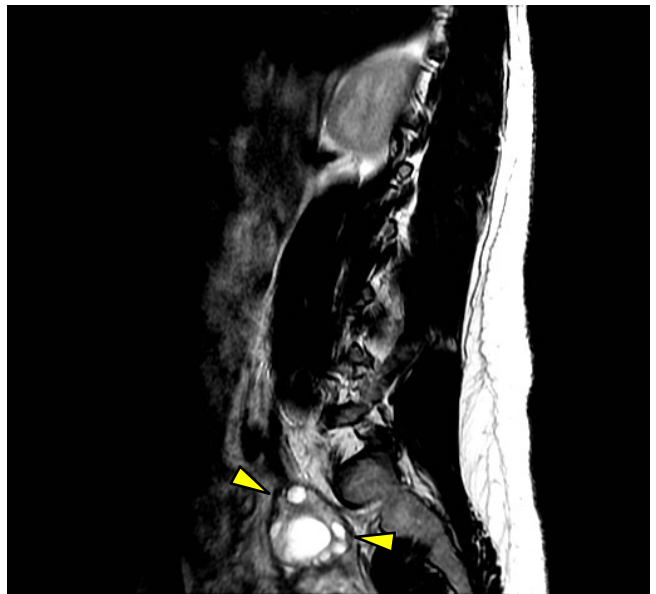


Figure 26:32. T2 weighted sagittal image revealing an ovary with multiple follicles, also referred to as a polycystic ovary.

Incidental findings of fluid-filled ovarian cysts and fluid in the pelvis may not be particularly uncommon findings in young women. Sometimes cysts and bowel contents are large enough to place pressure on the bladder and cause a sense of urinary urgency.

Polycystic Ovaries



Figures 26:33 and 26:34. Polycystic ovaries found on T2 weighted sagittal images. Note the “string of pearls” finding on the image on the right. The string of pearls appearance of follicles (cysts) is characteristic of polycystic ovarian syndrome.

What is Polycystic Ovarian Syndrome?

Polycystic Ovarian Syndrome gets its name from the characteristic enlarged ovaries with multiple small cysts around the outer edge of the ovary (or ovaries). The exact cause of PCOS is not known; in fact, I question whether the polycystic portion of the disease is a result of a more insidious underlying condition that results in ovarian disease and not the other way around.

PCOS results in the ovaries producing too much androgen (hormones associated with male characteristics). The symptoms commonly attributed to PCOS include obesity (though about 50% of the patients with PCOS are not obese), excessive facial and body hair, increased muscle size, reduced breast size, acne, and amenorrhea. Other effects include fertility issues, insulin resistance, type 2 diabetes, hypercholesterolemia, infrequent ovulation, and heart disease. Patients with PCOS are also at greater risk for hypertension, sleep apnea, and fatty liver disease. PCOS affects 5-10% of women in their childbearing years.

Diagnosis

The diagnosis of PCOS is difficult and probably should involve an interdisciplinary team. PCOS may be diagnosed by the presence of excessive androgen activity, infrequent ovulation, sporadic or absent menstrual cycles, and polycystic ovaries. Excessive androgen activity can be accessed clinically and in the lab through testing levels of androstenedione and testosterone. The ovaries can be visualized radiographically by diagnostic ultrasound and MRI.

Gallbladder

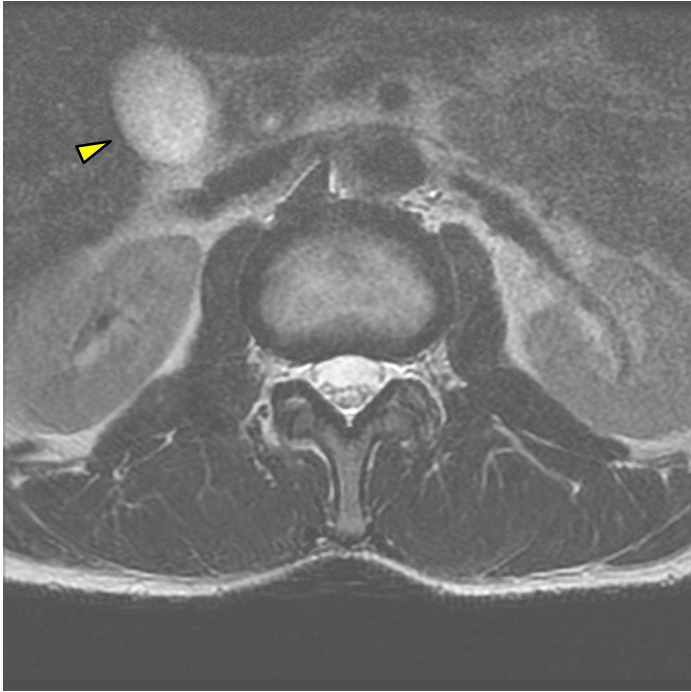


Figure 26:35. Normal gallbladder. T2 weighted axial image of a normal gallbladder.

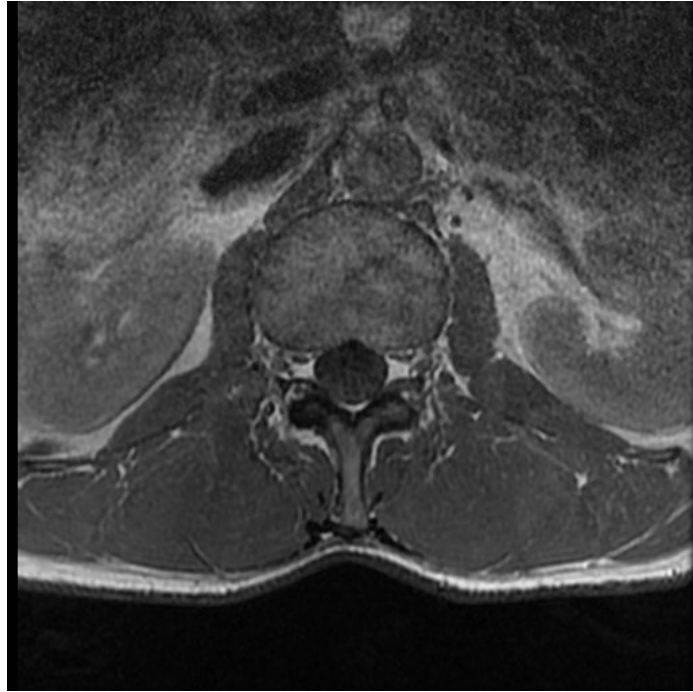
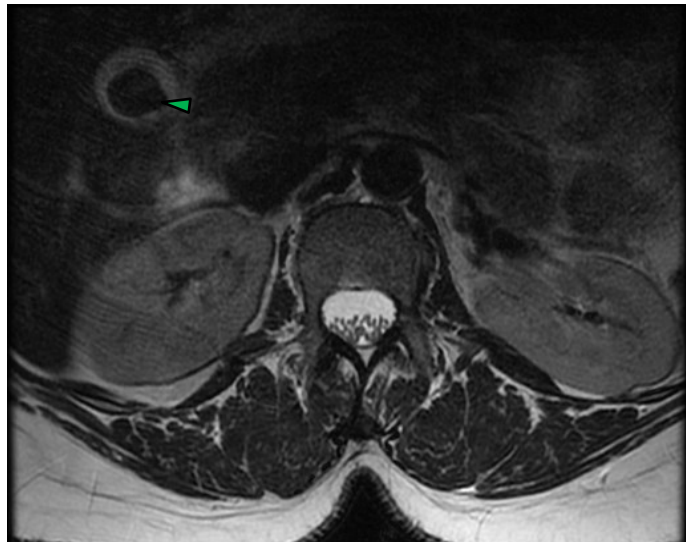


Figure 26:36. T1 weighted image of the same anatomy as 26:35, depicting a normal gallbladder.

The gallbladder is a small pear-shaped bladder that is nestled under the liver. It has a cyst-like appearance in T2 weighted images, but may be hard to distinguish from the liver in T1 weighted imagery.



Figures 26:37 and 26:38. Gallstone (cholelithiasis). T2 weighted axial images of a gallstone. The yellow arrow points to the light-colored fluid within the gallbladder. The green arrow points to the dark-colored gallstone.

Hypoplastic Kidney

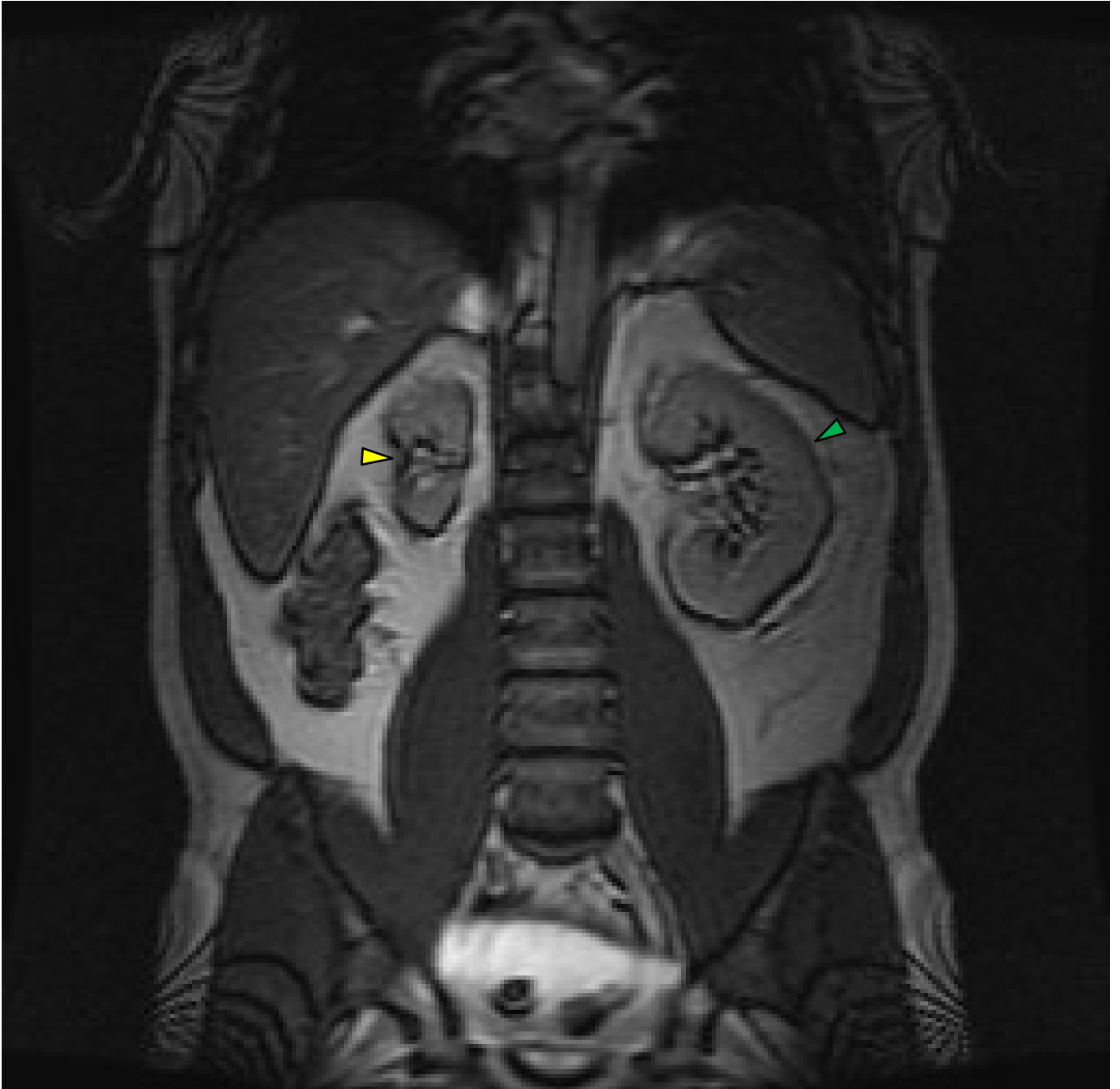


Figure 26:39. Hypoplastic right kidney (yellow arrow) identified as a coincidental finding on a lumbar MRI. The normal-sized left kidney is identified by the green arrow.

Polycystic Liver and Kidney Disease



Figure 26:40. Coronal image of polycystic liver disease with renal involvement. This patient had dozens of renal and liver cysts.

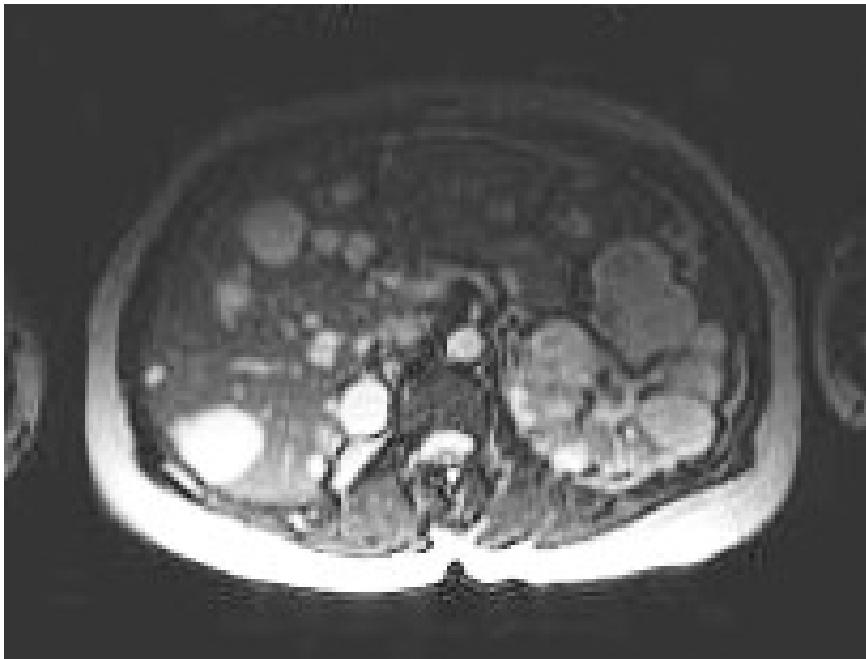


Figure 26:41. Axial image of polycystic liver disease with renal involvement.

Polycystic Liver and Kidney Disease

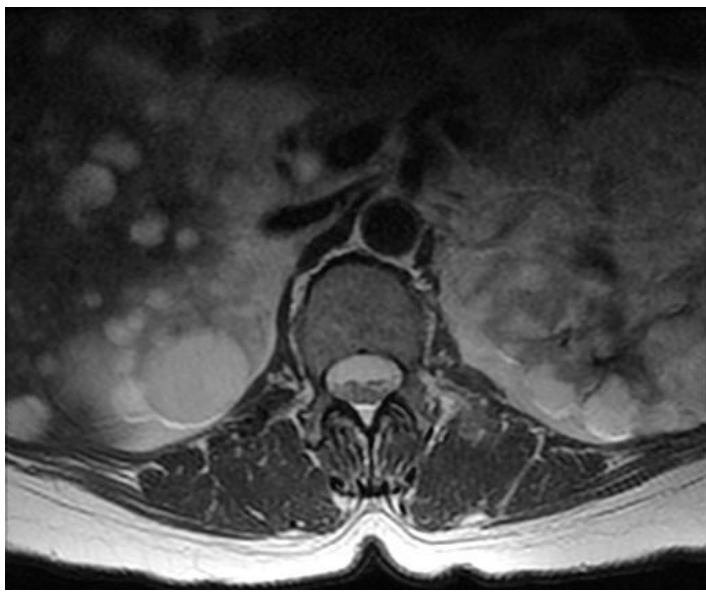


Figure 26:42. Numerous cysts of the kidneys and liver in a T2 axial image.



Figure 26:43. Multiple benign cysts of the kidneys and liver in a coronal image.

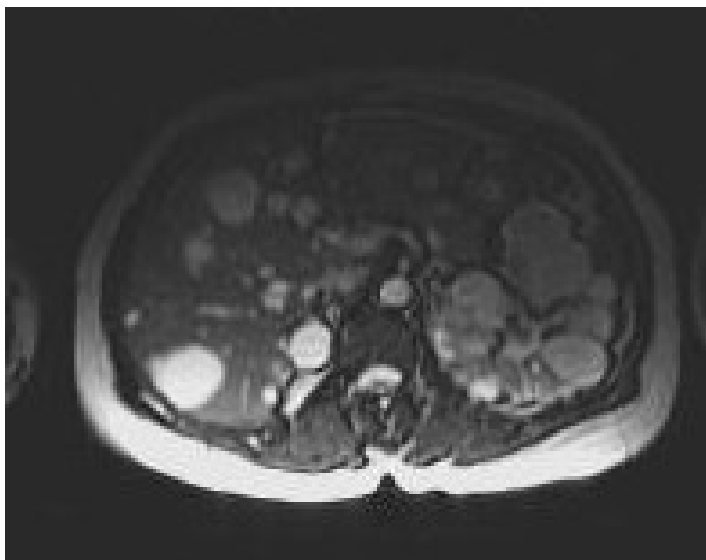


Figure 26:44. Multiple benign cysts of the kidneys and liver in an axial image.

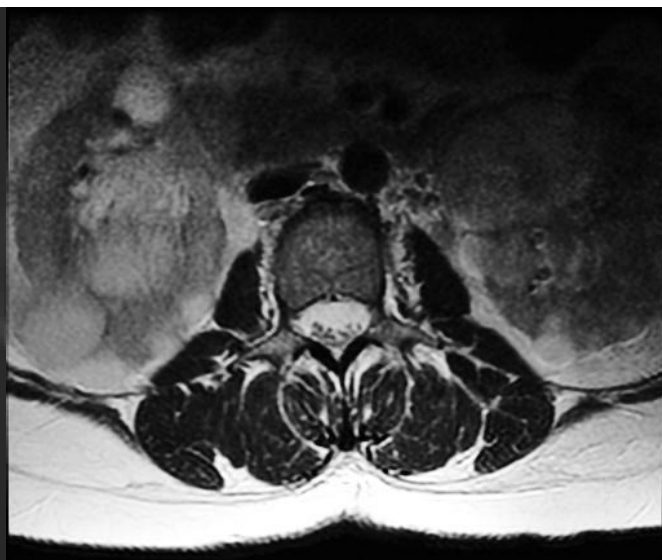
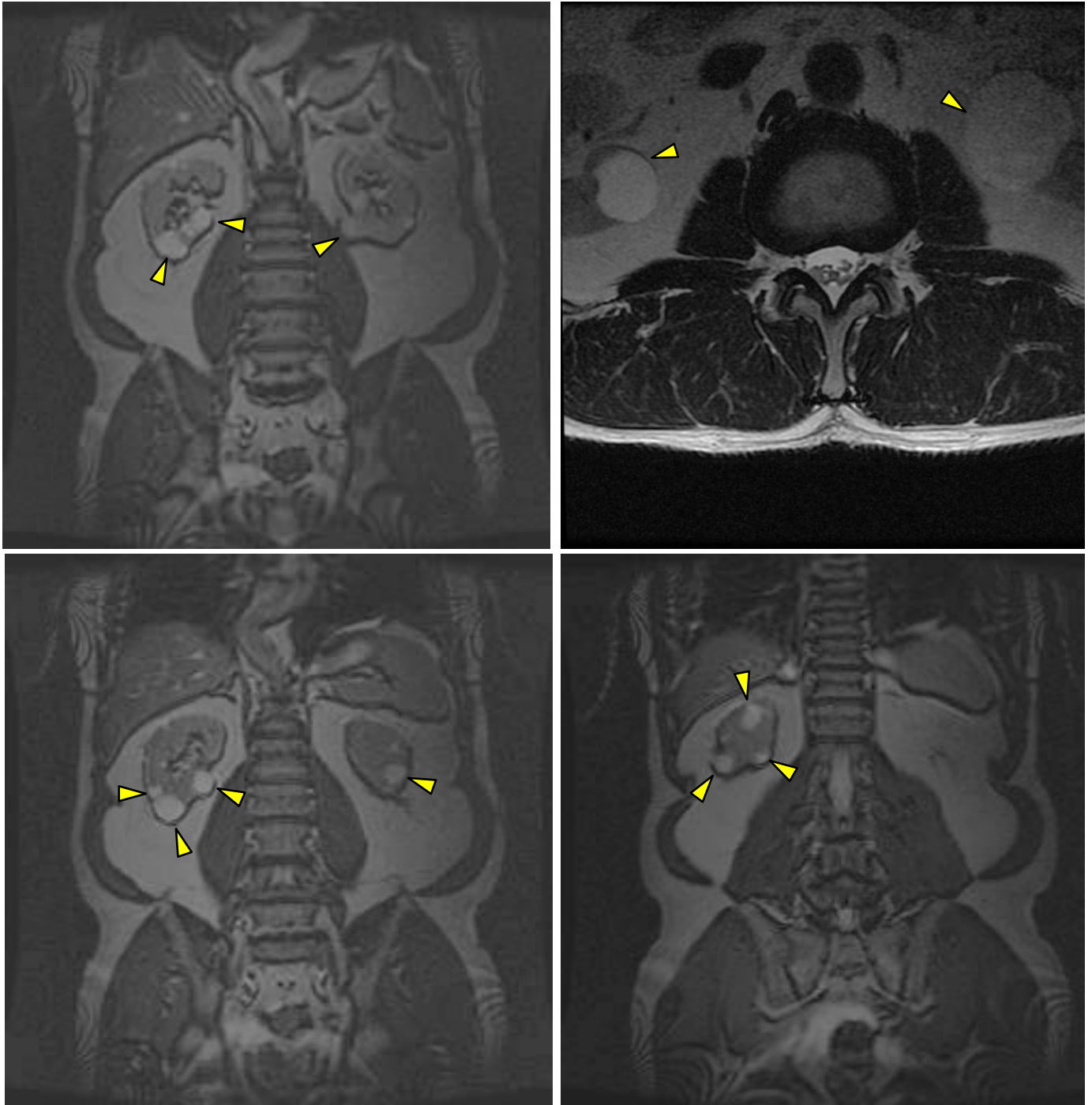


Figure 26:45. Renal cysts visible in an axial T2 weighted image.

Benign Cysts in Kidneys



Figures 26:46-49. Multiple benign cysts of the kidneys.

Kidney Transplant



Figure 26:50. Transplanted kidney anterior to L5 and the sacrum in this T2W sagittal.

The dysfunctional or diseased kidneys are not replaced when a transplant occurs. The surgeon will leave the dysfunctional kidneys in place and just insert the new kidney in the abdomen near the bladder and new sources of blood supply.

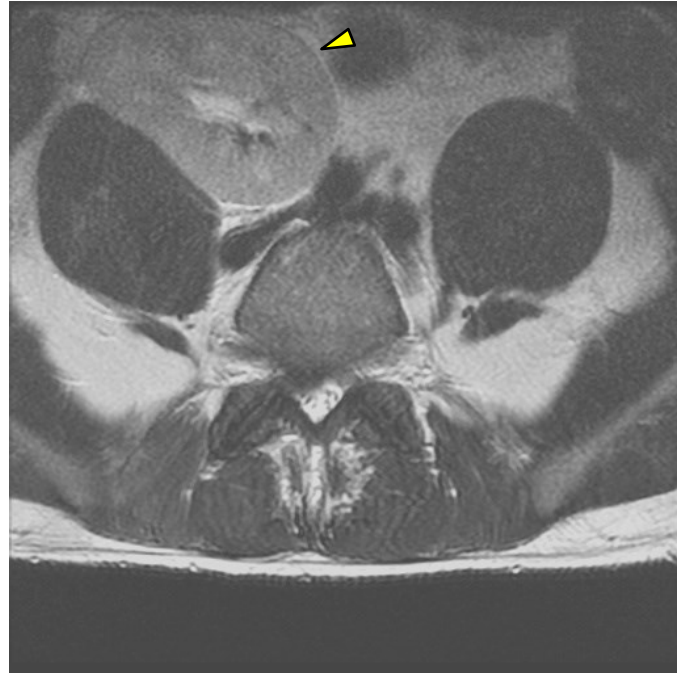


Figure 26:51. Transplanted kidney anterior to L5 and the sacrum in this T2W axial.



Figure 26:52. Transplanted kidney anterior to L5 and the sacrum in this T2W sagittal.

Suggested Reading

Wang JG, Anderson RA, Graham GM 3rd, Chu MC, Sauer MV, Guarnaccia MM, Lobo RA. The effect of cinnamon extract on insulin resistance parameters in polycystic ovary syndrome: a pilot study. *Fertility Sterility*. 2007 Jul;88(1):240-3.

Hoeger, KM. Obesity and Lifestyle Management in Polycystic Ovary Syndrome. *Clinical Obstetrics and Gynecology*. 2007; 50: 277-294.

Johns Hopkins News Release:

http://www.hopkinsmedicine.org/news/media/releases/physicians_have_less_respect_for_obese_patients_study_suggests

Wilde S, Scott-Barrett S. Radiological appearances of uterine fibroids. *Indian J Radiol Imaging*. 2009 August; 19(3): 222–231.

Tahvanainen E, Tahvanainen P, Kääriäinen H, Höckerstedt K. Polycystic liver and kidney diseases. *Ann Med*. 2005;37(8):546-55.

Wu JS, Hochman MG. Soft-tissue tumors and tumorlike lesions: a systematic imaging approach. November 2009 *Radiology*, 253, 297-316.

Other Assorted Findings on MRI

27



Asymmetrical Iliopsoas Muscles

Not all radiographic findings that fit neatly into categories can make up an entire chapter. This chapter will cover several small categories of MRI presentations. The theme of each presentation will change from page to page. This page will focus on the asymmetry of the iliopsoas muscles.

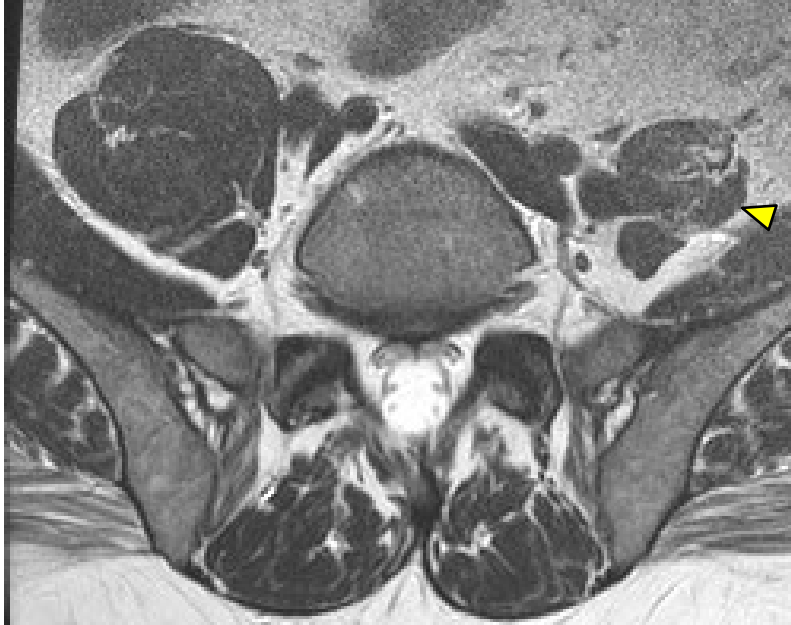


Figure 27:1. T2 axial image showing atrophy of the left iliopsoas muscle.



Figure 27:2. Another T2 axial image showing atrophy of the left iliopsoas muscle.

Baastrup's

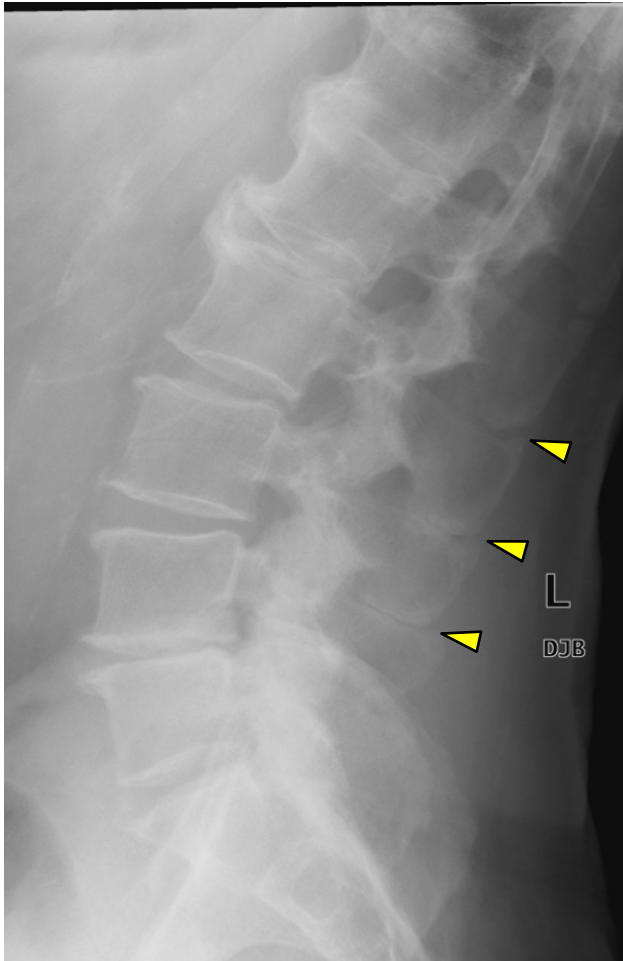


Figure 27:3. This plain film radiograph demonstrates the spinous processes abutting each other.

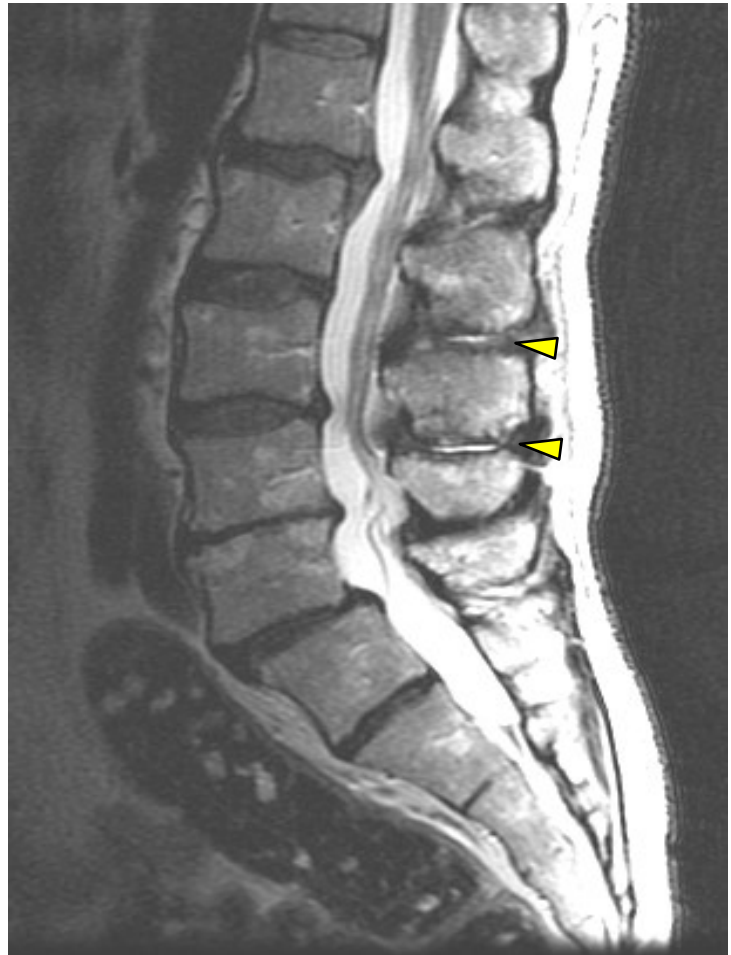


Figure 27:4. T2WI demonstrates effusion in the interspinous bursa as a hyperintense signal.

Baastrup's disease (the use of the word disease is a misnomer as it is a condition not a disease) is a condition known as kissing spinous disease. The spinous processes are enlarged to the point at which they cause approximation or contact between the spinous processes. The condition was named by Christian Baastrup, a Danish radiologist in 1933.

Anatomical, postural, and degeneration components may combine to contribute to this condition. Baastrup's may or may not be symptomatic.

The approximation of the spinous processes can be seen on plain film radiographs, but MRI will show edema within the interspinous bursa. Note the hyperintense signal of the interspinous bursa in this T2WI.



Figure 27:5. Normal. This MRI of a normal spine demonstrates the typical spacing between the spinous processes.

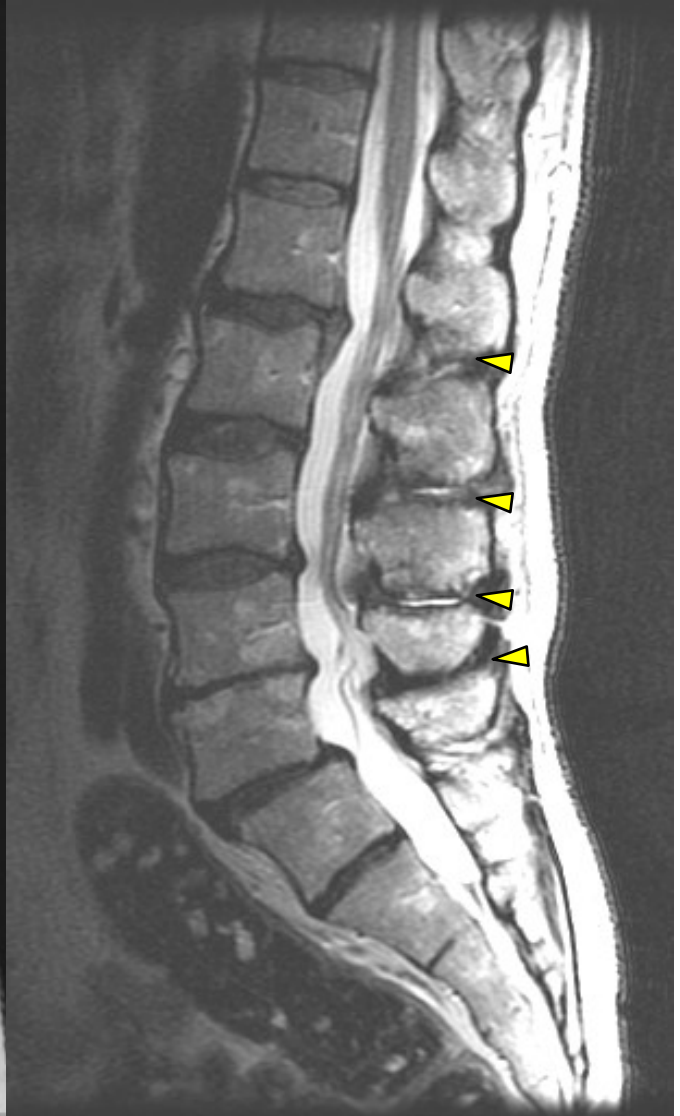
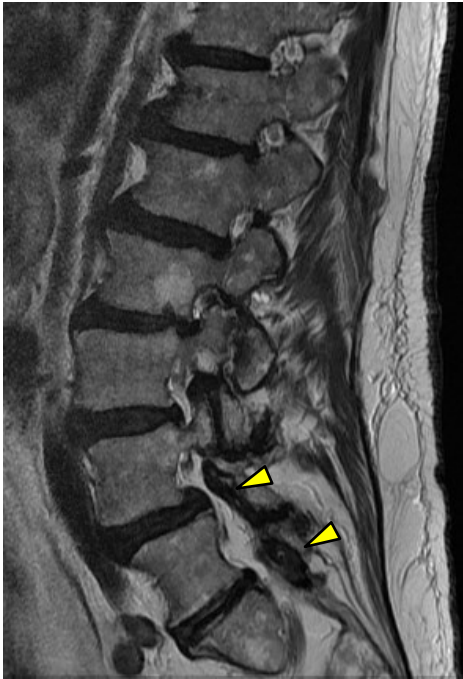


Figure 27:6. This MRI of a patient with Baastrup's is presented to show the difference of this condition next to a normal spine. In this patient, degenerative disc disease and a degenerative spondylolisthesis increase the interspinal compression characteristic of this condition.

Ligamentum Flavum Hypertrophy



Figures 27:7 and 27:8. T2 sagittal images showing hypertrophy of the ligamentum flavum in a degenerative lumbar spine.

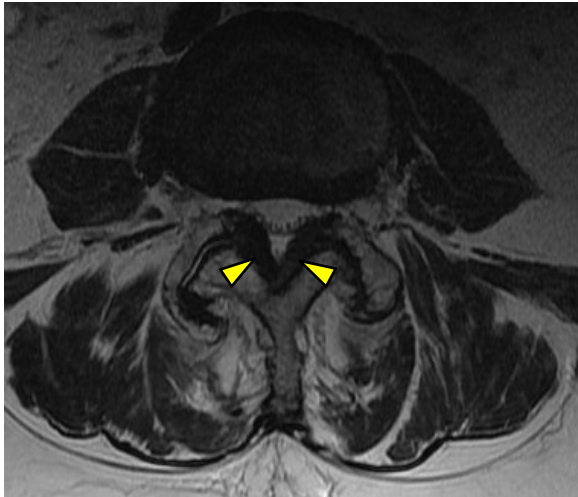


Figure 27:9. T2 axial image of hypertrophy of the ligamentum flavum and facets.

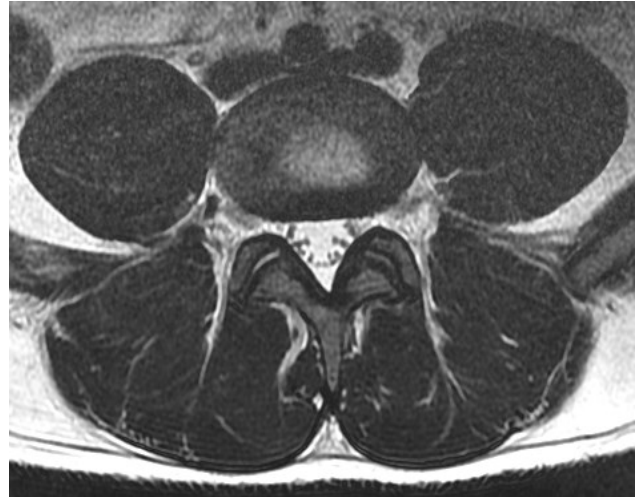


Figure 27:10. This T2 axial image reveals a relatively normal ligamentum flavum and facets.

Ligamentum flavum hypertrophy is an insidiously progressive finding that gradually contributes to central canal stenosis. Ligaments appear dark in these T2 weighted images.

Neurogenic Bladder

Normal urination occurs through a complex neurological synchronization of muscle contraction, muscle relaxation, reflexes, responsiveness, and consciousness. The neurology of urination is complex and reliant upon coordination between sympathetic, parasympathetic, and somatic nervous systems, and executive volition.

The two functions of the bladder are storage and voiding. Either of these can be affected by neurologic compromise. While MSK practitioners frequently think of incontinence in association with neurologic compromise, urinary retention is another condition that can result. Either retention of urine or incontinence of urine can happen depending on the location of the neurological insult.

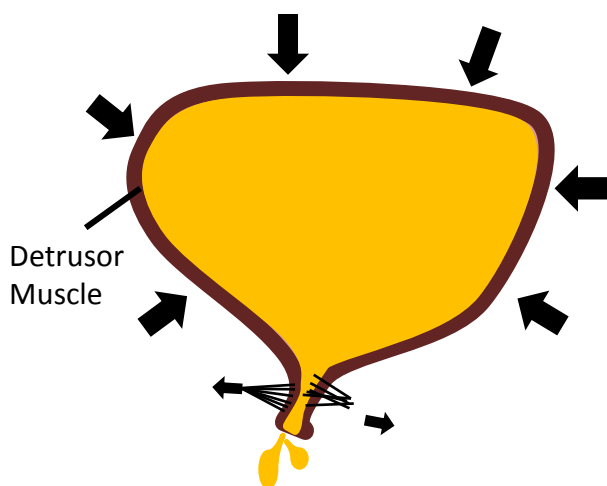


Figure 27:11. In normal voiding there is a coordinated contraction of the detrusor muscle and opening of the sphincters that allows normal urination.

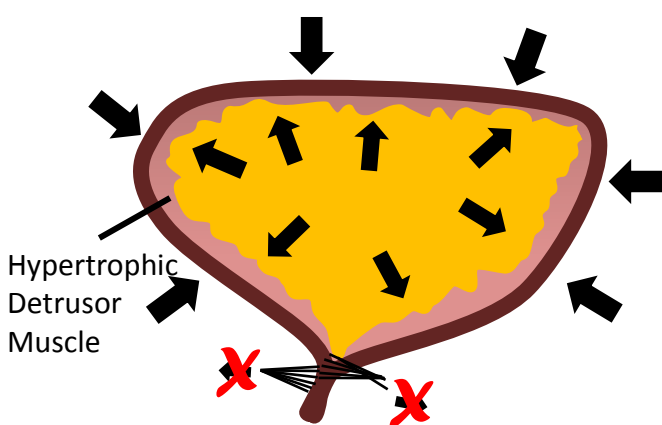


Figure 27:12. In neurogenic urinary retention the sphincters do not open and urine is retained. The detrusor muscle contracts to overcome the resistance of the sphincter. In time, the detrusor muscle will hypertrophy to the point that the thickened muscle can be recognized on MRI.

In a simplified explanation of urination, we can say that the urinary sphincters open and allow urine to escape while the bladder's detrusor muscle contracts to push the urine out of the bladder. In patients with neurological incontinence, the sphincter does not appropriately retain urine flow, and urine leaks out. In neurological urinary retention the sphincter does not open to allow urine to exit. This may result in hypertrophy of the detrusor muscle which strains to push urine through a closed sphincter.

Other urinary obstructions such as prostate hypertrophy, urethral obstruction, or cancer may also result in detrusor hypertrophy.

While evidence of a neurogenic bladder may be evident on MRI, MRI is not the medium of choice for making a diagnosis of neurogenic bladder.

Neurogenic Bladder

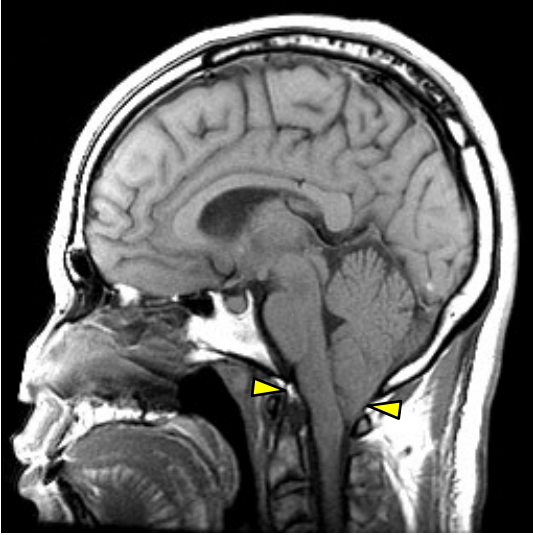


Figure 27:13. Chiari malformation (downward displacement of the cerebellar tonsils/hindbrain through the foramen magnum).

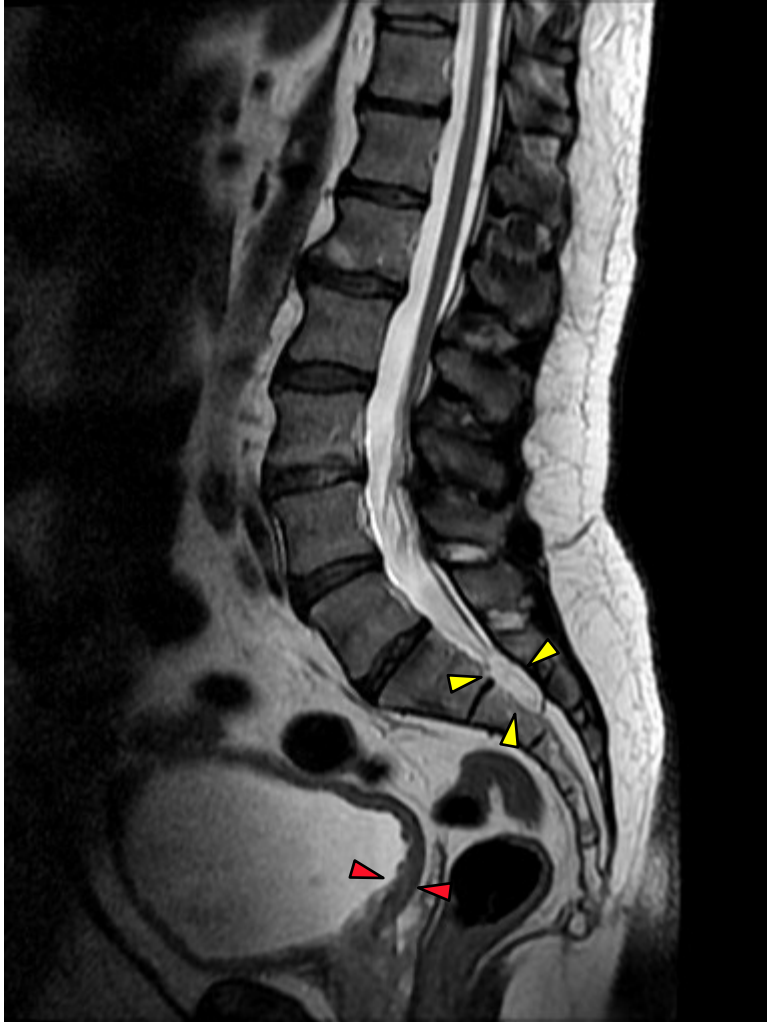


Figure 27:15. Thickening of the detrusor muscle (red arrows) of the bladder in this patient with a tethered cord syndrome resulting from a lipoma anchoring the filum terminale to the sacrum (yellow arrows). Neurogenic urinary retention can cause a greatly distended bladder .

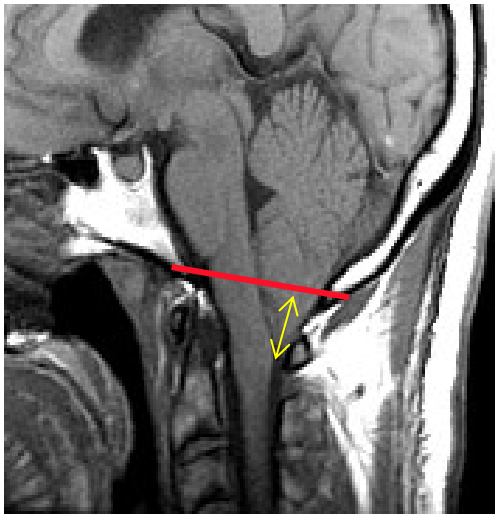
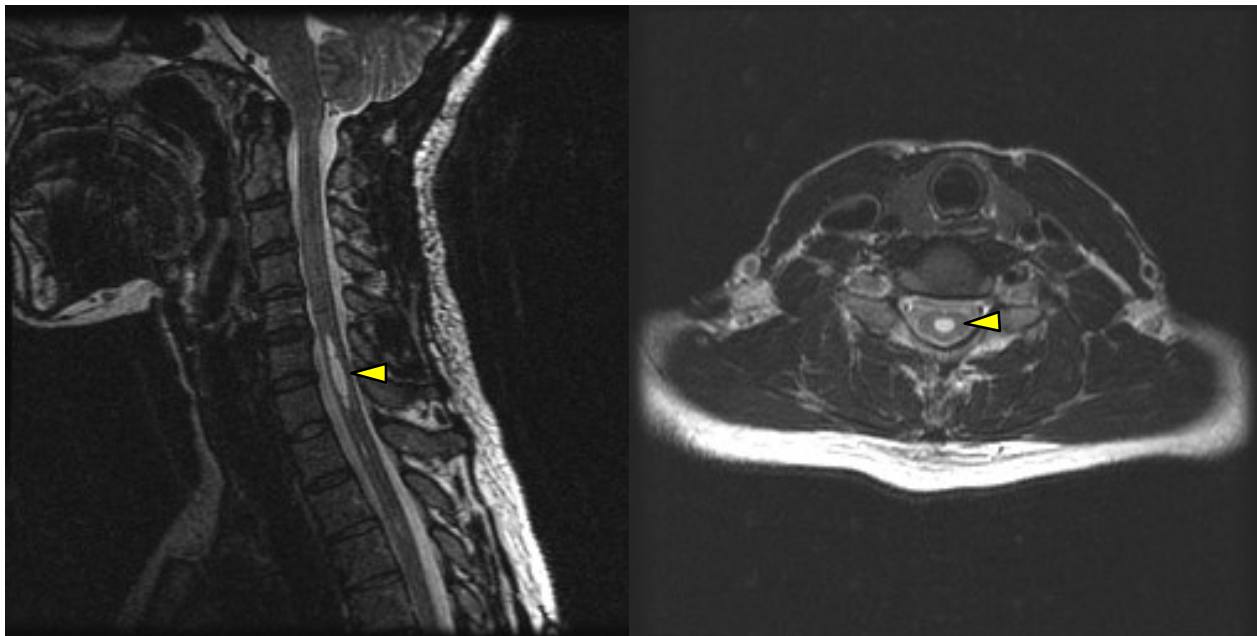


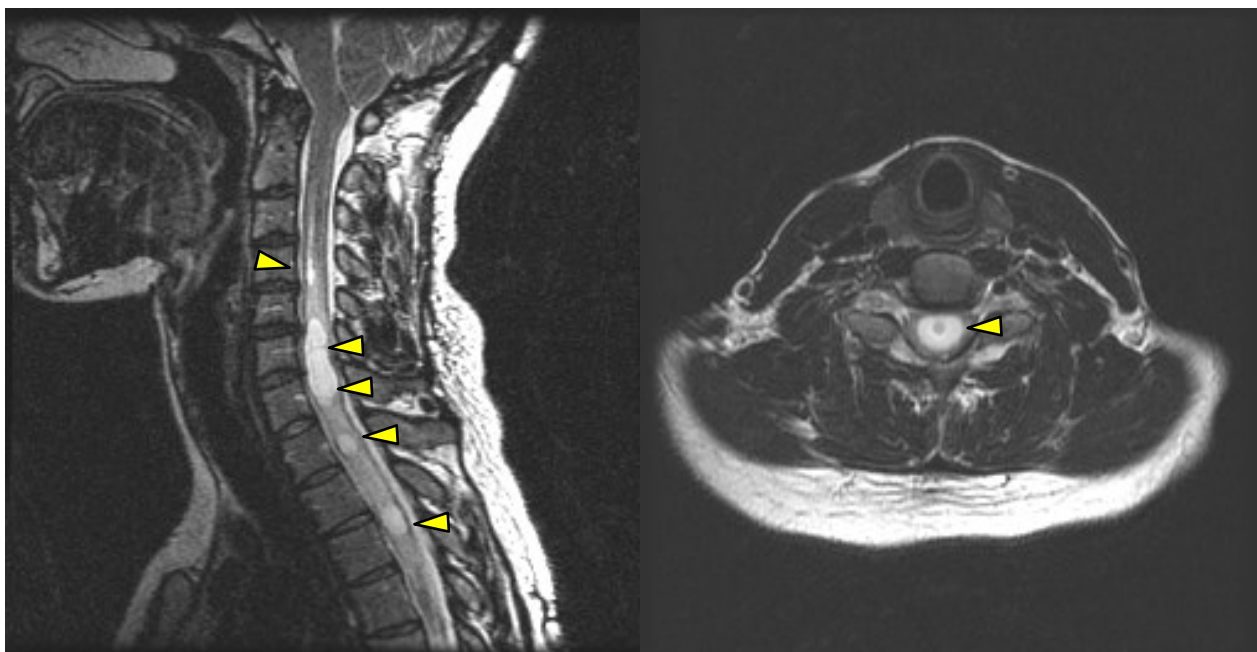
Figure 27:14. Chiari malformation is diagnosed by measuring the extent of downward displacement. This is done by drawing a line from the ophisthion to basion (the anterior and posterior margins of the foramen magnum) and measuring the distance from the line to the most inferior portion of the cerebellar tonsils. Normally this should be less than 3mm.

Lipomas of the filum terminale can become so large that they anchor or “tether” the spinal cord. This can result in neurologic compromise. There is also a greater likelihood of Chiari malformation, syrinx, and syringomyelia in patients with a tethered cord.

Neurogenic Bladder Syrinx



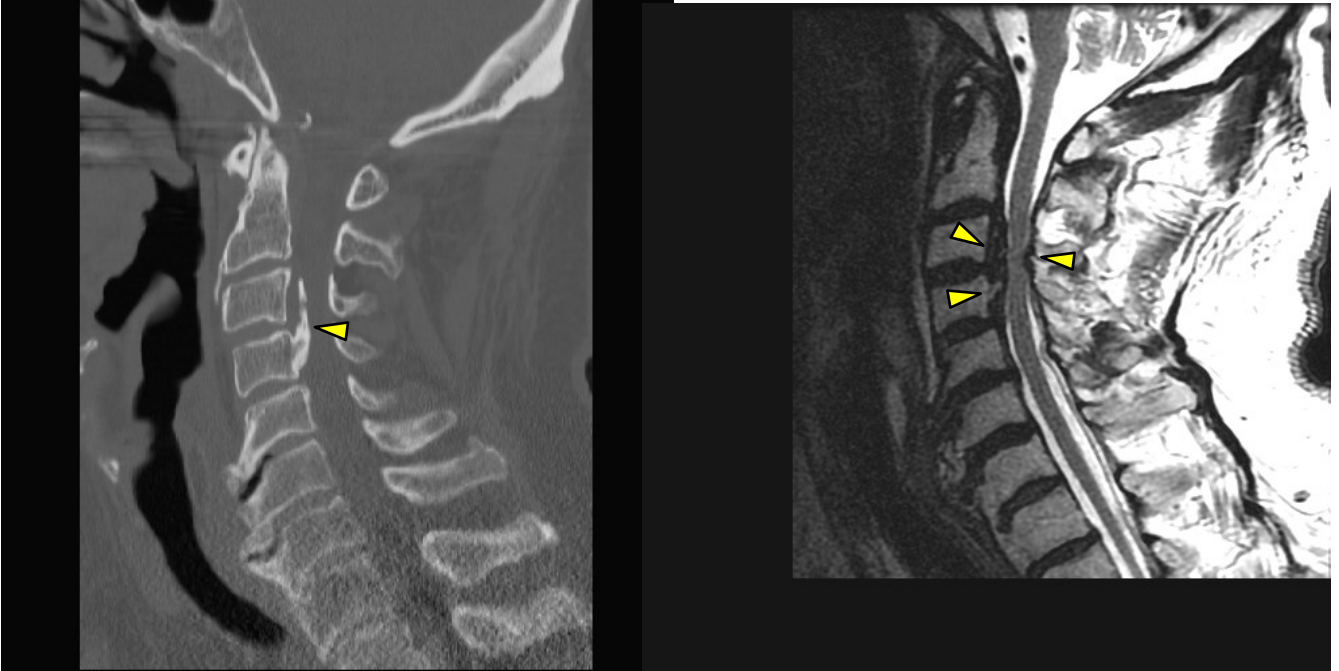
Figures 27:16 and 27:17. These two T2W images show the CSF-filled dilation of the central spinal canal. These findings are consistent with a syrinx.



Figures 27:18 and 27:19. The sagittal image on the left reveals several central spinal canal dilations. The axial image on the right shows the extent.

Dilation of the central spinal canal and filling with CSF is called a syrinx. A syrinx may result in a syringomyelia (syrinx progression and damage to the spinal cord). This can result in significant neurologic compromise including motor weakness, headaches, inability to distinguish hot or cold, and other symptoms including neurogenic bladder. Syringes are caused by congenital anomalies, trauma, spinal cord tumors, tethered cord, and Chiari malformations.

Neurogenic Bladder: Cervical Spondylotic Myelopathy



Figures 27:20 and 27:21. These two images (sagittal CT on the left and T2W sagittal MRI on the right) show the effects of cervical spondylotic occlusion of the central canal. This can result in myelopathy.

The most common cause of spinal cord pathology in patients over 55 is cervical spondylotic myelopathy (CSM). CSM is caused by the slow progression of osteophytic spurs within the spinal canal to the point that the spinal cord is compressed, producing myelopathy. The symptoms of CSM progress slowly—so slowly that the gravity of this condition is often missed and/or attributed to other age-related conditions.

The indistinct presentation of CSM leads to a broad number of potentially different diagnoses, including spinal cord tumors, syrinx (with syringomyelia), ALS, MS, normal pressure hydrocephalus, cerebral hemisphere disease, and peripheral neuropathy. It takes an alert clinician to identify when spondylosis progresses to CSM. In addition to particular radiographic findings, the following characteristic symptoms are attributed to CSM:

- gait spasticity
- upper extremity numbness and loss of fine motor control
- neck pain
- motor weakness in the extremities
- upper and lower motor neuron findings
- bowel and bladder signs
- Lhermitte's sign (electrical shock with cervical flexion).

Conus Medullaris Cyst



Figure 27:22. This FLETA sagittal image clearly shows a fluid-filled ovoid cyst at the conus medullaris. The cyst is hyperintense in this image.

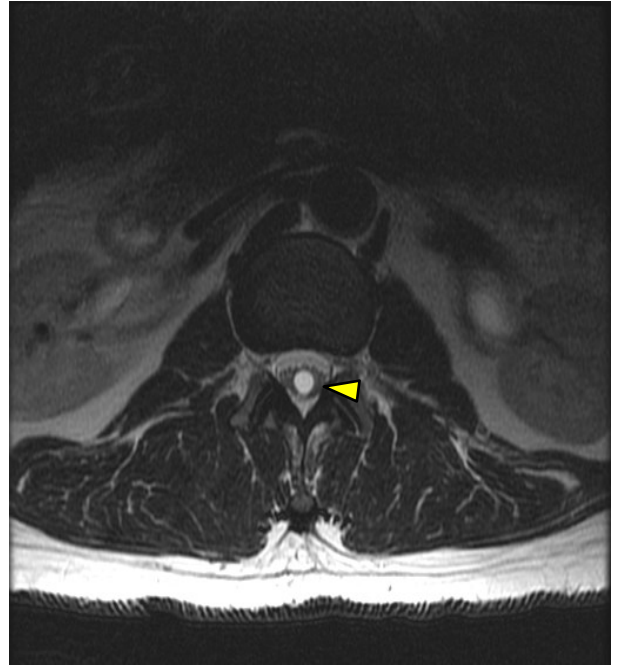


Figure 27:23. This T2W axial image displays the cyst as a hyperintense circular image.

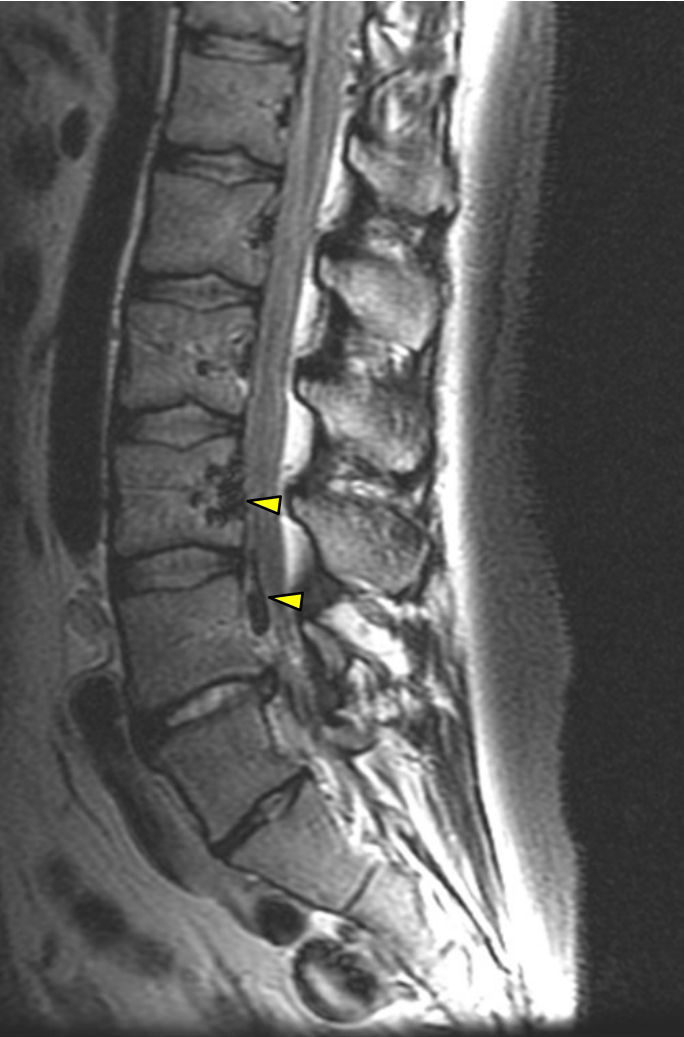
There are many reasons that a cystic cavity can form in the spinal cord. It might present as an incidental finding, or it may cause serious complications such as conus medullaris syndrome or cauda equina syndrome. Cystic cord lesions should be evaluated by a neurosurgeon.

Comparing T1WI, T2WI, and fat-suppressed images is useful in differentiating cystic lesions from lipomas.



Figure 27:24. This T1W sagittal image displays the cyst as a hypointense (darkened) ovoid image.

Engorged Epidural Plexus



rest, shows minimal enlargement of the veins of the epidural plexus in a patient with agenesis of the inferior vena cava.

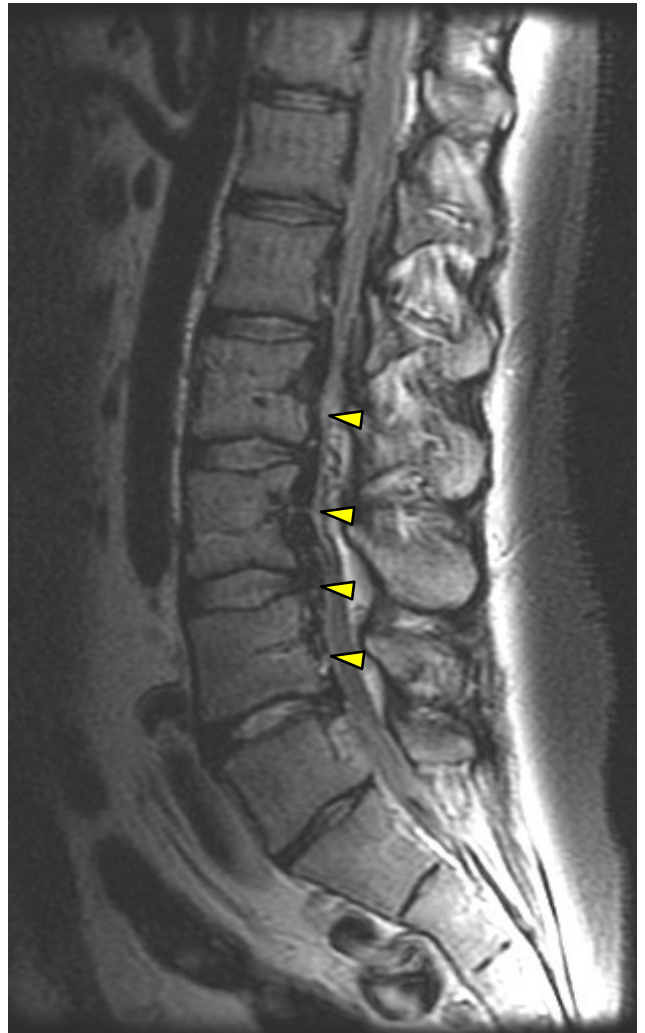


Figure 27:26. This image was taken after the patient exercised for 20 minutes riding a recumbent bike and then immediately entered the MRI tube. This image shows significant engorgement of the epidural plexus with displacement of the thecal sac.

In the stenosis or absence of the normal inferior vena cava, blood flow may be diverted to the epidural plexus. The epidural plexus may contribute to the transport of blood back to the heart from the lower extremities. This has been reported to occur in cases of inferior vena cava thrombosis, agenesis of the inferior vena cava, and in the occlusion of inferior vena cava flow from liver disease. This phenomenon may displace the cauda equina or nerve roots and can be symptomatic.

In one study reviewing 9640 patients' MRIs, Paksoy found that 13 patients had inferior vena cava obstruction resulting in epidural venous engorgement. A busy practitioner could conceivably see several of these cases in a career.

Large Non-Displaced Discs

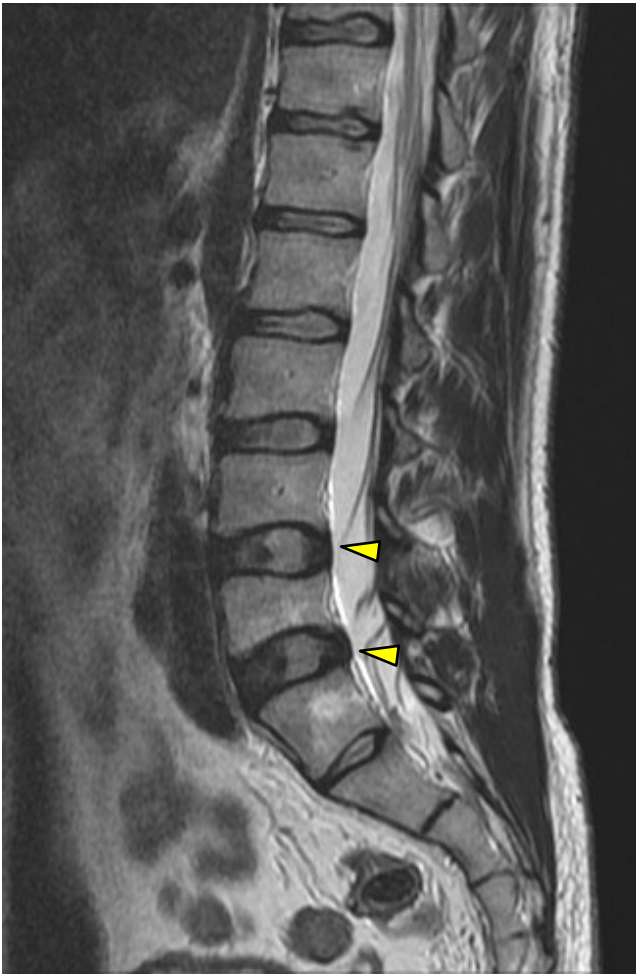


Figure 27:27. T2 weighted sagittal image of large intervertebral discs. This is a normal variant.

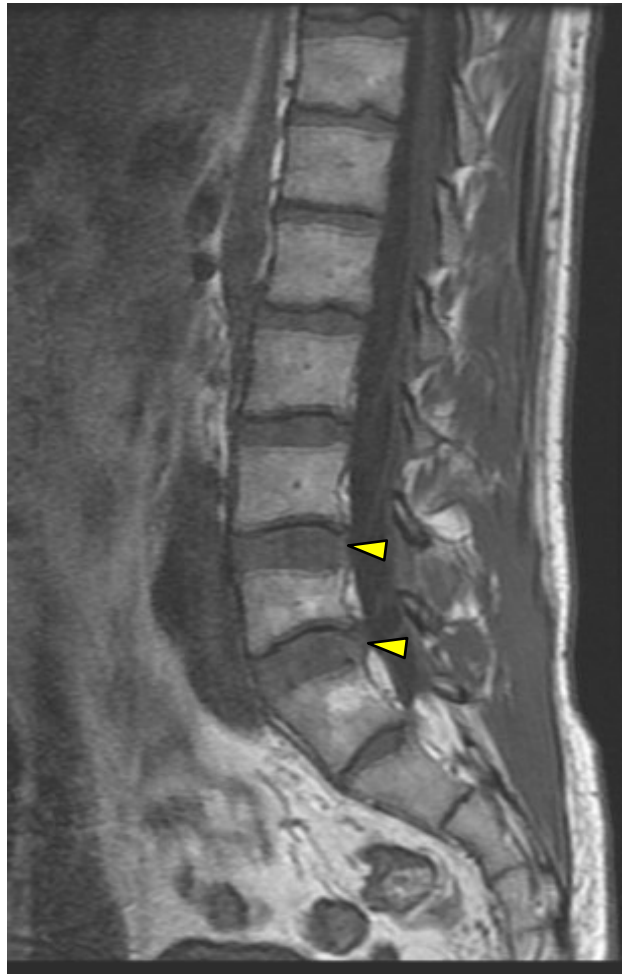


Figure 27:28. T1 weighted sagittal image of the large intervertebral discs.

These images show a normal variant: abnormally large disc height without displacement.

Intranuclear Cleft

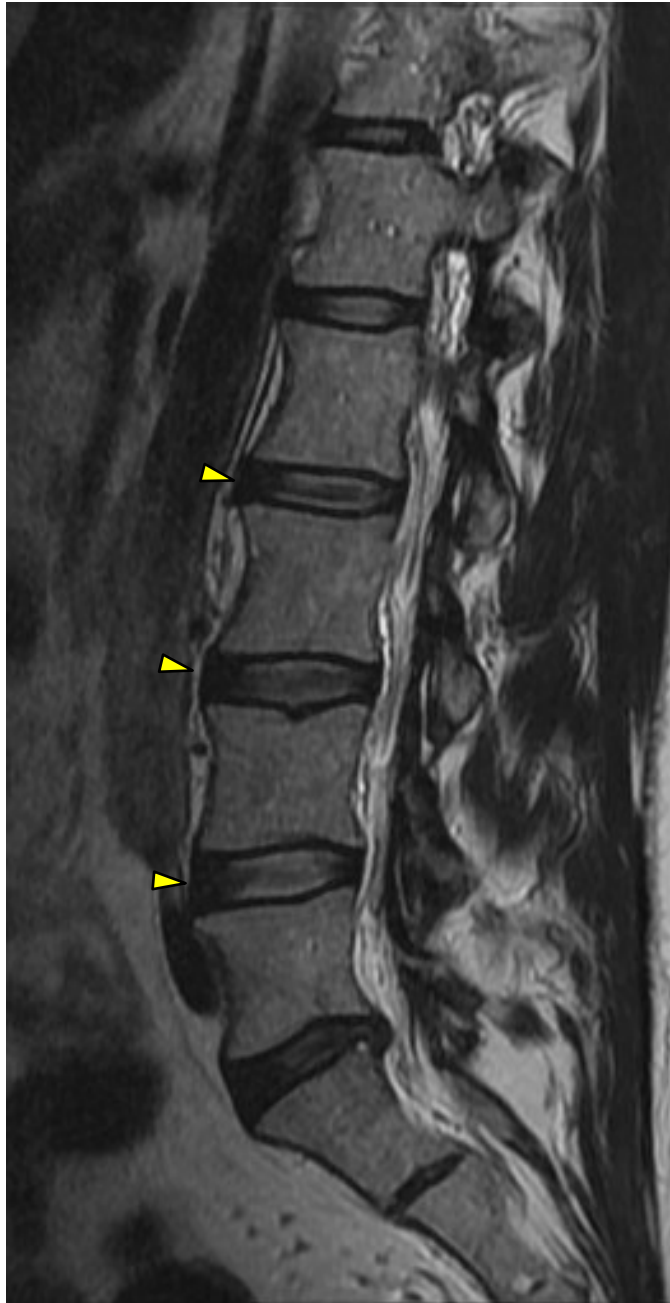


Figure 27:29. This T2 weighted sagittal image shows the normal variant of intranuclear clefts. This is a normal sign of aging.

This T2 weighted sagittal image demonstrates lines through the intervertebral discs. This is an early sign of aging (constant in those 30 years old and older). This is a normal variant known as an intranuclear cleft.

Sebaceous Cyst



Figure 27:30. Sagittal T1 weighted image.

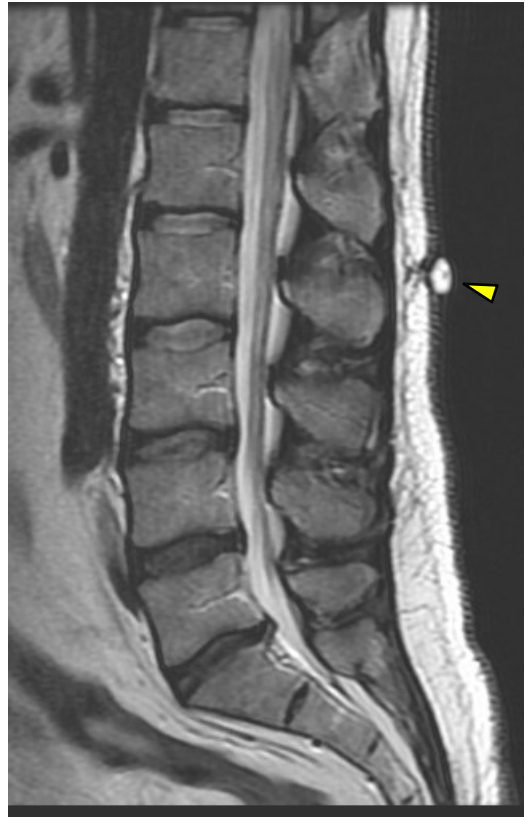


Figure 27:31. Sagittal T2 weighted image.

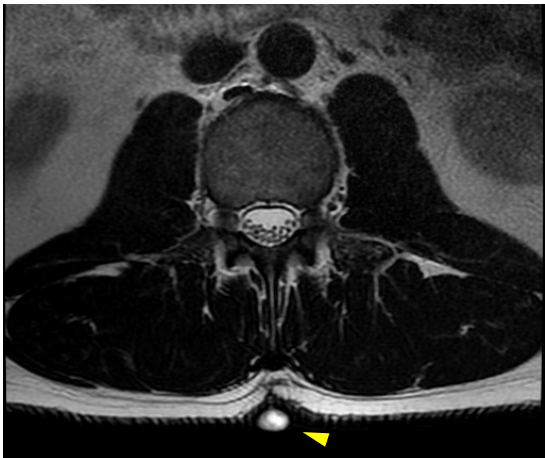


Figure 27:32. Axial T2 weighted image.

Sebaceous cysts are not typically a source of great concern to MSK practitioners outside of being an occasional source of pain and infection. Nonetheless, a back pain specialist should be able to discern the difference of this common lesion from normal and from more significant cystic lesions. These images reveal a sebaceous cyst posterior to the spinous process of L2.

Suggested Reading

Kamerath J, Morgan WE. Absent inferior vena cava resulting in exercise-induced epidural venous plexus congestion and lower extremity numbness: a case report and review of the literature. *Spine (Phila Pa 1976)*. 2010 Aug 15;35(18):E921-4.

Paksoy Y, Gormus N. Epidural venous plexus enlargements presenting with radiculopathy and back pain in patients with inferior vena cava obstruction or occlusion. *Spine (Phila Pa 1976)*. 2004 Nov 1;29(21):2419-24.

Aguila L, Piraino DW, Modic MT, et al. The intranuclear cleft of the intervertebral disk: magnetic resonance imaging. *Radiology* April 1985 155:155-158.

Fukuda K, Ozaki T, Tsumura N, Sengoku A, Nomi M, Yanagiuchi A, Nishida K, Kuroda R, Iguchi T. Neurogenic bladder associated with pure cervical spondylotic myelopathy: clinical characteristics and recovery after surgery. *Spine (Phila Pa 1976)*. 2013 Jan 15;38(2):104-11. doi: 10.1097/BRS.0b013e318267af02.

Milhorat TH, Bolognese PA, Nishikawa M, Francomano CA, McDonnell NB, Roonprapunt C, Kula RW. Association of Chiari malformation type I and tethered cord syndrome: preliminary results of sectioning filum terminale. *Surg Neurol*. 2009 Jul;72(1):20-35. doi: 10.1016/j.surneu.2009.03.008.

Baastrop CI. Proc.spin. vert.lumb. und einige zwischen diesen liegenden Gelenkbildungen mit pathologischen Prozessen in dieser Region. Fortschritte auf dem Gebiete der Rontgenstrahlen, 1933, 48:430-435.

Coleman LT, Zimmerman RA, Rorke LB. Ventriculus Terminalis of the Conus Medullaris: MR Findings in Children. *AJNR Am J Neuroradiol* 16:1421-1426, August 1995.

Lai SW, Chan WP, Chen CY, Chien JC, Chu JS, Chiu WT. MRI of epidermoid cyst of the conus medullaris. *Spinal Cord*. 2005 May;43(5):320-3.

Wu JS, Hochman MG. Soft-tissue tumors and tumorlike lesions: a systematic imaging approach. November 2009 *Radiology*, 253, 297-316.

Chen CK, Yeh L, Resnick D et-al. Intraspinal posterior epidural cysts associated with Baastrop's disease: report of 10 patients. *AJR Am J Roentgenol*. 2004;182(1): 191-4.

Rutherford EE, Tarplett LJ, Davies EM et-al. Lumbar spine fusion and stabilization: hardware, techniques, and imaging appearances. *Radiographics*. 27 (6): 1737-49.

Upright MRI

28



The Case for Upright MRI



Figure 28:1. T1 weighted sagittal image taken in supine position. Image provided by FONAR Corporation and used with permission.



Figure 28:2. T1 weighted sagittal image of the same patient taken weight bearing. Instability of L4 is clearly visible on a weighted view, but not visible on a supine image. Image provided by FONAR Corporation and used with permission.

While lying supine may be comfortable for the patient and lends for a more stable study with less motion artifacts, it also may inhibit the visualization of certain lesions. Lumbar disc lesions, listhesis, ligament integrity disorders, stenosis, and stability disorders may be better visualized in an upright or dynamic/kinetic image. The images on this page show that an unstable L4 appears normal when viewed supine (figure 28:1), but it is evident when viewed in a weight-bearing dynamic image (weight bearing in flexion).

Upright MRIs



Figure 28:3. T2 weighted sagittal image taken in supine position. Image provided by FONAR Corporation and used with permission.



Figure 28:4. T2 weighted sagittal image of the same patient taken weight bearing. Instability of L3 is clearly visible on a weighted view, but not visible on a supine image. Image provided by FONAR Corporation and used with permission.

Timing of the Image

One of the aspects of MRI that is rarely discussed is the time of day the study is taken. The intervertebral disc has hydrodynamics that are time and position dependent. The discs are hydrophilic and absorb water when lying down. Conversely, as the day progresses with a person weight bearing, the discs lose hydration. This explains why people are taller in the morning and shorter as the day progresses. It may also explain why some spinal conditions are more symptomatic in the morning and regress as the day progresses. A common complaint is that it is difficult to put shoes on in the morning, but easy to take them off in the evening.

It may be better to take MRIs of suspected disc herniations in the morning than in the later part of the day. Taking an MRI at the time and position of greatest pain may yield the most valuable images.

Claustrophobia

Conventional MRI tubes are enclosed, confining and loud. This causes problems for patients who are claustrophobic. Claustrophobic patients frequently are sedated to acquire an MRI study. Upright MRIs are open and reduce the effect of claustrophobia.

Upright MRIs

Currently most MRIs are performed with the patient lying supine; while the supine position is easy for putting a patient in a position that is stable and less apt to move, it may not be the optimal view for visualizing particular spinal lesions such as spondylolisthesis.



Figure 28:5-7. In addition to allowing the patient to be upright for an MRI, some machines allow the patient to be positioned in various postures. For some patients this would allow the patient to have an image taken with reduced pain, but this feature can also be used to take an image while in a provocative (painful or symptom producing) posture. Images provided by FONAR Corporation and used with permission.

The premise behind the concept of upright MRI is that visualization of some lesions may be position dependent. An intervertebral foramina occlusion may be evident in lumbar extension, but invisible while supine. A disc herniation may be evident when visualized while weight bearing and exacerbated in truncal flexion, but not visible or not as evident when the patient lies supine. Some patients have conditions that are worse with particular positions. By placing the patient in the position of provocation during an MRI study, it may be possible to “capture” an image when the lesion is most visible.

Upright MRIs are gaining popularity, but most MRI tubes are still horizontal. To obtain an upright MRI may require a purposeful effort on the part of the requesting provider.

Upright MRIs

Figure 28:8. Disc pressure is affected by body position. Weight bearing MRI allows the image to be taken in the position that is most provocative or the position of increased disc pressure. Currently most MRIs are taken with the patient in the position that provides the lower level of disc load: supine.

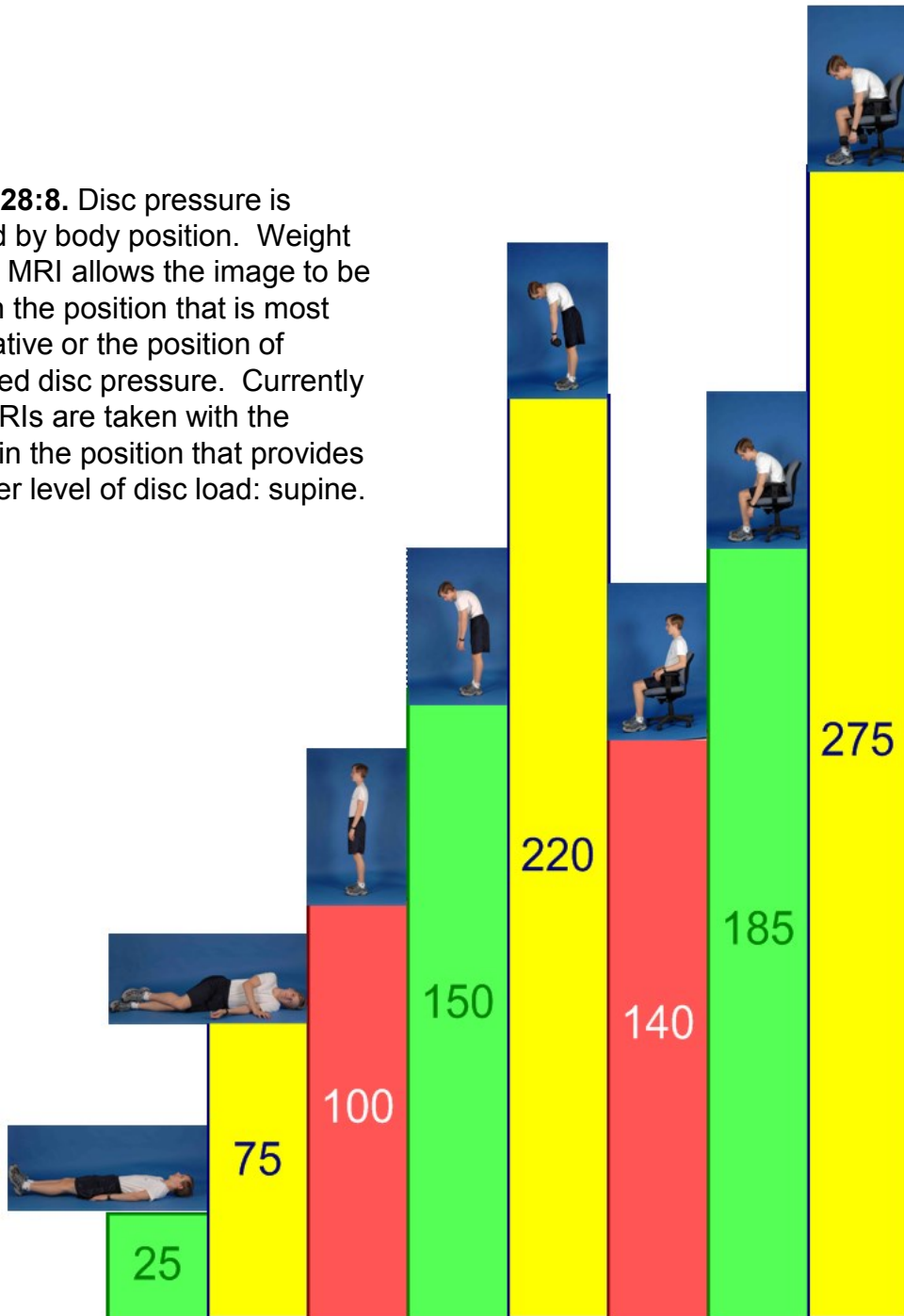


Image from TheLumbarDisc.com

Based on:

Nachemson A: The Load on Lumbar Disks in Different Positions of the Body, Clin. Orthop., 45:107-122, 1966

Suggested Reading

Hong SW, et al., Missed spondylolisthesis in static MRIs but found in dynamic MRIs in the patients with low back pain. *The Spine Journal*, 7 (2007) p 69S.

Nachemson AL. Disc pressure measurements. January/February 1981 - Volume 6 - Issue 1, pp: 1-106.

Nachemson AL. The load on lumbar disks in different positions of the body, *Clin Orthop*, 45:107-122, 1966.

http://www.fonar.com/pdf/Spine_Journal_UCLA_study.pdf

Artifacts

29



Artifacts

Artifacts are a common finding on MRI. An artifact is an alteration of the MRI images in a manner that creates distortion. A detailed explanation of what causes these artifacts would require a discussion about the physics of MRI. That discussion will not take place in this book. This chapter will instead point out some common artifacts seen in MR and provide a superficial description of what causes the artifact.

The three main categories of MRI artifacts are (1) patient-triggered artifacts, (2) processing or signal-triggered artifacts, or (3) machine-generated artifacts.

Patient-triggered artifacts include motion artifacts, flow artifacts, and metal artifacts. A blurred or distorted image from the patient moving during the procedure is called a motion artifact. Variations in blood flow speed will alter the MR machine's ability to achieve an optimal image. Metal artifacts are distorted images caused by the presence of metal in or near the patient. Ferrous metals will have the greatest impact on the quality of the MRI image. This is one reason, along with safety, that titanium (a non-ferrous metal) is preferred for surgical implantation.

Processing or signal-triggered artifacts include chemical shift artifacts, partial volume artifacts, wrap around artifacts, and ringing artifacts (aka Gibb's phenomenon). Chemical shift artifacts occur at anatomical points of interface between fat and water.

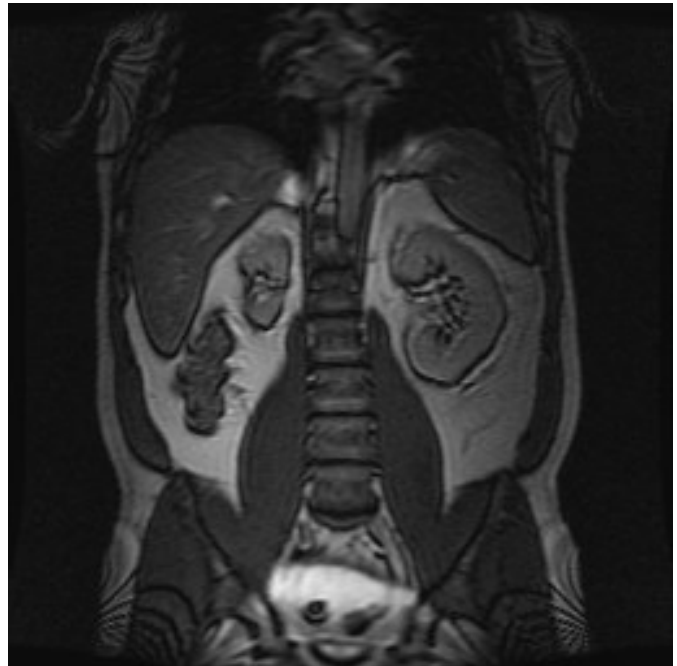
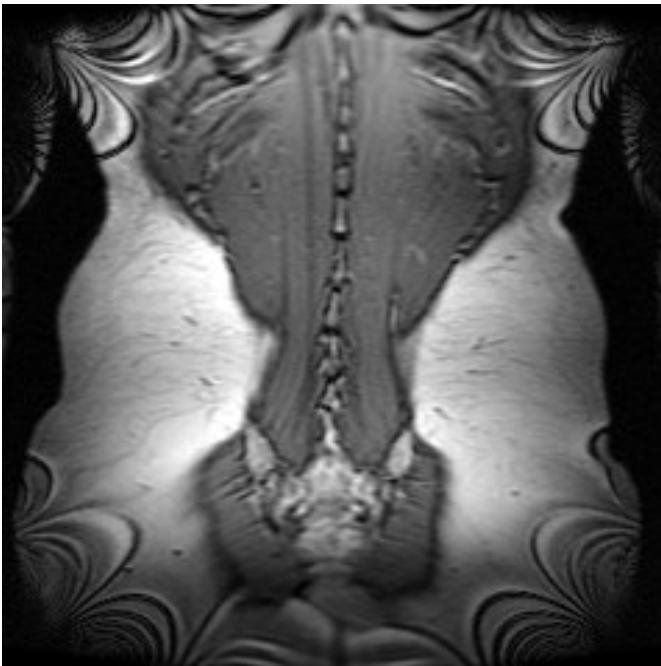
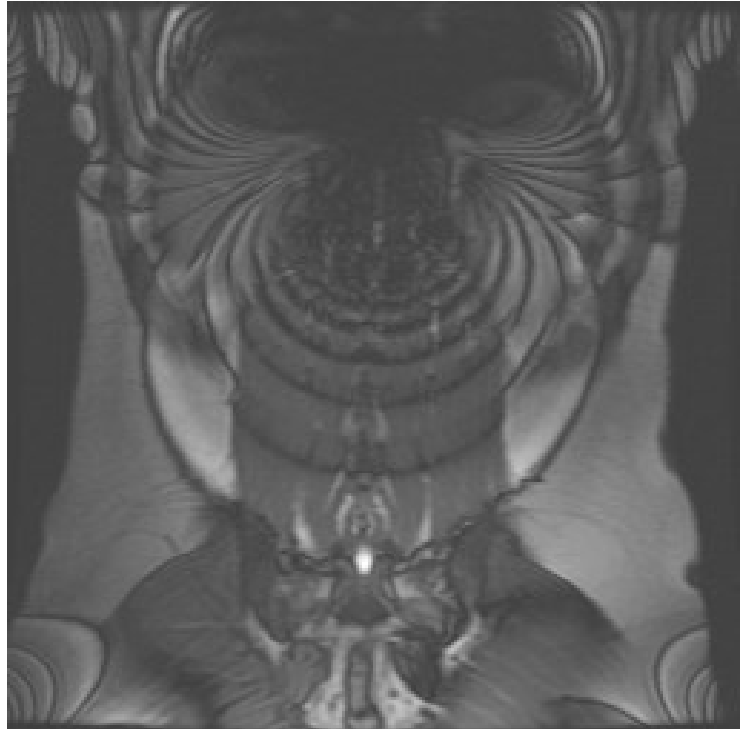
Partial volume artifacts arise from variations the size of the anatomic structure versus the size of the pixel used to depict the anatomic structure. Items smaller than the pixels that represent them in the computerized image may appear distorted or be absent from the image.

Wrap around artifacts occur when there is a spatial cartography error and portions of the anatomy which should be viewed on one side of the image are visible on the opposite side of the image. This is the result of corruption in the processing of the image.

Ringing artifacts are the production of a series of parallel lines of alternating high and low intensity signals. This phenomenon occurs near sharply contrasted boundaries.

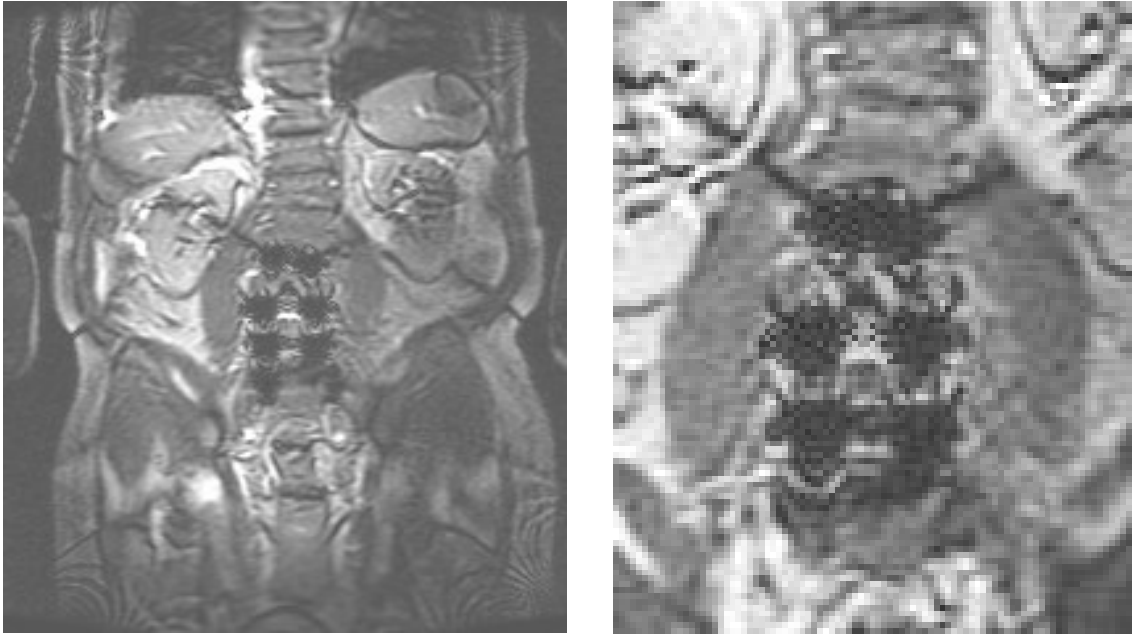
The subject of machine-generated MR artifacts is an escalating body of information. There are many ways that the MR machine, hardware, other mechanical factors, and radiofrequency waves can disrupt normal MRIs. Other than to introduce the concept that there is a broad field of machine-generated artifacts, this book will not attempt to delve into this subject.

Artifacts

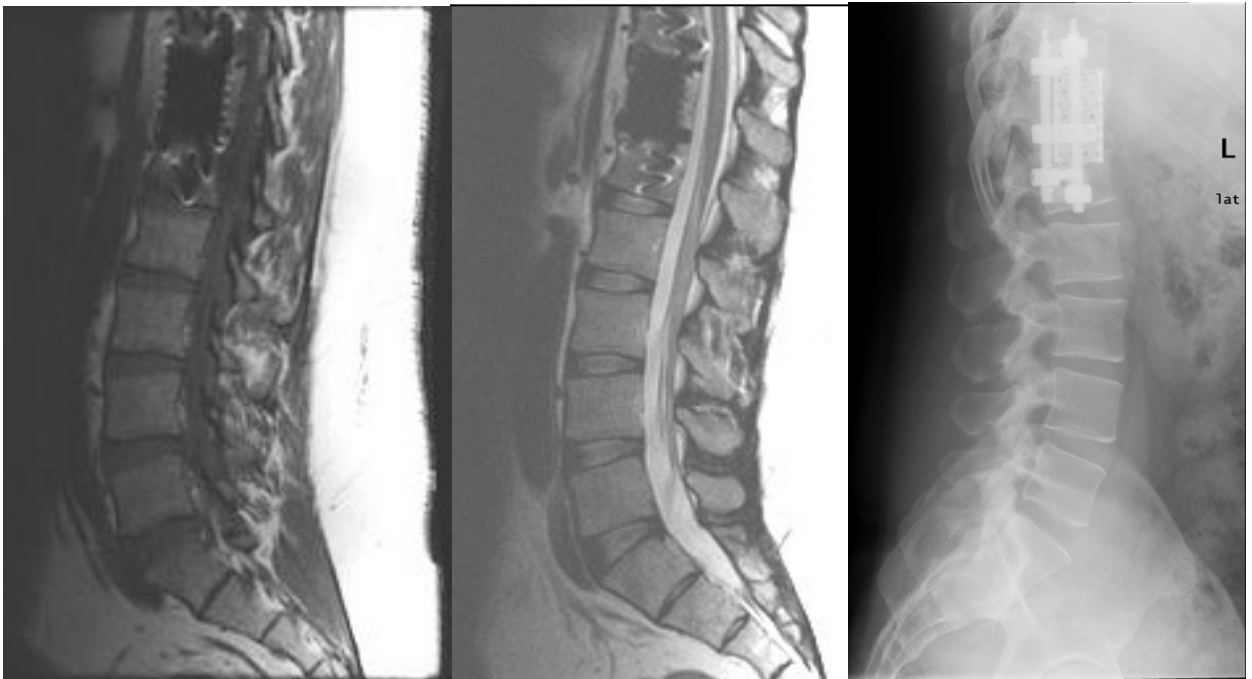


Figures 29:1-4. Lumbar MRIs are subject to the appearance of various artifacts that may be distracting and are of no clinical significance. These images show spiral distortion artifacts that degrade the image quality, but are not clinically relevant.

Metal Artifacts

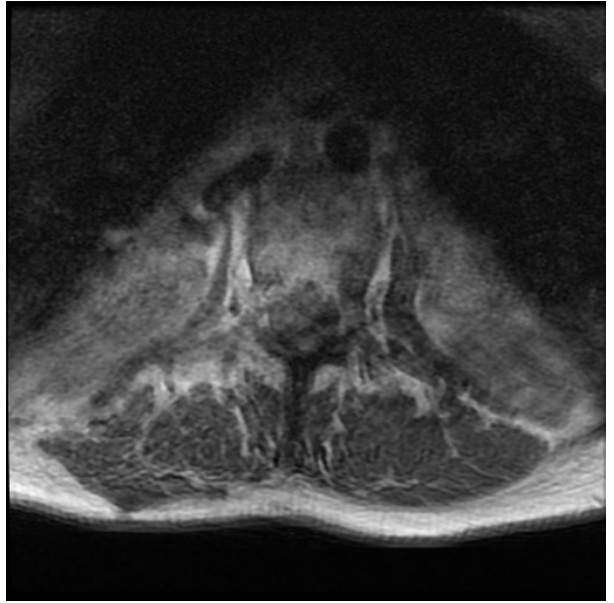


Figures 29:5 and 29:6. Post-surgical metallic artifacts. These transpedicular titanium screws have a spider-like appearance in these coronal images.



Figures 29:7 and 29:8. Post-surgical metallic artifacts. These images show a metallic artifact left by the surgical repair of fractures of T11, T12, and L1. The images from left to right are a T1 weighted sagittal, a T2 weighted sagittal, and a plain film lateral lumbar radiograph.

Artifacts



Figures 29:9 and 29:10. Motion artifacts. These two axial images show motion artifacts. The patient moved during the study, degrading the diagnostic quality of the study.

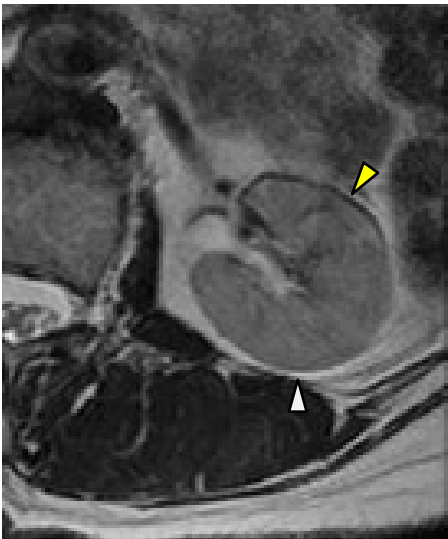


Figure 29:11. Chemical shift artifact. Note the black line (yellow arrow) at the margin of the kidney and the surrounding fat, as well as the white line (white arrow). Black line and white line artifacts are created at fat/water interfaces.



Figure 29:12. This plain film lateral lumbar radiograph reveals a surgically implanted medical device, in this case a spinal cord stimulator. This device contains ferrous metal and taking an MRI of this patient could prove to be disastrous.

Suggested Reading

Smith TB, Nayak KS. MRI artifacts and correction strategies. *Imaging Med.* (2010) 2(4).

Erasmus LJ, Hurter D, Naudé M, Kritzinger HG, Acho S. A short overview of MRI artefacts *SA Journal of Radiology*, August 2004.

Systematic Sequence of Interpretation



Systematic Interpretation of the Lumbar MRI

After hundreds of pages of learning the details of what can be found in a lumbar MR, looking at an MRI can be daunting unless you have a system of review. At this point I would like to reintroduce the system that we first purposed in Chapter 2. This system ensures that you cover the images in a logical manner. The next pages expand on how to analyze axial and sagittal sequences in detail. As you develop an eye for the subtleties found in lumbar MRI, you will find that sticking to a system of observation will help you to avoid missing important findings. With time you will become more and more proficient in streaming through MRIs and be able to scan MRI without referring to these notes.

Sequence of Systematic Interpretation of Lumbar MRI Images

1. Verify patient identifiers and date of examination.
2. Confirm that the images and the studies are in order if using film rather than digitized images.
3. View the sagittal T2 weighted images from left to right.
4. View the sagittal T1 weighted images from left to right.
5. View and analyze the T2 weighted axial images from caudal to cephalad.
6. View and analyze the T1 weighted axial images from caudal to cephalad.
7. Review your findings and compare to the radiologist's report.
8. Determine if the radiographic findings are clinically significant or coincidental findings.
9. Integrate collaborative MRI findings into patient care.

Sequential Analysis of Sagittal Images

1. Identify the left-right orientation. Sagittal images represent anatomic slices in a vertical plane which travel through the body from posterior to anterior and divides the body into right and left components. Scroll from left to right. If you are unable to identify the orientation of the sagittal images, remember that the aorta is on the left (right in the MRI) and that the inferior vena cava lies on the right (left in the MRI). The aorta typically has greater girth and a more symmetrically round appearance.

2. Analyze the spine from a global view. Scan through the sagittal images and look for larger, more obvious findings:

Alignment of the spine – Spondylolisthesis and retrolisthesis can be usually be discerned on sagittal inspection. Scoliosis can be a little more difficult. On sagittal imagery a scoliosis will present with partial views of structures and a contorted view of the spinal canal and vertebral bodies.

Vertebral body shape – Identify endplate disruption, Schmorl's nodes, compression fractures, block vertebrae, and fusion.

Vertebral body content – Analyze the cortical bone for edema, tumors, fatty infiltration, and hemangiomas.

Posterior Elements – Evaluate the facets, the pars, spinous processes, pedicles, and the lamina.

End plates – Look for sclerotic changes and alterations in signal intensity. Also look for disruptions or fractures of the endplates.

3. Intervertebral foramina:

The IVF should be a light-colored peanut-shaped image with a gray dot in the middle. The light color is due to the fact that it is in the foramina. When displaced, the light-colored fat will alter in shape. The gray dot in the foramina is the exiting nerve root.

4. The discs and the canal:

Look for alterations in disc height. Increased disc height may occur with discitis. Loss of disc height and reduced water content is indicative of degeneration. Disc tears and derangements may also be observed in sagittal imagery. Note disruptions of the thecal sac, the cauda equina, and nerve roots.

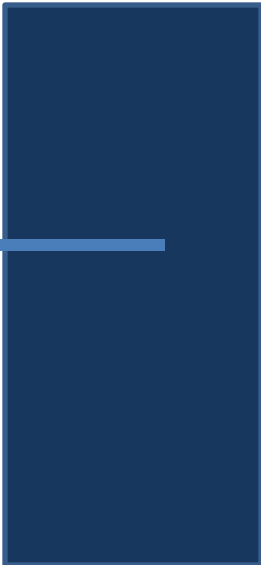
High intensity zones (HIZ) may be observed in T2 weighted images. These bright-colored zones indicate the presence of disc tears, scarring, or vascularization of the annulus.

The cord should terminate at about the level of L1. Increased signal (brightness) on T2 weighted images may indicate cysts, tumors, syrinxes, or demyelination.

Sequential Analysis of Axial Images

1. Identify left and right. Axial images are backwards; structures that you see on the left of an axial image represent structures found on the right of the patient.
2. Begin your analysis caudally proceeding cephalad. The sacrum will be easily recognizable. Observe the S1 nerve roots. Look for perineural (Tarlovs' cysts) which occur most commonly at the S2 and S1 nerve roots.
3. As you scroll superiorly, observe the L5-S1 disc. Note the circumferential margin of the disc, and inspect it for derangement. Scroll past the disc to the L5 vertebra. Note that L5 is commonly shaped like a lemon when viewed axially. Observe the bony integrity of L5. Look for elongation of the central canal which may be indicative of a spondylolisthesis.
4. The canal should be intact and not effaced. Look for effacement or disruption of the thecal sac by discs, osteophytes, or spondylosis, or other space-occupying lesions.
5. Look at the lumbar discs and evaluate for tears, herniations, nerve compression, and degeneration.
6. Identify the ligamentum flavum, and look for signs of hypertrophy and subsequent stenosis.
7. Evaluate the posterior elements of the vertebrae. Look for pars defects, spina bifida, facet hypertrophy, and overall posterior ring integrity.
8. Examine the retroperitoneal space.
9. In addition to examining the spinal structures, evaluate and note the paraspinal muscles, multifidus muscles, iliopsoas muscles, the great vessels, and the kidneys.
10. After scrolling up the lumbar spine, reverse directions and descend the spine to follow the course of the nerve roots. Start cephalad and scroll (if using a computer) caudally. If looking at film, move from slide to slide. Follow the migration of the nerve rootlets from the cauda equina from their posterior central location to the lateral anterior portion of the thecal sac and then leaving the sac as traversing nerve roots.

Appendix



Shades of Gray

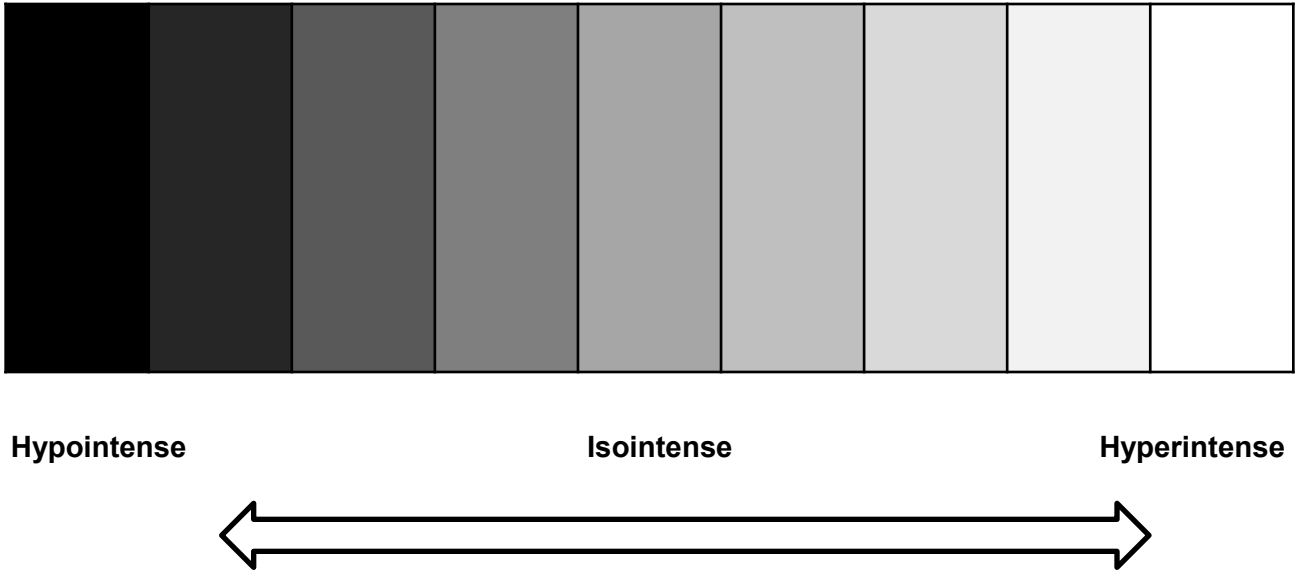


Figure 1. Shades of gray. Interpreting findings on MRI is not always black or white. When we use terms like hypointense or hyperintense, we are not saying that the image will be black or white, but will tend toward darkness or lightness on a grayscale continuum.

Which Radiological Studies Should You Order?

Develop a relationship with your radiologist, and be willing to consult with the radiologist prior to ordering radiological studies. Explain the history, and work with the radiologist to determine the best study for each patient.

Trauma	<ul style="list-style-type: none">•Plain films may be used initially to determine if there is an unstable injury or displacement•Non-contrast CT•MRI to evaluate cord integrity
Tumors	MRI with contrast enhancement
Inflammation and Vascular Disorders	MRI with contrast enhancement
Scoliosis	Plain films, unless pathology is suspected, then MRI
Congenital anomalies	MRI without contrast enhancement
Infections	MRI with contrast enhancement
Nerve Root Compression	MRI
Spondylolisthesis	<ul style="list-style-type: none">•Plain film radiographs•CT•MRI if there is a need to evaluate neuronal involvement

Note: There is an inherent danger in using contrast enhancements. These risks include allergic reaction, shock, and death.

CTs are less expensive than MRI and are the medium of choice for head and neck trauma. They utilize significant doses of radiation and increase the risk of cancer.

MRI Image Type

MRI image types enhance various tissue types differently. This allows the differentiation of tissues by the specialist. The various types of MRI images are as follows:

- 1. T1 Weighted Image** Water densities are dark; fat densities are bright. T1WI have greater anatomic detail than T2WI.
- 2. T2 Weighted Image** Water and fat densities are bright; muscle appears intermediate in intensity.
- 3. Fat Suppressed T2 Weighted Image** Water densities are bright; fat is suppressed and dark.
- 4. Intermediate T2 Weighted Image** Ligaments and cartilage are viewed as very dark.
- 5. Gadolinium Enhanced T1 Weighted Image** Gadolinium is an injected enhancement. It is used to identify pathology.
- 6. Fast Spin Echo (FSE)** Frequently used in T2 weighted musculoskeletal imaging. Allows quicker image acquisition. Fat is bright on T2 weighted images. Marrow or subcutaneous pathology may not show unless fat suppression is used.
- 7. FSE STIR (Short T1 Inversion Recovery)** Decreased signal intensity (brightness) from fat and an increased signal from fluid and edema. This is useful in identifying soft tissue and marrow pathologies.
- 8. Proton Density** Proton density uses a mixture of T1 and T2 images. It is characterized by enhanced anatomical detail and poor tissue contrast.
- 9. Fat Saturation** Fat saturation employs a “spoiler” pulse that neutralizes the fat signal without affecting the water and gadolinium signal. Fat saturation is used with T1 weighted images to distinguish a hemorrhage from a lipoma. When used with FSE T2 weighted images, fat saturation can enhance marrow or soft tissue pathology.
- 10. FIESTA (Fast Imaging Employing Steady sTate Acquisition)** This method of image acquisition captures structures rapidly and provides high quality images of fluid-filled structures.

William E. Morgan practices in Bethesda's Walter Reed National Military Medical Center, the President's Hospital. He has been credentialed at five hospitals and serves as a consultant to various United States government executive health clinics in Washington, D.C., caring for government leaders. He has served as a consultant to the White House, the Veterans Administration, the U.S. Navy, and the U.S. Army. Dr. Morgan holds faculty adjunct appointments at institutions of higher learning: He is a professor for New York Chiropractic College and assistant professor for F Edward Hébert School of Medicine. Additionally he is on the Board of Trustees for Palmer College of Chiropractic.

Dr. Morgan is the team chiropractor for the United States Naval Academy football team. A veteran of military service, he has served in Naval Special Warfare Unit One, Marine Corps Recon, and in a Mobile Dive and Salvage Unit.

Dr. Morgan is a 1985 graduate of Palmer College of Chiropractic-West. In addition to many other awards, he has received the American Chiropractic Association's Chiropractor of the Year Award. He has also been featured on CCN.com and has been interviewed by the Washington Post. William Morgan has written dozens of articles on integrated medicine, chiropractic, and health care. Dr. Morgan uses MRI in an integrated clinical setting on a daily basis and is well suited to share this knowledge in a practical and engaging manner.

He can be contacted through his website: DrMorgan.info



The Lumbar MRI in Clinical Practice is written for the busy practitioner. It combines easy to understand schematics, illustrations and explanations with an exhaustive gallery of lumbar MRIs. This book will quickly immerse the reader with practical applications. This book is the perfect companion for any specialist or resident who treats the lumbar spine:

- Physical Medicine and Rehabilitation Specialists
- Orthopedists
- Neurologists
- Neurosurgeons
- Chiropractors
- Physical Therapists
- Team Physicians

You will not get lost in the details with this manual, it does not delve deeply into the details of MRI physics, but it does tell you what you need to look for on a lumbar MRI to make a difference in your patient's care.

